DEPARTMENT OF ENERGY
Environmental Management Los Alamos Field Office (EM-LA)
Los Alamos, New Mexico 87544

EMLA-2020-1452-02-001 May 28, 2020

Mr. Kevin Pierard
Bureau Chief
Hazardous Waste Bureau
New Mexico Environment Department
2905 Rodeo Park Drive East, Building 1
Santa Fe, NM 87505-6313

Subject: Submittal of the Fate and Transport Modeling and Risk Assessment Report for RDX Contamination in Deep Groundwater

Dear Mr. Pierard:

Enclosed please find two hard copies with electronic files of the "Fate and Transport Modeling and Risk Assessment Report for RDX Contamination in Deep Groundwater." Submittal of this report fulfills fiscal year 2020 Milestone #7 of Appendix B of the 2016 Compliance Order on Consent (Consent Order). The report includes a comprehensive present-day risk assessment and predictions for future fate and transport of RDX (Royal Demolition Explosive) in the regional aquifer. The report reflects discussions held in several pre-submission meetings with the New Mexico Environment Department and the U.S. Environmental Protection Agency on September 9, 2019; January 28, 2020; March 31, 2020; and April 13, 2020.

This report addresses the 2016 Consent Order benchmark of evaluating whether there is a need for cleanup "triggered by potential unacceptable risk…." The overall conclusions of the risk assessment presented in this report are (1) there is no current or reasonably foreseeable future unacceptable risk to human health associated with RDX contamination in the regional aquifer and (2) based on land use controls restricting potable groundwater wells, there is no current, potential, or reasonably foreseeable future unacceptable risk to human health from drinking groundwater from the perched-intermediate groundwater. The U.S. Department of Energy Environmental Management Los Alamos Field Office (EM-LA) and Newport News Nuclear BWXT-Los Alamos, LLC (N3B) recommend long-term groundwater monitoring to monitor the plume and ensure protection of human health. To implement a comprehensive and protective monitoring program, EM-LA and N3B propose a long-term monitoring plan. The monitoring plan would include action levels that would be used for early identification of changed conditions that could indicate the potential for unacceptable risk to human health or plume expansion beyond that bounded by the fate and transport model. EM-LA and N3B will collaborate with NMED in establishing criteria to determine when groundwater conditions have the potential to cause an unacceptable risk to human health and the necessary response actions to be taken.

If you have any questions, please contact Pat McGuire at (315) 420-5629 (patrick.mcguire@em-la.doe.gov) or Cheryl Rodriguez at (505) 414-0450 (cheryl.rodriguez@em.doe.gov).

Sincerely,

Lee Bishop
Digitally signed by Lee Bishop
Date: 2020.05.28 12:40:34 -06'00'

Arturo Q. Duran
Compliance and Permitting Manager
Environmental Management
Los Alamos Field Office

Enclosures:

1. Two hard copies with electronic files – Fate and Transport Modeling and Risk Assessment Report for RDX Contamination in Deep Groundwater (EM2020-0135)

CC (letter with hard-copy enclosure[s]):
Patrick McGuire, N3B
Cheryl Rodriguez, EM-LA

CC (letter with CD/DVD enclosure[s]):
Laurie King, EPA Region 6, Dallas, TX
Scott Ellinger, EPA Region 6, Dallas, TX
Raymond Martinez, San Ildefonso Pueblo, NM
Dino Chavarria, Santa Clara Pueblo, NM
Chris Catechis, NMED-DOE-OB
Steve Yanicak, NMED-DOE-OB
emla.docs@em.doe.gov
n3brecords@em-la.doe.gov
Public Reading Room (EPRR)
PRS Website

CC (letter emailed without enclosures):
William Alexander, N3B
Emily Day, N3B
Danny Katzman, N3B
Kim Lebak, N3B
Joseph Legare, N3B
Dana Lindsay, N3B
Frazer Lockhart, N3B
Elizabeth Lowes, N3B

Pamela Maestas, N3B
Glenn Morgan, N3B
Bruce Robinson, N3B
Bradley Smith, N3B
M. Lee Bishop, EM-LA
Stephen Hoffman, EM-LA
Thomas Johnson Jr., EM-LA
David Nickless, EM-LA
Hai Shen, EM-LA
Ben Underwood, EM-LA

May 2020
EM2020-0135

Fate and Transport Modeling and Risk Assessment Report for RDX Contamination in Deep Groundwater

N3B Los Alamos

EM2020-0135

Fate and Transport Modeling and Risk Assessment Report for RDX Contamination in Deep Groundwater

May 2020

Responsible program director:

Bruce Robinson		Program Director	Water Program	5/28/20
Printed Name	Signature	Title	Organization	Date

Responsible N3B representative:

Bradley Smith		Acting Program Manager	N3B Environmental Remediation Program	5/28/20
Printed Name	Signature	Title	Organization	Date

Responsible DOE EM-LA representative:

Arturo Q. Duran	Lee Bishop Digitally signed by Lee Bishop Date: 2020.05.28 12:41:49 -06'00'	Compliance and Permitting Manager	Office of Quality and Regulatory Compliance	
Printed Name	Signature	Title	Organization	Date

EXECUTIVE SUMMARY

This risk assessment and fate and transport model report for Royal Demolition Explosive (RDX) contamination in deep groundwater at Los Alamos National Laboratory (LANL or the Laboratory) fulfills a requirement of the 2016 Compliance Order on Consent (Consent Order) Appendix B fiscal year 2020 milestones and targets. Appendix B Milestone 7 is described as a report that will present a fate and transport evaluation and risk assessment for RDX in deep groundwater (i.e., perched-intermediate groundwater and the regional aquifer).

Operations and standard industrial practices at LANL mesa-top facilities between 1951 and 1996 led to the release of RDX to the facilities’ process water outfall, adjacent and underlying soils, and alluvial sediments and surface water in Cañon de Valle (where the treated water was discharged). Two remedial actions (between 2000 and 2010) removed much of this surficial and near-surface RDX. However, recharge from precipitation has carried RDX down to the perched-intermediate zone and ultimately to the regional aquifer. Groundwater monitoring data indicate that RDX concentrations exceed the New Mexico tap water screening level (9.66 µg/L) in some wells in the southwestern portion of LANL.

This risk assessment report has been prepared to evaluate potential risks associated with exposure to RDX in groundwater and to determine the probability that RDX might encroach on water-supply wells at some time in the future. A calibrated probabilistic fate and transport model, developed to support this risk assessment report, provides long-term predictions of the spatial extent and associated concentrations of RDX in the regional aquifer.

This report integrates applicable information from groundwater-related investigations and modeling and addresses potential groundwater-related risks by evaluation of the following assessment scenarios:

- Scenario 1: Evaluating risk to human health under current conditions, where land-use control restricting potable groundwater wells is exercised by LANL within the facility’s administrative boundary. The evaluation of scenario 1, which takes into account the location of water-supply wells with respect to the impacted groundwater bodies and the extent of contamination within the impacted groundwater bodies, leads to the conclusion that there is no present-day risk to human health from groundwater contamination, either within or outside of LANL administrative boundaries.
- Scenario 2: Performing a screening-level groundwater risk assessment for RDX and all other detected constituents under present-day and potential future baseline conditions. This screening-level assessment indicates that concentrations of chemicals detected in perched-intermediate groundwater warrant institutional controls to eliminate the possibility of the use of impacted groundwater for consumption now and in the foreseeable future.
- Scenario 3: Evaluating future plume expansion in the regional aquifer, as predicted by the fate and transport model, focusing on the probability that RDX will reach existing water-supply wells. The fate and transport model indicates that by 2070 the plume will expand approximately 2600 ft and there is a 0% probability that RDX will reach any of the three nearest water-supply wells (approximately 17,000 ft from the RDX plume) in the reasonably foreseeable future.

CONTENTS

Figures

Tables

Appendixes

1.0 INTRODUCTION

This risk assessment and fate and transport model report for dissolved phase Royal Demolition Explosive (RDX) contamination in a portion of deep groundwater at Los Alamos National Laboratory (LANL or the Laboratory) Technical Area 16 (TA-16) fulfills the requirements of the 2016 Compliance Order on Consent (Consent Order) Appendix B milestones and targets for fiscal year 2020. Appendix B Milestone 7 requires a report that presents a fate and transport evaluation and risk assessment for RDX in deep groundwater. Deep groundwater in this report refers to both the perched-intermediate zone beneath TA-16 and the underlying regional aquifer.

The geographic setting of LANL is on the Pajarito Plateau, which consists of fingerlike mesas separated by canyons. The Pajarito Plateau is bounded by the Jemez Mountains to the west and the Rio Grande to the east. Groundwater migrates generally from west to east but with some local perturbations due to the manner in which the alluvial fans that form the groundwater-bearing unit’s matrix were deposited and due to northeast-trending faults and fractures that cut across the RDX primary source and the infiltration zone at Cañon de Valle.

The original sources of the RDX at LANL are mesa-top facilities and an outfall to Cañon de Valle, which were active from 1951 to 1996. Standard industrial practices at the time led to the release of RDX to the facilities’ process water outfall, adjacent and underlying soils, and alluvial sediments and surface water in Cañon de Valle (where the treated water was discharged). Two remedial actions (between 2000 and 2010) removed much of this surficial and near-surface RDX (N3B 2019, 700561).

RDX is present in a localized perched-intermediate groundwater zone above the regional aquifer and in a portion of the regional aquifer in the southwestern portion of LANL. Groundwater monitoring data indicate that RDX concentrations exceed the New Mexico tap water screening level (9.66 µg/L) in some wells.

The Consent Order provides a process to follow when a sample result shows a compound’s concentration exceeds a screening level. Section IX.C of the Consent Order states

> …the corrective action process employs both screening levels and cleanup levels. Screening levels are contaminant concentrations that indicate the potential for unacceptable risk. If contaminants are present at concentrations above screening levels, it does not necessarily indicate that cleanup is required, but it does indicate that additional risk evaluation is needed to determine the potential need for cleanup. Cleanup levels are the contaminant concentrations that indicate when cleanup objectives are met. The need for cleanup is triggered by potential unacceptable risk and not by exceedance of screening levels.

Further, Section IX.F of the Consent Order states “NMED’s tap water screening levels shall be used as groundwater screening levels for protection of human health if groundwater is a current or reasonably foreseeable source of drinking water.”

The scope of this risk assessment focuses on the potential exposures to deep groundwater contaminants. Screening of potential health risks pertaining to residual contamination in surface and near-surface soil and sediment, alluvial groundwater, springs, and shallow groundwater in areas overlying deep groundwater is presented in separate reports, including the “Phase III RFI Report for Solid Waste Management Unit 16-021(c)-99” (LANL 2003, 077965), “Investigation Report for Water Canyon/ Cañon de Valle” (LANL 2011, 207069), and the “Supplemental Investigation Report for S-Site Aggregate Area, Revision 1” (N3B 2019, 700414).

Information on radioactive materials and radionuclides, including the results of sampling and analysis of radioactive constituents, is voluntarily provided to the New Mexico Environment Department (NMED) in accordance with U.S. Department of Energy (DOE) policy.

The remaining parts of section 1 introduce the purpose and objective of this report and the regulatory context. Section 2 presents the conceptual site model. Sections 3, 4, and 5 describe the assessments performed and results for Scenarios 1, 2, and 3, respectively. Section 6 presents conclusions and recommendations. References and map data sources are found in section 7. The report appendixes include Acronyms and Abbreviations, Metric Conversion Table, and Data Qualifier Definitions (Appendix A), Data Preparation Protocol, Time Plots, Box Plots, and ProUCL Files for Chemicals of Potential Concern (Appendix B), Probabilistic Groundwater Modeling of the Royal Demotion Explosive Plume at Los Alamos National Laboratory to Support Risk Assessment (Appendix C), and Perched-Intermediate Groundwater Database Query (Appendix D, on CD included with this document).

1.1 Report Purpose and Objectives

The objective of this risk assessment report is to present a comprehensive description of the potential risks to human health related to contamination in perched-intermediate and regional groundwater at TA-16. Achieving this objective involved evaluating potential risks under three assessment scenarios related to present-day and potential future site conditions:

- Scenario 1: Present-day conditions within and outside LANL boundaries, including LANL land-use controls
- Scenario 2: Present-day conditions within and outside LANL boundaries, excluding LANL land-use controls
- Scenario 3: Potential future conditions at the existing water-supply wells in the regional aquifer

The Scenario 1 assessment considered the present-day spatial extent of groundwater contamination in deep groundwater in reference to the location of LANL administrative boundaries. Scenario 1 assessed current conditions and the potential for complete present-day exposure pathways for contaminants in perched-intermediate groundwater and the regional aquifer.

The Scenario 2 screening-level risk assessment evaluated potential human health risks under present-day conditions in the absence of land use controls. This assessment used groundwater risk-based screening levels published by NMED and the U.S. Environmental Protection Agency (EPA) to evaluate potential risks to a hypothetical future resident who might have a domestic water-supply well drawing groundwater from an impacted groundwater body.

Scenario 3 applies the results of RDX fate and transport modeling in the regional aquifer to evaluate the probability that RDX could reach regional aquifer water-supply wells at some time in the reasonably foreseeable future.

1.2 Regulatory Context

NMED issued the Consent Order to DOE pursuant to Section 74-4-10 of the New Mexico Hazardous Waste Act. The Consent Order was also issued under Section 74-9-36.D of the New Mexico Solid Waste Act and 20.9.9.14 New Mexico Administrative Code (NMAC) for the limited purpose of addressing the corrective action activities, including requirements, concerning groundwater contaminants listed at 20.6.2.3103 NMAC, toxic pollutants listed at 20.6.2.7.T(2) NMAC, and explosive compounds as defined in this report.

The Consent Order provides the process by which investigation and remediation of contamination from legacy waste management activities at the Laboratory occurs. The Consent Order both guides and governs the ongoing cleanup of legacy waste at the Laboratory through a campaign-based approach and the annual planning process. The annual planning process allows for revisions to cleanup campaigns based on actual work progress, changed conditions, and funding, with the DOE Environmental Management Los Alamos Field Office (EM-LA) updating the milestones and targets listed in the Consent Order Appendix B Milestones and Targets table.

EM-LA proposed to use the annual planning process described in Section VIII.C of the Consent Order to discuss and establish a new target date for the final corrective measures evaluation (CME) report based upon the recommendations in the "Investigation Report for Royal Demolition Explosive in Deep Groundwater," (hereafter, DGIR) (N3B 2019, 700561). EM-LA proposed to delay the CME report target in Appendix B so that a fate and transport model and risk assessment report, consistent with the Consent Order process, could be prepared and submitted to NMED. During the 2018 annual planning process, the Appendix B milestone table showed a CME being submitted in August 2020. During the 2019 planning process, the fate and transport model and risk assessment report for deep groundwater submission date was set as May 29, 2020, and a target date for the CME was set at December 18, 2020.

1.2.1 Applicable Regulations and Guidance for Human Health Risk Assessment

The primary guidance applied for the methodology employed in the human health risk assessment is NMED's soil screening guidance for human health risk assessment (NMED 2019, 700550). Risk-based groundwater screening levels are provided in this guidance for the purpose of supporting soil screening for the leaching-to-groundwater pathway. These groundwater screening levels are applied in this risk assessment. NMED (2019, 700550) also describes relevant methodology for conducting a screening-level risk assessment that, although published for the purpose of soil screening, can be applied to groundwater risk assessment.

Groundwater concentrations are also evaluated in the context of applicable regulatory standards for groundwater, specifically New Mexico Water Quality Control Commission standards (20 6.2.3103 NMAC Parts A and B) and EPA maximum contaminant levels (MCLs), which can be found at https://www.nrc.gov/docs/ML1307/ML13078A040.pdf.

2.0 CONCEPTUAL SITE MODEL

2.1 Site Description

RDX impacts on groundwater are associated with operations at TA-16, which is located in the southwestern corner of the Laboratory and covers 2410 acres (3.8 mi^2). Figure 2.1-1 shows the boundary of TA-16 within the Laboratory. Bandelier National Monument borders TA-16 along NM 4 to the south. The Santa Fe National Forest, along NM 501, borders TA-16 to the west. To the north and east, TA-16 is bordered by TA-08, TA-09, TA-11, TA-14, TA-15, TA-37, and TA-49. TA-16 is fenced and posted along NM 4. Water Canyon, a 200-ft-deep ravine with steep walls, separates NM 4 from active sites at TA-16. Cañon de Valle forms the northern border of TA-16.

Building 16-260, located on the north side of TA-16 (Figure 2.1-2), has been used for processing and machining high explosives (HE) since 1951. Water is used to machine HE, which is slightly water soluble. Effluent from machining operations contains dissolved HE and may contain entrained HE cuttings. At building 16-260, effluent treatment consists of routing the water to 13 settling sumps to recover any entrained HE cuttings. From 1951 to 1996, the water from these sumps was discharged to the 260 Outfall

(Figure 2.1-2) that drained into Cañon de Valle. In 1994, outfall discharge volumes were measured at several million gallons per year. The discharge volumes were probably greater during the 1950s when HE production output from building 260 was substantially greater than it was in the 1990s (LANL 1994, 076858).

In the past, barium was a constituent of certain HE formulations and inert components and was present in the outfall effluent from building 16-260. The HE machining building (16-260) and associated sumps, drainlines, and troughs discharged effluent into the 260 Outfall drainage channel. The 260 Outfall drainage channel consisted of a settling pond and an upper and lower drainage channel that extends from the 260 Outfall downgradient to the confluence of the drainage and Cañon de Valle. The former approximately 50-ft-long × 20-ft-wide settling pond was located within the upper drainage channel, approximately 45 ft below the 260 Outfall. The drainage channel runs approximately 600 ft northeast from the 260 Outfall to the bottom of Cañon de Valle. Historically, HE-containing water from the outfall entered the former settling pond and drained into the 260 Outfall drainage channel. Current management of this waste stream includes pumping the sumps and treating the water at the TA-16 HE wastewater treatment plant.

2.2 Conceptual Exposure Model of Current and Future Land Use

Current and future land use at TA-16, according to the Laboratory’s 25-year site plan for 2013 to 2037 (LANL 2012, 601095), is designated as HE research, development, testing, assembly, and production, in addition to weapons engineering tritium research. Most areas within TA-16 are active sites for the Weapons Engineering Technology Division of the Laboratory. As described in the site plan, construction of new facilities is planned during this 25-year period. As shown in Figure 2.1-2, many roads and utilities are present at the site.

In addition, on Laboratory property there are institutional controls and safeguards that govern access and land use at TA-16. Security controls prevent unknowing entry and minimize the possibility for unauthorized entry of persons or livestock onto TA-16, thus ensuring no unauthorized land use, including installation of a water-supply well. There are also requirements for land transfer. Land transfer protocols govern any transfer of property from DOE to another entity. These land transfer protocols require a notice to NMED when DOE intends to transfer property.

2.2.1 Potentially Complete Human Exposure Pathways

The assessment of potential risks related to domestic use of groundwater was evaluated employing the exposure model associated with NMED tap water screening levels (NMED 2019, 700550; inputs to soil screening for the leaching-to-groundwater pathway). This exposure model is consistent with the model used by EPA for calculation of residential tap water regional screening levels. The exposure pathways addressed in the NMED and EPA tap water screening levels include

1. ingestion of drinking water,
2. dermal absorption from water while bathing, and
3. inhalation of volatile chemicals released from water into indoor air.

It is important to recognize the implications of the assumed duration of exposure used in the calculation of these tap water screening levels. For chemicals with screening levels based on the assessment endpoint of cancer risk, such as RDX, this is a 26-yr exposure duration. The tap water exposure concentration that is associated with these screening levels is the average concentration across a 26-yr period. This is true regardless of what value from a data set is used to represent the exposure concentration. This is discussed in relation to the Scenario 2 risk screening for baseline conditions in section 4 of this report.

One other potentially complete exposure pathway related to tap water is ingestion of produce products contaminated through irrigation of crops with impacted tap water and of livestock products contaminated through livestock ingesting impacted tap water. As discussed below, the potential contribution of exposures from food-ingestion pathways is expected to be small for organic chemicals dissolved in tap water relative to the pathways that are addressed in the NMED and EPA tap water exposure models. Therefore, these pathways are not included in the risk-based groundwater criteria used in this risk assessment report.

2.2.2 Bioaccumulation Considerations for Organic Chemicals in Plant Tissues

Plant and animal uptake and retention of organic chemicals is related to the lipophilicity of such chemicals, as well as their resistance to metabolism once they are absorbed into plant or animal tissues. NMED guidance for ecological risk assessment (NMED 2017, 602274, Equation 11) describes how plant concentrations of organic chemicals can be estimated based on a chemical’s octanol-water partition coefficient (K_{ow}), within a range of K_{ow} between approximately 1 and 10 (Travis and Arms 1988, 059108). Concentrations of more soluble organic chemicals in plants are predicted to be greater than those of less soluble chemicals. However, man-made organic chemicals are not expected to become concentrated in plant tissues because, unlike essential nutrients and certain endogenous organic molecules, such chemicals are not actively transported across the cell membranes of plants. Therefore, human intake of organic chemicals from direct ingestion of contaminated water is always likely to be far greater than from ingestion of produce irrigated with contaminated water.

2.2.3 Bioaccumulation Considerations for Organic Chemicals in Animal Tissues

Bioaccumulation of certain organic chemicals in lipid-rich animal tissues can be of concern. Organic chemicals that are known to bioaccumulate in animal tissues, such as polychlorinated biphenyls (PCBs), dioxins-furans, and certain organochlorine pesticides, generally share the physical properties of being largely insoluble in water and also resistant to metabolism. Appendix D of NMED’s soil screening guidance for human health risk assessments (NMED 2019, 700550) discusses PCBs as an example of a persistent environmental pollutant that possesses these properties. Because of their low solubility, and tendency to adsorb onto soils and sediments, such chemicals are not typically encountered in groundwater. RDX has a generally low to negligible water solubility at 59.7 mg/L at 25°C. RDX is not very lipid soluble, and therefore has a low potential for bioaccumulation in aquatic species (https://www.atsdr.cdc.gov/toxprofiles/tp78-c6.pdf). RDX is not expected to bioaccumulate in livestock through ingestion of contaminated water.

2.3 Conceptual Site Model of Contaminant Occurrence and Transport

This section presents a summary of the conceptual site model as it pertains to assessing risk to human health. Additional details on the perched-intermediate groundwater system and the regional aquifer can be found in the DGIR (N3B 2019, 700561).

Based on data collected from previous investigations showing the spatial distribution of HE constituents in the Cañon de Valle watershed, the 260 Outfall was the most significant source for releases of HE (and in particular, RDX) at TA-16 (N3B 2019, 700561).

The direction of groundwater flow in the perched-intermediate groundwater zones is predominantly from west to east (Figure 2.3-1). As shown in Figure 2.3-2, the regional groundwater table beneath the Pajarito Plateau has a generally east-sloping gradient that extends from an elevation of approximately 6600 ft at the Pajarito fault to approximately 5500 ft at the Rio Grande, over a distance of approximately 9.3 mi.

The vertical transport pathway for RDX found in perched-intermediate groundwater zones in the lower vadose zone and in the regional aquifer is downward percolation of canyon-floor infiltration through the upper vadose zone. Infiltration through the vadose zone is expected to be predominantly vertical and controlled by gravity as modified by the hydrogeological properties of the various stratigraphic units. Hydraulic properties of stratigraphic and structural features (e.g., laterally discontinuous silt layers, faults) appear to be locally significant. Significant vertical anisotropy occurs because of the layered nature of the stratigraphic units, and horizontal hydraulic conductivities within stratigraphic units are significantly greater than vertical hydraulic conductivities across bedding within and between units. As a result, downward percolating moisture is likely to be diverted laterally at capillary barriers associated with bedding contacts in the stratigraphic sequence.

Two main horizons (or zones) of perched-intermediate groundwater occur in the lower vadose zone as a result of perching on less permeable strata. These perched-intermediate zones are characterized by complex, lateral-discontinuous pathways for the transport of RDX in the vadose zone via “stair-stepping” that likely follows dips of beds within the geologic units. Both perched-intermediate zones contain RDX at concentrations greater than the 9.66-µg/L NMED tap water screening level. RDX concentrations are greater in the upper perched-intermediate zone than the lower perched-intermediate zone, and perched-intermediate RDX concentrations are greater than those observed in the regional aquifer (N3B 2019, 700561). Concentrations of RDX that exceed 100 µg/L have been measured in the upper perched-intermediate zone in intermediate wells CdV-16-2(i)r and CdV-16-4ip.

The estimated mass of RDX in both the upper and lower perched-intermediate zones combined is estimated to be between 263 kg and 1478 kg (N3B 2019, 700561). The approximate boundaries of the upper perched-intermediate groundwater zone, and the approximate area where RDX concentrations exceed the NMED tap water screening level, are shown in Figure 2.3-1.

The regional groundwater system is a complex heterogeneous system that consists of a shallow, predominantly unconfined zone and a deep, predominantly confined zone. Vertical hydraulic stratification in the regional aquifer is indicated by pronounced vertical differences in hydraulic heads in multiscreen wells and a lack of vertical propagation of pumping drawdown caused by pumping tests and pumping of municipal water-supply wells. There are no clearly defined laterally continuous aquitards or confining layers that provide hydraulic separation between the shallow and deep zones of the regional aquifer. The vertical hydraulic separation is likely caused by pronounced vertical aquifer anisotropy caused by the complex depositional layering of the Puye Formation, with the lateral permeability substantially higher than the vertical permeability.

The regional groundwater zone contains between 35 and 415 kg of RDX according to inventory performed in 2017 (LANL 2018, 602963).

3.0 ASSESSMENT SCENARIO 1: EVALUATION OF CURRENT CONDITIONS

The objective of Scenario 1 is to evaluate potential risks from dissolved phase RDX in deep groundwater under present-day conditions, which includes institutional controls exercised by LANL within its administrative boundaries. These controls prohibit and prevent the drilling, installation, and operation of potable groundwater wells within or in the vicinity of the area of impacted groundwater.

As shown in Figure 2.3-1, the approximate present-day spatial extent of RDX above the NMED tap water screening level in upper perched-intermediate groundwater is primarily within TA-16, with some extension into adjacent regions of TA-09 and TA-14. However, the extent of RDX within upper perched-intermediate groundwater is wholly contained within LANL administrative boundaries (Figure 2.1-1). As indicated in the water table contours in Figure 2.3-1, and discussed in section 2.3, the predominant direction of groundwater migration of perched-intermediate groundwater is from west to east. This west-to-east migration direction is also characteristic of the regional aquifer (Figure 2.3-2).

The estimated extent of RDX in the regional aquifer is depicted in Figure 2.3-3. The approximate area of RDX deep groundwater concentrations shown in Figure 2.3-3 is indicated by the cluster of monitoring wells (R-25, R-63, R-68, R-69, R-47, and R-18) in and around Cañon de Valle. A comparison of the spatial extent of RDX in the regional aquifer with that of RDX in upper perched-intermediate groundwater shows that RDX concentrations in the regional aquifer extend farther to the north-northeast. However, the extent of RDX in the regional aquifer is about 3 mi from the nearest LANL administrative boundary. Figure 2.3-2 shows the location of LANL administrative boundaries, along with the location of downgradient regional aquifer municipal supply wells PM-2, PM-4, and PM-5.

In summary, the factors that support a conclusion that there is no potential current human exposure to site-related groundwater contamination are the following:

- No water-supply wells exist in impacted perched-intermediate groundwater. Therefore, there are no present-day exposures to contaminants in the perched-intermediate zone.
- The current boundaries of the dissolved-phase RDX in the regional aquifer above the NMED tap water screening levels are at least 3 mi from the nearest existing water-supply well. Therefore, there are no present-day exposures to RDX via this pathway.
- The extent of detectable concentrations of RDX in the perched-intermediate groundwater zone and the regional aquifer are entirely within the LANL administrative boundary. In addition, the entire extent of the perched-intermediate zone is within that boundary. No exposures are taking place because of migration off-site.

4.0 ASSESSMENT SCENARIO 2: EVALUATION OF RISK UNDER BASELINE CONDITIONS

This section presents a screening-level groundwater risk assessment for all detected constituents under an assumption that no land use controls are exercised and that no engineering controls or future remediation takes place to mitigate groundwater concentrations of possible contaminants. The assessment evaluates potential risks using data from monitoring wells. Risks are evaluated separately for each of the nine monitoring wells, since any future exposure would pertain to groundwater pumped from a single, hypothetical, domestic well at a particular location.

4.1 Identification of Wells for the Screening-Level Risk Assessment

As discussed in section 2.3, contaminants related to releases from TA-16 migrate vertically through the vadose zone to reach deep groundwater. Observed contaminant concentrations are higher in perched-intermediate groundwater than in the regional aquifer. The screening assessment protectively assumes that a hypothetical future well is screened in the perched-intermediate zone, where contaminant concentrations are highest.

As discussed in the DGIR (N3B 2019, 700561), groundwater monitoring at TA-16 and in downgradient areas is conducted under an annual interim facility-wide groundwater monitoring plan. Groundwater monitoring wells where sampling of perched-intermediate groundwater is performed are identified in Table 3.1-2 of the DGIR. Wells with screens in the perched-intermediate zone used to support the RDX vadose zone model (discussed in section C-2.2.2.2 of the fate and transport model report [Appendix C]) were also reviewed to support identification of wells and well screens for this screening-level risk assessment. Other candidate wells were identified by review of maps and figures published in the DGIR and discussion with subject matter experts at LANL. The initial list of candidate wells and well screens is shown in Table 4.1-1.

Well R-25c is a dry well; therefore, no usable analytical data for perched-intermediate groundwater exist for this well.

Three of the wells shown in Table 4.1-1 (16-26644, R-26 PZ-2, and MSC-16-02665) are screened in fractures in shallow tuff bedrock at a depth below ground surface (bgs) of between approximately 94 and 180 ft. Data from these wells were not used in this assessment because the occurrence of only localized and limited availability of groundwater in shallow bedrock is inconsistent with the water production requirements of a domestic supply well. As noted below, MSC-16-02665 in particular is screened in a zone of bedrock that is only intermittently saturated.

Section 3.2.2.1 of the DGIR (N3B 2019, 700561) describes the characteristics of these shallow bedrock wells:

> Most shallow boreholes (<200 ft) drilled on TA-16 mesas are dry; however, three wells, 16-260E-02712, MSC-16-02665, and 90LP-SE-16-02669, are intermittently saturated and one well, 16-26644, is perennially saturated (Figure 3.2-2). The spotty distribution of groundwater associated with the springs and shallow boreholes supports the interpretation that the shallow bedrock perched-groundwater occurs as ribbons of saturation that are stratigraphically controlled.

R-26 PZ-2 is a shallow borehole (<200 ft) completed in the Tshirege Member tuff. Analytical data for well R-26 PZ-2 are related to water sampled during piezometer tests. Since these piezometers are not constructed as monitoring wells for collection of decision-level data, results from the piezometers are considered screening-level data and are therefore not used in this risk assessment. Section 3.1.2 of the DGIR (N3B 2019, 700561) notes that water from well 16-26644 is chemically similar to the surface system comprising the Cañon de Valle springs and base flows.

Drilling activities in 2000 caused screen 1 and screen 2 of well R-25 to become plugged with concrete/stainless-steel shavings. The presence of the stainless-steel shavings in screens 1 and 2 have led to some stainless-steel corrosion and nonrepresentativeness of data collected from those screens. The Westbay sampling system used in well R-25 does not allow purging of the well before sampling, and therefore the corroding metal resulted in anomalously large values reported for several analytes. Therefore, samples from these intervals have not been included in the data set used for this risk assessment.

A subset of the wells shown in Table 4.1-1 has been identified as representative of groundwater background conditions. These wells are identified in Table 3.2-2 of “Groundwater Background Investigation Report, Revision 5” (LANL 2016, 601920) and include PCI-2, R-26 (screen 1), R-27(i), and R-47(i). These wells are used to support identification of chemicals of potential concern (COPCs) in the perched-intermediate wells evaluated in this assessment.

The final list of site characterization and background wells is shown in Table 4.1-2. Note that, per discussion in section 4.2, well CdV-R-37-2 is not included in this list because of the lack of usable analytical data. Additionally, note that there is only a single sample, obtained in 2019, available from well

R-63(i). Although results from a single sample are inadequate to characterize groundwater concentrations for this well, these data have been included in the assessment to provide a potential indication of chemical and radionuclide groundwater concentrations in this well.

4.2 Data Retrieval and Preparation

The perched-intermediate well list discussed in section 4.1 was used to query data in LANL's Environmental Information Management (EIM) database. In EIM, the view V_LANL_REPORT_CHEM_SWTS was used to query the data for the well list. The results of this query were downloaded on March 6, 2020.

The final data set, with Data Removal field flags and the associated Data Removal Reason field defined, is provided in Appendix D (on CD included with this document).

The following provides an overview of the data filters applied to the EIM data query for this risk assessment: (1) sample purpose = regular (REG), (2) sample type = water (W) or groundwater (WG), (3) best value flag = YES, and (4) sample usage code = investigation (INV) or blank. No data related to screening samples, well testing or development samples, tracer study samples, or quality control samples were included in the data set. A complete description of the data filters applied, as well as the selected analytical method in cases where the same analyte was measured by multiple methods for the same sample, is provided in Appendix B.

After the data preparation filters described above were applied, no usable groundwater data were identified in well CdV-R-37-2. Therefore, this well is not included in this risk assessment.

The following logic was applied with regard to handling of data qualifiers:

- Do not use data if qualifier = R (rejected).
- If qualifier contains a U, data are used and result is considered not detected.
- For all other qualifiers, data are used and considered detected.

4.2.1 Data Filters Related to Evaluation of Temporal Trends

Evaluation of temporal trends was performed by review of plots that show patterns of constituent concentrations over time. Some data collected very early within a time series may not be representative because of an initial period of stabilization of newly constructed wells or because of changes in the nature and extent of the plume over time. Because the intention of the risk assessment evaluation is to evaluate current and potential future groundwater conditions, the data plots were reviewed to identify early sample results that are not representative of current conditions for either of the reasons above. Temporal plots of the data reviewed to identify time trends are provided in Appendix B, Attachment B-1 (on CD included with this document).

The plots for inorganic chemicals and radionuclides were reviewed to support development of the data set used to perform statistical tests comparing site and background groundwater concentrations (see section 4.3). Based on this review, the following inorganic chemical data were removed from the data set:

1. Inorganic chemical results for samples collected before 2010 in well CdV-16-2(i)r were removed. Review of the temporal plots showed anomalously high values for several inorganic chemicals, including aluminum, barium, copper, iron, lead, magnesium, potassium, sodium, uranium, vanadium, and zinc.

2. Inorganic chemical results for samples collected before 2003 in well R-19 were removed. Review of the temporal plots showed anomalously high values for several inorganic chemicals in these early samples, including barium, copper, iron, manganese, nitrate-nitrite as nitrogen, potassium, strontium, and zinc.
3. Inorganic chemical results for samples collected before 2003 in well R-25 were removed. Review of the temporal plots showed anomalously high values for several inorganic chemicals in these early samples, including barium, calcium, chromium, iron, manganese, potassium, selenium, thallium, uranium, and vanadium.

A summary of the analytical data in both site wells and background wells (see Table 4.1-2) applied in the risk assessment to identify COPCs is provided in Table 4.2-1. This data summary is presented for each analyte and well combination and includes the number of samples; number of detected values; and the minimum, maximum, median, and mean of the detected values and nondetections.

Removal of the early inorganic chemical results from wells CdV-16-2(i)r, R-19, and R-25 leaves adequate data to characterize current groundwater concentrations of these analytes. The data set for inorganic chemicals in well CdV-16-2(i)r is from 2006 through 2019, the data set for inorganic chemicals in well R-19 begins in 2000 and ends in 2019, and the data set for inorganic chemicals in well R-25 begins in 2000 and ends in 2016. There are many more-recent sampling events in these wells to characterize concentrations of inorganic chemicals that are more representative of current conditions.

Review of the temporal plots for well R-25b showed anomalously high values for molybdenum, uranium, and zinc in samples collected before 2010. However, no samples were systematically removed from well R-25b because the number of potentially impacted inorganic chemicals in early samples appears limited relative to wells CdV-16-2(i)r, R-19, and R-25.

Temporal plots of organic COPCs were also reviewed to determine whether additional trimming of the data set could be warranted at some wells. Although there is some indication of possible trends for certain organic chemicals, these trends are noisy and uncertain. For example, concentrations of RDX appear to be declining over time at wells CdV-9-1(i), CdV-16-4ip, and R-25b but appear to be increasing at well CdV-16-2(i)r. The potential for possible temporal trends to influence the results of the risk assessment screening for organic chemicals, inorganic chemicals, and radionuclides is discussed in the uncertainty analysis in section 4.6.3. Time plots for data trimming are provided in Attachment B-1 (on CD included with this document).

The relatively large short-term variability observed for some analytes in wells CdV-16-4ip and R-25 is likely related to the fact that data from two well screens at different depths were aggregated for these wells.

4.3 Data Evaluation and Identification of COPCs

COPCs were identified for each monitoring well, because local aquifer concentrations are applicable to exposure from water pumped from a single, hypothetical, domestic well. Unlike in soil assessments, where a receptor is assumed to roam at random across an exposure unit, the exposure source in a groundwater risk assessment is the groundwater that is pumped at the location where a well is drilled.

Organic chemicals detected in one or more samples at a monitoring well are evaluated directly in the screening assessment presented in section 4.6 of this report. Sometimes this resulted in organic COPCs being evaluated in the assessment even though concentrations may not be representative of current groundwater conditions. For example, several noncarcinogenic polycyclic aromatic hydrocarbons were identified in a single, early sample at well R-19. Although these results are not representative of more recent groundwater samples, they were included in the risk screening to demonstrate that the measured concentrations are, in any case, of negligible toxicological concern.

For inorganic chemicals and radionuclides, where there are commonly background levels of naturally occurring analytes in groundwater, statistical tests and data visualization plots are used to identify analytes present at concentrations exceeding background levels. The data visualization plots are provided for organic chemicals as well, to facilitate data review.

Box-and whisker plots (box plots) were constructed to facilitate comparisons of the site and background data for each analyte. The box plots divide the data into four sections, each containing 25% of the data. The length of the central box indicates the spread of the central 50% of the data, while the length of the whiskers shows the breadth of the tails of the distribution. Potential outliers are those data that lie beyond the whiskers, which extend to 1.5 times the interquartile range (75th percentile minus the 25th percentile) from either end of the central box. The box plot also demonstrates the shape of the data in the following manner. If the upper box and whisker are approximately the same length as the lower box and whisker, then the data are distributed symmetrically. If the upper box and whisker are longer than the lower box and whisker, then the data are right-skewed. If the upper box and whisker are shorter than the lower box and whisker, then the data are left-skewed. Box plots for all analytes are provided in Appendix B, Attachment B-2 (on CD included with this document).

As discussed in section 4.2.1, temporal data plots were constructed to allow visualization of potential patterns of increasing or decreasing concentrations over time. These plots are useful in conjunction with box plots for determining when potential outliers were measured during the sampling period. As noted above, the temporal data plots were reviewed to identify where early sampling results for one or more analytes are very different from the more-recent results in a monitoring well. Inclusion of analytical data that are clearly not representative of current conditions is inappropriate because the intention of the risk assessment evaluation is to evaluate current and potential future groundwater conditions. A set of temporal data plots for the final data set used in this screening-level risk assessment, subsequent to the trimming of early sample results for inorganic chemicals in some wells as discussed in section 4.2.1, is provided in Appendix B, Attachment B-3 (on CD included with this document). Hence, the box plots in Appendix B, Attachment B-2 and temporal data plots in Appendix B, Attachment B-3 both reflect the final data set used in the screening assessment.

Statistical background comparisons were conducted for all inorganic chemicals and radionuclides. The null hypothesis of each of the four chosen statistical tests is that site and background concentrations are of the same source. Analyte concentrations were considered to be potentially above background concentrations if any of the statistical tests failed this hypothesis test, using a p-value of 0.05. The box plots and temporal data plots were also reviewed in conjunction with the results of the statistical tests to identify COPCs. Additionally, the range of the data were sometimes compared with risk-based criteria and regulatory standards to support decisions on COPC identification. Complete results from the statistical background comparisons, with notes describing information taken from review of the box plots and temporal plots, are presented in Table 4.3-1.

The Student’s t-test and the Gehan test (Gehan 1965, 055611; Gilbert and Simpson 1992, 054952) were used to compare the mean and the median of the distributions of metals concentrations at the site and background wells, respectively. The quantile and the slippage tests were used to compare the upper tails of the distributions relative to background. A more detailed description of these four tests is provided in section B-2.0 of Appendix B.

The final list of COPCs for each site well, including detected organic chemicals and inorganic chemicals and radionuclides present at concentrations above background levels, is shown in Table 4.3-2.

4.4 Identification of Risk-Based Screening Criteria and Regulatory Standards

A domestic water-supply well is assumed to exist in the impacted perched-intermediate groundwater zone for the Scenario 2 risk assessment. This assumption indicates that residential land use is the limiting (most protective) potential future exposure scenario. Under residential land use assumptions, both children and adults are evaluated, where children are considered to be potentially more sensitive to adverse effects than adults. Also, relative to an industrial or commercial scenario, individual daily consumption rates are likely to be greater under residential land use assumptions where individuals may be at home for the majority of their waking hours.

NMED tap water screening levels, described in Section 2.4 of NMED's soil screening guidance (NMED 2019, 700550) are used as inputs to soil screening for the leaching-to-groundwater pathway discussed in that guidance. In this assessment, these screening levels were preferentially used to evaluate potential health risks related to groundwater exposure in a residence. Section IX.F of the Consent Order states "NMED's tap water screening levels shall be used as groundwater screening levels for protection of human health if groundwater is a current or reasonably foreseeable source of drinking water."

If tap water screening levels are not included in NMED's soil screening guidance (NMED 2019, 700550) for one or more chemicals, EPA regional screening levels (RSLs) for tap water were applied. This hierarchy of sources is consistent with Section 1.1 of NMED's soil screening guidance (NMED 2019, 700550), and in accordance with that guidance, RSLs based on a carcinogenic endpoint were adjusted to the NMED 1×10^{-5} risk threshold, since RSLs for carcinogenic effects are derived using a risk threshold of 1×10^{-6}. As noted in section 2.2.1 of this report, the same exposure pathways are addressed in both NMED and EPA tap water screening criteria. EPA tap water RSLs are the values published in November 2019 at https://www.epa.gov/risk/regional-screening-levels-rsls-generic-tables.

For radionuclides, EPA's preliminary remediation goal (PRG) calculator was used to calculate tap water ingestion PRGs using a target risk of 1×10^{-5}. For consistency with the chemical screening criteria, potential exposures to radionuclides in groundwater were evaluated for both tap water ingestion and inhalation of gas-phase radionuclides. As discussed in section 2.2.1, ingestion of garden produce was not included in the PRGs developed for this screening. Default PRG calculator inputs for the tap water ingestion and inhalation pathways for the residential scenario were used to calculate radionuclide PRGs.

Radionuclide PRGs were calculated with the PRG calculator option "Does not assume secular equilibrium, provide results for progeny throughout chain (with decay)." For long-lived radionuclides, such as uranium-234, uranium-235, and uranium-238, secular equilibrium within the uranium or actinium decay chains requires many millennia. Such an assumption of secular equilibrium is inconsistent with the assumed release and transport of specific radionuclides that are being evaluated as possible COPCs related to LANL operations. However, secular equilibrium with short-lived progeny (i.e., half-life < approximately 1 yr) is accounted for in developing radionuclide PRGs. The contributions of short-lived progeny to PRG for a parent radionuclide are included in the parent radionuclide's PRG. The method of adding the contribution of short-lived progeny to the PRG of a parent radionuclide is by the inverse sum of reciprocals. For a parent radionuclide, X_parent, and short-lived progeny, X_progeny, the calculation proceeds as

$$X\_total = 1 / ((1 / X\_parent) + (1 / X\_progeny)) \qquad \textbf{Equation 1}$$

NMED and EPA risk-based screening criteria for chemical COPCs for both cancer and noncancer endpoints, and for radionuclide PRGs, are provided in Table 4.4-1.

Groundwater concentrations of COPCs are also compared with regulatory standards, specifically, New Mexico groundwater protection standards (NMAC 20.6.2.3103, Parts A and B) and EPA National Primary Drinking Water Regulations tap water MCLs. These regulatory standards for COPCs are provided in Table 4.4-2.

4.5 Identification of Exposure Point Concentrations

In principle, estimates of average groundwater concentrations at assessment locations over the time periods pertaining to noncancer health effects of RDX (6 yr) and carcinogenic effects of RDX (26 yr) are of interest. As stated in section 2.2.1, regardless of what statistic is used to represent the exposure point concentration (EPC) (even when using maxima), the characteristics of the exposure model are such that the EPC represents an average concentration in groundwater pumped from the well during the entire exposure duration. For assessment of exposure to tap water from a domestic water well, average aquifer concentrations across a well screen length are the appropriate basis for estimating EPCs because of the physical characteristics of the perched-intermediate zone described in section 2.3 that limit the volume and rate at which groundwater can be pumped.

A separate set of COPCs and associated EPCs was developed for each individual monitoring well. EPCs for the screening assessment are estimated using the protocol described in NMED’s soil screening guidance (NMED 2019, 700550). As an initial estimation, average groundwater concentrations over a residential exposure period are represented by the maximum detected concentration at a well. Secondly, for COPCs where data support estimation of a 95% upper confidence limit (UCL) at a well, the 95% UCL is used to represent groundwater EPCs in the cumulative risk screening for perched-intermediate groundwater.

Calculation of UCLs of the mean concentrations was done using the EPA ProUCL 5.1.002 software (EPA 2015, 601725). Consistent with the ProUCL v5.1 Technical Guide (EPA 2015, 601724), and NMED soil screening guidance (NMED 2019, 700550), a minimum of eight samples and five detections in a data set were required to calculate UCLs. ProUCL documentation strongly recommends against using the maximum detected concentration for the EPC. The maximum detected concentration was used to represent the EPC only when there was an insufficient number of samples or number of detections to calculate a UCL.

To prepare the data set for calculating 95% UCLs, COPC nondetection data were first imputed to a value equal to one-half of the associated detection limit. This approach was chosen because of concerns that the Kaplan-Meier method (often applied in the ProUCL software) for imputing values for nondetection data can sometimes produce artificially low estimates of 95% UCLs, particularly when there is a wide range of nondetection values such as occurs for some analytes in this data set. The Kaplan-Meier imputation method substitutes a nondetection with the next lowest detected value except it uses the detection limit for the nondetection when there is no lower-valued detection. When there is a large gap between nondetections and the next lowest detected value, this can result in underestimation of the mean, and hence of the UCL of the mean. Data that span many years often suffer from this type of effect, because detection limits have usually decreased over time. Investigation of these data revealed that this was the case for too many of the chemicals to allow reliance on UCL methods that included the Kaplan-Meier imputation approach. Consequently, the substitution approach of using half the detection limit was chosen so that UCLs, and hence risk, would not be underestimated.

The data set with nondetection results assigned a value of one-half of the detection limit was then used in ProUCL to calculate 95% UCLs for each COPC. Specifically, the 95% Student's t-test UCL (*t*-UCL) and the 95% bias-corrected and accelerated (BCA) bootstrap UCL were chosen from the ProUCL output to represent the 95% UCL. For each COPC and well combination, the larger of these two UCLs was protectively used as the 95% UCL. Additionally, if the selected 95% UCL was ever greater than the highest detected value, the maximum detected concentration was used as the EPC instead.

The *t*-UCL and BCA bootstrap methods were selected for estimating 95% UCLs because of their general robustness. If the data come from an underlying normal distribution, then the *t*-UCL is appropriate. If the data are sufficiently skewed, then the BCA bootstrap method is likely to provide a more realistic estimate of a 95% UCL. The methodology described here was chosen because ProUCL's suggested 95% UCL is sometimes unrealistic in cases where small sample size results in low power for ProUCL's goodness-of-fit tests. Because small sample sizes result in low statistical power to determine that a data set does not belong to a statistical distribution, ProUCL may select a parametric 95% UCL when there is little evidence that the data follow an underlying distribution.

A set of box plots for individual COPCs showing the mean and 95% UCL in relation to the site well data are provided in Appendix B, Attachment B-4 (on CD included with this document) to support review of the reasonableness of the 95% UCL estimates. Note that nondetection results in the Appendix B, Attachment B-4 plots are shown as one-half of the sample analytical detection limit to represent the value used in the calculation of the 95% UCL. Input and output data files for ProUCL calculations are provided in Appendix B, Attachment B-5 (on CD included with this document).

Table 4.5-1 summarizes minimum detected value, maximum detected value, mean, 95% UCL concentrations, and the selected EPC for all site wells and COPCs.

4.6 Screening-Level Risk Assessment Results

4.6.1 Assessment of Cancer Risk and Chemical Hazard

The screening-level risk assessment evaluated the ratios of groundwater EPCs and risk-based groundwater concentrations. Screening for COPCs, performed on a per-well basis, included (1) incremental lifetime cancer risk (cancer risk) and noncancer hazard quotient (HQ) assessment endpoints for chemicals and (2) cancer risk for radionuclides.

As discussed in section 4.5, the risk-based screening follows the general protocol described in NMED's soil screening guidance (NMED 2019, 700550). First, maximum detected concentrations are compared with screening criteria, and a sum-of-ratios is calculated for cancer and noncancer endpoints. Next, for analytes and wells where data support estimation of a 95% UCL, the 95% UCL is also used to represent groundwater EPCs in the cumulative risk screening for the perched-intermediate zone.

For both cancer risk and HQ, the water concentration at each well (initially the maximum detected value, and then the EPC estimated as described in section 4.5) was divided by the tap water screening value, and these ratios were summed for each assessment endpoint. For cancer risk, the resulting ratios were multiplied by 1×10^{-5} to express the sum-of-ratios as the equivalent cancer risk. The HQ sum-of-ratios, referred to as a hazard index (HI), does not require this adjustment because the target HQ is 1.

Table 4.6-1 displays the cumulative risk-screening summary results for chemicals and radionuclides in perched-intermediate groundwater for the nine groundwater monitoring wells evaluated in the risk assessment screening. Cancer risks calculated using maximum detected COPC concentrations as well as EPCs exceeded the 1×10^{-5} risk threshold in all wells excepting CdV-37-1(i), R-19, and R-63(i). The highest cancer risk calculated using EPCs (1×10^{-4}) was for monitoring wells CdV-16-4ip and CdV-16-2(i)r. Cancer risk results calculated using EPCs for the remaining wells were between 2×10^{-5} and 6×10^{-5}. HIs exceed the threshold value of 1 only at monitoring wells CdV-16-4ip and CdV-16-2(i)r. Cancer risks described in this paragraph were almost entirely related to chemical COPCs; the contribution of radionuclide COPCs to cancer risks above the 1×10^{-5} risk threshold was negligible.

Tables 4.6-2 through 4.6-10 display the full cumulative risk screening results for chemicals by well, showing the individual contribution of all chemical COPCs to the cancer risk sum and HI. With the exception of well R-25b, RDX was the dominant contributor to cancer risks above the threshold of 1×10^{-5} at all monitoring wells. RDX was also the dominant contributor to HI values at or above 1 in monitoring wells CdV-16-4ip and CdV-16-2(i)r. Table 4.6-11 indicates the major contributors to cancer risk and HI above thresholds at each monitoring well, with EPCs used to represent groundwater concentrations.

RDX is clearly the most significant contributor to cancer risk and HI values above thresholds. The sole exception is well R-25b, where 3 halogenated volatile organic compounds (VOCs) contribute 90% of the total cancer risk of 6×10^{-5}. These 3 VOCs were each detected in the same 2 of the 11 groundwater samples that compose the R-25b data set. These samples were the last 2 samples acquired from well R-25b, where the last sample was obtained in 2017. The similar VOC bromoform was also detected in these samples, although it is a negligible contributor to calculated health effects. These 4 VOCs were not detected in any of the other 8 site wells.

Table 4.6-12 displays the full cumulative risk-screening results for radionuclide COPCs, which consist of tritium, uranium-234, and uranium-238. Relative to chemical cancer risks, radionuclide COPCs were negligible contributors to cancer risks above the 1×10^{-5} risk threshold. Cancer risk results for radionuclides, calculated using EPCs to represent groundwater concentrations, were below the 1×10^{-5} risk threshold and ranged from 6×10^{-7} to 6×10^{-6}. Most of the radionuclide cancer risk was contributed by tritium when this analyte was a COPC in a monitoring well.

4.6.2 Comparison of EPCs with Regulatory Standards

Table 4.6-13 presents a comparison of maximum detected values and EPCs with regulatory standards (20.6.2.3103 NMAC and EPA MCLs) . The only exceedance of an 20.6.2.3103 NMAC Part A human health standard was for the COPC nitrate-nitrite as nitrogen in well CdV-9-1(i). The EPC of 1300 µg/L exceeded the Part A standard of 1000 µg/L, as well as the primary MCL standard, which is also 1000 µg/L.

There were three occurrences of an EPC at a monitoring well exceeding a secondary MCL, where secondary MCLs are guidelines related to possible cosmetic or aesthetic effects. The iron EPC of 330 µg/L at CdV-16-1(i) exceeded the secondary MCL of 300 µg/L. Also, the aluminum secondary MCL of 50 to 200 µg/L was exceeded at wells R-25 (600 µg/L) and R-25b (360 µg/L).

4.6.3 Uncertainty Analysis

The assessment presented in this report is specifically a screening-level evaluation of potential risks related to consumption of groundwater in the vicinity of TA-16. As a screening assessment, it is proper that the assessment include protective assumptions intended to ensure that potential risks are not inadvertently overlooked. This is important because it implies that the tabulated risk estimates are intentionally biased high. In this context, a tabulated residential cancer risk estimate of 1×10^{-5} should not be interpreted to indicate that this level of potential risk is likely or anticipated. Rather, it signifies that one can conclude with reasonable assurance that potential cancer risks would not exceed 1×10^{-5} should a residence be sited in the area and obtain domestic water from impacted groundwater.

The major uncertainties and biases in the risk assessment screening results are discussed below.

1. The representativeness of EPCs for characterizing average COPC concentrations in the volume of groundwater that would be pumped from a domestic well during the assumed residential exposure period

   A potentially important aspect of this topic is (1) the application of the ProUCL approach to avoid computing a 95% UCL when there are fewer than 5 detected values and (2) the application of NMED guidance (NMED 2019, 700550) to represent the EPC as the maximum value under these circumstances. For RDX, where detection frequency is generally high in the impacted wells, a 95% UCL was calculated for those wells. However, this approach affects the risk results for well R-25b, where 3 halogenated VOCs contribute 90% of the total cancer risk of 6×10^{-5}. Because these VOCs were detected in only 2 of the 11 groundwater samples available for well R-25b, the average groundwater concentration for the entire exposure duration is represented by a single data point, which is the maximum detected value. As shown in Table 4.5-1, the maximum concentrations of chlorodibromomethane, bromodichloromethane, and chloroform were approximately 3 to 5 times larger than the average value across all 11 samples.

2. Whether the perched-intermediate groundwater zone has adequate transmissivity to support a domestic well, which commonly requires that at least a few gallons per minute be produced in a pump test

   To mitigate this uncertainty in wells R-25 and CdV-16-4ip, the data from both screened intervals from which perched-intermediate groundwater were available were combined. As noted in section 2.3, the heterogeneity and limited areal extent of the paleo channels where groundwater flow is dominant presents significant challenges to effectively removing water at the rate required for a domestic well. Ultimately, if an attempted well were to be insufficiently productive in the perched-intermediate groundwater zone, it is likely the driller would continue to drill and obtain water from the regional aquifer. The use of perched-intermediate groundwater data is a protective assumption since concentrations or RDX (the main risk-driver) are lower in the regional aquifer.

3. The likelihood that a single-residence well would be financially feasible

   This uncertainty could potentially be evaluated by review of existing well information in New Mexico, but within the context of this screening assessment, this is, like the assumption of adequate water production from the perched-intermediate zone, a protective assumption required to conduct the screening assessment.

4. The uncertainty in the dose-response information for key risk-drivers

   Ingestion of RDX, and associated cancer risk, is the main contributor to screening assessment results above the NMED threshold of 1×10^{-5}. EPA's "Guidelines for Carcinogen Risk Assessment" (https://www.epa.gov/risk/guidelines-carcinogen-risk-assessment) describes five recommended standard descriptors of the weight of evidence of a chemicals' carcinogenicity: (1) carcinogenic to humans, (2) likely to be carcinogenic to humans, (3) suggestive evidence of carcinogenic potential, (4) inadequate information to assess carcinogenic potential, and (5) not likely to be carcinogenic to humans. RDX has been assigned the third descriptor, suggestive evidence of carcinogenic potential, which indicates the weight of evidence from animal studies is suggestive of carcinogenicity, and a concern for potential carcinogenic effects in humans exists, but the data are judged to be insufficient for supporting a stronger conclusion. The oral slope factor used to calculate the NMED and EPA tap water criteria is based on a 2-yr dietary study in mice, which included 4 dose groups and a control group, and 85 mice per sex per group. The oral slope factor was derived from increased incidence of hepatocellular adenomas or carcinomas and alveolar/bronchiolar adenomas or carcinomas in female mice. Details of this study can be found in EPA's toxicological review for RDX, available online through the Integrated Risk Information System (IRIS) database at https://cfpub.epa.gov/ncea/iris/iris_documents/documents/toxreviews/0313tr.pdf.

5. The residential exposure assumptions applied in the NMED and EPA tap water screening criteria

   The main protective biases applied in these exposure models are that for a hypothetical individual, most or all of water consumption will occur at home and the individual will reside in the home from birth for an exposure period of 26 yr. The exposure period of 26 yr corresponds to the 90th percentile of the key population mobility study described in EPA's "Exposure Factors Handbook" (EPA 2011, 208374). From the same study, the average length of time that an individual resides at a residence is 12 yr. Since cancer risk scales linearly with the duration of exposure, the degree of protective bias associated with that specific exposure assumption is a bit more than twofold.

4.7 Screening Assessment Conclusions

Concentrations of chemicals in perched-intermediate groundwater necessitate that institutional controls be maintained to eliminate the possibility of contaminated groundwater being accessed for consumption in the foreseeable future. This conclusion is based on a screening-level assessment that indicates potential cancer risks exceed NMED's cancer risk threshold of 1×10^{-5} at six of the monitoring wells evaluated in this assessment. RDX is the most significant contributor to cancer risk and HI values above NMED's regulatory thresholds of 1×10^{-5} and 1, respectively. However, NMED's cancer risk threshold of $1\text{x}10^{-5}$ is at the midpoint of the risk management range of 1×10^{-6} to 1×10^{-4} that EPA has used to evaluate cancer risk across the country as described in the "National Oil and Hazardous Substances Pollution Contingency Plan" (40 Code of Federal Regulations 300.430) The HI for non-cancer risk was exceeded at two of the wells, CdV-16-2(i)r (HI = 1.6) and CdV-16-4ip (HI = 2.5). While there is evidence of a slight potential risk for non-cancer effects, the cancer risk is the larger concern.

5.0 ASSESSMENT SCENARIO 3: EVALUATION OF FUTURE CONDITIONS AT EXISTING WATER-SUPPLY WELLS

The objective of Scenario 3 is to evaluate the probability that RDX could reach any of the downgradient regional aquifer water-supply wells PM-2, PM-4, or PM-5, at some time in the reasonably foreseeable future. Evaluation of Scenario 3 applies the results of RDX fate and transport modeling in the regional aquifer, which is discussed in detail in Appendix C of this report. No risk assessment calculations related to modeled RDX concentrations at future times and locations are included in this evaluation because Scenario 3 evaluates the migration of RDX in the regional aquifer and the potential that it could reach the water supply wells.

As discussed in Appendix C, fate and transport modeling of RDX in the regional aquifer was conducted using a probabilistic RDX regional aquifer model (RRM) that applied high-performance computing to predict regional aquifer concentrations over space and time. The model was calibrated with measured RDX groundwater concentrations over time, up to December 2019, and also with measurements of hydraulic head in regional aquifer wells. The objective of the calibration work is to develop a model that matches the observed pattern of RDX concentrations in monitoring wells through the present day, thus providing a measure of assurance in predicted future concentrations at those locations and in downgradient areas where monitoring data are unavailable. The RRM thus provides spatially and temporally explicit estimates of hydraulic head and RDX concentration, with associated measures of uncertainty, at all modeling points within the spatial domain of the model.

The RRM was run through the year 2070, or about 50 yr beyond the time of the last data used for model calibration. The 50-yr timeframe was selected to represent a reasonably foreseeable future time period. The area and depth of the RDX plume in the regional aquifer is shown in Figure 5.1-1 and Figure C-3.3-2 of Appendix C. Uncertainty in the areal extent of RDX is shown in Figure C-3.3-2 as lines encompassing the area where RDX concentrations exceed the NMED tap water screening level of 9.66 µg/L. These lines show where this boundary lies for the 5th, 50th, and 95th percentiles of the probabilistic model runs. The 95th percentile boundary is where RDX concentrations are below 9.66 µg/L for 95% of model runs. A color-scaled heat map is also provided in Figure C-3.3-2, showing where RDX concentrations as low as 0.1 µg/L exist in the model run representing the 50th percentile of all runs. The predicted 0.1-µg/L boundary extends in a southeasterly direction as far as monitoring well R-58, the location of which can be seen in Figure 5.1-1.

In Figure 5.1-1, the dashed lines represent the 5% cases of the probabilistic simulation, solid lines represent the median, and dotted lines represent the 95% cases. The red line shows the 9.66-µg/kg isopleth area (where this concentration corresponds to NMED's tap water screening level for RDX), and the black line shows the 1-µg/kg isopleth. Concentrations out to a minimum value of 0.1 µg/kg are plotted in the heat map.

The RRM assumes a steady-state recharge rate and associated flux of RDX to the regional aquifer from the vadose zone throughout the modeling period. The mass of RDX introduced to the regional aquifer over time through this steady-state assumption can be compared with the estimated mass of RDX in the hydrologic system at TA-16 as a point of reference for the protectiveness of the modeling results. As noted in section C-3.1 of Appendix C and discussed in section 2.10.1 of the DGIR (N3B 2019, 700561), there is an estimated RDX mass of between approximately 1500 and 3600 kg distributed among all components of the hydrologic system at TA-16. By the year 2020, the RRM had applied an estimated inventory of 429 kg of RDX (Appendix C) in the regional aquifer, which is close to the upper bound of between 35 and 415 kg of RDX in the regional aquifer provided in the DGIR. The maintenance of the steady-state assumption for this source concentration of RDX results in complete movement of a 1500-kg RDX inventory (the lower-bound) into the regional aquifer by about year 2070, which is the duration of the modeling period. If the upper bound of the total RDX inventory is assumed, all RDX would move into the regional aquifer by about 2150. After all inventory above the regional aquifer is exhausted, RDX concentrations must necessarily decrease within the regional aquifer.

The RRM uses a continuous source input of RDX in the hydraulic windows from a variable time of onset until the end of the modeling period (2070). This assumption is made for the following reasons. First, there is no indication in the regional aquifer data that an end time of input from the vadose zone has been reached; thus it would be difficult to develop a meaningful distribution of end time for hydraulic window RDX concentration. Second, under this assumption, the movement of RDX from the vadose zone into the regional aquifer is approximately 1500 kg by 2070, which is the lower bound of recent inventory estimates (N3B 2019, 700561). In the median forward case, exhaustion of the upper bound inventory estimate would not occur until approximately 2150. Therefore, if inventory estimates in the system are accurate, a decrease in RDX concentrations arriving at the regional aquifer would likely occur between 2070 and 2150.

As discussed in Appendix C, heat maps of the RDX plume indicate that the plume expansion is slow and that RDX concentrations gradually dilute as the center of the plume expands in the regional aquifer. Based on the model results, there is a 0% probability that RDX will reach any of the downgradient water-supply wells PM-2, PM-4, or PM-5, during the modeling period. The modeling indicates that the bounding case has the plume expanding approximately 2600 ft, thus the leading edge of the plume would be approximately 2.5 mi from the nearest water-supply wells. Without completion of the pathway to the water-supply wells, RDX in the regional aquifer will not pose an unacceptable risk to human health for the reasonably foreseeable future.

6.0 CONCLUSIONS AND RECOMMENDATIONS

This risk assessment report has been prepared to evaluate potential risks associated with exposure to RDX in groundwater and to determine the probability that RDX might encroach on existing water-supply wells at some time in the future. A calibrated probabilistic fate and transport model (Appendix C), developed to support this risk assessment report, provides long-term predictions of the spatial extent and associated concentrations of RDX in the regional aquifer.

This report integrates applicable information from groundwater-related investigations and modeling and addresses potential groundwater-related risks by evaluation of the following assessment scenarios:

- Scenario 1: Evaluating risk to human health under current conditions, where land use control restricting potable groundwater wells is exercised by LANL within the facility's administrative boundary
- Scenario 2: Performing a screening-level groundwater risk assessment for RDX and all other detected constituents under present-day and potential future baseline conditions
- Scenario 3: Evaluating future plume expansion in the regional aquifer, as predicted by the fate and transport model, focusing on the probability that RDX will reach existing water-supply wells

The principal conclusions of this risk assessment report with respect to the three assessment scenarios follow:

- Assessment Scenario 1 Conclusions: There is no present-day risk to human health from groundwater contamination, either within or outside of LANL administrative boundaries, for the following reasons:
    - ❖ No water-supply wells exist in the impacted perched-intermediate groundwater body. Therefore, there are no present-day exposures to RDX in perched-intermediate groundwater.
    - ❖ RDX in the regional aquifer is approximately 3 mi from nearest existing water-supply wells. Therefore, there are no present-day exposures to contaminants in the regional aquifer.
    - ❖ The extent of RDX in both perched-intermediate groundwater and the regional aquifer is currently within LANL administrative boundaries. Additionally, the downgradient extent of the perched-intermediate groundwater zone is well within these LANL boundaries, so near-term migration to locations outside of the LANL boundary is not considered feasible.
- Assessment Scenario 2 Conclusions: The screening-level assessment indicates that at six of the wells evaluated, potential risks exceed NMED's risk threshold, with RDX being the most significant contributor to these risks. Based on these results, concentrations of chemicals detected in perched-intermediate groundwater warrant institutional controls to eliminate the possibility of the use of contaminated groundwater for consumption now and in the foreseeable future.

- Assessment Scenario 3 Conclusions: The RRM indicates that by 2070 the plume could expand downgradient by no more than 2600 ft. There is a 0% probability that RDX will reach any of the three nearest water-supply wells, which are more than 3 mi away, in the reasonably foreseeable future.

The overall conclusions of this risk assessment are (1) there is no current or reasonably foreseeable future unacceptable risk to human health associated with RDX contamination in the regional aquifer and (2) based on land use controls restricting potable groundwater wells, there is no current, potential, or reasonably foreseeable future unacceptable risk to human health from drinking groundwater from the perched-intermediate groundwater. As stated in the Consent Order Section IX.C “If contaminants are present at concentrations above screening levels, it does not necessarily indicate that cleanup is required, but it does indicate that additional risk evaluation is needed to determine the potential need for cleanup.” This risk assessment report meets the Consent Order benchmark of determining that there is no need for cleanup “triggered by potential unacceptable risk and not by exceedance of screening levels.” Therefore, EM-LA and Newport News Nuclear BWXT-Los Alamos, LLC (N3B) recommend that long-term groundwater monitoring be conducted to ensure protection of human health and to monitor fate and transport of the plume compared with the modeling results.

To implement this recommendation, a comprehensive and protective monitoring program and a long-term monitoring plan will be developed. The initial plan will include a monitoring well network evaluation to ensure the set of wells is sufficient to collect the necessary data to detect expected or unexpected expansion of the RDX plume. EM-LA and N3B will collaborate with NMED in establishing criteria to determine when groundwater conditions have the potential to cause an unacceptable risk to human health and the necessary response actions to be taken.

7.0 REFERENCES AND MAP DATA SOURCES

7.1 References

The following reference list includes documents cited in this report. Parenthetical information following each reference provides the author(s), publication date, and ERID, ESHID, or EMID. This information is also included in text citations. ERIDs were assigned by the Laboratory’s Associate Directorate for Environmental Management (IDs through 599999); ESHIDs were assigned by the Laboratory’s Associate Directorate for Environment, Safety, and Health (IDs 600000 through 699999); and EMIDs are assigned by N3B (IDs 700000 and above). IDs are used to locate documents in N3B’s Records Management System and in the Master Reference Set. The NMED Hazardous Waste Bureau and N3B maintain copies of the Master Reference Set. The set ensures that NMED has the references to review documents. The set is updated when new references are cited in documents.

EPA (U.S. Environmental Protection Agency), September 2011. “Exposure Factors Handbook: 2011 Edition,” EPA/600/R-09/052F, Office of Research and Development, Washington, D.C. (EPA 2011, 208374)

EPA (U.S. Environmental Protection Agency), October 2015. “ProUCL Version 5.1.002 User Guide,” Statistical Software for Environmental Applications for Data Sets with and without Nondetect Observations, EPA/600/R-07/041, Office of Research and Development, Washington, D.C. (EPA 2015, 601725)

EPA (U.S. Environmental Protection Agency), October 2015. “ProUCL Version 5.1.002 Technical Guide,” Statistical Software for Environmental Applications for Data Sets with and without Nondetect Observations, EPA/600/R-07/041, Office of Research and Development, Washington, D.C. (EPA 2015, 601724)

Gehan, E.A., June 1965. “A Generalized Wilcoxon Test for Comparing Arbitrarily Singly-Censored Samples,” *Biometrika,* Vol. 52, No. 1 and 2, pp. 203–223. (Gehan 1965, 055611)

Gilbert, R.O., and J.C. Simpson, December 1992. “Statistical Methods for Evaluating the Attainment of Cleanup Standards, Volume 3: Reference-Based Standards for Soils and Solid Media,” document prepared for the U.S. Environmental Protection Agency, Pacific Northwest Laboratory, Richland, Washington. (Gilbert and Simpson 1992, 054952)

LANL (Los Alamos National Laboratory), May 9, 1994. “Process Flow Reductions from Waste Minimization for Value Engineering Study,” Los Alamos National Laboratory, Los Alamos, New Mexico. (LANL 1994, 076858)

LANL (Los Alamos National Laboratory), September 2003. “Phase III RFI Report for Solid Waste Management Unit 16-021(c)-99,” Los Alamos National Laboratory document LA-UR-03-5248, Los Alamos, New Mexico. (LANL 2003, 077965)

LANL (Los Alamos National Laboratory), September 2011. “Investigation Report for Water Canyon/ Cañon de Valle,” Los Alamos National Laboratory document LA-UR-11-5478, Los Alamos, New Mexico. (LANL 2011, 207069)

LANL (Los Alamos National Laboratory), July 12, 2012. “Twenty-Five Year Site Plan, FY2013 - FY2037,” Los Alamos National Laboratory document LA-UR-12-22913, Los Alamos, New Mexico. (LANL 2012, 601095)

LANL (Los Alamos National Laboratory), October 27, 2016. “Groundwater Background Investigation Report, Revision 5,” Los Alamos National Laboratory document LA-UR-16-27907, Los Alamos, New Mexico. (LANL 2016, 601920)

LANL (Los Alamos National Laboratory), March 2018. “Compendium of Technical Reports Related to the Deep Groundwater Investigation for the RDX Project at Los Alamos National Laboratory,” Los Alamos National Laboratory document LA-UR-18-21326, Los Alamos, New Mexico. (LANL 2018, 602963)

N3B (Newport News Nuclear BWXT-Los Alamos, LLC), April 2019. “Supplemental Investigation Report for S-Site Aggregate Area, Revision 1,” Newport News Nuclear BWXT-Los Alamos, LLC, document EM2019-0048, Los Alamos, New Mexico. (N3B 2019, 700414)

N3B (Newport News Nuclear BWXT-Los Alamos, LLC), August 2019. “Investigation Report for Royal Demolition Explosive in Deep Groundwater,” Newport News Nuclear BWXT-Los Alamos, LLC, document EM2019-0235, Los Alamos, New Mexico. (N3B 2019, 700561)

NMED (New Mexico Environment Department), March 2017. “Risk Assessment Guidance for Site Investigations and Remediation, Volume 2, Soil Screening Guidance for Ecological Risk Assessments,” Hazardous Waste Bureau and Ground Water Quality Bureau, Santa Fe, New Mexico. (NMED 2017, 602274)

NMED (New Mexico Environment Department), June 19, 2019. “Risk Assessment Guidance for Site Investigations and Remediation, Volume 1, Soil Screening Guidance for Human Health Risk Assessments,” February 2019 (Revision 2, 6/19/19), Hazardous Waste Bureau and Ground Water Quality Bureau, Santa Fe, New Mexico. (NMED 2019, 700550)

Travis, C.C., and A.D. Arms, 1988. “Bioconcentration of Organics in Beef, Milk, and Vegetation,” *Environmental Science & Technology,* Vol. 22, No. 3, pp. 271-274. (Travis and Arms 1988, 059108)

7.2 Map Data Sources

Monitoring well and spring point features; Former LANL ER-DB Database pull; 02 February 2004; As published 02 February 2004.

Infiltration area outline; Los Alamos National Laboratory, ER-ES, As published, project folder 11-0015; \\172.30.0.10\n3b-shares\GIS Data and Projects\11-Projects\11-0057\gdb\gdb_11-057.mdb\infiltration_lines_buffer; 2012.

SWMU or AOC; Los Alamos National Laboratory, Site Planning & Project Initiation Group, Infrastructure Planning Office; September 2007; As published 13 August 2010.

Structures; Los Alamos National Laboratory, KSL Site Support Services, Planning, Locating and Mapping Section; 06 January 2004; As published 29 November 2010.

Contours, 100, 20-ft interval; Los Alamos National Laboratory, Site Planning & Project Initiation Group, Infrastructure Planning Office; September 2007; As published 13 August 2010.

Paved Road; Los Alamos National Laboratory, FWO Site Support Services, Planning, Locating and Mapping Section; 06 January 2004; As published 29 November 2010.

Unpaved Road; Los Alamos National Laboratory, ER-ES, As published, GIS projects folder; \\slip\GIS\Projects\14-Projects\14-0062\project_data.gdb; digitized_site_features; digitized_road; 2017.

Drainage Channel; Los Alamos National Laboratory, ER-ES, As published, GIS projects folder; \\slip\GIS\Projects\11-Projects\11-0108\\gdb\gdb_11-0108_generic.mdb; drainage; 2017.

Watersheds; Los Alamos National Laboratory, ENV Environmental Remediation and Surveillance Program; EP2006-0942; 1:2,500 Scale Data; 27 October 2006

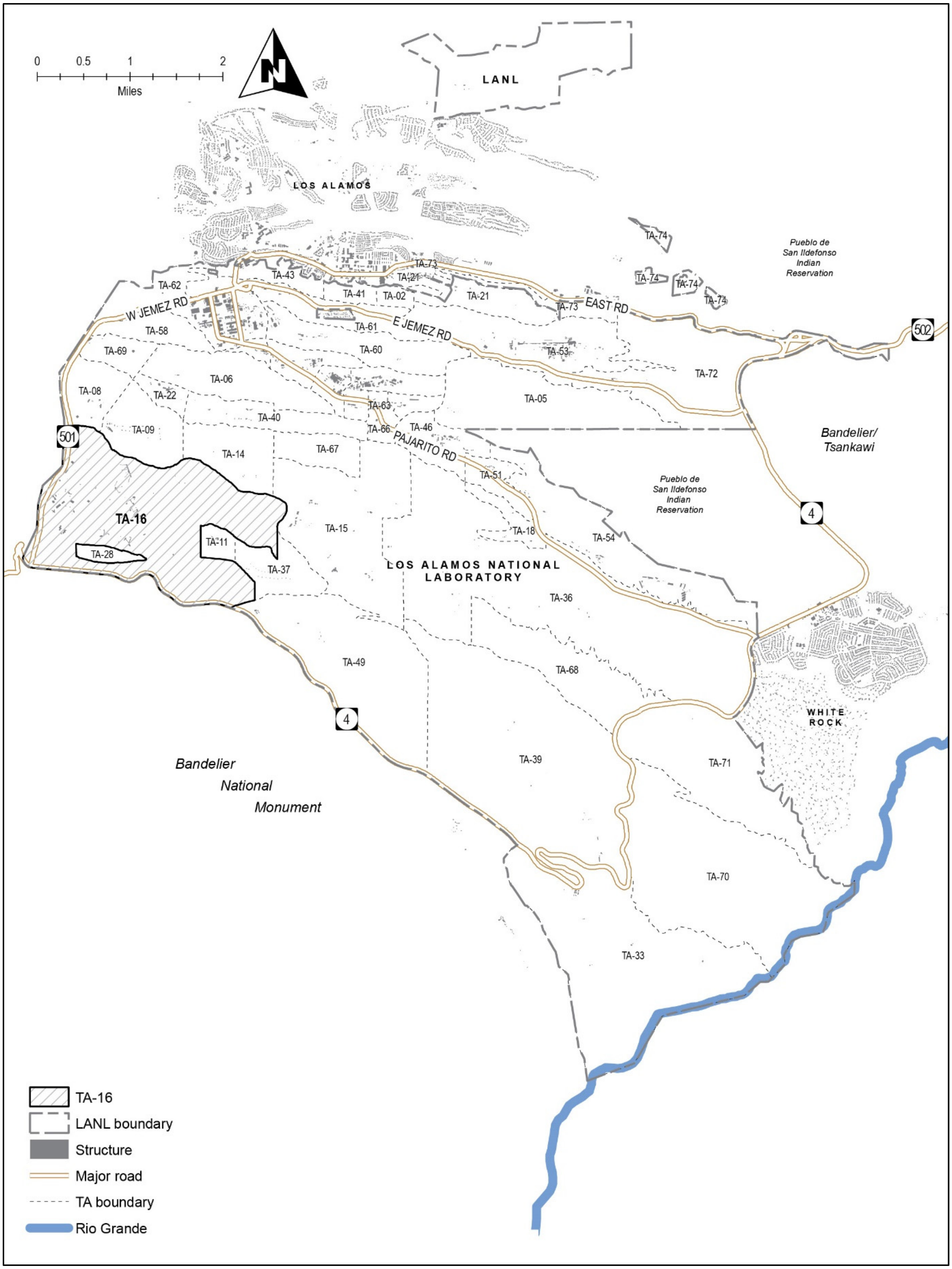

Figure 2.1-1 Location of TA-16 within the LANL boundary

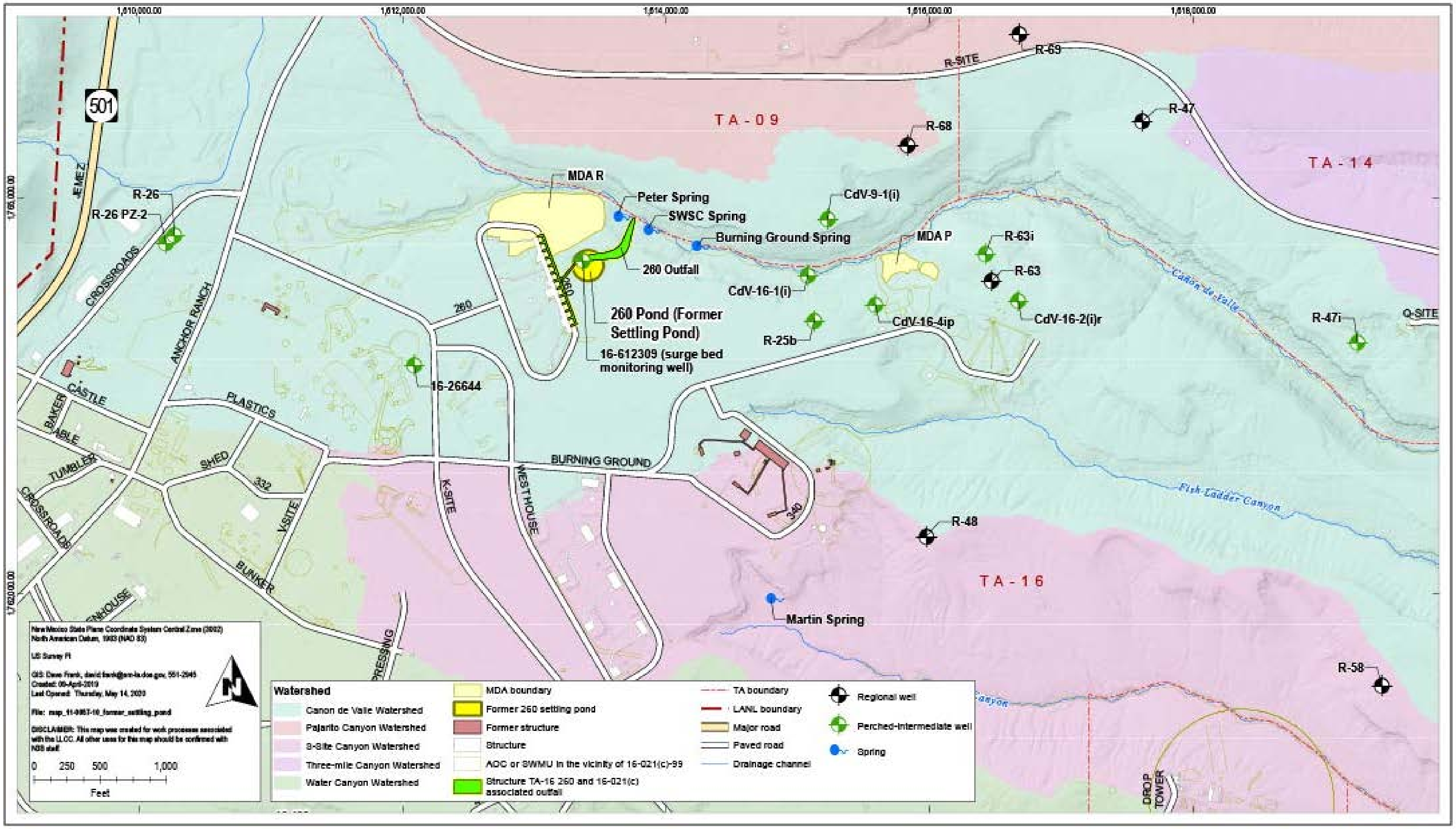

Figure 2.1-2 TA-16 site map

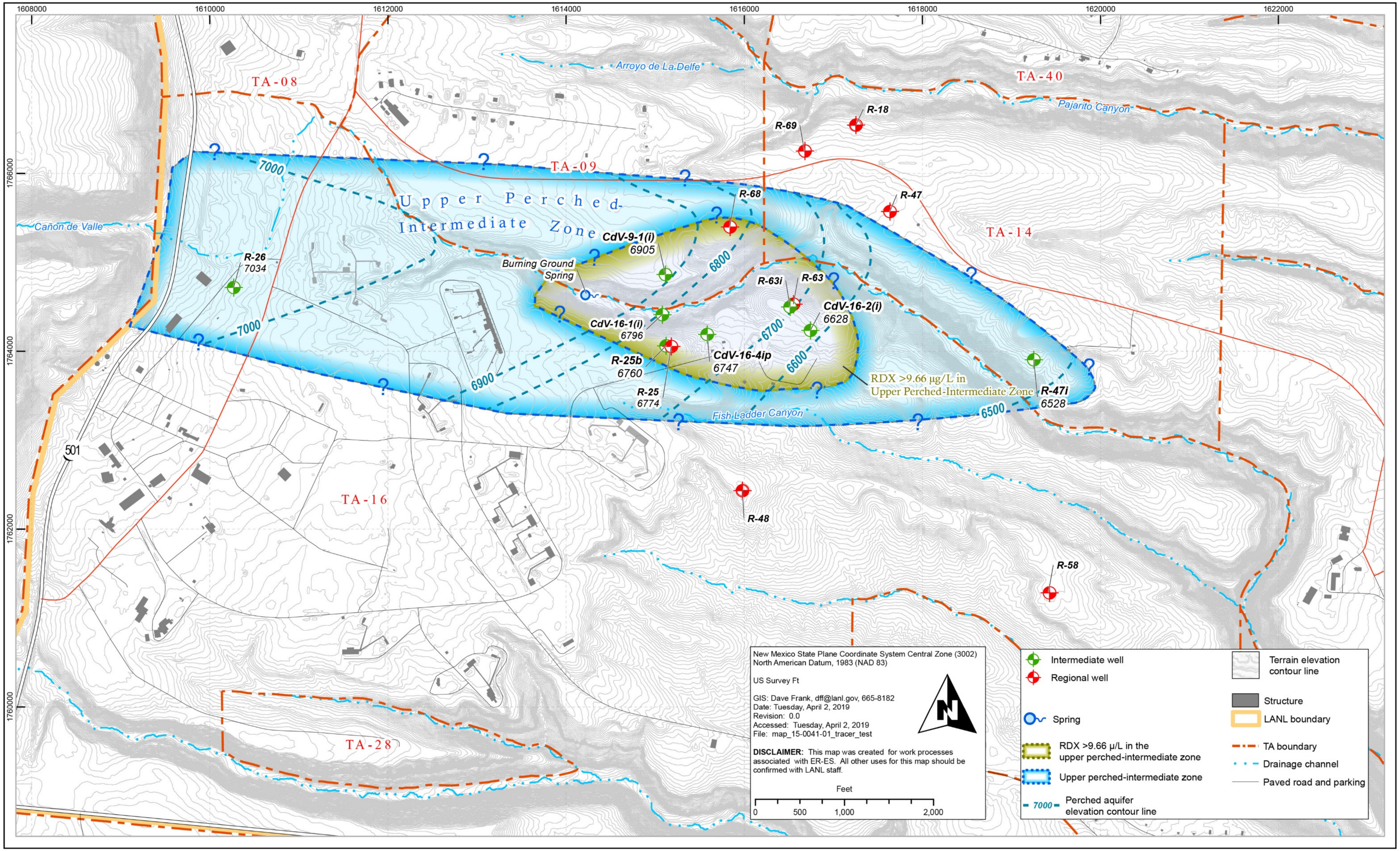

Figure 2.3-1 Spatial extent of the upper perched-intermediate groundwater zone and associated RDX concentrations above the NMED tap water screening criterion

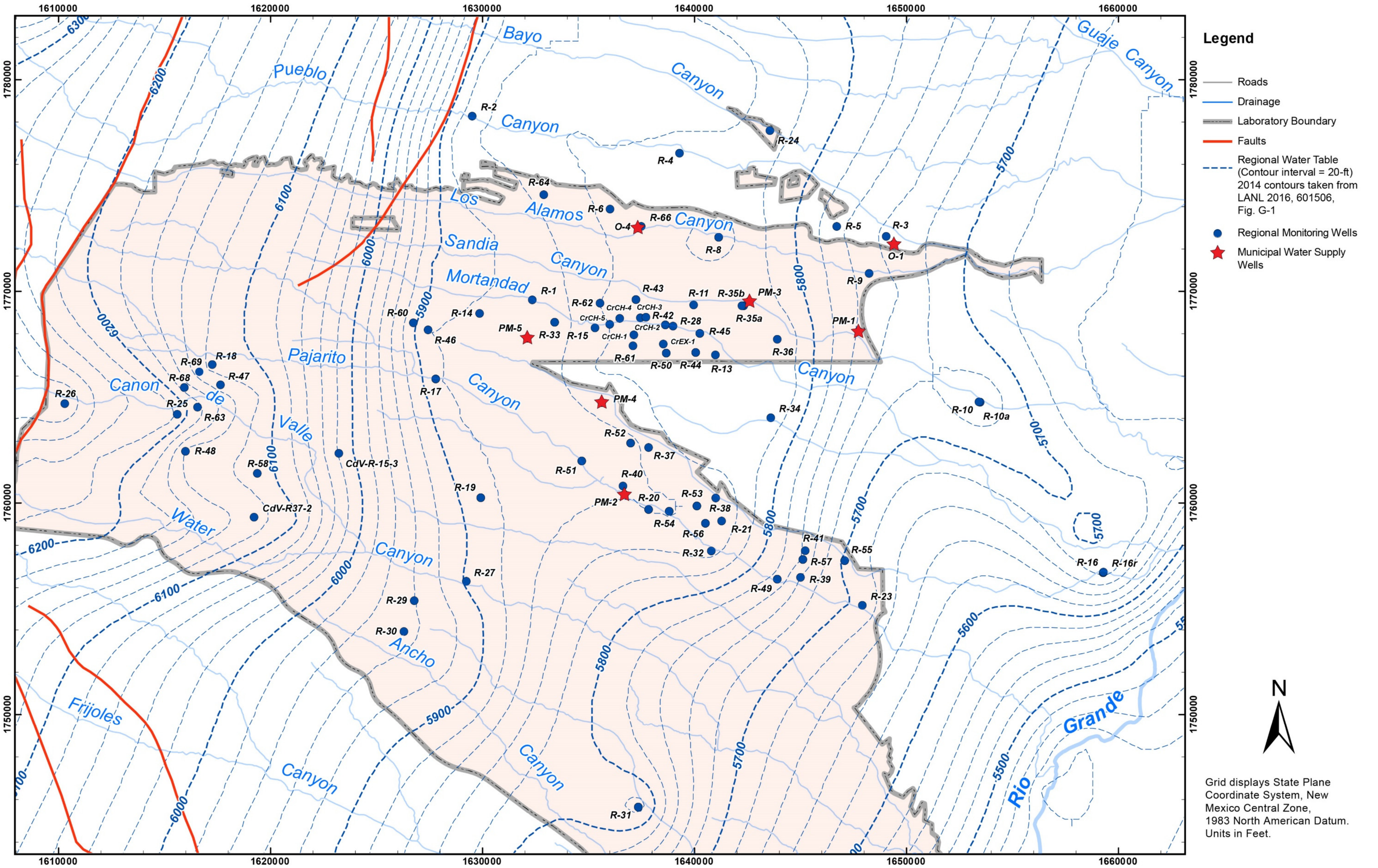

Figure 2.3-2 Location of LANL administrative boundary and municipal supply wells in the regional aquifer relative to TA-16 monitoring wells

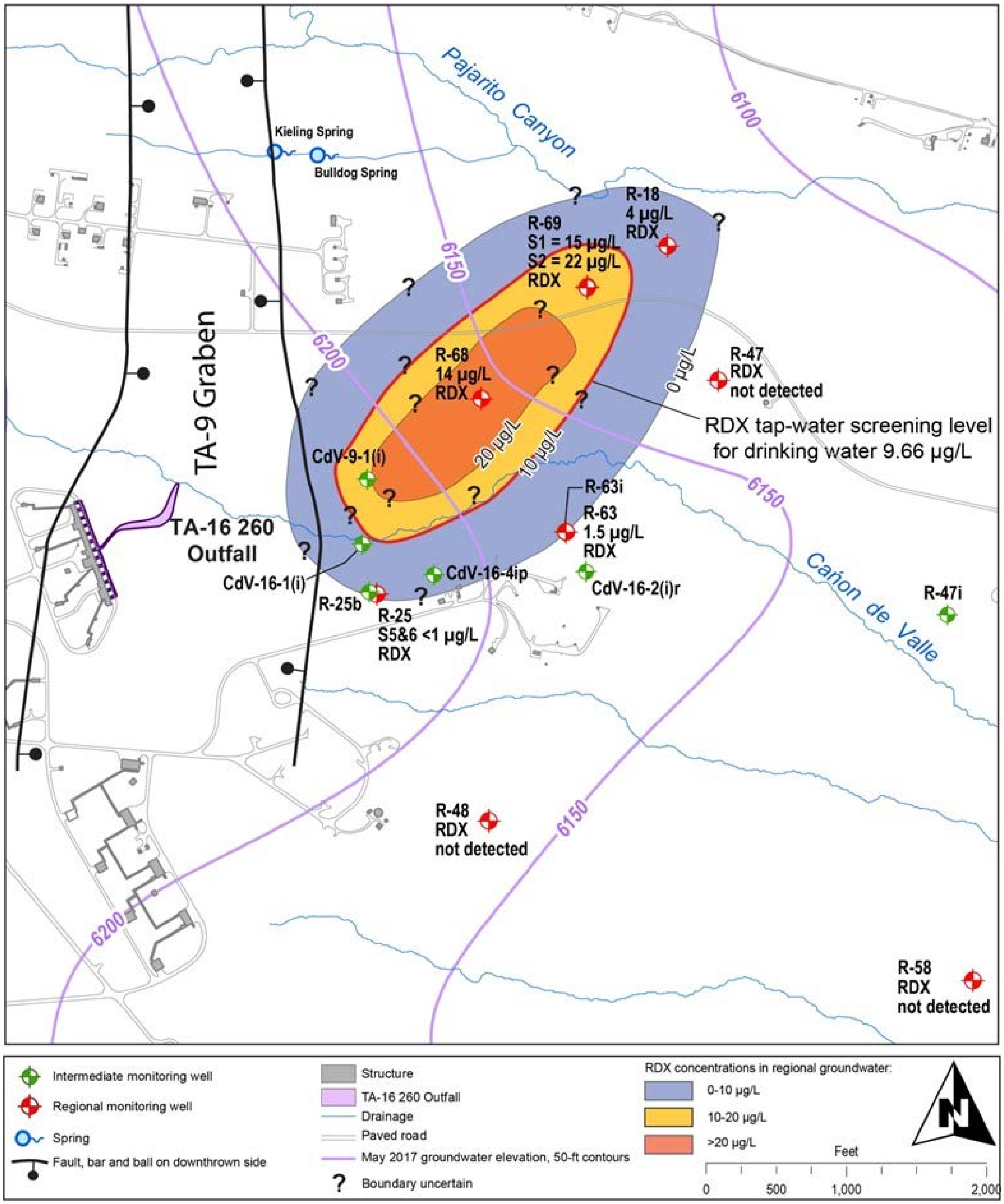

Figure 2.3-3 Approximate extent of RDX in the regional aquifer

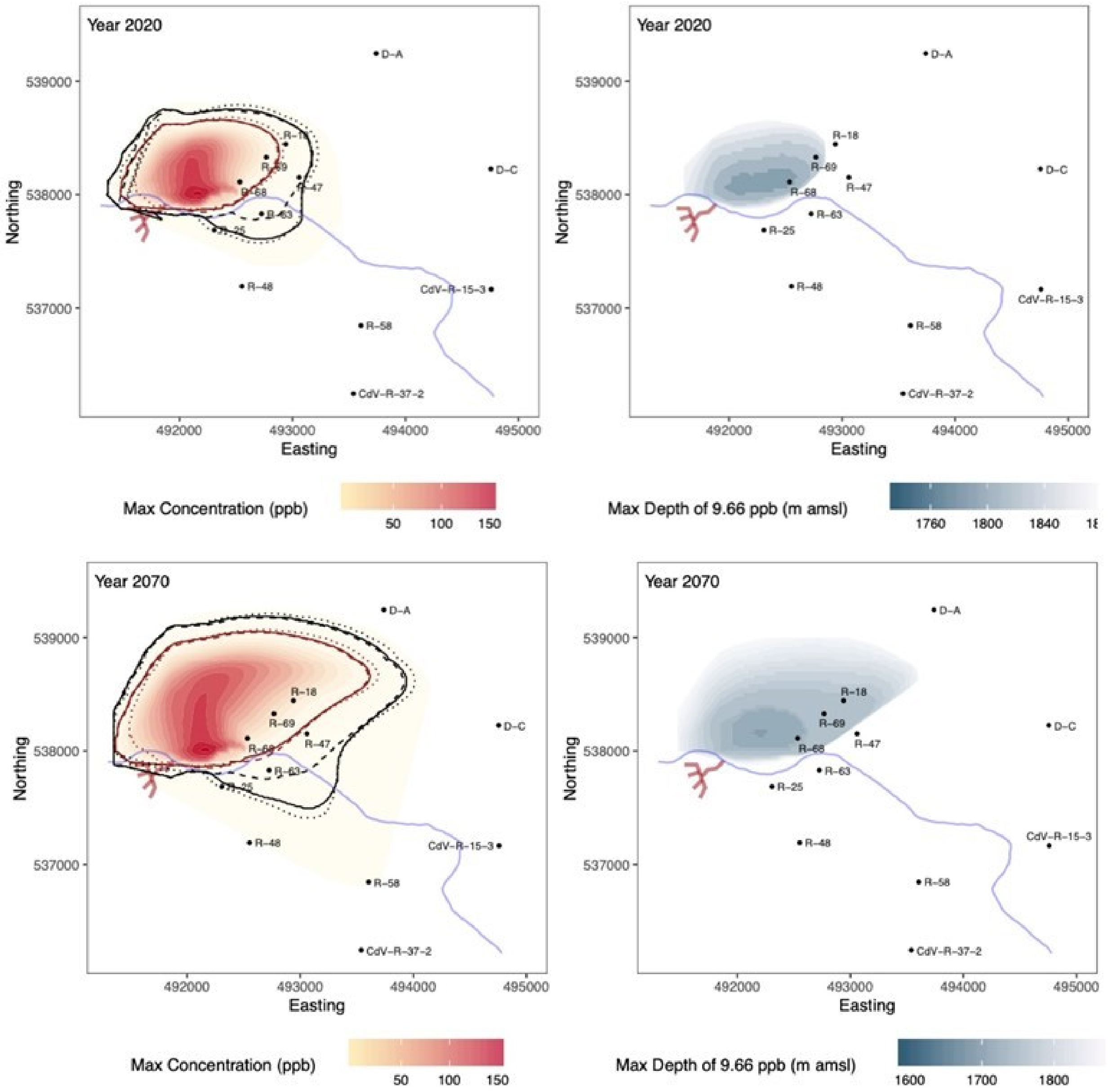

Figure 5.1-1 Heat maps of RDX concentrations and plume thickness at years 2020 and 2070

Table 4.1-1
Initial List of Perched-Intermediate Wells Considered for the Risk Assessment

Location ID	Northing	Easting	Hydrostratigraphic Unit	Geologic Unit	Top of Screen (ft bgs)	Bottom of Screen (ft bgs)	Number of Water Level Data Points Available	Used In DGIR	Used In Vadose Zone Model
16-26644	1763721.08	1612085.66	Intermediate Perched	Qbt 3	129.0	144.0	7507	Yes	No
CdV-16-1(i)	1764415.20	1615078.20	Intermediate Perched	Qbo	624.0	634.0	9106	Yes	Yes
CdV-16-2(i)r	1764219.40	1616673.24	Intermediate Perched	Tpf	850.0	859.7	8556	Yes	Yes
CdV-16-4ip S1*	1764195.74	1615587.07	Intermediate Perched	Tpf	815.6	879.2	6374	Yes	Yes
CdV-16-4ip S2	1764195.74	1615587.07	Intermediate	Tpf	1110.0	1141.1	1	Yes	No
CdV-37-1(i)	1757798.61	1624592.30	Intermediate Perched	Tpf	632.0	652.5	8411	Yes	No
CdV-9-1(i) S1	1764875.09	1615113.20	Intermediate Perched	Tpf	937.4	992.4	5446	Yes	Yes
R-25 S1	1764060.50	1615178.42	Intermediate	Qbo	737.6	758.4	10,129	Yes	Yes
R-25 S2	1764060.50	1615178.42	Intermediate	Tpf	882.6	893.4	10,127	Yes	Yes
R-25 S3	1764060.50	1615178.42	Intermediate	Tpf	1054.6	1064.6	8893	Yes	Yes
R-25 S4	1764060.50	1615178.42	Intermediate	Tpf	1184.6	1194.6	10,137	Yes	Yes
R-25b	1764074.70	1615125.60	Intermediate Perched	Qbo	750.0	770.8	8795	Yes	Yes
R-26 PZ-2	1764660.61	1610201.96	Intermediate	Qbt3	150.0	180.0	8531	Yes	Yes
R-26 S1	1764721.12	1610267.23	Intermediate Perched	Qct	651.8	669.9	8826	Yes	Yes
R-27(i)	1756302.42	1629129.03	Intermediate	Tpf	619.0	629.0	7422	Yes	No
R-47(i)	1763907.91	1619250.01	Intermediate Perched	Tpf	840.0	860.6	7543	Yes	Yes
R-63(i)	1764507.14	1616520.27	Intermediate Perched	Tpf	1122.5	1189.0	7166	Yes	Yes
CdV-R-37-2 S1	1759327.28	1619218.96	Intermediate	Tpf	914.4	939.5	363	No	No
R-19 S1	1760252.10	1629918.40	Intermediate Perched	Qbog	827.2	843.6	841	No	No
R-19 S2	1760252.10	1629918.40	Intermediate Perched	Tp	893.3	909.6	6698	No	No
R-25c	1764083.07	1615073.72	Intermediate Perched	Tpf	1039.6	1060.0	16	No	No
MSC-16-02665	1762530.55	1614427.59	Intermediate Perched	Qbt 3	93.5	123.5	0	No	No
PCI-2	1765872.63	1627648.27	Intermediate Perched	Tpf	512.0	522.0	10,757	No	No

* S = Screen.

Table 4.1-2
Final List of Perched-Intermediate Wells Used in the Risk Assessment

Well Name	Site Well or Background Well[a]	Screen Depth (ft)
CdV-16-1(i)	Site	624–634
CdV-16-2(i)r	Site	850–860
CdV-16-4ip (S1 + S2)[b]	Site	816–880; 1110–1141
CdV-37-1(i)	Site	632–653
CdV-9-1(i) (S1)	Site	937–992
PCI-2	Background	512–522
R-19 (S2)[c]	Site	893–910
R-25 (S3 and S4)[d]	Site	1055–1065; 1185–1195
R-25b	Site	750–771
R-26 S1	Background	652–670
R-27(i)	Background	619–629
R-47(i)	Background	840–861
R-63(i)	Site	1123–1189

[a] Background wells are identified in “Groundwater Background Investigation Report, Rev. 5” (LANL 2016, 601920).

[b] S = Screen.

[c] No usable data were identified in the first well screened interval.

[d] Damage to well screens 1 and 2 compromised more recent data; see section 4.1.

Table 4.2-1
Analytical Data Summary for Site and Background Wells

Parameter Name	Parameter Code	Well	Analytical Method	Analytical Method Category[a]	Geological Unit Code[a]	No. Samples	No. Detects	Unit	Mean Detect	Median Detect	Min Detect	Max Detect	Mean ND[b]	Median ND	Min ND	Max ND
1,5-naphthalenedisulfonic acid	1655-29-4	CdV-16-1(i)	SW-846:8330	HEXP[c]	Qbo	1	1	µg/L	20,714	20,714	20,714	20,714	— [d]	—	—	—
Acenaphthene	83-32-9	CdV-16-1(i)	SW-846:8270C, SW-846:8270D, SW-846:8270DGCMS_SIM, SW-846:8310	SVOC[e]	Qbo	9	0	µg/L	—	—	—	—	0.70133333	0.962	0.104	1.11
Acenaphthylene	208-96-8	CdV-16-1(i)	SW-846:8270C, SW-846:8270D, SW-846:8270DGCMS_SIM, SW-846:8310	SVOC	Qbo	9	0	µg/L	—	—	—	—	0.70133333	0.962	0.104	1.11
Acetone	67-64-1	CdV-16-1(i)	SW-846:8260B	VOC[f]	Qbo	23	1	µg/L	1.84	1.84	1.84	1.84	9.64090909	10	1.5	63.5
Acidity or alkalinity of a solution	pH	CdV-16-1(i)	EPA:150.1	General Chemistry	Qbo	25	25	SU	7.2576	7.13	6.96	8.4	—	—	—	—
Alkalinity-CO3	ALK-CO3	CdV-16-1(i)	EPA:310.1	General Chemistry	Qbo	26	0	µg/L	—	—	—	—	1431.73077	1000	725	4000
Alkalinity-CO3+HCO3	ALK-CO3+HCO3	CdV-16-1(i)	EPA:310.1	General Chemistry	Qbo	28	28	µg/L	61,967.107	59,100	54,700	79,579	—	—	—	—
Alkalinity-HCO3	ALK-HCO3	CdV-16-1(i)	EPA:310.1	General Chemistry	Qbo	1	1	µg/L	54,600	54,600	54,600	54,600	—	—	—	—
Aluminum	Al	CdV-16-1(i)	EPA:200.7, SW-846:6010B, SW 846:6010C	Inorganic	Qbo	41	1	µg/L	69	69	69	69	139.03	200	1	200
Amino-2,6-dinitrotoluene[4-]	19406-51-0	CdV-16-1(i)	SW-846:8321A_MOD, SW-846:8330B, SW-846:8321A(M)	LCMS/MS[g] High Explosives, LCMS/MS Perchlorate	Qbo	30	29	µg/L	0.1891379	0.184	0.134	0.292	0.325	0.325	0.325	0.325
Amino-4,6-dinitrotoluene[2-]	35572-78-2	CdV-16-1(i)	SW-846:8321A_MOD, SW_846:8330B, SW-846:8321A(M)	LCMS/MS High Explosives, LCMS/MS Perchlorate	Qbo	29	19	µg/L	0.1215737	0.114	0.0841	0.193	0.18051	0.17145	0.0816	0.325
Ammonia as nitrogen	NH3-N	CdV-16-1(i)	EPA:350.1	General Chemistry	Qbo	25	10	µg/L	95.02	35.15	24.8	353	44.1933333	44	10	150
Anthracene	120-12-7	CdV-16-1(i)	SW-846:8270C, SW-846:8270D, SW-846:8270DGCMS_SIM, SW-846:8310	SVOC	Qbo	9	0	µg/L	—	—	—	—	0.70133333	0.962	0.104	1.11
Antimony	Sb	CdV-16-1(i)	EPA:200.8, SW-846:6020	Inorganic	Qbo	41	0	µg/L	—	—	—	—	1.90243902	2	0.5	3
Arsenic	As	CdV-16-1(i)	EPA:200.8, SW-846:6010B, SW-846:6020	Inorganic	Qbo	41	6	µg/L	2.118845	2.32	0.3431	3.02	4.77142857	5	1.5	6
Barium	Ba	CdV-16-1(i)	EPA:200.7, SW-846:6010B, SW-846:6010C	Inorganic	Qbo	41	41	µg/L	16.558317	16.5	14.7	17.9	—	—	—	—
Benzo(g,h,i)perylene	191-24-2	CdV-16-1(i)	SW-846:8270C, SW-846:8270D, SW-846:8270DGCMS_SIM, SW-846:8310	SVOC	Qbo	8	0	µg/L	—	—	—	—	0.611375	0.653	0.051	1.11
Benzoic acid	65-85-0	CdV-16-1(i)	SW-846:8270C, SW-846:8270D	SVOC	Qbo	8	0	µg/L	—	—	—	—	16.44	20.45	6.12	22.2
Beryllium	Be	CdV-16-1(i)	EPA:200.8, SW-846:6010B, SW-846:6010C, SW-846:6020	Inorganic	Qbo	41	5	µg/L	0.168	0.17	0.15	0.2	3.64166667	5	0.1	5
Bis(2-ethylhexyl)phthalate	117-81-7	CdV-16-1(i)	SW-846:8270C, SW-846:8270D	SVOC	Qbo	9	2	µg/L	3.695	3.695	3	4.39	8.65428571	10.3	3.06	11.1
Boron	B	CdV-16-1(i)	EPA:200.7, SW-846:6010B, SW-846:6010C	Inorganic	Qbo	41	41	µg/L	60.754171	60.7	29.521	78.9	—	—	—	—
Bromide	Br(-1)	CdV-16-1(i)	EPA:300.0	General Chemistry	Qbo	29	20	µg/L	86.8045	86.1	44.987	117	152.666667	200	41	200
Bromodichloromethane	75-27-4	CdV-16-1(i)	SW-846:8260B	VOC	Qbo	23	0	µg/L	—	—	—	—	0.87826087	1	0.3	1

Table 4.2-1 (continued)

Parameter Name	Parameter Code	Well	Analytical Method	Analytical Method Category[a]	Geological Unit Code[a]	No. Samples	No. Detects	Unit	Mean Detect	Median Detect	Min Detect	Max Detect	Mean ND	Median ND	Min ND	Max ND
Bromoform	75-25-2	CdV-16-1(i)	SW-846:8260B	VOC	Qbo	23	0	µg/L	—	—	—	—	0.87826087	1	0.3	1
Butanone[2-]	78-93-3	CdV-16-1(i)	SW-846:8260B	VOC	Qbo	23	1	µg/L	11.6	11.6	11.6	11.6	4.36363636	5	1.5	5
Cadmium	Cd	CdV-16-1(i)	EPA:200.8, SW-846:6020	Inorganic	Qbo	41	0	µg/L	—	—	—	—	0.66878049	1	0.1	1
Calcium	Ca	CdV-16-1(i)	EPA:200.7, SW-846:6010B, SW-846:6010C	Inorganic	Qbo	41	41	µg/L	13,251.171	13,200	11,300	14,700	—	—	—	—
Carbon disulfide	75-15-0	CdV-16-1(i)	SW-846:8260B	VOC	Qbo	23	0	µg/L	—	—	—	—	4.39130435	5	1.5	5
Chloride	Cl(-1)	CdV-16-1(i)	EPA:300.0	General Chemistry	Qbo	28	28	µg/L	7936.7143	7335	5780	22378	—	—	—	—
Chlorobenzene	108-90-7	CdV-16-1(i)	SW-846:8260B	VOC	Qbo	23	0	µg/L	—	—	—	—	0.87826087	1	0.3	1
Chlorodibromomethane	124-48-1	CdV-16-1(i)	SW-846:8260B	VOC	Qbo	23	0	µg/L	—	—	—	—	0.87826087	1	0.3	1
Chloroform	67-66-3	CdV-16-1(i)	SW-846:8260B	VOC	Qbo	23	0	µg/L	—	—	—	—	0.87826087	1	0.3	1
Chloromethane	74-87-3	CdV-16-1(i)	SW-846:8260B	VOC	Qbo	23	0	µg/L	—	—	—	—	0.87826087	1	0.3	1
Chromium	Cr	CdV-16-1(i)	EPA:200.8, SW-846:6010B, SW-846:6020	Inorganic	Qbo	41	11	µg/L	2.6472727	2.5	1.2	4.48	6.00833333	6.5	1	10
Cobalt	Co	CdV-16-1(i)	EPA:200.8, SW-846:6010B, SW-846:6010C	Inorganic	Qbo	41	1	µg/L	1.13	1.13	1.13	1.13	3.3	5	1	5
Copper	Cu	CdV-16-1(i)	EPA:200.8, SW-846:6010B, SW-846:6010C	Inorganic	Qbo	41	39	µg/L	13.177513	10.8	3.7	63.2	6.28	6.28	3	9.56
Cyanide (total)	CN (Total)	CdV-16-1(i)	EPA:335.3, EPA:335.4	Inorganic	Qbo	16	0	µg/L	—	—	—	—	3.94875	5	1.5	5
DNX[h]	DNX	CdV-16-1(i)	SW-846:8321A_MOD, SW-846:8330B, SW-846:8330RDX	LCMS/MS High Explosives	Qbo	21	19	µg/L	0.1786316	0.148	0.106	0.452	0.5	0.5	0.5	0.5
Fluoranthene	206-44-0	CdV-16-1(i)	SW-846:8270C, SW-846:8270D, SW-846:8270DGCMS_SIM, SW-846:8310	SVOC	Qbo	9	0	µg/L	—	—	—	—	0.65033333	0.962	0.051	1.11
Fluoride	F(-1)	CdV-16-1(i)	EPA:300.0	General Chemistry	Qbo	28	23	µg/L	116.63957	105	42.8	402.51	59.2	33	30	100
Gross alpha	GrossA	CdV-16-1(i)	EPA:900	RAD[i]	Qbo	7	2	pCi/L	2.765	2.765	1.38	4.15	1.1584	1.06	-1.27	2.67
Gross beta	GrossB	CdV-16-1(i)	EPA:900	RAD	Qbo	7	5	pCi/L	3.158	3.32	2.47	3.63	1.905	1.905	1.34	2.47
Gross gamma	GrossG	CdV-16-1(i)	EPA:901.1	RAD	Qbo	3	0	pCi/L	—	—	—	—	48.81	58.1	0.73	87.6
Hardness	Hardness	CdV-16-1(i)	SM:A2340B	Inorganic	Qbo	34	34	µg/L	55,785.294	55,800	46,800	62,400	—	—	—	—
Heptachlor	76-44-8	CdV-16-1(i)	SW-846:8081A	PESTPCB[j]	Qbo	2	1	µg/L	0.0165	0.0165	0.0165	0.0165	0.022	0.022	0.022	0.022
Hexachlorobutadiene	87-68-3	CdV-16-1(i)	SW-846:8260B	VOC	Qbo	20	0	µg/L	—	—	—	—	0.86	1	0.3	1
HMX[k]	2691-41-0	CdV-16-1(i)	SW-846:8321A_MOD, SW-846:8330B, SW-846:8321A(M)	LCMS/MS High Explosives, LCMS/MS Perchlorate	Qbo	30	30	µg/L	1.7153333	1.66	1.21	2.53	—	—	—	—
Iron	Fe	CdV-16-1(i)	EPA:200.7, SW-846:6010B, SW-846:6010C	Inorganic	Qbo	41	11	µg/L	364.82727	48.6	29.4	2750	75.46	100	10	100
Lead	Pb	CdV-16-1(i)	EPA:200.8, SW-846:6020	Inorganic	Qbo	41	5	µg/L	3.038414	0.72	0.2591	12.7	1.45833333	2	0.5	2
Lithium	Li	CdV-16-1(i)	EPA:200.7	Inorganic	Qbo	1	1	µg/L	5.8417	5.8417	5.8417	5.8417	—	—	—	—
Magnesium	Mg	CdV-16-1(i)	EPA:200.7, SW-846:6010B, SW-846:6010C	Inorganic	Qbo	41	41	µg/L	5534.2049	5560	4500	6210	—	—	—	—
Manganese	Mn	CdV-16-1(i)	EPA:200.7, SW-846:6010B, SW-846:6010C, SW-846:6020	Inorganic	Qbo	41	29	µg/L	5.0124207	3.8	2.2	13.6	6	6	2	10

Table 4.2-1 (continued)

Parameter Name	Parameter Code	Well	Analytical Method	Analytical Method Category[a]	Geological Unit Code[a]	No. Samples	No. Detects	Unit	Mean Detect	Median Detect	Min Detect	Max Detect	Mean ND	Median ND	Min ND	Max ND
Mercury	Hg	CdV-16-1(i)	EPA:200.8, EPA:245.2, SW-846:7470A	Inorganic	Qbo	52	1	µg/L	0.071	0.071	0.071	0.071	0.14572549	0.2	0.03	0.2
Methyl tert-butyl ether	1634-04-4	CdV-16-1(i)	SW-846:8260B	VOC	Qbo	18	16	µg/L	1.202875	1.16	0.966	1.48	1.195	1.195	1	1.39
Methyl-2-pentanone[4-]	108-10-1	CdV-16-1(i)	SW-846:8260B	VOC	Qbo	23	0	µg/L	—	—	—	—	4.39130435	5	1.5	5
Methylene chloride	75-09-2	CdV-16-1(i)	SW-846:8260B	VOC	Qbo	23	0	µg/L	—	—	—	—	6.83478261	10	1	10
MNX[l]	MNX	CdV-16-1(i)	SW-846:8321A_MOD, SW-846:8330B, SW-846:8330RDX	LCMS/MS High Explosives	Qbo	21	19	µg/L	0.2971579	0.3	0.141	0.391	0.5	0.5	0.5	0.5
Molybdenum	Mo	CdV-16-1(i)	EPA:200.8, SW-846:6010B, SW-846:6020	Inorganic	Qbo	41	31	µg/L	1.5570645	1.1	0.535	3.6	1.5186	1.065	0.631	3.3
Nickel	Ni	CdV-16-1(i)	EPA:200.8, SW-846:6010B, SW-846:6020	Inorganic	Qbo	41	41	µg/L	4.9947976	4.45	1.69	13.2	—	—	—	—
Nitrate	NO3	CdV-16-1(i)	EPA:300.0	General Chemistry	Qbo	1	1	µg/L	3927.1	3927.1	3927.1	3927.1	—	—	—	—
Nitrate-nitrite as nitrogen	NO3+NO2-N	CdV-16-1(i)	EPA:353.1, EPA:353.2	General Chemistry	Qbo	27	27	µg/L	844.7037	880	510	1090	—	—	—	—
Nitrotoluene[2-]	88-72-2	CdV-16-1(i)	SW-846:8321A_MOD, SW-846:8330B, SW-846:8321A(M)	LCMS/MS High Explosives, LCMS/MS Perchlorate	Qbo	29	0	µg/L	—	—	—	—	0.24397241	0.272	0.0837	0.325
Oxygen-18/oxygen-16 ratio from nitrate	O18O16-NO3	CdV-16-1(i)	Generic:Oxygen Isotope Ratio	General Chemistry	Qbo	1	1	permil	-0.28189	-0.2819	-0.2819	-0.2819	—	—	—	—
Perchlorate	ClO4	CdV-16-1(i)	SW-846:6850, SW846 6850 Modified	LCMS/MS Perchlorate	Qbo	27	27	µg/L	0.5188519	0.521	0.461	0.577	—	—	—	—
Perfluorooctanoic acid	335-67-1	CdV-16-1(i)	EPA:537M	LCMS/MS PFAS[m]	Qbo	1	1	µg/L	0.00115	0.0012	0.0012	0.0012	—	—	—	—
Phenanthrene	85-01-8	CdV-16-1(i)	SW-846:8270C, SW-846:8270D, SW-846:8270DGCMS_SIM, SW-846:8310	SVOC	Qbo	9	0	µg/L	—	—	—	—	0.70133333	0.962	0.104	1.11
Potassium	K	CdV-16-1(i)	EPA:200.7, SW-846:6010B, SW-846:6010C	Inorganic	Qbo	41	41	µg/L	2387.6098	2400	1722	2700	—	—	—	—
Pyrene	129-00-0	CdV-16-1(i)	SW-846:8270C, SW-846:8270D, SW-846:8270DGCMS_SIM, SW-846:8310	SVOC	Qbo	9	0	µg/L	—	—	—	—	0.65033333	0.962	0.051	1.11
Radium-226	Ra-226	CdV-16-1(i)	EPA:903.1	RAD	Qbo	2	0	pCi/L	—	—	—	—	0.304	0.304	0.255	0.353
Radium-228	Ra-228	CdV-16-1(i)	EPA:904	RAD	Qbo	2	0	pCi/L	—	—	—	—	0.314	0.314	0.251	0.377
RDX	121-82-4	CdV-16-1(i)	SW-846:8330, SW-846:8321A_MOD, SW-846:8330B, SW-846:8321A(M)	HEXP, LCMS/MS High Explosives, LCMS/MS Perchlorate	Qbo	31	31	µg/L	28.570968	28.1	22.2	37.4	—	—	—	—
Selenium	Se	CdV-16-1(i)	EPA:200.8, SW-846:6010B, SW-846:6020	Inorganic	Qbo	41	0	µg/L	—	—	—	—	4.31707317	5	1	6
Silicon dioxide	SiO2	CdV-16-1(i)	EPA:200.7, SW-846:6010B, SW-846:6010C	Inorganic	Qbo	31	31	µg/L	58,063	57,600	52,800	63,200	—	—	—	—
Silver	Ag	CdV-16-1(i)	EPA:200.8, SW-846:6010B, SW-846:6020	Inorganic	Qbo	41	0	µg/L	—	—	—	—	0.81463415	1	0.2	1
Sodium	Na	CdV-16-1(i)	EPA:200.7, SW-846:6010B, SW-846:6010C	Inorganic	Qbo	41	41	µg/L	12353.463	12000	10300	23600	—	—	—	—

Table 4.2-1 (continued)

Parameter Name	Parameter Code	Well	Analytical Method	Analytical Method Category[a]	Geological Unit Code[a]	No. Samples	No. Detects	Unit	Mean Detect	Median Detect	Min Detect	Max Detect	Mean ND	Median ND	Min ND	Max ND
Strontium	Sr	CdV-16-1(i)	EPA:200.7, SW-846:6010B, SW-846:6010C	Inorganic	Qbo	41	41	µg/L	94.587244	94.5	76.1	110	—	—	—	—
Styrene	100-42-5	CdV-16-1(i)	SW-846:8260B	VOC	Qbo	23	0	µg/L	—	—	—	—	0.87826087	1	0.3	1
Sulfate	SO4(-2)	CdV-16-1(i)	EPA:300.0	General Chemistry	Qbo	28	28	µg/L	9839.5357	9635	8670	12,500	—	—	—	—
Temperature	TEMP	CdV-16-1(i)	EPA:170.0	VOC	Qbo	13	13	deg C	2.9230769	3	1	4	—	—	—	—
Tetrachloroethene	127-18-4	CdV-16-1(i)	SW-846:8260B	VOC	Qbo	23	21	µg/L	1.0935238	1.11	0.79	1.49	1.245	1.245	1	1.49
Thallium	Tl	CdV-16-1(i)	EPA:200.8, SW-846:6020	Inorganic	Qbo	41	6	µg/L	0.5341667	0.4875	0.41	0.74	1.23868571	1	0.3	2
Tin	Sn	CdV-16-1(i)	EPA:200.8, SW-846:6010B, SW-846:6010C	Inorganic	Qbo	35	1	µg/L	10	10	10	10	12.5294118	10	1	100
TNX[n]	TNX	CdV-16-1(i)	SW-846:8321A_MOD, SW-846:8330B, SW-846:8330RDX	LCMS/MS High Explosives	Qbo	21	19	µg/L	0.2303158	0.226	0.163	0.362	0.5	0.5	0.5	0.5
Toluene	108-88-3	CdV-16-1(i)	SW-846:8260B	VOC	Qbo	23	9	µg/L	17.166444	3.04	0.268	119	0.8	1	0.3	1
Total dissolved solids	TDS	CdV-16-1(i)	EPA:160.1	General Chemistry	Qbo	24	24	µg/L	151845.83	148,500	94,300	194,000	—	—	—	—
Total Kjeldahl nitrogen	TKN	CdV-16-1(i)	EPA:351.2	General Chemistry	Qbo	23	9	µg/L	197.34444	138	36	520	76.0357143	100	10	100
Total organic carbon	TOC	CdV-16-1(i)	SW-846:9060	General Chemistry	Qbo	23	22	µg/L	1897.3636	1050	639	16,900	1040	1040	1040	1040
Total phosphate as phosphorus	PO4-P	CdV-16-1(i)	EPA:365.4	General Chemistry	Qbo	27	14	µg/L	50.1	42.7	22.8	107	56.6769231	52	24	88.4
Trichlorobenzene[1,2,3-]	87-61-6	CdV-16-1(i)	SW-846:8260B	VOC	Qbo	20	0	µg/L	—	—	—	—	0.86	1	0.3	1
Trichloroethene	79-01-6	CdV-16-1(i)	SW-846:8260B	VOC	Qbo	23	0	µg/L	—	—	—	—	0.87826087	1	0.3	1
Trinitrobenzene[1,3,5-]	99-35-4	CdV-16-1(i)	SW-846:8321A_MOD, SW-846:8330B, SW-846:8321A(M)	LCMS/MS High Explosives, LCMS/MS Perchlorate	Qbo	29	0	µg/L	—	—	—	—	0.24345517	0.272	0.0816	0.325
Trinitrotoluene[2,4,6-]	118-96-7	CdV-16-1(i)	SW-846:8321A_MOD, SW-846:8330B, SW-846:8321A(M)	LCMS/MS High Explosives, LCMS/MS Perchlorate	Qbo	29	0	µg/L	—	—	—	—	0.24345517	0.272	0.0816	0.325
Tritium	H-3	CdV-16-1(i)	Generic:LLEE, Generic:Low_Level_Tritium	RAD	Qbo	8	8	pCi/L	55.3415	63.595	26.645	68.264	—	—	—	—
Uranium	U	CdV-16-1(i)	EPA:200.8, SW-846:6020	Inorganic	Qbo	41	40	µg/L	0.443151	0.435	0.3	0.62	0.359	0.359	0.359	0.359
Uranium-234	U-234	CdV-16-1(i)	HASL-300:ISOU	RAD	Qbo	8	8	pCi/L	0.397625	0.4045	0.293	0.462	—	—	—	—
Uranium-235/236	U-235/236	CdV-16-1(i)	HASL-300:ISOU	RAD	Qbo	8	0	pCi/L	—	—	—	—	0.021035	0.015	-0.0147	0.0855
Uranium-238	U-238	CdV-16-1(i)	HASL-300:ISOU	RAD	Qbo	8	8	pCi/L	0.17175	0.1475	0.112	0.28	—	—	—	—
Vanadium	V	CdV-16-1(i)	EPA:200.8, SW-846:6010B, SW-846:6010C	Inorganic	Qbo	41	37	µg/L	2.6780838	2.6	1.5	4.73	2.85	3.05	1.2	4.1
Zinc	Zn	CdV-16-1(i)	EPA:200.7, SW-846:6010B, SW-846:6010C	Inorganic	Qbo	41	36	µg/L	23.897417	24	4.9	70.7	10.47	12.3	5.48	14.7
Acenaphthene	83-32-9	CdV-16-2(i)r	SW-846:8270C, SW-846:8270D, SW-846:8270DGCMS_SIM, SW-846:8310	SVOC	Tpf	10	0	µg/L	—	—	—	—	0.7811	1.035	0.105	1.12
Acenaphthylene	208-96-8	CdV-16-2(i)r	SW-846:8270C, SW-846:8270D, SW-846:8270DGCMS_SIM, SW-846:8310	SVOC	Tpf	10	0	µg/L	—	—	—	—	0.7811	1.035	0.105	1.12
Acetone	67-64-1	CdV-16-2(i)r	SW-846:8260B	VOC	Tpf	23	1	µg/L	7.81	7.81	7.81	7.81	7.05272727	10	1.5	10

Table 4.2-1 (continued)

Parameter Name	Parameter Code	Well	Analytical Method	Analytical Method Category[a]	Geological Unit Code[a]	No. Samples	No. Detects	Unit	Mean Detect	Median Detect	Min Detect	Max Detect	Mean ND	Median ND	Min ND	Max ND
Acidity or Alkalinity of a solution	pH	CdV-16-2(i)r	EPA:150.1	General Chemistry	Tpf	19	19	SU	7.4094737	7.35	7.11	7.85	—	—	—	—
Alkalinity-CO3	ALK-CO3	CdV-16-2(i)r	EPA:310.1	General Chemistry	Tpf	19	0	µg/L	—	—	—	—	1486.84211	1000	1000	4000
Alkalinity-CO3+HCO3	ALK-CO3+HCO3	CdV-16-2(i)r	EPA:310.1	General Chemistry	Tpf	19	19	µg/L	51342.105	51,400	44,800	55,800	—	—	—	—
Aluminum	Al	CdV-16-2(i)r	SW-846:6010B, SW-846:6010C	Inorganic	Tpf	24	2	µg/L	197	197	165	229	170	200	68	200
Amino-2,6-dinitrotoluene[4-]	19406-51-0	CdV-16-2(i)r	SW-846:8321A_MOD, SW-846:8330B	LCMS/MS High Explosives	Tpf	33	20	µg/L	0.12414	0.121	0.0958	0.166	0.29855385	0.325	0.0842	0.325
Amino-4,6-dinitrotoluene[2-]	35572-78-2	CdV-16-2(i)r	SW-846:8321A_MOD, SW-846:8330B	LCMS/MS High Explosives	Tpf	32	1	µg/L	0.182	0.182	0.182	0.182	0.2243	0.263	0.0816	0.325
Ammonia as nitrogen	NH3-N	CdV-16-2(i)r	EPA:350.1	General Chemistry	Tpf	19	13	µg/L	70.961538	43.5	22	234	72.0333333	57.4	32	154
Anthracene	120-12-7	CdV-16-2(i)r	SW-846:8270C, SW-846:8270D, SW-846:8270DGCMS_SIM, SW-846:8310	SVOC	Tpf	10	0	µg/L	—	—	—	—	0.7811	1.035	0.105	1.12
Antimony	Sb	CdV-16-2(i)r	SW-846:6020	Inorganic	Tpf	24	0	µg/L	—	—	—	—	2.58333333	3	1	3
Arsenic	As	CdV-16-2(i)r	SW-846:6020	Inorganic	Tpf	24	4	µg/L	2.6475	2.285	2.12	3.9	4.6385	5	2	5
Barium	Ba	CdV-16-2(i)r	SW-846:6010B, SW-846:6010C	Inorganic	Tpf	24	24	µg/L	2.5175	2.42	1.95	3.55	—	—	—	—
Benzo(g,h,i)perylene	191-24-2	CdV-16-2(i)r	SW-846:8270C, SW-846:8270D, SW-846:8270DGCMS_SIM, SW-846:8310	SVOC	Tpf	9	0	µg/L	—	—	—	—	0.64973333	1.03	0.0505	1.12
Benzoic acid	65-85-0	CdV-16-2(i)r	SW-846:8270C, SW-846:8270D	SVOC	Tpf	9	0	µg/L	—	—	—	—	17.9444444	20.8	6	21.7
Beryllium	Be	CdV-16-2(i)r	SW-846:6010B, SW-846:6010C	Inorganic	Tpf	24	0	µg/L	—	—	—	—	4.16666667	5	1	5
Bis(2-ethylhexyl)phthalate	117-81-7	CdV-16-2(i)r	SW-846:8270C, SW-846:8270D	SVOC	Tpf	10	0	µg/L	—	—	—	—	9.28	10.45	3	11.2
Boron	B	CdV-16-2(i)r	SW-846:6010B, SW-846:6010C	Inorganic	Tpf	24	21	µg/L	26.97619	27.5	17.7	37.5	38.3333333	50	15	50
Bromide	Br(-1)	CdV-16-2(i)r	EPA:300.0	General Chemistry	Tpf	19	4	µg/L	75.15	76.05	69.1	79.4	164.533333	200	67	200
Bromodichloromethane	75-27-4	CdV-16-2(i)r	SW-846:8260B	VOC	Tpf	23	0	µg/L	—	—	—	—	0.84782609	1	0.3	1
Bromoform	75-25-2	CdV-16-2(i)r	SW-846:8260B	VOC	Tpf	23	0	µg/L	—	—	—	—	0.84782609	1	0.3	1
Butanone[2-]	78-93-3	CdV-16-2(i)r	SW-846:8260B	VOC	Tpf	23	1	µg/L	11.7	11.7	11.7	11.7	4.20454545	5	1.5	5
Cadmium	Cd	CdV-16-2(i)r	SW-846:6020	Inorganic	Tpf	24	0	µg/L	—	—	—	—	0.85416667	1	0.3	1
Calcium	Ca	CdV-16-2(i)r	SW-846:6010B, SW-846:6010C	Inorganic	Tpf	24	24	µg/L	9817.9167	9875	8510	11,100	—	—	—	—
Carbon disulfide	75-15-0	CdV-16-2(i)r	SW-846:8260B	VOC	Tpf	23	0	µg/L	—	—	—	—	4.23913043	5	1.5	5
Chloride	Cl(-1)	CdV-16-2(i)r	EPA:300.0	General Chemistry	Tpf	19	19	µg/L	2823.6842	3020	1950	3280	—	—	—	—
Chlorobenzene	108-90-7	CdV-16-2(i)r	SW-846:8260B	VOC	Tpf	23	0	µg/L	—	—	—	—	0.84782609	1	0.3	1
Chlorodibromomethane	124-48-1	CdV-16-2(i)r	SW-846:8260B	VOC	Tpf	23	0	µg/L	—	—	—	—	0.84782609	1	0.3	1
Chloroform	67-66-3	CdV-16-2(i)r	SW-846:8260B	VOC	Tpf	23	0	µg/L	—	—	—	—	0.84782609	1	0.3	1
Chloromethane	74-87-3	CdV-16-2(i)r	SW-846:8260B	VOC	Tpf	23	1	µg/L	2.7	2.7	2.7	2.7	0.84090909	1	0.3	1
Chromium	Cr	CdV-16-2(i)r	SW-846:6020	Inorganic	Tpf	24	3	µg/L	2.6833333	2.66	2.5	2.89	8.33333333	10	3	10
Cobalt	Co	CdV-16-2(i)r	SW-846:6010B, SW-846:6010C	Inorganic	Tpf	24	0	µg/L	—	—	—	—	4.16666667	5	1	5
Copper	Cu	CdV-16-2(i)r	SW-846:6010B, SW-846:6010C	Inorganic	Tpf	24	8	µg/L	4.94	4.395	3.14	9.4	8.25	10	3	10
Cyanide (total)	CN (Total)	CdV-16-2(i)r	EPA:335.4	Inorganic	Tpf	15	0	µg/L	—	—	—	—	3.89	5	1.67	5
DNX	DNX	CdV-16-2(i)r	SW-846:8321A_MOD, SW-846:8330B, SW-846:8330RDX	LCMS/MS High Explosives	Tpf	26	20	µg/L	0.20135	0.176	0.081	0.385	0.3657	0.5	0.0842	0.5

Table 4.2-1 (continued)

Parameter Name	Parameter Code	Well	Analytical Method	Analytical Method Category[a]	Geological Unit Code[a]	No. Samples	No. Detects	Unit	Mean Detect	Median Detect	Min Detect	Max Detect	Mean ND	Median ND	Min ND	Max ND
Fluoranthene	206-44-0	CdV-16-2(i)r	SW-846:8270C, SW-846:8270D, SW-846:8270DGCMS_SIM, SW-846:8310	SVOC	Tpf	10	0	µg/L	—	—	—	—	0.68876	1.035	0.0505	1.12
Fluoride	F(-1)	CdV-16-2(i)r	EPA:300.0	General Chemistry	Tpf	19	19	µg/L	148.19474	142	75.6	248	—	—	—	—
Gross alpha	GrossA	CdV-16-2(i)r	EPA:900	RAD	Tpf	8	0	pCi/L	—	—	—	—	0.956	1.435	-0.565	2.08
Gross beta	GrossB	CdV-16-2(i)r	EPA:900	RAD	Tpf	8	0	pCi/L	—	—	—	—	1.00895913	1.045	0.00067	1.74
Gross gamma	GrossG	CdV-16-2(i)r	EPA:901.1	RAD	Tpf	5	0	pCi/L	—	—	—	—	82.03	84.8	8.55	142
Hardness	Hardness	CdV-16-2(i)r	SM:A2340B	Inorganic	Tpf	24	24	µg/L	34,762.5	35,100	30,400	38,800	—	—	—	—
Heptachlor	76-44-8	CdV-16-2(i)r	SW-846:8081A	PESTPCB	Tpf	2	0	µg/L	—	—	—	—	0.02295	0.02295	0.0206	0.0253
Hexachlorobutadiene	87-68-3	CdV-16-2(i)r	SW-846:8260B	VOC	Tpf	22	0	µg/L	—	—	—	—	0.84090909	1	0.3	1
HMX	2691-41-0	CdV-16-2(i)r	SW-846:8321A_MOD, SW-846:8330B	LCMS/MS High Explosives	Tpf	33	32	µg/L	0.8444063	0.925	0.155	1.98	0.0842	0.0842	0.0842	0.0842
Iron	Fe	CdV-16-2(i)r	SW-846:6010B, SW-846:6010C	Inorganic	Tpf	24	3	µg/L	128.83333	156	54.5	176	86.6666667	100	30	100
Lead	Pb	CdV-16-2(i)r	SW-846:6020	Inorganic	Tpf	24	2	µg/L	0.64	0.64	0.569	0.711	1.65909091	2	0.5	2
Magnesium	Mg	CdV-16-2(i)r	SW-846:6010B, SW-846:6010C	Inorganic	Tpf	24	24	µg/L	2490	2540	2180	2840	—	—	—	—
Manganese	Mn	CdV-16-2(i)r	SW-846:6010B, SW-846:6010C	Inorganic	Tpf	24	3	µg/L	6.63	4.85	2.24	12.8	8.0952381	10	2	10
Mercury	Hg	CdV-16-2(i)r	EPA:245.2	Inorganic	Tpf	38	0	µg/L	—	—	—	—	0.165	0.2	0.067	0.2
Methyl tert-butyl ether	1634-04-4	CdV-16-2(i)r	SW-846:8260B	VOC	Tpf	19	16	µg/L	0.47875	0.475	0.31	0.64	0.76666667	1	0.3	1
Methyl-2-pentanone[4-]	108-10-1	CdV-16-2(i)r	SW-846:8260B	VOC	Tpf	23	1	µg/L	5.35	5.35	5.35	5.35	4.20454545	5	1.5	5
Methylene chloride	75-09-2	CdV-16-2(i)r	SW-846:8260B	VOC	Tpf	23	0	µg/L	—	—	—	—	6.82869565	10	1	10
MNX	MNX	CdV-16-2(i)r	SW-846:8321A_MOD, SW-846:8330B, SW-846:8330RDX	LCMS/MS High Explosives	Tpf	26	23	µg/L	0.4212609	0.449	0.16	0.667	0.2814	0.26	0.0842	0.5
Molybdenum	Mo	CdV-16-2(i)r	SW-846:6020	Inorganic	Tpf	24	21	µg/L	1.0073333	0.971	0.84	1.38	1.004	0.933	0.819	1.26
Nickel	Ni	CdV-16-2(i)r	SW-846:6020	Inorganic	Tpf	24	10	µg/L	0.8824	0.687	0.52	1.8	1.43342857	1.93	0.6	2
Nitrate-nitrite as nitrogen	NO3+NO2-N	CdV-16-2(i)r	EPA:353.2	General Chemistry	Tpf	19	19	µg/L	626.68421	607	498	763	—	—	—	—
Nitrotoluene[2-]	88-72-2	CdV-16-2(i)r	SW-846:8321A_MOD, SW-846:8330B	LCMS/MS High Explosives	Tpf	32	0	µg/L	—	—	—	—	0.22810313	0.263	0.0837	0.325
Oxygen-18/oxygen-16 ratio from nitrate	O18O16-NO3	CdV-16-2(i)r	Generic:Oxygen Isotope Ratio	General Chemistry	Tpf	2	2	permil	3.68095	3.681	2.0179	5.344	—	—	—	—
Perchlorate	ClO4	CdV-16-2(i)r	SW-846:6850	LCMS/MS Perchlorate	Tpf	19	19	µg/L	0.3121053	0.314	0.242	0.385	—	—	—	—
Perfluorooctanoic acid	335-67-1	CdV-16-2(i)r	EPA:537M	LCMS/MS PFAS	Tpf	1	1	µg/L	0.0108	0.0108	0.0108	0.0108	—	—	—	—
Phenanthrene	85-01-8	CdV-16-2(i)r	SW-846:8270C, SW-846:8270D, SW-846:8270DGCMS_SIM, SW-846:8310	SVOC	Tpf	10	0	µg/L	—	—	—	—	0.7722	1.0005	0.105	1.12
Potassium	K	CdV-16-2(i)r	SW-846:6010B, SW-846:6010C	Inorganic	Tpf	24	22	µg/L	303	304	204	543	332.5	332.5	324	341
Pyrene	129-00-0	CdV-16-2(i)r	SW-846:8270C, SW-846:8270D, SW-846:8270DGCMS_SIM, SW-846:8310	SVOC	Tpf	10	0	µg/L	—	—	—	—	0.68876	1.035	0.0505	1.12
Radium-226	Ra-226	CdV-16-2(i)r	EPA:903.1	RAD	Tpf	1	0	pCi/L	—	—	—	—	0.285	0.285	0.285	0.285
Radium-228	Ra-228	CdV-16-2(i)r	EPA:904	RAD	Tpf	1	0	pCi/L	—	—	—	—	-0.0291	-0.0291	-0.0291	-0.0291

Table 4.2-1 (continued)

Parameter Name	Parameter Code	Well	Analytical Method	Analytical Method Category[a]	Geological Unit Code[a]	No. Samples	No. Detects	Unit	Mean Detect	Median Detect	Min Detect	Max Detect	Mean ND	Median ND	Min ND	Max ND
RDX	121-82-4	CdV-16-2(i)r	SW-846:8321A_MOD, SW-846:8330B	LCMS/MS High Explosives	Tpf	33	32	µg/L	83.091875	89.2	1.34	128	46.1	46.1	46.1	46.1
Selenium	Se	CdV-16-2(i)r	SW-846:6020	Inorganic	Tpf	24	0	µg/L	—	—	—	—	4.375	5	2	5
Silicon dioxide	SiO2	CdV-16-2(i)r	SW-846:6010B, SW-846:6010C	Inorganic	Tpf	19	19	µg/L	60,831.579	61,400	53,300	63,800	—	—	—	—
Silver	Ag	CdV-16-2(i)r	SW-846:6020	Inorganic	Tpf	24	0	µg/L	—	—	—	—	0.85416667	1	0.3	1
Sodium	Na	CdV-16-2(i)r	SW-846:6010B, SW-846:6010C	Inorganic	Tpf	24	24	µg/L	12,550	12,600	10,900	13,300	—	—	—	—
Strontium	Sr	CdV-16-2(i)r	SW-846:6010B, SW-846:6010C	Inorganic	Tpf	24	24	µg/L	61.845833	62.5	56.1	67.8	—	—	—	—
Styrene	100-42-5	CdV-16-2(i)r	SW-846:8260B	VOC	Tpf	23	0	µg/L	—	—	—	—	0.84782609	1	0.3	1
Sulfate	SO4(-2)	CdV-16-2(i)r	EPA:300.0	General Chemistry	Tpf	19	19	µg/L	4217.3684	4310	3190	5000	—	—	—	—
Temperature	TEMP	CdV-16-2(i)r	EPA:170.0	VOC	Tpf	16	16	deg C	2.3125	2	1	4	—	—	—	—
Tetrachloroethene	127-18-4	CdV-16-2(i)r	SW-846:8260B	VOC	Tpf	23	22	µg/L	0.5580909	0.53	0.289	0.92	1	1	1	1
Thallium	Tl	CdV-16-2(i)r	SW-846:6020	Inorganic	Tpf	24	0	µg/L	—	—	—	—	1.58333333	2	0.6	2
Tin	Sn	CdV-16-2(i)r	SW-846:6010B, SW-846:6010C	Inorganic	Tpf	24	2	µg/L	5.42	5.42	2.93	7.91	15.9090909	10	2.5	50
TNX	TNX	CdV-16-2(i)r	SW-846:8321A_MOD, SW-846:8330B, SW-846:8330RDX	LCMS/MS High Explosives	Tpf	26	19	µg/L	0.1348632	0.134	0.0887	0.193	0.38488571	0.5	0.0842	0.5
Toluene	108-88-3	CdV-16-2(i)r	SW-846:8260B	VOC	Tpf	23	15	µg/L	3.0840667	1.81	0.321	12	0.65	0.65	0.3	1
Total dissolved solids	TDS	CdV-16-2(i)r	EPA:160.1	General Chemistry	Tpf	19	19	µg/L	119,694.74	120,000	62,900	161,000	—	—	—	—
Total Kjeldahl nitrogen	TKN	CdV-16-2(i)r	EPA:351.2	General Chemistry	Tpf	17	4	µg/L	232.575	164.5	36.3	565	77.2846154	100	33	100
Total organic carbon	TOC	CdV-16-2(i)r	SW-846:9060	General Chemistry	Tpf	17	16	µg/L	575.1875	587.5	354	919	674	674	674	674
Total phosphate as phosphorus	PO4-P	CdV-16-2(i)r	EPA:365.4	General Chemistry	Tpf	19	7	µg/L	100.91429	80.8	21.1	278	58.4583333	47.1	30.7	155
Trichlorobenzene[1,2,3-]	87-61-6	CdV-16-2(i)r	SW-846:8260B	VOC	Tpf	21	0	µg/L	—	—	—	—	0.83333333	1	0.3	1
Trichloroethene	79-01-6	CdV-16-2(i)r	SW-846:8260B	VOC	Tpf	23	14	µg/L	0.3923571	0.37	0.293	0.57	0.84444444	1	0.3	1
Trinitrobenzene[1,3,5-]	99-35-4	CdV-16-2(i)r	SW-846:8321A_MOD, SW-846:8330B	LCMS/MS High Explosives	Tpf	32	10	µg/L	0.11405	0.1026	0.0856	0.16	0.23607727	0.266	0.0825	0.325
Trinitrotoluene[2,4,6-]	118-96-7	CdV-16-2(i)r	SW-846:8321A_MOD, SW-846:8330B	LCMS/MS High Explosives	Tpf	32	0	µg/L	—	—	—	—	0.22744688	0.263	0.0816	0.325
Tritium	H-3	CdV-16-2(i)r	EPA:906.0, Generic:LLEE, Generic:Low_Level_Tritium	RAD	Tpf	11	9	pCi/L	7.2240222	7.567	4.993	8.4686	52.95	52.95	35.3	70.6
Uranium	U	CdV-16-2(i)r	SW-846:6020	Inorganic	Tpf	24	21	µg/L	0.2889524	0.283	0.214	0.394	0.30333333	0.302	0.25	0.358
Uranium-234	U-234	CdV-16-2(i)r	HASL-300:ISOU	RAD	Tpf	9	8	pCi/L	0.213	0.1995	0.139	0.348	0.244	0.244	0.244	0.244
Uranium-235/236	U-235/236	CdV-16-2(i)r	HASL-300:ISOU	RAD	Tpf	9	0	pCi/L	—	—	—	—	0.02570111	0.013	0.00389	0.106
Uranium-238	U-238	CdV-16-2(i)r	HASL-300:ISOU	RAD	Tpf	9	9	pCi/L	0.1136333	0.0975	0.0714	0.203	—	—	—	—
Vanadium	V	CdV-16-2(i)r	SW-846:6010B, SW-846:6010C	Inorganic	Tpf	24	13	µg/L	1.2615385	1.23	1.01	1.66	4.27272727	5	1	5
Zinc	Zn	CdV-16-2(i)r	SW-846:6010B, SW-846:6010C	Inorganic	Tpf	24	24	µg/L	17.299583	15.65	9.19	33.3	—	—	—	—
Acenaphthene	83-32-9	CDV-16-4ip	SW-846:8270C, SW-846:8270D, SW-846:8270DGCMS_SIM, SW-846:8310	SVOC	Tpf	13	0	µg/L	—	—	—	—	0.82807692	1	0.101	1.15
Acenaphthylene	208-96-8	CDV-16-4ip	SW-846:8270C, SW-846:8270D, SW-846:8270DGCMS_SIM, SW-846:8310	SVOC	Tpf	13	0	µg/L	—	—	—	—	0.82807692	1	0.101	1.15
Acetone	67-64-1	CDV-16-4ip	SW-846:8260B	VOC	Tpf	20	2	µg/L	39.6	39.6	10.5	68.7	7.53611111	10	1.5	10

Table 4.2-1 (continued)

Parameter Name	Parameter Code	Well	Analytical Method	Analytical Method Category[a]	Geological Unit Code[a]	No. Samples	No. Detects	Unit	Mean Detect	Median Detect	Min Detect	Max Detect	Mean ND	Median ND	Min ND	Max ND
Acidity or alkalinity of a solution	pH	CDV-16-4ip	EPA:150.1	General Chemistry	Tpf	28	28	SU	7.4428571	7.45	7.08	7.67	—	—	—	—
Alkalinity-CO3	ALK-CO3	CDV-16-4ip	EPA:310.1	General Chemistry	Tpf	28	0	µg/L	—	—	—	—	1534.82143	1000	725	4000
Alkalinity-CO3+HCO3	ALK-CO3+HCO3	CDV-16-4ip	EPA:310.1	General Chemistry	Tpf	28	28	µg/L	49,157.143	49,900	43,700	52,100	—	—	—	—
Aluminum	Al	CDV-16-4ip	SW-846:6010B, SW-846:6010C	Inorganic	Tpf	28	0	µg/L	—	—	—	—	171.714286	200	68	200
Amino-2,6-dinitrotoluene[4-]	19406-51-0	CDV-16-4ip	SW-846:8321A_MOD, SW-846:8330B	LCMS/MS High Explosives	Tpf	29	28	µg/L	1.9696429	1.87	1.47	2.67	0.27	0.27	0.27	0.27
Amino-4,6-dinitrotoluene[2-]	35572-78-2	CDV-16-4ip	SW-846:8321A_MOD, SW-846:8330B	LCMS/MS High Explosives	Tpf	28	0	µg/L	—	—	—	—	0.20116786	0.259	0.0816	0.284
Ammonia as nitrogen	NH3-N	CDV-16-4ip	EPA:350.1	General Chemistry	Tpf	28	12	µg/L	77.541667	49.1	24.3	194	59.84375	52.2	17	143
Anthracene	120-12-7	CDV-16-4ip	SW-846:8270C, SW-846:8270D, SW-846:8270DGCMS_SIM, SW-846:8310	SVOC	Tpf	13	0	µg/L	—	—	—	—	0.82807692	1	0.101	1.15
Antimony	Sb	CDV-16-4ip	SW-846:6020	Inorganic	Tpf	28	0	µg/L	—	—	—	—	2.57142857	3	1	3
Arsenic	As	CDV-16-4ip	SW-846:6020	Inorganic	Tpf	28	4	µg/L	2.3775	2.39	1.87	2.86	4.6125	5	1.7	5
Barium	Ba	CDV-16-4ip	SW-846:6010B, SW-846:6010C	Inorganic	Tpf	28	27	µg/L	4.0192593	3.14	2.2	8.56	3.74	3.74	3.74	3.74
Benzo(g,h,i)perylene	191-24-2	CDV-16-4ip	SW-846:8270C, SW-846:8270D, SW-846:8270DGCMS_SIM, SW-846:8310	SVOC	Tpf	13	0	µg/L	—	—	—	—	0.75600769	1	0.0515	1.15
Benzoic acid	65-85-0	CDV-16-4ip	SW-846:8270C, SW-846:8270D	SVOC	Tpf	13	0	µg/L	—	—	—	—	18.7423077	20	6.25	23
Beryllium	Be	CDV-16-4ip	SW-846:6010B, SW-846:6010C	Inorganic	Tpf	28	0	µg/L	—	—	—	—	4.14285714	5	1	5
Bis(2-ethylhexyl)phthalate	117-81-7	CDV-16-4ip	SW-846:8270C, SW-846:8270D	SVOC	Tpf	13	0	µg/L	—	—	—	—	9.37	10	3.13	11.5
Boron	B	CDV-16-4ip	SW-846:6010B, SW-846:6010C	Inorganic	Tpf	28	27	µg/L	65.392593	63.7	15.1	115	50	50	50	50
Bromide	Br(-1)	CDV-16-4ip	EPA:300.0	General Chemistry	Tpf	28	11	µg/L	80.690909	79.3	72	96.9	160.882353	200	67	200
Bromodichloromethane	75-27-4	CDV-16-4ip	SW-846:8260B	VOC	Tpf	20	0	µg/L	—	—	—	—	0.825	1	0.3	1
Bromoform	75-25-2	CDV-16-4ip	SW-846:8260B	VOC	Tpf	20	0	µg/L	—	—	—	—	0.825	1	0.3	1
Butanone[2-]	78-93-3	CDV-16-4ip	SW-846:8260B	VOC	Tpf	20	0	µg/L	—	—	—	—	4.125	5	1.5	5
Cadmium	Cd	CDV-16-4ip	SW-846:6020	Inorganic	Tpf	28	0	µg/L	—	—	—	—	0.84321429	1	0.11	1
Calcium	Ca	CDV-16-4ip	SW-846:6010B, SW-846:6010C	Inorganic	Tpf	28	28	µg/L	10,565	10,700	9470	11,600	—	—	—	—
Carbon disulfide	75-15-0	CDV-16-4ip	SW-846:8260B	VOC	Tpf	20	0	µg/L	—	—	—	—	4.125	5	1.5	5
Chloride	Cl(-1)	CDV-16-4ip	EPA:300.0	General Chemistry	Tpf	28	28	µg/L	3388.5714	3500	1500	4150	—	—	—	—
Chlorobenzene	108-90-7	CDV-16-4ip	SW-846:8260B	VOC	Tpf	20	0	µg/L	—	—	—	—	0.825	1	0.3	1
Chlorodibromomethane	124-48-1	CDV-16-4ip	SW-846:8260B	VOC	Tpf	20	0	µg/L	—	—	—	—	0.825	1	0.3	1
Chloroform	67-66-3	CDV-16-4ip	SW-846:8260B	VOC	Tpf	20	0	µg/L	—	—	—	—	0.825	1	0.3	1
Chloromethane	74-87-3	CDV-16-4ip	SW-846:8260B	VOC	Tpf	20	0	µg/L	—	—	—	—	0.825	1	0.3	1
Chromium	Cr	CDV-16-4ip	SW-846:6020	Inorganic	Tpf	28	4	µg/L	2.5325	2.53	2.34	2.73	8.20833333	10	2	10
Cobalt	Co	CDV-16-4ip	SW-846:6010B, SW-846:6010C	Inorganic	Tpf	28	0	µg/L	—	—	—	—	4.14285714	5	1	5
Copper	Cu	CDV-16-4ip	SW-846:6010B, SW-846:6010C	Inorganic	Tpf	28	0	µg/L	—	—	—	—	8.5	10	3	10
Cyanide (total)	CN (Total)	CDV-16-4ip	EPA:335.4	Inorganic	Tpf	17	0	µg/L	—	—	—	—	3.82470588	5	1.67	5
DNX	DNX	CDV-16-4ip	SW-846:8321A_MOD, SW-846:8330B, SW-846:8330RDX	LCMS/MS High Explosives	Tpf	24	24	µg/L	0.3058333	0.284	0.202	0.578	—	—	—	—

Table 4.2-1 (continued)

Parameter Name	Parameter Code	Well	Analytical Method	Analytical Method Category[a]	Geological Unit Code[a]	No. Samples	No. Detects	Unit	Mean Detect	Median Detect	Min Detect	Max Detect	Mean ND	Median ND	Min ND	Max ND
Fluoranthene	206-44-0	CDV-16-4ip	SW-846:8270C, SW-846:8270D, SW-846:8270DGCMS_SIM, SW-846:8310	SVOC	Tpf	13	0	µg/L	—	—	—	—	0.75600769	1	0.0515	1.15
Fluoride	F(-1)	CDV-16-4ip	EPA:300.0	General Chemistry	Tpf	28	28	µg/L	108.73929	99.5	49.9	282	—	—	—	—
Gross alpha	GrossA	CDV-16-4ip	EPA:900	RAD	Tpf	5	0	pCi/L	—	—	—	—	0.9284	0.842	0.465	1.62
Gross beta	GrossB	CDV-16-4ip	EPA:900	RAD	Tpf	5	0	pCi/L	—	—	—	—	0.8278	0.937	-0.149	1.48
Hardness	Hardness	CDV-16-4ip	SM:A2340B	Inorganic	Tpf	28	28	µg/L	39,082.143	39,150	35,400	43,500	—	—	—	—
Hexachlorobutadiene	87-68-3	CDV-16-4ip	SW-846:8260B	VOC	Tpf	20	0	µg/L	—	—	—	—	0.825	1	0.3	1
HMX	2691-41-0	CDV-16-4ip	SW-846:8321A_MOD, SW-846:8330B	LCMS/MS High Explosives	Tpf	29	29	µg/L	9.0641379	9.17	6.33	11.8	—	—	—	—
Iron	Fe	CDV-16-4ip	SW-846:6010B, SW-846:6010C	Inorganic	Tpf	28	2	µg/L	69.45	69.45	33.9	105	86.5384615	100	30	100
Lead	Pb	CDV-16-4ip	SW-846:6020	Inorganic	Tpf	28	0	µg/L	—	—	—	—	1.67857143	2	0.5	2
Magnesium	Mg	CDV-16-4ip	SW-846:6010B, SW-846:6010C	Inorganic	Tpf	28	28	µg/L	3091.0714	3065	2800	3540	—	—	—	—
Manganese	Mn	CDV-16-4ip	SW-846:6010B, SW-846:6010C	Inorganic	Tpf	28	5	µg/L	8.88	6.87	2.34	14.6	7.91304348	10	2	10
Mercury	Hg	CDV-16-4ip	EPA:245.2	Inorganic	Tpf	45	0	µg/L	—	—	—	—	0.20453333	0.2	0.067	2
Methyl tert-butyl ether	1634-04-4	CDV-16-4ip	SW-846:8260B	VOC	Tpf	20	18	µg/L	0.5855556	0.6	0.32	0.8	0.65	0.65	0.3	1
Methyl-2-pentanone[4-]	108-10-1	CDV-16-4ip	SW-846:8260B	VOC	Tpf	20	0	µg/L	—	—	—	—	4.125	5	1.5	5
Methylene chloride	75-09-2	CDV-16-4ip	SW-846:8260B	VOC	Tpf	20	0	µg/L	—	—	—	—	7.75	10	1	10
MNX	MNX	CDV-16-4ip	SW-846:8321A_MOD, SW-846:8330B, SW-846:8330RDX	LCMS/MS High Explosives	Tpf	24	24	µg/L	0.5874167	0.6005	0.273	0.92	—	—	—	—
Molybdenum	Mo	CDV-16-4ip	SW-846:6020	Inorganic	Tpf	28	20	µg/L	0.5855	0.5765	0.514	0.734	0.617375	0.6075	0.546	0.686
Nickel	Ni	CDV-16-4ip	SW-846:6020	Inorganic	Tpf	28	17	µg/L	0.7288824	0.693	0.526	1.19	1.26372727	1.15	0.6	2
Nitrate-nitrite as nitrogen	NO3+NO2-N	CDV-16-4ip	EPA:353.2	General Chemistry	Tpf	28	28	µg/L	868.71429	882.5	433	1120	—	—	—	—
Nitrotoluene[2-]	88-72-2	CDV-16-4ip	SW-846:8321A_MOD, SW-846:8330B	LCMS/MS High Explosives	Tpf	28	0	µg/L	—	—	—	—	0.201925	0.259	0.0837	0.284
Oxygen-18/oxygen-16 ratio from nitrate	O18O16-NO3	CDV-16-4ip	Generic:Oxygen Isotope Ratio	General Chemistry	Tpf	2	2	permil	8.19985	8.1999	5.3747	11.025	—	—	—	—
Perchlorate	ClO4	CDV-16-4ip	SW-846:6850	LCMS/MS Perchlorate	Tpf	28	28	µg/L	0.35375	0.359	0.246	0.397	—	—	—	—
Perfluorooctanoic acid	335-67-1	CDV-16-4ip	EPA:537M	LCMS/MS PFAS	Tpf	1	1	µg/L	0.0117	0.0117	0.0117	0.0117	—	—	—	—
Phenanthrene	85-01-8	CDV-16-4ip	SW-846:8270C, SW-846:8270D, SW-846:8270DGCMS_SIM, SW-846:8310	SVOC	Tpf	13	0	µg/L	—	—	—	—	0.82807692	1	0.101	1.15
Potassium	K	CDV-16-4ip	SW-846:6010B, SW-846:6010C	Inorganic	Tpf	28	28	µg/L	961.60714	960.5	554	1320	—	—	—	—
Pyrene	129-00-0	CDV-16-4ip	SW-846:8270C, SW-846:8270D, SW-846:8270DGCMS_SIM, SW-846:8310	SVOC	Tpf	13	0	µg/L	—	—	—	—	0.75600769	1	0.0515	1.15
RDX	121-82-4	CDV-16-4ip	SW-846:8321A_MOD, SW-846:8330B	LCMS/MS High Explosives	Tpf	29	29	µg/L	132.24138	131	104	177	—	—	—	—
Selenium	Se	CDV-16-4ip	SW-846:6020	Inorganic	Tpf	28	0	µg/L	—	—	—	—	4.33928571	5	1.5	5
Silicon dioxide	SiO2	CDV-16-4ip	SW-846:6010B, SW-846:6010C	Inorganic	Tpf	28	28	µg/L	60,271.429	59,800	55,500	67,100	—	—	—	—
Silver	Ag	CDV-16-4ip	SW-846:6020	Inorganic	Tpf	28	0	µg/L	—	—	—	—	0.84642857	1	0.2	1

Table 4.2-1 (continued)

Parameter Name	Parameter Code	Well	Analytical Method	Analytical Method Category[a]	Geological Unit Code[a]	No. Samples	No. Detects	Unit	Mean Detect	Median Detect	Min Detect	Max Detect	Mean ND	Median ND	Min ND	Max ND
Sodium	Na	CDV-16-4ip	SW-846:6010B, SW-846:6010C	Inorganic	Tpf	28	28	µg/L	10,034.643	9970	8480	12,700	—	—	—	—
Strontium	Sr	CDV-16-4ip	SW-846:6010B, SW-846:6010C	Inorganic	Tpf	28	28	µg/L	61.45	61.3	55.7	71.9	—	—	—	—
Styrene	100-42-5	CDV-16-4ip	SW-846:8260B	VOC	Tpf	20	0	µg/L	—	—	—	—	0.825	1	0.3	1
Sulfate	SO4(-2)	CDV-16-4ip	EPA:300.0	General Chemistry	Tpf	28	28	µg/L	3693.2143	3680	2410	5660	—	—	—	—
Temperature	TEMP	CDV-16-4ip	EPA:170.0	VOC	Tpf	16	16	deg C	2.375	2	1	4	—	—	—	—
Tetrachloroethene	127-18-4	CDV-16-4ip	SW-846:8260B	VOC	Tpf	20	20	µg/L	0.9145	0.92	0.73	1.12	—	—	—	—
Thallium	Tl	CDV-16-4ip	SW-846:6020	Inorganic	Tpf	28	0	µg/L	—	—	—	—	1.5875	2	0.45	2
Tin	Sn	CDV-16-4ip	SW-846:6010B, SW-846:6010C	Inorganic	Tpf	28	1	µg/L	8.06	8.06	8.06	8.06	15.462963	10	2.5	100
TNX	TNX	CDV-16-4ip	SW-846:8321A_MOD, SW-846:8330B, SW-846:8330RDX	LCMS/MS High Explosives	Tpf	24	24	µg/L	0.2610833	0.228	0.129	1.1	—	—	—	—
Toluene	108-88-3	CDV-16-4ip	SW-846:8260B	VOC	Tpf	20	0	µg/L	—	—	—	—	0.825	1	0.3	1
Total dissolved solids	TDS	CDV-16-4ip	EPA:160.1	General Chemistry	Tpf	28	28	µg/L	117,489.29	120,500	42,900	156,000	—	—	—	—
Total Kjeldahl nitrogen	TKN	CDV-16-4ip	EPA:351.2	General Chemistry	Tpf	23	9	µg/L	134.41111	132	46.3	266	81.8714286	100	33	100
Total organic carbon	TOC	CDV-16-4ip	SW-846:9060	General Chemistry	Tpf	23	22	µg/L	698.63636	666.5	401	1110	530	530	530	530
Total phosphate as phosphorus	PO4-P	CDV-16-4ip	EPA:365.4	General Chemistry	Tpf	28	14	µg/L	49.735714	42.8	22.5	91.8	56.0357143	50	38.9	95.4
Trichlorobenzene[1,2,3-]	87-61-6	CDV-16-4ip	SW-846:8260B	VOC	Tpf	20	1	µg/L	0.9	0.9	0.9	0.9	0.81578947	1	0.3	1
Trichloroethene	79-01-6	CDV-16-4ip	SW-846:8260B	VOC	Tpf	20	20	µg/L	0.6435	0.645	0.45	0.79	—	—	—	—
Trinitrobenzene[1,3,5-]	99-35-4	CDV-16-4ip	SW-846:8321A_MOD, SW-846:8330B	LCMS/MS High Explosives	Tpf	28	12	µg/L	0.1156583	0.1175	0.0867	0.158	0.2096625	0.2625	0.0833	0.284
Trinitrotoluene[2,4,6-]	118-96-7	CDV-16-4ip	SW-846:8321A_MOD, SW-846:8330B	LCMS/MS High Explosives	Tpf	28	0	µg/L	—	—	—	—	0.20116786	0.259	0.0816	0.284
Tritium	H-3	CDV-16-4ip	Generic:Low_Level_Tritium	RAD	Tpf	7	7	pCi/L	13.724571	10.401	8.407	33.114	—	—	—	—
Uranium	U	CDV-16-4ip	SW-846:6020	Inorganic	Tpf	28	27	µg/L	0.4844074	0.476	0.36	0.705	0.412	0.412	0.412	0.412
Uranium-234	U-234	CDV-16-4ip	HASL-300:ISOU	RAD	Tpf	5	5	pCi/L	0.2814	0.278	0.239	0.346	—	—	—	—
Uranium-235/236	U-235/236	CDV-16-4ip	HASL-300:ISOU	RAD	Tpf	5	0	pCi/L	—	—	—	—	0.02661	0.0199	0.00805	0.0695
Uranium-238	U-238	CDV-16-4ip	HASL-300:ISOU	RAD	Tpf	5	5	pCi/L	0.1712	0.175	0.141	0.197	—	—	—	—
Vanadium	V	CDV-16-4ip	SW-846:6010B, SW-846:6010C	Inorganic	Tpf	28	28	µg/L	2.4971429	2.475	1.52	3.45	—	—	—	—
Zinc	Zn	CDV-16-4ip	SW-846:6010B, SW-846:6010C	Inorganic	Tpf	28	4	µg/L	7.93	7.65	4.02	12.4	8.36083333	10	3.3	10
Acenaphthene	83-32-9	CDV-37-1(i)	SW-846:8270C, SW-846:8270D, SW-846:8270DGCMS_SIM, SW-846:8310	SVOC	Tpf	5	0	µg/L	—	—	—	—	0.4932	0.521	0.103	1
Acenaphthylene	208-96-8	CDV-37-1(i)	SW-846:8270C, SW-846:8270D, SW-846:8270DGCMS_SIM, SW-846:8310	SVOC	Tpf	5	0	µg/L	—	—	—	—	0.4932	0.521	0.103	1
Acetone	67-64-1	CDV-37-1(i)	SW-846:8260B	VOC	Tpf	11	2	µg/L	3.44	3.44	2.47	4.41	6.22888889	10	1.5	10
Acidity or alkalinity of a solution	pH	CDV-37-1(i)	EPA:150.1	General Chemistry	Tpf	17	17	SU	7.4670588	7.44	7.15	7.82	—	—	—	—
Alkalinity-CO3	ALK-CO3	CDV-37-1(i)	EPA:310.1	General Chemistry	Tpf	17	0	µg/L	—	—	—	—	1367.64706	1000	1000	4000
Alkalinity-CO3+HCO3	ALK-CO3+HCO3	CDV-37-1(i)	EPA:310.1	General Chemistry	Tpf	17	17	µg/L	54,670.588	53,800	51,500	65,400	—	—	—	—
Aluminum	Al	CDV-37-1(i)	SW-846:6010B, SW-846:6010C	Inorganic	Tpf	17	2	µg/L	138	138	116	160	164.8	200	68	200

Table 4.2-1 (continued)

Parameter Name	Parameter Code	Well	Analytical Method	Analytical Method Category[a]	Geological Unit Code[a]	No. Samples	No. Detects	Unit	Mean Detect	Median Detect	Min Detect	Max Detect	Mean ND	Median ND	Min ND	Max ND
Amino-2,6-dinitrotoluene[4-]	19406-51-0	CDV-37-1(i)	SW-846:8321A_MOD, SW-846:8330B	LCMS/MS High Explosives	Tpf	11	0	µg/L	—	—	—	—	0.19171818	0.259	0.0842	0.325
Amino-4,6-dinitrotoluene[2-]	35572-78-2	CDV-37-1(i)	SW-846:8321A_MOD, SW-846:8330B	LCMS/MS High Explosives	Tpf	11	0	µg/L	—	—	—	—	0.19171818	0.259	0.0842	0.325
Ammonia as nitrogen	NH3-N	CDV-37-1(i)	EPA:350.1	General Chemistry	Tpf	17	8	µg/L	47.75	35.25	16.7	94	43.8111111	44	17	91.4
Anthracene	120-12-7	CDV-37-1(i)	SW-846:8270C, SW-846:8270D, SW-846:8270DGCMS_SIM, SW-846:8310	SVOC	Tpf	5	0	µg/L	—	—	—	—	0.4932	0.521	0.103	1
Antimony	Sb	CDV-37-1(i)	SW-846:6020	Inorganic	Tpf	17	4	µg/L	0.7695	0.7365	0.575	1.03	2.07476923	3	0.972	3
Arsenic	As	CDV-37-1(i)	SW-846:6020	Inorganic	Tpf	17	2	µg/L	2.705	2.705	2.61	2.8	4.26	5	2	5.9
Barium	Ba	CDV-37-1(i)	SW-846:6010B, SW-846:6010C	Inorganic	Tpf	17	17	µg/L	9.6288235	7.88	6.44	18.6	—	—	—	—
Benzo(g,h,i)perylene	191-24-2	CDV-37-1(i)	SW-846:8270C, SW-846:8270D, SW-846:8270DGCMS_SIM, SW-846:8310	SVOC	Tpf	5	0	µg/L	—	—	—	—	0.30474	0.103	0.0521	1
Benzoic Acid	65-85-0	CDV-37-1(i)	SW-846:8270C, SW-846:8270D	SVOC	Tpf	5	0	µg/L	—	—	—	—	15.384	20	6.32	20.4
Beryllium	Be	CDV-37-1(i)	SW-846:6010B, SW-846:6010C	Inorganic	Tpf	17	0	µg/L	—	—	—	—	3.82352941	5	1	5
Bis(2-ethylhexyl)phthalate	117-81-7	CDV-37-1(i)	SW-846:8270C, SW-846:8270D	SVOC	Tpf	5	0	µg/L	—	—	—	—	7.692	10	3.16	10.2
Boron	B	CDV-37-1(i)	SW-846:6010B, SW-846:6010C	Inorganic	Tpf	17	1	µg/L	17.4	17.4	17.4	17.4	39.0625	50	15	50
Bromide	Br(-1)	CDV-37-1(i)	EPA:300.0	General Chemistry	Tpf	17	0	µg/L	—	—	—	—	160.882353	200	67	200
Bromodichloromethane	75-27-4	CDV-37-1(i)	SW-846:8260B	VOC	Tpf	11	0	µg/L	—	—	—	—	0.68181818	1	0.3	1
Bromoform	75-25-2	CDV-37-1(i)	SW-846:8260B	VOC	Tpf	11	0	µg/L	—	—	—	—	0.68181818	1	0.3	1
Butanone[2-]	78-93-3	CDV-37-1(i)	SW-846:8260B	VOC	Tpf	11	0	µg/L	—	—	—	—	3.40909091	5	1.5	5
Cadmium	Cd	CDV-37-1(i)	SW-846:6020	Inorganic	Tpf	17	0	µg/L	—	—	—	—	0.79411765	1	0.3	1
Calcium	Ca	CDV-37-1(i)	SW-846:6010B, SW-846:6010C	Inorganic	Tpf	17	17	µg/L	9383.5294	9370	8590	10,200	—	—	—	—
Carbon Disulfide	75-15-0	CDV-37-1(i)	SW-846:8260B	VOC	Tpf	11	0	µg/L	—	—	—	—	3.40909091	5	1.5	5
Chloride	Cl(-1)	CDV-37-1(i)	EPA:300.0	General Chemistry	Tpf	17	17	µg/L	1271.7647	1220	1140	1720	—	—	—	—
Chlorobenzene	108-90-7	CDV-37-1(i)	SW-846:8260B	VOC	Tpf	11	0	µg/L	—	—	—	—	0.68181818	1	0.3	1
Chlorodibromomethane	124-48-1	CDV-37-1(i)	SW-846:8260B	VOC	Tpf	11	0	µg/L	—	—	—	—	0.68181818	1	0.3	1
Chloroform	67-66-3	CDV-37-1(i)	SW-846:8260B	VOC	Tpf	11	0	µg/L	—	—	—	—	0.68181818	1	0.3	1
Chloromethane	74-87-3	CDV-37-1(i)	SW-846:8260B	VOC	Tpf	11	0	µg/L	—	—	—	—	0.68181818	1	0.3	1
Chromium	Cr	CDV-37-1(i)	SW-846:6020	Inorganic	Tpf	17	1	µg/L	3.36	3.36	3.36	3.36	7.51875	10	3	10
Cobalt	Co	CDV-37-1(i)	SW-846:6010B, SW-846:6010C	Inorganic	Tpf	17	1	µg/L	1.12	1.12	1.12	1.12	3.75	5	1	5
Copper	Cu	CDV-37-1(i)	SW-846:6010B, SW-846:6010C	Inorganic	Tpf	17	0	µg/L	—	—	—	—	7.94117647	10	3	10
Cyanide (total)	CN (Total)	CDV-37-1(i)	EPA:335.4	Inorganic	Tpf	9	0	µg/L	—	—	—	—	3.15	1.67	1.67	5
DNX	DNX	CDV-37-1(i)	SW-846:8321A_MOD, SW-846:8330B, SW-846:8330RDX	LCMS/MS High Explosives	Tpf	10	0	µg/L	—	—	—	—	0.20249	0.1773	0.0842	0.5
Fluoranthene	206-44-0	CDV-37-1(i)	SW-846:8270C, SW-846:8270D, SW-846:8270DGCMS_SIM, SW-846:8310	SVOC	Tpf	5	0	µg/L	—	—	—	—	0.30474	0.103	0.0521	1
Fluoride	F(-1)	CDV-37-1(i)	EPA:300.0	General Chemistry	Tpf	17	17	µg/L	153.21176	144	78.6	312	—	—	—	—
Gross alpha	GrossA	CDV-37-1(i)	EPA:900	RAD	Tpf	4	0	pCi/L	—	—	—	—	-0.0968	-0.0836	-1.67	1.45

Table 4.2-1 (continued)

Parameter Name	Parameter Code	Well	Analytical Method	Analytical Method Category[a]	Geological Unit Code[a]	No. Samples	No. Detects	Unit	Mean Detect	Median Detect	Min Detect	Max Detect	Mean ND	Median ND	Min ND	Max ND
Gross beta	GrossB	CDV-37-1(i)	EPA:900	RAD	Tpf	4	1	pCi/L	5.24	5.24	5.24	5.24	0.39433333	0.158	-0.855	1.88
Hardness	Hardness	CDV-37-1(i)	SM:A2340B	Inorganic	Tpf	17	17	µg/L	32,894.118	32,700	30,300	36,000	—	—	—	—
Hexachlorobutadiene	87-68-3	CDV-37-1(i)	SW-846:8260B	VOC	Tpf	11	0	µg/L	—	—	—	—	0.68181818	1	0.3	1
HMX	2691-41-0	CDV-37-1(i)	SW-846:8321A_MOD, SW-846:8330B	LCMS/MS High Explosives	Tpf	11	0	µg/L	—	—	—	—	0.19171818	0.259	0.0842	0.325
Iron	Fe	CDV-37-1(i)	SW-846:6010B, SW-846:6010C	Inorganic	Tpf	17	5	µg/L	46.98	47.7	31	62.9	67.05	77.3	30	100
Lead	Pb	CDV-37-1(i)	SW-846:6020	Inorganic	Tpf	17	0	µg/L	—	—	—	—	1.55882353	2	0.5	2
Magnesium	Mg	CDV-37-1(i)	SW-846:6010B, SW-846:6010C	Inorganic	Tpf	17	17	µg/L	2297.0588	2290	2130	2570	—	—	—	—
Manganese	Mn	CDV-37-1(i)	SW-846:6010B, SW-846:6010C	Inorganic	Tpf	17	12	µg/L	10.159167	7.35	2.17	22.8	2	2	2	2
Mercury	Hg	CDV-37-1(i)	EPA:245.2	Inorganic	Tpf	26	0	µg/L	—	—	—	—	0.14884615	0.2	0.067	0.2
Methyl tert-butyl ether	1634-04-4	CDV-37-1(i)	SW-846:8260B	VOC	Tpf	11	0	µg/L	—	—	—	—	0.68181818	1	0.3	1
Methyl-2-pentanone[4-]	108-10-1	CDV-37-1(i)	SW-846:8260B	VOC	Tpf	11	0	µg/L	—	—	—	—	3.40909091	5	1.5	5
Methylene chloride	75-09-2	CDV-37-1(i)	SW-846:8260B	VOC	Tpf	11	0	µg/L	—	—	—	—	5.90909091	10	1	10
MNX	MNX	CDV-37-1(i)	SW-846:8321A_MOD, SW-846:8330B, SW-846:8330RDX	LCMS/MS High Explosives	Tpf	10	0	µg/L	—	—	—	—	0.20249	0.1773	0.0842	0.5
Molybdenum	Mo	CDV-37-1(i)	SW-846:6020	Inorganic	Tpf	17	15	µg/L	1.2908667	1.11	0.993	2.14	1.365	1.365	1.04	1.69
Nickel	Ni	CDV-37-1(i)	SW-846:6020	Inorganic	Tpf	17	17	µg/L	3.6258824	2.83	1.41	7.07	—	—	—	—
Nitrate-nitrite as nitrogen	NO3+NO2-N	CDV-37-1(i)	EPA:353.2	General Chemistry	Tpf	17	16	µg/L	134.84375	117	27.4	255	250	250	250	250
Nitrotoluene[2-]	88-72-2	CDV-37-1(i)	SW-846:8321A_MOD, SW-846:8330B	LCMS/MS High Explosives	Tpf	11	0	µg/L	—	—	—	—	0.1927	0.259	0.0863	0.325
Perchlorate	ClO4	CDV-37-1(i)	SW-846:6850	LCMS/MS Perchlorate	Tpf	16	16	µg/L	0.134625	0.127	0.108	0.257	—	—	—	—
Phenanthrene	85-01-8	CDV-37-1(i)	SW-846:8270C, SW-846:8270D, SW-846:8270DGCMS_SIM, SW-846:8310	SVOC	Tpf	5	0	µg/L	—	—	—	—	0.4932	0.521	0.103	1
Potassium	K	CDV-37-1(i)	SW-846:6010B, SW-846:6010C	Inorganic	Tpf	17	17	µg/L	509.17647	513	323	736	—	—	—	—
Pyrene	129-00-0	CDV-37-1(i)	SW-846:8270C, SW-846:8270D, SW-846:8270DGCMS_SIM, SW-846:8310	SVOC	Tpf	5	0	µg/L	—	—	—	—	0.30474	0.103	0.0521	1
Radium-226	Ra-226	CDV-37-1(i)	EPA:903.1	RAD	Tpf	1	0	pCi/L	—	—	—	—	0.0379	0.0379	0.0379	0.0379
Radium-228	Ra-228	CDV-37-1(i)	EPA:904	RAD	Tpf	1	1	pCi/L	2.66	2.66	2.66	2.66	—	—	—	—
RDX	121-82-4	CDV-37-1(i)	SW-846:8321A_MOD, SW-846:8330B	LCMS/MS High Explosives	Tpf	11	0	µg/L	—	—	—	—	0.19171818	0.259	0.0842	0.325
Selenium	Se	CDV-37-1(i)	SW-846:6020	Inorganic	Tpf	17	0	µg/L	—	—	—	—	4.11764706	5	2	5
Silicon dioxide	SiO2	CDV-37-1(i)	SW-846:6010B, SW-846:6010C	Inorganic	Tpf	17	17	µg/L	61,629.412	62,200	57,100	64,500	—	—	—	—
Silver	Ag	CDV-37-1(i)	SW-846:6020	Inorganic	Tpf	17	0	µg/L	—	—	—	—	0.79411765	1	0.3	1
Sodium	Na	CDV-37-1(i)	SW-846:6010B, SW-846:6010C	Inorganic	Tpf	17	17	µg/L	11,568.824	10,600	9480	15,100	—	—	—	—
Strontium	Sr	CDV-37-1(i)	SW-846:6010B, SW-846:6010C	Inorganic	Tpf	17	17	µg/L	48.6	49.2	45.6	51	—	—	—	—
Styrene	100-42-5	CDV-37-1(i)	SW-846:8260B	VOC	Tpf	11	0	µg/L	—	—	—	—	0.68181818	1	0.3	1
Sulfate	SO4(-2)	CDV-37-1(i)	EPA:300.0	General Chemistry	Tpf	17	17	µg/L	2505.2941	2050	1430	5130	—	—	—	—
Temperature	TEMP	CDV-37-1(i)	EPA:170.0	VOC	Tpf	10	10	deg C	2.6	2	2	4	—	—	—	—

Table 4.2-1 (continued)

Parameter Name	Parameter Code	Well	Analytical Method	Analytical Method Category[a]	Geological Unit Code[a]	No. Samples	No. Detects	Unit	Mean Detect	Median Detect	Min Detect	Max Detect	Mean ND	Median ND	Min ND	Max ND
Tetrachloroethene	127-18-4	CDV-37-1(i)	SW-846:8260B	VOC	Tpf	11	0	µg/L	—	—	—	—	0.68181818	1	0.3	1
Thallium	Tl	CDV-37-1(i)	SW-846:6020	Inorganic	Tpf	17	0	µg/L	—	—	—	—	1.31323529	1	0.325	2
Tin	Sn	CDV-37-1(i)	SW-846:6010B, SW-846:6010C	Inorganic	Tpf	17	0	µg/L	—	—	—	—	14.8529412	10	2.5	50
TNX	TNX	CDV-37-1(i)	SW-846:8321A_MOD, SW-846:8330B, SW-846:8330RDX	LCMS/MS High Explosives	Tpf	10	0	µg/L	—	—	—	—	0.20249	0.1773	0.0842	0.5
Toluene	108-88-3	CDV-37-1(i)	SW-846:8260B	VOC	Tpf	11	0	µg/L	—	—	—	—	0.68181818	1	0.3	1
Total dissolved solids	TDS	CDV-37-1(i)	EPA:160.1	General Chemistry	Tpf	17	17	µg/L	117,864.71	121,000	84,300	157,000	—	—	—	—
Total Kjeldahl nitrogen	TKN	CDV-37-1(i)	EPA:351.2	General Chemistry	Tpf	11	1	µg/L	61.6	61.6	61.6	61.6	77.36	89.8	33	162
Total organic carbon	TOC	CDV-37-1(i)	SW-846:9060	General Chemistry	Tpf	11	11	µg/L	697.63636	648	346	1160	—	—	—	—
Total phosphate as phosphorus	PO4-P	CDV-37-1(i)	EPA:365.4	General Chemistry	Tpf	17	4	µg/L	101.225	90.9	25.1	198	50.5615385	50	28	87
Trichlorobenzene[1,2,3-]	87-61-6	CDV-37-1(i)	SW-846:8260B	VOC	Tpf	11	0	µg/L	—	—	—	—	0.68181818	1	0.3	1
Trichloroethene	79-01-6	CDV-37-1(i)	SW-846:8260B	VOC	Tpf	11	0	µg/L	—	—	—	—	0.68181818	1	0.3	1
Trinitrobenzene[1,3,5-]	99-35-4	CDV-37-1(i)	SW-846:8321A_MOD, SW-846:8330B	LCMS/MS High Explosives	Tpf	11	0	µg/L	—	—	—	—	0.19171818	0.259	0.0842	0.325
Trinitrotoluene[2,4,6-]	118-96-7	CDV-37-1(i)	SW-846:8321A_MOD, SW-846:8330B	LCMS/MS High Explosives	Tpf	11	0	µg/L	—	—	—	—	0.19171818	0.259	0.0842	0.325
Tritium	H-3	CDV-37-1(i)	Generic:Low_Level_Tritium	RAD	Tpf	6	0	pCi/L	—	—	—	—	-0.0293333	0.022	-1.539	1.126
Uranium	U	CDV-37-1(i)	SW-846:6020	Inorganic	Tpf	17	16	µg/L	0.443	0.425	0.293	0.623	0.2	0.2	0.2	0.2
Uranium-234	U-234	CDV-37-1(i)	HASL-300:ISOU	RAD	Tpf	4	4	pCi/L	0.26375	0.265	0.243	0.282	—	—	—	—
Uranium-235/236	U-235/236	CDV-37-1(i)	HASL-300:ISOU	RAD	Tpf	4	0	pCi/L	—	—	—	—	0.0169725	0.0184	0.00569	0.0254
Uranium-238	U-238	CDV-37-1(i)	HASL-300:ISOU	RAD	Tpf	4	3	pCi/L	0.1586667	0.156	0.152	0.168	0.0763	0.0763	0.0763	0.0763
Vanadium	V	CDV-37-1(i)	SW-846:6010B, SW-846:6010C	Inorganic	Tpf	17	5	µg/L	1.534	1.49	1.26	1.79	3.33	4.105	1	5
Zinc	Zn	CDV-37-1(i)	SW-846:6010B, SW-846:6010C	Inorganic	Tpf	17	15	µg/L	11.643333	10.3	3.61	30.7	6.65	6.65	3.3	10
Acenaphthene	83-32-9	CDV-9-1(i)	SW-846:8270D, SW-846:8270DGCMS_SIM	SVOC	Tpf	9	0	µg/L	—	—	—	—	0.66011111	1	0.1	1.08
Acenaphthylene	208-96-8	CDV-9-1(i)	SW-846:8270D, SW-846:8270DGCMS_SIM	SVOC	Tpf	9	0	µg/L	—	—	—	—	0.66011111	1	0.1	1.08
Acetone	67-64-1	CDV-9-1(i)	SW-846:8260B	VOC	Tpf	12	2	µg/L	10.545	10.545	2.59	18.5	6.6	10	1.5	10
Acidity or alkalinity of a solution	pH	CDV-9-1(i)	EPA:150.1	General Chemistry	Tpf	12	12	SU	7.4575	7.38	7.23	7.83	—	—	—	—
Alkalinity-CO3	ALK-CO3	CDV-9-1(i)	EPA:310.1	General Chemistry	Tpf	12	0	µg/L	—	—	—	—	2020.83333	1450	1000	4000
Alkalinity-CO3+HCO3	ALK-CO3+HCO3	CDV-9-1(i)	EPA:310.1	General Chemistry	Tpf	12	12	µg/L	63,600	64,100	57,600	66,800	—	—	—	—
Aluminum	Al	CDV-9-1(i)	SW-846:6010C	Inorganic	Tpf	12	1	µg/L	189	189	189	189	140	200	68	200
Amino-2,6-dinitrotoluene[4-]	19406-51-0	CDV-9-1(i)	SW-846:8321A_MOD, SW-846:8330B	LCMS/MS High Explosives	Tpf	17	17	µg/L	0.3519412	0.306	0.199	0.769	—	—	—	—
Amino-4,6-dinitrotoluene[2-]	35572-78-2	CDV-9-1(i)	SW-846:8321A_MOD, SW-846:8330B	LCMS/MS High Explosives	Tpf	17	17	µg/L	0.3428824	0.34	0.29	0.47	—	—	—	—
Ammonia as nitrogen	NH3-N	CDV-9-1(i)	EPA:350.1	General Chemistry	Tpf	12	4	µg/L	49.85	51.4	33.4	63.2	92.5875	90.3	57.4	149
Anthracene	120-12-7	CDV-9-1(i)	SW-846:8270D, SW-846:8270DGCMS_SIM	SVOC	Tpf	9	0	µg/L	—	—	—	—	0.66011111	1	0.1	1.08
Antimony	Sb	CDV-9-1(i)	SW-846:6020	Inorganic	Tpf	12	0	µg/L	—	—	—	—	2.16666667	3	1	3

Table 4.2-1 (continued)

Parameter Name	Parameter Code	Well	Analytical Method	Analytical Method Category[a]	Geological Unit Code[a]	No. Samples	No. Detects	Unit	Mean Detect	Median Detect	Min Detect	Max Detect	Mean ND	Median ND	Min ND	Max ND
Arsenic	As	CDV-9-1(i)	SW-846:6020	Inorganic	Tpf	12	4	µg/L	2.26	2.125	2.01	2.78	3.865	5	1.92	5
Barium	Ba	CDV-9-1(i)	SW-846:6010C	Inorganic	Tpf	12	12	µg/L	4.9283333	4.98	2.94	7.07	—	—	—	—
Benzo(g,h,i)perylene	191-24-2	CDV-9-1(i)	SW-846:8270D, SW-846:8270DGCMS_SIM	SVOC	Tpf	9	0	µg/L	—	—	—	—	0.66011111	1	0.1	1.08
Benzoic acid	65-85-0	CDV-9-1(i)	SW-846:8270D	SVOC	Tpf	9	0	µg/L	—	—	—	—	15.0133333	20	6	21.5
Beryllium	Be	CDV-9-1(i)	SW-846:6010C	Inorganic	Tpf	12	0	µg/L	—	—	—	—	3.33333333	5	1	5
Bis(2-ethylhexyl)phthalate	117-81-7	CDV-9-1(i)	SW-846:8270D	SVOC	Tpf	9	0	µg/L	—	—	—	—	7.51222222	10	3	10.8
Boron	B	CDV-9-1(i)	SW-846:6010C	Inorganic	Tpf	12	10	µg/L	35.08	31.75	27.5	52.4	15	15	15	15
Bromide	Br(-1)	CDV-9-1(i)	EPA:300.0	General Chemistry	Tpf	12	11	µg/L	501.80909	164	74.5	2440	67	67	67	67
Bromodichloromethane	75-27-4	CDV-9-1(i)	SW-846:8260B	VOC	Tpf	12	0	µg/L	—	—	—	—	0.70833333	1	0.3	1
Bromoform	75-25-2	CDV-9-1(i)	SW-846:8260B	VOC	Tpf	12	0	µg/L	—	—	—	—	0.70833333	1	0.3	1
Butanone[2-]	78-93-3	CDV-9-1(i)	SW-846:8260B	VOC	Tpf	12	1	µg/L	4.35	4.35	4.35	4.35	3.40909091	5	1.5	5
Cadmium	Cd	CDV-9-1(i)	SW-846:6020	Inorganic	Tpf	12	0	µg/L	—	—	—	—	0.70833333	1	0.3	1
Calcium	Ca	CDV-9-1(i)	SW-846:6010C	Inorganic	Tpf	12	12	µg/L	13,489.167	13,950	8070	16,700	—	—	—	—
Carbon disulfide	75-15-0	CDV-9-1(i)	SW-846:8260B	VOC	Tpf	12	1	µg/L	1.5	1.5	1.5	1.5	3.40909091	5	1.5	5
Chloride	Cl(-1)	CDV-9-1(i)	EPA:300.0	General Chemistry	Tpf	12	12	µg/L	17,348.333	12,650	9130	66,500	—	—	—	—
Chlorobenzene	108-90-7	CDV-9-1(i)	SW-846:8260B	VOC	Tpf	12	0	µg/L	—	—	—	—	0.70833333	1	0.3	1
Chlorodibromomethane	124-48-1	CDV-9-1(i)	SW-846:8260B	VOC	Tpf	12	0	µg/L	—	—	—	—	0.70833333	1	0.3	1
Chloroform	67-66-3	CDV-9-1(i)	SW-846:8260B	VOC	Tpf	12	0	µg/L	—	—	—	—	0.70833333	1	0.3	1
Chloromethane	74-87-3	CDV-9-1(i)	SW-846:8260B	VOC	Tpf	12	0	µg/L	—	—	—	—	0.70833333	1	0.3	1
Chromium	Cr	CDV-9-1(i)	SW-846:6020	Inorganic	Tpf	12	2	µg/L	2.17	2.17	2.16	2.18	6.5	6.5	3	10
Cobalt	Co	CDV-9-1(i)	SW-846:6010C	Inorganic	Tpf	12	0	µg/L	—	—	—	—	3.38166667	5	1	5
Copper	Cu	CDV-9-1(i)	SW-846:6010C	Inorganic	Tpf	12	0	µg/L	—	—	—	—	7.08333333	10	3	10
Cyanide (total)	CN (Total)	CDV-9-1(i)	EPA:335.4	Inorganic	Tpf	12	0	µg/L	—	—	—	—	3.6125	5	1.67	5
DNX	DNX	CDV-9-1(i)	SW-846:8321A_MOD, SW-846:8330B	LCMS/MS High Explosives	Tpf	17	4	µg/L	0.11855	0.103	0.0892	0.179	0.15392308	0.087	0.0821	0.272
Fluoranthene	206-44-0	CDV-9-1(i)	SW-846:8270D, SW-846:8270DGCMS_SIM	SVOC	Tpf	9	0	µg/L	—	—	—	—	0.66011111	1	0.1	1.08
Fluoride	F(-1)	CDV-9-1(i)	EPA:300.0	General Chemistry	Tpf	12	12	µg/L	122.475	107	78.2	239	—	—	—	—
Gross alpha	GrossA	CDV-9-1(i)	EPA:900	RAD	Tpf	4	1	pCi/L	2.01	2.01	2.01	2.01	1.244	0.945	0.927	1.86
Gross beta	GrossB	CDV-9-1(i)	EPA:900	RAD	Tpf	4	1	pCi/L	2.83	2.83	2.83	2.83	0.68466667	0.875	-0.021	1.2
Hardness	Hardness	CDV-9-1(i)	SM:A2340B	Inorganic	Tpf	12	12	µg/L	51,416.667	53,500	31,700	62,900	—	—	—	—
Hexachlorobutadiene	87-68-3	CDV-9-1(i)	SW-846:8260B	VOC	Tpf	12	0	µg/L	—	—	—	—	0.7125	1	0.3	1
HMX	2691-41-0	CDV-9-1(i)	SW-846:8321A_MOD, SW-846:8330B	LCMS/MS High Explosives	Tpf	17	17	µg/L	1.4786471	1.3	0.728	3.46	—	—	—	—
Iron	Fe	CDV-9-1(i)	SW-846:6010C	Inorganic	Tpf	12	2	µg/L	88.4	88.4	50.8	126	65	65	30	100
Lead	Pb	CDV-9-1(i)	SW-846:6020	Inorganic	Tpf	12	0	µg/L	—	—	—	—	1.375	2	0.5	2
Magnesium	Mg	CDV-9-1(i)	SW-846:6010C	Inorganic	Tpf	12	12	µg/L	4368.3333	4550	2820	5130	—	—	—	—
Manganese	Mn	CDV-9-1(i)	SW-846:6010C	Inorganic	Tpf	12	4	µg/L	4.9325	4.22	2.79	8.5	5	2	2	10

Table 4.2-1 (continued)

Parameter Name	Parameter Code	Well	Analytical Method	Analytical Method Category[a]	Geological Unit Code[a]	No. Samples	No. Detects	Unit	Mean Detect	Median Detect	Min Detect	Max Detect	Mean ND	Median ND	Min ND	Max ND
Mercury	Hg	CDV-9-1(i)	EPA:245.2	Inorganic	Tpf	24	0	µg/L	—	—	—	—	0.14458333	0.2	0.067	0.2
Methyl tert-butyl ether	1634-04-4	CDV-9-1(i)	SW-846:8260B	VOC	Tpf	12	11	µg/L	0.81	0.82	0.36	1.24	0.3	0.3	0.3	0.3
Methyl-2-pentanone[4-]	108-10-1	CDV-9-1(i)	SW-846:8260B	VOC	Tpf	12	0	µg/L	—	—	—	—	3.54166667	5	1.5	5
Methylene chloride	75-09-2	CDV-9-1(i)	SW-846:8260B	VOC	Tpf	12	0	µg/L	—	—	—	—	5.54833333	5.755	1	10
MNX	MNX	CDV-9-1(i)	SW-846:8321A_MOD, SW-846:8330B	LCMS/MS High Explosives	Tpf	17	14	µg/L	0.1700857	0.1465	0.0852	0.414	0.08573333	0.086	0.0842	0.087
Molybdenum	Mo	CDV-9-1(i)	SW-846:6020	Inorganic	Tpf	12	12	µg/L	1.15	0.948	0.844	2.23	—	—	—	—
Nickel	Ni	CDV-9-1(i)	SW-846:6020	Inorganic	Tpf	12	8	µg/L	0.756125	0.69	0.547	1.17	0.95	0.6	0.6	2
Nitrate-nitrite as nitrogen	NO3+NO2-N	CDV-9-1(i)	EPA:353.2	General Chemistry	Tpf	12	12	µg/L	1133.0833	1080	945	1650	—	—	—	—
Nitrotoluene[2-]	88-72-2	CDV-9-1(i)	SW-846:8321A_MOD, SW-846:8330B	LCMS/MS High Explosives	Tpf	17	2	µg/L	0.10755	0.1076	0.0941	0.121	0.14530667	0.0882	0.0841	0.272
Oxygen-18/oxygen-16 ratio from Nitrate	O18O16-NO3	CDV-9-1(i)	Generic:Oxygen Isotope Ratio	General Chemistry	Tpf	2	2	permil	3.8822	3.8822	3.775	3.9894	—	—	—	—
Perchlorate	ClO4	CDV-9-1(i)	SW-846:6850	LCMS/MS Perchlorate	Tpf	12	12	µg/L	0.4519167	0.4365	0.404	0.532	—	—	—	—
Perfluorooctanoic acid	335-67-1	CDV-9-1(i)	EPA:537M	LCMS/MS PFAS	Tpf	1	1	µg/L	0.00217	0.0022	0.0022	0.0022	—	—	—	—
Phenanthrene	85-01-8	CDV-9-1(i)	SW-846:8270D, SW-846:8270DGCMS_SIM	SVOC	Tpf	9	0	µg/L	—	—	—	—	0.66011111	1	0.1	1.08
Potassium	K	CDV-9-1(i)	SW-846:6010C	Inorganic	Tpf	12	12	µg/L	1755.8333	1835	1020	2220	—	—	—	—
Pyrene	129-00-0	CDV-9-1(i)	SW-846:8270D, SW-846:8270DGCMS_SIM	SVOC	Tpf	9	0	µg/L	—	—	—	—	0.66011111	1	0.1	1.08
RDX	121-82-4	CDV-9-1(i)	SW-846:8321A_MOD, SW-846:8330B	LCMS/MS High Explosives	Tpf	17	17	µg/L	19.742941	18.1	8.03	37.3	—	—	—	—
Selenium	Se	CDV-9-1(i)	SW-846:6020	Inorganic	Tpf	12	1	µg/L	3.76	3.76	3.76	3.76	3.63636364	5	2	5
Silicon dioxide	SiO2	CDV-9-1(i)	SW-846:6010C	Inorganic	Tpf	12	12	µg/L	47,483.333	46,950	44,300	51,400	—	—	—	—
Silver	Ag	CDV-9-1(i)	SW-846:6020	Inorganic	Tpf	12	0	µg/L	—	—	—	—	0.70833333	1	0.3	1
Sodium	Na	CDV-9-1(i)	SW-846:6010C	Inorganic	Tpf	12	12	µg/L	17,633.333	17,200	13,200	23,800	—	—	—	—
Strontium	Sr	CDV-9-1(i)	SW-846:6010C	Inorganic	Tpf	12	12	µg/L	82.058333	86.5	47.7	104	—	—	—	—
Styrene	100-42-5	CDV-9-1(i)	SW-846:8260B	VOC	Tpf	12	0	µg/L	—	—	—	—	0.70833333	1	0.3	1
Sulfate	SO4(-2)	CDV-9-1(i)	EPA:300.0	General Chemistry	Tpf	12	12	µg/L	7625.8333	7525	6470	9490	—	—	—	—
Temperature	TEMP	CDV-9-1(i)	EPA:170.0	VOC	Tpf	18	18	deg C	2.7611111	3	1	5	—	—	—	—
Tetrachloroethene	127-18-4	CDV-9-1(i)	SW-846:8260B	VOC	Tpf	12	12	µg/L	1.0816667	1.065	0.87	1.35	—	—	—	—
Thallium	Tl	CDV-9-1(i)	SW-846:6020	Inorganic	Tpf	12	0	µg/L	—	—	—	—	1.41666667	2	0.6	2
Tin	Sn	CDV-9-1(i)	SW-846:6010C	Inorganic	Tpf	12	1	µg/L	3.18	3.18	3.18	3.18	7.41818182	10	2.5	10
TNX	TNX	CDV-9-1(i)	SW-846:8321A_MOD, SW-846:8330B	LCMS/MS High Explosives	Tpf	16	5	µg/L	0.16986	0.126	0.0863	0.35	0.11863636	0.086	0.0821	0.272
Toluene	108-88-3	CDV-9-1(i)	SW-846:8260B	VOC	Tpf	12	1	µg/L	0.85	0.85	0.85	0.85	0.68181818	1	0.3	1
Total dissolved solids	TDS	CDV-9-1(i)	EPA:160.1	General Chemistry	Tpf	12	12	µg/L	13,3916.67	130,500	117,000	166,000	—	—	—	—
Total Kjeldahl nitrogen	TKN	CDV-9-1(i)	EPA:351.2	General Chemistry	Tpf	12	3	µg/L	97.033333	112	37.1	142	95.8444444	100	33	169
Total organic carbon	TOC	CDV-9-1(i)	SW-846:9060	General Chemistry	Tpf	12	11	µg/L	1147.2727	1030	534	2300	1010	1010	1010	1010

Table 4.2-1 (continued)

Parameter Name	Parameter Code	Well	Analytical Method	Analytical Method Category[a]	Geological Unit Code[a]	No. Samples	No. Detects	Unit	Mean Detect	Median Detect	Min Detect	Max Detect	Mean ND	Median ND	Min ND	Max ND
Total Phosphate as phosphorus	PO4-P	CDV-9-1(i)	EPA:365.4	General Chemistry	Tpf	12	6	µg/L	56.716667	54.9	30.5	99.2	56.7333333	52.6	40.4	93.9
Trichlorobenzene[1,2,3-]	87-61-6	CDV-9-1(i)	SW-846:8260B	VOC	Tpf	12	0	µg/L	—	—	—	—	0.70833333	1	0.3	1
Trichloroethene	79-01-6	CDV-9-1(i)	SW-846:8260B	VOC	Tpf	12	12	µg/L	0.5083333	0.505	0.31	0.74	—	—	—	—
Trinitrobenzene[1,3,5-]	99-35-4	CDV-9-1(i)	SW-846:8321A_MOD, SW-846:8330B	LCMS/MS High Explosives	Tpf	17	0	µg/L	—	—	—	—	0.15855882	0.087	0.0821	0.272
Trinitrotoluene[2,4,6-]	118-96-7	CDV-9-1(i)	SW-846:8321A_MOD, SW-846:8330B	LCMS/MS High Explosives	Tpf	17	6	µg/L	0.1235833	0.1063	0.0897	0.209	0.18189091	0.254	0.0825	0.272
Tritium	H-3	CDV-9-1(i)	Generic:Low_Level_Tritium	RAD	Tpf	6	6	pCi/L	14.295167	15.592	7.472	16.423	—	—	—	—
Uranium	U	CDV-9-1(i)	SW-846:6020	Inorganic	Tpf	12	11	µg/L	0.7576364	0.739	0.526	0.967	0.624	0.624	0.624	0.624
Uranium-234	U-234	CDV-9-1(i)	HASL-300:ISOU	RAD	Tpf	4	4	pCi/L	0.56575	0.5445	0.49	0.684	—	—	—	—
Uranium-235/236	U-235/236	CDV-9-1(i)	HASL-300:ISOU	RAD	Tpf	4	0	pCi/L	—	—	—	—	0.0346	0.0344	0.0255	0.0441
Uranium-238	U-238	CDV-9-1(i)	HASL-300:ISOU	RAD	Tpf	4	4	pCi/L	0.32675	0.3245	0.252	0.406	—	—	—	—
Vanadium	V	CDV-9-1(i)	SW-846:6010C	Inorganic	Tpf	12	12	µg/L	1.8083333	1.79	1.11	2.71	—	—	—	—
Zinc	Zn	CDV-9-1(i)	SW-846:6010C	Inorganic	Tpf	12	7	µg/L	5.1857143	4.77	3.49	7.83	10	10	10	10
Acenaphthene	83-32-9	PCI-2	SW-846:8270C, SW-846:8270D, SW-846:8270DGCMS_SIM, SW-846:8310	SVOC	Tpf	14	0	µg/L	—	—	—	—	0.57207143	0.5075	0.1	1
Acenaphthylene	208-96-8	PCI-2	SW-846:8270C, SW-846:8270D, SW_846:8270DGCMS_SIM, SW-846:8310	SVOC	Tpf	14	0	µg/L	—	—	—	—	0.57207143	0.5075	0.1	1
Acetone	67-64-1	PCI-2	SW-846:8260B	VOC	Tpf	14	1	µg/L	2.99	2.99	2.99	2.99	7.38461538	10	1.5	10
Acidity or Alkalinity of a solution	pH	PCI-2	EPA:150.1	General Chemistry	Tpf	23	23	SU	7.5552174	7.53	7.2	7.86	—	—	—	—
Alkalinity-CO3	ALK-CO3	PCI-2	EPA:310.1	General Chemistry	Tpf	23	0	µg/L	—	—	—	—	1358.69565	1000	1000	4000
Alkalinity-CO3+HCO3	ALK-CO3+HCO3	PCI-2	EPA:310.1	General Chemistry	Tpf	23	23	µg/L	51,139.13	51,600	44,000	55,000	—	—	—	—
Aluminum	Al	PCI-2	SW-846:6010B, SW-846:6010C	Inorganic	Tpf	22	0	µg/L	—	—	—	—	176.681818	200	68	215
Amino-2,6-dinitrotoluene[4-]	19406-51-0	PCI-2	SW-846:8321A_MOD, SW-846:8330B	LCMS/MS High Explosives	Tpf	11	0	µg/L	—	—	—	—	0.19828182	0.265	0.0851	0.278
Amino-4,6-dinitrotoluene[2-]	35572-78-2	PCI-2	SW-846:8321A_MOD, SW-846:8330B	LCMS/MS High Explosives	Tpf	11	0	µg/L	—	—	—	—	0.19828182	0.265	0.0851	0.278
Ammonia as nitrogen	NH3-N	PCI-2	EPA:350.1	General Chemistry	Tpf	22	8	µg/L	66.025	60.3	18.2	127	40.8142857	48.4	17	50
Anthracene	120-12-7	PCI-2	SW-846:8270C, SW-846:8270D, SW-846:8270DGCMS_SIM, SW-846:8310	SVOC	Tpf	14	0	µg/L	—	—	—	—	0.57207143	0.5075	0.1	1
Antimony	Sb	PCI-2	SW-846:6020, SW-846:6020B	Inorganic	Tpf	22	0	µg/L	—	—	—	—	2.5	3	1	3
Arsenic	As	PCI-2	SW-846:6020, SW-846:6020B	Inorganic	Tpf	22	5	µg/L	2.454	2.4	1.96	3.04	4.64705882	5	2	5
Barium	Ba	PCI-2	SW-846:6010B, SW-846:6010C	Inorganic	Tpf	22	22	µg/L	5.4286364	4.25	3.3	19.8	—	—	—	—
Benzo(g,h,i)perylene	191-24-2	PCI-2	SW-846:8270C, SW-846:8270D, SW-846:8270DGCMS_SIM, SW-846:8310	SVOC	Tpf	14	1	µg/L	0.0301	0.0301	0.0301	0.0301	0.5365	0.309	0.0515	1
Benzoic acid	65-85-0	PCI-2	SW-846:8270C, SW-846:8270D	SVOC	Tpf	14	0	µg/L	—	—	—	—	13.4757143	13	6	21.1
Beryllium	Be	PCI-2	SW-846:6010B, SW-846:6010C	Inorganic	Tpf	22	0	µg/L	—	—	—	—	4.09090909	5	1	5
Bis(2-ethylhexyl)phthalate	117-81-7	PCI-2	SW-846:8270C, SW-846:8270D	SVOC	Tpf	14	0	µg/L	—	—	—	—	5.94835714	6.5	0.3	10.5

Table 4.2-1 (continued)

Parameter Name	Parameter Code	Well	Analytical Method	Analytical Method Category[a]	Geological Unit Code[a]	No. Samples	No. Detects	Unit	Mean Detect	Median Detect	Min Detect	Max Detect	Mean ND	Median ND	Min ND	Max ND
Boron	B	PCI-2	SW-846:6010B, SW-846:6010C	Inorganic	Tpf	22	1	µg/L	16.9	16.9	16.9	16.9	41.6666667	50	15	50
Bromide	Br(-1)	PCI-2	EPA:300.0	General Chemistry	Tpf	23	0	µg/L	—	—	—	—	171.086957	200	67	200
Bromodichloromethane	75-27-4	PCI-2	SW-846:8260B	VOC	Tpf	14	0	µg/L	—	—	—	—	0.75	1	0.3	1
Bromoform	75-25-2	PCI-2	SW-846:8260B	VOC	Tpf	14	0	µg/L	—	—	—	—	0.75	1	0.3	1
Butanone[2-]	78-93-3	PCI-2	SW-846:8260B	VOC	Tpf	14	0	µg/L	—	—	—	—	3.75	5	1.5	5
Cadmium	Cd	PCI-2	SW-846:6020, SW-846:6020B	Inorganic	Tpf	22	0	µg/L	—	—	—	—	0.84090909	1	0.3	1
Calcium	Ca	PCI-2	SW-846:6010B, SW-846:6010C	Inorganic	Tpf	22	22	µg/L	8790.4545	8890	8060	9450	—	—	—	—
Carbon Disulfide	75-15-0	PCI-2	SW-846:8260B	VOC	Tpf	14	0	µg/L	—	—	—	—	3.75	5	1.5	5
Chloride	Cl(-1)	PCI-2	EPA:300.0	General Chemistry	Tpf	23	23	µg/L	1390.4783	1420	341	1690	—	—	—	—
Chlorobenzene	108-90-7	PCI-2	SW-846:8260B	VOC	Tpf	14	0	µg/L	—	—	—	—	0.75	1	0.3	1
Chlorodibromomethane	124-48-1	PCI-2	SW-846:8260B	VOC	Tpf	14	0	µg/L	—	—	—	—	0.75	1	0.3	1
Chloroform	67-66-3	PCI-2	SW-846:8260B	VOC	Tpf	14	0	µg/L	—	—	—	—	0.75	1	0.3	1
Chloromethane	74-87-3	PCI-2	SW-846:8260B	VOC	Tpf	14	0	µg/L	—	—	—	—	0.75	1	0.3	1
Chromium	Cr	PCI-2	SW-846:6020, SW-846:6020B	Inorganic	Tpf	22	0	µg/L	—	—	—	—	7.64318182	10	3	10
Cobalt	Co	PCI-2	SW-846:6010B, SW-846:6010C	Inorganic	Tpf	22	1	µg/L	1.99	1.99	1.99	1.99	4.04761905	5	1	5
Copper	Cu	PCI-2	SW-846:6010B, SW-846:6010C	Inorganic	Tpf	22	0	µg/L	—	—	—	—	8.40909091	10	3	10
Cyanide (total)	CN (Total)	PCI-2	EPA:335.3, EPA:335.4	Inorganic	Tpf	14	0	µg/L	—	—	—	—	3.81071429	5	1.67	5
DNX	DNX	PCI-2	SW-846:8321A_MOD	LCMS/MS High Explosives	Tpf	2	0	µg/L	—	—	—	—	0.2665	0.2665	0.266	0.267
Fluoranthene	206-44-0	PCI-2	SW-846:8270C, SW-846:8270D, SW-846:8270DGCMS_SIM, SW-846:8310	SVOC	Tpf	14	0	µg/L	—	—	—	—	0.50225714	0.3085	0.0515	1
Fluoride	F(-1)	PCI-2	EPA:300.0	General Chemistry	Tpf	23	23	µg/L	186.00435	181	91.1	379	—	—	—	—
Gross alpha	GrossA	PCI-2	EPA:900	RAD	Tpf	10	0	pCi/L	—	—	—	—	0.47422	0.4645	-1.33	1.96
Gross beta	GrossB	PCI-2	EPA:900	RAD	Tpf	10	1	pCi/L	8.05	8.05	8.05	8.05	0.91784444	0.693	-0.29	2.28
Gross gamma	GrossG	PCI-2	EPA:901.1	RAD	Tpf	2	0	pCi/L	—	—	—	—	22.3	22.3	21.9	22.7
Hardness	Hardness	PCI-2	SM:A2340B	Inorganic	Tpf	22	22	µg/L	31,013.636	31,300	29,300	33,200	—	—	—	—
Hexachlorobutadiene	87-68-3	PCI-2	SW-846:8260B	VOC	Tpf	14	0	µg/L	—	—	—	—	0.75	1	0.3	1
HMX	2691-41-0	PCI-2	SW-846:8321A_MOD, SW-846:8330B	LCMS/MS High Explosives	Tpf	11	0	µg/L	—	—	—	—	0.19828182	0.265	0.0851	0.278
Iron	Fe	PCI-2	SW-846:6010B, SW-846:6010C	Inorganic	Tpf	22	2	µg/L	45.4	45.4	33.2	57.6	85.79	100	30	100
Lead	Pb	PCI-2	SW-846:6020, SW-846:6020B	Inorganic	Tpf	22	0	µg/L	—	—	—	—	1.65909091	2	0.5	2
Magnesium	Mg	PCI-2	SW-846:6010B, SW-846:6010C	Inorganic	Tpf	22	22	µg/L	2203.6364	2225	2010	2370	—	—	—	—
Manganese	Mn	PCI-2	SW-846:6010B, SW-846:6010C	Inorganic	Tpf	22	6	µg/L	6.22	4.87	2.09	11.5	7.5	10	2	10
Mercury	Hg	PCI-2	EPA:245.2, SW-846:7470A	Inorganic	Tpf	34	0	µg/L	—	—	—	—	0.16182353	0.2	0.067	0.2
Methyl tert-butyl ether	1634-04-4	PCI-2	SW-846:8260B	VOC	Tpf	14	0	µg/L	—	—	—	—	0.75	1	0.3	1
Methyl-2-pentanone[4-]	108-10-1	PCI-2	SW-846:8260B	VOC	Tpf	14	0	µg/L	—	—	—	—	3.75	5	1.5	5
Methylene chloride	75-09-2	PCI-2	SW-846:8260B	VOC	Tpf	14	0	µg/L	—	—	—	—	6.79642857	10	1	10

Table 4.2-1 (continued)

Parameter Name	Parameter Code	Well	Analytical Method	Analytical Method Category[a]	Geological Unit Code[a]	No. Samples	No. Detects	Unit	Mean Detect	Median Detect	Min Detect	Max Detect	Mean ND	Median ND	Min ND	Max ND
MNX	MNX	PCI-2	SW-846:8321A_MOD	LCMS/MS High Explosives	Tpf	2	0	µg/L	—	—	—	—	0.2665	0.2665	0.266	0.267
Molybdenum	Mo	PCI-2	SW-846:6020, SW-846:6020B	Inorganic	Tpf	22	21	µg/L	1.007381	1.03	0.829	1.2	1.3	1.3	1.3	1.3
Nickel	Ni	PCI-2	SW-846:6020, SW-846:6020B	Inorganic	Tpf	22	10	µg/L	0.8044	0.6835	0.502	1.8	1.43408333	2	0.6	2
Nitrate-nitrite as nitrogen	NO3+NO2-N	PCI-2	EPA:353.2	General Chemistry	Tpf	22	21	µg/L	121.04762	117	67	178	50	50	50	50
Nitrotoluene[2-]	88-72-2	PCI-2	SW-846:8321A_MOD, SW-846:8330B	LCMS/MS High Explosives	Tpf	11	0	µg/L	—	—	—	—	0.19905455	0.265	0.0872	0.278
Perchlorate	ClO4	PCI-2	SW-846:6850	LCMS/MS Perchlorate	Tpf	22	22	µg/L	0.1756818	0.1765	0.145	0.202	—	—	—	—
Perfluorooctanoic acid	335-67-1	PCI-2	EPA:537M	LCMS/MS PFAS	Tpf	1	0	µg/L	—	—	—	—	0.000643	0.00064	0.00064	0.00064
Phenanthrene	85-01-8	PCI-2	SW-846:8270C, SW-846:8270D, SW-846:8270DGCMS_SIM, SW-846:8310	SVOC	Tpf	14	0	µg/L	—	—	—	—	0.57207143	0.5075	0.1	1
Potassium	K	PCI-2	SW-846:6010B, SW-846:6010C	Inorganic	Tpf	22	22	µg/L	312.68182	314.5	165	444	—	—	—	—
Pyrene	129-00-0	PCI-2	SW-846:8270C, SW-846:8270D, SW-846:8270DGCMS_SIM, SW-846:8310	SVOC	Tpf	14	0	µg/L	—	—	—	—	0.50225714	0.3085	0.0515	1
RDX	121-82-4	PCI-2	SW-846:8321A_MOD, SW-846:8330B	LCMS/MS High Explosives	Tpf	11	0	µg/L	—	—	—	—	0.19828182	0.265	0.0851	0.278
Selenium	Se	PCI-2	SW-846:6020, SW-846:6020B	Inorganic	Tpf	22	0	µg/L	—	—	—	—	4.13909091	5	1.06	5
Silicon dioxide	SiO2	PCI-2	SW-846:6010B, SW-846:6010C	Inorganic	Tpf	23	23	µg/L	69,234.783	69,100	61,000	76,500	—	—	—	—
Silver	Ag	PCI-2	SW-846:6020, SW-846:6020B	Inorganic	Tpf	22	1	µg/L	0.108	0.108	0.108	0.108	0.83333333	1	0.3	1
Sodium	Na	PCI-2	SW-846:6010B, SW-846:6010C	Inorganic	Tpf	22	22	µg/L	11,713.636	11,500	10,700	14,000	—	—	—	—
Strontium	Sr	PCI-2	SW-846:6010B, SW-846:6010C	Inorganic	Tpf	22	22	µg/L	48.368182	48.1	44.4	67.8	—	—	—	—
Styrene	100-42-5	PCI-2	SW-846:8260B	VOC	Tpf	14	0	µg/L	—	—	—	—	0.75	1	0.3	1
Sulfate	SO4(-2)	PCI-2	EPA:300.0	General Chemistry	Tpf	23	22	µg/L	1617.5455	1680	576	1790	1670	1670	1670	1670
Temperature	TEMP	PCI-2	EPA:170.0	VOC	Tpf	12	12	deg C	2.5	2	2	4	—	—	—	—
Tetrachloroethene	127-18-4	PCI-2	SW-846:8260B	VOC	Tpf	14	0	µg/L	—	—	—	—	0.75	1	0.3	1
Thallium	Tl	PCI-2	SW-846:6020, SW-846:6020B	Inorganic	Tpf	22	1	µg/L	0.354	0.354	0.354	0.354	1.34909524	1	0.331	2
Tin	Sn	PCI-2	SW-846:6010B, SW-846:6010C	Inorganic	Tpf	22	0	µg/L	—	—	—	—	16.0227273	10	2.5	100
TNX	TNX	PCI-2	SW-846:8321A_MOD	LCMS/MS High Explosives	Tpf	2	0	µg/L	—	—	—	—	0.2665	0.2665	0.266	0.267
Toluene	108-88-3	PCI-2	SW-846:8260B	VOC	Tpf	14	0	µg/L	—	—	—	—	0.75	1	0.3	1
Total dissolved solids	TDS	PCI-2	EPA:160.1	General Chemistry	Tpf	23	23	µg/L	114,304.35	120,000	67,100	134,000	—	—	—	—
Total Kjeldahl nitrogen	TKN	PCI-2	EPA:351.2	General Chemistry	Tpf	15	3	µg/L	119.93333	106	49.8	204	77.6666667	100	33	100
Total organic carbon	TOC	PCI-2	SW-846:9060, SW-846:9060A	General Chemistry	Tpf	15	9	µg/L	467.33333	454	337	852	698.333333	765	330	1000
Total phosphate as phosphorus	PO4-P	PCI-2	EPA:365.4	General Chemistry	Tpf	23	4	µg/L	79.7	43.65	27.5	204	42.6736842	49	20	84.2
Trichlorobenzene[1,2,3-]	87-61-6	PCI-2	SW-846:8260B	VOC	Tpf	14	0	µg/L	—	—	—	—	0.75	1	0.3	1
Trichloroethene	79-01-6	PCI-2	SW-846:8260B	VOC	Tpf	14	0	µg/L	—	—	—	—	0.75	1	0.3	1

Table 4.2-1 (continued)

Parameter Name	Parameter Code	Well	Analytical Method	Analytical Method Category[a]	Geological Unit Code[a]	No. Samples	No. Detects	Unit	Mean Detect	Median Detect	Min Detect	Max Detect	Mean ND	Median ND	Min ND	Max ND
Trinitrobenzene[1,3,5-]	99-35-4	PCI-2	SW-846:8321A_MOD, SW-846:8330B	LCMS/MS High Explosives	Tpf	11	0	µg/L	—	—	—	—	0.19828182	0.265	0.0851	0.278
Trinitrotoluene[2,4,6-]	118-96-7	PCI-2	SW-846:8321A_MOD, SW-846:8330B	LCMS/MS High Explosives	Tpf	11	0	µg/L	—	—	—	—	0.19828182	0.265	0.0851	0.278
Tritium	H-3	PCI-2	Generic:Low_Level_Tritium	RAD	Tpf	5	0	pCi/L	—	—	—	—	-0.8984	0.694	-8.284	1.82
Uranium	U	PCI-2	SW-846:6020, SW-846:6020B	Inorganic	Tpf	22	19	µg/L	0.3432105	0.334	0.285	0.576	0.33066667	0.332	0.309	0.351
Uranium-234	U-234	PCI-2	HASL-300:ISOU	RAD	Tpf	10	10	pCi/L	0.2198	0.2215	0.144	0.288	—	—	—	—
Uranium-235/236	U-235/236	PCI-2	HASL-300:ISOU	RAD	Tpf	10	1	pCi/L	0.0547	0.0547	0.0547	0.0547	0.01407556	0.0105	0	0.0578
Uranium-238	U-238	PCI-2	HASL-300:ISOU	RAD	Tpf	10	9	pCi/L	0.1222333	0.124	0.0921	0.161	0.0816	0.0816	0.0816	0.0816
Vanadium	V	PCI-2	SW-846:6010B, SW-846:6010C	Inorganic	Tpf	22	20	µg/L	1.4305	1.42	1.14	1.78	4.135	4.135	3.27	5
Zinc	Zn	PCI-2	SW-846:6010B, SW-846:6010C	Inorganic	Tpf	22	7	µg/L	4.3328571	4.25	2.6	5.45	9.10666667	10	3.3	10
Acenaphthene	83-32-9	R-19	SW-846:8270, SW-846:8270C, SW-846:8270D, SW-846:8310	SVOC	Tp	8	1	µg/L	0.18	0.18	0.18	0.18	5.05671429	1	0.315	11
Acenaphthylene	208-96-8	R-19	SW-846:8270, SW-846:8270C, SW-846:8270D, SW-846:8310	SVOC	Tp	8	1	µg/L	0.16	0.16	0.16	0.16	5.05671429	1	0.315	11
Acetone	67-64-1	R-19	SW-846:8260, SW-846:8260B	VOC	Tp	9	1	µg/L	3.1	3.1	3.1	3.1	15.91375	10	2.31	30
Acidity or alkalinity of a solution	pH	R-19	EPA:150.1	General Chemistry	Tp	17	17	SU	8.1505882	8.32	6.23	8.79	—	—	—	—
Alkalinity-CO3	ALK-CO3	R-19	EPA:310.1	General Chemistry	Tp	17	7	µg/L	2634.2857	2120	1070	5230	1135	1000	1000	1450
Alkalinity-CO3+HCO3	ALK-CO3+HCO3	R-19	EPA:310.1	General Chemistry	Tp	17	17	µg/L	73,600	74,300	68,300	80,200	—	—	—	—
Alkalinity-HCO3	ALK-HCO3	R-19	EPA:310.1	General Chemistry	Tp	2	2	µg/L	67,900	67,900	67,200	68,600	—	—	—	—
Aluminum	Al	R-19	SW-846:6010B, SW-846:6010C	Inorganic	Tp	21	1	µg/L	217	217	217	217	176.9	200	68	200
Amino-2,6-dinitrotoluene[4-]	19406-51-0	R-19	SW-846:8330, SW-846:8321A_MOD, SW-846:8330B, SW-846:8321A(M)	HEXP, LCMS/MS High Explosives, LCMS/MS Perchlorate	Tp	14	0	µg/L	—	—	—	—	0.21904286	0.258	0.0846	0.325
Amino-4,6-dinitrotoluene[2-]	35572-78-2	R-19	SW-846:8330, SW-846:8321A_MOD, SW-846:8330B, SW-846:8321A(M)	HEXP, LCMS/MS High Explosives, LCMS/MS Perchlorate	Tp	14	0	µg/L	—	—	—	—	0.23068571	0.2785	0.0846	0.325
Ammonia as nitrogen	NH3-N	R-19	EPA:350.1	General Chemistry	Tp	15	5	µg/L	42.88	39	31.7	58	49.45	50	24	80
Anthracene	120-12-7	R-19	SW-846:8270, SW-846:8270C, SW-846:8270D, SW-846:8310	SVOC	Tp	8	1	µg/L	0.2	0.2	0.2	0.2	5.05671429	1	0.315	11
Antimony	Sb	R-19	SW-846:6020	Inorganic	Tp	22	0	µg/L	—	—	—	—	2.11636364	2	0.28	3
Arsenic	As	R-19	SW-846:6010B, SW-846:6020	Inorganic	Tp	22	1	µg/L	2.14	2.14	2.14	2.14	4.53238095	5	2	6
Barium	Ba	R-19	SW-846:6010B, SW-846:6010C	Inorganic	Tp	22	22	µg/L	25.090909	25	22.4	28.2	—	—	—	—
Benzo(g,h,i)perylene	191-24-2	R-19	SW-846:8270, SW-846:8270C, SW-846:8270D, SW-846:8310	SVOC	Tp	8	0	µg/L	—	—	—	—	4.4529	1.1	0.0526	11
Benzoic acid	65-85-0	R-19	SW-846:8270, SW-846:8270C, SW-846:8270D	SVOC	Tp	6	0	µg/L	—	—	—	—	35.8683333	38.75	6.31	56
Beryllium	Be	R-19	SW-846:6010B, SW-846:6010C	Inorganic	Tp	22	0	µg/L	—	—	—	—	4.01436364	5	0.158	5
Bis(2-ethylhexyl)phthalate	117-81-7	R-19	SW-846:8270, SW-846:8270C, SW-846:8270D	SVOC	Tp	6	2	µg/L	0.39	0.39	0.17	0.61	8.675	11	1.7	11

Table 4.2-1 (continued)

Parameter Name	Parameter Code	Well	Analytical Method	Analytical Method Category[a]	Geological Unit Code[a]	No. Samples	No. Detects	Unit	Mean Detect	Median Detect	Min Detect	Max Detect	Mean ND	Median ND	Min ND	Max ND
Bismuth-214	Bi-214	R-19	EPA:901.1, Generic:Gamma Spec.	RAD	Tp	4	0	pCi/L	—	—	—	—	4.5875	4.175	3	7
Boron	B	R-19	SW-846:6010B, SW-846:6010C	Inorganic	Tp	22	11	µg/L	16.027273	15.2	12.7	20.9	50	50	50	50
Bromide	Br(-1)	R-19	EPA:300.0	General Chemistry	Tp	15	0	µg/L	—	—	—	—	180.533333	200	41	200
Bromodichloromethane	75-27-4	R-19	SW-846:8260, SW-846:8260B	VOC	Tp	9	0	µg/L	—	—	—	—	2.25555556	1	0.3	5
Bromoform	75-25-2	R-19	SW-846:8260, SW-846:8260B	VOC	Tp	9	0	µg/L	—	—	—	—	2.25555556	1	0.3	5
Butanone[2-]	78-93-3	R-19	SW-846:8260, SW-846:8260B	VOC	Tp	9	0	µg/L	—	—	—	—	9.61111111	5	1.5	20
Cadmium	Cd	R-19	SW-846:6020	Inorganic	Tp	22	1	µg/L	0.156	0.156	0.156	0.156	0.78952381	1	0.04	1
Calcium	Ca	R-19	SW-846:6010B, SW-846:6010C	Inorganic	Tp	22	22	µg/L	16,390.909	16,500	14,600	17,700	—	—	—	—
Carbon Disulfide	75-15-0	R-19	SW-846:8260, SW-846:8260B	VOC	Tp	9	0	µg/L	—	—	—	—	4.61111111	5	1.5	5
Chloride	Cl(-1)	R-19	EPA:300.0	General Chemistry	Tp	17	17	µg/L	2759.4118	2720	2420	3120	—	—	—	—
Chlorobenzene	108-90-7	R-19	SW-846:8260, SW-846:8260B	VOC	Tp	9	0	µg/L	—	—	—	—	2.25555556	1	0.3	5
Chlorodibromomethane	124-48-1	R-19	SW-846:8260, SW-846:8260B	VOC	Tp	9	0	µg/L	—	—	—	—	2.25555556	1	0.3	5
Chloroform	67-66-3	R-19	SW-846:8260, SW-846:8260B	VOC	Tp	9	0	µg/L	—	—	—	—	2.25555556	1	0.3	5
Chloromethane	74-87-3	R-19	SW-846:8260, SW-846:8260B	VOC	Tp	9	0	µg/L	—	—	—	—	3.92222222	1	0.3	10
Chromium	Cr	R-19	SW-846:6010B, SW-846:6020	Inorganic	Tp	22	14	µg/L	6.1335714	3.01	1.5	46.6	6.4975	7.49	1	10
Cobalt	Co	R-19	SW-846:6010B, SW-846:6010C	Inorganic	Tp	22	1	µg/L	1.04	1.04	1.04	1.04	4.00390476	5	0.541	5
Copper	Cu	R-19	SW-846:6010B, SW-846:6010C	Inorganic	Tp	22	0	µg/L	—	—	—	—	8.35909091	10	1.39	10
Cyanide (total)	CN (Total)	R-19	SW-846:9012A, EPA:335.3, EPA:335.4	General Chemistry, Inorganic	Tp	6	0	µg/L	—	—	—	—	2.935	2.11	1.67	5
DNX	DNX	R-19	SW-846:8321A_MOD, SW-846:8330RDX	LCMS/MS High Explosives	Tp	5	0	µg/L	—	—	—	—	0.42	0.5	0.291	0.5
Fluoranthene	206-44-0	R-19	SW-846:8270, SW-846:8270C, SW-846:8270D, SW-846:8310	SVOC	Tp	8	1	µg/L	0.19	0.19	0.19	0.19	4.9176	1	0.0526	11
Fluoride	F(-1)	R-19	EPA:300.0	General Chemistry	Tp	17	17	µg/L	571.11765	565	409	849	—	—	—	—
Gross alpha	GrossA	R-19	EPA:900, Generic:GrossAB	RAD	Tp	16	3	pCi/L	5.6466667	3.73	3.51	9.7	0.77515385	0.53	-0.119	2.28
Gross beta	GrossB	R-19	EPA:900, Generic:GrossAB	RAD	Tp	16	3	pCi/L	2.86	3.26	1.79	3.53	0.748	0.645	-0.368	2.44
Gross gamma	GrossG	R-19	EPA:901.1, Generic:Gross Gamma	RAD	Tp	13	1	pCi/L	132	132	132	132	33.9733333	20	7.62	108
Hardness	Hardness	R-19	EPA:200.7, SM:A2340B	Inorganic	Tp	22	22	µg/L	52,740.909	53,200	47,600	56,800	—	—	—	—
Heptachlor	76-44-8	R-19	SW-846:8080, SW-846:8081	PESTPCB	Tp	4	0	µg/L	—	—	—	—	0.0465	0.0545	0.021	0.056
Hexachlorobutadiene	87-68-3	R-19	SW-846:8260, SW-846:8260B	VOC	Tp	8	0	µg/L	—	—	—	—	2.4125	1	0.3	5
HMX	2691-41-0	R-19	SW-846:8330, SW-846:8321A_MOD, SW-846:8330B, SW-846:8321A(M)	HEXP, LCMS/MS High Explosives, LCMS/MS Perchlorate	Tp	14	0	µg/L	—	—	—	—	0.27261429	0.2785	0.0846	1
Iron	Fe	R-19	SW-846:6010B, SW-846:6010C	Inorganic	Tp	22	5	µg/L	79.06	26	25	281	87.9411765	100	12.6	100
Lead	Pb	R-19	SW-846:6020	Inorganic	Tp	22	0	µg/L	—	—	—	—	1.61818182	2	0.05	2
Magnesium	Mg	R-19	SW-846:6010B, SW-846:6010C	Inorganic	Tp	22	22	µg/L	2867.2727	2900	2510	3120	—	—	—	—
Manganese	Mn	R-19	SW-846:6010B, SW-846:6010C	Inorganic	Tp	22	4	µg/L	3.7775	3.03	2.25	6.8	8.16055556	10	1	10
Mercury	Hg	R-19	EPA:245.1, EPA:245.2	Inorganic	Tp	25	0	µg/L	—	—	—	—	0.165136	0.2	0.0472	0.2
Methyl tert-butyl ether	1634-04-4	R-19	SW-846:8260B	VOC	Tp	4	0	µg/L	—	—	—	—	0.825	1	0.3	1

Table 4.2-1 (continued)

Parameter Name	Parameter Code	Well	Analytical Method	Analytical Method Category[a]	Geological Unit Code[a]	No. Samples	No. Detects	Unit	Mean Detect	Median Detect	Min Detect	Max Detect	Mean ND	Median ND	Min ND	Max ND
Methyl-2-pentanone[4-]	108-10-1	R-19	SW-846:8260, SW-846:8260B	VOC	Tp	9	0	µg/L	—	—	—	—	9.61111111	5	1.5	20
Methylene chloride	75-09-2	R-19	SW-846:8260, SW-846:8260B	VOC	Tp	9	0	µg/L	—	—	—	—	5.94222222	5	1.38	10
MNX	MNX	R-19	SW-846:8321A_MOD, SW-846:8330RDX	LCMS/MS High Explosives	Tp	4	0	µg/L	—	—	—	—	0.4	0.4045	0.291	0.5
Molybdenum	Mo	R-19	SW-846:6010B, SW-846:6020	Inorganic	Tp	22	19	µg/L	1.6542105	1.35	1.12	6.2	1.68333333	1.51	1.43	2.11
Nickel	Ni	R-19	SW-846:6010B, SW-846:6020	Inorganic	Tp	22	11	µg/L	3.3546364	0.745	0.51	28.6	1.79027273	2	0.5	2.92
Nitrate-nitrite as nitrogen	NO3+NO2-N	R-19	EPA:353.1, EPA:353.2	General Chemistry	Tp	17	17	µg/L	356.11765	360	128	496	—	—	—	—
Nitrotoluene[2-]	88-72-2	R-19	SW-846:8330, SW-846:8321A_MOD, SW-846:8330B, SW-846:8321A(M)	HEXP, LCMS/MS High Explosives, LCMS/MS Perchlorate	Tp	14	0	µg/L	—	—	—	—	0.27276429	0.2785	0.0867	1
Perchlorate	ClO4	R-19	EPA:314.0, SW-846:6850, SW846 6850 Modified	General Chemistry, LCMS/MS Perchlorate	Tp	17	16	µg/L	0.340125	0.3405	0.299	0.381	4	4	4	4
Phenanthrene	85-01-8	R-19	SW-846:8270, SW-846:8270C, SW-846:8270D, SW-846:8310	SVOC	Tp	8	1	µg/L	0.24	0.24	0.24	0.24	5.05671429	1	0.315	11
Potassium	K	R-19	SW-846:6010B, SW-846:6010C	Inorganic	Tp	22	22	µg/L	1005.2273	1005	897	1060	—	—	—	—
Pyrene	129-00-0	R-19	SW-846:8270, SW-846:8270C, SW-846:8270D, SW-846:8310	SVOC	Tp	8	1	µg/L	0.19	0.19	0.19	0.19	4.9176	1	0.0526	11
Radium-226	Ra-226	R-19	EPA:903.1	RAD	Tp	1	0	pCi/L	—	—	—	—	0.0884	0.0884	0.0884	0.0884
Radium-228	Ra-228	R-19	EPA:901.1	RAD	Tp	1	0	pCi/L	—	—	—	—	3.79	3.79	3.79	3.79
RDX	121-82-4	R-19	SW-846:8330, SW-846:8321A_MOD, SW-846:8330B, SW-846:8321A(M)	HEXP, LCMS/MS High Explosives, LCMS/MS Perchlorate	Tp	14	1	µg/L	0.098	0.098	0.098	0.098	0.21666154	0.266	0.0846	0.325
Selenium	Se	R-19	SW-846:6010B, SW-846:6020	Inorganic	Tp	22	1	µg/L	2.8	2.8	2.8	2.8	4.52952381	5	2	5
Silicon dioxide	SiO2	R-19	SW-846:6010B, SW-846:6010C	Inorganic	Tp	18	18	µg/L	70,777.778	71,200	64,800	74,700	—	—	—	—
Silver	Ag	R-19	SW-846:6010B, SW-846:6020	Inorganic	Tp	22	0	µg/L	—	—	—	—	0.88045455	1	0.2	1
Sodium	Na	R-19	SW-846:6010B, SW-846:6010C	Inorganic	Tp	22	22	µg/L	14463.636	14,550	13,100	15,300	—	—	—	—
Strontium	Sr	R-19	SW-846:6010B, SW-846:6010C	Inorganic	Tp	22	22	µg/L	70.309091	70.85	56.6	77.2	—	—	—	—
Styrene	100-42-5	R-19	SW-846:8260, SW-846:8260B	VOC	Tp	9	0	µg/L	—	—	—	—	2.25555556	1	0.3	5
Sulfate	SO4(-2)	R-19	EPA:300.0	General Chemistry	Tp	17	17	µg/L	3226.4706	3270	2570	3560	—	—	—	—
Suspended sediment concentration	SSC	R-19	EPA:160.2	General Chemistry	Tp	1	0	µg/L	—	—	—	—	2000	2000	2000	2000
Temperature	TEMP	R-19	EPA:170.0	VOC	Tp	2	2	deg C	2	2	2	2	—	—	—	—
Tetrachloroethene	127-18-4	R-19	SW-846:8260, SW-846:8260B	VOC	Tp	9	0	µg/L	—	—	—	—	2.25555556	1	0.3	5
Thallium	Tl	R-19	SW-846:6020	Inorganic	Tp	22	2	µg/L	0.407	0.407	0.294	0.52	1.0663	1	0.066	2
Tin	Sn	R-19	SW-846:6010B, SW-846:6010C	Inorganic	Tp	22	0	µg/L	—	—	—	—	21.5463636	10	2.5	100
TNX	TNX	R-19	SW-846:8321A_MOD, SW-846:8330RDX	LCMS/MS High Explosives	Tp	5	0	µg/L	—	—	—	—	0.42	0.5	0.291	0.5
Toluene	108-88-3	R-19	SW-846:8260, SW-846:8260B	VOC	Tp	9	1	µg/L	0.54	0.54	0.54	0.54	2.4125	1	0.3	5
Total dissolved solids	TDS	R-19	EPA:160.1	General Chemistry	Tp	17	17	µg/L	152,294.12	151,000	145,000	164,000	—	—	—	—

Table 4.2-1 (continued)

Parameter Name	Parameter Code	Well	Analytical Method	Analytical Method Category[a]	Geological Unit Code[a]	No. Samples	No. Detects	Unit	Mean Detect	Median Detect	Min Detect	Max Detect	Mean ND	Median ND	Min ND	Max ND
Total Kjeldahl nitrogen	TKN	R-19	EPA:351.2	General Chemistry	Tp	8	1	µg/L	324	324	324	324	90.4285714	100	33	100
Total organic carbon	TOC	R-19	SW-846:9060	General Chemistry	Tp	7	6	µg/L	504.5	420	304	924	240	240	240	240
Total phosphate as phosphorus	PO4-P	R-19	EPA:365.4	General Chemistry	Tp	17	8	µg/L	86.1	79.75	51	139	63.5444444	64	48.9	81
Total suspended solids	TSS	R-19	EPA:160.2	General Chemistry	Tp	2	0	µg/L	—	—	—	—	1132	1132	734	1530
Trichlorobenzene[1,2,3-]	87-61-6	R-19	SW-846:8260, SW-846:8260B	VOC	Tp	7	0	µg/L	—	—	—	—	2.61428571	1	0.3	5
Trichloroethene	79-01-6	R-19	SW-846:8260, SW-846:8260B	VOC	Tp	9	0	µg/L	—	—	—	—	2.25555556	1	0.3	5
Trinitrobenzene[1,3,5-]	99-35-4	R-19	SW-846:8330, SW-846:8321A_MOD, SW-846:8330B, SW-846:8321A(M)	HEXP, LCMS/MS High Explosives, LCMS/MS Perchlorate	Tp	14	0	µg/L	—	—	—	—	0.2314	0.2785	0.0846	0.325
Trinitrotoluene[2,4,6-]	118-96-7	R-19	SW-846:8330, SW-846:8321A_MOD, SW-846:8330B, SW-846:8321A(M)	HEXP, LCMS/MS High Explosives, LCMS/MS Perchlorate	Tp	14	0	µg/L	—	—	—	—	0.21904286	0.258	0.0846	0.325
Tritium	H-3	R-19	EPA:906.0, Generic:LLEE, Generic:Low_Level_Tritium, Generic:Tritium	RAD	Tp	14	0	pCi/L	—	—	—	—	-5.3084143	0.0966	-158	80.5
Uranium	U	R-19	SW-846:6020	Inorganic	Tp	22	22	µg/L	0.2773182	0.2785	0.214	0.344	—	—	—	—
Uranium-234	U-234	R-19	Generic:Alpha-Spec, HASL-300:ISOU	RAD	Tp	19	19	pCi/L	0.2625263	0.256	0.192	0.332	—	—	—	—
Uranium-235/236	U-235/236	R-19	Generic:Alpha-Spec, HASL-300:ISOU	RAD	Tp	19	1	pCi/L	0.041	0.041	0.041	0.041	0.014425	0.00656	-0.0175	0.0929
Uranium-238	U-238	R-19	Generic:Alpha-Spec, HASL-300:ISOU	RAD	Tp	19	17	pCi/L	0.1134882	0.114	0.0786	0.171	0.0665	0.0665	0.0498	0.0832
Vanadium	V	R-19	SW-846:6010B, SW-846:6010C	Inorganic	Tp	22	20	µg/L	2.0715	1.945	1.2	3.1	2.43	2.43	2.18	2.68
Zinc	Zn	R-19	SW-846:6010B, SW-846:6010C	Inorganic	Tp	21	15	µg/L	9.164	5.73	3	44.4	10.49	10	7.64	17.2
Acenaphthene	83-32-9	R-25	SW-846:8270, SW-846:8270C	SVOC	Tpf	5	0	µg/L	—	—	—	—	1.058	1.06	1	1.1
Acenaphthylene	208-96-8	R-25	SW-846:8270, SW-846:8270C	SVOC	Tpf	5	0	µg/L	—	—	—	—	1.058	1.06	1	1.1
Acetone	67-64-1	R-25	SW-846:8260, SW-846:8260B	VOC	Tpf	18	2	µg/L	2.705	2.705	2.01	3.4	13.75	10	5	30
Acidity or alkalinity of a solution	pH	R-25	EPA:150.1	General Chemistry	Tpf	16	16	SU	7.518125	7.19	6.58	11.8	—	—	—	—
Alkalinity-CO3	ALK-CO3	R-25	EPA:310.1	General Chemistry	Tpf	16	1	µg/L	38,100	38,100	38,100	38,100	1223.33333	1000	725	4000
Alkalinity-CO3+HCO3	ALK-CO3+HCO3	R-25	EPA:310.1	General Chemistry	Tpf	16	16	µg/L	81600	68,000	59,400	286,000	—	—	—	—
Alkalinity-HCO3	ALK-HCO3	R-25	EPA:310.1	General Chemistry	Tpf	1	1	µg/L	75300	75,300	75,300	75,300	—	—	—	—
Aluminum	Al	R-25	SW-846:6010B, SW-846:6010C	Inorganic	Tpf	24	4	µg/L	235.75	131.5	76	604	173.6	200	68	200
Amino-2,6-dinitrotoluene[4-]	19406-51-0	R-25	SW-846:8330, SW-846:8321A_MOD, SW-846:8321A(M)	HEXP, LCMS/MS High Explosives, LCMS/MS Perchlorate	Tpf	20	2	µg/L	0.4945	0.4945	0.389	0.6	0.29916667	0.3045	0.1	1.04
Amino-4,6-dinitrotoluene[2-]	35572-78-2	R-25	SW-846:8330, SW-846:8321A_MOD, SW-846:8321A(M)	HEXP, LCMS/MS High Explosives, LCMS/MS Perchlorate	Tpf	20	4	µg/L	0.2635	0.1555	0.093	0.65	0.31	0.3045	0.1	1.04
Ammonia as nitrogen	NH3-N	R-25	EPA:350.1	General Chemistry	Tpf	16	8	µg/L	626.1	218.5	20	2660	44.475	40	10	106
Anthracene	120-12-7	R-25	SW-846:8270, SW-846:8270C	SVOC	Tpf	5	0	µg/L	—	—	—	—	1.058	1.06	1	1.1
Antimony	Sb	R-25	SW-846:6020	Inorganic	Tpf	24	1	µg/L	0.67	0.67	0.67	0.67	2.09913043	3	0.28	3

Table 4.2-1 (continued)

Parameter Name	Parameter Code	Well	Analytical Method	Analytical Method Category[a]	Geological Unit Code[a]	No. Samples	No. Detects	Unit	Mean Detect	Median Detect	Min Detect	Max Detect	Mean ND	Median ND	Min ND	Max ND
Arsenic	As	R-25	SW-846:6020, SW-846:6010B	Inorganic	Tpf	24	2	µg/L	2.295	2.295	1.7	2.89	4.32909091	5	1.5	6
Barium	Ba	R-25	SW-846:6010B, SW-846:6010C	Inorganic	Tpf	24	24	µg/L	21.708333	20.3	18.7	40.4	—	—	—	—
Benzo(g,h,i)perylene	191-24-2	R-25	SW-846:8270, SW-846:8270C	SVOC	Tpf	5	0	µg/L	—	—	—	—	1.058	1.06	1	1.1
Benzoic Acid	65-85-0	R-25	SW-846:8270, SW-846:8270C	SVOC	Tpf	4	0	µg/L	—	—	—	—	21.4	21.4	20.6	22.2
Beryllium	Be	R-25	SW-846:6010B, SW-846:6010C	Inorganic	Tpf	23	0	µg/L	—	—	—	—	3.95652174	5	1	5
Bis(2-ethylhexyl)phthalate	117-81-7	R-25	SW-846:8270, SW-846:8270C	SVOC	Tpf	5	0	µg/L	—	—	—	—	8.74	10.3	1.8	10.8
Bismuth-214	Bi-214	R-25	Generic:Gamma Spec.	RAD	Tpf	2	0	pCi/L	—	—	—	—	27.5	27.5	25	30
Boron	B	R-25	SW-846:6010B, SW-846:6010C	Inorganic	Tpf	24	24	µg/L	29.15	27.7	12.3	61.6	—	—	—	—
Bromide	Br(-1)	R-25	EPA:300.0	General Chemistry	Tpf	15	11	µg/L	103.50909	101	72	154	133	133	66	200
Bromodichloromethane	75-27-4	R-25	SW-846:8260, SW-846:8260B	VOC	Tpf	18	0	µg/L	—	—	—	—	1.88888889	1	1	5
Bromoform	75-25-2	R-25	SW-846:8260, SW-846:8260B	VOC	Tpf	18	0	µg/L	—	—	—	—	1.88888889	1	1	5
Butanone[2-]	78-93-3	R-25	SW-846:8260, SW-846:8260B	VOC	Tpf	18	0	µg/L	—	—	—	—	8.33333333	5	5	20
Cadmium	Cd	R-25	SW-846:6020	Inorganic	Tpf	24	0	µg/L	—	—	—	—	0.735	1	0.04	1
Calcium	Ca	R-25	SW-846:6010B, SW-846:6010C	Inorganic	Tpf	24	24	µg/L	34,870.833	24,250	18,600	106,000	—	—	—	—
Carbon disulfide	75-15-0	R-25	SW-846:8260, SW-846:8260B	VOC	Tpf	18	1	µg/L	1.36	1.36	1.36	1.36	5	5	5	5
Chloride	Cl(-1)	R-25	EPA:300.0	General Chemistry	Tpf	16	16	µg/L	8541.25	8075	6330	11,500	—	—	—	—
Chlorobenzene	108-90-7	R-25	SW-846:8260, SW-846:8260B	VOC	Tpf	18	3	µg/L	1.3066667	0.89	0.73	2.3	1.26666667	1	1	5
Chlorodibromomethane	124-48-1	R-25	SW-846:8260, SW-846:8260B	VOC	Tpf	18	0	µg/L	—	—	—	—	1.88888889	1	1	5
Chloroform	67-66-3	R-25	SW-846:8260, SW-846:8260B	VOC	Tpf	18	0	µg/L	—	—	—	—	1.88888889	1	1	5
Chloromethane	74-87-3	R-25	SW-846:8260, SW-846:8260B	VOC	Tpf	18	0	µg/L	—	—	—	—	3	1	1	10
Chromium	Cr	R-25	SW-846:6020, SW-846:6010B	Inorganic	Tpf	24	5	µg/L	3.546	4	2.04	4.6	7.35421053	10	1	10.7
Cobalt	Co	R-25	SW-846:6010B, SW-846:6010C	Inorganic	Tpf	24	4	µg/L	8.5875	6.735	1.18	19.7	3.70705	5	0.541	5
Copper	Cu	R-25	SW-846:6010B, SW-846:6010C	Inorganic	Tpf	23	2	µg/L	3.555	3.555	2.66	4.45	8.33333333	10	3	10
Cyanide (total)	CN (Total)	R-25	SW-846:9012A, EPA:335.3, EPA:335.4	General Chemistry, Inorganic	Tpf	8	1	µg/L	-1.47	-1.47	-1.47	-1.47	3.03142857	1.72	1.5	5
DNX	DNX	R-25	SW-846:8321A_MOD, SW-846:8330RDX	LCMS/MS High Explosives	Tpf	11	6	µg/L	0.1403333	0.1395	0.101	0.18	0.3766	0.5	0.11	0.5
Fluoranthene	206-44-0	R-25	SW-846:8270, SW-846:8270C	SVOC	Tpf	5	0	µg/L	—	—	—	—	1.058	1.06	1	1.1
Fluoride	F(-1)	R-25	EPA:300.0	General Chemistry	Tpf	16	14	µg/L	126.37857	111	67.9	277	44.15	44.15	33	55.3
Gross alpha	GrossA	R-25	EPA:900, Generic:GrossAB	RAD	Tpf	7	1	pCi/L	3.09	3.09	3.09	3.09	0.919	1.13	0.22	1.6
Gross beta	GrossB	R-25	EPA:900, Generic:GrossAB	RAD	Tpf	8	0	pCi/L	—	—	—	—	0.9251875	1.2	0.0316	1.7
Gross gamma	GrossG	R-25	EPA:901.1, Generic:Gross Gamma	RAD	Tpf	9	2	pCi/L	168.5	168.5	153	184	65.4257143	75.2	6.35	113
Hardness	Hardness	R-25	SM:A2340B, EPA:200.7	Inorganic	Tpf	24	24	µg/L	106,279.17	81,600	66,000	285,000	—	—	—	—
Heptachlor	76-44-8	R-25	SW-846:8081A	PESTPCB	Tpf	2	0	µg/L	—	—	—	—	0.02085	0.02085	0.02	0.0217
Hexachlorobutadiene	87-68-3	R-25	SW-846:8260, SW-846:8260B	VOC	Tpf	17	0	µg/L	—	—	—	—	1.94117647	1	1	5
HMX	2691-41-0	R-25	SW-846:8330, SW-846:8321A_MOD, SW-846:8321A(M)	HEXP, LCMS/MS High Explosives, LCMS/MS Perchlorate	Tpf	20	7	µg/L	1.0585714	0.134	0.115	4.9	0.36676923	0.325	0.08	1.04

Table 4.2-1 (continued)

Parameter Name	Parameter Code	Well	Analytical Method	Analytical Method Category[a]	Geological Unit Code[a]	No. Samples	No. Detects	Unit	Mean Detect	Median Detect	Min Detect	Max Detect	Mean ND	Median ND	Min ND	Max ND
Iron	Fe	R-25	SW-846:6010B, SW-846:6010C	Inorganic	Tpf	24	13	µg/L	157.93846	153	32.3	524	77.5363636	100	18	168
Lead	Pb	R-25	SW-846:6020	Inorganic	Tpf	24	1	µg/L	0.336	0.336	0.336	0.336	1.60869565	2	0.5	2
Magnesium	Mg	R-25	SW-846:6010B, SW-846:6010C	Inorganic	Tpf	24	23	µg/L	4865.2174	4970	3660	5610	300	300	300	300
Manganese	Mn	R-25	SW-846:6010B, SW-846:6010C	Inorganic	Tpf	24	20	µg/L	18.5145	9.215	2	52.7	10	10	10	10
Mercury	Hg	R-25	EPA:245.2, EPA:245.1	Inorganic	Tpf	26	0	µg/L	—	—	—	—	0.22758462	0.2	0.0472	2
Methyl tert-butyl ether	1634-04-4	R-25	SW-846:8260B	VOC	Tpf	9	9	µg/L	1.1044444	1.09	0.94	1.31	—	—	—	—
Methyl-2-pentanone[4-]	108-10-1	R-25	SW-846:8260, SW-846:8260B	VOC	Tpf	18	0	µg/L	—	—	—	—	8.33333333	5	5	20
Methylene chloride	75-09-2	R-25	SW-846:8260, SW-846:8260B	VOC	Tpf	18	1	µg/L	0.85	0.85	0.85	0.85	6.72352941	5.8	1.1	10
MNX	MNX	R-25	SW-846:8321A_MOD, SW-846:8330RDX	LCMS/MS High Explosives	Tpf	11	10	µg/L	0.2203	0.197	0.13	0.42	0.5	0.5	0.5	0.5
Molybdenum	Mo	R-25	SW-846:6020, SW-846:6010B	Inorganic	Tpf	24	9	µg/L	1.2185556	0.414	0.294	7.4	1.20706667	0.623	0.39	2.5
Nickel	Ni	R-25	SW-846:6020, SW-846:6010B	Inorganic	Tpf	24	21	µg/L	3.3219048	2.71	0.75	11	2.00333333	1.96	1.4	2.65
Nitrate-nitrite as nitrogen	NO3+NO2-N	R-25	EPA:353.2, EPA:353.1	General Chemistry	Tpf	16	12	µg/L	677.125	763.5	58.5	1230	91.5	53	10	250
Nitrotoluene[2-]	88-72-2	R-25	SW-846:8330, SW-846:8321A_MOD, SW-846:8321A(M)	HEXP, LCMS/MS High Explosives, LCMS/MS Perchlorate	Tpf	20	2	µg/L	0.602	0.602	0.104	1.1	0.39072222	0.325	0.1	1.04
Perchlorate	ClO4	R-25	SW-846:6850, EPA:314.0, SW846 6850 Modified	LCMS/MS Perchlorate, General Chemistry	Tpf	15	13	µg/L	0.3514077	0.452	0.0521	0.53	2.1	2.1	0.2	4
Phenanthrene	85-01-8	R-25	SW-846:8270, SW-846:8270C	SVOC	Tpf	4	0	µg/L	—	—	—	—	1.065	1.08	1	1.1
Potassium	K	R-25	SW-846:6010B, SW-846:6010C	Inorganic	Tpf	24	24	µg/L	1095.9583	701	401	10300	—	—	—	—
Pyrene	129-00-0	R-25	SW-846:8270, SW-846:8270C	SVOC	Tpf	5	0	µg/L	—	—	—	—	1.058	1.06	1	1.1
RDX	121-82-4	R-25	SW-846:8330, SW-846:8321A_MOD, SW-846:8321A(M)	HEXP, LCMS/MS High Explosives, LCMS/MS Perchlorate	Tpf	20	18	µg/L	14.17	14.75	1.9	26.7	7.95	7.95	3.4	12.5
Selenium	Se	R-25	SW-846:6020, SW-846:6010B	Inorganic	Tpf	24	0	µg/L	—	—	—	—	4.28375	5	2.5	5
Silicon dioxide	SiO2	R-25	SW-846:6010B, SW-846:6010C	Inorganic	Tpf	17	17	µg/L	51,464.706	53,900	12,500	56,700	—	—	—	—
Silver	Ag	R-25	SW-846:6020, SW-846:6010B	Inorganic	Tpf	24	1	µg/L	0.87	0.87	0.87	0.87	0.81891304	1	0.2	1
Sodium	Na	R-25	SW-846:6010B, SW-846:6010C	Inorganic	Tpf	24	24	µg/L	9452.0833	9505	5680	19600	—	—	—	—
Strontium	Sr	R-25	SW-846:6010B, SW-846:6010C	Inorganic	Tpf	24	24	µg/L	139.67083	115	96.9	366	—	—	—	—
Styrene	100-42-5	R-25	SW-846:8260, SW-846:8260B	VOC	Tpf	18	1	µg/L	1	1	1	1	1.70588235	1	1	5
Sulfate	SO4(-2)	R-25	EPA:300.0	General Chemistry	Tpf	16	16	µg/L	30,841.25	19,800	9310	207,000	—	—	—	—
Suspended sediment Concentration	SSC	R-25	EPA:160.2	General Chemistry	Tpf	1	1	µg/L	8000	8000	8000	8000	—	—	—	—
Tetrachloroethene	127-18-4	R-25	SW-846:8260, SW-846:8260B	VOC	Tpf	18	11	µg/L	0.7654545	0.83	0.31	1.21	3.28571429	5	1	5
Thallium	Tl	R-25	SW-846:6020	Inorganic	Tpf	24	2	µg/L	0.53	0.53	0.41	0.65	1.19659091	1	0.02	2
Tin	Sn	R-25	SW-846:6010B, SW-846:6010C	Inorganic	Tpf	24	1	µg/L	2.51	2.51	2.51	2.51	22.5330435	10	2.5	100
TNX	TNX	R-25	SW-846:8321A_MOD, SW-846:8330RDX	LCMS/MS High Explosives	Tpf	11	8	µg/L	0.1475	0.1395	0.12	0.2	0.362	0.5	0.086	0.5

Table 4.2-1 (continued)

Parameter Name	Parameter Code	Well	Analytical Method	Analytical Method Category[a]	Geological Unit Code[a]	No. Samples	No. Detects	Unit	Mean Detect	Median Detect	Min Detect	Max Detect	Mean ND	Median ND	Min ND	Max ND
Toluene	108-88-3	R-25	SW-846:8260, SW-846:8260B	VOC	Tpf	17	5	µg/L	4.128	0.94	0.24	15	0.98416667	1	0.81	1
Total dissolved solids	TDS	R-25	EPA:160.1	General Chemistry	Tpf	16	16	µg/L	188,812.5	160,500	117,000	459,000	—	—	—	—
Total Kjeldahl nitrogen	TKN	R-25	EPA:351.2	General Chemistry	Tpf	12	5	µg/L	111.04	105	13	189	89.8571429	100	29	100
Total organic carbon	TOC	R-25	SW-846:9060	General Chemistry	Tpf	10	9	µg/L	1227.5556	928	617	3040	330	330	330	330
Total phosphate as phosphorus	PO4-P	R-25	EPA:365.4	General Chemistry	Tpf	16	11	µg/L	401.31818	122	35	3350	123.92	128	75.6	174
Total suspended solids	TSS	R-25	EPA:160.2	General Chemistry	Tpf	1	1	µg/L	2400	2400	2400	2400	—	—	—	—
Trichlorobenzene[1,2,3-]	87-61-6	R-25	SW-846:8260, SW-846:8260B	VOC	Tpf	15	0	µg/L	—	—	—	—	2.06666667	1	1	5
Trichloroethene	79-01-6	R-25	SW-846:8260, SW-846:8260B	VOC	Tpf	18	12	µg/L	0.60375	0.615	0.31	0.9	3.66666667	5	1	5
Trinitrobenzene[1,3,5-]	99-35-4	R-25	SW-846:8330, SW-846:8321A_MOD, SW-846:8321A(M)	HEXP, LCMS/MS High Explosives, LCMS/MS Perchlorate	Tpf	20	1	µg/L	0.315	0.315	0.315	0.315	0.29763158	0.284	0.1	1.04
Trinitrotoluene[2,4,6-]	118-96-7	R-25	SW-846:8330, SW-846:8321A_MOD, SW-846:8321A(M)	HEXP, LCMS/MS High Explosives, LCMS/MS Perchlorate	Tpf	20	1	µg/L	0.36	0.36	0.36	0.36	0.29763158	0.284	0.1	1.04
Tritium	H-3	R-25	Generic:Tritium, EPA:906.0, Generic:LLEE, Generic:Low_Level_Tritium, Generic:LSC	RAD	Tpf	11	10	pCi/L	38.42104	34.293	30.654	67.942	0	0	0	0
Uranium	U	R-25	SW-846:6020	Inorganic	Tpf	24	23	µg/L	0.5863478	0.614	0.127	0.812	0.2	0.2	0.2	0.2
Uranium-234	U-234	R-25	HASL-300:ISOU	RAD	Tpf	15	13	pCi/L	0.4541538	0.4	0.315	0.733	0.11015	0.11015	0.0213	0.199
Uranium-235/236	U-235/236	R-25	HASL-300:ISOU	RAD	Tpf	15	0	pCi/L	—	—	—	—	0.022762	0.022	0.00296	0.0545
Uranium-238	U-238	R-25	HASL-300:ISOU	RAD	Tpf	15	14	pCi/L	0.2772143	0.225	0.15	0.47	0.00776	0.00776	0.00776	0.00776
Vanadium	V	R-25	SW-846:6010B, SW-846:6010C	Inorganic	Tpf	24	7	µg/L	2.1542857	1.2	1.01	7.7	3.90588235	5	1	5
Zinc	Zn	R-25	SW-846:6010B, SW-846:6010C	Inorganic	Tpf	24	19	µg/L	8.2105263	7.4	2.4	20.1	8.994	9.27	7.8	10
Acenaphthene	83-32-9	R-25b	SW-846:8270C, SW-846:8270DGCMS_SIM, SW-846:8310	SVOC	Qbo	4	0	µg/L	—	—	—	—	0.55875	0.5075	0.1	1.12
Acenaphthylene	208-96-8	R-25b	SW-846:8270C, SW-846:8270DGCMS_SIM, SW-846:8310	SVOC	Qbo	4	0	µg/L	—	—	—	—	0.55875	0.5075	0.1	1.12
Acetone	67-64-1	R-25b	SW-846:8260B	VOC	Qbo	11	0	µg/L	—	—	—	—	9.63181818	10	5.95	10
Acidity or alkalinity of a solution	pH	R-25b	EPA:150.1	General Chemistry	Qbo	18	18	SU	7.6711111	7.71	7.23	7.91	—	—	—	—
Alkalinity-CO3	ALK-CO3	R-25b	EPA:310.1	General Chemistry	Qbo	18	0	µg/L	—	—	—	—	1277.77778	1000	1000	4000
Alkalinity-CO3+HCO3	ALK-CO3+HCO3	R-25b	EPA:310.1	General Chemistry	Qbo	18	18	µg/L	72,988.889	66,900	54,600	123,000	—	—	—	—
Aluminum	Al	R-25b	SW-846:6010B, SW-846:6010C	Inorganic	Qbo	19	8	µg/L	400.875	274.5	111	1010	200	200	200	200
Amino-2,6-dinitrotoluene[4-]	19406-51-0	R-25b	SW-846:8321A_MOD	LCMS/MS High Explosives	Qbo	11	2	µg/L	0.143	0.143	0.117	0.169	0.266	0.266	0.255	0.275
Amino-4,6-dinitrotoluene[2-]	35572-78-2	R-25b	SW-846:8321A_MOD	LCMS/MS High Explosives	Qbo	11	1	µg/L	0.165	0.165	0.165	0.165	0.2778	0.2675	0.255	0.325
Ammonia as nitrogen	NH3-N	R-25b	EPA:350.1	General Chemistry	Qbo	18	9	µg/L	74.722222	75.9	17.8	172	43.6666667	48.2	31	50

Table 4.2-1 (continued)

Parameter Name	Parameter Code	Well	Analytical Method	Analytical Method Category[a]	Geological Unit Code[a]	No. Samples	No. Detects	Unit	Mean Detect	Median Detect	Min Detect	Max Detect	Mean ND	Median ND	Min ND	Max ND
Anthracene	120-12-7	R-25b	SW-846:8270C, SW-846:8270DGCMS_SIM, SW-846:8310	SVOC	Qbo	4	0	µg/L	—	—	—	—	0.55875	0.5075	0.1	1.12
Antimony	Sb	R-25b	SW-846:6020	Inorganic	Qbo	19	1	µg/L	1.26	1.26	1.26	1.26	2.94444444	3	2	3
Arsenic	As	R-25b	SW-846:6020	Inorganic	Qbo	19	11	µg/L	3.4554545	3.39	1.94	5.37	5	5	5	5
Barium	Ba	R-25b	SW-846:6010B, SW-846:6010C	Inorganic	Qbo	19	18	µg/L	17.062222	12.45	8.41	40.6	14.8	14.8	14.8	14.8
Benzo(g,h,i)perylene	191-24-2	R-25b	SW-846:8270C, SW-846:8270DGCMS_SIM, SW-846:8310	SVOC	Qbo	4	0	µg/L	—	—	—	—	0.330375	0.0755	0.0505	1.12
Benzoic Acid	65-85-0	R-25b	SW-846:8270C, SW-846:8270D	SVOC	Qbo	4	0	µg/L	—	—	—	—	18.525	20.4	10.8	22.5
Beryllium	Be	R-25b	SW-846:6010B, SW-846:6010C	Inorganic	Qbo	19	0	µg/L	—	—	—	—	5	5	5	5
Bis(2-ethylhexyl)phthalate	117-81-7	R-25b	SW-846:8270C, SW-846:8270D	SVOC	Qbo	4	0	µg/L	—	—	—	—	9.245	10.2	5.38	11.2
Boron	B	R-25b	SW-846:6010B, SW-846:6010C	Inorganic	Qbo	19	12	µg/L	23.483333	20.7	15.5	51.4	46.6714286	50	26.7	50
Bromide	Br(-1)	R-25b	EPA:300.0	General Chemistry	Qbo	18	2	µg/L	73	73	71.4	74.6	200	200	200	200
Bromodichloromethane	75-27-4	R-25b	SW-846:8260B	VOC	Qbo	11	2	µg/L	1.63	1.63	1.08	2.18	1	1	1	1
Bromoform	75-25-2	R-25b	SW-846:8260B	VOC	Qbo	11	2	µg/L	1.255	1.255	0.72	1.79	1	1	1	1
Butanone[2-]	78-93-3	R-25b	SW-846:8260B	VOC	Qbo	11	0	µg/L	—	—	—	—	5	5	5	5
Cadmium	Cd	R-25b	SW-846:6020	Inorganic	Qbo	19	0	µg/L	—	—	—	—	1	1	1	1
Calcium	Ca	R-25b	SW-846:6010B, SW-846:6010C	Inorganic	Qbo	19	19	µg/L	11,548.947	11,700	6240	14,900	—	—	—	—
Carbon disulfide	75-15-0	R-25b	SW-846:8260B	VOC	Qbo	11	0	µg/L	—	—	—	—	5	5	5	5
Chloride	Cl(-1)	R-25b	EPA:300.0	General Chemistry	Qbo	18	18	µg/L	2531.1111	2085	1770	4850	—	—	—	—
Chlorobenzene	108-90-7	R-25b	SW-846:8260B	VOC	Qbo	11	0	µg/L	—	—	—	—	1	1	1	1
Chlorodibromomethane	124-48-1	R-25b	SW-846:8260B	VOC	Qbo	11	2	µg/L	2.255	2.255	1.47	3.04	1	1	1	1
Chloroform	67-66-3	R-25b	SW-846:8260B	VOC	Qbo	11	2	µg/L	2.855	2.855	1.62	4.09	1	1	1	1
Chloromethane	74-87-3	R-25b	SW-846:8260B	VOC	Qbo	11	0	µg/L	—	—	—	—	1	1	1	1
Chromium	Cr	R-25b	SW-846:6020	Inorganic	Qbo	19	6	µg/L	3.7016667	3.675	1.7	5.34	9.55384615	10	4.2	10
Cobalt	Co	R-25b	SW-846:6010B, SW-846:6010C	Inorganic	Qbo	19	2	µg/L	3.815	3.815	2.2	5.43	5	5	5	5
Copper	Cu	R-25b	SW-846:6010B, SW-846:6010C	Inorganic	Qbo	19	7	µg/L	8.6957143	7.47	3.99	15.9	10	10	10	10
Cyanide (total)	CN (Total)	R-25b	EPA:335.3, EPA:335.4	Inorganic	Qbo	10	0	µg/L	—	—	—	—	5	5	5	5
DNX	DNX	R-25b	SW-846:8321A_MOD, SW-846:8330RDX	LCMS/MS High Explosives	Qbo	9	0	µg/L	—	—	—	—	0.318	0.266	0.255	0.5
Fluoranthene	206-44-0	R-25b	SW-846:8270C, SW-846:8270DGCMS_SIM, SW-846:8310	SVOC	Qbo	4	0	µg/L	—	—	—	—	0.330375	0.0755	0.0505	1.12
Fluoride	F(-1)	R-25b	EPA:300.0	General Chemistry	Qbo	18	18	µg/L	130.86111	129.5	54.8	226	—	—	—	—
Gross alpha	GrossA	R-25b	EPA:900	RAD	Qbo	3	1	pCi/L	3.92	3.92	3.92	3.92	0.69825	0.69825	-0.0235	1.42
Gross beta	GrossB	R-25b	EPA:900	RAD	Qbo	3	3	pCi/L	2.96	3.68	1.42	3.78	—	—	—	—
Gross gamma	GrossG	R-25b	EPA:901.1	RAD	Qbo	2	0	pCi/L	—	—	—	—	31.8	31.8	25.8	37.8
Hardness	Hardness	R-25b	SM:A2340B	Inorganic	Qbo	19	19	µg/L	44,163.158	45,200	24,800	52,300	—	—	—	—
Hexachlorobutadiene	87-68-3	R-25b	SW-846:8260B	VOC	Qbo	11	0	µg/L	—	—	—	—	1	1	1	1
HMX	2691-41-0	R-25b	SW-846:8321A_MOD	LCMS/MS High Explosives	Qbo	12	9	µg/L	0.3321111	0.271	0.155	0.656	0.26666667	0.266	0.265	0.269

Table 4.2-1 (continued)

Parameter Name	Parameter Code	Well	Analytical Method	Analytical Method Category[a]	Geological Unit Code[a]	No. Samples	No. Detects	Unit	Mean Detect	Median Detect	Min Detect	Max Detect	Mean ND	Median ND	Min ND	Max ND
Iron	Fe	R-25b	SW-846:6010B, SW-846:6010C	Inorganic	Qbo	19	10	µg/L	214.27	143	32.5	600	94.1222222	100	47.1	100
Lead	Pb	R-25b	SW-846:6020	Inorganic	Qbo	19	5	µg/L	1.1822	0.819	0.512	2.25	2	2	2	2
Magnesium	Mg	R-25b	SW-846:6010B, SW-846:6010C	Inorganic	Qbo	19	19	µg/L	3722.6316	3750	2230	4400	—	—	—	—
Manganese	Mn	R-25b	SW-846:6010B, SW-846:6010C	Inorganic	Qbo	19	10	µg/L	37.551	24.3	4.3	102	10	10	10	10
Mercury	Hg	R-25b	EPA:245.2	Inorganic	Qbo	26	0	µg/L	—	—	—	—	0.2	0.2	0.2	0.2
Methyl tert-butyl ether	1634-04-4	R-25b	SW-846:8260B	VOC	Qbo	11	0	µg/L	—	—	—	—	1	1	1	1
Methyl-2-pentanone[4-]	108-10-1	R-25b	SW-846:8260B	VOC	Qbo	11	0	µg/L	—	—	—	—	5	5	5	5
Methylene chloride	75-09-2	R-25b	SW-846:8260B	VOC	Qbo	11	0	µg/L	—	—	—	—	10	10	10	10
MNX	MNX	R-25b	SW-846:8321A_MOD, SW-846:8330RDX	LCMS/MS High Explosives	Qbo	9	0	µg/L	—	—	—	—	0.318	0.266	0.255	0.5
Molybdenum	Mo	R-25b	SW-846:6020	Inorganic	Qbo	19	18	µg/L	9.3607222	4.115	0.62	40.3	0.965	0.965	0.965	0.965
Nickel	Ni	R-25b	SW-846:6020	Inorganic	Qbo	19	15	µg/L	2.3094667	2.13	0.627	5.6	1.79	2	1.16	2
Nitrate-nitrite as nitrogen	NO3+NO2-N	R-25b	EPA:353.2	General Chemistry	Qbo	18	17	µg/L	538.95882	597	41.3	930	715	715	715	715
Nitrotoluene[2-]	88-72-2	R-25b	SW-846:8321A_MOD	LCMS/MS High Explosives	Qbo	11	0	µg/L	—	—	—	—	0.27672727	0.266	0.255	0.325
Perchlorate	ClO4	R-25b	SW-846:6850	LCMS/MS Perchlorate	Qbo	16	16	µg/L	0.2810625	0.289	0.208	0.313	—	—	—	—
Phenanthrene	85-01-8	R-25b	SW-846:8270C, SW-846:8270DGCMS_SIM, SW-846:8310	SVOC	Qbo	4	0	µg/L	—	—	—	—	0.55875	0.5075	0.1	1.12
Potassium	K	R-25b	SW-846:6010B, SW-846:6010C	Inorganic	Qbo	19	19	µg/L	1893.6842	1420	1180	4220	—	—	—	—
Pyrene	129-00-0	R-25b	SW-846:8270C, SW-846:8270DGCMS_SIM, SW-846:8310	SVOC	Qbo	4	0	µg/L	—	—	—	—	0.330375	0.0755	0.0505	1.12
Radium-226	Ra-226	R-25b	EPA:903.1	RAD	Qbo	1	1	pCi/L	1.27	1.27	1.27	1.27	—	—	—	—
Radium-228	Ra-228	R-25b	EPA:904	RAD	Qbo	1	1	pCi/L	0.879	0.879	0.879	0.879	—	—	—	—
RDX	121-82-4	R-25b	SW-846:8321A_MOD	LCMS/MS High Explosives	Qbo	12	12	µg/L	3.5201667	3.36	0.144	8.49	—	—	—	—
Selenium	Se	R-25b	SW-846:6020	Inorganic	Qbo	19	0	µg/L	—	—	—	—	5	5	5	5
Silicon dioxide	SiO2	R-25b	SW-846:6010B, SW-846:6010C	Inorganic	Qbo	18	18	µg/L	57,422.222	56,200	49,300	69,800	—	—	—	—
Silver	Ag	R-25b	SW-846:6020	Inorganic	Qbo	19	0	µg/L	—	—	—	—	1	1	1	1
Sodium	Na	R-25b	SW-846:6010B, SW-846:6010C	Inorganic	Qbo	19	19	µg/L	47,714.211	14,100	8710	246,000	—	—	—	—
Strontium	Sr	R-25b	SW-846:6010B, SW-846:6010C	Inorganic	Qbo	19	19	µg/L	73.457895	72.2	50.8	91.9	—	—	—	—
Styrene	100-42-5	R-25b	SW-846:8260B	VOC	Qbo	11	0	µg/L	—	—	—	—	1	1	1	1
Sulfate	SO4(-2)	R-25b	EPA:300.0	General Chemistry	Qbo	18	18	µg/L	7283.3333	4615	2250	21000	—	—	—	—
Tetrachloroethene	127-18-4	R-25b	SW-846:8260B	VOC	Qbo	11	3	µg/L	0.3433333	0.33	0.32	0.38	1	1	1	1
Thallium	Tl	R-25b	SW-846:6020	Inorganic	Qbo	19	0	µg/L	—	—	—	—	1.66968421	2	0.724	2
Tin	Sn	R-25b	SW-846:6010B, SW-846:6010C	Inorganic	Qbo	19	3	µg/L	6.2566667	4.46	3.91	10.4	17.5	10	10	50
TNX	TNX	R-25b	SW-846:8321A_MOD, SW-846:8330RDX	LCMS/MS High Explosives	Qbo	9	0	µg/L	—	—	—	—	0.318	0.266	0.255	0.5
Toluene	108-88-3	R-25b	SW-846:8260B	VOC	Qbo	11	0	µg/L	—	—	—	—	1	1	1	1

Table 4.2-1 (continued)

Parameter Name	Parameter Code	Well	Analytical Method	Analytical Method Category[a]	Geological Unit Code[a]	No. Samples	No. Detects	Unit	Mean Detect	Median Detect	Min Detect	Max Detect	Mean ND	Median ND	Min ND	Max ND
Total dissolved solids	TDS	R-25b	EPA:160.1	General Chemistry	Qbo	18	18	µg/L	373,150	124,500	32,900	2E+06	—	—	—	—
Total Kjeldahl nitrogen	TKN	R-25b	EPA:351.2	General Chemistry	Qbo	12	4	µg/L	193.85	139	89.4	408	119.25	100	100	254
Total organic carbon	TOC	R-25b	SW-846:9060	General Chemistry	Qbo	12	12	µg/L	145,859.08	861.5	505	693,000	—	—	—	—
Total phosphate as phosphorus	PO4-P	R-25b	EPA:365.4	General Chemistry	Qbo	18	13	µg/L	139.94615	119	19.5	531	97.36	106	50	143
Trichlorobenzene[1,2,3-]	87-61-6	R-25b	SW-846:8260B	VOC	Qbo	11	0	µg/L	—	—	—	—	1	1	1	1
Trichloroethene	79-01-6	R-25b	SW-846:8260B	VOC	Qbo	11	0	µg/L	—	—	—	—	1	1	1	1
Trinitrobenzene[1,3,5-]	99-35-4	R-25b	SW-846:8321A_MOD	LCMS/MS High Explosives	Qbo	11	0	µg/L	—	—	—	—	0.27672727	0.266	0.255	0.325
Trinitrotoluene[2,4,6-]	118-96-7	R-25b	SW-846:8321A_MOD	LCMS/MS High Explosives	Qbo	11	0	µg/L	—	—	—	—	0.27672727	0.266	0.255	0.325
Tritium	H-3	R-25b	Generic:Low_Level_Tritium	RAD	Qbo	1	0	pCi/L	—	—	—	—	1.289	1.289	1.289	1.289
Uranium	U	R-25b	SW-846:6020	Inorganic	Qbo	19	19	µg/L	1.1376842	1.11	0.264	3.12	—	—	—	—
Uranium-234	U-234	R-25b	HASL-300:ISOU	RAD	Qbo	4	4	pCi/L	1.10425	1.22	0.207	1.77	—	—	—	—
Uranium-235/236	U-235/236	R-25b	HASL-300:ISOU	RAD	Qbo	4	1	pCi/L	0.0615	0.0615	0.0615	0.0615	0.01793333	0.014	0.0118	0.028
Uranium-238	U-238	R-25b	HASL-300:ISOU	RAD	Qbo	4	4	pCi/L	0.3875	0.433	0.13	0.554	—	—	—	—
Vanadium	V	R-25b	SW-846:6010B, SW-846:6010C	Inorganic	Qbo	19	19	µg/L	3.0047368	2.8	2	6.41	—	—	—	—
Zinc	Zn	R-25b	SW-846:6010B, SW-846:6010C	Inorganic	Qbo	19	18	µg/L	110.92222	29	7.5	1420	10	10	10	10
Acenaphthene	83-32-9	R-26	SW-846:8270C, SW-846:8270D, SW-846:8270DGCMS_SIM, SW-846:8310	SVOC	Qct	14	0	µg/L	—	—	—	—	0.88428571	1.04	0.1	1.2
Acenaphthylene	208-96-8	R-26	SW-846:8270C, SW-846:8270D, SW-846:8270DGCMS_SIM, SW-846:8310	SVOC	Qct	14	0	µg/L	—	—	—	—	0.88428571	1.04	0.1	1.2
Acetone	67-64-1	R-26	SW-846:8260B	VOC	Qct	23	2	µg/L	9.645	9.645	4.79	14.5	6.18952381	5	1.5	10
Acidity or alkalinity of a solution	pH	R-26	EPA:150.1	General Chemistry	Qct	24	24	SU	7.7279167	7.725	7.33	7.96	—	—	—	—
Alkalinity-CO3	ALK-CO3	R-26	EPA:310.1	General Chemistry	Qct	25	0	µg/L	—	—	—	—	1224	1000	725	4000
Alkalinity-CO3+HCO3	ALK-CO3+HCO3	R-26	EPA:310.1	General Chemistry	Qct	27	27	µg/L	48,874.074	47,300	43,200	94,500	—	—	—	—
Alkalinity-HCO3	ALK-HCO3	R-26	EPA:310.1	General Chemistry	Qct	1	1	µg/L	47,600	47,600	47,600	47,600	—	—	—	—
Aluminum	Al	R-26	SW-846:6010B, SW-846:6010C	Inorganic	Qct	38	0	µg/L	—	—	—	—	134	134	68	200
Amino-2,6-dinitrotoluene[4-]	19406-51-0	R-26	SW-846:8330, SW-846:8321A_MOD, SW-846:8330B	HEXP, LCMS/MS High Explosives	Qct	23	0	µg/L	—	—	—	—	0.31073043	0.273	0.0833	1
Amino-4,6-dinitrotoluene[2-]	35572-78-2	R-26	SW-846:8330, SW-846:8321A_MOD, SW-846:8330B	HEXP, LCMS/MS High Explosives	Qct	23	0	µg/L	—	—	—	—	0.31073043	0.273	0.0833	1
Ammonia as nitrogen	NH3-N	R-26	EPA:350.1	General Chemistry	Qct	25	8	µg/L	49.1625	37	18.5	115	60.4529412	50	10	250
Anthracene	120-12-7	R-26	SW-846:8270C, SW-846:8270D, SW-846:8270DGCMS_SIM, SW-846:8310	SVOC	Qct	14	0	µg/L	—	—	—	—	0.88428571	1.04	0.1	1.2
Antimony	Sb	R-26	SW-846:6020	Inorganic	Qct	38	0	µg/L	—	—	—	—	1.68421053	1.5	0.5	3
Arsenic	As	R-26	SW-846:6010B, SW-846:6020	Inorganic	Qct	38	8	µg/L	2.44	2.39	1.7	3.48	4.46666667	5	1.5	6
Barium	Ba	R-26	SW-846:6010B, SW-846:6010C	Inorganic	Qct	38	37	µg/L	7.7756757	7.7	6.39	10	9.45	9.45	9.45	9.45

Table 4.2-1 (continued)

Parameter Name	Parameter Code	Well	Analytical Method	Analytical Method Category[a]	Geological Unit Code[a]	No. Samples	No. Detects	Unit	Mean Detect	Median Detect	Min Detect	Max Detect	Mean ND	Median ND	Min ND	Max ND
Benzo(g,h,i)perylene	191-24-2	R-26	SW-846:8270C, SW-846:8270D, SW-846:8270DGCMS_SIM, SW-846:8310	SVOC	Qct	14	0	µg/L	—	—	—	—	0.8155	1.04	0.0521	1.2
Benzoic acid	65-85-0	R-26	SW-846:8270C, SW-846:8270D	SVOC	Qct	13	1	µg/L	14.6	14.6	14.6	14.6	19.6583333	21.5	6	24.1
Beryllium	Be	R-26	SW-846:6010B, SW-846:6010C, SW-846:6020	Inorganic	Qct	38	0	µg/L	—	—	—	—	2.85789474	3	0.1	5
Bis(2-ethylhexyl)phthalate	117-81-7	R-26	SW-846:8270C, SW-846:8270D	SVOC	Qct	13	0	µg/L	—	—	—	—	9.19153846	10.2	3	12
Bismuth-214	Bi-214	R-26	EPA:901.1	RAD	Qct	3	1	pCi/L	13.8	13.8	13.8	13.8	4.67	4.67	3.41	5.93
Boron	B	R-26	SW-846:6010B, SW-846:6010C	Inorganic	Qct	38	1	µg/L	13.3	13.3	13.3	13.3	30.1351351	15	10	50
Bromide	Br(-1)	R-26	EPA:300.0	General Chemistry	Qct	27	2	µg/L	74.25	74.25	70.2	78.3	131.88	200	41	200
Bromodichloromethane	75-27-4	R-26	SW-846:8260B	VOC	Qct	24	0	µg/L	—	—	—	—	0.85416667	1	0.3	1
Bromoform	75-25-2	R-26	SW-846:8260B	VOC	Qct	24	0	µg/L	—	—	—	—	0.85416667	1	0.3	1
Butanone[2-]	78-93-3	R-26	SW-846:8260B	VOC	Qct	24	0	µg/L	—	—	—	—	4.27083333	5	1.5	5
Cadmium	Cd	R-26	SW-846:6020	Inorganic	Qct	38	1	µg/L	0.18	0.18	0.18	0.18	0.56540541	0.3	0.1	1
Calcium	Ca	R-26	SW-846:6010B, SW-846:6010C	Inorganic	Qct	38	38	µg/L	7576.0526	7520	7150	8600	—	—	—	—
Carbon disulfide	75-15-0	R-26	SW-846:8260B	VOC	Qct	24	0	µg/L	—	—	—	—	4.27083333	5	1.5	5
Chloride	Cl(-1)	R-26	EPA:300.0	General Chemistry	Qct	27	27	µg/L	1172.5926	1180	1060	1250	—	—	—	—
Chlorobenzene	108-90-7	R-26	SW-846:8260B	VOC	Qct	24	0	µg/L	—	—	—	—	0.85416667	1	0.3	1
Chlorodibromomethane	124-48-1	R-26	SW-846:8260B	VOC	Qct	24	0	µg/L	—	—	—	—	0.85416667	1	0.3	1
Chloroform	67-66-3	R-26	SW-846:8260B	VOC	Qct	24	0	µg/L	—	—	—	—	0.85416667	1	0.3	1
Chloromethane	74-87-3	R-26	SW-846:8260B	VOC	Qct	24	1	µg/L	0.36	0.36	0.36	0.36	0.84782609	1	0.3	1
Chromium	Cr	R-26	SW-846:6010B, SW-846:6020	Inorganic	Qct	38	20	µg/L	4.311	2.76	1.6	25.1	5.63111111	3.88	1	10
Cobalt	Co	R-26	SW-846:6010B, SW-846:6010C	Inorganic	Qct	38	1	µg/L	1.1	1.1	1.1	1.1	3.05405405	5	1	5
Copper	Cu	R-26	SW-846:6010B, SW-846:6010C	Inorganic	Qct	34	0	µg/L	—	—	—	—	6.91176471	10	3	10
Cyanide (total)	CN (Total)	R-26	SW-846:9012A, EPA:335.3, EPA:335.4	General Chemistry, Inorganic	Qct	22	2	µg/L	4.94	4.94	3.97	5.91	2.944	2.265	1.5	5
DNX	DNX	R-26	SW-846:8321A_MOD, SW-846:8330B, SW-846:8330RDX	LCMS/MS High Explosives	Qct	17	0	µg/L	—	—	—	—	0.32107647	0.273	0.0833	0.5
Fluoranthene	206-44-0	R-26	SW-846:8270C, SW-846:8270D, SW-846:8270DGCMS_SIM, SW-846:8310	SVOC	Qct	14	0	µg/L	—	—	—	—	0.8155	1.04	0.0521	1.2
Fluoride	F(-1)	R-26	EPA:300.0	General Chemistry	Qct	27	25	µg/L	121.884	114	38.7	273	97.5	97.5	30	165
Gross alpha	GrossA	R-26	EPA:900	RAD	Qct	10	0	pCi/L	—	—	—	—	0.08996	0.2043	-1.35	1.56
Gross beta	GrossB	R-26	EPA:900	RAD	Qct	10	6	pCi/L	3.14	3.255	1.96	3.85	1.17025	0.9465	0.218	2.57
Gross gamma	GrossG	R-26	EPA:901.1	RAD	Qct	6	0	pCi/L	—	—	—	—	64.9166667	68.65	14	101
Hardness	Hardness	R-26	SM:A2340B	Inorganic	Qct	32	32	µg/L	31,009.375	30,950	28,900	34,800	—	—	—	—
Heptachlor	76-44-8	R-26	SW-846:8081A	PESTPCB	Qct	6	0	µg/L	—	—	—	—	0.02171667	0.0222	0.02	0.0232
Hexachlorobutadiene	87-68-3	R-26	SW-846:8260B	VOC	Qct	21	0	µg/L	—	—	—	—	0.83333333	1	0.3	1
HMX	2691-41-0	R-26	SW-846:8330, SW-846:8321A_MOD, SW-846:8330B	HEXP, LCMS/MS High Explosives	Qct	23	0	µg/L	—	—	—	—	0.31073043	0.273	0.0833	1

Table 4.2-1 (continued)

Parameter Name	Parameter Code	Well	Analytical Method	Analytical Method Category[a]	Geological Unit Code[a]	No. Samples	No. Detects	Unit	Mean Detect	Median Detect	Min Detect	Max Detect	Mean ND	Median ND	Min ND	Max ND
Iron	Fe	R-26	SW-846:6010B, SW-846:6010C	Inorganic	Qct	38	6	µg/L	53.333333	45.3	24.8	109	64.1875	65	18	211
Lead	Pb	R-26	SW-846:6020	Inorganic	Qct	38	0	µg/L	—	—	—	—	1.25	1.25	0.5	2
Magnesium	Mg	R-26	SW-846:6010B, SW-846:6010C	Inorganic	Qct	38	38	µg/L	2907.8947	2905	2660	3240	—	—	—	—
Manganese	Mn	R-26	SW-846:6010B, SW-846:6010C, SW-846:6020	Inorganic	Qct	38	8	µg/L	2.695	2.53	1.2	4.86	5.658	2.37	1	10
Mercury	Hg	R-26	EPA:245.2, SW-846:7470A	Inorganic	Qct	48	0	µg/L	—	—	—	—	0.13291667	0.185	0.03	0.2
Methyl tert-butyl ether	1634-04-4	R-26	SW-846:8260B	VOC	Qct	19	0	µg/L	—	—	—	—	0.81578947	1	0.3	1
Methyl-2-pentanone[4-]	108-10-1	R-26	SW-846:8260B	VOC	Qct	24	0	µg/L	—	—	—	—	4.27083333	5	1.5	5
Methylene chloride	75-09-2	R-26	SW-846:8260B	VOC	Qct	24	0	µg/L	—	—	—	—	6.34208333	5	1	10
MNX	MNX	R-26	SW-846:8321A_MOD, SW-846:8330B, SW-846:8330RDX	LCMS/MS High Explosives	Qct	16	0	µg/L	—	—	—	—	0.30989375	0.271	0.0833	0.5
Molybdenum	Mo	R-26	SW-846:6010B, SW-846:6020	Inorganic	Qct	38	28	µg/L	0.9941786	0.962	0.78	1.4	1.804	2	0.99	2
Nickel	Ni	R-26	SW-846:6010B, SW-846:6020	Inorganic	Qct	38	17	µg/L	2.5021765	1.48	0.654	14.9	1.2447619	1.1	0.5	2.35
Nitrate-nitrite as nitrogen	NO3+NO2-N	R-26	EPA:353.1, EPA:353.2	General Chemistry	Qct	30	30	µg/L	344.12333	365	77.7	459	—	—	—	—
Nitrotoluene[2-]	88-72-2	R-26	SW-846:8330, SW-846:8321A_MOD, SW-846:8330B	HEXP, LCMS/MS High Explosives	Qct	23	0	µg/L	—	—	—	—	0.31119565	0.273	0.0854	1
Perchlorate	ClO4	R-26	SW-846:6850, SW846 6850 Modified	LCMS/MS Perchlorate	Qct	26	26	µg/L	0.2310385	0.2325	0.204	0.254	—	—	—	—
Phenanthrene	85-01-8	R-26	SW-846:8270C, SW-846:8270D, SW-846:8270DGCMS_SIM, SW-846:8310	SVOC	Qct	13	0	µg/L	—	—	—	—	0.86846154	1.02	0.1	1.2
Potassium	K	R-26	SW-846:6010B, SW-846:6010C	Inorganic	Qct	38	38	µg/L	2195.2632	2170	2050	2450	—	—	—	—
Pyrene	129-00-0	R-26	SW-846:8270C, SW-846:8270D, SW-846:8270DGCMS_SIM, SW-846:8310	SVOC	Qct	14	0	µg/L	—	—	—	—	0.8155	1.04	0.0521	1.2
Radium-226	Ra-226	R-26	EPA:901.1, EPA:903.1	RAD	Qct	6	1	pCi/L	0.373	0.373	0.373	0.373	2	0.274	0.152	5.93
Radium-228	Ra-228	R-26	EPA:904	RAD	Qct	4	2	pCi/L	1.023	1.023	0.646	1.4	0.4725	0.4725	0.384	0.561
RDX	121-82-4	R-26	SW-846:8330, SW-846:8321A_MOD, SW-846:8330B	HEXP, LCMS/MS High Explosives	Qct	23	0	µg/L	—	—	—	—	0.31073043	0.273	0.0833	1
Selenium	Se	R-26	SW-846:6010B, SW-846:6020	Inorganic	Qct	38	0	µg/L	—	—	—	—	4.15789474	5	1	6
Silicon dioxide	SiO2	R-26	SW-846:6010B, SW-846:6010C	Inorganic	Qct	30	30	µg/L	57,176.667	57,300	52,100	61,100	—	—	—	—
Silver	Ag	R-26	SW-846:6010B, SW-846:6020	Inorganic	Qct	38	0	µg/L	—	—	—	—	0.73947368	1	0.2	1
Sodium	Na	R-26	SW-846:6010B, SW-846:6010C	Inorganic	Qct	38	38	µg/L	8456.0526	8445	7910	9120	—	—	—	—
Strontium	Sr	R-26	SW-846:6010B, SW-846:6010C	Inorganic	Qct	38	38	µg/L	45.007895	45	41.6	49	—	—	—	—
Styrene	100-42-5	R-26	SW-846:8260B	VOC	Qct	24	0	µg/L	—	—	—	—	0.85416667	1	0.3	1
Sulfate	SO4(-2)	R-26	EPA:300.0	General Chemistry	Qct	27	26	µg/L	1189.1923	1200	799	1420	1210	1210	1210	1210
Suspended sediment concentration	SSC	R-26	EPA:160.2	General Chemistry	Qct	1	0	µg/L	—	—	—	—	4750	4750	4750	4750
Temperature	TEMP	R-26	EPA:170.0	VOC	Qct	10	10	deg C	2.4	2	2	3	—	—	—	—
Tetrachloroethene	127-18-4	R-26	SW-846:8260B	VOC	Qct	24	0	µg/L	—	—	—	—	0.85416667	1	0.3	1
Thallium	Tl	R-26	SW-846:6020	Inorganic	Qct	38	2	µg/L	0.405	0.405	0.4	0.41	1.00127778	0.6	0.3	2

Table 4.2-1 (continued)

Parameter Name	Parameter Code	Well	Analytical Method	Analytical Method Category[a]	Geological Unit Code[a]	No. Samples	No. Detects	Unit	Mean Detect	Median Detect	Min Detect	Max Detect	Mean ND	Median ND	Min ND	Max ND
Tin	Sn	R-26	SW-846:6010B, SW-846:6010C	Inorganic	Qct	32	1	µg/L	4.71	4.71	4.71	4.71	10.7258065	10	2.5	50
TNX	TNX	R-26	SW-846:8321A_MOD, SW-846:8330B, SW-846:8330RDX	LCMS/MS High Explosives	Qct	17	0	µg/L	—	—	—	—	0.32107647	0.273	0.0833	0.5
Toluene	108-88-3	R-26	SW-846:8260B	VOC	Qct	24	4	µg/L	0.73	0.86	0.31	0.89	0.825	1	0.3	1
Total dissolved solids	TDS	R-26	EPA:160.1	General Chemistry	Qct	24	23	µg/L	94,539.13	97,000	62,900	126,000	108,000	108,000	108,000	108000
Total Kjeldahl nitrogen	TKN	R-26	EPA:351.2	General Chemistry	Qct	31	8	µg/L	202.175	54	24	656	81.3608696	76.4	10	500
Total organic carbon	TOC	R-26	SW-846:9060	General Chemistry	Qct	23	13	µg/L	512.23077	436	206	1120	598.7	481.5	132	1000
Total phosphate as phosphorus	PO4-P	R-26	EPA:365.4	General Chemistry	Qct	30	12	µg/L	72.2	70.6	38.8	111	47.8666667	49.55	10	98.9
Trichlorobenzene[1,2,3-]	87-61-6	R-26	SW-846:8260B	VOC	Qct	21	0	µg/L	—	—	—	—	0.83333333	1	0.3	1
Trichloroethene	79-01-6	R-26	SW-846:8260B	VOC	Qct	24	0	µg/L	—	—	—	—	0.85416667	1	0.3	1
Trinitrobenzene[1,3,5-]	99-35-4	R-26	SW-846:8330, SW-846:8321A_MOD, SW-846:8330B	HEXP, LCMS/MS High Explosives	Qct	23	0	µg/L	—	—	—	—	0.31073043	0.273	0.0833	1
Trinitrotoluene[2,4,6-]	118-96-7	R-26	SW-846:8330, SW-846:8321A_MOD, SW-846:8330B	HEXP, LCMS/MS High Explosives	Qct	23	0	µg/L	—	—	—	—	0.31073043	0.273	0.0833	1
Tritium	H-3	R-26	Generic:LLEE, Generic:Low_Level_Tritium	RAD	Qct	13	0	pCi/L	—	—	—	—	0.13623077	0.1288	-1.328	1.35
Uranium	U	R-26	SW-846:6020	Inorganic	Qct	38	36	µg/L	0.33275	0.328	0.282	0.607	0.317	0.317	0.304	0.33
Uranium-234	U-234	R-26	HASL-300:ISOU	RAD	Qct	14	14	pCi/L	0.212	0.206	0.142	0.257	—	—	—	—
Uranium-235/236	U-235/236	R-26	HASL-300:ISOU	RAD	Qct	14	0	pCi/L	—	—	—	—	0.01760643	0.01565	-0.0082	0.05
Uranium-238	U-238	R-26	HASL-300:ISOU	RAD	Qct	14	14	pCi/L	0.1225857	0.1215	0.0853	0.175	—	—	—	—
Vanadium	V	R-26	SW-846:6010B, SW-846:6010C	Inorganic	Qct	38	38	µg/L	8.3910526	8.355	7.35	9.68	—	—	—	—
Zinc	Zn	R-26	SW-846:6010B, SW-846:6010C	Inorganic	Qct	38	28	µg/L	8.5882143	9.04	2.31	19.6	4.395	3.3	2	10
Acenaphthene	83-32-9	R-27i	SW-846:8270C, SW-846:8270D, SW-846:8270DGCMS_SIM, SW-846:8310	SVOC	Tpf	8	0	µg/L	—	—	—	—	0.610625	0.5265	0.103	1.08
Acenaphthylene	208-96-8	R-27i	SW-846:8270C, SW-846:8270D, SW-846:8270DGCMS_SIM, SW-846:8310	SVOC	Tpf	8	0	µg/L	—	—	—	—	0.610625	0.5265	0.103	1.08
Acetone	67-64-1	R-27i	SW-846:8260B	VOC	Tpf	8	0	µg/L	—	—	—	—	7.875	10	1.5	10
Acidity or alkalinity of a solution	pH	R-27i	EPA:150.1	General Chemistry	Tpf	14	14	SU	7.4257143	7.38	7.29	7.81	—	—	—	—
Alkalinity-CO3	ALK-CO3	R-27i	EPA:310.1	General Chemistry	Tpf	14	0	µg/L	—	—	—	—	1350	1000	1000	4000
Alkalinity-CO3+HCO3	ALK-CO3+HCO3	R-27i	EPA:310.1	General Chemistry	Tpf	14	14	µg/L	54,735.714	50,000	47,100	125,000	—	—	—	—
Aluminum	Al	R-27i	SW-846:6010B, SW-846:6010C	Inorganic	Tpf	14	0	µg/L	—	—	—	—	181.142857	200	68	200
Amino-2,6-dinitrotoluene[4-]	19406-51-0	R-27i	SW-846:8321A_MOD	LCMS/MS High Explosives	Tpf	5	0	µg/L	—	—	—	—	0.2652	0.263	0.258	0.279
Amino-4,6-dinitrotoluene[2-]	35572-78-2	R-27i	SW-846:8321A_MOD	LCMS/MS High Explosives	Tpf	5	0	µg/L	—	—	—	—	0.2652	0.263	0.258	0.279
Ammonia as nitrogen	NH3-N	R-27i	EPA:350.1	General Chemistry	Tpf	14	0	µg/L	—	—	—	—	41.1571429	48.4	17	88
Anthracene	120-12-7	R-27i	SW-846:8270C, SW-846:8270D, SW-846:8270DGCMS_SIM, SW-846:8310	SVOC	Tpf	8	0	µg/L	—	—	—	—	0.610625	0.5265	0.103	1.08
Antimony	Sb	R-27i	SW-846:6020	Inorganic	Tpf	14	0	µg/L	—	—	—	—	2.71428571	3	1	3

Table 4.2-1 (continued)

Parameter Name	Parameter Code	Well	Analytical Method	Analytical Method Category[a]	Geological Unit Code[a]	No. Samples	No. Detects	Unit	Mean Detect	Median Detect	Min Detect	Max Detect	Mean ND	Median ND	Min ND	Max ND
Arsenic	As	R-27i	SW-846:6020	Inorganic	Tpf	14	1	µg/L	1.73	1.73	1.73	1.73	4.64769231	5	2	7.72
Barium	Ba	R-27i	SW-846:6010B, SW-846:6010C	Inorganic	Tpf	14	14	µg/L	10.064286	9.605	8.97	13.7	—	—	—	—
Benzo(g,h,i)perylene	191-24-2	R-27i	SW-846:8270C, SW-846:8270D, SW-846:8270DGCMS_SIM, SW-846:8310	SVOC	Tpf	8	0	µg/L	—	—	—	—	0.4921625	0.3145	0.0521	1.08
Benzoic Acid	65-85-0	R-27i	SW-846:8270C, SW-846:8270D	SVOC	Tpf	8	0	µg/L	—	—	—	—	15.79625	20.2	6.25	21.5
Beryllium	Be	R-27i	SW-846:6010B, SW-846:6010C	Inorganic	Tpf	14	0	µg/L	—	—	—	—	4.42857143	5	1	5
Bis(2-ethylhexyl)phthalate	117-81-7	R-27i	SW-846:8270C, SW-846:8270D	SVOC	Tpf	8	0	µg/L	—	—	—	—	7.191125	10.1	0.313	10.8
Boron	B	R-27i	SW-846:6010B, SW-846:6010C	Inorganic	Tpf	14	0	µg/L	—	—	—	—	45	50	15	50
Bromide	Br(-1)	R-27i	EPA:300.0	General Chemistry	Tpf	14	0	µg/L	—	—	—	—	181	200	67	200
Bromodichloromethane	75-27-4	R-27i	SW-846:8260B	VOC	Tpf	8	0	µg/L	—	—	—	—	0.825	1	0.3	1
Bromoform	75-25-2	R-27i	SW-846:8260B	VOC	Tpf	8	0	µg/L	—	—	—	—	0.825	1	0.3	1
Butanone[2-]	78-93-3	R-27i	SW-846:8260B	VOC	Tpf	8	0	µg/L	—	—	—	—	4.125	5	1.5	5
Cadmium	Cd	R-27i	SW-846:6020	Inorganic	Tpf	14	0	µg/L	—	—	—	—	0.9	1	0.3	1
Calcium	Ca	R-27i	SW-846:6010B, SW-846:6010C	Inorganic	Tpf	14	14	µg/L	8612.1429	8625	8080	9150	—	—	—	—
Carbon disulfide	75-15-0	R-27i	SW-846:8260B	VOC	Tpf	8	0	µg/L	—	—	—	—	4.125	5	1.5	5
Chloride	Cl(-1)	R-27i	EPA:300.0	General Chemistry	Tpf	14	14	µg/L	1352.1429	1335	1220	1790	—	—	—	—
Chlorobenzene	108-90-7	R-27i	SW-846:8260B	VOC	Tpf	8	0	µg/L	—	—	—	—	0.825	1	0.3	1
Chlorodibromomethane	124-48-1	R-27i	SW-846:8260B	VOC	Tpf	8	0	µg/L	—	—	—	—	0.825	1	0.3	1
Chloroform	67-66-3	R-27i	SW-846:8260B	VOC	Tpf	8	0	µg/L	—	—	—	—	0.825	1	0.3	1
Chloromethane	74-87-3	R-27i	SW-846:8260B	VOC	Tpf	8	0	µg/L	—	—	—	—	0.825	1	0.3	1
Chromium	Cr	R-27i	SW-846:6020	Inorganic	Tpf	14	2	µg/L	2.1	2.1	2.07	2.13	8.83333333	10	3	10
Cobalt	Co	R-27i	SW-846:6010B, SW-846:6010C	Inorganic	Tpf	14	0	µg/L	—	—	—	—	4.42857143	5	1	5
Copper	Cu	R-27i	SW-846:6010B, SW-846:6010C	Inorganic	Tpf	14	0	µg/L	—	—	—	—	9	10	3	10
Cyanide (total)	CN (Total)	R-27i	EPA:335.4	Inorganic	Tpf	6	0	µg/L	—	—	—	—	3.89	5	1.67	5
DNX	DNX	R-27i	SW-846:8321A_MOD, SW-846:8330RDX	LCMS/MS High Explosives	Tpf	3	0	µg/L	—	—	—	—	0.342	0.266	0.26	0.5
Fluoranthene	206-44-0	R-27i	SW-846:8270C, SW-846:8270D, SW-846:8270DGCMS_SIM, SW-846:8310	SVOC	Tpf	8	0	µg/L	—	—	—	—	0.4921625	0.3145	0.0521	1.08
Fluoride	F(-1)	R-27i	EPA:300.0	General Chemistry	Tpf	14	14	µg/L	177.07143	169	141	219	—	—	—	—
Gross alpha	GrossA	R-27i	EPA:900	RAD	Tpf	8	0	pCi/L	—	—	—	—	0.2475	0.284	-0.658	1.12
Gross beta	GrossB	R-27i	EPA:900	RAD	Tpf	8	1	pCi/L	4.02	4.02	4.02	4.02	0.95857143	0.713	0.426	2
Hardness	Hardness	R-27i	SM:A2340B	Inorganic	Tpf	14	14	µg/L	31,671.429	31,600	29,700	33,300	—	—	—	—
Hexachlorobutadiene	87-68-3	R-27i	SW-846:8260B	VOC	Tpf	8	1	µg/L	0.37	0.37	0.37	0.37	0.8	1	0.3	1
HMX	2691-41-0	R-27i	SW-846:8321A_MOD	LCMS/MS High Explosives	Tpf	5	0	µg/L	—	—	—	—	0.2652	0.263	0.258	0.279
Iron	Fe	R-27i	SW-846:6010B, SW-846:6010C	Inorganic	Tpf	14	0	µg/L	—	—	—	—	85.2714286	100	30	100
Lead	Pb	R-27i	SW-846:6020	Inorganic	Tpf	14	0	µg/L	—	—	—	—	1.78571429	2	0.5	2
Magnesium	Mg	R-27i	SW-846:6010B, SW-846:6010C	Inorganic	Tpf	14	14	µg/L	2469.2857	2475	2290	2640	—	—	—	—

Table 4.2-1 (continued)

Parameter Name	Parameter Code	Well	Analytical Method	Analytical Method Category[a]	Geological Unit Code[a]	No. Samples	No. Detects	Unit	Mean Detect	Median Detect	Min Detect	Max Detect	Mean ND	Median ND	Min ND	Max ND
Manganese	Mn	R-27i	SW-846:6010B, SW-846:6010C	Inorganic	Tpf	14	5	µg/L	4.788	2.98	2.06	10.6	8.22222222	10	2	10
Mercury	Hg	R-27i	EPA:245.2	Inorganic	Tpf	20	0	µg/L	—	—	—	—	0.1734	0.2	0.067	0.2
Methyl tert-butyl ether	1634-04-4	R-27i	SW-846:8260B	VOC	Tpf	8	0	µg/L	—	—	—	—	0.825	1	0.3	1
Methyl-2-pentanone[4-]	108-10-1	R-27i	SW-846:8260B	VOC	Tpf	8	0	µg/L	—	—	—	—	4.125	5	1.5	5
Methylene chloride	75-09-2	R-27i	SW-846:8260B	VOC	Tpf	8	0	µg/L	—	—	—	—	7.75	10	1	10
MNX	MNX	R-27i	SW-846:8321A_MOD, SW-846:8330RDX	LCMS/MS High Explosives	Tpf	3	0	µg/L	—	—	—	—	0.342	0.266	0.26	0.5
Molybdenum	Mo	R-27i	SW-846:6020	Inorganic	Tpf	14	13	µg/L	1.6053846	1.59	1.42	1.91	1.65	1.65	1.65	1.65
Nickel	Ni	R-27i	SW-846:6020	Inorganic	Tpf	14	7	µg/L	0.7214286	0.749	0.55	0.875	1.27557143	1.09	0.6	2
Nitrate-nitrite as nitrogen	NO3+NO2-N	R-27i	EPA:353.2	General Chemistry	Tpf	14	11	µg/L	121.04545	99.7	58	377	163.333333	190	50	250
Nitrotoluene[2-]	88-72-2	R-27i	SW-846:8321A_MOD	LCMS/MS High Explosives	Tpf	5	0	µg/L	—	—	—	—	0.2652	0.263	0.258	0.279
Perchlorate	ClO4	R-27i	SW-846:6850	LCMS/MS Perchlorate	Tpf	13	13	µg/L	0.1199	0.12	0.0957	0.134	—	—	—	—
Phenanthrene	85-01-8	R-27i	SW-846:8270C, SW-846:8270D, SW-846:8270DGCMS_SIM, SW-846:8310	SVOC	Tpf	8	0	µg/L	—	—	—	—	0.610625	0.5265	0.103	1.08
Potassium	K	R-27i	SW-846:6010B, SW-846:6010C	Inorganic	Tpf	14	14	µg/L	861.85714	898	673	981	—	—	—	—
Pyrene	129-00-0	R-27i	SW-846:8270C, SW-846:8270D, SW-846:8270DGCMS_SIM, SW-846:8310	SVOC	Tpf	8	0	µg/L	—	—	—	—	0.4921625	0.3145	0.0521	1.08
RDX	121-82-4	R-27i	SW-846:8321A_MOD	LCMS/MS High Explosives	Tpf	5	0	µg/L	—	—	—	—	0.2652	0.263	0.258	0.279
Selenium	Se	R-27i	SW-846:6020	Inorganic	Tpf	14	0	µg/L	—	—	—	—	4.57142857	5	2	5
Silicon dioxide	SiO2	R-27i	SW-846:6010B, SW-846:6010C	Inorganic	Tpf	14	14	µg/L	68,292.857	68,250	63,900	71,100	—	—	—	—
Silver	Ag	R-27i	SW-846:6020	Inorganic	Tpf	14	0	µg/L	—	—	—	—	0.9	1	0.3	1
Sodium	Na	R-27i	SW-846:6010B, SW-846:6010C	Inorganic	Tpf	14	14	µg/L	9880	9835	9450	10,600	—	—	—	—
Strontium	Sr	R-27i	SW-846:6010B, SW-846:6010C	Inorganic	Tpf	14	14	µg/L	46.85	46.65	44.9	49.9	—	—	—	—
Styrene	100-42-5	R-27i	SW-846:8260B	VOC	Tpf	8	0	µg/L	—	—	—	—	0.825	1	0.3	1
Sulfate	SO4(-2)	R-27i	EPA:300.0	General Chemistry	Tpf	14	14	µg/L	1865.7143	1855	1370	2770	—	—	—	—
Temperature	TEMP	R-27i	EPA:170.0	VOC	Tpf	4	4	deg C	2	2	2	2	—	—	—	—
Tetrachloroethene	127-18-4	R-27i	SW-846:8260B	VOC	Tpf	8	0	µg/L	—	—	—	—	0.825	1	0.3	1
Thallium	Tl	R-27i	SW-846:6020	Inorganic	Tpf	14	1	µg/L	0.354	0.354	0.354	0.354	1.55384615	2	0.6	2
Tin	Sn	R-27i	SW-846:6010B, SW-846:6010C	Inorganic	Tpf	14	0	µg/L	—	—	—	—	17.5	10	2.5	50
TNX	TNX	R-27i	SW-846:8321A_MOD, SW-846:8330RDX	LCMS/MS High Explosives	Tpf	3	0	µg/L	—	—	—	—	0.342	0.266	0.26	0.5
Toluene	108-88-3	R-27i	SW-846:8260B	VOC	Tpf	8	0	µg/L	—	—	—	—	0.825	1	0.3	1
Total dissolved solids	TDS	R-27i	EPA:160.1	General Chemistry	Tpf	14	14	µg/L	122,064.29	119,500	82,900	157,000	—	—	—	—
Total Kjeldahl nitrogen	TKN	R-27i	EPA:351.2	General Chemistry	Tpf	8	1	µg/L	527	527	527	527	199.385714	100	33	500
Total organic carbon	TOC	R-27i	SW-846:9060	General Chemistry	Tpf	8	6	µg/L	491.5	438.5	330	780	665	665	330	1000
Total phosphate as phosphorus	PO4-P	R-27i	EPA:365.4	General Chemistry	Tpf	14	3	µg/L	128.76667	150	39.3	197	45.2909091	50	20	70

Table 4.2-1 (continued)

Parameter Name	Parameter Code	Well	Analytical Method	Analytical Method Category[a]	Geological Unit Code[a]	No. Samples	No. Detects	Unit	Mean Detect	Median Detect	Min Detect	Max Detect	Mean ND	Median ND	Min ND	Max ND
Trichlorobenzene[1,2,3-]	87-61-6	R-27i	SW-846:8260B	VOC	Tpf	8	1	µg/L	0.31	0.31	0.31	0.31	0.8	1	0.3	1
Trichloroethene	79-01-6	R-27i	SW-846:8260B	VOC	Tpf	8	0	µg/L	—	—	—	—	0.825	1	0.3	1
Trinitrobenzene[1,3,5-]	99-35-4	R-27i	SW-846:8321A_MOD	LCMS/MS High Explosives	Tpf	5	0	µg/L	—	—	—	—	0.2652	0.263	0.258	0.279
Trinitrotoluene[2,4,6-]	118-96-7	R-27i	SW-846:8321A_MOD	LCMS/MS High Explosives	Tpf	5	0	µg/L	—	—	—	—	0.2652	0.263	0.258	0.279
Tritium	H-3	R-27i	Generic:Low_Level_Tritium	RAD	Tpf	8	0	pCi/L	—	—	—	—	0.213375	0.2705	-0.594	1.128
Uranium	U	R-27i	SW-846:6020	Inorganic	Tpf	14	11	µg/L	0.2632727	0.263	0.24	0.294	0.27066667	0.265	0.25	0.297
Uranium-234	U-234	R-27i	HASL-300:ISOU	RAD	Tpf	8	8	pCi/L	0.19625	0.203	0.139	0.257	—	—	—	—
Uranium-235/236	U-235/236	R-27i	HASL-300:ISOU	RAD	Tpf	8	1	pCi/L	0.0553	0.0553	0.0553	0.0553	0.01674143	0.0131	0.00723	0.044
Uranium-238	U-238	R-27i	HASL-300:ISOU	RAD	Tpf	8	8	pCi/L	0.10755	0.1035	0.0827	0.138	—	—	—	—
Vanadium	V	R-27i	SW-846:6010B, SW-846:6010C	Inorganic	Tpf	14	11	µg/L	1.7590909	1.63	1.33	2.45	5	5	5	5
Zinc	Zn	R-27i	SW-846:6010B, SW-846:6010C	Inorganic	Tpf	14	5	µg/L	5.43	5.01	4.27	7.68	9.25555556	10	3.3	10
Acenaphthene	83-32-9	R-47i	SW-846:8270C, SW-846:8270D, SW-846:8310	SVOC	Tpf	5	0	µg/L	—	—	—	—	0.6942	0.532	0.309	1.09
Acenaphthylene	208-96-8	R-47i	SW-846:8270C, SW-846:8270D, SW-846:8310	SVOC	Tpf	5	0	µg/L	—	—	—	—	0.6942	0.532	0.309	1.09
Acetone	67-64-1	R-47i	SW-846:8260B	VOC	Tpf	12	0	µg/L	—	—	—	—	6.45833333	10	1.5	10
Acidity or alkalinity of a solution	pH	R-47i	EPA:150.1	General Chemistry	Tpf	20	20	SU	7.5825	7.555	7.29	7.97	—	—	—	—
Alkalinity-CO3	ALK-CO3	R-47i	EPA:310.1	General Chemistry	Tpf	20	0	µg/L	—	—	—	—	1712.5	1000	1000	4000
Alkalinity-CO3+HCO3	ALK-CO3+HCO3	R-47i	EPA:310.1	General Chemistry	Tpf	20	20	µg/L	57,875	57,900	50,500	70,900	—	—	—	—
Aluminum	Al	R-47i	SW-846:6010B, SW-846:6010C	Inorganic	Tpf	21	3	µg/L	143.36667	143	73.1	214	163.333333	200	68	200
Amino-2,6-dinitrotoluene[4-]	19406-51-0	R-47i	SW-846:8321A_MOD, SW-846:8330B	LCMS/MS High Explosives	Tpf	18	0	µg/L	—	—	—	—	0.18311111	0.1725	0.0808	0.325
Amino-4,6-dinitrotoluene[2-]	35572-78-2	R-47i	SW-846:8321A_MOD, SW-846:8330B	LCMS/MS High Explosives	Tpf	18	0	µg/L	—	—	—	—	0.18311111	0.1725	0.0808	0.325
Ammonia as nitrogen	NH3-N	R-47i	EPA:350.1	General Chemistry	Tpf	20	9	µg/L	46.888889	45	24.2	84.8	52.2545455	50	17	134
Anthracene	120-12-7	R-47i	SW-846:8270C, SW-846:8270D, SW-846:8310	SVOC	Tpf	5	0	µg/L	—	—	—	—	0.6942	0.532	0.309	1.09
Antimony	Sb	R-47i	SW-846:6020	Inorganic	Tpf	21	2	µg/L	0.546	0.546	0.541	0.551	2.47368421	3	1	3
Arsenic	As	R-47i	SW-846:6020	Inorganic	Tpf	21	5	µg/L	2.444	2.56	1.92	2.83	4.319375	5	2	7.57
Barium	Ba	R-47i	SW-846:6010B, SW-846:6010C	Inorganic	Tpf	21	21	µg/L	6.4809524	6.02	3.67	13.1	—	—	—	—
Benzo(g,h,i)perylene	191-24-2	R-47i	SW-846:8270C, SW-846:8270D, SW-846:8310	SVOC	Tpf	5	0	µg/L	—	—	—	—	0.50664	0.309	0.051	1.09
Benzoic acid	65-85-0	R-47i	SW-846:8270C, SW-846:8270D	SVOC	Tpf	5	1	µg/L	32.6	32.6	32.6	32.6	17.4475	20.95	6.19	21.7
Beryllium	Be	R-47i	SW-846:6010B, SW-846:6010C	Inorganic	Tpf	21	0	µg/L	—	—	—	—	4.04761905	5	1	5
Bis(2-ethylhexyl)phthalate	117-81-7	R-47i	SW-846:8270C, SW-846:8270D	SVOC	Tpf	5	0	µg/L	—	—	—	—	8.978	10.3	3.09	10.9
Boron	B	R-47i	SW-846:6010B, SW-846:6010C	Inorganic	Tpf	21	9	µg/L	18.3	18.1	15.6	22.4	38.3333333	50	15	50
Bromide	Br(-1)	R-47i	EPA:300.0	General Chemistry	Tpf	20	3	µg/L	72.866667	72.1	70.8	75.7	160.882353	200	67	200
Bromodichloromethane	75-27-4	R-47i	SW-846:8260B	VOC	Tpf	12	0	µg/L	—	—	—	—	0.70833333	1	0.3	1

Table 4.2-1 (continued)

Parameter Name	Parameter Code	Well	Analytical Method	Analytical Method Category[a]	Geological Unit Code[a]	No. Samples	No. Detects	Unit	Mean Detect	Median Detect	Min Detect	Max Detect	Mean ND	Median ND	Min ND	Max ND
Bromoform	75-25-2	R-47i	SW-846:8260B	VOC	Tpf	12	0	µg/L	—	—	—	—	0.70833333	1	0.3	1
Butanone[2-]	78-93-3	R-47i	SW-846:8260B	VOC	Tpf	12	0	µg/L	—	—	—	—	3.54166667	5	1.5	5
Cadmium	Cd	R-47i	SW-846:6020	Inorganic	Tpf	21	0	µg/L	—	—	—	—	0.83333333	1	0.3	1
Calcium	Ca	R-47i	SW-846:6010B, SW-846:6010C	Inorganic	Tpf	21	21	µg/L	10,057.143	9990	9120	109,00	—	—	—	—
Carbon disulfide	75-15-0	R-47i	SW-846:8260B	VOC	Tpf	12	0	µg/L	—	—	—	—	3.54166667	5	1.5	5
Chloride	Cl(-1)	R-47i	EPA:300.0	General Chemistry	Tpf	20	20	µg/L	2507.5	2370	1870	3970	—	—	—	—
Chlorobenzene	108-90-7	R-47i	SW-846:8260B	VOC	Tpf	12	0	µg/L	—	—	—	—	0.70833333	1	0.3	1
Chlorodibromomethane	124-48-1	R-47i	SW-846:8260B	VOC	Tpf	12	0	µg/L	—	—	—	—	0.70833333	1	0.3	1
Chloroform	67-66-3	R-47i	SW-846:8260B	VOC	Tpf	12	0	µg/L	—	—	—	—	0.70833333	1	0.3	1
Chloromethane	74-87-3	R-47i	SW-846:8260B	VOC	Tpf	12	0	µg/L	—	—	—	—	0.70833333	1	0.3	1
Chromium	Cr	R-47i	SW-846:6020	Inorganic	Tpf	21	8	µg/L	3.5775	2.8	2.01	8.22	7.30769231	10	3	10
Cobalt	Co	R-47i	SW-846:6010B, SW-846:6010C	Inorganic	Tpf	21	0	µg/L	—	—	—	—	4.04761905	5	1	5
Copper	Cu	R-47i	SW-846:6010B, SW-846:6010C	Inorganic	Tpf	21	1	µg/L	4.19	4.19	4.19	4.19	8.25	10	3	10
Cyanide (total)	CN (Total)	R-47i	EPA:335.4	Inorganic	Tpf	12	0	µg/L	—	—	—	—	3.6125	5	1.67	5
DNX	DNX	R-47i	SW-846:8321A_MOD, SW-846:8330B, SW-846:8330RDX	LCMS/MS High Explosives	Tpf	17	0	µg/L	—	—	—	—	0.19929412	0.087	0.0808	0.5
Fluoranthene	206-44-0	R-47i	SW-846:8270C, SW-846:8270D, SW-846:8310	SVOC	Tpf	5	0	µg/L	—	—	—	—	0.50664	0.309	0.051	1.09
Fluoride	F(-1)	R-47i	EPA:300.0	General Chemistry	Tpf	20	20	µg/L	146.345	140	79.3	310	—	—	—	—
Gross alpha	GrossA	R-47i	EPA:900	RAD	Tpf	4	1	pCi/L	11.4	11.4	11.4	11.4	0.522	0.691	-0.505	1.38
Gross beta	GrossB	R-47i	EPA:900	RAD	Tpf	4	1	pCi/L	13.7	13.7	13.7	13.7	0.71166667	0.809	0.365	0.961
Gross gamma	GrossG	R-47i	EPA:901.1	RAD	Tpf	1	0	pCi/L	—	—	—	—	271	271	271	271
Hardness	Hardness	R-47i	SM:A2340B	Inorganic	Tpf	21	21	µg/L	35,138.095	34,800	32,300	38,400	—	—	—	—
Heptachlor	76-44-8	R-47i	SW-846:8081A	PESTPCB	Tpf	1	0	µg/L	—	—	—	—	0.0204	0.0204	0.0204	0.0204
Hexachlorobutadiene	87-68-3	R-47i	SW-846:8260B	VOC	Tpf	12	0	µg/L	—	—	—	—	0.70833333	1	0.3	1
HMX	2691-41-0	R-47i	SW-846:8321A_MOD, SW-846:8330B	LCMS/MS High Explosives	Tpf	18	0	µg/L	—	—	—	—	0.18311111	0.1725	0.0808	0.325
Iron	Fe	R-47i	SW-846:6010B, SW-846:6010C	Inorganic	Tpf	21	5	µg/L	129.42	55.6	41.6	359	78.125	100	30	100
Lead	Pb	R-47i	SW-846:6020	Inorganic	Tpf	21	2	µg/L	0.578	0.578	0.571	0.585	1.60526316	2	0.5	2
Magnesium	Mg	R-47i	SW-846:6010B, SW-846:6010C	Inorganic	Tpf	21	21	µg/L	2431.9048	2410	2310	2720	—	—	—	—
Manganese	Mn	R-47i	SW-846:6010B, SW-846:6010C	Inorganic	Tpf	21	7	µg/L	33.707143	24.4	3.3	95.2	7.14285714	10	2	10
Mercury	Hg	R-47i	EPA:245.2	Inorganic	Tpf	32	0	µg/L	—	—	—	—	0.1584375	0.2	0.067	0.2
Methyl tert-butyl ether	1634-04-4	R-47i	SW-846:8260B	VOC	Tpf	12	0	µg/L	—	—	—	—	0.70833333	1	0.3	1
Methyl-2-pentanone[4-]	108-10-1	R-47i	SW-846:8260B	VOC	Tpf	12	0	µg/L	—	—	—	—	3.54166667	5	1.5	5
Methylene chloride	75-09-2	R-47i	SW-846:8260B	VOC	Tpf	12	0	µg/L	—	—	—	—	6.25	10	1	10
MNX	MNX	R-47i	SW-846:8321A_MOD, SW-846:8330B, SW-846:8330RDX	LCMS/MS High Explosives	Tpf	17	0	µg/L	—	—	—	—	0.19929412	0.087	0.0808	0.5
Molybdenum	Mo	R-47i	SW-846:6020	Inorganic	Tpf	21	20	µg/L	2.6795	2.04	1.27	8.16	1.45	1.45	1.45	1.45
Nickel	Ni	R-47i	SW-846:6020	Inorganic	Tpf	21	16	µg/L	1.668875	1.185	0.574	4.93	1.006	0.6	0.6	2

Table 4.2-1 (continued)

Parameter Name	Parameter Code	Well	Analytical Method	Analytical Method Category[a]	Geological Unit Code[a]	No. Samples	No. Detects	Unit	Mean Detect	Median Detect	Min Detect	Max Detect	Mean ND	Median ND	Min ND	Max ND
Nitrate-nitrite as nitrogen	NO3+NO2-N	R-47i	EPA:353.2	General Chemistry	Tpf	20	20	µg/L	381.45	408.5	130	489	—	—	—	—
Nitrotoluene[2-]	88-72-2	R-47i	SW-846:8321A_MOD, SW-846:8330B	LCMS/MS High Explosives	Tpf	18	0	µg/L	—	—	—	—	0.18417222	0.17355	0.0828	0.325
Oxygen-18/Oxygen-16 Ratio from Nitrate	O18O16-NO3	R-47i	Generic:Oxygen Isotope Ratio	General Chemistry	Tpf	2	2	permil	0.36645	0.3665	-1.2922	2.0251	—	—	—	—
Perchlorate	ClO4	R-47i	SW-846:6850	LCMS/MS Perchlorate	Tpf	19	19	µg/L	0.2495263	0.25	0.222	0.286	—	—	—	—
Perfluorooctanoic acid	335-67-1	R-47i	EPA:537M	LCMS/MS PFAS	Tpf	1	0	µg/L	—	—	—	—	0.000728	0.00073	0.00073	0.00073
Phenanthrene	85-01-8	R-47i	SW-846:8270C, SW-846:8270D, SW-846:8310	SVOC	Tpf	5	0	µg/L	—	—	—	—	0.6942	0.532	0.309	1.09
Potassium	K	R-47i	SW-846:6010B, SW-846:6010C	Inorganic	Tpf	21	20	µg/L	483.7	415	347	882	568	568	568	568
Pyrene	129-00-0	R-47i	SW-846:8270C, SW-846:8270D, SW-846:8310	SVOC	Tpf	5	0	µg/L	—	—	—	—	0.50664	0.309	0.051	1.09
Radium-226	Ra-226	R-47i	EPA:903.1	RAD	Tpf	1	1	pCi/L	4.86	4.86	4.86	4.86	—	—	—	—
Radium-228	Ra-228	R-47i	EPA:904	RAD	Tpf	1	0	pCi/L	—	—	—	—	0.0894	0.0894	0.0894	0.0894
RDX	121-82-4	R-47i	SW-846:8321A_MOD, SW-846:8330B	LCMS/MS High Explosives	Tpf	18	0	µg/L	—	—	—	—	0.18311111	0.1725	0.0808	0.325
Selenium	Se	R-47i	SW-846:6020	Inorganic	Tpf	21	1	µg/L	2.77	2.77	2.77	2.77	4.0765	5	1.53	5
Silicon dioxide	SiO2	R-47i	SW-846:6010B, SW-846:6010C	Inorganic	Tpf	20	20	µg/L	58,810	58,850	54,900	62,500	—	—	—	—
Silver	Ag	R-47i	SW-846:6020	Inorganic	Tpf	21	0	µg/L	—	—	—	—	0.83333333	1	0.3	1
Sodium	Na	R-47i	SW-846:6010B, SW-846:6010C	Inorganic	Tpf	21	21	µg/L	15,866.667	14,800	11,700	30,300	—	—	—	—
Strontium	Sr	R-47i	SW-846:6010B, SW-846:6010C	Inorganic	Tpf	21	21	µg/L	53.12381	52.4	46	66	—	—	—	—
Styrene	100-42-5	R-47i	SW-846:8260B	VOC	Tpf	12	0	µg/L	—	—	—	—	0.70833333	1	0.3	1
Sulfate	SO4(-2)	R-47i	EPA:300.0	General Chemistry	Tpf	20	20	µg/L	6545	4975	3440	18,500	—	—	—	—
Temperature	TEMP	R-47i	EPA:170.0	VOC	Tpf	16	16	deg C	2.5625	2	2	4	—	—	—	—
Tetrachloroethene	127-18-4	R-47i	SW-846:8260B	VOC	Tpf	12	0	µg/L	—	—	—	—	0.70833333	1	0.3	1
Thallium	Tl	R-47i	SW-846:6020	Inorganic	Tpf	21	0	µg/L	—	—	—	—	1.42857143	2	0.6	2
Tin	Sn	R-47i	SW-846:6010B, SW-846:6010C	Inorganic	Tpf	21	2	µg/L	5.235	5.235	3.09	7.38	12.6315789	10	2.5	50
TNX	TNX	R-47i	SW-846:8321A_MOD, SW-846:8330B, SW-846:8330RDX	LCMS/MS High Explosives	Tpf	17	0	µg/L	—	—	—	—	0.19929412	0.087	0.0808	0.5
Toluene	108-88-3	R-47i	SW-846:8260B	VOC	Tpf	12	0	µg/L	—	—	—	—	0.70833333	1	0.3	1
Total dissolved solids	TDS	R-47i	EPA:160.1	General Chemistry	Tpf	20	20	µg/L	122,255	126,000	81,400	151,000	—	—	—	—
Total Kjeldahl nitrogen	TKN	R-47i	EPA:351.2	General Chemistry	Tpf	14	5	µg/L	138.42	106	39.7	309	73.8666667	100	33	100
Total organic carbon	TOC	R-47i	SW-846:9060	General Chemistry	Tpf	14	14	µg/L	2648.2143	2590	429	4960	—	—	—	—
Total phosphate as phosphorus	PO4-P	R-47i	EPA:365.4	General Chemistry	Tpf	20	9	µg/L	66.122222	46.3	26.9	150	51.3	50	27.1	95.6
Trichlorobenzene[1,2,3-]	87-61-6	R-47i	SW-846:8260B	VOC	Tpf	12	0	µg/L	—	—	—	—	0.70833333	1	0.3	1
Trichloroethene	79-01-6	R-47i	SW-846:8260B	VOC	Tpf	12	0	µg/L	—	—	—	—	0.72166667	1	0.3	1
Trinitrobenzene[1,3,5-]	99-35-4	R-47i	SW-846:8321A_MOD, SW-846:8330B	LCMS/MS High Explosives	Tpf	18	0	µg/L	—	—	—	—	0.18311111	0.1725	0.0808	0.325

Table 4.2-1 (continued)

Parameter Name	Parameter Code	Well	Analytical Method	Analytical Method Category[a]	Geological Unit Code[a]	No. Samples	No. Detects	Unit	Mean Detect	Median Detect	Min Detect	Max Detect	Mean ND	Median ND	Min ND	Max ND
Trinitrotoluene[2,4,6-]	118-96-7	R-47i	SW-846:8321A_MOD, SW-846:8330B	LCMS/MS High Explosives	Tpf	18	0	µg/L	—	—	—	—	0.18311111	0.1725	0.0808	0.325
Tritium	H-3	R-47i	Generic:Low_Level_Tritium	RAD	Tpf	6	1	pCi/L	2.484	2.484	2.484	2.484	0.52884	0.5152	-0.232	1.689
Uranium	U	R-47i	SW-846:6020	Inorganic	Tpf	21	21	µg/L	0.4266667	0.34	0.219	0.774	—	—	—	—
Uranium-234	U-234	R-47i	HASL-300:ISOU	RAD	Tpf	4	4	pCi/L	0.38625	0.3895	0.303	0.463	—	—	—	—
Uranium-235/236	U-235/236	R-47i	HASL-300:ISOU	RAD	Tpf	4	0	pCi/L	—	—	—	—	0.0244425	0.01455	0.00897	0.0597
Uranium-238	U-238	R-47i	HASL-300:ISOU	RAD	Tpf	4	3	pCi/L	0.16	0.158	0.158	0.164	0.0694	0.0694	0.0694	0.0694
Vanadium	V	R-47i	SW-846:6010B, SW-846:6010C	Inorganic	Tpf	21	15	µg/L	1.3966667	1.36	1.02	2.08	3.98	5	1	5
Zinc	Zn	R-47i	SW-846:6010B, SW-846:6010C	Inorganic	Tpf	21	7	µg/L	7.0671429	4.95	3.53	12	8.56428571	10	3.3	10
Acetone	67-64-1	R-63i	SW-846:8260B	VOC	Tpf	1	1	µg/L	1.92	1.92	1.92	1.92	—	—	—	—
Acidity or alkalinity of a solution	pH	R-63i	EPA:150.1	General Chemistry	Tpf	1	1	SU	9.31	9.31	9.31	9.31	—	—	—	—
Alkalinity-CO3	ALK-CO3	R-63i	EPA:310.1	General Chemistry	Tpf	1	1	µg/L	37,000	37,000	37,000	37,000	—	—	—	—
Alkalinity-CO3+HCO3	ALK-CO3+HCO3	R-63i	EPA:310.1	General Chemistry	Tpf	1	1	µg/L	89,000	89,000	89,000	89,000	—	—	—	—
Aluminum	Al	R-63i	SW-846:6010C	Inorganic	Tpf	1	0	µg/L	—	—	—	—	68	68	68	68
Amino-2,6-dinitrotoluene[4-]	19406-51-0	R-63i	SW-846:8330B	LCMS/MS High Explosives	Tpf	1	0	µg/L	—	—	—	—	0.0908	0.0908	0.0908	0.0908
Amino-4,6-dinitrotoluene[2-]	35572-78-2	R-63i	SW-846:8330B	LCMS/MS High Explosives	Tpf	1	0	µg/L	—	—	—	—	0.0908	0.0908	0.0908	0.0908
Ammonia as nitrogen	NH3-N	R-63i	EPA:350.1	General Chemistry	Tpf	1	1	µg/L	48.6	48.6	48.6	48.6	—	—	—	—
Antimony	Sb	R-63i	SW-846:6020	Inorganic	Tpf	1	0	µg/L	—	—	—	—	1	1	1	1
Arsenic	As	R-63i	SW-846:6020	Inorganic	Tpf	1	1	µg/L	3.03	3.03	3.03	3.03	—	—	—	—
Barium	Ba	R-63i	SW-846:6010C	Inorganic	Tpf	1	1	µg/L	10.9	10.9	10.9	10.9	—	—	—	—
Beryllium	Be	R-63i	SW-846:6010C	Inorganic	Tpf	1	0	µg/L	—	—	—	—	1	1	1	1
Boron	B	R-63i	SW-846:6010C	Inorganic	Tpf	1	0	µg/L	—	—	—	—	15	15	15	15
Bromide	Br(-1)	R-63i	EPA:300.0	General Chemistry	Tpf	1	0	µg/L	—	—	—	—	67	67	67	67
Bromodichloromethane	75-27-4	R-63i	SW-846:8260B	VOC	Tpf	1	0	µg/L	—	—	—	—	0.3	0.3	0.3	0.3
Bromoform	75-25-2	R-63i	SW-846:8260B	VOC	Tpf	1	0	µg/L	—	—	—	—	0.3	0.3	0.3	0.3
Butanone[2-]	78-93-3	R-63i	SW-846:8260B	VOC	Tpf	1	0	µg/L	—	—	—	—	1.5	1.5	1.5	1.5
Cadmium	Cd	R-63i	SW-846:6020	Inorganic	Tpf	1	0	µg/L	—	—	—	—	0.3	0.3	0.3	0.3
Calcium	Ca	R-63i	SW-846:6010C	Inorganic	Tpf	1	1	µg/L	12,900	12,900	12,900	12,900	—	—	—	—
Carbon Disulfide	75-15-0	R-63i	SW-846:8260B	VOC	Tpf	1	0	µg/L	—	—	—	—	1.5	1.5	1.5	1.5
Chloride	Cl(-1)	R-63i	EPA:300.0	General Chemistry	Tpf	1	1	µg/L	1790	1790	1790	1790	—	—	—	—
Chlorobenzene	108-90-7	R-63i	SW-846:8260B	VOC	Tpf	1	0	µg/L	—	—	—	—	0.3	0.3	0.3	0.3
Chlorodibromomethane	124-48-1	R-63i	SW-846:8260B	VOC	Tpf	1	0	µg/L	—	—	—	—	0.3	0.3	0.3	0.3
Chloroform	67-66-3	R-63i	SW-846:8260B	VOC	Tpf	1	0	µg/L	—	—	—	—	0.3	0.3	0.3	0.3
Chloromethane	74-87-3	R-63i	SW-846:8260B	VOC	Tpf	1	0	µg/L	—	—	—	—	0.3	0.3	0.3	0.3
Chromium	Cr	R-63i	SW-846:6020	Inorganic	Tpf	1	0	µg/L	—	—	—	—	3	3	3	3
Cobalt	Co	R-63i	SW-846:6010C	Inorganic	Tpf	1	0	µg/L	—	—	—	—	1	1	1	1
Copper	Cu	R-63i	SW-846:6010C	Inorganic	Tpf	1	0	µg/L	—	—	—	—	3	3	3	3

Table 4.2-1 (continued)

Parameter Name	Parameter Code	Well	Analytical Method	Analytical Method Category[a]	Geological Unit Code[a]	No. Samples	No. Detects	Unit	Mean Detect	Median Detect	Min Detect	Max Detect	Mean ND	Median ND	Min ND	Max ND
Cyanide (total)	CN (Total)	R-63i	EPA:335.4	Inorganic	Tpf	1	0	µg/L	—	—	—	—	1.67	1.67	1.67	1.67
DNX	DNX	R-63i	SW-846:8330B	LCMS/MS High Explosives	Tpf	1	0	µg/L	—	—	—	—	0.0908	0.0908	0.0908	0.0908
Fluoride	F(-1)	R-63i	EPA:300.0	General Chemistry	Tpf	1	1	µg/L	270	270	270	270	—	—	—	—
Hardness	Hardness	R-63i	SM:A2340B	Inorganic	Tpf	1	1	µg/L	46,700	46,700	46,700	46,700	—	—	—	—
Hexachlorobutadiene	87-68-3	R-63i	SW-846:8260B	VOC	Tpf	1	0	µg/L	—	—	—	—	0.3	0.3	0.3	0.3
HMX	2691-41-0	R-63i	SW-846:8330B	LCMS/MS High Explosives	Tpf	1	0	µg/L	—	—	—	—	0.0908	0.0908	0.0908	0.0908
Iron	Fe	R-63i	SW-846:6010C	Inorganic	Tpf	1	1	µg/L	37.3	37.3	37.3	37.3	—	—	—	—
Lead	Pb	R-63i	SW-846:6020	Inorganic	Tpf	1	0	µg/L	—	—	—	—	0.5	0.5	0.5	0.5
Magnesium	Mg	R-63i	SW-846:6010C	Inorganic	Tpf	1	1	µg/L	3530	3530	3530	3530	—	—	—	—
Manganese	Mn	R-63i	SW-846:6010C	Inorganic	Tpf	1	1	µg/L	5.67	5.67	5.67	5.67	—	—	—	—
Mercury	Hg	R-63i	EPA:245.2	Inorganic	Tpf	2	0	µg/L	—	—	—	—	0.067	0.067	0.067	0.067
Methyl tert-butyl ether	1634-04-4	R-63i	SW-846:8260B	VOC	Tpf	1	0	µg/L	—	—	—	—	0.3	0.3	0.3	0.3
Methyl-2-pentanone[4-]	108-10-1	R-63i	SW-846:8260B	VOC	Tpf	1	0	µg/L	—	—	—	—	1.5	1.5	1.5	1.5
Methylene chloride	75-09-2	R-63i	SW-846:8260B	VOC	Tpf	1	1	µg/L	1.42	1.42	1.42	1.42	—	—	—	—
MNX	MNX	R-63i	SW-846:8330B	LCMS/MS High Explosives	Tpf	1	0	µg/L	—	—	—	—	0.0908	0.0908	0.0908	0.0908
Molybdenum	Mo	R-63i	SW-846:6020	Inorganic	Tpf	1	1	µg/L	2.39	2.39	2.39	2.39	—	—	—	—
Nickel	Ni	R-63i	SW-846:6020	Inorganic	Tpf	1	1	µg/L	0.75	0.75	0.75	0.75	—	—	—	—
Nitrate-nitrite as nitrogen	NO3+NO2-N	R-63i	EPA:353.2	General Chemistry	Tpf	1	1	µg/L	561	561	561	561	—	—	—	—
Nitrotoluene[2-]	88-72-2	R-63i	SW-846:8330B	LCMS/MS High Explosives	Tpf	1	0	µg/L	—	—	—	—	0.093	0.093	0.093	0.093
Perchlorate	ClO4	R-63i	SW-846:6850	LCMS/MS Perchlorate	Tpf	1	1	µg/L	0.223	0.223	0.223	0.223	—	—	—	—
Potassium	K	R-63i	SW-846:6010C	Inorganic	Tpf	1	1	µg/L	1250	1250	1250	1250	—	—	—	—
RDX	121-82-4	R-63i	SW-846:8330B	LCMS/MS High Explosives	Tpf	1	1	µg/L	0.31	0.31	0.31	0.31	—	—	—	—
Selenium	Se	R-63i	SW-846:6020	Inorganic	Tpf	1	0	µg/L	—	—	—	—	2	2	2	2
Silicon dioxide	SiO2	R-63i	SW-846:6010C	Inorganic	Tpf	1	1	µg/L	53,000	53,000	53,000	53,000	—	—	—	—
Silver	Ag	R-63i	SW-846:6020	Inorganic	Tpf	1	0	µg/L	—	—	—	—	0.3	0.3	0.3	0.3
Sodium	Na	R-63i	SW-846:6010C	Inorganic	Tpf	1	1	µg/L	22,000	22,000	22,000	22,000	—	—	—	—
Strontium	Sr	R-63i	SW-846:6010C	Inorganic	Tpf	1	1	µg/L	66.3	66.3	66.3	66.3	—	—	—	—
Styrene	100-42-5	R-63i	SW-846:8260B	VOC	Tpf	1	0	µg/L	—	—	—	—	0.3	0.3	0.3	0.3
Sulfate	SO4(-2)	R-63i	EPA:300.0	General Chemistry	Tpf	1	1	µg/L	3730	3730	3730	3730	—	—	—	—
Temperature	TEMP	R-63i	EPA:170.0	VOC	Tpf	2	2	deg C	2	2	2	2	—	—	—	—
Tetrachloroethene	127-18-4	R-63i	SW-846:8260B	VOC	Tpf	1	0	µg/L	—	—	—	—	0.3	0.3	0.3	0.3
Thallium	Tl	R-63i	SW-846:6020	Inorganic	Tpf	1	0	µg/L	—	—	—	—	0.6	0.6	0.6	0.6
Tin	Sn	R-63i	SW-846:6010C	Inorganic	Tpf	1	0	µg/L	—	—	—	—	2.5	2.5	2.5	2.5

Table 4.2-1 (continued)

Parameter Name	Parameter Code	Well	Analytical Method	Analytical Method Category[a]	Geological Unit Code[a]	No. Samples	No. Detects	Unit	Mean Detect	Median Detect	Min Detect	Max Detect	Mean ND	Median ND	Min ND	Max ND
TNX	TNX	R-63i	SW-846:8330B	LCMS/MS High Explosives	Tpf	1	0	µg/L	—	—	—	—	0.0908	0.0908	0.0908	0.0908
Toluene	108-88-3	R-63i	SW-846:8260B	VOC	Tpf	1	0	µg/L	—	—	—	—	0.3	0.3	0.3	0.3
Total dissolved solids	TDS	R-63i	EPA:160.1	General Chemistry	Tpf	1	1	µg/L	124,000	124,000	124,000	124,000	—	—	—	—
Total Kjeldahl nitrogen	TKN	R-63i	EPA:351.2	General Chemistry	Tpf	1	1	µg/L	94.2	94.2	94.2	94.2	—	—	—	—
Total organic carbon	TOC	R-63i	SW-846:9060	General Chemistry	Tpf	1	1	µg/L	823	823	823	823	—	—	—	—
Total phosphate as phosphorus	PO4-P	R-63i	EPA:365.4	General Chemistry	Tpf	1	1	µg/L	100	100	100	100	—	—	—	—
Trichlorobenzene[1,2,3-]	87-61-6	R-63i	SW-846:8260B	VOC	Tpf	1	0	µg/L	—	—	—	—	0.3	0.3	0.3	0.3
Trichloroethene	79-01-6	R-63i	SW-846:8260B	VOC	Tpf	1	0	µg/L	—	—	—	—	0.3	0.3	0.3	0.3
Trinitrobenzene[1,3,5-]	99-35-4	R-63i	SW-846:8330B	LCMS/MS High Explosives	Tpf	1	0	µg/L	—	—	—	—	0.0908	0.0908	0.0908	0.0908
Trinitrotoluene[2,4,6-]	118-96-7	R-63i	SW-846:8330B	LCMS/MS High Explosives	Tpf	1	0	µg/L	—	—	—	—	0.0908	0.0908	0.0908	0.0908
Uranium	U	R-63i	SW-846:6020	Inorganic	Tpf	1	1	µg/L	0.943	0.943	0.943	0.943	—	—	—	—
Vanadium	V	R-63i	SW-846:6010C	Inorganic	Tpf	1	1	µg/L	1.41	1.41	1.41	1.41	—	—	—	—
Zinc	Zn	R-63i	SW-846:6010C	Inorganic	Tpf	1	0	µg/L	—	—	—	—	6.32	6.32	6.32	6.32

Note: This table summarizes the analytical data used to identify COPCs and calculate EPCs for the risk assessment.

[a] These fields concatenate entries from all samples for the analyte and well combination.

[b] ND = Nondetection,

[c] HEXP = High explosives.

[d] — = Not applicable.

[e] SVOC = Semivolatile organic compound.

[f] VOC = Volatile organic compound.

[g] LCMS/MS = Liquid chromatography mass spectrometry/mass spectrometry.

[h] DNX = Hexahydro-1,3-dinitro-5-nitro-1,3,5-triazine.

[i] RAD = Radionuclides.

[j] PESTPCB = Pesticides/PCBs.

[k] HMX = Her Majesty's Explosive.

[l] MNX = Hexahydro-1-nitroso-3,5-dinitro-1,3,5-triazine.

[m] PFAS = Per- and polyfluoroalkyl substances.

[n] TNX = 2,4,6-trinitroxylene.

Table 4.3-1
Statistical Background Comparison Test Results and Identification of COPCs for Inorganic Chemicals and Radionuclides

Analyte	Two-Sample t-test	Gehan Test	Quantile Test (0.75)	Quantile Test (0.90)	Slippage Test	Notes on Stat Tests	COPC Identification Notes
Aluminum	0.00677	0.1768	0.06279	0.06279	0.03655		Identified as a COPC in R-25 and R-25b. Statistical test results without these wells are 0.28, 0.46, 0.54, 0.54, and 0.37.
Ammonia as nitrogen	0.01484	0.0176	0.04016	0.01008	0.001298		Not a COPC. Ammonia is not recognized as a potential health hazard by EPA or NMED.
Antimony	0.2593	0.3275	1	1	0.05832		
Arsenic	0.2078	0.2681	0.7854	0.6305	0.06389		
Barium	1.425e-15	1.016e-05	4.97e-14	3.196e-06	5.98e-09		Plots show elevated concentrations in a number of wells. Identified as a COPC in all wells where there are one or more detections for simplicity since max concentrations for all wells are far below screening levels.
Beryllium	0.1423	0.1323	1	1	—[a]	Slippage: No detects in background	
Boron	1.606e-24	5.603e-06	8.873e-15	3.196e-06	6.142e-21		Plots show the range of detects in most wells are above the range of background well detects. Identified as a COPC in all wells where there are one or more detections for simplicity since max concentrations for all wells are far below screening levels.
Bromide	0.02459	0.7058	0.1729	0.1729	9.655e-08		Not a COPC. No toxicity data or regulatory criteria.
Cadmium	0.1518	0.1494	1	1	1		
Calcium	1.076e-11	0	8.546e-16	3.196e-06	7.587e-30		Essential nutrient per Section 5.2 of NMED 2019, 700550.
Cesium	NC[b]	NC	NC	NC	NC	All:less than 2 observations in site or background	
Chloride	1.529e-12	0	3.721e-14	1.646e-05	3.721e-14		Essential nutrient per Section 5.2 of NMED 2019, 700550. Maximum below NMAC and MCL standard of 250 mg/L.
Chromium	0.4566	0.2772	0.7225	0.8736	0.6643		
Cobalt	0.07145	0.2144	0.2916	0.2916	0.1703		Identified as a COPC in R-25. Statistical test results without this well are 0.20, 0.21, 0.60, 0.60, and 0.33.
Copper	1.129e-06	0.0446	1.799e-05	1.799e-05	9.774e-09		An early outlier result exists in CdV-16-1(i). Identified as a COPC in two wells (CdV-16-1(i) and R-25b based on review of plots. Statistical test results w/o these wells are 0.23, 0.50, 1, 1 and 0.067.
Cyanide (total)	0.5005	0.2027	1	1	1		
Fluoride	0.07989	0.9921	0.9193	0.009958	0.0002975		Identified as a COPC in R-19. Statistical test results without these wells are 1, 1, 1, 0.80, and 0.62.
Hardness	1.651e-15	0	7.833e-15	1.603e-05	4.737e-35		A measure that's analogous to calcium and magnesium.
Iron	0.01249	0.01946	0.006069	0.002832	0.1271		An early outlier result exists in CdV-16-1(i). In later years, the box plot shows potentially elevated concentrations in at least three other wells [R-19, CdV-16-2(i)r, and R-25b]. Identified as a COPC in all wells where there are one or more detections for simplicity since max concentrations other than the single outlier are far below screening levels.
Lead	0.06189	0.1798	0.4405	0.4405	0.02382		Not identified as a COPC. A single outlier result from 2005 exists in CdV-16-1(i), but all subsequent detections in this well are below the nominal detection limit. The slippage test result without this value is 0.088. Both stat tests and review of plots indicate no differences between site and background wells subsequent to the early outlier result in CdV-16-1(i).
Lithium	NC	NC	NC	NC	NC	All:less than 2 observations in site or background	
Magnesium	4.182e-28	0	8.546e-16	3.196e-06	1.989e-23		No toxicity data or regulatory criteria. Essential nutrient per Section 5.2 of NMED 2019, 700550.
Manganese	0.08557	0.05722	0.1559	0.03501	0.4405		Plots show potentially elevated in wells R-25 and R-25b. Identified as a COPC these wells. Statistical test results w/o R-25 and R-25b are 0.80, 0.37, 0.76, 0.76, 1.
Mercury	0.03332	0.1307	0.1268	0.1268	—	Slippage: No detects in background	Not a COPC. The box plot shows detects all within the range of NDs[c], with a few outlier ND values, and max detect < screening level.
Molybdenum	0.1015	0.9996	0.9935	0.3093	0.1271		

Table 4.3-1 (continued)

Analyte	Two-Sample t-test	Gehan Test	Quantile Test (0.75)	Quantile Test (0.90)	Slippage Test	Notes on Stat Tests	COPC Identification Notes
Nickel	1.484e-06	3.965e-06	1.953e-07	0.0005081	0.6643		Outlier result in R-19. Plots show potentially elevated results in R-25, CdV-16-1(i), and CdV-37-1(i). Identified as a COPC in all wells where there are one or more detections for simplicity since max concentrations in wells near background levels are far below screening levels.
Nitrate	NC	NC	NC	NC	NC	All:less than 2 observations in site or background	
Nitrate-nitrite as nitrogen	8.044e-28	0	1.72e-14	1.254e-05	3.36e-30		Plots show potentially elevated concentrations in most wells. Identified as a COPC in all wells where there are one or more detections for simplicity since max concentrations in wells near background levels are far below screening levels.
Nitrite	NC	NC	NC	NC	NC	All:less than 2 observations in site or background	
Perchlorate	5.113e-16	0	1.537e-13	3.01e-05	2.901e-35		Plots show potentially elevated concentrations in most wells. Identified as a COPC in all wells where there are one or more detections for simplicity since max concentrations in wells near background levels are far below screening levels.
Potassium	0.1286	0.01878	0.8563	5.823e-05	0.0004759		No toxicity data or regulatory criteria. Essential nutrient per Section 5.2 of NMED 2019, 700550.
Selenium	0.1856	0.2766	0.7384	0.7384	0.3634		
Silver	0.1307	0.2011	1	1	0.5		
Sodium	0.007582	2.603e-07	0.004634	0.6305	0.1271		No toxicity data or regulatory criteria. Essential nutrient per Section 5.2 of NMED 2019, 700550.
Strontium	5.632e-27	0	8.546e-16	3.196e-06	5.281e-26		Plots show potentially elevated concentrations in most wells. Identified as a COPC in all wells where there are one or more detections for simplicity since max concentrations in wells near background levels are far below screening levels.
Sulfate	5.996e-05	0	8.895e-08	0.009958	0.007698		An early outlier result exists in R-25. Plots show potentially elevated concentrations in most wells. Identified as a COPC in all wells for simplicity since max concentrations in wells near background levels are far below the NMAC and MCL standards.
Thallium	0.08002	0.07917	1	1	0.0212		Not a COPC. Although slippage is <0.05, the box plot shows that the detects are all well within the range of NDs and the plots are identical in form.
Tin	0.1409	0.1614	0.1996	0.4039	0.1752		
Titanium	NC	NC	NC	NC	NC	All:less than 2 observations in site or background	
Total organic carbon	0.04275	0.006923	0.2934	0.9586	0.1854		No toxicity data or regulatory criteria; organic (carbon-containing) compounds with potential toxicity are assessed individually.
Total phosphate as phosphorus	0.04075	0.00138	0.02212	0.05863	0.1659		No toxicity data or regulatory criteria. Essential nutrient per Section 5.2 of NMED 2019, 700550.
Uranium	2.023e-09	2.163e-09	1.135e-06	0.0005081	0.0004759		Plots show elevated concentrations in many wells. Identified as a COPC in all wells where there are one or more detections for simplicity since max concentrations for all wells are far below screening levels and regulatory standards.
Vanadium	1	0.991	1	1	1		
Zinc	0.01911	6.37e-08	1.717e-07	3.012e-06	3.984e-08		An early outlier result exists in R-25b. Plots show elevated concentrations in many wells. Identified as a COPC in all wells where there are one or more detections for simplicity since max concentrations for all wells are far below screening levels.
Actinium-228	NC	NC	NC	NC	NC	All:less than 2 observations in site or background	
Americium-241	0.1356	0.2214	1	1	—	Slippage: No detects in background	
Antimony-124	NC	NC	NC	NC	NC	All:less than 2 observations in site or background	

Table 4.3-1 (continued)

Analyte	Two-Sample t-test	Gehan Test	Quantile Test (0.75)	Quantile Test (0.90)	Slippage Test	Notes on Stat Tests	COPC Identification Notes
Antimony-125	NC	NC	NC	NC	NC	All:less than 2 observations in site or background	
Barium-133	NC	NC	NC	NC	NC	All:less than 2 observations in site or background	
Barium-140	NC	NC	NC	NC	NC	All:less than 2 observations in site or background	
Beryllium-7	NC	NC	NC	NC	NC	All:less than 2 observations in site or background	
Bismuth-211	0.2979	0.2819	1	1	—	Slippage: No detects in background	
Bismuth-212	NC	NC	NC	NC	NC	All:less than 2 observations in site or background	
Bismuth-214	0.5036	0.3981	1	1	1		
Cadmium-109	NC	NC	NC	NC	NC	All:less than 2 observations in site or background	
Cerium-139	0.9023	0.9495	1	1	—	Slippage: No detects in background	
Cerium-141	NC	NC	NC	NC	NC	All:less than 2 observations in site or background	
Cerium-144	NC	NC	NC	NC	NC	All:less than 2 observations in site or background	
Cesium-134	0.8086	0.8492	1	1	—	Slippage: No detects in background	
Cesium-137	0.6788	0.667	1	1	—	Slippage: No detects in background	
Chromium-51	NC	NC	NC	NC	NC	All:less than 2 observations in site or background	
Cobalt-57	NC	NC	NC	NC	NC	All:less than 2 observations in site or background	
Cobalt-60	0.4916	0.2539	1	1	—	Slippage: No detects in background	
Europium-152	0.6387	0.6019	1	1	—	Slippage: No detects in background	
Europium-154	NC	NC	NC	NC	NC	All:less than 2 observations in site or background	
Europium-155	NC	NC	NC	NC	NC	All:less than 2 observations in site or background	
Gross alpha	0.1507	0.00114	0.01388	0.08397	1		Plots show potentially elevated concentrations in R-19, R-25, and R-25b. Identified as a COPC in all wells where there are one or more detections for simplicity since max concentrations are below the NMAC and MCL standards.
Gross alpha/beta	NC	NC	NC	NC	NC	All:less than 2 observations in site or background	
Gross beta	0.8897	0.7497	0.7657	0.8088	1		
Gross gamma	0.5336	0.7252	0.7006	0.7959	—	Slippage: No detects in background	
Iodine-129	NC	NC	NC	NC	NC	All:less than 2 observations in site or background	
Iron-59	NC	NC	NC	NC	NC	All:less than 2 observations in site or background	
Lanthanum-140	NC	NC	NC	NC	NC	All:less than 2 observations in site or background	

Table 4.3-1 (continued)

Analyte	Two-Sample t-test	Gehan Test	Quantile Test (0.75)	Quantile Test (0.90)	Slippage Test	Notes on Stat Tests	COPC Identification Notes
Lead-211	NC	NC	NC	NC	NC	All:less than 2 observations in site or background	
Lead-212	0.6652	0.6972	1	1	—	Slippage: No detects in background	
Lead-214	0.9323	0.7807	1	1	—	Slippage: No detects in background	
Manganese-54	NC	NC	NC	NC	NC	All:less than 2 observations in site or background	
Mercury-203	0.8226	0.9101	1	1	—	Slippage: No detects in background	
Neptunium-237	0.2593	0.6122	1	1	—	Slippage: No detects in background	
Neptunium-239	NC	NC	NC	NC	NC	All:less than 2 observations in site or background	
Niobium-95	NC	NC	NC	NC	NC	All:less than 2 observations in site or background	
Plutonium-238	0.2931	0.1632	1	1	—	Slippage: No detects in background	
Plutonium-239/240	0.4126	0.1273	1	1	—	Slippage: No detects in background	
Potassium-40	0.4463	0.7409	1	1	—	Slippage: No detects in background	
Protactinium-231	NC	NC	NC	NC	NC	All:less than 2 observations in site or background	
Protactinium-233	NC	NC	NC	NC	NC	All:less than 2 observations in site or background	
Protactinium-234m	NC	NC	NC	NC	NC	All:less than 2 observations in site or background	
Radium-223	NC	NC	NC	NC	NC	All:less than 2 observations in site or background	
Radium-224	NC	NC	NC	NC	NC	All:less than 2 observations in site or background	
Radium-226	0.9235	0.9007	0.8776	0.7308	1		
Radium-228	0.2056	0.4276	0.5758	0.5455	0.5		
Radon-219	NC	NC	NC	NC	NC	All:less than 2 observations in site or background	
Rhodium-106	NC	NC	NC	NC	NC	All:less than 2 observations in site or background	
Ruthenium-103	NC	NC	NC	NC	NC	All:less than 2 observations in site or background	
Ruthenium-106	0.2074	0.5	1	1	—	Slippage: No detects in background	
Selenium-75	NC	NC	NC	NC	NC	All:less than 2 observations in site or background	
Sodium-22	0.998	0.9953	1	1	—	Slippage: No detects in background	
Strontium-85	0.5204	0.3274	1	1	—	Slippage: No detects in background	
Strontium-90	0.5913	0.684	1	1	—	Slippage: No detects in background	
Technetium-99	NC	NC	NC	NC	NC	All:less than 2 observations in site or background	
Thallium-208	0.7404	0.5	1	1	—	Slippage: No detects in background	
Thorium-227	0.4523	0.5	1	1	—	Slippage: No detects in background	

Table 4.3-1 (continued)

Analyte	Two-Sample t-test	Gehan Test	Quantile Test (0.75)	Quantile Test (0.90)	Slippage Test	Notes on Stat Tests	COPC Identification Notes
Thorium-228	NC	NC	NC	NC	NC	All:less than 2 observations in site or background	
Thorium-230	NC	NC	NC	NC	NC	All:less than 2 observations in site or background	
Thorium-231	NC	NC	NC	NC	NC	All:less than 2 observations in site or background	
Thorium-232	NC	NC	NC	NC	NC	All:less than 2 observations in site or background	
Thorium-234	0.6429	0.6023	1	1	—	Slippage: No detects in background	
Tin-113	0.5732	0.348	1	1	—	Slippage: No detects in background	
Tritium	2.585e-07	4.416e-07	9.603e-06	0.01343	3.671e-11		Plots show concentrations are elevated in many wells. Identified as a COPC in all wells where there are one or more detections for simplicity since max concentrations for all wells are far below screening levels and regulatory standard.
Uranium-234	5.831e-05	2.309e-06	0.0004643	0.006873	0.004213		Plots show concentrations are potentially elevated in many wells. Identified as a COPC in all wells where there are one or more detections for simplicity since max concentrations in wells near background levels are far below screening levels.
Uranium-235	0.5749	0.8531	1	1	—	Slippage: No detects in background	
Uranium-235/236	0.4232	0.267	0.868	0.7697	0.6531		
Uranium-238	2.108e-05	0.001743	4.419e-05	0.006873	6.483e-06		Plots show concentrations are potentially elevated in many wells. Identified as a COPC in all wells where there are one or more detections for simplicity since max concentrations in wells near background levels are far below SLs.
Yttrium-88	0.1939	0.3274	1	1	—	Slippage: No detects in background	
Zinc-65	NC	NC	NC	NC	NC	All:less than 2 observations in site or background	
Zirconium-95	NC	NC	NC	NC	NC	All:less than 2 observations in site or background	

Note: Yellow shading indicates a p-value for the statistical test below the significance threshold of 0.05 (meaning there is less than a 1 in 20 probability that site well concentrations are not larger than background well concentrations.)

[a] — = Not applicable.

[b] NC = Not calculated.

[c] ND = Nondetection.

Table 4.3-2
Final List of COPCs, by Site Well

COPC	CdV-16-1(i)	CdV-16-2(i)r	CdV-16-4ip	CdV-37-1(i)	CdV-9-1(i)	R-19	R-25	R-25b	R-63i
Aluminum	No	No	No	No	No	No	Yes	Yes	No
Barium	Yes	Yes	Yes	Yes	Yes	Yes	Yes	Yes	Yes
Boron	Yes	Yes	Yes	Yes	Yes	Yes	Yes	Yes	No
Copper	Yes	No	No	No	No	No	No	Yes	No
Fluoride	No	No	No	No	No	Yes	No	No	No
Iron	Yes	Yes	Yes	Yes	Yes	Yes	Yes	Yes	Yes
Manganese	Yes	No	No	No	No	No	Yes	Yes	No
Nickel	Yes	Nickel	Nickel	Nickel	Nickel	Nickel	Nickel	Nickel	Nickel
Nitrate-nitrite as nitrogen	Yes	Yes	Yes	Yes	Yes	Yes	Yes	Yes	Yes
Perchlorate	Yes	Yes	Yes	Yes	Yes	Yes	Yes	Yes	Yes
Strontium	Yes	Yes	Yes	Yes	Yes	Yes	Yes	Yes	Yes
Sulfate	Yes	Yes	Yes	Yes	Yes	Yes	Yes	Yes	Yes
Uranium	Yes	Yes	Yes	Yes	Yes	Yes	Yes	Yes	Yes
Zinc	Yes	Yes	Yes	Yes	Yes	Yes	Yes	Yes	No
Gross alpha	Yes	No	No	No	Yes	Yes	Yes	Yes	No
Tritium	Yes	Yes	Yes	No	Yes	No	Yes	No	No
Uranium-234	Yes	Yes	Yes	Yes	Yes	Yes	Yes	Yes	No
Uranium-238	Yes	Yes	Yes	Yes	Yes	Yes	Yes	Yes	No
Naphthalenedisulfonic acid[1,5-]	Yes	No	No	No	No	No	No	No	No
Acetone	Yes	Yes	Yes	Yes	Yes	Yes	Yes	No	Yes
Amino-2,6-dinitrotoluene[4-]	Yes	Yes	Yes	No	Yes	No	Yes	Yes	No
Amino-4,6-dinitrotoluene[2-]	Yes	Yes	No	No	Yes	No	Yes	Yes	No
Anthracene	No	No	No	No	No	Yes	No	No	No
Bis(2-ethylhexyl)phthalate	Yes	No	No	No	No	Yes	No	No	No
Bromodichloromethane	No	No	No	No	No	No	No	Yes	No
Bromoform	No	No	No	No	No	No	No	Yes	No
Butanone[2-]	Yes	Yes	No	No	Yes	No	No	No	No
Carbon disulfide	No	No	No	No	Yes	No	Yes	No	No
Chlorobenzene	No	No	No	No	No	No	Yes	No	No
Chlorodibromomethane	No	No	No	No	No	No	No	Yes	No
Chloroform	No	No	No	No	No	No	No	Yes	No
Chloromethane	No	Yes	No	No	No	No	No	No	No
DNX[a]	No	Yes	Yes	No	Yes	No	Yes	No	No
Fluoranthene	No	No	No	No	No	Yes	No	No	No

Table 4.3-2 (continued)

COPC	CdV-16-1(i)	CdV-16-2(i)r	CdV-16-4ip	CdV-37-1(i)	CdV-9-1(i)	R-19	R-25	R-25b	R-63i
Heptachlor	Yes	No	No	No	No	No	No	No	No
HMX[b]	Yes	Yes	Yes	No	Yes	No	Yes	Yes	No
Methyl tert-butyl ether	Yes	Yes	Yes	No	Yes	No	Yes	No	No
Methyl-2-pentanone[4-]	No	Yes	No	No	No	No	No	No	No
Methylene chloride	No	No	No	No	No	No	Yes	No	Yes
MNX[c]	Yes	Yes	Yes	No	Yes	No	Yes	No	No
Nitrotoluene[2-]	No	No	No	No	Yes	No	Yes	No	No
Perfluorooctanoic acid	Yes	Yes	Yes	No	Yes	No	No	No	No
Phenanthrene	No	No	No	No	No	Yes	No	No	No
Pyrene	No	No	No	No	No	Yes	No	No	No
RDX	Yes	Yes	Yes	No	Yes	Yes	Yes	Yes	Yes
Styrene	No	No	No	No	No	No	Yes	No	No
Tetrachloroethene	Yes	Yes	Yes	No	Yes	No	Yes	Yes	No
TNX[d]	Yes	Yes	Yes	No	Yes	No	Yes	No	No
Toluene	Yes	Yes	No	No	Yes	Yes	Yes	No	No
Trichlorobenzene[1,2,3-]	No	No	Yes	No	No	No	No	No	No
Trichloroethene	No	Yes	Yes	No	Yes	No	Yes	No	No
Trinitrobenzene[1,3,5-]	No	Yes	Yes	No	No	No	Yes	No	No
Trinitrotoluene[2,4,6-]	No	No	No	No	Yes	No	Yes	No	No

[a] DNX = Hexahydro-1,3-dinitro-5-nitro-1,3,5-triazine.

[b] HMX = Her Majesty's Explosive.

[c] MNX = Hexahydro-1-nitroso-3,5-dinitro-1,3,5-triazine.

[d] TNX = 2,4,6-trinitroxylene.

Table 4.4-1
NMED and EPA Risk-Based Tap Water Screening Criteria

COPC	CAS[a] Identifier (or Parameter Code)	NMED SL[b]; Noncarcinogenic µg/L	NMED SL; Carcinogenic µg/L	EPA RSL[c]; Noncarcinogenic µg/L	EPA RSL; Carcinogenic µg/L	EPA PRG[d] pCi/L	Notes
Aluminum	7429-90-5	1.99E+04	NA[e]	20,000	NA	—[f]	
Barium	7440-39-3	3.28E+03	NA	3800	NA	—	
Boron	7440-42-8	3.95E+03	NA	4000	NA	—	
Copper	7440-50-8	7.90E+02	NA	800	NA	—	
Fluoride	16984-48-8	1.18E+03	NA	800	NA	—	
Iron	7439-89-6	1.38E+04	NA	14,000	NA	—	
Manganese	7439-96-5	2.02E+03	NA	430	NA	—	EPA value for manganese as “manganese (non-diet)”
Nickel	7440-02-0	3.72E+02	NA	390	NA	—	EPA value for nickel as “nickel soluble salts"
Nitrate-nitrite as nitrogen	E701177	1.68E+04	NA	NA	NA	—	
Perchlorate	14797-73-0	1.38E+01	NA	14	NA	—	
Strontium	7440-24-6	1.18E+04	NA	12,000	NA	—	
Sulfate	14996-02-2	NL[g]	NL	NL	NL	—	
Uranium	7440-61-1	5.92E+01	NA	4	NA	—	
Zinc	7440-66-6	5.96E+03	NA	6000	NA	—	
Tritium	10028-17-8	NA	NA	NA	NA	1.45E+02	
Uranium-234	7440-61-1	NA	NA	NA	NA	7.39E+00	
Uranium-238	7440-61-1	NA	NA	NA	NA	5.86E+00	
Naphthalenedisulfonic acid[1,5-]	1655-29-4	NL	NL	NL	NL	—	
Acetone	67-64-1	1.41E+04	NA	1.40E+04	NA	—	
Amino-2,6-dinitrotoluene[4-]	19406-51-0	NL	NL	39	NA	—	
Amino-4,6-dinitrotoluene[2-]	35572-78-2	NL	NL	39	NA	—	
Anthracene	120-12-7	1.72E+03	NA	1800	NA	—	
Bis(2-ethylhexyl)phthalate	117-81-7	4.01E+02	5.56E+01	400	56	—	
Bromodichloromethane	75-27-4	3.77E+02	1.34E+00	380	1.3	—	
Bromoform	75-25-2	3.76E+02	3.29E+01	380	33	—	
Butanone[2-]	78-93-3	5.56E+03	NA	5600	NA	—	Synonym: methyl ethyl ketone (MEK)
Carbon disulfide	75-15-0	8.10E+02	NA	810	NA	—	
Chlorobenzene	108-90-7	7.76E+01	NA	78	NA	—	
Chlorodibromomethane	124-48-1	3.78E+02	1.68E+00	380	8.7	—	Synonym: dibromochloromethane
Chloroform	67-66-3	9.72E+01	2.29E+00	97	2.2	—	
Chloromethane	74-87-3	1.88E+02	2.03E+01	190	NA	—	
DNX[h]	DNX	7.96E+01	9.66E+00	80	9.7	—	An RDX degradation product; RDX used as a toxicity surrogate.
Fluoranthene	206-44-0	8.02E+02	NA	800	NA	—	
Heptachlor	76-44-8	2.72E+00	2.21E-02	1.3	0.014	—	
HMX[i]	2691-41-0	1.00E+03	NA	1000	NA	—	

Table 4.4-1 (continued)

COPC	CAS[a] Identifier (or Parameter Code)	NMED SL[b]; Noncarcinogenic µg/L	NMED SL; Carcinogenic µg/L	EPA RSL[c]; Noncarcinogenic µg/L	EPA RSL; Carcinogenic µg/L	EPA PRG[d] pCi/L	Notes
Methyl tert-butyl ether	1634-04-4	6.26E+03	NA	6300	140	—	
Methyl-2-pentanone[4-]	108-10-1	1.24E+03	NA	6300	NA	—	Synonym: methyl isobutyl ketone (MIBK)
Methylene chloride	75-09-2	1.06E+02	1.18E+02	110	110	—	Synonym: dichloromethane
MNX[j]	MNX	7.96E+01	9.66E+00	80	9.7	—	An RDX degradation product; RDX used as a toxicity surrogate.
Nitrotoluene[2-]	88-72-2	1.61E+01	3.14E+00	16	3.1	—	
Perfluorooctanoic acid	335-67-1	7.00E-02	NA	NL	NL	—	
Phenanthrene	85-01-8	1.70E+02	NA	NL	NL	—	
Pyrene	129-00-0	1.17E+02	NA	120	NA	—	
RDX	121-82-4	7.96E+01	9.66E+00	80	9.7	—	
Styrene	100-42-5	1.21E+03	NA	1200	NA	—	
Tetrachloroethene	127-18-4	4.03E+01	1.13E+02	41	110	—	
TNX[k]	TNX	7.96E+01	9.66E+00	80	9.7	—	An RDX degradation product; RDX used as a toxicity surrogate.
Toluene	108-88-3	1.09E+03	NA	1100	NA	—	
Trichlorobenzene[1,2,3-]	87-61-6	NL	NL	7	NA	—	
Trichloroethene	79-01-6	2.82E+00	2.59E+00	2.8	4.9	—	
Trinitrobenzene[1,3,5-]	99-35-4	NL	NL	590	NA	—	
Trinitrotoluene[2,4,6-]	118-96-7	9.80E+00	2.53E+01	9.8	25	—	

[a] CAS = Chemical Abstracts Service.

[b] NMED SL = Tap water screening level (NMED 2019, 700550).

[c] EPA RSL = Tap water regional screening level https://www.epa.gov/risk/regional-screening-levels-rsls-generic-tables.

[d] EPA PRG = Calculated tap water preliminary remediation goal.

[e] NA = Not available; no toxicity criteria published for this chemical.

[f] — = Not applicable; EPA preliminary remediation goals apply to radionuclides.

[g] NL = Not listed; this chemical is not listed in the reference.

[h] DNX = Hexahydro-1,3-dinitro-5-nitro-1,3,5-triazine.

[i] HMX = Her Majesty's Explosive.

[j] MNX = Hexahydro-1-nitroso-3,5-dinitro-1,3,5-triazine.

[k] TNX = 2,4,6-trinitroxylene.

Table 4.4-2
NMED Groundwater Standards and EPA Tap Water Maximum Contaminant Levels

COPC	CAS[a] Identifier (or Parameter Code)	NMAC; Part A	NMAC; Part B	Primary MCL or TT[b]	Secondary MCL
Aluminum	7429-90-5	NA[c]	NA	NA	50
Barium	7440-39-3	2000	NA	2000	NA
Boron	7440-42-8	NA	NA	NA	NA
Copper	7440-50-8	NA	1000	1300	1000
Fluoride	16984-48-8	1600	NA	4000	2000
Iron	7439-89-6	NA	1000	NA	300
Manganese	7439-96-5	NA	200	NA	50
Nickel	7440-02-0	NA	NA	NA	NA
Nitrate-nitrite as nitrogen[d]	E701177	1000	NA	1000	NA
Perchlorate	14797-73-0	NA	NA	NA	NA
Strontium	7440-24-6	NA	NA	NA	NA
Sulfate	14996-02-2	NA	600,000	NA	250,000
Uranium	7440-61-1	30	NA	30	NA
Zinc	7440-66-6	NA	10,000	NA	5000
Naphthalenedisulfonic acid[1,5-]	1655-29-4	NA	NA	NA	NA
Acetone	67-64-1	NA	NA	NA	NA
Amino-2,6-dinitrotoluene[4-]	19406-51-0	NA	NA	NA	NA
Amino-4,6-dinitrotoluene[2-]	35572-78-2	NA	NA	NA	NA
Anthracene	120-12-7	NA	NA	NA	NA
Bis(2-ethylhexyl)phthalate	117-81-7	NA	NA	400	NA
Bromodichloromethane	75-27-4	NA	NA	NA	NA
Bromoform	75-25-2	NA	NA	NA	NA
Butanone[2-]	78-93-3	NA	NA	NA	NA
Carbon disulfide	75-15-0	NA	NA	NA	NA
Chlorobenzene	108-90-7	NA	NA	100	NA
Chlorodibromomethane	124-48-1	NA	NA	NA	NA
Chloroform	67-66-3	100	NA	NA	NA
Chloromethane	74-87-3	NA	NA	NA	NA
DNX[e]	DNX	NA	NA	NA	NA
Fluoranthene	206-44-0	NA	NA	NA	NA
Heptachlor	76-44-8	NA	NA	0.4	NA
HMX[f]	2691-41-0	NA	NA	NA	NA
Methyl tert-butyl ether	1634-04-4	NA	100	NA	NA
Methyl-2-pentanone[4-]	108-10-1	NA	NA	NA	NA
Methylene chloride	75-09-2	5	NA	5	NA
MNX[g]	MNX	NA	NA	NA	NA

Table 4.4-2 (continued)

COPC	CAS[a] Identifier (or Parameter Code)	NMAC; Part A	NMAC; Part B	Primary MCL or TT[b]	Secondary MCL
Nitrotoluene[2-]	88-72-2	NA	NA	NA	NA
Perfluorooctanoic acid	335-67-1	NA	NA	NA	NA
Phenanthrene	85-01-8	NA	NA	NA	NA
Pyrene	129-00-0	NA	NA	NA	NA
RDX	121-82-4	NA	NA	NA	NA
Styrene	100-42-5	100	NA	100	NA
Tetrachloroethene	127-18-4	5	NA	5	NA
TNX[h]	TNX	NA	NA	NA	NA
Toluene	108-88-3	1000	NA	1000	NA
Trichlorobenzene[1,2,3-]	87-61-6	NA	NA	NA	NA
Trichloroethene	79-01-6	5	NA	5	NA
Trinitrobenzene[1,3,5-]	99-35-4	NA	NA	NA	NA
Trinitrotoluene[2,4,6-]	118-96-7	NA	NA	NA	NA
Gross alpha (pCi/L)	GROSSA	NA	NA	15	NA
Tritium (pCi/L)	10028-17-8	NA	NA	20,000[i]	NA

Note: Units are in µg/L unless otherwise noted.

[a] CAS = Chemical Abstracts Service.

[b] TT = Treatment technique.

[c] NA = Not available; no standard published for this chemical.

[d] Nitrate-nitrite as nitrogen protectively represented as nitrite (NO_2 as N) from 20.6.2 NMAC.

[e] DNX = Hexahydro-1,3-dinitro-5-nitro-1,3,5-triazine.

[f] HMX = Her Majesty's Explosive.

[g] MNX = Hexahydro-1-nitroso-3,5-dinitro-1,3,5-triazine.

[h] TNX = 2,4,6-trinitroxylene.

[i] The tritium MCL of 20,000 pCi/L is equivalent to 4-mrem/year MCL for beta and photon emitters.

Table 4.5-1
Groundwater Exposure Point Concentrations

COPC Name	Site Well	Category	No. of Analyses[a]	No. of Detects[b]	Min Detect (µg/L)	Max Detect (µg/L)	Mean Concentration[c] (µg/L)	EPC[d] (µg/L)	EPC Method[e]
Naphthalenedisulfonic acid[1,5-]	CdV-16-1(i)	Organic	1	1	20,714	20,714	20,714	20,714	Max detected concentration
Acetone	CdV-16-1(i)	Organic	23	1	1.84	1.84	4.690869565	1.84	Max detected concentration
Amino-2,6-dinitrotoluene[4-]	CdV-16-1(i)	Organic	30	29	0.134	0.292	0.18825	0.198	95% Student's-t UCL
Amino-4,6-dinitrotoluene[2-]	CdV-16-1(i)	Organic	29	19	0.0841	0.193	0.110774138	0.124	95% Student's-t UCL
Barium	CdV-16-1(i)	Inorganic	41	41	14.7	17.9	16.55831707	16.73	95% Student's-t UCL
Bis(2-ethylhexyl)phthalate	CdV-16-1(i)	Organic	9	2	3	4.39	4.186666667	4.39	Max detected concentration
Boron	CdV-16-1(i)	Inorganic	41	41	29.521	78.9	60.75417073	63.46	95% Student's-t UCL
Butanone[2-]	CdV-16-1(i)	Organic	23	1	11.6	11.6	2.591304348	11.6	Max detected concentration
Copper	CdV-16-1(i)	Inorganic	41	39	3.7	63.2	12.68787805	16.21	95% BCA Bootstrap UCL
DNX[f]	CdV-16-1(i)	Organic	21	19	0.106	0.452	0.185428571	0.227	95% BCA Bootstrap UCL
Gross alpha	CdV-16-1(i)	Rad	7	2	1.38	4.15	1.203714286	4.15	Max detected concentration
Heptachlor	CdV-16-1(i)	Organic	2	1	0.0165	0.0165	0.01375	0.0165	Max detected concentration
HMX[g]	CdV-16-1(i)	Organic	30	30	1.21	2.53	1.715333333	1.828	95% BCA Bootstrap UCL
Iron	CdV-16-1(i)	Inorganic	41	11	29.4	2750	125.4878049	334.2	95% BCA Bootstrap UCL
Manganese	CdV-16-1(i)	Inorganic	41	29	2.2	13.6	4.423419512	5.331	95% BCA Bootstrap UCL
Methyl tert-butyl ether	CdV-16-1(i)	Organic	18	16	0.966	1.48	1.135611111	1.235	95% Student's-t UCL
MNX[h]	CdV-16-1(i)	Organic	21	19	0.141	0.391	0.292666667	0.314	95% Student's-t UCL
Nickel	CdV-16-1(i)	Inorganic	41	41	1.69	13.2	4.994797561	5.687	95% BCA Bootstrap UCL
Nitrate-nitrite as nitrogen	CdV-16-1(i)	Inorganic	27	27	510	1090	844.7037037	894.7	95% Student's-t UCL
Perchlorate	CdV-16-1(i)	Inorganic	27	27	0.461	0.577	0.518851852	0.528	95% Student's-t UCL
Perfluorooctanoic acid	CdV-16-1(i)	Organic	1	1	0.00115	0.00115	0.00115	0.0012	Max detected concentration
RDX	CdV-16-1(i)	Organic	31	31	22.2	37.4	28.57096774	29.63	95% Student's-t UCL
Strontium	CdV-16-1(i)	Inorganic	41	41	76.1	110	94.5872439	95.79	95% Student's-t UCL

Table 4.5-1 (continued)

COPC Name	Site Well	Category	No. of Analyses[a]	No. of Detects[b]	Min Detect (µg/L)	Max Detect (µg/L)	Mean Concentration[c] (µg/L)	EPC[d] (µg/L)	EPC Method[e]
Sulfate	CdV-16-1(i)	Inorganic	28	28	8670	12,500	9839.535714	10,215	95% BCA Bootstrap UCL
Tetrachloroethene	CdV-16-1(i)	Organic	23	21	0.79	1.49	1.052565217	1.141	95% Student's-t UCL
TNX[i]	CdV-16-1(i)	Organic	21	19	0.163	0.362	0.232190476	0.251	95% BCA Bootstrap UCL
Toluene	CdV-16-1(i)	Organic	23	9	0.268	119	6.960782609	22.9	95% BCA Bootstrap UCL
Tritium	CdV-16-1(i)	Rad	8	8	26.645	68.264	55.3415	67.03	95% Student's-t UCL
Uranium	CdV-16-1(i)	Inorganic	41	40	0.3	0.62	0.436720488	0.463	95% Student's-t UCL
Uranium-234	CdV-16-1(i)	Rad	8	8	0.293	0.462	0.397625	0.436	95% Student's-t UCL
Uranium-238	CdV-16-1(i)	Rad	8	8	0.112	0.28	0.17175	0.214	95% BCA Bootstrap UCL
Zinc	CdV-16-1(i)	Inorganic	41	36	4.9	70.7	21.6215122	26.33	95% BCA Bootstrap UCL
Acetone	CdV-16-2(i)r	Organic	23	1	7.81	7.81	3.712608696	7.81	Max detected concentration
Amino-2,6-dinitrotoluene[4-]	CdV-16-2(i)r	Organic	33	20	0.0958	0.166	0.134042424	0.142	95% Student's-t UCL
Amino-4,6-dinitrotoluene[2-]	CdV-16-2(i)r	Organic	32	1	0.182	0.182	0.114332813	0.182	Max detected concentration
Barium	CdV-16-2(i)r	Inorganic	24	24	1.95	3.55	2.5175	2.671	95% BCA Bootstrap UCL
Boron	CdV-16-2(i)r	Inorganic	24	21	17.7	37.5	26	28.08	95% Student's-t UCL
Butanone[2-]	CdV-16-2(i)r	Organic	23	1	11.7	11.7	2.519565217	11.7	Max detected concentration
Chloromethane	CdV-16-2(i)r	Organic	23	1	2.7	2.7	0.519565217	2.7	Max detected concentration
DNX	CdV-16-2(i)r	Organic	26	20	0.081	0.385	0.197080769	0.226	95% BCA Bootstrap UCL
HMX	CdV-16-2(i)r	Organic	33	32	0.155	1.98	0.820093939	0.969	95% Student's-t UCL
Iron	CdV-16-2(i)r	Inorganic	24	3	54.5	176	54.02083333	176	Max detected concentration
Methyl tert-butyl ether	CdV-16-2(i)r	Organic	19	16	0.31	0.64	0.463684211	0.513	95% Student's-t UCL
Methyl-2-pentanone[4-]	CdV-16-2(i)r	Organic	23	1	5.35	5.35	2.243478261	5.35	Max detected concentration
MNX	CdV-16-2(i)r	Organic	26	23	0.16	0.667	0.388888462	0.439	95% Student's-t UCL
Nickel	CdV-16-2(i)r	Inorganic	24	10	0.52	1.8	0.78575	0.922	95% Student's-t UCL
Nitrate-nitrite as nitrogen	CdV-16-2(i)r	Inorganic	19	19	498	763	626.6842105	654	95% Student's-t UCL
Perchlorate	CdV-16-2(i)r	Inorganic	19	19	0.242	0.385	0.312105263	0.324	95% Student's-t UCL
Perfluorooctanoic acid	CdV-16-2(i)r	Organic	1	1	0.0108	0.0108	0.0108	0.0108	Max detected concentration

Table 4.5-1 (continued)

COPC Name	Site Well	Category	No. of Analyses[a]	No. of Detects[b]	Min Detect (µg/L)	Max Detect (µg/L)	Mean Concentration[c] (µg/L)	EPC[d] (µg/L)	EPC Method[e]
RDX	CdV-16-2(i)r	Organic	33	32	1.34	128	81.27242424	89.59	95% Student's-t UCL
Strontium	CdV-16-2(i)r	Inorganic	24	24	56.1	67.8	61.84583333	62.91	95% Student's-t UCL
Sulfate	CdV-16-2(i)r	Inorganic	19	19	3190	5000	4217.368421	4377	95% Student's-t UCL
Tetrachloroethene	CdV-16-2(i)r	Organic	23	22	0.289	0.92	0.555565217	0.612	95% BCA Bootstrap UCL
TNX	CdV-16-2(i)r	Organic	26	19	0.0887	0.193	0.150365385	0.171	95% BCA Bootstrap UCL
Toluene	CdV-16-2(i)r	Organic	23	15	0.321	12	2.124391304	3.423	95% BCA Bootstrap UCL
Trichloroethene	CdV-16-2(i)r	Organic	23	14	0.293	0.57	0.404043478	0.446	95% Student's-t UCL
Trinitrobenzene[1,3,5-]	CdV-16-2(i)r	Organic	32	10	0.0856	0.16	0.116792188	0.13	95% Student's-t UCL
Tritium	CdV-16-2(i)r	Rad	11	9	4.993	8.4686	10.7242	8.4686	UCL greater than max detect
Uranium	CdV-16-2(i)r	Inorganic	24	21	0.214	0.394	0.271791667	0.294	95% Student's-t UCL
Uranium-234	CdV-16-2(i)r	Rad	9	8	0.139	0.348	0.202888889	0.247	95% BCA Bootstrap UCL
Uranium-238	CdV-16-2(i)r	Rad	9	9	0.0714	0.203	0.113633333	0.14	95% Student's-t UCL
Zinc	CdV-16-2(i)r	Inorganic	24	24	9.19	33.3	17.29958333	19.58	95% BCA Bootstrap UCL
Acetone	CDV-16-4ip	Organic	20	2	10.5	68.7	7.35125	68.7	Max detected concentration
Amino-2,6-dinitrotoluene[4-]	CDV-16-4ip	Organic	29	28	1.47	2.67	1.90637931	2.06	95% Student's-t UCL
Barium	CDV-16-4ip	Inorganic	28	27	2.2	8.56	3.9425	4.674	95% BCA Bootstrap UCL
Boron	CDV-16-4ip	Inorganic	28	27	15.1	115	63.95	70.14	95% Student's-t UCL
DNX	CDV-16-4ip	Organic	24	24	0.202	0.578	0.305833333	0.344	95% BCA Bootstrap UCL
HMX	CDV-16-4ip	Organic	29	29	6.33	11.8	9.064137931	9.445	95% Student's-t UCL
Iron	CDV-16-4ip	Inorganic	28	2	33.9	105	45.13928571	105	Max detected concentration
Methyl tert-butyl ether	CDV-16-4ip	Organic	20	18	0.32	0.8	0.5595	0.616	95% Student's-t UCL
MNX	CDV-16-4ip	Organic	24	24	0.273	0.92	0.587416667	0.631	95% Student's-t UCL
Nickel	CDV-16-4ip	Inorganic	28	17	0.526	1.19	0.690767857	0.772	95% BCA Bootstrap UCL
Nitrate-nitrite as nitrogen	CDV-16-4ip	Inorganic	28	28	433	1120	868.7142857	917.6	95% Student's-t UCL
Perchlorate	CDV-16-4ip	Inorganic	28	28	0.246	0.397	0.35375	0.365	95% Student's-t UCL
Perfluorooctanoic acid	CDV-16-4ip	Organic	1	1	0.0117	0.0117	0.0117	0.0117	Max detected concentration

Table 4.5-1 (continued)

COPC Name	Site Well	Category	No. of Analyses[a]	No. of Detects[b]	Min Detect (µg/L)	Max Detect (µg/L)	Mean Concentration[c] (µg/L)	EPC[d] (µg/L)	EPC Method[e]
RDX	CDV-16-4ip	Organic	29	29	104	177	132.2413793	137.6	95% BCA Bootstrap UCL
Strontium	CDV-16-4ip	Inorganic	28	28	55.7	71.9	61.45	62.79	95% BCA Bootstrap UCL
Sulfate	CDV-16-4ip	Inorganic	28	28	2410	5660	3693.214286	3878	95% BCA Bootstrap UCL
Tetrachloroethene	CDV-16-4ip	Organic	20	20	0.73	1.12	0.9145	0.961	95% Student's-t UCL
TNX	CDV-16-4ip	Organic	24	24	0.129	1.1	0.261083333	0.371	95% BCA Bootstrap UCL
Trichlorobenzene[1,2,3-]	CDV-16-4ip	Organic	20	1	0.9	0.9	0.4325	0.9	Max detected concentration
Trichloroethene	CDV-16-4ip	Organic	20	20	0.45	0.79	0.6435	0.68	95% Student's-t UCL
Trinitrobenzene[1,3,5-]	CDV-16-4ip	Organic	28	12	0.0867	0.158	0.109471429	0.121	95% Student's-t UCL
Tritium	CDV-16-4ip	Rad	7	7	8.407	33.114	13.72457143	33.114	Max detected concentration
Uranium	CDV-16-4ip	Inorganic	28	27	0.36	0.705	0.474464286	0.502	95% Student's-t UCL
Uranium-234	CDV-16-4ip	Rad	5	5	0.239	0.346	0.2814	0.346	Max detected concentration
Uranium-238	CDV-16-4ip	Rad	5	5	0.141	0.197	0.1712	0.197	Max detected concentration
Zinc	CDV-16-4ip	Inorganic	28	4	4.02	12.4	4.716071429	12.4	Max detected concentration
Acetone	CDV-37-1(i)	Organic	11	2	2.47	4.41	3.173636364	4.41	Max detected concentration
Barium	CDV-37-1(i)	Inorganic	17	17	6.44	18.6	9.628823529	11.27	95% BCA Bootstrap UCL
Boron	CDV-37-1(i)	Inorganic	17	1	17.4	17.4	19.40588235	17.4	Max detected concentration
Iron	CDV-37-1(i)	Inorganic	17	5	31	62.9	37.48235294	44.74	95% Student's-t UCL
Nickel	CDV-37-1(i)	Inorganic	17	17	1.41	7.07	3.625882353	4.436	95% BCA Bootstrap UCL
Nitrate-nitrite as nitrogen	CDV-37-1(i)	Inorganic	17	16	27.4	255	134.2647059	159.5	95% BCA Bootstrap UCL
Perchlorate	CDV-37-1(i)	Inorganic	16	16	0.108	0.257	0.134625	0.159	95% BCA Bootstrap UCL
Strontium	CDV-37-1(i)	Inorganic	17	17	45.6	51	48.6	49.34	95% Student's-t UCL
Sulfate	CDV-37-1(i)	Inorganic	17	17	1430	5130	2505.294118	2971	95% BCA Bootstrap UCL
Uranium	CDV-37-1(i)	Inorganic	17	16	0.293	0.623	0.422823529	0.475	95% Student's-t UCL
Uranium-234	CDV-37-1(i)	Rad	4	4	0.243	0.282	0.26375	0.282	Max detected concentration
Uranium-238	CDV-37-1(i)	Rad	4	3	0.152	0.168	0.1285375	0.168	Max detected concentration
Zinc	CDV-37-1(i)	Inorganic	17	15	3.61	30.7	10.66470588	14.25	95% BCA Bootstrap UCL

Table 4.5-1 (continued)

COPC Name	Site Well	Category	No. of Analyses[a]	No. of Detects[b]	Min Detect (µg/L)	Max Detect (µg/L)	Mean Concentration[c] (µg/L)	EPC[d] (µg/L)	EPC Method[e]
Acetone	CDV-9-1(i)	Organic	12	2	2.59	18.5	4.5075	18.5	Max detected concentration
Amino-2,6-dinitrotoluene[4-]	CDV-9-1(i)	Organic	17	17	0.199	0.769	0.351941176	0.426	95% BCA Bootstrap UCL
Amino-4,6-dinitrotoluene[2-]	CDV-9-1(i)	Organic	17	17	0.29	0.47	0.342882353	0.365	95% BCA Bootstrap UCL
Barium	CDV-9-1(i)	Inorganic	12	12	2.94	7.07	4.928333333	5.434	95% Student's-t UCL
Boron	CDV-9-1(i)	Inorganic	12	10	27.5	52.4	30.48333333	37.49	95% Student's-t UCL
Butanone[2-]	CDV-9-1(i)	Organic	12	1	4.35	4.35	1.925	4.35	Max detected concentration
Carbon disulfide	CDV-9-1(i)	Organic	12	1	1.5	1.5	1.6875	1.5	Max detected concentration
DNX	CDV-9-1(i)	Organic	17	4	0.0892	0.179	0.086747059	0.179	Max detected concentration
Gross alpha	CDV-9-1(i)	Rad	4	1	2.01	2.01	0.969	2.01	Max detected concentration
HMX	CDV-9-1(i)	Organic	17	17	0.728	3.46	1.478647059	1.821	95% BCA Bootstrap UCL
Iron	CDV-9-1(i)	Inorganic	12	2	50.8	126	41.81666667	126	Max detected concentration
Methyl tert-butyl ether	CDV-9-1(i)	Organic	12	11	0.36	1.24	0.755	0.926	95% Student's-t UCL
MNX	CDV-9-1(i)	Organic	17	14	0.0852	0.414	0.147635294	0.192	95% BCA Bootstrap UCL
Nickel	CDV-9-1(i)	Inorganic	12	8	0.547	1.17	0.662416667	0.808	95% Student's-t UCL
Nitrate-nitrite as nitrogen	CDV-9-1(i)	Inorganic	12	12	945	1650	1133.083333	1252	95% BCA Bootstrap UCL
Nitrotoluene[2-]	CDV-9-1(i)	Organic	17	2	0.0941	0.121	0.076758824	0.121	Max detected concentration
Perchlorate	CDV-9-1(i)	Inorganic	12	12	0.404	0.532	0.451916667	0.472	95% Student's-t UCL
Perfluorooctanoic acid	CDV-9-1(i)	Organic	1	1	0.00217	0.00217	0.00217	0.0022	Max detected concentration
RDX	CDV-9-1(i)	Organic	17	17	8.03	37.3	19.74294118	22.78	95% BCA Bootstrap UCL
Strontium	CDV-9-1(i)	Inorganic	12	12	47.7	104	82.05833333	90.02	95% Student's-t UCL
Sulfate	CDV-9-1(i)	Inorganic	12	12	6470	9490	7625.833333	8097	95% BCA Bootstrap UCL
Tetrachloroethene	CDV-9-1(i)	Organic	12	12	0.87	1.35	1.081666667	1.164	95% Student's-t UCL
TNX	CDV-9-1(i)	Organic	16	5	0.0863	0.35	0.0938625	0.143	95% BCA Bootstrap UCL
Toluene	CDV-9-1(i)	Organic	12	1	0.85	0.85	0.383333333	0.85	Max detected concentration
Trichloroethene	CDV-9-1(i)	Organic	12	12	0.31	0.74	0.508333333	0.567	95% Student's-t UCL
Trinitrotoluene[2,4,6-]	CDV-9-1(i)	Organic	17	6	0.0897	0.209	0.102464706	0.123	95% Student's-t UCL

Table 4.5-1 (continued)

COPC Name	Site Well	Category	No. of Analyses[a]	No. of Detects[b]	Min Detect (µg/L)	Max Detect (µg/L)	Mean Concentration[c] (µg/L)	EPC[d] (µg/L)	EPC Method[e]
Tritium	CDV-9-1(i)	Rad	6	6	7.472	16.423	14.29516667	16.423	Max detected concentration
Uranium	CDV-9-1(i)	Inorganic	12	11	0.526	0.967	0.7205	0.812	95% Student's-t UCL
Uranium-234	CDV-9-1(i)	Rad	4	4	0.49	0.684	0.56575	0.684	Max detected concentration
Uranium-238	CDV-9-1(i)	Rad	4	4	0.252	0.406	0.32675	0.406	Max detected concentration
Zinc	CDV-9-1(i)	Inorganic	12	7	3.49	7.83	5.108333333	5.763	95% BCA Bootstrap UCL
Acetone	R-19	Organic	9	1	3.1	3.1	7.417222222	3.1	Max detected concentration
Anthracene	R-19	Organic	8	1	0.2	0.2	2.2373125	0.2	Max detected concentration
Barium	R-19	Inorganic	22	22	22.4	28.2	25.09090909	25.61	95% Student's-t UCL
Bis(2-ethylhexyl)phthalate	R-19	Organic	6	2	0.17	0.61	3.021666667	0.61	Max detected concentration
Boron	R-19	Inorganic	22	11	12.7	20.9	20.51363636	20.9	UCL greater than max detect
Fluoranthene	R-19	Organic	8	1	0.19	0.19	2.1752	0.19	Max detected concentration
Fluoride	R-19	Inorganic	17	17	409	849	571.1176471	618.3	95% BCA Bootstrap UCL
Gross alpha	R-19	Rad	16	3	3.51	9.7	1.37365625	9.7	Max detected concentration
Iron	R-19	Inorganic	22	5	25	281	51.94545455	84.42	95% BCA Bootstrap UCL
Nickel	R-19	Inorganic	22	11	0.51	28.6	2.124886364	5.936	95% BCA Bootstrap UCL
Nitrate-nitrite as nitrogen	R-19	Inorganic	17	17	128	496	356.1176471	390.9	95% Student's-t UCL
Perchlorate	R-19	Inorganic	17	16	0.299	0.381	0.437764706	0.381	UCL greater than max detect
Phenanthrene	R-19	Organic	8	1	0.24	0.24	2.2423125	0.24	Max detected concentration
Pyrene	R-19	Organic	8	1	0.19	0.19	2.1752	0.19	Max detected concentration
RDX	R-19	Organic	14	1	0.098	0.098	0.107592857	0.098	Max detected concentration
Strontium	R-19	Inorganic	22	22	56.6	77.2	70.30909091	71.95	95% Student's-t UCL
Sulfate	R-19	Inorganic	17	17	2570	3560	3226.470588	3316	95% Student's-t UCL
Toluene	R-19	Organic	9	1	0.54	0.54	1.132222222	0.54	Max detected concentration
Uranium	R-19	Inorganic	22	22	0.214	0.344	0.277318182	0.29	95% Student's-t UCL
Uranium-234	R-19	Rad	19	19	0.192	0.332	0.262526316	0.278	95% Student's-t UCL
Uranium-238	R-19	Rad	19	17	0.0786	0.171	0.105042105	0.118	95% Student's-t UCL

Table 4.5-1 (continued)

COPC Name	Site Well	Category	No. of Analyses[a]	No. of Detects[b]	Min Detect (µg/L)	Max Detect (µg/L)	Mean Concentration[c] (µg/L)	EPC[d] (µg/L)	EPC Method[e]
Zinc	R-19	Inorganic	21	15	3	44.4	8.044285714	13.47	95% BCA Bootstrap UCL
Acetone	R-25	Organic	18	2	2.01	3.4	6.411666667	3.4	Max detected concentration
Aluminum	R-25	Inorganic	24	4	76	604	111.625	604	Max detected concentration
Amino-2,6-dinitrotoluene[4-]	R-25	Organic	20	2	0.389	0.6	0.184075	0.6	Max detected concentration
Amino-4,6-dinitrotoluene[2-]	R-25	Organic	20	4	0.093	0.65	0.1767	0.65	Max detected concentration
Barium	R-25	Inorganic	24	24	18.7	40.4	21.70833333	24.11	95% BCA Bootstrap UCL
Boron	R-25	Inorganic	24	24	12.3	61.6	29.15	32.84	95% BCA Bootstrap UCL
Carbon disulfide	R-25	Organic	18	1	1.36	1.36	2.436666667	1.36	Max detected concentration
Chlorobenzene	R-25	Organic	18	3	0.73	2.3	0.745555556	2.3	Max detected concentration
DNX	R-25	Organic	11	6	0.101	0.18	0.162136364	0.18	UCL greater than max detect
Gross alpha	R-25	Rad	7	1	3.09	3.09	0.835285714	3.09	Max detected concentration
HMX	R-25	Organic	20	7	0.115	4.9	0.4897	1.346	95% BCA Bootstrap UCL
Iron	R-25	Inorganic	24	13	32.3	524	103.31875	161.9	95% BCA Bootstrap UCL
Manganese	R-25	Inorganic	24	20	2	52.7	16.26208333	23.13	95% BCA Bootstrap UCL
Methyl tert-butyl ether	R-25	Organic	9	9	0.94	1.31	1.104444444	1.177	95% Student's-t UCL
Methylene chloride	R-25	Organic	18	1	0.85	0.85	3.222222222	0.85	Max detected concentration
MNX	R-25	Organic	11	10	0.13	0.42	0.223	0.275	95% BCA Bootstrap UCL
Nickel	R-25	Inorganic	24	21	0.75	11	3.031875	4.072	95% BCA Bootstrap UCL
Nitrate-nitrite as nitrogen	R-25	Inorganic	16	12	58.5	1230	519.28125	700.4	95% Student's-t UCL
Nitrotoluene[2-]	R-25	Organic	20	2	0.104	1.1	0.236025	1.1	Max detected concentration
Perchlorate	R-25	Inorganic	15	13	0.0521	0.53	0.444553333	0.53	UCL greater than max detect
RDX	R-25	Organic	20	18	1.9	26.7	13.1505	16.15	95% Student's-t UCL
Strontium	R-25	Inorganic	24	24	96.9	366	139.6708333	168.7	95% BCA Bootstrap UCL
Styrene	R-25	Organic	18	1	1	1	0.861111111	1	Max detected concentration
Sulfate	R-25	Inorganic	16	16	9310	207000	30841.25	66423	95% BCA Bootstrap UCL
Tetrachloroethene	R-25	Organic	18	11	0.31	1.21	1.106666667	1.21	UCL greater than max detect

Table 4.5-1 (continued)

COPC Name	Site Well	Category	No. of Analyses[a]	No. of Detects[b]	Min Detect (µg/L)	Max Detect (µg/L)	Mean Concentration[c] (µg/L)	EPC[d] (µg/L)	EPC Method[e]
TNX	R-25	Organic	11	8	0.12	0.2	0.156636364	0.19	95% Student's-t UCL
Toluene	R-25	Organic	17	5	0.24	15	1.561470588	4.35	95% BCA Bootstrap UCL
Trichloroethene	R-25	Organic	18	12	0.31	0.9	1.013611111	0.9	UCL greater than max detect
Trinitrobenzene[1,3,5-]	R-25	Organic	20	1	0.315	0.315	0.157125	0.315	Max detected concentration
Trinitrotoluene[2,4,6-]	R-25	Organic	20	1	0.36	0.36	0.159375	0.36	Max detected concentration
Tritium	R-25	Rad	11	10	30.6544	67.942	34.92821818	43.48	95% Student's-t UCL
Uranium	R-25	Inorganic	24	23	0.127	0.812	0.566083333	0.634	95% Student's-t UCL
Uranium-234	R-25	Rad	15	13	0.315	0.733	0.400943333	0.488	95% Student's-t UCL
Uranium-238	R-25	Rad	15	14	0.15	0.47	0.258992	0.32	95% Student's-t UCL
Zinc	R-25	Inorganic	24	19	2.4	20.1	7.436875	9.171	95% BCA Bootstrap UCL
Aluminum	R-25b	Inorganic	19	8	111	1010	226.6842105	357.7	95% BCA Bootstrap UCL
Amino-2,6-dinitrotoluene[4-]	R-25b	Organic	11	2	0.117	0.169	0.134818182	0.169	Max detected concentration
Amino-4,6-dinitrotoluene[2-]	R-25b	Organic	11	1	0.165	0.165	0.141272727	0.165	Max detected concentration
Barium	R-25b	Inorganic	19	18	8.41	40.6	16.55368421	21.57	95% BCA Bootstrap UCL
Boron	R-25b	Inorganic	19	12	15.5	51.4	23.42894737	27.72	95% BCA Bootstrap UCL
Bromodichloromethane	R-25b	Organic	11	2	1.08	2.18	0.705454545	2.18	Max detected concentration
Bromoform	R-25b	Organic	11	2	0.72	1.79	0.637272727	1.79	Max detected concentration
Chlorodibromomethane	R-25b	Organic	11	2	1.47	3.04	0.819090909	3.04	Max detected concentration
Chloroform	R-25b	Organic	11	2	1.62	4.09	0.928181818	4.09	Max detected concentration
Copper	R-25b	Inorganic	19	7	3.99	15.9	6.361578947	8.103	95% BCA Bootstrap UCL
Gross alpha	R-25b	Rad	3	1	3.92	3.92	1.539416667	3.92	Max detected concentration
HMX	R-25b	Organic	12	9	0.155	0.656	0.282416667	0.376	95% BCA Bootstrap UCL
Iron	R-25b	Inorganic	19	10	32.5	600	135.0657895	214.4	95% BCA Bootstrap UCL
Manganese	R-25b	Inorganic	19	10	4.3	102	22.13210526	37.6	95% BCA Bootstrap UCL
Nickel	R-25b	Inorganic	19	15	0.627	5.6	2.011684211	2.696	95% BCA Bootstrap UCL
Nitrate-nitrite as nitrogen	R-25b	Inorganic	18	17	41.3	930	528.8777778	632.5	95% Student's-t UCL

Table 4.5-1 (continued)

COPC Name	Site Well	Category	No. of Analyses[a]	No. of Detects[b]	Min Detect (µg/L)	Max Detect (µg/L)	Mean Concentration[c] (µg/L)	EPC[d] (µg/L)	EPC Method[e]
Perchlorate	R-25b	Inorganic	16	16	0.208	0.313	0.2810625	0.293	95% Student's-t UCL
RDX	R-25b	Organic	12	12	0.144	8.49	3.520166667	4.873	95% Student's-t UCL
Strontium	R-25b	Inorganic	19	19	50.8	91.9	73.45789474	77.24	95% Student's-t UCL
Sulfate	R-25b	Inorganic	18	18	2250	21000	7283.333333	10077	95% BCA Bootstrap UCL
Tetrachloroethene	R-25b	Organic	11	3	0.32	0.38	0.457272727	0.38	Max detected concentration
Uranium	R-25b	Inorganic	19	19	0.264	3.12	1.137684211	1.454	95% BCA Bootstrap UCL
Uranium-234	R-25b	Rad	4	4	0.207	1.77	1.10425	1.77	Max detected concentration
Uranium-238	R-25b	Rad	4	4	0.13	0.554	0.3875	0.554	Max detected concentration
Zinc	R-25b	Inorganic	19	18	7.5	1420	105.3473684	327.7	95% BCA Bootstrap UCL
Acetone	R-63i	Organic	1	1	1.92	1.92	1.92	1.92	Max detected concentration
Barium	R-63i	Inorganic	1	1	10.9	10.9	10.9	10.9	Max detected concentration
Iron	R-63i	Inorganic	1	1	37.3	37.3	37.3	37.3	Max detected concentration
Methylene chloride	R-63i	Organic	1	1	1.42	1.42	1.42	1.42	Max detected concentration
Nickel	R-63i	Inorganic	1	1	0.75	0.75	0.75	0.75	Max detected concentration
Nitrate-nitrite as nitrogen	R-63i	Inorganic	1	1	561	561	561	561	Max detected concentration
Perchlorate	R-63i	Inorganic	1	1	0.223	0.223	0.223	0.223	Max detected concentration

Table 4.5-1 (continued)

COPC Name	Site Well	Category	No. of Analyses[a]	No. of Detects[b]	Min Detect (µg/L)	Max Detect (µg/L)	Mean Concentration[c] (µg/L)	EPC[d] (µg/L)	EPC Method[e]
RDX	R-63i	Organic	1	1	0.31	0.31	0.31	0.31	Max detected concentration
Strontium	R-63i	Inorganic	1	1	66.3	66.3	66.3	66.3	Max detected concentration
Sulfate	R-63i	Inorganic	1	1	3730	3730	3730	3730	Max detected concentration
Uranium	R-63i	Inorganic	1	1	0.943	0.943	0.943	0.943	Max detected concentration

[a] No. of Analyses = The number of samples for the analyte.

[b] No. of Detects = Number of detected results (values with validation qualifiers other than those containing “U”).

[c] The arithmetic mean was calculated using one-half of the detection limit to represent the concentration of U-qualified (non-detect) results. Because ProUCL software uses various methods to represent the concentration for nondetections, some of these mean values could be below the 95% UCL estimate when detected concentrations are small relative to the detection limit.

[d] EPC = Exposure point concentration. The 95% UCL if there were at least eight samples and five detected values; otherwise the maximum detected value.

[e] EPC Method = Basis of the 95% UCL calculation. See ProUCL software output for details.

[f] DNX = Hexahydro-1,3-dinitro-5-nitro-1,3,5-triazine.

[g] HMX = Her Majesty’s Explosive.

[h] MNX = Hexahydro-1-nitroso-3,5-dinitro-1,3,5-triazine.

[i] TNX = 2,4,6-trinitroxylene.

Table 4.6-1

Summary of Screening-Level Risk Assessment Results

Screening Results for Chemical COPCs					Screening Results for Radionuclide COPCs		
	Cancer Risk		Hazard Index			Cancer Risk	
Well	Cancer Risk (using Max Detect)	Cancer Risk (using EPCs)	Sum of Ratios (using Max Detect)	Sum of Ratios (using EPCs)	Well	Cancer Risk (using Max Detect)	Cancer Risk (using EPCs)
CdV-16-1(i)	5E-05	4E-05	1	0.7	CdV-16-1(i)	6E-06	6E-06
CdV-16-2(i)r	1E-04	1E-04	2	2	CdV-16-2(i)r	3E-06	1E-06
CDV-16-4ip	2E-04	1E-04	3	2	CDV-16-4ip	3E-06	3E-06
CDV-37-1(i)	0E+00	0E+00	0.09	0.06	CDV-37-1(i)	7E-07	7E-07
CDV-9-1(i)	4E-05	3E-05	1	0.8	CDV-9-1(i)	3E-06	3E-06
R-19	2E-07	2E-07	1	0.9	R-19	7E-07	6E-07
R-25	4E-05	2E-05	1	0.9	R-25	6E-06	4E-06
R-25b	6E-05	6E-05	0.8	0.4	R-25b	3E-06	3E-06
R-63i	4E-07	4E-07	0.1	0.1	R-63i	NA*	NA

Notes: Purple shading indicates chemical hazard index > 1. Blue shading indicates chemical cancer risk > 1E-05.

*NA = Not available.

Table 4.6-2

Cumulative Risk Assessment Screening for Chemicals in Well CdV-16-1(i)

COPC Name	Category	Cancer Risk (Max)	Cancer Risk (EPC)	Non-cancer Risk (Max)	Non-cancer Risk (EPC)
Naphthalenedisulfonic acid[1,5-]	Organic	NA[a]	NA	NA	NA
Acetone	Organic	NA	NA	1.31E-04	1.31E-04
Amino-2,6-dinitrotoluene[4-]	Organic	NA	NA	7.49E-03	5.08E-03
Amino-4,6-dinitrotoluene[2-]	Organic	NA	NA	4.95E-03	3.18E-03
Barium	Inorganic	NA	NA	5.46E-03	5.10E-03
Bis(2-ethylhexyl)phthalate	Organic	7.89E-07	7.89E-07	1.09E-02	1.09E-02
Boron	Inorganic	NA	NA	2.00E-02	1.61E-02

Table 4.6-2 (continued)

COPC Name	Category	Cancer Risk (Max)	Cancer Risk (EPC)	Non-cancer Risk (Max)	Non-cancer Risk (EPC)
Butanone[2-]	Organic	NA	NA	2.08E-03	2.08E-03
Copper	Inorganic	NA	NA	8.00E-02	2.05E-02
DNX[b]	Organic	4.68E-07	2.35E-07	5.68E-03	2.85E-03
Heptachlor	Organic	7.46E-06	7.46E-06	6.07E-03	6.07E-03
HMX[c]	Organic	NA	NA	2.53E-03	1.83E-03
Iron	Inorganic	NA	NA	1.99E-01	2.42E-02
Manganese	Inorganic	NA	NA	6.74E-03	2.64E-03
Methyl tert-butyl ether	Organic	1.03E-07	8.63E-08	2.37E-04	1.97E-04
MNX[d]	Organic	4.05E-07	3.25E-07	4.91E-03	3.94E-03
Nickel	Inorganic	NA	NA	3.55E-02	1.53E-02
Nitrate-nitrite as nitrogen	Inorganic	NA	NA	6.49E-02	5.33E-02
Perchlorate	Inorganic	NA	NA	4.17E-02	3.82E-02
Perfluorooctanoic acid	Organic	NA	NA	1.64E-02	1.64E-02
RDX	Organic	3.87E-05	3.07E-05	4.70E-01	3.72E-01
Strontium	Inorganic	NA	NA	9.28E-03	8.09E-03
Sulfate	Inorganic	NA	NA	NA	NA
Tetrachloroethene	Organic	1.32E-07	1.01E-07	3.70E-02	2.83E-02
TNX[e]	Organic	3.75E-07	2.60E-07	4.55E-03	3.15E-03
Toluene	Organic	NA	NA	1.09E-01	2.09E-02
Uranium	Inorganic	NA	NA	1.05E-02	7.82E-03
Zinc	Inorganic	NA	NA	1.19E-02	4.42E-03
	Risk/Hazard	**5E-05**	**4E-05**	**1**	**0.7**

[a] NA = Not available.

[b] DNX = Hexahydro-1,3-dinitro-5-nitro-1,3,5-triazine.

[c] HMX = Her Majesty's Explosive.

[d] MNX = Hexahydro-1-nitroso-3,5-dinitro-1,3,5-triazine.

[e] TNX = 2,4,6-trinitroxylene.

Table 4.6-3
Cumulative Risk Assessment Screening for Chemicals in Well CdV-16-2(i)r

COPC Name	Category	Cancer Risk (Max)	Cancer Risk (EPC)	Non-cancer Risk (Max)	Non-cancer Risk (EPC)
Acetone	Organic	NA[a]	NA	5.55E-04	5.55E-04
Amino-2,6-dinitrotoluene[4-]	Organic	NA	NA	4.26E-03	3.64E-03
Amino-4,6-dinitrotoluene[2-]	Organic	NA	NA	4.67E-03	4.67E-03
Barium	Inorganic	NA	NA	1.08E-03	8.15E-04
Boron	Inorganic	NA	NA	9.50E-03	7.11E-03
Butanone[2-]	Organic	NA	NA	2.10E-03	2.10E-03
Chloromethane	Organic	1.33E-06	1.33E-06	1.44E-02	1.44E-02
DNX[b]	Organic	3.99E-07	2.34E-07	4.84E-03	2.84E-03
HMX[c]	Organic	NA	NA	1.98E-03	9.68E-04
Iron	Inorganic	NA	NA	1.27E-02	1.27E-02
Methyl tert-butyl ether	Organic	4.47E-08	3.59E-08	1.02E-04	8.20E-05
Methyl-2-pentanone[4-]	Organic	NA	NA	4.30E-03	4.30E-03
MNX[d]	Organic	6.91E-07	4.55E-07	8.38E-03	5.52E-03
Nickel	Inorganic	NA	NA	4.84E-03	2.48E-03
Nitrate-nitrite as nitrogen	Inorganic	NA	NA	4.55E-02	3.90E-02
Perchlorate	Inorganic	NA	NA	2.79E-02	2.34E-02
Perfluorooctanoic acid	Organic	NA	NA	1.54E-01	1.54E-01
RDX	Organic	1.33E-04	9.28E-05	1.61E+00	1.13E+00
Strontium	Inorganic	NA	NA	5.72E-03	5.31E-03
Sulfate	Inorganic	NA	NA	NA	NA
Tetrachloroethene	Organic	8.15E-08	5.42E-08	2.28E-02	1.52E-02
TNX[e]	Organic	2.00E-07	1.77E-07	2.42E-03	2.15E-03
Toluene	Organic	NA	NA	1.10E-02	3.13E-03

Table 4.6-3 (continued)

COPC Name	Category	Cancer Risk (Max)	Cancer Risk (EPC)	Non-cancer Risk (Max)	Non-cancer Risk (EPC)
Trichloroethene	Organic	2.20E-06	1.72E-06	2.02E-01	1.58E-01
Trinitrobenzene[1,3,5-]	Organic	NA	NA	2.71E-04	2.20E-04
Uranium	Inorganic	NA	NA	6.65E-03	4.96E-03
Zinc	Inorganic	NA	NA	5.59E-03	3.28E-03
	Risk/Hazard	**1E-04**	**1E-04**	**2**	**1.6**

[a] NA = Not available.

[b] DNX = Hexahydro-1,3-dinitro-5-nitro-1,3,5-triazine.

[c] HMX = Her Majesty's Explosive.

[d] MNX = Hexahydro-1-nitroso-3,5-dinitro-1,3,5-triazine.

[e] TNX = 2,4,6-trinitroxylene.

Table 4.6-4
Cumulative Risk Assessment Screening for Chemicals in Well CdV-16-4ip

COPC Name	Category	Cancer Risk (Max)	Cancer Risk (EPC)	Non-cancer Risk (Max)	Non-cancer Risk (EPC)
Acetone	Organic	NA[a]	NA	4.88E-03	4.88E-03
Amino-2,6-dinitrotoluene[4-]	Organic	NA	NA	6.85E-02	5.28E-02
Barium	Inorganic	NA	NA	2.61E-03	1.43E-03
Boron	Inorganic	NA	NA	2.91E-02	1.78E-02
DNX[b]	Organic	5.98E-07	3.56E-07	7.26E-03	4.32E-03
HMX[c]	Organic	NA	NA	1.18E-02	9.43E-03
Iron	Inorganic	NA	NA	7.60E-03	7.60E-03
Methyl tert-butyl ether	Organic	5.59E-08	4.31E-08	1.28E-04	9.84E-05
MNX[d]	Organic	9.53E-07	6.53E-07	1.16E-02	7.93E-03
Nickel	Inorganic	NA	NA	3.20E-03	2.08E-03
Nitrate-nitrite as nitrogen	Inorganic	NA	NA	6.67E-02	5.47E-02

Table 4.6-4 (continued)

COPC Name	Category	Cancer Risk (Max)	Cancer Risk (EPC)	Non-cancer Risk (Max)	Non-cancer Risk (EPC)
Perchlorate	Inorganic	NA	NA	2.87E-02	2.64E-02
Perfluorooctanoic acid	Organic	NA	NA	1.67E-01	1.67E-01
RDX	Organic	1.83E-04	1.42E-04	2.22E+00	1.73E+00
Strontium	Inorganic	NA	NA	6.07E-03	5.30E-03
Sulfate	Inorganic	NA	NA	NA	NA
Tetrachloroethene	Organic	9.92E-08	8.51E-08	2.78E-02	2.38E-02
TNX[e]	Organic	1.14E-06	3.84E-07	1.38E-02	4.66E-03
Trichlorobenzene[1,2,3-]	Organic	NA	NA	1.29E-01	1.29E-01
Trichloroethene	Organic	3.05E-06	2.62E-06	2.80E-01	2.41E-01
Trinitrobenzene[1,3,5-]	Organic	NA	NA	2.68E-04	2.05E-04
Uranium	Inorganic	NA	NA	1.19E-02	8.47E-03
Zinc	Inorganic	NA	NA	2.08E-03	2.08E-03
	Risk/Hazard	**2E-04**	**1E-04**	**3**	**2.5**

[a] NA = Not available.

[b] DNX = Hexahydro-1,3-dinitro-5-nitro-1,3,5-triazine.

[c] HMX = Her Majesty's Explosive.

[d] MNX = Hexahydro-1-nitroso-3,5-dinitro-1,3,5-triazine.

[e] TNX = 2,4,6-trinitroxylene.

Table 4.6-5
Cumulative Risk Assessment Screening for Chemicals in Well CdV-37-1(i)

COPC Name	Category	Cancer Risk (Max)	Cancer Risk (EPC)	Non-cancer Risk (Max)	Non-cancer Risk (EPC)
Acetone	Organic	NA*	NA	3.14E-04	3.14E-04
Barium	Inorganic	NA	NA	5.68E-03	3.44E-03
Boron	Inorganic	NA	NA	4.41E-03	4.41E-03
Iron	Inorganic	NA	NA	4.55E-03	3.24E-03
Nickel	Inorganic	NA	NA	1.90E-02	1.19E-02
Nitrate-nitrite as nitrogen	Inorganic	NA	NA	1.52E-02	9.50E-03
Perchlorate	Inorganic	NA	NA	1.86E-02	1.15E-02
Strontium	Inorganic	NA	NA	4.30E-03	4.16E-03
Sulfate	Inorganic	NA	NA	NA	NA
Uranium	Inorganic	NA	NA	1.05E-02	8.02E-03
Zinc	Inorganic	NA	NA	5.15E-03	2.39E-03
	Risk/Hazard	**0E+00**	**0E+00**	**0.09**	**0.06**

* NA = Not available.

Table 4.6-6
Cumulative Risk Assessment Screening for Chemicals in Well CdV-9-1(i)

COPC Name	Category	Cancer Risk (Max)	Cancer Risk (EPC)	Non-cancer Risk (Max)	Non-cancer Risk (EPC)
Acetone	Organic	NA[a]	NA	1.32E-03	1.32E-03
Amino-2,6-dinitrotoluene[4-]	Organic	NA	NA	1.97E-02	1.09E-02
Amino-4,6-dinitrotoluene[2-]	Organic	NA	NA	1.21E-02	9.36E-03
Barium	Inorganic	NA	NA	2.16E-03	1.66E-03
Boron	Inorganic	NA	NA	1.33E-02	9.49E-03
Butanone[2-]	Organic	NA	NA	7.82E-04	7.82E-04
Carbon disulfide	Organic	NA	NA	1.85E-03	1.85E-03

Table 4.6-6 (continued)

COPC Name	Category	Cancer Risk (Max)	Cancer Risk (EPC)	Non-cancer Risk (Max)	Non-cancer Risk (EPC)
DNX[b]	Organic	1.85E-07	1.85E-07	2.25E-03	2.25E-03
HMX[c]	Organic	NA	NA	3.46E-03	1.82E-03
Iron	Inorganic	NA	NA	9.12E-03	9.12E-03
Methyl tert-butyl ether	Organic	8.67E-08	6.47E-08	1.98E-04	1.48E-04
MNX[d]	Organic	4.29E-07	1.99E-07	5.20E-03	2.41E-03
Nickel	Inorganic	NA	NA	3.15E-03	2.17E-03
Nitrate-nitrite as nitrogen	Inorganic	NA	NA	9.83E-02	7.46E-02
Nitrotoluene[2-]	Organic	3.85E-07	3.85E-07	7.52E-03	7.52E-03
Perchlorate	Inorganic	NA	NA	3.85E-02	3.41E-02
Perfluorooctanoic acid	Organic	NA	NA	3.10E-02	3.10E-02
RDX	Organic	3.86E-05	2.36E-05	4.69E-01	2.86E-01
Strontium	Inorganic	NA	NA	8.78E-03	7.60E-03
Sulfate	Inorganic	NA	NA	NA	NA
Tetrachloroethene	Organic	1.20E-07	1.03E-07	3.35E-02	2.89E-02
TNX[e]	Organic	3.62E-07	1.48E-07	4.40E-03	1.80E-03
Toluene	Organic	NA	NA	7.78E-04	7.78E-04
Trichloroethene	Organic	2.86E-06	2.19E-06	2.62E-01	2.01E-01
Trinitrotoluene[2,4,6-]	Organic	8.24E-08	4.85E-08	2.13E-02	1.26E-02
Uranium	Inorganic	NA	NA	1.63E-02	1.37E-02
Zinc	Inorganic	NA	NA	1.31E-03	9.67E-04
Risk/Hazard		**4E-05**	**3E-05**	**1**	**0.8**

[a] NA = Not available.

[b] DNX = Hexahydro-1,3-dinitro-5-nitro-1,3,5-triazine.

[c] HMX = Her Majesty's Explosive.

[d] MNX = Hexahydro-1-nitroso-3,5-dinitro-1,3,5-triazine.

[e] TNX = 2,4,6-trinitroxylene.

Table 4.6-7
Cumulative Risk Assessment Screening for Chemicals in Well R-19

COPC Name	Category	Cancer Risk (Max)	Cancer Risk (EPC)	Non-cancer Risk (Max)	Non-cancer Risk (EPC)
Acetone	Organic	NA*	NA	2.20E-04	2.20E-04
Anthracene	Organic	NA	NA	1.16E-04	1.16E-04
Barium	Inorganic	NA	NA	8.60E-03	7.81E-03
Bis(2-ethylhexyl)phthalate	Organic	1.10E-07	1.10E-07	1.52E-03	1.52E-03
Boron	Inorganic	NA	NA	5.29E-03	5.29E-03
Fluoranthene	Organic	NA	NA	2.37E-04	2.37E-04
Fluoride	Inorganic	NA	NA	1.06E+00	7.73E-01
Iron	Inorganic	NA	NA	2.03E-02	6.11E-03
Nickel	Inorganic	NA	NA	7.69E-02	1.60E-02
Nitrate-nitrite as nitrogen	Inorganic	NA	NA	2.96E-02	2.33E-02
Perchlorate	Inorganic	NA	NA	2.76E-02	2.76E-02
Phenanthrene	Organic	NA	NA	1.41E-03	1.41E-03
Pyrene	Organic	NA	NA	1.62E-03	1.62E-03
RDX	Organic	1.01E-07	1.01E-07	1.23E-03	1.23E-03
Strontium	Inorganic	NA	NA	6.52E-03	6.07E-03
Sulfate	Inorganic	NA	NA	NA	NA
Toluene	Organic	NA	NA	4.94E-04	4.94E-04
Uranium	Inorganic	NA	NA	5.81E-03	4.90E-03
Zinc	Inorganic	NA	NA	7.45E-03	2.26E-03
Risk/Hazard		**2E-07**	**2E-07**	**1**	**0.9**

* NA = Not available.

Table 4.6-8
Cumulative Risk Assessment Screening for Chemicals in Well R-25

COPC Name	Category	Cancer Risk (Max)	Cancer Risk (EPC)	Non-cancer Risk (Max)	Non-cancer Risk (EPC)
Acetone	Organic	NA[a]	NA	2.42E-04	2.42E-04
Aluminum	Inorganic	NA	NA	3.03E-02	3.03E-02
Amino-2,6-dinitrotoluene[4-]	Organic	NA	NA	1.54E-02	1.54E-02
Amino-4,6-dinitrotoluene[2-]	Organic	NA	NA	1.67E-02	1.67E-02
Barium	Inorganic	NA	NA	1.23E-02	7.36E-03
Boron	Inorganic	NA	NA	1.56E-02	8.32E-03
Carbon disulfide	Organic	NA	NA	1.68E-03	1.68E-03
Chlorobenzene	Organic	NA	NA	2.96E-02	2.96E-02
DNX[b]	Organic	1.86E-07	1.86E-07	2.26E-03	2.26E-03
HMX[c]	Organic	NA	NA	4.89E-03	1.34E-03
Iron	Inorganic	NA	NA	3.79E-02	1.17E-02
Manganese	Inorganic	NA	NA	2.61E-02	1.15E-02
Methyl tert-butyl ether	Organic	9.16E-08	8.23E-08	2.09E-04	1.88E-04
Methylene chloride	Organic	7.21E-08	7.21E-08	7.98E-03	7.98E-03
MNX[d]	Organic	4.35E-07	2.85E-07	5.28E-03	3.45E-03
Nickel	Inorganic	NA	NA	2.96E-02	1.09E-02
Nitrate-nitrite as nitrogen	Inorganic	NA	NA	7.33E-02	4.17E-02
Nitrotoluene[2-]	Organic	3.50E-06	3.50E-06	6.83E-02	6.83E-02
Perchlorate	Inorganic	NA	NA	3.83E-02	3.83E-02
RDX	Organic	2.76E-05	1.67E-05	3.35E-01	2.03E-01
Strontium	Inorganic	NA	NA	3.09E-02	1.42E-02
Styrene	Organic	NA	NA	8.30E-04	8.30E-04
Sulfate	Inorganic	NA	NA	NA	NA
Tetrachloroethene	Organic	1.07E-07	1.07E-07	3.00E-02	3.00E-02
TNX[e]	Organic	2.07E-07	1.97E-07	2.51E-03	2.39E-03

Table 4.6-8 (continued)

COPC Name	Category	Cancer Risk (Max)	Cancer Risk (EPC)	Non-cancer Risk (Max)	Non-cancer Risk (EPC)
Toluene	Organic	NA	NA	1.37E-02	3.98E-03
Trichloroethene	Organic	3.47E-06	3.47E-06	3.19E-01	3.19E-01
Trinitrobenzene[1,3,5-]	Organic	NA	NA	5.34E-04	5.34E-04
Trinitrotoluene[2,4,6-]	Organic	1.42E-07	1.42E-07	3.67E-02	3.67E-02
Uranium	Inorganic	NA	NA	1.37E-02	1.07E-02
Zinc	Inorganic	NA	NA	3.37E-03	1.54E-03
Risk/Hazard		**4E-05**	**2E-05**	**1**	**0.9**

[a] NA = Not available.

[b] DNX = Hexahydro-1,3-dinitro-5-nitro-1,3,5-triazine.

[c] HMX = Her Majesty's Explosive.

[d] MNX = Hexahydro-1-nitroso-3,5-dinitro-1,3,5-triazine.

[e] TNX = 2,4,6-trinitroxylene.

Table 4.6-9
Cumulative Risk Assessment Screening for Chemicals in Well R-25b

COPC Name	Category	Cancer Risk (Max)	Cancer Risk (EPC)	Non-cancer Risk (Max)	Non-cancer Risk (EPC)
Aluminum	Inorganic	NA[a]	NA	5.07E-02	1.80E-02
Amino-2,6-dinitrotoluene[4-]	Organic	NA	NA	4.33E-03	4.33E-03
Amino-4,6-dinitrotoluene[2-]	Organic	NA	NA	4.23E-03	4.23E-03
Barium	Inorganic	NA	NA	1.24E-02	6.58E-03
Boron	Inorganic	NA	NA	1.30E-02	7.02E-03
Bromodichloromethane	Organic	1.62E-05	1.62E-05	5.78E-03	5.78E-03
Bromoform	Organic	5.45E-07	5.45E-07	4.76E-03	4.76E-03
Chlorodibromomethane	Organic	1.81E-05	1.81E-05	8.05E-03	8.05E-03
Chloroform	Organic	1.78E-05	1.78E-05	4.21E-02	4.21E-02
Copper	Inorganic	NA	NA	2.01E-02	1.03E-02
HMX[b]	Organic	NA	NA	6.55E-04	3.76E-04
Iron	Inorganic	NA	NA	4.34E-02	1.55E-02
Manganese	Inorganic	NA	NA	5.06E-02	1.86E-02
Nickel	Inorganic	NA	NA	1.51E-02	7.25E-03
Nitrate-nitrite as nitrogen	Inorganic	NA	NA	5.54E-02	3.77E-02
Perchlorate	Inorganic	NA	NA	2.26E-02	2.12E-02
RDX	Organic	8.79E-06	5.05E-06	1.07E-01	6.12E-02
Strontium	Inorganic	NA	NA	7.76E-03	6.52E-03
Sulfate	Inorganic	NA	NA	NA	NA
Tetrachloroethene	Organic	3.37E-08	3.37E-08	9.42E-03	9.42E-03
Uranium	Inorganic	NA	NA	5.27E-02	2.45E-02
Zinc	Inorganic	NA	NA	2.38E-01	5.50E-02
Risk/Hazard		**6E-05**	**6E-05**	**0.8**	**0.4**

[a] NA = Not available.

[b] HMX = Her Majesty's Explosive.

Table 4.6-10

Cumulative Risk Assessment Screening for Chemicals in Well R-63i

COPC Name	Category	Cancer Risk (Max)	Cancer Risk (EPC)	Non-cancer Risk (Max)	Non-cancer Risk (EPC)
Acetone	Organic	NA*	NA	1.37E-04	1.37E-04
Barium	Inorganic	NA	NA	3.33E-03	3.33E-03
Iron	Inorganic	NA	NA	2.70E-03	2.70E-03
Methylene chloride	Organic	1.20E-07	1.20E-07	1.33E-02	1.33E-02
Nickel	Inorganic	NA	NA	2.02E-03	2.02E-03
Nitrate-nitrite as nitrogen	Inorganic	NA	NA	3.34E-02	3.34E-02
Perchlorate	Inorganic	NA	NA	1.61E-02	1.61E-02
RDX	Organic	3.21E-07	3.21E-07	3.89E-03	3.89E-03
Strontium	Inorganic	NA	NA	5.60E-03	5.60E-03
Sulfate	Inorganic	NA	NA	NA	NA
Uranium	Inorganic	NA	NA	1.59E-02	1.59E-02
Risk/Hazard		**4E-07**	**4E-07**	**0.1**	**0.1**

* NA = Not available.

Table 4.6-11
Major Contributors to Calculated Health Effects Above Threshold in Site Wells

CdV-16-1(i)	
Cancer Risk	**HI**
4E-05	0.7
RDX Contribution to Risk	**RDX Contribution to HI**
77%	55%
Risk From All Other COPCs	**HI From All Other COPCs**
9E-06	0.3
CdV-16-2(i)r	
Cancer Risk	**HI**
1E-04	1.6
RDX Contribution to Risk	**RDX Contribution to HI**
96%	70%
Risk From All Other COPCs	**HI From All Other COPCs**
4E-06	0.5
CdV-16-4ip	
Cancer Risk	**HI**
1E-04	2.5
RDX Contribution to Risk	**RDX Contribution to HI**
97%	69%
Risk From All Other COPCs	**Hi From All Other COPCs**
4E-06	0.8
CdV-37-1(i)	
Cancer Risk	**HI**
0E+00	0.1
R-19	
Cancer Risk	**HI**
2E-07	0.9
R-63i	
Cancer Risk	**HI**
4E-07	0.1

Table 4.6-11 (continued)

<table>
<tr><td colspan="4">CdV-9-1(i)</td></tr>
<tr><td colspan="2">Cancer Risk</td><td colspan="2">HI</td></tr>
<tr><td colspan="2">3E-05</td><td colspan="2">0.8</td></tr>
<tr><td>RDX Contribution to Risk</td><td colspan="2">RDX Contribution to HI</td><td>Tricholorethene Contribution to HI</td></tr>
<tr><td>88%</td><td colspan="2">38%</td><td>27%</td></tr>
<tr><td colspan="2">Risk From All Other COPCs</td><td colspan="2">HI From All Other COPCs</td></tr>
<tr><td colspan="2">3E-06</td><td colspan="2">0.3</td></tr>
<tr><td colspan="4">R-25</td></tr>
<tr><td colspan="2">Cancer Risk</td><td colspan="2">HI</td></tr>
<tr><td colspan="2">2E-05</td><td colspan="2">0.9</td></tr>
<tr><td>RDX Contribution to Risk</td><td colspan="2">RDX Contribution to HI</td><td>Tricholorethene Contribution to HI</td></tr>
<tr><td>68%</td><td colspan="2">22%</td><td>34%</td></tr>
<tr><td colspan="2">Risk From All Other COPCs</td><td colspan="2">HI From All Other COPCs</td></tr>
<tr><td colspan="2">8E-06</td><td colspan="2">0.4</td></tr>
<tr><td colspan="4">R-25b</td></tr>
<tr><td colspan="2">Cancer Risk</td><td colspan="2">HI</td></tr>
<tr><td colspan="2">6E-05</td><td colspan="2">0.4</td></tr>
<tr><td colspan="2">Chlorodibromomethane Contribution to Risk</td><td colspan="2">Chloroform Contribution to Risk</td></tr>
<tr><td colspan="2">31%</td><td colspan="2">31%</td></tr>
<tr><td colspan="2">Bromodichloromethane Contribution to Risk</td><td colspan="2">Risk From All Other COPCs</td></tr>
<tr><td colspan="2">28%</td><td colspan="2">6E-06</td></tr>
</table>

Table 4.6-12
Cumulative Risk Assessment Screening for Radionuclides, All Wells

COPC Name	Site Well	Cancer Risk (using Max and PRG)	Cancer Risk (using EPC and PRG)
Gross alpha	CdV-16-1(i)	NA*	NA
Tritium	CdV-16-1(i)	4.71E-06	4.62E-06
Uranium-234	CdV-16-1(i)	6.25E-07	5.90E-07
Uranium-238	CdV-16-1(i)	4.78E-07	3.65E-07
Total Excess Cancer Risk		**6E-06**	**6E-06**
Tritium	CdV-16-2(i)r	2.44E-06	5.84E-07
Uranium-234	CdV-16-2(i)r	4.71E-07	3.34E-07
Uranium-238	CdV-16-2(i)r	3.47E-07	2.39E-07
Total Excess Cancer Risk		**3E-06**	**1E-06**
Tritium	CDV-16-4ip	2.28E-06	2.28E-06
Uranium-234	CDV-16-4ip	4.68E-07	4.68E-07
Uranium-238	CDV-16-4ip	3.36E-07	3.36E-07
Total Excess Cancer Risk		**3E-06**	**3E-06**
Uranium-234	CDV-37-1(i)	3.82E-07	3.82E-07
Uranium-238	CDV-37-1(i)	2.87E-07	2.87E-07
Total Excess Cancer Risk		**7E-07**	**7E-07**
Gross alpha	CDV-9-1(i)	NA	NA
Tritium	CDV-9-1(i)	1.13E-06	1.13E-06
Uranium-234	CDV-9-1(i)	9.26E-07	9.26E-07
Uranium-238	CDV-9-1(i)	6.93E-07	6.93E-07
Total Excess Cancer Risk		**3E-06**	**3E-06**
Gross alpha	R-19	NA	NA
Uranium-234	R-19	4.49E-07	3.76E-07
Uranium-238	R-19	2.92E-07	2.02E-07
Total Excess Cancer Risk		**7E-07**	**7E-07**
Gross alpha	R-25	NA	NA
Tritium	R-25	4.69E-06	3.00E-06
Uranium-234	R-25	9.92E-07	6.60E-07
Uranium-238	R-25	8.03E-07	5.46E-07
Total Excess Cancer Risk		**6E-06**	**4E-06**
Gross alpha	R-25b	NA	NA
Uranium-234	R-25b	2.40E-06	2.40E-06
Uranium-238	R-25b	9.46E-07	9.46E-07
Total Excess Cancer Risk		**3E-06**	**3E-06**

* NA = Not available.

Table 4.6-13
Comparison of EPCs for Site Wells with Regulatory Standards

COPC Name	Site Well	EPC (µg/L or pCi/L)	NMAC; Part A (µg/L)	NMAC; Part B (µg/L)	Primary MCL or TT[a] (µg/L)	Secondary MCL (µg/L)
Naphthalenedisulfonic acid[1,5-]	CdV-16-1(i)	2.1E+04	NA[b]	NA	NA	NA
Acetone	CdV-16-1(i)	1.8E+00	NA	NA	NA	NA
Amino-2,6-dinitrotoluene[4-]	CdV-16-1(i)	2.0E-01	NA	NA	NA	NA
Amino-4,6-dinitrotoluene[2-]	CdV-16-1(i)	1.2E-01	NA	NA	NA	NA
Barium	CdV-16-1(i)	1.7E+01	2.0E+03	NA	2.0E+03	NA
Bis(2-ethylhexyl)phthalate	CdV-16-1(i)	4.4E+00	NA	NA	4.0E+02	NA
Boron	CdV-16-1(i)	6.3E+01	NA	NA	NA	NA
Butanone[2-]	CdV-16-1(i)	1.2E+01	NA	NA	NA	NA
Copper	CdV-16-1(i)	1.6E+01	NA	1.0E+03	1.3E+03	1.0E+03
DNX[c]	CdV-16-1(i)	2.3E-01	NA	NA	NA	NA
Heptachlor	CdV-16-1(i)	1.7E-02	NA	NA	4.0E-01	NA
HMX[d]	CdV-16-1(i)	1.8E+00	NA	NA	NA	NA
Iron	CdV-16-1(i)	3.3E+02	NA	1.0E+03	NA	3.0E+02
Manganese	CdV-16-1(i)	5.3E+00	NA	2.0E+02	NA	5.0E+01
Methyl tert-butyl ether	CdV-16-1(i)	1.2E+00	NA	1.0E+02	NA	NA
MNX[e]	CdV-16-1(i)	3.1E-01	NA	NA	NA	NA
Nickel	CdV-16-1(i)	5.7E+00	NA	NA	NA	NA
Nitrate-nitrite as nitrogen	CdV-16-1(i)	8.9E+02	1.0E+03	NA	1.0E+03	NA
Perchlorate	CdV-16-1(i)	5.3E-01	NA	NA	NA	NA
Perfluorooctanoic acid	CdV-16-1(i)	1.2E-03	NA	NA	NA	NA
RDX	CdV-16-1(i)	3.0E+01	NA	NA	NA	NA
Strontium	CdV-16-1(i)	9.6E+01	NA	NA	NA	NA
Sulfate	CdV-16-1(i)	1.0E+04	NA	6.0E+05	NA	2.5E+05
Tetrachloroethene	CdV-16-1(i)	1.1E+00	5.0E+00	NA	5.0E+00	NA
TNX[f]	CdV-16-1(i)	2.5E-01	NA	NA	NA	NA

Table 4.6-13 (continued)

COPC Name	Site Well	EPC (µg/L or pCi/L)	NMAC; Part A (µg/L)	NMAC; Part B (µg/L)	Primary MCL or TT (µg/L)	Secondary MCL (µg/L)
Toluene	CdV-16-1(i)	2.3E+01	1.0E+03	NA	1.0E+03	NA
Uranium	CdV-16-1(i)	4.6E-01	3.0E+01	NA	3.0E+01	NA
Zinc	CdV-16-1(i)	2.6E+01	NA	1.0E+04	NA	5.0E+03
Gross alpha	CdV-16-1(i)	4.2E+00	NA	NA	1.5E+01	NA
Tritium	CdV-16-1(i)	6.7E+01	NA	NA	2.0E+04	NA
Uranium-234	CdV-16-1(i)	4.4E-01	NA	NA	NA	NA
Uranium-238	CdV-16-1(i)	2.1E-01	NA	NA	NA	NA
Acetone	CdV-16-2(i)r	7.8E+00	NA	NA	NA	NA
Amino-2,6-dinitrotoluene[4-]	CdV-16-2(i)r	1.4E-01	NA	NA	NA	NA
Amino-4,6-dinitrotoluene[2-]	CdV-16-2(i)r	1.8E-01	NA	NA	NA	NA
Barium	CdV-16-2(i)r	2.7E+00	2.0E+03	NA	2.0E+03	NA
Boron	CdV-16-2(i)r	2.8E+01	NA	NA	NA	NA
Butanone[2-]	CdV-16-2(i)r	1.2E+01	NA	NA	NA	NA
Chloromethane	CdV-16-2(i)r	2.7E+00	NA	NA	NA	NA
DNX	CdV-16-2(i)r	2.3E-01	NA	NA	NA	NA
HMX	CdV-16-2(i)r	9.7E-01	NA	NA	NA	NA
Iron	CdV-16-2(i)r	1.8E+02	NA	1.0E+03	NA	3.0E+02
Methyl tert-butyl ether	CdV-16-2(i)r	5.1E-01	NA	1.0E+02	NA	NA
Methyl-2-pentanone[4-]	CdV-16-2(i)r	5.4E+00	NA	NA	NA	NA
MNX	CdV-16-2(i)r	4.4E-01	NA	NA	NA	NA
Nickel	CdV-16-2(i)r	9.2E-01	NA	NA	NA	NA
Nitrate-nitrite as nitrogen	CdV-16-2(i)r	6.5E+02	1.0E+03	NA	1.0E+03	NA
Perchlorate	CdV-16-2(i)r	3.2E-01	NA	NA	NA	NA
Perfluorooctanoic acid	CdV-16-2(i)r	1.1E-02	NA	NA	NA	NA
RDX	CdV-16-2(i)r	9.0E+01	NA	NA	NA	NA
Strontium	CdV-16-2(i)r	6.3E+01	NA	NA	NA	NA

Table 4.6-13 (continued)

COPC Name	Site Well	EPC (µg/L or pCi/L)	NMAC; Part A (µg/L)	NMAC; Part B (µg/L)	Primary MCL or TT (µg/L)	Secondary MCL (µg/L)
Sulfate	CdV-16-2(i)r	4.4E+03	NA	6.0E+05	NA	2.5E+05
Tetrachloroethene	CdV-16-2(i)r	6.1E-01	5.0E+00	NA	5.0E+00	NA
TNX	CdV-16-2(i)r	1.7E-01	NA	NA	NA	NA
Toluene	CdV-16-2(i)r	3.4E+00	1.0E+03	NA	1.0E+03	NA
Trichloroethene	CdV-16-2(i)r	4.5E-01	5.0E+00	NA	5.0E+00	NA
Trinitrobenzene[1,3,5-]	CdV-16-2(i)r	1.3E-01	NA	NA	NA	NA
Uranium	CdV-16-2(i)r	2.9E-01	3.0E+01	NA	3.0E+01	NA
Zinc	CdV-16-2(i)r	2.0E+01	NA	1.0E+04	NA	5.0E+03
Tritium	CdV-16-2(i)r	8.5E+00	NA	NA	2.0E+04	NA
Uranium-234	CdV-16-2(i)r	2.5E-01	NA	NA	NA	NA
Uranium-238	CdV-16-2(i)r	1.4E-01	NA	NA	NA	NA
Acetone	CDV-16-4ip	6.9E+01	NA	NA	NA	NA
Amino-2,6-dinitrotoluene[4-]	CDV-16-4ip	2.1E+00	NA	NA	NA	NA
Barium	CDV-16-4ip	4.7E+00	2.0E+03	NA	2.0E+03	NA
Boron	CDV-16-4ip	7.0E+01	NA	NA	NA	NA
DNX	CDV-16-4ip	3.4E-01	NA	NA	NA	NA
HMX	CDV-16-4ip	9.4E+00	NA	NA	NA	NA
Iron	CDV-16-4ip	1.1E+02	NA	1.0E+03	NA	3.0E+02
Methyl tert-butyl ether	CDV-16-4ip	6.2E-01	NA	1.0E+02	NA	NA
MNX	CDV-16-4ip	6.3E-01	NA	NA	NA	NA
Nickel	CDV-16-4ip	7.7E-01	NA	NA	NA	NA
Nitrate-nitrite as nitrogen	CDV-16-4ip	9.2E+02	1.0E+03	NA	1.0E+03	NA
Perchlorate	CDV-16-4ip	3.7E-01	NA	NA	NA	NA
Perfluorooctanoic acid	CDV-16-4ip	1.2E-02	NA	NA	NA	NA
RDX	CDV-16-4ip	1.4E+02	NA	NA	NA	NA
Strontium	CDV-16-4ip	6.3E+01	NA	NA	NA	NA

Table 4.6-13 (continued)

COPC Name	Site Well	EPC (µg/L or pCi/L)	NMAC; Part A (µg/L)	NMAC; Part B (µg/L)	Primary MCL or TT (µg/L)	Secondary MCL (µg/L)
Sulfate	CDV-16-4ip	3.9E+03	NA	6.0E+05	NA	2.5E+05
Tetrachloroethene	CDV-16-4ip	9.6E-01	5.0E+00	NA	5.0E+00	NA
TNX	CDV-16-4ip	3.7E-01	NA	NA	NA	NA
Trichlorobenzene[1,2,3-]	CDV-16-4ip	9.0E-01	NA	NA	NA	NA
Trichloroethene	CDV-16-4ip	6.8E-01	5.0E+00	NA	5.0E+00	NA
Trinitrobenzene[1,3,5-]	CDV-16-4ip	1.2E-01	NA	NA	NA	NA
Uranium	CDV-16-4ip	5.0E-01	3.0E+01	NA	3.0E+01	NA
Zinc	CDV-16-4ip	1.2E+01	NA	1.0E+04	NA	5.0E+03
Tritium	CDV-16-4ip	3.3E+01	NA	NA	2.0E+04	NA
Uranium-234	CDV-16-4ip	3.5E-01	NA	NA	NA	NA
Uranium-238	CDV-16-4ip	2.0E-01	NA	NA	NA	NA
Acetone	CDV-37-1(i)	4.4E+00	NA	NA	NA	NA
Barium	CDV-37-1(i)	1.1E+01	2.0E+03	NA	2.0E+03	NA
Boron	CDV-37-1(i)	1.7E+01	NA	NA	NA	NA
Iron	CDV-37-1(i)	4.5E+01	NA	1.0E+03	NA	3.0E+02
Nickel	CDV-37-1(i)	4.4E+00	NA	NA	NA	NA
Nitrate-nitrite as nitrogen	CDV-37-1(i)	1.6E+02	1.0E+03	NA	1.0E+03	NA
Perchlorate	CDV-37-1(i)	1.6E-01	NA	NA	NA	NA
Strontium	CDV-37-1(i)	4.9E+01	NA	NA	NA	NA
Sulfate	CDV-37-1(i)	3.0E+03	NA	6.0E+05	NA	2.5E+05
Uranium	CDV-37-1(i)	4.8E-01	3.0E+01	NA	3.0E+01	NA
Zinc	CDV-37-1(i)	1.4E+01	NA	1.0E+04	NA	5.0E+03
Uranium-234	CDV-37-1(i)	2.8E-01	NA	NA	NA	NA
Uranium-238	CDV-37-1(i)	1.7E-01	NA	NA	NA	NA
Acetone	CDV-9-1(i)	1.9E+01	NA	NA	NA	NA
Amino-2,6-dinitrotoluene[4-]	CDV-9-1(i)	4.3E-01	NA	NA	NA	NA

Table 4.6-13 (continued)

COPC Name	Site Well	EPC (µg/L or pCi/L)	NMAC; Part A (µg/L)	NMAC; Part B (µg/L)	Primary MCL or TT (µg/L)	Secondary MCL (µg/L)
Amino-4,6-dinitrotoluene[2-]	CDV-9-1(i)	3.7E-01	NA	NA	NA	NA
Barium	CDV-9-1(i)	5.4E+00	2.0E+03	NA	2.0E+03	NA
Boron	CDV-9-1(i)	3.7E+01	NA	NA	NA	NA
Butanone[2-]	CDV-9-1(i)	4.4E+00	NA	NA	NA	NA
Carbon disulfide	CDV-9-1(i)	1.5E+00	NA	NA	NA	NA
DNX	CDV-9-1(i)	1.8E-01	NA	NA	NA	NA
HMX	CDV-9-1(i)	1.8E+00	NA	NA	NA	NA
Iron	CDV-9-1(i)	1.3E+02	NA	1.0E+03	NA	3.0E+02
Methyl tert-butyl ether	CDV-9-1(i)	9.3E-01	NA	1.0E+02	NA	NA
MNX	CDV-9-1(i)	1.9E-01	NA	NA	NA	NA
Nickel	CDV-9-1(i)	8.1E-01	NA	NA	NA	NA
Nitrate-nitrite as nitrogen	CDV-9-1(i)	1.3E+03	1.0E+03	NA	1.0E+03	NA
Nitrotoluene[2-]	CDV-9-1(i)	1.2E-01	NA	NA	NA	NA
Perchlorate	CDV-9-1(i)	4.7E-01	NA	NA	NA	NA
Perfluorooctanoic acid	CDV-9-1(i)	2.2E-03	NA	NA	NA	NA
RDX	CDV-9-1(i)	2.3E+01	NA	NA	NA	NA
Strontium	CDV-9-1(i)	9.0E+01	NA	NA	NA	NA
Sulfate	CDV-9-1(i)	8.1E+03	NA	6.0E+05	NA	2.5E+05
Tetrachloroethene	CDV-9-1(i)	1.2E+00	5.0E+00	NA	5.0E+00	NA
TNX	CDV-9-1(i)	1.4E-01	NA	NA	NA	NA
Toluene	CDV-9-1(i)	8.5E-01	1.0E+03	NA	1.0E+03	NA
Trichloroethene	CDV-9-1(i)	5.7E-01	5.0E+00	NA	5.0E+00	NA
Trinitrotoluene[2,4,6-]	CDV-9-1(i)	1.2E-01	NA	NA	NA	NA
Uranium	CDV-9-1(i)	8.1E-01	3.0E+01	NA	3.0E+01	NA
Zinc	CDV-9-1(i)	5.8E+00	NA	1.0E+04	NA	5.0E+03
Gross alpha	CDV-9-1(i)	2.0E+00	NA	NA	1.5E+01	NA

Table 4.6-13 (continued)

COPC Name	Site Well	EPC (µg/L or pCi/L)	NMAC; Part A (µg/L)	NMAC; Part B (µg/L)	Primary MCL or TT (µg/L)	Secondary MCL (µg/L)
Tritium	CDV-9-1(i)	1.6E+01	NA	NA	2.0E+04	NA
Uranium-234	CDV-9-1(i)	6.8E-01	NA	NA	NA	NA
Uranium-238	CDV-9-1(i)	4.1E-01	NA	NA	NA	NA
Acetone	R-19	3.1E+00	NA	NA	NA	NA
Anthracene	R-19	2.0E-01	NA	NA	NA	NA
Barium	R-19	2.6E+01	2.0E+03	NA	2.0E+03	NA
Bis(2-ethylhexyl)phthalate	R-19	6.1E-01	NA	NA	4.0E+02	NA
Boron	R-19	2.1E+01	NA	NA	NA	NA
Fluoranthene	R-19	1.9E-01	NA	NA	NA	NA
Fluoride	R-19	6.2E+02	1.6E+03	NA	4.0E+03	2.0E+03
Iron	R-19	8.4E+01	NA	1.0E+03	NA	3.0E+02
Nickel	R-19	5.9E+00	NA	NA	NA	NA
Nitrate-nitrite as nitrogen	R-19	3.9E+02	1.0E+03	NA	1.0E+03	NA
Perchlorate	R-19	3.8E-01	NA	NA	NA	NA
Phenanthrene	R-19	2.4E-01	NA	NA	NA	NA
Pyrene	R-19	1.9E-01	NA	NA	NA	NA
RDX	R-19	9.8E-02	NA	NA	NA	NA
Strontium	R-19	7.2E+01	NA	NA	NA	NA
Sulfate	R-19	3.3E+03	NA	6.0E+05	NA	2.5E+05
Toluene	R-19	5.4E-01	1.0E+03	NA	1.0E+03	NA
Uranium	R-19	2.9E-01	3.0E+01	NA	3.0E+01	NA
Zinc	R-19	1.3E+01	NA	1.0E+04	NA	5.0E+03
Gross alpha	R-19	9.7E+00	NA	NA	1.5E+01	NA
Uranium-234	R-19	2.8E-01	NA	NA	NA	NA
Uranium-238	R-19	1.2E-01	NA	NA	NA	NA
Acetone	R-25	3.4E+00	NA	NA	NA	NA

Table 4.6-13 (continued)

COPC Name	Site Well	EPC (µg/L or pCi/L)	NMAC; Part A (µg/L)	NMAC; Part B (µg/L)	Primary MCL or TT (µg/L)	Secondary MCL (µg/L)
Aluminum	R-25	6.0E+02	NA	NA	NA	5.0E+01
Amino-2,6-dinitrotoluene[4-]	R-25	6.0E-01	NA	NA	NA	NA
Amino-4,6-dinitrotoluene[2-]	R-25	6.5E-01	NA	NA	NA	NA
Barium	R-25	2.4E+01	2.0E+03	NA	2.0E+03	NA
Boron	R-25	3.3E+01	NA	NA	NA	NA
Carbon disulfide	R-25	1.4E+00	NA	NA	NA	NA
Chlorobenzene	R-25	2.3E+00	NA	NA	1.0E+02	NA
DNX	R-25	1.8E-01	NA	NA	NA	NA
HMX	R-25	1.3E+00	NA	NA	NA	NA
Iron	R-25	1.6E+02	NA	1.0E+03	NA	3.0E+02
Manganese	R-25	2.3E+01	NA	2.0E+02	NA	5.0E+01
Methyl tert-butyl ether	R-25	1.2E+00	NA	1.0E+02	NA	NA
Methylene chloride	R-25	8.5E-01	5.0E+00	NA	5.0E+00	NA
MNX	R-25	2.8E-01	NA	NA	NA	NA
Nickel	R-25	4.1E+00	NA	NA	NA	NA
Nitrate-nitrite as nitrogen	R-25	7.0E+02	1.0E+03	NA	1.0E+03	NA
Nitrotoluene[2-]	R-25	1.1E+00	NA	NA	NA	NA
Perchlorate	R-25	5.3E-01	NA	NA	NA	NA
RDX	R-25	1.6E+01	NA	NA	NA	NA
Strontium	R-25	1.7E+02	NA	NA	NA	NA
Styrene	R-25	1.0E+00	1.0E+02	NA	1.0E+02	NA
Sulfate	R-25	6.6E+04	NA	6.0E+05	NA	2.5E+05
Tetrachloroethene	R-25	1.2E+00	5.0E+00	NA	5.0E+00	NA
TNX	R-25	1.9E-01	NA	NA	NA	NA
Toluene	R-25	4.4E+00	1.0E+03	NA	1.0E+03	NA
Trichloroethene	R-25	9.0E-01	5.0E+00	NA	5.0E+00	NA

Table 4.6-13 (continued)

COPC Name	Site Well	EPC (µg/L or pCi/L)	NMAC; Part A (µg/L)	NMAC; Part B (µg/L)	Primary MCL or TT (µg/L)	Secondary MCL (µg/L)
Trinitrobenzene[1,3,5-]	R-25	3.2E-01	NA	NA	NA	NA
Trinitrotoluene[2,4,6-]	R-25	3.6E-01	NA	NA	NA	NA
Uranium	R-25	6.3E-01	3.0E+01	NA	3.0E+01	NA
Zinc	R-25	9.2E+00	NA	1.0E+04	NA	5.0E+03
Gross alpha	R-25	3.1E+00	NA	NA	1.5E+01	NA
Tritium	R-25	4.3E+01	NA	NA	2.0E+04	NA
Uranium-234	R-25	4.9E-01	NA	NA	NA	NA
Uranium-238	R-25	3.2E-01	NA	NA	NA	NA
Aluminum	R-25b	3.6E+02	NA	NA	NA	5.0E+01
Amino-2,6-dinitrotoluene[4-]	R-25b	1.7E-01	NA	NA	NA	NA
Amino-4,6-dinitrotoluene[2-]	R-25b	1.7E-01	NA	NA	NA	NA
Barium	R-25b	2.2E+01	2.0E+03	NA	2.0E+03	NA
Boron	R-25b	2.8E+01	NA	NA	NA	NA
Bromodichloromethane	R-25b	2.2E+00	NA	NA	NA	NA
Bromoform	R-25b	1.8E+00	NA	NA	NA	NA
Chlorodibromomethane	R-25b	3.0E+00	NA	NA	NA	NA
Chloroform	R-25b	4.1E+00	1.0E+02	NA	NA	NA
Copper	R-25b	8.1E+00	NA	1.0E+03	1.3E+03	1.0E+03
HMX	R-25b	3.8E-01	NA	NA	NA	NA
Iron	R-25b	2.1E+02	NA	1.0E+03	NA	3.0E+02
Manganese	R-25b	3.8E+01	NA	2.0E+02	NA	5.0E+01
Nickel	R-25b	2.7E+00	NA	NA	NA	NA
Nitrate-nitrite as nitrogen	R-25b	6.3E+02	1.0E+03	NA	1.0E+03	NA
Perchlorate	R-25b	2.9E-01	NA	NA	NA	NA
RDX	R-25b	4.9E+00	NA	NA	NA	NA
Strontium	R-25b	7.7E+01	NA	NA	NA	NA

Table 4.6-13 (continued)

COPC Name	Site Well	EPC (µg/L or pCi/L)	NMAC; Part A (µg/L)	NMAC; Part B (µg/L)	Primary MCL or TT (µg/L)	Secondary MCL (µg/L)
Sulfate	R-25b	1.0E+04	NA	6.0E+05	NA	2.5E+05
Tetrachloroethene	R-25b	3.8E-01	5.0E+00	NA	5.0E+00	NA
Uranium	R-25b	1.5E+00	3.0E+01	NA	3.0E+01	NA
Zinc	R-25b	3.3E+02	NA	1.0E+04	NA	5.0E+03
Gross alpha	R-25b	3.9E+00	NA	NA	1.5E+01	NA
Uranium-234	R-25b	1.8E+00	NA	NA	NA	NA
Uranium-238	R-25b	5.5E-01	NA	NA	NA	NA
Acetone	R-63i	1.9E+00	NA	NA	NA	NA
Barium	R-63i	1.1E+01	2.0E+03	NA	2.0E+03	NA
Iron	R-63i	3.7E+01	NA	1.0E+03	NA	3.0E+02
Methylene chloride	R-63i	1.4E+00	5.0E+00	NA	5.0E+00	NA
Nickel	R-63i	7.5E-01	NA	NA	NA	NA
Nitrate-nitrite as nitrogen	R-63i	5.6E+02	1.0E+03	NA	1.0E+03	NA
Perchlorate	R-63i	2.2E-01	NA	NA	NA	NA
RDX	R-63i	3.1E-01	NA	NA	NA	NA
Strontium	R-63i	6.6E+01	NA	NA	NA	NA
Sulfate	R-63i	3.7E+03	NA	6.0E+05	NA	2.5E+05
Uranium	R-63i	9.4E-01	3.0E+01	NA	3.0E+01	NA

[a] TT = Treatment technique.

[b] NA = Not available.

[c] DNX = Hexahydro-1,3-dinitro-5-nitro-1,3,5-triazine.

[d] HMX = Her Majesty’s Explosive.

[e] MNX = Hexahydro-1-nitroso-3,5-dinitro-1,3,5-triazine.

[f] TNX = 2,4,6-trinitroxylene.

Appendix A

Acronyms and Abbreviations, Metric Conversion Table, and Data Qualifier Definitions

A-1.0 ACRONYMS AND ABBREVIATIONS

2-D	two-dimensional
3-D	three-dimensional
amsl	above mean sea level
ASTM	American Society for Testing and Materials
BCA	bias-corrected and accelerated
bgs	below ground surface
CAS	Chemical Abstracts Service
CB	consistent Bayes
CdV	Cañon de Valle
CME	corrective measures evaluation
Consent Order	Compliance Order on Consent
COPC	chemical of potential concern
CSM	conceptual site model
DGIR	deep groundwater investigation report
DOE	Department of Energy (U.S.)
DNX	hexahydro-1,3-dinitro-5-nitro-1,3,5-triazine
EIM	Environmental Information Management (database)
EM-LA	Environmental Management Los Alamos Field Office (DOE)
EPA	Environmental Protection Agency (U.S.)
EPC	exposure point concentration
FEHM	Finite Element Heat and Mass transfer code
HASL	Health and Safety Laboratory
HE	high explosives
HI	hazard index
HMX	Her Majesty’s Explosive
HPC	high-performance computing
HQ	hazard quotient
IRIS	Integrated Risk Information System (EPA database)
LANL	Los Alamos National Laboratory
LCMS/MS	liquid chromatography mass spectrometry/mass spectrometry
LCS	laboratory control sample
LHS	Latin Hypercube Sampling
LM	Levenberg-Marquardt
LPZ	lower perched-intermediate zone
MADS	Model Analysis and Decision Support
MBR	mountain-block recharge
MC	Monte Carlo

MCL	maximum contaminant level
MCMC	Markov Chain Monte Carlo
MDC	minimum detectable concentration
MFR	mountain-front recharge
ML	machine learning
MLMM	machine learning meta model
MNX	hexahydro-1-nitroso-3,5-dinitro-1,3,5-triazine
N3B	Newport News Nuclear BWXT-Los Alamos, LLC
NA	not available
NC	not calculated
ND	nondetection
NL	not listed
NMAC	New Mexico Administrative Code
NMED	New Mexico Environment Department
OF	objective function
P&D	Pipe and Disk (analytical screening tool)
PAH	polycyclic aromatic hydrocarbon
PCB	polychlorinated biphenyl
PFAS	per- and polyfluoroalkyl substances
PRG	preliminary remediation goal
PZ	piezometer
RDX	Royal Demolition Explosive
RFI	Resource Conservation and Recovery Act facility investigation
RL	reporting limit
RPD	relative percent difference
RRM	RDX regional aquifer model
RSL	regional screening level (EPA)
RVZM	RDX vadose zone model
S	screen
SA	sensitivity analysis
SD	standard deviation
SIMS	secondary ion mass spectrometry
SL	screening level
SVOC	semivolatile organic compound
SZ	saturated zone
TA	technical area
TNX	2,4,6-trinitroxylene
TT	treatment technique

UCL	upper confidence limit
UPZ	upper perched-intermediate zone
UZ	unsaturated zone
VOC	volatile organic compound
VOI	value of information
VZ	vadose zone
XGB	extreme gradient boosting

A-2.0 METRIC CONVERSION TABLE

Multiply SI (Metric) Unit	by	To Obtain U.S. Customary Unit
kilometers (km)	0.622	miles (mi)
kilometers (km)	3281	feet (ft)
meters (m)	3.281	feet (ft)
meters (m)	39.37	inches (in.)
centimeters (cm)	0.03281	feet (ft)
centimeters (cm)	0.394	inches (in.)
millimeters (mm)	0.0394	inches (in.)
micrometers or microns (µm)	0.0000394	inches (in.)
square kilometers (km^2)	0.3861	square miles (mi^2)
hectares (ha)	2.5	acres
square meters (m^2)	10.764	square feet (ft^2)
cubic meters (m^3)	35.31	cubic feet (ft^3)
kilograms (kg)	2.2046	pounds (lb)
grams (g)	0.0353	ounces (oz)
grams per cubic centimeter (g/cm^3)	62.422	pounds per cubic foot (lb/ft^3)
milligrams per kilogram (mg/kg)	1	parts per million (ppm)
micrograms per gram (µg/g)	1	parts per million (ppm)
liters (L)	0.26	gallons (gal.)
milligrams per liter (mg/L)	1	parts per million (ppm)
degrees Celsius (°C)	9/5 + 32	degrees Fahrenheit (°F)

A-3.0 DATA QUALIFIER DEFINITIONS

Data Qualifier	Definition
U	The analyte was analyzed for but not detected.
J	The analyte was positively identified, and the associated numerical value is estimated to be more uncertain than would normally be expected for that analysis.
J+	The analyte was positively identified, and the result is likely to be biased high.
J-	The analyte was positively identified, and the result is likely to be biased low.
UJ	The analyte was not positively identified in the sample, and the associated value is an estimate of the sample-specific detection or quantitation limit.
R	The data are rejected as a result of major problems with quality assurance/quality control parameters.

Appendix B

Data Preparation Protocol, Time Plots, Box Plots, and ProUCL Files for Chemicals of Potential Concern

B-1.0 DATA PREPARATION PROTOCOL

The data preparation protocol applied to the Environmental Information Management (EIM) data query is similar to that described in section 3.1 of the “Investigation Report for Royal Demolition Explosive in Deep Groundwater” (N3B 2019, 700561):

The data set evaluated to screening values included the following filters: (1) sample purpose – regular (REG), (2) sample type – water (W) and groundwater (WG), (3) best value – yes, and (4) sample usage code – investigation (INV) or blank. No screening values, test data, or field duplicates were included in the data set.

For the data set created by the EIM data query for this assessment, a “removal_flag” field was added to the data file and flagged with Y (yes, remove from data set) or N (no, do not remove from data set) to indicate records that should be removed because they are not applicable to evaluating current groundwater conditions. The removal_flag = Y reasons based on the initial review are provided in the following list:

- SAMPLE_TYPE
    - ❖ Remove EM (engineered material), R (rock), S (soil), and WIP (industrial process water)
    - ❖ Keep WG (groundwater), W (water)
- EXCAVATED_FLAG
    - ❖ Keep N (no)
    - ❖ Keep NA (not available)
    - ❖ Remove Y (yes)
- SAMPLE_PURPOSE
    - ❖ Remove EQB (equipment blank), FB (field blank), PEB (performance equipment blank), FTB (field trip blank), FD (field duplicate), and TEST
    - ❖ Keep REG
- LAB_MATRIX
    - ❖ Remove GAS, SD (solid)
    - ❖ Keep W (water)
- VALIDATION_STATUS_CODE
    - ❖ Remove NOVAL (not validated)
    - ❖ Keep VAL (validated)
    - ❖ Keep NA (not available)
- SAMPLE_USAGE_CODE
    - ❖ Remove CONST (well under construction)
    - ❖ Remove DEV (well development)
    - ❖ Remove PUMT (pump/aquifer test)

  - Remove QC (quality control)
  - Remove SCR (screening samples for screening purposes only)
  - Remove TEST (well testing samples collected from sampling system, not for monitoring)
  - Remove TRACER (tracer study for groundwater wells for the purpose of water dispersion studies)
  - Remove WST (waste classification samples collected for waste determination purposes only)
  - Keep INV (investigation)
  - Keep NA (not available)

- SAMPLE_PLAN_NAME
  - Remove CDV-9-1i Initial Drilling and Purge Sampling
  - Remove FY09; Direct waste Decon Fluids for Well PCI-2, TA-18
  - Remove R-25(b) Well Development
  - Remove R-26 Piezometer Sampling
  - Remove R-26 Piezometer Sampling 2
  - Remove Westbay Reliability Assessment Part 1: No-Purge Samples
  - Remove Westbay Reliability Assessment Part 2: Sampling during Initial Purge
  - Remove R-63-i – Bailed Sample
  - Keep all other sampling plan names
- BEST_VALUE_FLAG
  - Remove N (no)
  - Remove NA (not available)
  - Keep Y (yes)
- USE_FLAG
  - Remove N (no)
  - Keep Y (yes)

B-1.1 Evaluation of Preferred Analytical Method

In some instances, an analyte was measured by multiple analytical methods for the same sample. The following analytes were analyzed by more than one method in a single sample:

- High explosives – 2,4-dinitrotoluene; 2,6-dinitrotoluene
  - Analyzed by 8321/8270 or 8330/8270
- Polycyclic aromatic hydrocarbons (PAHs) – acenaphthene, acenaphthylene, anthracene, benzo(g,h,i)perylene, chrysene, fluoranthene, phenanthrene, pyrene
  - Analyzed by 8270/8270SIM

- Volatile organic compounds (VOCs)/Semivolatile organic compounds (SVOCs) – hexachlorobutadiene; 1,2-dichlorobenzene
  - ❖ Analyzed by 8260/8270
- Metals – antimony, beryllium, cadmium, lead, thallium
  - ❖ Analyzed by 6010/6020
- Radionuclide – americium-241 (Am-241)
  - ❖ Analyzed by generic gamma spectroscopy/Health and Safety Laboratory (HASL) 300 Am-241 (alpha spectroscopy)
- Radionuclide – radium-226 (Ra-226)
  - ❖ Analyzed by 901.1 and 903.1
- Radionuclide – uranium-238 (U-238)
  - ❖ Analyzed by 901.1 and generic alpha spectroscopy
- Metal/radionuclide – uranium
  - ❖ Analyzed by American Society for Testing and Materials (ASTM) D3972-90 (alpha spectroscopy)/6020

Table B-1.1-1 provides a summary of the analytical methods selected for these analytes. Details of the selection rationale are provided below.

High explosives – 2,4-dinitrotoluene; 2,6-dinitrotoluene

- Prefer 8231 over 8270
  - ❖ All results are nondetections (ND).
  - ❖ Reporting limits (RLs) for 8321 are ~3× lower.
  - ❖ No qualifications of particular concern are in the data chosen for retention.
  - ❖ One 8321 result was qualified UJ for a holding-time exceedance.
- Prefer 8330 over 8270
  - ❖ All results are ND.
  - ❖ RLs for 8330 are ~5–10× lower.
  - ❖ Most 8330 analyses used a mass spectrometer detector, which gives greater certainty in the identification.
  - ❖ No qualifications of particular concern have been applied to the data chosen for retention.
- Comparability – The data seem to be split across these three analyses.

PAHs – acenaphthene, acenaphthylene, anthracene, benzo(g,h,i)perylene, chrysene, fluoranthene, phenanthrene, pyrene

- Prefer 8270SIM over 8270
    - ❖ All results are ND.
    - ❖ RLs for secondary ion mass spectrometry (SIMS) are generally 3–10× lower.
    - ❖ No qualifications.
- Comparability – Most results are from 8270 analyses and not SIMS. However, the preparation and separation portions of the analyses are the same and both also use a mass spectrometer for detection. In SIMS, the mass spectrometer looks only for the selected masses, which provides the greater sensitivity. (There were some analyses by 8310; this analysis has problems with interferences.)

VOCs/SVOCs – hexachlorobutadiene, 1,2-dichlorobenzene

- Prefer 8260 over 8270
    - ❖ Most results are ND.
    - ❖ RLs for 8260 are ~10× lower.
    - ❖ No qualifications of particular concern are in the data chosen for retention. A few 8260 results are qualified for either holding-time exceedance or low laboratory control sample (LCS) recovery.
- Comparability – Looking at the full water matrix data set, most analyses per performed by 8260.

Metals – antimony, beryllium, cadmium, lead, thallium

- Prefer 6020 over 6010
    - ❖ Most results are ND.
    - ❖ 6020 generally has lower RLs.
    - ❖ No qualifications of particular concern are in the data chosen for retention. A few results qualified for a high duplicate relative percent difference (RPD).
    - ❖ 6020 detected results are often (but not exclusively) higher than the paired 6010 result, but not substantially higher.
- Comparability – Both 6010 and 6020 use the same “separation” process (plasma) but have different detectors so, analytically, they are slightly less comparable. Method 6010 is more robust for groundwater analyses when there are high concentrations of dissolved solids, but the total dissolved solids results in the database are fairly low, so that is probably not an issue. The mass spectrometer is more sensitive than the optical system used in 6010, so 6020 usually has lower detection limits. Analytically, these are reasonably comparable methods.
    - ❖ Beryllium was analyzed more by 6010.
    - ❖ Antimony, cadmium, lead, thallium were analyzed more by 6020.

Perchlorate

- Prefer 6850 over 314.0

  - ❖ 6580 has lower RLs.
  - ❖ No qualifications of particular concern. A few results were qualified, but the reason codes were not defined. Likely the qualifications were for a low LCS recovery and/or RPD between the LCS and LCS duplicate.
- Comparability – Most analyses were performed by 6850.

Total phosphate as phosphorus

- Prefer 365.4 over 300.0
  - ❖ 365.4 specific to phosphate
  - ❖ Fewer interferences since phosphate is the only analyte
  - ❖ One result was censored for a method blank detection. No other qualifications were of concern.
- Comparability – Most results were reported by 365.4.

Radionuclide – Am-241

- Prefer HASL 300 over generic gamma spectroscopy
  - ❖ HASL method uses a chemical separation specific for americium.
  - ❖ Minimum detectable concentration (MDC) and uncertainties are orders of magnitude lower.
  - ❖ No qualifications
- Comparability – The methods are not analytically comparable.
  - ❖ There are four results above the MDC. Two detections were by HASL in samples where the result was <gamma MDC and the gamma result was <MDC. The other two detections were in the same sample, with the gamma result 3 orders of magnitude higher.
  - ❖ Most analyses were performed by alpha spectroscopy.

Radionuclide – Ra-226

- Prefer 903.1 over 901.1
  - ❖ 901.1 is a gamma spectroscopy screening method while 903.1 performs a chemical separation of Ra-226 and then counts it via alpha spectrometry.
  - ❖ MDC and uncertainties are orders of magnitude lower.
  - ❖ No qualifications
- Comparability – most analyses performed by 903.1

Radionuclide – U-238

- Prefer generic alpha spectroscopy over 901.1
  - ❖ 901.1 is a gamma spectroscopy screening method while even a generic alpha spectroscopy probably performs a chemical separation of uranium and then counts it via alpha spectrometry.

  - ❖ MDC and uncertainties are orders of magnitude lower.
  - ❖ The result was qualified, but the code is not defined. The laboratory may have qualified the result as a nondetection even though it was above the MDC. This is not a concern.
- Comparability – Most analyses were performed by HASL 300, which is an alpha spectroscopy method.

Metal/radionuclide – uranium

- Use either ASTM D3972-90 (alpha spectroscopy) or 6020.
  - ❖ Only one affected sample was analyzed twice by 6020 and once by an alpha spectroscopy method; the three results are virtually the same.
  - ❖ None of the results are qualified.
  - ❖ Alpha spectroscopy may have better identification because there is a chemical speciation before counting.
- Comparability – Of the analyses reporting nonspeciated uranium, about 90% were performed by either 6010 or 6020.

Evaluation of temporal trends in the prepared data set was performed by review of time plots that show potential patterns of increasing or decreasing concentrations over time for each analyte. The plots were reviewed to identify early sample results that are not representative of current conditions for specific analytes or analytical suites, and these results were then removed to produce the trimmed data set used in the screening assessment. Attachment B-1 shows the time plots for data trimming. (on CD included with this document).

B-2.0 DESCRIPTION OF STATISTICAL TESTS USED FOR BACKGROUND COMPARISONS

The following four tests were used to support evaluation of whether concentrations of inorganic chemicals and radionuclides in groundwater from the site wells were elevated relative to corresponding concentrations in the background wells. Tests that evaluate a shift in the central tendency of the data (t-test and Gehan test) address whether concentrations in the site wells are broadly elevated. This is complemented by the use of tests that evaluate shifts in the upper tails of the distributions (quantile and slippage tests) to determine whether concentrations in one or a few wells might be elevated, even if there are relatively few samples from these wells. Box plots comparing the analytical results of site wells and background wells are shown in Attachment B-2 (on CD included with this document).

Student’s two sample t-test. The t-test tests for equality of the means of the site and background concentrations. The theoretical basis of the test assumes that concentrations are normally distributed at both site and background locations, though the test is fairly robust with respect to this assumption, if sufficient data are available. This test does not directly accommodate data reported as nondetections (i.e., data reported as below some detection limit). A substitution method is required for the censored data. In practice, a value of one-half the detection limit (censoring limit) is commonly used. The t-test is run as a one-sided test, significant only if the site mean concentration is higher than the background mean, not assuming equal variances for the site and background distributions.

Gehan test. The Gehan test is a modification of the Wilcoxon rank sum test that tests for a location shift in the site concentrations (i.e., a shift of the entire distribution), and was first presented in “A Generalized Wilcoxon Test for Comparing Arbitrarily Singly-Censored Samples” (Gehan 1965, 055611). This nonparametric test ignores the actual concentrations measured and uses only the rank of the concentrations, and thus it can detect any upward shift of the site concentration distribution with respect to background. The Gehan test is less efficient than the t-test (i.e., it generally requires more data than the t-test to detect a difference between site and background), but it is more robust to outliers (i.e., less likely to produce a spurious significant result because of one or two outliers).

Quantile Test. The quantile test is a nonparametric test of the equality of some quantile of the site and background distributions (Gilbert and Simpson 1992, 054952). That is, it statistically compares the numbers of values greater than the specified quantile that come from the site and background data. Any quantile can be tested if sufficient data are available—the more extreme the quantile, the greater the sample size required. Commonly used quantiles are the 75th, 80th, or 90th percentiles. For purposes of this report, the 75th and 90th percentiles are discussed. The quantile test can accommodate nondetections provided that the detection limit is below the appropriate quantile of the background data set. If the detection limit is higher than the quantile, the nondetection data point is not used by the test.

Slippage Test. The slippage test is a nonparametric test that compares the extreme tails of the site and background distributions (Gilbert and Simpson 1992, 054952). Since the tail of a distribution can be estimated well only with a very large data set, the slippage test has low power for small data sets. The test statistic relies on the maximum concentration in the background data, and thus it is not robust to outliers in the background data set. The test is robust to outliers in the site data set. Nondetections for the slippage test are handled in the same way as the quantile test. The nondetection is used if the detection limit is below the maximum detected concentration in the background data set.

Attachment B-3 (on CD included with this document) presents time plots for the final data set used in the screening, subsequent to data trimming supported by the plots described in Attachment B-1 (on CD included with this document). Attachment B-4 (on CD included with this document) presents box plots for chemicals of potential concern that include the 95% upper confidence limit (UCL) line. These plots support review of the reasonableness of the calculated 95% UCL by displaying the value relative to the underlying data distribution. Attachment B-5 (on CD included with this document) presents the ProUCL software output files associated with the 95% UCL calculations.

B-3.0 REFERENCES

The following reference list includes documents cited in this appendix. Parenthetical information following each reference provides the author(s), publication date, and ERID, ESHID, or EMID. This information is also included in text citations. ERIDs were assigned by the Laboratory's Associate Directorate for Environmental Management (IDs through 599999); ESHIDs were assigned by the Laboratory's Associate Directorate for Environment, Safety, and Health (IDs 600000 through 699999); and EMIDs are assigned by Newport News Nuclear BWXT-Los Alamos, LLC (N3B) (IDs 700000 and above). IDs are used to locate documents in N3B's Records Management System and in the Master Reference Set. The NMED Hazardous Waste Bureau and N3B maintain copies of the Master Reference Set. The set ensures that NMED has the references to review documents. The set is updated when new references are cited in documents.

Gehan, E.A., June 1965. "A Generalized Wilcoxon Test for Comparing Arbitrarily Singly-Censored Samples," *Biometrika,* Vol. 52, No. 1 and 2, pp. 203–223. (Gehan 1965, 055611)

Gilbert, R.O., and J.C. Simpson, December 1992. "Statistical Methods for Evaluating the Attainment of Cleanup Standards, Volume 3: Reference-Based Standards for Soils and Solid Media," document prepared for the U.S. Environmental Protection Agency, Pacific Northwest Laboratory, Richland, Washington. (Gilbert and Simpson 1992, 054952)

N3B (Newport News Nuclear BWXT-Los Alamos, LLC), August 2019. "Investigation Report for Royal Demolition Explosive in Deep Groundwater," Newport News Nuclear BWXT-Los Alamos, LLC, document EM2019-0235, Los Alamos, New Mexico. (N3B 2019, 700561)

Table B-1.1-1
Identification of Preferred Analytical Method for Analytes with Multiple Measurements in a Single Sample

Analytical Group	Compounds/Analytes	Methods Used	Method to Retain
High Explosive	2,4-dinitrotoluene 2,6-dinitrotoluene	8231 and 8270	8231
High Explosive	2,4-dinitrotoluene 2,6-dinitrotoluene	8330 and 8270	8330
PAHs	Acenaphthene Acenaphthylene Anthracene Benzo(g,h,i)perylene Chrysene Fluoranthene Phenanthrene Pyrene	8270 and 8270SIM	8270SIM
VOC/SVOC	Hexachlorobutadiene 1,2-dichlorobenzene	8260 and 8270	8260
Metals	Antimony Beryllium Cadmium Lead Thallium	6010 and 6020	6010
General Chemistry	Perchlorate	314.0 and 6850	6850
	Total phosphate as phosphorous	300.0 and 365.4	365.4
Radionuclides	Am-241	Generic gamma spectroscopy and HASL 300 Am-241	HASL 300 Am-241
	Ra-226	901.1 and 903.1	903.1
	U-238	901.1 and generic alpha spectroscopy	Alpha spectroscopy
Radionuclide/Metal	Uranium	ASTM D3972-90 and 6020	6020

Attachment B-1

Time Plots for Data Trimming
(on CD included with this document)

Attachment B-2

Box Plots
(on CD included with this document)

Attachment B-3

Time Plot Final Data Set
(on CD included with this document)

Attachment B-4

Box Plots with 95% UCL Line
(on CD included with this document)

Attachment B-5

ProUCL Files
(on CD included with this document)

Appendix C

Probabilistic Groundwater Modeling of the Royal Demotion Explosive Plume at Los Alamos National Laboratory to Support Risk Assessment

EXECUTIVE SUMMARY

A dissolved phase plume of the organic compound hexahydro-1,3,5-trinitro-1,3,5-triazine (Royal Demolition Explosive [RDX]) with concentrations greater than the New Mexico tap water drinking standard of 9.66 ppb is present in the upper portions of the regional aquifer near the southwestern boundary of Los Alamos National Laboratory (LANL). This risk assessment for exposure to regional aquifer groundwater is supported with long-term predictions of RDX concentrations provided by a calibrated, probabilistic, numerical fate and transport model run to the year 2070. The fate and transport modeling of the regional aquifer was conducted with innovative computational and statistical methods that use high-performance computing resources to support the risk assessment. This modeling leverages prior work performed at the chromium plume site in the central LANL area, with extensive updates in terms of data, software, model, and analytical tools. Results of the calibration demonstrate excellent matches to concentration data, water levels near the plume, and hydraulic gradients. Final model results with uncertainty show that in 2070 no simulations reach the water-supply wells, nor do they reach an arc of monitoring locations approximately one-third of the way between the plume and the water-supply wells.

The RDX Regional aquifer Model (RRM) was developed as the primary decision support tool for analysis of downgradient RDX concentrations. The RRM is informed by the conceptual site model and is calibrated using site RDX concentration data and hydraulic head measurements, along with other analyses. The model is calibrated using data through December 2019. Model inputs are described with informative prior distributions. Where data are scarce, other lines of evidence are used to inform the distributions, including the multiphase RDX Vadose Zone Model (RVZM) and Pipe & Disk (P&D) analytical screening tool. This hierarchical structure is a robust approach to distribution development that incorporates all available lines of evidence for every parameter used as an input to the RRM.

Calibration is performed using a classical nonlinear optimization routine—Levenberg-Marquardt (LM) optimization—which is then used to initialize a Markov Chain Monte Carlo (MCMC) calibration. The MCMC calibration simulates model parameter uncertainty, ultimately providing updated distributions for all model parameters. The challenges of the calibration include high temporal and spatial resolution, high-dimensional parameter space (including spatially heterogeneous hydraulic conductivities), comparatively sparse data, and low RDX concentrations. The result of the predictive forward runs is spatially and temporally explicit estimates of head and concentration with uncertainty at all modeled points in space and time.

LM calibration results show very close matches between simulated and observed values at the site. All wells with observed RDX concentrations have matches in the simulated results, including multiple screens showing a vertical concentration gradient. The clear trend in the RDX data observed at R-18 is matched closely at the beginning, middle, and end of the trend. The simulation shows 0 concentrations at all wells where no RDX is observed. Hydraulic gradients local to the plume are also matched in both direction and magnitude. This is significant because the overall regional gradient is from west to east, but local to the plume there is a northeast gradient of variable magnitude between wells where RDX has been observed in the regional aquifer. Water levels match closely local to the plume, with the simulation heads being within 3 m of all observed data. Vertical gradients are accurately represented at R-25 between screens 5 and 6, though they match less well (residual = −1.2 m at screen 7) between screens 6 and 7. Likewise, the vertical gradient at R-69 is not strong enough in the simulation (residual = −2.8 m at screen 2). Hydraulic head residuals increase east of the plume beyond the region of primary decision interest, where the hydraulic gradient flattens and the model resolution decreases to 125 m. Even in this low-resolution region, hydraulic heads are within 11 m of observed data.

Probabilistic model simulations of the calibrated model provide uncertainty bounds between 1.6 ppb and 10.6 ppb in either direction depending on the well. Wells R-18 and R-69 both indicate that concentrations will increase in the future (continuing the upward trend at R-18 until approximately 2035 and at R-69 for the next few years before leveling off). Simulation results suggest that concentrations are likely to be relatively stable in coming years at R-68, even after accounting for uncertainty in the trend. Well R-47 is the only well with 0 ppb targets that suggest potential to increase above the 0.1-ppb level in the next 50 yr; even at R-47, only a few simulations at the edges of the posterior predictive distribution reach 0.15 ppb.

All decision locations (i.e., PM- wells and a monitoring arc closer to the plume) show 0% of simulations exceeding 0.1 ppb of RDX between now and 2070. Maps of the plume in both 2020 and 2070 suggest that expansion is slow. As a result, additions of dissolved RDX from the perched-intermediate groundwater are offset by the influx of groundwater in the regional aquifer.

CONTENTS

Figures

Tables

C-1.0 INTRODUCTION

C-1.1 Background

This risk assessment report for Royal Demolition Explosive (RDX) contamination in deep groundwater at Los Alamos National Laboratory (LANL or the Laboratory) Technical Area 16 (TA-16) fulfills a requirement of the 2016 Compliance Order on Consent (Consent Order) Appendix B milestones and targets for fiscal year 2020. Appendix B Milestone 7 requires a report that presents a fate and transport evaluation and risk assessment for RDX in deep groundwater. Deep groundwater in this report refers to the perched-intermediate zone beneath TA-16 and the regional aquifer. This appendix meets the requirement for an RDX fate and transport evaluation.

In 2019, Newport News Nuclear BWXT-Los Alamos, LLC (N3B) submitted the “Investigation Report for Royal Demolition Explosive in Deep Groundwater” (hereafter, DGIR) to the New Mexico Environment Department (NMED) (N3B 2019, 700561). The DGIR presented results of previous investigations and studies, including results on the nature and extent of RDX in deep groundwater and an updated conceptual site model (CSM). The predictive modeling of the RDX plume at LANL, which is summarized in this report draws from prior work and supports the continual characterization and evaluation of RDX in groundwater, including scenario 3 in this risk assessment report. Scenario 3 applies the results of this RDX fate and transport modeling in the regional aquifer to evaluate the probability that RDX could reach regional aquifer water-supply wells at some time in the reasonably foreseeable future (i.e., 50-yr time period).

The modeling conducted for this report draws from a conceptual model that derives from work that began in 1998 and reflects refinements presented as recently as the DGIR (N3B 2019, 700561). The data collected from these studies, including the relative quantification of recharge sources (mountain-block recharge [MBR], mountain-front recharge [MFR], and local), as well as more accurate conceptualizations of geologic surfaces and structures, were used in the creation of a three-dimensional (3-D) RDX Vadose Zone model (RVZM) of the site, presented in the “Compendium of Technical Reports Related to the Deep Groundwater Investigation for the RDX Project at Los Alamos National Laboratory” (RDX compendium) (LANL 2018, 602963). The RVZM was built using the Finite Element Heat and Mass transfer code (FEHM). These data and the preliminary vadose zone (VZ) FEHM model contributed to the creation and calibration of the RDX Regional aquifer Model (RRM) used for further plume classification and prediction.

C-1.2 Conceptual Site Model

Early activities at TA-16 supported the development of the first implosion-type atomic bombs. The high explosives (HE) components of the implosion design were developed, manufactured, and tested at TA-16 during World War II. TA-16 was the principal site that manufactured HE castings and lenses to produce a means of detonating an explosive charge (McGehee et al. 2003, 700541).

Building 260, located on the north side of TA-16, has been used for processing and machining HE since 1951, including RDX (hexahydro-1,3,5-trinitro-1,3,5-triazine) Water is used in the machining process. The HE is slightly water soluble, and effluent from machining operations contains dissolved and entrained HE cuttings. At building 260, effluent treatment consists of routing the effluent to 13 settling sumps to recover any entrained HE cuttings. From 1951 to 1996, the water from these sumps was discharged to the 260 Outfall that drained into Cañon de Valle.

The 260 Outfall drainage channel consisted of the outfall, a former settling pond, and the upper and lower portions of the drainage channel leading to Cañon de Valle. From 1951 to 1996, the water from the building 260 sumps was discharged to the 260 Outfall, with millions of gallons discharged per year. Discharges from the 260 Outfall were greatest in the 1950s and then fell significantly, although they were sustained at low levels for more than 30 yr afterward (Gard and Newman 2005, 093651, p.19). There are limited data on the amounts of HE-containing discharge released from the 260 Outfall into Cañon de Valle between 1950 and 1996, when the outfall was decommissioned and remediation programs commenced.

Water containing HE and barium flowed from the sumps into the settling pond to capture entrained HE cuttings in the concrete trough and ultimately to the 260 Outfall, located 200 ft east of building 260. The outfall discharged into Cañon de Valle, providing a pathway for contaminants to enter the alluvial groundwater, VZ, and deeper groundwater (LANL 2003, 077965).

The 260 Outfall is the primary source of HE that impacted groundwater at TA-16 (LANL 2011, 203711). The 260 Outfall released large quantities of contaminants, particularly RDX, at high concentrations and large volumes of water that provided a significant hydrologic driving force for infiltration of contaminants (LANL 2011, 203711; LANL 2012, 213573).

The physical systems presented in the CSM describe the fate and transport of RDX in groundwater beneath the TA-16 area. The development of the CSM began with Phase I site characterization (LANL 2011, 206324). Subsequent soil, sediment, surface water, springs, alluvial groundwater, shallow- and deep- perched-intermediate groundwater, and regional groundwater investigations formed and continue to influence the current CSM.

C-1.2.1 Geologic Context

The RDX project area lies on the western edge of the Pajarito Plateau. Underlying the plateau is a geologic feature consisting of roughly 250 m of varying sequences of poorly consolidated tuffaceous materials known as the Bandelier Tuff. The sequences of the Bandelier Tuff were deposited from volcanic eruptions roughly 1.25 and1.6 million yr ago from the Valles Caldera to the west and can be generally classified into two members: the lower (1.6 million yr) Otowi Member and the upper (1.25 million yr) Tshirege Member. Separating the deposition of these two members was a brief pause in geologic activity when the Cerro Toledo Formation erosional sediments were deposited. Below the Bandelier Tuff in the RDX project area lies the Puye Formation (unconsolidated alluvial sediments sourced from the Jemez Mountains volcanic field to the west that predate the deposition of the Bandelier Tuff). The Tschicoma Formation, a thick lobe of massive to brecciated dacite lavas, lies deep in the stratigraphic section beneath the project area.

There is a large variety of surficial deposits at TA-16, in both the canyons and on top of mesas. Holocene alluvium and colluvium can be found within the canyons while older alluvial fans compose part of the mesa-top sediments. The poorly sorted alluvium within Cañon de Valle and other local drainages is made up of medium- and fine-grained sands and volcanic cobbles, gravels, and sands derived from the Tshirege Member and the Tschicoma Formation. Within the canyons proximal to RDX site, this alluvium ranges between 5–9 ft in thickness (LANL 1998, 059577). These deposits perennially contain alluvial groundwater. Mesa tops at TA-16 include widespread remnants of gravel deposits from early Pleistocene streams draining the Sierra de los Valles, which predated the incision of the modern canyons (Reneau et al. 1996, 055539). Because of their thickness and high porosity, mesa-top alluvial fans may also play a role in storing water from storm runoff and snowmelt (N3B 2019, 700561). Figure C-1.2-1 shows a vertical profile of the geologic sequences of the Bandelier Tuff and the underlying coarse alluvial Puye sediments.

Following the deposition of the Bandelier Tuff, erosion and faulting have modified the geology. Erosion of the tuff has created fingerlike mesas and canyons that extend west to east. TA-16 sits on one of these mesas located south of, and adjacent to, Cañon de Valle. The TA-16 260 Outfall discharged directly into the Cañon de Valle canyon bottom.

Extensive faulting has also been observed at the western edge of the Pajarito Plateau, known as the Pajarito Fault System (Figure C-1.2-2). The Pajarito Fault System is a narrow band of normal faults that trend to the north/northeast. Deep-seated normal faulting is expressed at the surface level by a mix of normal faults of variable magnitudes and monoclines (Gardner et al. 1999, 063492).

The Pajarito fault has extensive influence on the thickness and relative location of geologic units at the mountain block/plateau interface. It is the principal structural feature in the area and most likely plays a key role in the transfer of groundwater from the mountain block to the plateau. Because of intense fracturing, the fault zone probably is also an important infiltration zone for MFR (N3B 2019, 700561). Faulting has the ability to create fast pathways or hydraulic windows to the subsurface. The 260 Outfall is located in the TA-09 graben, an area that is suspected to be coincident with an area of high infiltration due to faulting and fractures (Figure C-1.2-3).

C-1.2.2 Hydrologic Context

The hydrologic system in the watershed includes surface water, springs, alluvial groundwater, shallow bedrock and perched-intermediate groundwater, and regional aquifer groundwater. Water Canyon and its main tributary, Cañon de Valle, have their headwaters west of the Laboratory in the Sierra de los Valles within the Santa Fe National Forest. Surface water in Cañon de Valle is predominantly ephemeral and seasonally dependent on snowmelt and storm runoff. Only short reaches with perennial flow occur in Cañon de Valle, and these reaches are dependent on spring discharges. Alluvial groundwater in Cañon de Valle is recharged by streamflow and runoff from local precipitation and snowmelt runoff.

Perched groundwater occurs at both shallow (referred to as shallow bedrock) and deep (referred to as perched-intermediate) levels of the VZ in the TA-16 area. Shallow bedrock groundwater zones occur at depths of 200 ft below ground surface (bgs) in upper units of the Tshirege Member of the Bandelier Tuff. Groundwater from these zones includes springs that discharge into canyons and small zones of saturation in tuff that are penetrated by shallow wells. Perched-intermediate groundwater occurs at depths of generally 600 ft bgs in the lower part of the VZ, primarily in the Cerro Toledo Formation, the Otowi Member of the Bandelier Tuff, and the Puye Formation. Groundwater in the two perched-intermediate zones is a mixture of MBR and MFR. MBR originates in the highlands west of the Pajarito fault zone and consists of diffuse subsurface infiltration of snowmelt and surface water that percolates through the rock and recharges the regional aquifer. MFR consists of mountain overland flow (generally streamflow) that infiltrates at the mountain front and the adjacent basin.

The regional groundwater table beneath Cañon de Valle has an easterly sloping gradient that extends from an elevation of approximately 6600 ft at the Pajarito fault to approximately 5500 ft at the Rio Grande, over a distance of approximately 9.3 mi. Much of the 1100-ft decline in elevation occurs within the 1.3-mi distance between the Pajarito fault zone (western edge of the Pajarito Plateau) and well R-63. Recharge of the regional aquifer takes place largely in the Jemez Mountains west of the Pajarito fault zone; however, the presence of HE in some regional aquifer monitoring wells indicates that local infiltration at TA-16 contributes to recharge of the regional aquifer.

RDX-contaminated water initially entered the hydrologic system at the land surface and was transported down to the regional aquifer. The deposition of a significant inventory of water containing RDX occurred in mesa-top settling ponds or within sediments in small drainages near outfalls. RDX from the 260 Outfall that mixed with surface water and alluvial groundwater in Cañon de Valle acted as a hydraulic driver for a line source of recharge to the VZ. The infiltration of surface water at outfalls in the surrounding areas moved soluble contaminants down into the shallow perched groundwater in the upper Tshirege Member. Infiltration into this perched zone mainly occurs through fast pathways such as Pajarito fault-related faulting and fractures. Ultimately, this resulted in the deposition of RDX within the VZ. Previous reports have divided the VZ into two parts: upper and lower. The upper VZ is defined as extending from the surface to a depth of about 600 ft. This section is composed of variably welded Bandelier Tuff and Cerro Toledo fluvial deposits. The upper VZ is, for the most part, unsaturated but contains thin ribbon-like zones of perched groundwater, some of which daylight as springs in the canyons.

The lower VZ extends from a depth of 600 ft to the top of the regional aquifer (between 1000 and 1300 ft bgs) and includes the lowermost deposits of the Bandelier Tuff as well as thick sequences of generally coarse and highly heterogeneous fluvial sediments of the Puye Formation. The lower VZ, as defined here, includes both of the perched-intermediate groundwater bodies that are often referred to as the upper and lower perched zones. Significant amounts of RDX have been observed in these zones.

C-1.2.2.1 Upper Vadose Zone

Dissolved-phase RDX initially migrated into the subsurface through surface water and alluvial groundwater pathways. Infiltration is more significant beneath canyons and gullies than mesa tops. The shallow bedrock beneath Cañon de Valle is composed of welded and relatively impermeable tuffs, and infiltration in this canyon bottom is thought to be strongest in areas where bedrock has been fractured. In the RDX site, faults along the TA-09 graben cut roughly perpendicular to the canyon axis, and large amounts of stream and alluvial water loss occur in this part of the canyon (N3B 2019, 700561). Infiltration also occurs outside of the canyon bottoms at the mesa tops in locations where sufficient water is stored or accumulates. This ponding creates higher hydrologic heads with the ability to drive infiltration. The 260 Outfall pond and adjacent drainages are two examples of locations with enough inundation to allow varying frequencies of seepage.

RDX containing wastewater was discharged from the 260 Outfall into Cañon de Valle, where it mixed with surface waters coming up from the canyon. The combined waters infiltrated into the alluvium and from there into the upper VZ. The amount of water that migrates through these vertical pathways is temporally variable and spatially dependent. Vertical movement is primarily controlled by gravity in unsaturated zones. However, water has the potential to move laterally at bedding contacts and in zones of perched water, which are driven by hydraulic gradients that generally trend to the east (LANL 2018, 602963). The result is that water tends to stairstep down through the VZ through a series of perched zones, likely expanding the lateral extent of the contaminant plume. This process occurs to a small degree in the upper VZ compared with the lower VZ, where much larger perched zones have been observed.

C-1.2.2.2 Lower Vadose Zone and Perched-Intermediate Groundwater

Two discrete perched-intermediate groundwater zones are believed to be below the RDX site in the lower VZ. The upper and lower perched-intermediate zones are separated by 80–150 ft of variably saturated rocks. Both zones have the potential to create a lateral pathway for contaminant transport. Because of the potential for lateral transport, contaminated water may leave the perched zones at a spatial location that is different from where the source entered the perched zone. Contaminated water eventually travels vertically from these zones, resulting in contaminated recharge to the regional aquifer.

Of the two perched-intermediate zones, the upper perched-intermediate zone (UPZ) is larger and more important for RDX lateral transport because of the spatial extent of saturation. The lower perched-intermediate zone (LPZ) is thought to be much smaller in its extent of saturation compared with the upper. The perched zones are generally continuous and in direct hydraulic communication locally, although that communication can be variable as a result of the heterogeneous geology present and the variable levels of saturation spatially. Perched groundwater appears to be supported by leaky confining beds made up of thin silt beds that are limited in their lateral extent.

The primary source of recharge to the perched-intermediate groundwater is thought to be dominated by MBR and MFR (N3B 2019, 700561). Monitoring of water levels in the perched-intermediate zones suggests that recharge from precipitation events at the surface is slow, and travel times are long, although there is evidence of fast pathways from the surface to the regional aquifer as well. These fast pathways could be the results of localized fault-related fracture networks. Geochemical analysis also suggests a large fraction of the perched water is similar to water sourced from the mountain block rather than from vertical infiltration sources above (LANL 2018, 602963). MBR and MFR are thought to occur where steep gradients in the regional water table intersect gently dipping transmissive geologic strata (N3B 2019, 700561), creating the perched-intermediate zones. That is, as groundwater flows eastward from the mountain block towards TA-16, some groundwater is diverted laterally into the VZ. While MBR is similar to MFR, MFR is considered to be recharge, which occurs more shallowly than MBR.

MFR is characterized by streamflow infiltration from upcanyon Cañon de Valle watershed drainages and the infiltration of overland flows. The MFR recharge to the perched-intermediate groundwater occurs in an area extending from the Pajarito fault zone to the TA-16 area. MBR is thought to make up approximately 66% of perched groundwater, with local MFR making up 34% (LANL 2018, 602963).

During the period of active releases at the 260 Outfall, wastewater containing RDX that had comingled with surface water infiltrated vertically and mixed with perched-intermediate water sustained by clean MBR and MFR, resulting in diluted RDX concentrations in the perched-intermediate groundwater. This contaminated water eventually flows from the perched-intermediate zones downward in VZ pathways and laterally in perched zones to recharge the regional aquifer.

The CSM for the RRM includes both RDX-free and RDX-contaminated sources of recharge from the perched-intermediate groundwater to the regional aquifer (section C-2.2.3.2.4).

C-1.2.2.3 Regional Aquifer Groundwater

The Puye Formation begins in the lower part of the VZ and is characterized by coarse and highly heterogeneous alluvial fan sediments. The Puye Formation is up to several thousand feet thick in some locations (LANL 2018, 602963). The regional aquifer water table at the RDX site is mostly within the Puye Formation.

At TA-16, the regional water table is located between 1000 and 1300 ft bgs, with higher water table levels to the west creating flow from west to east. The regional groundwater system is heterogeneous and complex, with unconfined conditions thought to exist near the water table and semiconfined conditions with depth (LANL 2011, 207069). However, because of complex geologic sequences, faulting, and heterogeneous aquifer materials, the site contains highly variable hydraulic gradients, both horizontally and vertically.

The shape of the regional water table is predominantly controlled by hydrologic recharge at the western boundary and discharge to the east. At the western boundary of the regional aquifer, recharge from the Sierra de los Valles mountain block provides higher hydraulic heads that force an overall west-to-east gradient. At the eastern boundary, the regional aquifer contributes to gaining stream conditions below the Rio Grande and is also expressed at the surface as discharges from springs in White Rock Canyon. Aside from the overall west-to-east hydraulic gradient within the aquifer, regional flows may also be influenced by local areas of infiltration (beneath canyons), heterogeneous lithology, and anisotropic aquifer properties. Pumping tests have shown a higher degree of lateral connectivity than vertical connectivity within the aquifer, suggesting hydraulic conductivities are generally higher laterally than vertically. Vertical differences in hydraulic heads and a lack of vertical propagation of pumping drawdown indicate some level of hydraulic stratification. This vertical anisotropy within the aquifer is likely caused by the depositional layering of the stratigraphic units that contain the regional aquifer.

C-1.2.3 RDX Transport Conceptual Model

RDX has been detected in surface water, springs, sediments, and alluvial, perched-intermediate, and regional groundwater at the site. The focus of the risk assessment is on RDX detected in the perched-intermediate zones and regional aquifer. The RDX transport conceptual model described here aims to briefly summarize the conceptualized modes and paths of RDX transport in these systems.

The primary source for RDX that has been detected in the perched-intermediate and regional groundwater at the site is largely thought to be the result of discharges of wastewater containing RDX from the TA-16 260 Outfall and pond to Cañon de Valle (Figure C-1.2-3). At the outfall, the water containing RDX was directly discharged into Cañon de Valle, where it mixed with surface water and alluvial groundwater in Cañon de Valle and infiltrated into the subsurface near the TA-09 graben (faults of the TA-09 graben are shown in the lower-right map of Figure C-1.2-4). Faulting in the TA-09 graben area intersects the canyon bottom, and significant stream loss has been observed in the vicinity of the faults (Figure C-1.2-3).

After infiltrating to the subsurface, water containing RDX is transported vertically via partially saturated flow through the porous geologic material of the Bandelier Tuff until it reaches saturated conditions in the perched-intermediate zones, though the potential exists for faster transport through fractures. There are two main perched zones at the RDX site, an upper and a lower zone (Figure C-1.2-5 and section C-1.2.2). The UPZ occurs around 600 ft bgs, and hydraulic heads in the LPZ indicate the LPZ is roughly 200 to 280 ft lower, 800 to 880 ft bgs (N3B 2019, 700561). A large portion of recharge to the perched-intermediate aquifers is understood to come from MFR and MBR that have no RDX (Figure C-1.2-4). This recharge composes the majority of total recharge to the perched zones, so it is most likely that water containing RDX is successively diluted by MFR and MBR each time it arrives at a perched zone.

The upper of the two perched-intermediate zones is larger and more extensive (Figure C-1.2-5). Concentrations over 100 ppb have been detected in the UPZ in intermediate wells CdV-16-2(i)r and CdV-16-4ip. The LPZ is much smaller in extent, and lower concentrations of RDX have been detected compared with the upper zone. Only a few monitoring wells have been completed in the LPZ, with concentrations detected around 20–23 ppb (R-25 screen 4 and CdV-16-4ip screen 2). Limited data exist for the lower zone, as the two well screens completed in this zone have been abandoned.

Once RDX arrives in the perched-intermediate saturated zones, it has a higher potential for lateral movement via saturated flow (Figure C-1.2-4). Eventual downward percolation from these perched zones provides contaminated recharge to the regional aquifer. Because of the potential for lateral transport in the perched-intermediate aquifer systems, RDX may not arrive at the regional aquifer in the same spatial location as it first infiltrated into the subsurface.

The degree of hydraulic communication between the perched-intermediate zones and the regional aquifer is thought to be relatively poor and spatially variable, depending on local hydrogeologic conditions and associated hydrostratigraphy (Figure C-1.2-4) (N3B 2019, 700561). Downward percolation and recharge to the regional aquifer is thought to occur through regions of preferential recharge or “hydraulic windows,” although these flows have not been directly observed. Although actual hydraulic windows are likely to have a high degree of irregularity, within the RRM sources of recharge are modeled as elliptical (section C-2.2.3.2), providing a large amount of flexibility in the shape and size of recharge windows.

Once water containing RDX reaches the regional aquifer, it mixes with and is diluted by clean regional groundwater as it is being transported via hydraulic gradients. Lateral hydraulic connectivity within the regional aquifer has been demonstrated through observed drawdown during drilling, well development, and well pump tests (N3B 2019, 700561). Water-level data from regional wells show a general west-to-east hydraulic gradient at the RDX site; however, aquifer heterogeneity and sources of recharge to the regional aquifer have the potential to modify this gradient, as shown by regional groundwater level contours in Figure C-1.2-5. To date, concentrations up to 22 ppb (regional well R-69 screen 2) have been detected in the regional aquifer. Figures C-1.2-6 and C-1.2-7 show the estimated horizontal and vertical extent of RDX in the regional aquifer. The purpose of the RRM is to simulate the transport of RDX in the future towards potential downgradient points of compliance in the regional aquifer.

C-1.3 Approach to Modeling

The modeling approach is designed to integrate all possible sources of information available to inform the decision in the hierarchical structure represented in Figure C-1.3-1. This structure is used to predict RDX fate and transport in both space and time, quantify the uncertainty associated with model predictions, and quantify the sensitivity of parameters and the value of information. Figure C-1.3-1 shows the framework that leads to this final decision space in which the RRM provides the platform for quantitatively integrating these sources of information to address stakeholders’ concerns and regulations. The numerical RRM is built using FEHM (Zyvoloski 2007, 700904) and is calibrated using the Model Analysis and Decision Support (MADS) software, available at https://mads.lanl.gov/. Distribution development that incorporates all available lines of evidence (shown at left of Figure C-1.3-1) is discussed in section C-2.2. The RRM itself is discussed in section C-2.1 and the calibration (shown at center of Figure C-1.3-1) is discussed in section C-2.3. Predictive forward modeling is discussed in section C-2.5 (Figure C-1.3-1).

The steps developed for the RRM modeling need to leverage all the lines of evidence available, including data, the RVZM, site CSM and expert knowledge, as well as other available analytical tools (Figure C-1.3-1). Next, they need to combine these elements with an effective model structure and calibration. In order to gather as much information as possible, analytical tools (section C-2.4) are used throughout the process to best understand the physics, statistics, and assumptions made throughout the modeling process. While these steps can be thought of as stepwise, an effective modeling workflow needs to be iterative, with analyses throughout the process able to improve upon assumptions and decisions made at any point in the modeling. Within each step of the process there are internal iterative loops that maximize the value of information to be gained as the model is improved.

C-1.3.1 Distribution Development Approach

Distribution development is the process shown at the far left of Figure C-1.3-1 where available lines of evidence are combined to form appropriate inputs to the RRM. An iterative approach to parameter distribution development is used for the RRM for the purpose of focusing effort where it will have the greatest benefit for reducing uncertainty in risk and dose (Figure C-1.3-2). After a target or goal for the distribution for the input parameter is defined, the method has four main steps that result in model implementation. In the first step, *screening*, high-level decisions are used to limit the scope of information collection. For example, will data collection be limited to certain contaminants, locations, or types of properties? Expert judgment or prior sensitivity analysis (SA) results may be used during screening. During the next step, *data collection*, the most relevant available sources are gathered. To determine relevance, some site assessment is performed first to identify the expected media types and aqueous environmental conditions at the site (usually part of the conceptual site model development). In the *filtering* step, data are culled based on the site assessment with consideration to the amount of data available, its quality, and relevance to the site. Exploratory data analysis is extremely useful for determining whether categorizations of the data have been appropriate, and new choices may be made if necessary. Finally, the data subsets are ready for *statistical analysis*, where distributions are developed using the statistical techniques deemed most appropriate for meeting the distributional goal and for the intended usage of the parameter in the model. The distributions are implemented in the model, and results are used to identify new areas of focus for parameter development, based on sensitivity and/or value of information analysis. More extensive explanation of this process is described by Jordan et al. (2017, 700881).

In the case of the RRM, these steps are described in detail for every parameter in section C-2.2.3. These steps include incorporating the CSM, gathering lines of evidence, filtering the data, and also the analytical tools used to understand the distributions in the context of the modeling described in section C-2.4.

C-1.3.2 Calibration Approach

The center of Figure C-1.3-1 depicts the next step in the overall approach, calibration. Like distribution development, calibration is also iterative (Figure C-1.3-3). First, the goals of the calibration must be defined, including answering the question: “what is this [calibration] run hoping to achieve?”. Those goals may affect the target implementation, weights, or some other part of the calibration structure. They may also affect the numerical parameters and tolerances needed for the high-performance computing (HPC) solver. Lastly, the setup may need to be adjusted, including parallelization scaling, software, and input/output structures.

A calibration is launched with these goals in mind, and, as it completes each iteration, the ModelWatcher program (section C-2.4.5) automatically updates an internal webpage for use in visualizing results as they are output. This software uses an extensive array of independent visualizations that help quantify the success of the run, including summary plots, 1:1 matches to data across iterations, residuals, inventory plots, objective function (OF) plots, parameter movement over time, and results versus data plots. Often, certain visualizations are built in the moment to analyze a specific goal of the particular calibration. The results from each calibration can then inform improvements for the next calibration.

C-1.3.3 Analysis Step of Modeling Approach

Distribution development and calibration can be thought of as step 1 and step 2 of this modeling approach (as they are shown in Figure C-1.3-1); however, results throughout the process inform both steps, and iteration also occurs in the larger loop shown in Figure C-1.3-4. This figure depicts a more complete picture of the iterative steps in the modeling approach. The first part of any robust modeling exercise is describing the decision context, or purpose of the model. This guides the modeling to be most effective in ways that constrain the uncertainty around a particular decision. In this case, the priority is on accurate plume characterization and estimation of downgradient concentrations at locations described in section C-2.5.1. Next the model is constructed, purple box in Figure C-1.3-4 (section C-2.1), and the input parameter space is described using all lines of existing evidence, light blue box in Figure C-1.3-4 (section C-2.2). The calibrations are conducted (section C-2.3) using the iterative process described above. Calibrations, either singly or using data from all runs, are then analyzed to understand and verify model performance and structure. These analytical tools are shown as yellow boxes in Figure C-1.3-4 and described in detail in section C-2.4. The structural analyses, including manual calibrations (section C-2.4.1) and suites of forward models (section C-2.4.2), are used to understand and check the model physics, structure, and input parameter space of the model. The sensitivity analyses, including consistent Bayes (section C-2.4.4) and machine learning meta model (section C-2.4.3) are used to understand the relationship between inputs and outputs in the model.

These analyses then inform improvements and updates to either the model structure (for example, making a change to the way boundary conditions are set up in the model) or to the distribution development (for example, identifying that a particular parameter is missing values that are critical to model performance). Performing the modeling in this iterative manner ensures that all assumptions are checked and rechecked both by subject matter experts—hydrologists or site experts—and by statisticians. These steps help to verify that the model is effective at reproducing the CSM and effective at representing the uncertainty in that model based on the available lines of evidence to inform the structure and inputs.

The ensuing sections describe each of the components discussed above in greater detail. Section C-2.1 describes the RRM construction—the spatial and temporal setting, the parameters used in the model, and the numerical code. The calibration is discussed in section C-2.3, including much more detail on classical calibration, Bayesian calibration, and target development. The results of the calibration are posterior parameter distributions that are informed both by the prior parameter distributions and by the constraints of the RRM calibration. Section C-2.5 describes the forward predictive modeling process and decision context.

C-2.0 METHODS, ANALYSIS, AND DISCUSSION

C-2.1 RDX Regional Aquifer Model

C-2.1.1 Model Domain

The RRM begins at the regional aquifer water table, which is approximately 300–400 m below the land surface. Water table elevations range from 1920 m above mean sea level (amsl) near the western edge of the domain, which approaches the mountain block, to 1616 m amsl near the Rio Grande, whose x, y coordinates define the eastern model boundary. The model covers an area of 221 km^2 horizontally and extends from the water table surface down to 1000 m amsl in the vertical direction; it is designed to represent the regional aquifer.

The main direction of groundwater flow in the regional aquifer is from west, where regional recharge enters the aquifer from the mountain block of Sierra de los Valles, to east, where discharge occurs along the Rio Grande River and White Rock Canyon springs. However, throughout the area there are local zones of infiltration, especially under canyons where precipitation is routed on the surface. Additionally, heterogeneity, faults, and anisotropy add to the complexity and direction of flow within the regional aquifer. The aquifer is a large, regional system with both confined and unconfined areas; however, there are no clearly defined confining layers to determine the extent and location of these different zones.

The focus of this report is where RDX is currently observed in the regional aquifer and the downgradient region. This includes R-25, R-63, R-18, R-68, and R-69. The focus of the calibration, implemented through weighting certain target data points (section C-2.3.3), is first to match the data in the vicinity of the plume, and next to match data further downgradient in the regional aquifer. The model is built at a regional scale so that there is opportunity to evaluate many downgradient locations or to allow the possibility of added detail and complexity in the future.

C-2.1.2 Model Grid

The model is discretized into a tetrahedral mesh with lateral spacing at 125 m using the LANL LaGriT mesh generator available at https://lagrit.lanl.gov/ (Gable et al. 1996, 700887). Two levels of refinement are used in areas of interest, which increases lateral resolution to 62.5 m and 31.25 m respectively. The z direction is variably refined, ranging from 6–24 m in thickness and decreasing with depth. The grid is connected according to Delaunay criteria and is quality tested both in terms of Voronoi volumes and negative coefficients. Materials are assigned to each node in the mesh based on the 13 hydrogeological units in the Geological Framework Model for the LANL region. The total number of nodes for the RRM mesh is 510,226 and the total number of elements is 2,883,589. The entire RRM and an inset in the region of interest for monitoring RDX concentrations is shown in Figure C-2.1-1.

The approach taken to generate the mesh leveraged existing mesh generation work for the chromium plume site in the regional aquifer (LANL 2018, 602964). A water table surface was generated based on water table mapping that was representative of the 2014 average water table levels. The year 2014 is used because this is the same year used to develop water table targets and it represents the most thorough description of the water table (interpolated between data points) available from recent years. The model is run to steady-state flow conditions (see section C-2.1.3), as opposed to using transient flow solutions. An average water table decline of 0.5–1 ft per yr is observed across the site, but a uniform change in water table elevation is not expected to alter flow directions for RDX transport.

The water table surface was smoothed to a resolution appropriate for the grid spacing. Using the Los Alamos Grid Toolbox (LaGriT) (https://lagrit.lanl.gov/), the 125-m by 125-m grid was interpolated onto the water table surface, and the surface was clipped to the shape of the RRM. Next, a process of two-dimensional (2-D) refinement was carried out in (1) the main refinement area of interest to improve transport simulations for the RDX plume and (2) wells near the area of interest. Refinement was conducted as an attempt to balance the total number of nodes on the mesh (fewer nodes result in more tractable runtimes) with enough detail to do transport simulations in the area where RDX has been observed in the regional aquifer.

The first level of refinement covers a larger area of interest (from 492100 to 494800 m easting and from 537300 to 539600 m northing in New Mexico State Plane coordinates) as well as major wells in the wider region of interest (R-17, R-19, CdV-R-15-3, CdV-R-37-2, R-58, R-48, and R-26). Note that no RDX has been detected at these wells. The second level of refinement includes wells where RDX has been detected (R-68, R-69, R-18, R-63, and R-25) as well as some area downstream of these wells (from 492100 to 494000 m easting and from 537600 to 538000 m northing).

After refining these regions in 2-D, copies are made and stacked at every z-coordinate needed for the orthogonal mesh (21 layers near the surface from 1790 to1926 m amsl, 10 layers from 1640 to 1790, 4 layers from 1520 to 1640, and 8 layers from 1000 to1520). From top to bottom, this leads to z-resolutions of 6.5 m near the surface, then 15 m, then 30 m, then 65 m. Reducing resolution deeper in the aquifer increases computational efficiency. This mesh is then clipped to the water table surface, resulting in a fully orthogonal, stair-stepping surface. The orthogonal mesh has faster runtimes than an irregular mesh. It also amounts to 30% fewer nodes than an equivalent irregular mesh for the same vertical resolution in the area of interest. This mesh is then converted from a hexagonal mesh to a tetrahedral mesh for use in FEHM.

Detailed quality checks on the mesh are made throughout the process, verifying that LaGriT correctly tags nodes as inside or outside the domain, tags facies and geologic units correctly, and maintains high aspect ratios (> 0.5) and positive volumes in all elements. Errors in the meshing step can affect FEHM groundwater modeling calculations, so verifying the accuracy of the mesh is a critical step for a robust groundwater model.

C-2.1.3 Model Operation, Initial, and Boundary Conditions

The FEHM code (Zyvoloski 2007, 700904) is used to simulate flow and transport in the RRM. The model represents the regional aquifer and is therefore considered saturated at every node. The main flow gradient in the model is developed by assigning head conditions to the western (mountain block) and eastern (Rio Grande) boundaries. Details of the data informing these boundary conditions are discussed in section C-2.2. Boundary conditions, like other model parameters, are drawn for each simulation from distributions and vary across the stochastic suite that is simulated. Despite this variability, the direction of flow in the model described by the constant head boundary distributions (section C-2.2.3.3.1) is largely west to east. Other boundaries conditions include no flow at the north and south boundaries and at the base of the model. On the surface of the RRM, hydraulic windows representing recharge from the VZ are applied, which vary according to their input distributions (section C-2.2.3.2).

Some material and transport properties are assigned on a node-by-node basis; others are homogeneous throughout the domain. Details of these assignments are discussed in the distribution development in section C-2.2.3. Time series of RDX concentrations and water levels are output for every well within the domain. Decision locations are added to these time series for predictive forward runs. Additionally, the model can be set up to output data of interest at every point in both space and time within the modeling domain. Outputting all data this way is memory intensive so for most modeling runs, especially those conducted stochastically, this is not done. One area where these data are explored in detail at all points in space and time is in the manual calibration step, described in section C-2.4.1.

There are 196 input parameters to the RRM that are informed by their prior distributions (section C-2.2) and then calibrated. Boundary condition parameters include west head (north and south with the intermediate gradient calculated), east head (similar to west head [section C-2.2.3.3.1]), and source characteristics. Material properties parameters (section C-2.2.3.1) include advective porosity and porosity, lateral and vertical K (as well as kriging parameters that distribute K in space), and dispersivity. Additionally, K_d and diffusivity are defined for the model. These parameter categories, the central value of their distributions, and the sources of information that informed the distribution are listed in section C-2.2.3.

The RRM input parameter set is calibrated using the Levenberg-Marquardt (LM) optimization (section C-2.3.2) and a Markov Chain Monte Carlo (MCMC) calibration (section C-2.3.4). Throughout the calibrations, the model is run in forward mode for diagnosing behavior, understanding input distributions, testing forward workflows (section C-2.4), and developing input distributions (posterior distributions) for forward Monte Carlo simulations. Ultimately, a suite of probabilistic predictive forward runs is performed using posterior parameter distributions to inform decision-making under uncertainty (section C-2.5).

C-2.2 RDX Regional Model Input Parameter Distribution Development

C-2.2.1 Overview

Representing uncertainty in model inputs often means finding a balance between uncertainty and physical reality. Developing wide distributions may seem conservative in principle, but this approach can lead to unrealistic model results. Characterizing the current state of knowledge of stochastic inputs presents many challenges, especially if the data available are limited or have limited relevance to the site. Relationships among these inputs may also be important to represent but are typically complex or difficult to define. Often special adjustments must be made to account for reduced credibility in particular data. If parameters are strongly related to one another, a correlation structure may be developed for input to the model. Other techniques such as regression models may be used to incorporate relationships between the information available and the desired parameters.

The process of developing distributions must consider details of the model in terms of what the distribution is meant to represent. Many parameters in the RRM at LANL must make a single draw and apply that draw to all space and time over which the model is run, for a single simulation. This simplification is often made for many reasons, and can often be beneficial, but also adds additional complexity in the distribution development process. Defining the distributional goals as they relate to the modeling process is an important step, and it takes place before evaluation of the data. Usually, the distributions developed are meant to characterize the average value of the parameter over the spatial and temporal domain of the model.

Distribution development requires consideration of many sources of information on the parameter where available, ideally from multiple references. Examples of different sources include data from different references but also from different conditions, measurement methods, or experimental types. Depending on these conditions and the reliability or relevance of particular references, different sources of data may each contribute valuable information but may have varying relevance to the site. In these cases, weighting data unequally is a useful way to incorporate the value of different sources of information to the distribution in question. As an example, aqueous dispersivity (section C-2.2.3.1.4) data are available for a variety of rock types. Only a few values are available for the desired rock type, and this is not enough data to develop a robust distribution. Therefore, dispersivity values from other rock types are included in distribution development but are down-weighted such that the best data (data from a specific geologic unit) have the most influence on the distribution developed. In another case, sorption coefficient (K_d), (section C-2.2.3.3.2) distributions in the model are meant to represent a known composite of multiple soil types. Data from these materials are weighted accordingly to develop a distribution for the weighted average K_d across soil types. Other cases include varying reliability of different sources, and weighting data according to the confidence in these sources.

In some cases, input parameters are correlated with one another. An example is advective porosity, which is positively correlated with total porosity and must be less than total porosity (section C-2.2.3.1.3). Paired data with both parameters must exist to discern the relationship between the two parameters and, if it is necessary, to build a correlation structure into the model. In general, correlated parameters may be represented in the model by a multivariate distribution, or perhaps more desirably, capturing the correlation within the developed distributions, which may be treated as independent from one another. In the example of porosity, this can be done by transforming advective porosity into a proportion of total porosity, which may be drawn independently from the distribution of total porosity. In the RRM, complex data and correlations are incorporated to meet the distributional goals of the model. These distributions ultimately amount to populating the model structure with all existing data and knowledge of the site in order to model uncertainty as accurately as possible given the available lines of evidence.

The RRM necessarily represents a simplification of the coupled hydrogeologic and chemical processes in the regional aquifer. From a statistical perspective, the model parameters are “conditioned” on this simplification that defines the physical process the parameter is intended to represent. No matter the amount or quality of data available, there is no way to know the true value of the parameter we want to represent. The data available represent a sample of the population as defined by the conditioning on the model structure. This disconnect is referred to as sampling error—the uncertainty resulting from not knowing every value in the population. Although it is not possible to explicitly address sampling error in distribution development, by assuming the sample is unbiased and representative, inferences can be made about the population using a variety of techniques.

Because the distribution of the average is typically of interest, bootstrapping methods are useful in distribution development. Bootstrapping methods sample the data with replacement and calculate the statistic of interest (in this case the average) from this sample. This process can be repeated many times (usually 1000 or more) to produce representative averages. Bootstrapping is particularly useful for data sets smaller than n=30 but should not be used for data sets smaller than n=7 or 8.

In some cases, the data represent measures of uncertainty rather than the raw data themselves, and this uncertainty should be accounted for in distribution development. Depending on the parameter and the source, this uncertainty may be a standard deviation or variance of raw values in a study that measured the parameter of interest directly for several individuals or areas. Some studies from which data are gathered for the RRM distribution development use models to derive values for the parameter, in which case the study may provide a single estimate of the parameter and a standard error of estimation. Other studies may have been conducted for some purpose other than estimating the parameter of interest, but they may provide the parameter for reference. In these cases, it is common to find a table with the estimate(s) of the parameter and some associated uncertainty without an explanation of what that uncertainty is meant to represent. This makes accounting for the uncertainty in distribution development challenging, and professional judgement may be required to make assumptions on the most likely meaning of the reported uncertainty.

When uncertainty estimates are available, Monte Carlo (MC) simulation is a useful technique to develop a distribution. Just as MC simulations can propagate uncertainty throughout a model, this method is also useful for representing uncertainty on a smaller scale, such as for a single parameter. By assuming some distributional form applies to the individual measurements reported, MC simulation techniques can be used to develop the distribution of interest. Typically, a normal or lognormal distribution is applied to each measurement. A draw is taken for each measurement to represent a plausible average from that source, and the average across all sources is taken to represent a plausible average for the parameter suitable for input to the model. This process is repeated many times to obtain a set of averages, which a final distribution can be fit to.

Modelers and statisticians work in conjunction to make decisions regarding the relevance and usage of sparse data. Combining subject matter modeling expertise and statistical expertise ensures that the distribution used adequately represents, but does not overstate, uncertainty in the parameter of interest. Although these decisions inevitably introduce subjectivity into the process, the resulting distribution tends to be more representative of the most likely values of the parameter of interest.

More extensive discussion of the distribution development process can be found in “Scaling Input Distributions for Probabilistic Models” (Black et al. 2019, 700892).

C-2.2.2 Available Data and Other Lines of Evidence

Distribution development combines all sources of available information, here called “lines of evidence,” into probability distributions representing the possible values of a given parameter at the spatial and temporal scale of the model. For the RRM, lines of evidence include observational data at the site (section C-2.2.2.1), information or data from reviews of available literature (section C-2.2.2.1), the RVZM (section C-2.2.2.2), and the Pipe and Disk (P&D) analytical screening tool (section C-2.2.2.3). Distributions are needed for each of approximately 200 calibrated parameters in the RRM. While there are approximately 200 calibrated parameters, some share the same input distribution when there is not enough available information to develop a separate distribution. For example, in the case of lateral hydraulic conductivity, K_x and K_y at a given location use unique parameter draws during each calibration iteration; however, there are no data to develop separate distributions for K_x and K_y, so their distributions are identical, even though their draws and, ultimately, calibrated values, will differ.

The approach to distribution development is described in detail in section C-1.3.1. The available sources of data and the distributions to which they contribute are discussed below. All unique distributions are shown in Table C-2.2-1 and are discussed individually in the sections that follow.

The RVZM is used as a line of evidence for some of the RRM parameters (section C-2.2.2.2). It also makes use of distribution development for other parameters, especially material properties, many of which it shares with the RRM. Parameters that are used in both the RVZM and RRM will include discussion of distribution development for both models.

C-2.2.2.1 Well Data and Literature

There is extensive data to be found in the literature for RRM distribution development. The data is considered in the context of the CSM and, if needed for a given distribution, additional lines of evidence are also considered. Literature used to inform distribution development varied by parameter; however, LANL site-specific data were always preferred. Some sources of information in the literature include borehole data (core samples), geophysical methods, and pumping test data. Databases are built to collect, store, and update this type of observational data. For all parameters, the RDX compendium, a collection of studies pertaining to the RDX project site and performed by LANL (LANL 2018, 602963), was searched for data and information. Many additional LANL reports were also used in data collection and are referenced and described in subsequent sections of this report. Peer-reviewed scientific literature and reports from analogous sites (e.g., the Nevada National Security Site) were reviewed, and data and/or information were extracted where they pertained to the RDX site and/or could be used to inform distribution development. Well-drilling logs were used for geophysical measurements taken, as wells were drilled in or near the RDX site. Finally, expert opinion, especially from LANL scientists and engineers, was used as source of information and to interpret data, for example in selection of representative porosity measurements from geophysical logs (section C-2.2.3.1.3).

C-2.2.2.2 RDX Vadose Zone Model

The RVZM is considered as another line of evidence in distribution development where no data or literature previously exist to inform the parameter. In particular, it is used to estimate travel times and pathways of RDX from its infiltration below the surficial alluvial aquifer to the top of the regional aquifer water table and to help formulate distributions of RDX concentration and recharge fluxes to the RRM.

The RVZM was initially developed by LANL and solves saturated/unsaturated isothermal flow and RDX transport in a near-rectangular prism whose west-east long axis follows Cañon de Valle between the Pajarito fault to the west and the extent of the Cañon de Valle alluvial aquifer to the east (LANL 2018, 602963). The estimated north-south extent of saturated perched-intermediate groundwater defines the model extent in that direction. The model domain is approximately 3 km long between the eastern and western boundaries, 1 km from north to south, and 650 m deep, extending from the land surface to about 40 m below the water table. The model uses the geologic framework WC15c (LANL 2018, 602963), which in the TA-16 area is based on the geologic mapping of Lewis et al. (2009, 111708) and well logs (Figure C-2.2-1). The model includes 13 hydrogeological units discretized over 41 vertical layers using the LaGriT mesh generator (Figure C-2.2-2). The Delaunay mesh has 345,050 tetrahedral elements and 60,516 nodes. Vertical layer resolution ranges from about 1 m to 16 m. Horizontal resolution is 40 m. The mesh conforms to the land surface, the top of Qbof (Otowi) and Tpf 3 (Puye), and to the water table surface of the regional aquifer. All other geological units are interpolated onto the elements of the mesh.

FEHM is used to solve for flow and transport using the Richards equation, which calculates water pressure and saturation at every node of the domain as well as water fluxes (Zyvoloski 2007, 700904). The model uses van Genuchten parameterization of water retention curve to link water pressure and water content. The Mualem model is used to calculate unsaturated permeability as a function of water content. The van Genuchten parameters, the residual and saturated water content, the porosity, and rock density of each of the 13 hydrostratigraphic units are given as fixed quantities (Table C-2.2-2), as described in the RDX compendium (LANL 2018, 602963).

C-2.2.2.2.1 Model Function to Inform the RDX Regional Model

The RVZM is an important tool to help develop certain highly uncertain distributions in the RRM, given the lack of other evidence to inform source (hydraulic window) characteristics (section C-2.2.3.2). Source characteristics include the timing of arrival, concentration, recharge rate, location, radius, and shape of hydraulic windows containing RDX and arriving at the regional aquifer. While the extent of the RVZM, whose northern boundary does not cover the highest measured RDX in the regional aquifer (R-69 screen 2), precludes it from being used for location distributions, it can still provide useful information for the other source parameters. Travel times and recharge rates are constrained by the flow physics of the RVZM. The RVZM is therefore also used in conjunction with the P&D tool (section C-2.2.2.3) to inform the travel time of RDX from the land surface to the regional aquifer. Recharge rates are also constrained by the physics in the RVZM, which uses infiltration distributions informed by surface data and maintenance of the observed perched zones. Because of these realistic constraints, and the accurately represented physics of flow, recharge rate distributions for the RRM use RVZM output. The calibration attempts to match concentrations throughout the RVZM, making it an appropriate tool to estimate concentration where the VZ and regional aquifer intersect. Given that it is one of the only available lines of evidence, that it explicitly accounts for uncertainty, and that it appropriately constrains the flow and transport with detailed physical calculations, the RVZM is an appropriate line of evidence for the aforementioned distributions.

C-2.2.2.2.2 Initial and Boundary Conditions

The CSM informs flow and transport boundary and initial conditions for the different zones of the model. In the RVZM, the representation of the regional aquifer is simplified: The regional aquifer has a nearly flat water table surface, below which all nodes are assigned full saturation and hydrostatic pressure (with atmospheric pressure at the top of the regional aquifer), and the water table elevation at nodes of side boundaries is fixed. Flow of groundwater is allowed to enter and leave the regional aquifer through the side boundaries. The bottom of the domain, about 40 m below the water table surface, is a no-flow boundary.

Perched-intermediate saturated zones above the regional aquifer are initially assigned full saturation and hydrostatic pressure condition. Two perched zones, upper and lower, referred to as the UPZ and LPZ, are initially defined based on the estimates of Lewis et al. (2009, 111708). As in the regional aquifer, pressure and saturation of nodes in these perched saturated zones that intersect the side boundaries are kept fixed. The perched zone saturated thickness can vary in space and time during the simulation and depends on influx of water at the land surface and at side boundaries. To maintain the extent of the perched zones and prevent drainage, a permeability reduction factor at the bottom of the UPZ and LPZ is assigned to nodes that define the bottom of these perched zones. The bottom of the UPZ cuts across multiple geological units. On the western boundary, a flux of water representing MBR is imposed at the nodes of the upper perched saturated zone shown in Figure C-2.2-3. All other UPZ boundary nodes have constant saturation and pressure, allowing water to either enter or leave this perched zone there. The LPZ does not intersect any side boundaries.

Three other fluxes of water are specified at the top boundary (Figure C-2.2-3). One defines background infiltration and is imposed over all top boundary nodes. A second flux sets the canyon infiltration, except over Cañon de Valle. The third flux controls infiltration over Cañon de Valle. These three water fluxes are constant in time. Distribution development for these fluxes is described in section C-2.2.2.2.3.

Initially, the concentration of RDX is set to zero for the entire domain. RDX enters the model domain via two areas, the 260 Outfall over Cañon de Valle, and the 260 Pond (modeled as one single node). The mass of RDX entering the top surface at these two locations is calculated as the product of the volume of RDX solution that entered the system times the RDX concentration. RDX is assumed to be at the solubility limit (44 mg/L). This mass of RDX is time dependent and depends on the estimated production conditions at these two locations.

C-2.2.2.2.3 Distribution Development for Parameters Used Only in the RDX Vadose Zone Model

Infiltration

Infiltration is the entry of water into the subsurface from the ground surface (e.g., Freeze and Cherry 1979, 088742, p. 211). It is a parameter used only in the RVZM, and not the RRM, because the VZ separates the ground surface from the saturated zone of the regional aquifer. Water reaching the regional aquifer is termed recharge and is discussed in section C-2.2.3.2.4.

Sources of information for infiltration include field studies conducted as part of the investigation report for Water Canyon and Cañon de Valle (LANL 2011, 206324), values used in modeling studies, simulation results (Levitt 2011, 700879), and literature review (Birdsell et al. 2005, 092048). One source (Kwicklis et al. 2005, 090069) combined field measurements and literature review. These authors made a composite of point estimates of infiltration at higher elevation areas (e.g., mesa tops) with estimates of streamflow gains and losses in channels to generate an infiltration map, which included the RDX project site and surrounding areas. Geochemical data were also collected to inform distribution development. Estimates from mixing models indicate that the regional aquifer is composed of 90% MBR recharge (LANL 2018, 602963, Attachment 3, Section 6, and Tables 6.2-1, 6.2-2, and 6.3-2), which does not percolate through the VZ at the RDX site and is expected to mitigate RDX concentrations in the regional aquifer via dilution.

All of the nodes at the land surface in the RVZM have an assigned value of infiltration. Each node is classified in one of four topographical groupings identified in Figure C-2.2-3: background, canyon, Cañon de Valle, or MBR. Background infiltration is associated with mesa tops surrounding the RDX project site, and it has the lowest mean value of the four groups. Canyon infiltration is associated with locations at the ground surface in canyons but is not specific to Cañon de Valle and the location downstream of the 260 Outfall. Cañon de Valle infiltration is specific to Cañon de Valle and the location downstream of the 260 Outfall. MBR is groundwater flow sourced from diffuse precipitation falling over the upgradient mountain block. MBR feeds the upper perched zones (and the regional aquifer) and comes in at the upstream, left-hand side of the RVZM (Figure C-2.2-3) in accordance with the CSM (Figure C-1.2-4).

For infiltration into the RVZM, raw data are available from 16 different references (e.g., LANL 2011, 206324), collected in a comprehensive literature review. A probability distribution was developed for the mean infiltration rate for each grouping of infiltration in the RVZM. The distributions are intended to describe the spatio-temporal average of infiltration for each grouping, and a double bootstrap method is employed. This method estimates uncertainty in the mean while accounting for the fact that data values were taken from different references. Truncated normal distributions are selected to fit the distribution of bootstrap sample means because sampling distributions of the mean typically follow a normal distribution-when the sample size is large enough (or when the sample size is small, and the independence and normality assumptions are met). The fitted distributions are displayed over the bootstrapped means and the collected data in Figure C-2.2-4.

Diffusivity in Variably Saturated Porous Media

The effective diffusion coefficient (D_e) is used for calculating the movement of solutes in water because of differences in concentration gradient in a porous medium. This section describes parameter distribution development for the RDX D_e distribution used in the RVZM. Section C-2.2.3.3.3 discusses diffusion in water in the RRM, and it provides additional details on background information about the effective diffusion coefficient, including how the diffusion coefficient is calculated from other parameters, a description of data compilation and calculations used to inform distribution development, and the approach taken to produce input distributions for contaminants in the probabilistic model.

The spatial and temporal scales captured by the distributions should align with the scale of the model and with how individual draws from these distributions are used. For each realization of the RRM and RVZMs, a single D_e will be sampled from a distribution and applied to all model cells in the domain, regardless of actual geologic material. D_e is assumed to be homogeneous in space and constant in time. Because D_e depends on tortuosity, which depends on porosity, the choice of homogeneous porosity for the RRM is related to the selection of homogeneous diffusivity. For the RVZM, which includes multiple geologic units with different porosities, a separate (wider) distribution for diffusivity is developed. In both cases, because realistic variability in site D_es is expected to occur at spatial scales much smaller than the model domain over which they are applied, these individual values are intended to represent possible average values. D_e must be >0; therefore, negative D_es will not be entered into the FEHM model, and there are no physical upper limits of D_e values.

Salinity, temperature, and pressure have the potential to change the density of water, which in turn can change the rate of diffusion of a given substance in water. For the RRM and RVZM, the magnitude of change of these parameters over the domain of the models has a negligible effect on density. Factors relating to the porous media (such as porosity and volumetric water content) provide the primary source of spatial variability in diffusivity.

The RVZM is expected to contain a greater variability of effective diffusivity over the path of RDX migration compared with the RRM, since it covers a much greater range of porosity in widely different geologic materials as well as a wide range of volumetric water content (θ_w). As this is a calibrated parameter, the classical calibration of the RVZM will select a diffusion coefficient consistent with history-matching of the site RDX data in conjunction with all other parameters. The effective liquid-phase diffusion coefficient in the RVZM is not expected to be a sensitive parameter, and therefore a wide range is selected for calibration of the RVZM. A uniform distribution with range (1e-11, 1e-9 m^2/s) was selected, which is expected to be wider than plausible average values for the entire model domain and reflects a great deal of uncertainty in appropriate average values for this parameter for the RVZM. The selected coefficient was evaluated for reasonability given the current state of knowledge of diffusivity through the materials in the RVZM.

C-2.2.2.2.4 Model Calibration

The RVZM is calibrated by adjusting a set of input parameters to best fit pre-defined targets. For the RVZM, this includes time-dependent RDX concentrations at wells and thicknesses of perched saturated zones, as described below. Calibration is performed using the LM technique with random initial guesses implemented in the MADS software (https://mads.lanl.gov/), which minimizes an OF that measures the fit of model results to targets. The LM calibration is conducted in a similar manner to that of the RRM, and more details about the LM algorithm and application are given in section C-2.3.2.

Calibrated input parameters in the RVZM include

- the horizontal and vertical permeability for 16 units (13 hydro-stratigraphic units and 3 additional zones in the Puye Formation),
- 3 permeability reduction factors at two perched saturated zones (including a 3 × 3-node “window” in the upper perched zone),
- 10 RDX partition coefficients,
- 1 RDX matrix diffusion coefficient,
- 4 boundary fluxes, and
- 3 dispersivity coefficients (1 for each axis direction, identical for all geological units).

In the results shown in Table C-2.2-3, 42 dispersivity coefficients, 1 for each axis direction and for each of the 13 hydrostratigraphic units plus the regional aquifer, were calibrated. These calibrations are discussed in detail below.

Targets

Two types of targets are used for calibration of the RVZM: (1) saturated thickness of perched-intermediate water zones and (2) RDX concentrations measured at wells. Upper- and lower-perched zone saturated thickness data are interpolated onto each node of a horizontal plane of the mesh. This yields 2252 target values (1126 for each perched zone). Time-dependent RDX concentrations at wells add another 226 to 350 targets, depending on when the data set was processed, as discussed below. RDX concentration target values use monthly averages. Wells include intermediate well screens CdV-16-1(i), CdV-16-2(i)r, CdV-16-4ip, CdV-9-1(i), R-25 screens S1 through S4, and R47i; and regional well screens R-25 S5 through S8, R-63, and R-68. Weighting is used to prioritize matches to data most relevant to the purpose of the RVZM in estimating quantities for the RRM. While this weighting could be revisited in future work, for the results presented here, saturated thicknesses are assigned a weight of 1 and RDX concentrations a weight of 5, except where noted otherwise.

C-2.2.2.2.5 RDX Vadose Zone Model Results

Three calibrations were used to inform distributions for the RRM. The first calibration uses the same set of calibrated parameters as the calibration described in Attachment 8 of the RDX compendium (LANL 2018, 602963) with added RDX concentration targets for regional well R-68. In this calibration the total number of targets for RDX concentration is 350 over the period from September 30, 1998, to December 31, 2018. This calibration uses a unique set of dispersivity for all hydrostratigraphic units. The second calibration uses an updated set of RDX concentration targets, which contained 347 data points collected between November 31, 2000, and December 31, 2018. This calibration uses 14 layer-specific dispersivities along the 3 orientation axes. Finally, the third calibration improves over the second calibration by assigning higher weights (25) to intermediate well CdV-9-1(i) and regional well R-68 in an attempt to obtain a better match at these important locations. The number of targets for RDX concentration for this third calibration is 226 based on data pulled in March 2019 that include RDX concentration between February 28, 2002, and March 31, 2019.

Results

Values of calibrated parameters are given for the best calibration with the lowest value of the OF (Calibration 3) in Tables C-2.2-3 through C-2.2-7. These tables also include values of calibrated parameters of earlier calibrations reported in the RDX compendium (LANL 2018, 602963, Attachment 8, Tables 4.0-1 and 4.0-2), and an improved calibration from LANL's Earth and Environmental Sciences (EES) Division (Neptune 2018, 700878), for comparison. In general, calibrated values show similar trends to earlier calibrations. Results from calibrations indicate that many possible combinations of parameter values yield good fits to the data and thus, more than one set of parameter values is possible. Note that Calibration 3 yields overall smaller values of sorption coefficients (Table C 2.2-6) in better accordance with data (Heerspink et al. 2017, 602560). Calibrations 2 and 3, which assign three dispersivities to each of the hydrostratigraphic units, also seem to yield a better fit.

To illustrate the goodness of fit, Figure C-2.2-5 shows targets versus simulated RDX concentration for the lowest OF value of Calibration 3, and Figure C-2.2-6 shows the time-dependent targets and simulated values for all the wells. The model reproduces measured RDX concentration relatively well. A perfect fit would show all colored data points in Figure C-2.2-5 on the diagonal line. Three wells, R-25 screen 1, R-63, and R-68, have values of RDX concentration that are underestimated. One well, R-25b, has trends that are unlikely to be represented with a continuum model such as that used here. Note also that Calibration 3, whose results are shown in Figure C-2.2-5 and Figure C-2.2-6, is the only calibration that resulted in a good fit for well CdV-9-1(i) screen 1, perhaps owing to the large weight assigned to this well. Modeled RDX concentration for well R-68 was zero in all calibrations, which is a result attributed to the model structure, as the simplified representation of the regional aquifer may not permit movement of contaminated water towards R-68.

The best calibrations on the basis of smallest OF value (all eight seeds from Calibration 1 and 2; four seeds from Calibration 3), were run in a forward mode to compute fluxes and RDX concentration entering the regional aquifer. These forward model results are used to inform distributions for the RRM, as described in section C-2.2.3.2.

C-2.2.2.3 Pipe and Disk Analytical Tool

Another line of evidence used to constrain the inputs to the RRM is the P&D screening tool. The P&D tool was developed by LANL to represent contaminant transport pathways through the VZ. The P&D approach, as described in the RDX compendium (LANL 2018, 602963), is a simplified model that uses analytical solutions for fast computational analyses of problems that would be cumbersome to set up and test in a full 3-D VZ/saturated zone (SZ) model. The P&D tool has been previously used to roughly estimate plausible source timing and location relative to R-18 and R-68 RDX concentration data (LANL 2018, 602963).

The setup of the model is that arbitrary numbers of pathways can be established in unsaturated zones ("pipes") between arbitrary numbers of saturated lenses ("disks"), such as the case at the RDX site. Figure C-2.2-7 shows a schematic of an example model geometry for a case with several pipes and disks. The bottom disk always represents the regional aquifer. The locations, footprint, and fluxes in the pipes can be calibrated against observed data.

The unsaturated (VZ) pipes are simulated as 1D, vertical conduits which have discrete contaminant transfer and diffusion properties. The disks representing the saturated zones represent a homogenous lateral flow field within each disk. The analytical solutions used by the P&D tool incorporate advanced concepts of anomalous diffusion to better represent the observed behavior of contaminant transport in porous media (O'Malley and Vesselinov 2014, 700891). However, the tool as a whole does not presently allow for important MBR dilution processes in the SZs or other complexities in the CSM. However, because of its simplicity, the model is computationally efficient and therefore can be run thousands of times to generate distributions of possible pathways through a VZ, where the user can constrain the potential number and locations of pipes and/or disks.

The P&D tool was used to inform the distribution for time of onset of RDX concentration at surface of the regional aquifer (section C-2.2.3.2.5). Although some historical data on land surface RDX releases are available to inform this parameter, that does not provide information about travel times through the thick VZ to the regional aquifer. Inferring the time of contaminant arrival at the regional aquifer from well data is not possible because these data are incomplete in their spatial and temporal coverage, and their reliability can be questionable because of incidental and temporary contamination as a result of drilling issues. For the primary RDX source, P&D tool results from a single source simulation were used to develop the distribution. For the secondary source, P&D tool results using two sources were used. The tool was also used to inform the source locations (section C-2.2.3.2.1) and source sizes (section C-2.2.3.2.2).

C-2.2.3 Distribution Development

In this section, each parameter in the RRM requiring a unique distribution is described in detail, including all available lines of evidence, data, statistical modeling, and final distribution. These parameters are divided into three categories: material properties, source characteristics (for hydraulic windows on the surface of the regional aquifer), and other.

While there are 196 calibrated parameters, many of these use the same distribution (for example, ***K*** values are drawn for 49 points throughout the model; however, these are based on 13 unique distributions). All unique distributions, and their central value, units, and sources of information, are shown in Table C-2.2-8. When distributions are uniform, the full range is given rather than a central value.

C-2.2.3.1 Material Properties Distributions

C-2.2.3.1.1 Hydraulic Conductivity

Distribution development for saturated hydraulic conductivity (***K***) and K anisotropy ($K_{vertical}/K_{horizontal}$ or K_z/K_{xy}) in RDX project area at LANL is needed because hydraulic conductivity estimates are used as input parameters at every spatial location within the RRM. Distribution development also covers the hydraulic conductivity needed for the RVZM, which includes additional geologic units in the unsaturated zone. Spatially, a value will be drawn from the K_{xy} (horizontal) and K_z (vertical) distributions to represent an average value over a spatial extent (volume). Spatial scale is determined by pilot point density (described below) and node spacing (described in section C-2.1.2). In the RVZM, the spatial scale of interest is the volume of each geologic unit, as a single value is applied to each unit. Temporally, draws from the distributions will be used throughout the entire model run (tens to hundreds of years). This is done under the assumption that material properties will stay close enough to constant over the modeled future, that any heterogeneity over time is not large enough relative to uncertainty over space that it needs to be captured, or that the variability can be ignored because of model assumptions of linearity relative to the output of interest. Potential sources of temporal variability in ***K*** can include effects from biofouling or precipitate formation due to amendment introduction; however, these effects are insignificant or not relevant to the RDX site.

Sources of spatial variability in $\mathbf{K}$ are related to complex geologic depositional processes that generate preferential flow paths (high K zones) and areas that resist flow (low K zones) in subsurface sediment and volcanic rock materials at the site.

Hydraulic conductivity is the coefficient of proportionality between the hydraulic head gradient and fluid flux in Darcy's Law (in one dimension),

$$q = -K\frac{dh}{dl}, \qquad \textbf{Equation C-1}$$

Where q = fluid flux [L/T],

K = the hydraulic conductivity along the direction of flow [L/T], and

dh/dl = the hydraulic head gradient [unitless].

Hydraulic conductivity is dependent on both the properties of the porous medium and the fluid of interest. For this reason, Equation C-2 is also commonly expressed in terms of intrinsic permeability k, where

$$k = K\frac{\mu}{\rho g}, \qquad \textbf{Equation C-2}$$

Where k = intrinsic permeability [L^2],

μ = the fluid viscosity [M/L·T], and

ρ = the fluid density [M/L^3],

g = the acceleration due to gravity [L/T^2].

In the RRM, the quantity of interest is hydraulic conductivity, K. In the RVZM, the values are entered as permeabilities, k. All hydraulic conductivities in this document are assumed to be for water at in-situ subsurface temperatures. The laboratory standard for hydraulic conductivity is defined as pure water at a temperature of 15.6°C (Fetter 1994, 070942). Conversions between K and k for the models are made using an equation of state defined in the FEHM model with reference temperature set to 20°C and pressure 1.0 MPa.

Extension of Equation C-1 into three dimensions turns K along the direction of flow into a tensor, $\mathbf{K}$, of which the diagonal components K_x, K_y, and K_z are used as model inputs. These are aligned with the x, y, and z directions of the model domain and are not related to the direction of fluid flow. In general, fluid flow across the site is from west to east with local variations to the north or south. In the geologic units at the site, it is not known whether K_x and K_y differ in overall distribution, although locally the horizontal anisotropy may be pronounced because of paleochannels and other features in the unit. Therefore, a single distribution is developed for both K_x and K_y and is referred to as K_{xy}.

The 1st and 99th percentiles of the distributions developed will be used to define the constraints used in the classical calibration (section C-2.3.2). Beyond the use of constraint development, the probability distributions themselves will be used as a source of prior information in the MCMC calibration (section C-2.3.4).

Information Collection

A database of ***K*** information from the LANL site was built, including data from single and multi-well aquifer tests, geophysical well logging, and laboratory tests on extracted core. The spatial scale of these data covers a wide range. All well test and column test data included are from wells on the Pajarito Plateau, the majority of which are not in the RDX site vicinity but include many of the same relevant geologic formations.

Methods for measuring hydraulic conductivity are divided into three categories that correspond to the spatial scale represented by the measurement: small, intermediate, and site-scale. Because of the scale dependence of hydraulic conductivities, appropriate spatial scaling is a critical component of distribution development. The scale of the ***K*** and *k* parameters as used in the RRM and RVZM are both best approximated as intermediate-scale.

Scale Dependence of Hydraulic Conductivity

Attempts to measure hydraulic conductivity (or permeabilities) in the laboratory and field has led to the understanding that values of hydraulic conductivity are a function of measurement scale (Schulze-Makuch et al. 1999, 700893). This is because of the dominance of connected fast paths in the overall hydraulic behavior. Figure C-2.2-8 shows the results of studies conducted at LANL for the Bandelier Tuff units Qbt 1v, Qbt 1g, and Qbt 2, along with local basalts. Within each geologic unit, relatively larger hydraulic conductivities are calculated when observed at large measurement scales (e.g., packer tests and field pneumatic analysis), and relatively smaller results are found when measuring at smaller scales (e.g., laboratory measurements). Because of this scaling affect, the scale of data collected must be considered when combining data together to develop parameter distributions. Data collected is sorted into three spatial scales, as discussed in the following sections.

Small-Scale Information

Data or information are classified as “small” scale if they correspond to a measurement taken with a very localized method of sampling. The two primary small-scale measurement techniques used at the site both occur during the drilling of boreholes. The first method is to retrieve borehole samples that have enough integrity to perform laboratory analysis. The other is particle-size analysis, which is then used to estimate hydraulic conductivities using, e.g., the Kozeny-Carman relationship (Schwartz and Zhang 2002, 700913):

$$K = \frac{\rho g}{\mu}\left[\frac{d^2\phi^3}{180(1-\phi)^2}\right], \qquad \textbf{Equation C-3}$$

Where d = the representative particle diameter of a mixture [L], and

ϕ = porosity [–].

This type of analysis was performed on geologic samples collected at another site of study at LANL known as the Chromium project area, with samples obtained from sonic coreholes CrCH-1, CrCH-2, CrCH-3, CrCH-4, and CrCH-5 (LANL 2018, 602964). These data are included in the hydraulic database despite the small scale potentially being unrepresentative of intermediate-scale hydraulic conductivities needed for the model.

In a laboratory, other methods can be used to obtain a ***K*** value from retrieved borehole samples. Much of the data used to inform distributions for the geologic units that make up the RVZM were based on laboratory analyses such as constant head or gas injection techniques (Springer 2005, 098534).

The other small-scale technique of determining hydraulic conductivity is using in situ borehole geophysical methods. Although hydraulic conductivities estimated in this way are available throughout the site, they are considered less reliable than the other methods discussed below and were not collected into the database at the present time. The only borehole geophysics measurement entered in the database is a combinable magnetic resonance data point for the Puye at R-26 in the RDX area (Kleinfelder 2005, 087846).

Intermediate-Scale Information

Shortly following installation of many of the operational and monitoring wells at the LANL site, a pumping test was performed on that well to characterize the aquifer formation around the well and to test for proper well function. These pumping test analyses are the primary source of intermediate-scale information. Typically, the analyses are recorded in a section or appendix in the well completion report (e.g., Appendix E of LANL 2017, 602539).

Pumping test analyses can be performed in a single-well format (the pumped well is also monitored for drawdown) or in a multi-well format (a nearby monitoring well is used for drawdown rather than or in addition to the pumped well itself). Both are considered intermediate scale for the purposes of this document. Most of the LANL pumping test analyses are of the single-well format, with some exceptions. In either case, drawdown versus time is plotted over the course of a pumping test and the recovery period and fit by one of many empirical or semi-analytical solutions for aquifer testing that exist in the literature. The appropriateness of the selected method depends on assumptions in that method relative to the true behavior of the aquifer (e.g., homogeneity, isotropy, confinement, etc.) and the well characteristics. Not all well completion reports include hydraulic conductivity estimates; some only present transmissivity, which can be converted to hydraulic conductivity only if the effective thickness of flow is known:

$$K = \frac{T}{b} \, , \qquad \textbf{Equation C-4}$$

Where T = transmissivity [L^2/T], and

b = effective thickness.

Methods of fitting the time-series drawdown data that appear commonly in LANL well completion reports include Theis and the related Cooper-Jacob method for confined aquifers, the Hantush equation for partially penetrating wells, and the Neuman method for unconfined aquifers (Schwartz and Zhang 2002, 700913). These analyses are highly subjective and typically represent an individual’s interpretation of the goodness of fit of a particular semi-analytical or empirical solution. The time selected for curve-fitting along the drawdown or recovery process is also a factor in the appropriateness of the hydraulic conductivity estimate. Typically, early data (either immediately after pumping begins or ends) is considered key for determining hydraulic conductivity because the factor b in Equation C-4 is known and is approximately the length of the well screen. However, early time data are also the most likely to suffer from casing-storage effects.

Another intermediate-scale single well pumping test method is referred to as the specific capacity method. It is typically only used to estimate a *lower* bound hydraulic conductivity because it does not account for well inefficiencies, and therefore the actual hydraulic conductivity may be greater. The specific capacity method described in McLin (2005, 090073) is typically used in this dataset.

Site-Scale Information

The only site scale data that was included in the database for ***K*** and anisotropy distribution development was sourced from a previous model for the RDX site (LANL 2011, 207069).

Vertical Anisotropy

Vertical anisotropy is difficult to estimate from pumping tests and was typically not within the scope of estimations made for LANL well completion reports (e.g., Broxton et al. 2002, 072640). No estimates were found in the literature for vertical anisotropy within the RDX area regional aquifer Puye sediments, but several estimates exist from analyses at the Chromium site. Wells at the Chromium site that were also screened within the Puye Formation were included.

Summary of Collected Data for Geologic Units at the RDX Site

Distributions for K_{xy} and anisotropy (K_z / K_{xy}) are generated for eight geology groups using data available in the new LANL-area hydraulic conductivity database. Limited data are available on K_z values at the RDX site; therefore, K_z distributions used in the RRM are developed using the anisotropy distributions and K_{xy} distributions, which are based on the collected data. For the RRM, the inputs are K_{xy} and K_z. For the RVZM, the inputs are horizontal and vertical permeability. The K_{xy} and K_z distributions are converted to permeability using Equation C-2 for input into the RVZM.

The data in the ***K*** database are classified based on the eight geology groups defined in Table C-2.2-9. All the data from the sub-geologies Tpf 2, Tvt 2, Tpf 3, Qbof, Qct, Qbt 1g, Qbt 1v-u, Qbt 2, Qbt 3, Qbt 3t, Qbt 4, Qbof G2, Qbof G3, Tf, Tpf, Tvt 1, Tt 2, Tt, Qbog, and Qbo are included in the analysis for each geologic group to allow different sub-geology types to influence distributions for the overall geologic group as a whole.

Records of the largest scale (site scale) had larger K_{xy} values, observed in Groups 5, 6, 7, and 8. The highest K_{xy} values observed in Groups 1 and 3 also came from the largest scale. However, it was generally not the case that K_{xy} values were always larger for records of the largest scale in those two groups. K_{xy} values do tend to be similar when drawn from the same well, showing signs of dependence by well, which is consistent with some of the records being estimates from wells, using the same data but different methods of calculation. Summaries of K_{xy} (ft/day), log10 transformed, are found in Table C-2.2-10.

As discussed, some of the well locations in the database are outside the RDX site. In order to understand how these values compare to data collected within the RDX area of interest, a comparison is made between "RDX Area" data and other data from the LANL site. These include the Chromium site area, TA-21, TA-49, TA-53, Mortandad, CdB, Potrillo, TA-54, and TA-16 (outside of the RDX site area). Observed K_{xy} (ft/day), $\log_{10}$ transformed, for each individual well in the database are shown by geology in Figure C-2.2-9. Observed K_{xy} (ft/day), $\log_{10}$ transformed, for each well in the database are shown by geology and area in Figure C-2.2-10. No hydraulic conductivities were observed for geology groups 4–8 in the RDX area.

There are some differences present across areas. For example, among Group 1 (Puye) records, the median K_{xy} in the other areas category is lower than the median K_{xy} in the RDX area. Also, the range of observed K_{xy} in Group 1 is largest for the RDX area, but the interquartile range is largest among records grouped into the other areas. It is worth noting that in Group 1, records from a previous model calibration are the only records for Tpf 2 and Tpf 3. At present, all data from around the site and from prior model calibrations were used in distribution development and no method was used to weight data from different areas differently. The inclusion of data from different areas or the decision to not weight by area may be revisited in the future; as of this revision, weighting was only done by scaling group where intermediate records were weighted twice as much as the other scaling groups because of the closer match to the modeling scale of the intermediate data.

Anisotropies (K_z/K_{xy}) for each of the eight geology groups are shown in Figure C-2.2-11. Data to inform distributions of anisotropy for these eight groups is limited, with Group 1 (Puye) having the most records (n = 26). Four groups (Groups 2, 4, 6, 8) have only one reported anisotropy value, two groups (Groups 5 and 7) have only two anisotropy values, and one group (Group 3) has only six values reported. Group 4 has the largest value reported (approximately 3150), but this is a model calibration value and is not expected to be realistic. More likely, the extremely high value represents missing model processes, structure, or unrealistic parameterization of other inputs. However, given a lack of alternative information to define this distribution, the model calibration value is used. Summary statistics of observed anisotropy values are provided in Table C-2.2-11. There are no small-scale values reported for anisotropy. Group 1 (Puye) has 5 site-scale values and 21 intermediate-scale. Group 3 (Otowi) has three site scale and three intermediate scale values. The other six groups have only site-scale values from the prior model calibration.

Distribution Development for Geological Units at the RDX Site

For the RDX models, distributions are developed for both K_{xy} and K_z for each geology grouping present in the model (Table C-2.2-1). Distributions for K_z are developed by applying the anisotropy distribution developed for a geologic unit to the K_{xy} distribution developed for that particular unit. This process results in a unique K_z distribution for each geologic unit.

For K_{xy} data across all geologic groups, records are averaged within a well before fitting a distribution. K_{xy} and K_z/K_{xy} values tend to be similar within a well, and wells with larger sample sizes tend to have smaller K_{xy} and K_z/K_{xy} values. Thus, averaging all data within a well is performed to reduce potential bias towards wells with greater amounts of data. The inclusion of all the records could also produce an erroneous, overly precise estimate, without accounting for any violations of dependence. The spatial scale of the well data was used to weight K_{xy} and K_z/K_{xy} values when computing averages, with the intermediate scale having a weight of 2 and all other scales assigned a weight of 1. Distributions for K_{xy} and K_z/K_{xy} for the geologic groups are fit using the calculated well averages. When averaging well data within a geologic group, wells that contained intermediate scale data were given a weight of 2, and wells lacking any intermediate scale were assigned a weight of 1. Records from prior model calibration are treated as if they were coming from separate wells.

Only one data point is available for K_z/K_{xy} of groups 2, 4, 6, and 8, so the distribution is centered at the single anisotropy value and the spread equal 2/2.57 = 0.78 (on the log10 scale) to allow the middle 99% of the distribution to fall within 2 magnitudes of the center in either direction. Plots of distributions for K_{xy} for all geologic groups are provided in Figure C-2.2-12. Plots of individual geologic groups are shown in Figures C-2.2-13 through C-2.2-20. Plots of anisotropy distributions are shown by geologic group in Figure C-2.2-21.

Distributions for K_z (in log10 ft/day) were obtained by simulating 1000 draws from the K_{xy} and K_z/K_{xy} distributions for each geologic unit (on the log10 scale). A draw for log10 K_{xy} and a draw for log10 K_z/K_{xy} were summed to obtain a draw for log10 K_z:

$$log_{10}(K_z) = log_{10}\left(\frac{K_z}{K_{xy}} \times K_{xy}\right) = log_{10}\left(\frac{K_z}{K_{xy}}\right) + log_{10}(K_{xy}). \qquad \textbf{Equation C-5}$$

Histograms of the draws for the mean log10 K_z are shown by geologic group in Figure C-2.2-22 with the estimated distribution obtained using the method of moments.

Final distributions for K_{xy} and K_z are converted to log10 m/s for use in the model (Table C-2.2-1).

RDX Vadose Zone Model Implementation

The RVZM domain contains all 8 geologic units for which distributions were developed. The RVZM uses permeability as inputs, rather than hydraulic conductivity, and therefore draws from the K_{xy} and K_z distributions are converted to permeability using Equation C-2. In the RVZM, each geologic unit is modeled as a homogeneous unit. For each model run, a single horizontal and vertical permeability value is drawn from each distribution and applied to the respective geologic unit.

RDX Regional Model Implementation Using Pilot Points and Kriging

The CSM of the RDX site suggests that the contaminated groundwater that has reached the regional aquifer is present near the water table and within a short depth into the saturated zone (Figure C-2.2-23). This is based on several wells that show contamination at the water table, with a decrease in concentration at lower depths (N3B 2019, 700561). The water table at the RDX site in the regional aquifer is largely within the Puye geologic unit. The Tschicoma unit is present to the southwest in the nearby model domain (Figure C-2.2-24) and includes several pilot points; therefore, distributions for both Puye and Tschicoma hydraulic conductivities are used. Figure C-2.2-24 shows regional and perched-intermediate wells at the RDX site used in the model along with geologic units observed at the regional aquifer water table. Distributions developed for the Puye and Tschicoma units are used in the RRM; however, a more complex implementation of these distributions is achieved using a pilot point and kriging approach.

The Puye Formation consists of alluvial sediments, while the Tschicoma formation is composed of dacitic lava flows. Both the Puye and Tschicoma formations have a high degree of heterogeneity.

In the Puye Formation, it is expected that K_{xy} varies over several orders of magnitude. The Puye Formation in the RDX site area is also characterized by strong vertical anisotropy (K_z/K_{xy}), which is thought to explain observations of aquifer behavior in response to pumping and pronounced vertical hydraulic head gradients (LANL 2011, 207069).

Given the heterogeneity of these formations, and the sensitivity of transport to local hydraulic conductivity, a heterogeneous field of $\boldsymbol{K}$ is generated within the Puye and Tschicoma formations on a node-by-node basis using the pilot point approach (Doherty 2003, 700894) and kriging interpolation. To create a heterogeneous $\boldsymbol{K}$ field for the model layering, distributions for $\boldsymbol{K}$ are established at multiple points within the model domain, values are selected from the distributions, and the values are then kriged to interpolate a smooth field over the entire model domain. The method is employed by sampling from narrower distributions at actual well locations that have hydraulic conductivity data derived from aquifer tests at that particular location (referred to as “anchor points”), and sampling from wider distributions representing an entire geological unit (either the Puye or Tschicoma) at points between the well anchor points (referred to as “pilot points”). This allows the distributions to be stochastic rather than deterministic.

Unique $\boldsymbol{K}$ distributions are developed for each anchor point based on data (aquifer tests, geophysical data, etc.) specific to the individual well location. Since anchor point distributions are based solely on data from an individual well, the resulting distributions are typically narrower as they use data from only a small local portion of a geologic unit. If insufficient data (i.e., less than two data points) are available to develop a distribution for an anchor point, anchor points are assigned a distribution by which geologic unit/group is represented within the well. In the case of R-26, wide uniform distributions were used because (1) there is only a single data point, (2) geologic complexity increases as the model approaches the mountain block, and (3) there are potential boundary effects at the edge of the model. This allows the LM calibration freedom to tweak the parameter value in order to match calibration targets, allowing the data to drive the results. K_{xy} distributions for all anchor points are shown in Figure C-2.2-25. No anisotropy data were available for the anchor points; therefore, anisotropy distributions were assigned to the anchor points based on the geology where the anchor point is located. Geologic unit assignments for each anchor point are included in Table C-2.2-12.

Unlike anchor points, ***K*** distributions are not developed individually for each pilot point because there is no location-specific data at each pilot point. Rather, the distribution for the pilot points is assigned by the geologic unit they are placed within in the model domain. In the RRM, all pilot points fall within either the Puye (Figure C-2.2-13) or Tschicoma (Figure C-2.2-14) distributions. The distributions for the geologic units (Figure C-2.2-12) incorporate data from multiple locations across a geologic unit, generally resulting in wider distribution than for the anchor points. Geologic unit assignments for each pilot point are included in Table C-2.2-13.

As described above, for each model run, values are drawn from the anchor and pilot point distributions and are interpolated using kriging to establish a continuous ***K*** field for the model domain. The values of K_{xy} and K_z drawn from distributions at both pilot and anchor point locations are interpolated to the FEHM mesh (section C-2.1.2) to provide a heterogeneous field of values in the model domain. The conceptual model of the plume location is used to designate the region with pilot and anchor points. Pilot points are distributed with greater density in the area of interest and where the density of data is higher. Outside the region with pilot and anchor points, the ***K*** field is homogeneous, with the value being a function of the pilot point and anchor point values, and the kriging parameters drawn.

C-2.2.3.1.2 Kriging Parameterization

Kriging is used to interpolate values of hydraulic conductivity to every node within the RRM domain from discrete values of hydraulic conductivity at the anchor and pilot point locations (described in section C-2.2.3.1.1).

Spatial interpolation between pilot and anchor points (“control points”) is performed using the MADS kriging package in Julia (https://github.com/madsjulia/Kriging.jl). The interpolation is based on a spherical variogram. The spherical variogram is parametrized by three parameters: the nugget is the small-scale variability of the data, the sill (or sigma) is the limit of the influence of variogram representing the maximum variability between pairs of points, and the range (or scale) is the distance after which the variogram levels off (the distance at which points are not spatially correlated) (Cressie 1993, 700911). The nugget is assumed to be 0 and the range and the sill are calibrated parameters in the RRM.

The control points consist of the anchor points and pilot points developed in section C-2.2.3.1.1. Anchor points are located at wells, where enough local information is available to develop an independent distribution for each anchor point. Pilot points are placed throughout the area of interest in order to provide additional heterogeneity options in the aquifer at locations without local data, where ***K*** values are less certain. Pilot points are assigned aquifer parameter distributions based on the geologic layer they are placed within. For example, a pilot point place in the Puye Formation would be assigned parameter distributions for hydraulic conductivity developed for the Puye Formation.

For each model run, hydraulic conductivities (K_x, K_y, K_z) at each anchor point and pilot point are drawn from their respective distributions (K_x and K_y are drawn from the same distribution, K_{xy}). Because of limited information about the kriging parameters, uniform distributions from previous modeling studies in the area were used for sigma and scale (LANL 2018, 602964). The control points and kriging parameters are then used to develop a continuous K field. The scale parameter will determine the spatial extent away from control points that will be modeled as heterogeneous for a given model run. Outside of this range, the aquifer system is treated as homogeneous. Figure C-2.2-26 shows an example for hydraulic conductivity in the x-direction (K_x), where the hashed lines depict locations where aquifer parameters are homogeneous. The value for the homogenous zone is determined by the kriging parameters and control point values. Specifically, the value calculated for this region represents a global mean based on the kriging and control point input values. Given that there is no scaling data, the krige scale and sigma distributions are uniform, with krige sigma = Uniform (0.1, 4.0), and krige scale = Uniform (50, 2000 m). The extent of the heterogeneous and homogeneous zones therefore varies, depending on the kriging parameters drawn.

C-2.2.3.1.3 Porosity and Advective Porosity

Total porosity, ϕ, is used in the FEHM models (RRM and RVZM) to define the volume fraction of a cell that is not occupied by solid rock material. Porosity varies with time, but temporal changes in porosity are usually not relevant to hydrogeologic applications. Spatially, porosity can vary widely, both between different materials and within different materials. In the RRM, the primary material of importance to the RDX plume is the Puye Formation (section C-2.2.3.1.1), so only data within the Puye unit were incorporated in the distribution. There is additional uncertainty because of measurement error and sampling error that must also be incorporated into the distribution.

In addition to total porosity, advective porosity, also referred to as mobile or effective porosity (ϕ_e), is another stochastic input to the model, and it is correlated with total porosity. Advective porosity is the porosity through which advective transport may occur. It is the quantity linking Darcy velocity to average linear (“advective”) velocity through porous media. Advective porosity is smaller than the total porosity because the total porosity may include dead-end pores or regions dominated by non-advective (i.e., diffusive) transport.

For each simulation of the model, advective porosity may not be greater than total porosity. As total porosity increases, a higher value of advective porosity is expected. In this model, the correlation is incorporated by developing a distribution for advective porosity as a proportion of the total porosity. After a draw is taken for total porosity for a simulation, a draw representing the advective fraction of total porosity (with a domain between 0 and 1) is taken independently, and the product of the two draws is equal to advective porosity. This prevents a low value of total porosity being combined with a high value of advective porosity, which is physically impossible and could result in unrealistic outcomes. Because the distribution developed for total porosity represents a distribution of the average site porosity, rather than a distribution of the underlying data, the distribution for the advective porosity fraction should be developed directly from its data rather than representing a second distribution of the average. This would amount to averaging twice. Therefore, the distribution for the advective porosity fraction should encompass the entire range of potential values from the data.

In the RVZM, distributions are not developed for each geologic unit. Deterministic values are retained from the RDX compendium (LANL 2018, 602963). The values used are presented in Table C-2.2-2.

Porosity measurements are available in the Puye Formation at LANL; much of this is derived from geophysical logging of wells, and the rest are from borehole samples analyzed in the laboratory (Figure C-2.2-27). However, in many cases some data may be unreliable. For example, R-42, which has geophysical log data for porosity, is a cased borehole, which makes measurements more difficult to interpret because they require additional environmental corrections to remove the effects of the casing strings. For other wells, data after a certain point in time or within a certain depth range are noticeably greater than nearby data. This effect is attributed to washouts, as confirmed by corresponding caliper data, and these measurements are also filtered for the washout sections. All Puye measurements are given in Figure C-2.2-28. X-shaped points indicate data that have been filtered out and are not used to inform the distributions.

For advective porosity, paired measurements are available for two wells in the RDX area: R-17 and R-26; these measurements were used to develop the distribution. Figure C-2.2-29 panel 1 shows the relationship of advective porosity to total porosity, with a 1:1 line for reference. Points perfectly along the line indicate advective porosity equal to total porosity. Figure C-2.2-29 panel 2 shows the same relationship, with advective porosity transformed to a percentage of total porosity.

Sample size is an important consideration in characterizing the distribution of the average. The more data available on a parameter, the more confident we are that we have characterized the complete distribution, and the less uncertain we are about the true average of the parameter. The Central Limit Theorem states that the standard error of uncertainty around the mean will be reduced by a factor of the square root of the sample size. This is an important concept in distribution development because this standard error reflects the width of the distribution developed. A distribution of the average informed by 100 values will be much wider than a distribution of the average informed by 10,000 values; to be exact, it will be 10 times wider.

A key assumption of this principle, and of many of the methods used to develop a distribution of the average, is that of independence. Porosity is an example of a violation of that assumption. A total of 4877 measurements are available for porosity, most from geophysical logging at 0.5-ft intervals, but these come from only eight wells. In addition, there are two estimates available from use in different model calibrations (Robinson et al. 2005, 092040; LANL 2018, 602963). Because similar biases and measurement error are expected for the same boreholes, additional measurements from the same wells do not provide much additional information. As a result, we are not as confident in the value of the mean with the 4877 measurements from eight wells as we would be if we had the same number of measurements from unique spatial locations. Reducing the variation by a factor of the square root of the sample size would produce a distribution that would be misleadingly narrow. Therefore, the sample size used should be equivalent to the number of independent pieces of information, which in this case is the number of wells plus the number of other values from other sources of information, such as the independent model calibrations.

The distribution for porosity was developed via a bootstrap simulation within boreholes. For each borehole, a random measured value for porosity was sampled from the empirical distribution. For each of the two data points deriving from model calibrations, the single estimated value was recorded. The weighted average was then calculated across all boreholes/model calibrations. Each borehole/model calibration was weighted according to its sample size. The sample sizes within boreholes ranged from 2 to 1339. This process was repeated 1000 times to obtain 1000 weighted averages, and a normal distribution was fit to the weighted averages (Figure C-2.2-30).

Because it is not realistic for advective porosity to be equal to total porosity, the paired measurements where this condition was met were excluded from distribution development. The underlying distribution is developed for the remainder of paired measurements. The distribution of the data appears approximately normal; however, gamma, Weibull, and generalized beta distribution fits were also tested. Goodness of fit statistics and visual examination showed that normal was the best-fitting distribution, so a normal distribution was fit directly to data. The final distribution is shown in Figure C-2.2-31.

C-2.2.3.1.4 Aqueous Dispersivity

Aqueous-phase (i.e., dissolved) RDX may be transported by advection. Therefore, it is subject to dispersive processes in the porous materials that comprise the VZ and SZs of the RVZM and RRM. The RVZM contains both SZ and VZ regions, whereas the RRM is saturated everywhere. Dispersion is a process that spreads out an advecting solute front as it migrates through a porous material. It arises from (1) differing pore sizes with correspondingly different flow velocities, and the existence of mobile and immobile zones to flow, (2) differing solute speeds within individual pores because of the no-slip boundary condition, (3) different path lengths for different tortuous routes taken through the pores, and (4) heterogeneity in the material (Fetter 1994, 070942). The dispersion coefficient has units of length (m) and is defined in three directions relative to the flow path: longitudinal (α_L), transverse horizontal (α_H), and transverse vertical (α_V).

Flow-Direction and Length-Scale Dependencies

Dispersivities are typically larger in the longitudinal (same direction as flow) direction than in transverse (perpendicular to flow) directions. For the 3-D RDX models (both RVZM and RRM), dispersivities are required in each direction. The relative importance of longitudinal dispersivity in a given transport situation depends on the Péclet number, a dimensionless ratio that compares the effectiveness of advective to diffusive transport (Fetter 2008, 700912). When liquid infiltration rates and hence velocities are very low, the effect of aqueous dispersion on solute transport is small, and the effect of diffusive transport is relatively higher. Where higher infiltration rates and velocities are found, dispersive transport would be expected to increase accordingly, and diffusive transport would be less influential.

For the RRM, the length scale of interest for the calculation of aqueous dispersivity is defined by the distance RDX transport occurs from an RDX source to a given downstream location of interest, which is on the order of hundreds to thousands of m. In the RVZM, transport occurs predominately downward, and the length scale of interest is the average vertical thickness of each geologic unit. Exceptions are made for lateral transport in the perched and regional groundwater in the RVZM. In these locations, the length scale of interest is a lateral distance assumed to be of the order of tens to hundreds of meters.

A single distribution is developed for dispersivity for each direction in the saturated zones in both the RRM and RVZM. Each geologic unit in the unsaturated areas of the RVZM will have a separate value drawn for dispersivity. It is assumed that the average dispersivity over the spatial volume of the material in the model is the quantity of interest. The value drawn from the distribution of the average will be applied over the entire time the model is run (tens to hundreds of years). This is done under the assumption that material properties will stay close enough to constant over the modeled future.

Dispersivities are also spatial scale-dependent (Gelhar et al. 1992, 102465) and are a function of the material properties (e.g., homogeneity of pore sizes) and water content (Stephens 1995, 700914). Some authors suggest unsaturated zone dispersivities are lower than in the saturated zone (Ho et al. 1999, 700883), while others note a maximum at intermediate saturation or increasing dispersivity with decreasing saturation (Stephens 1995, 700914). Because dispersion produces an apparent diffusive-like distribution of solutes, it is typically combined with diffusion coefficients into a single effective “hydrodynamic” dispersion term in numerical models (Fetter 1994, 070942). The RRM handles dispersion in this way. Diffusion parameters are described in section C-2.2.3.3.3.

Treatment of Uncertainty

Values of dispersivity in the RVZM and RRM are highly uncertain because the primary geologic stratum of interest in the regional aquifer, the Puye Formation (Tpf), and the layers that comprise the VZ, are extremely heterogeneous. Therefore, distributions of dispersivity are needed for both the RVZM and RRM. First, available information about aqueous dispersivity coefficients relevant to materials at the RDX project area was assembled. Then distributions were developed that appropriately described the potential values for dispersivity in the RVZM and RRM. In this work, three values of aqueous dispersivities (longitudinal, transverse, and vertical) were developed.

Sources of uncertainty in dispersivity include spatial heterogeneity in geologic materials not captured by the model, uncertainty in velocity and water content, the influence of pore structure (e.g., dead-end pores) and fracturing, whether laboratory-scale samples were tested as undisturbed or repacked materials, experimental error, and variability in methods among sources in the literature. These sources of uncertainty are considered in distribution development in a way that is consistent with the spatial and temporal scales of the RVZM and RRM. Dispersivity data span a wide range of rock types, saturation conditions (VZ, SZ, or both), and experimental conditions and scales. In theory, since dispersivity depends on the porous medium structure, different materials are expected to have different dispersivities. However, site-specific data are rarely available and various rules of thumb for dispersivity are commonly used across materials instead, e.g., $\alpha_L = 0.1L$ (Gelhar et al. 1992, 102465), where L is a length scale. In this work, the relationship between the aqueous dispersivity coefficient and length scale is estimated from available data by weighting information sources according to relevance of the information to the site and relative quality of the information. Uncertainty in the relationship was also quantified and used in developing the distributions of aqueous dispersivity as a function of scale length.

Information Collection

An extensive review of both peer-reviewed and white paper literature (e.g., reports from performance assessments) was performed, and dispersivity data from over 16 sources were compiled into a master database. The intention was to include data from a wide range of available sources, so that distributions developed based on the data reflect the uncertainty in the subsurface environment at the site, and to have the database be as complete as possible to promote flexibility in including and excluding data based on expert judgment of the applicability to the site and overall quality of the source. The database sources included the following types of documents, in generally decreasing order of completeness of information:

1. Papers containing original experimental data, typically found in peer-reviewed journals and including extensive information about experimental conditions, methodology, and uncertainty.
2. Literature reviews (LR), which provide references to the original data, and generally contain less information about specific experimental conditions and methods.
3. Model description white papers, which describe dispersivity values selected by researchers for a particular modeling application. These papers sometimes provide an explanation of the methods used to select the values, often based on a combination of literature review, such as the papers in category 2 above, site-specific data if available, and expert judgment. This category includes the values used (VU) for previous modeling at Area G (French et al. 2008, 106890).

All data that could be obtained from these source types were entered into the database, including (when available): dispersivity values, type of value (e.g., average, empirical fit), range of values, spread (e.g., standard deviation), number of samples, rock or soil type/texture, location, length scale, saturation (saturated or unsaturated), and other relevant information. When length scale was uncertain, it was inferred based on other information in the source (e.g., model dimensions).

A great deal of dispersivity data are summarized across many rock types in two seminal references (Gelhar et al. 1992, 102465; Neuman 1990, 090184). Both sources give estimated regression equations. The raw data in Gelhar et al. (1992, 102465) was used instead of the regression equation because it is more easily combined with observations from other sources. The raw data from Neuman (1990, 090184) were not available, so the regression equation was used. Because there are so few data that apply specifically to the materials in the RVZM and RRM, groupings for which different distributions are developed are broad. For longitudinal dispersivity, a single distribution is developed for the RRM, and a separate distribution is developed for the RVZM. For transverse horizontal and transverse vertical dispersivity, a single distribution is developed for each direction based on the relationship of each to longitudinal dispersivity.

Longitudinal Dispersivity

The data used in distribution development are shown in Figure C-2.2-32. The sizes of the points reflect the relative influence of each in the final distribution, according to quality of information and relevance to the site (see Weighting section below). The shape of the points indicates source type: papers reporting experiments (Exp), literature reviews (LR), model application papers (Model), and reported values used in modeling (VU). The line is not a regression fit to the points, but rather an additional source of data (Neuman 1990, 090184) used in distribution development.

Transverse Dispersivity

Transverse dispersivity values paired with longitudinal dispersivity values were given only in Gelhar et al. (1992, 102465). Because these data were given the same weights for both the SZ and the VZ, the same distribution was applied to both the RVZM and the RRM for each direction. Two distributions are developed: one for the relationship between longitudinal dispersivity and transverse horizontal dispersivity, and the other for the relationship between longitudinal dispersivity and transverse vertical dispersivity. The data available from Gelhar et al. (1992, 102465) are plotted in Figure C-2.2-33. Similar to Figure C-2.2-32, the regression line, which is a “rule of thumb” presented in the literature, represents additional data incorporated into distribution development.

Flow-Direction and Length-Scale Analysis

The format for dispersivity used in the RRM is in terms of model coordinate system x, y, and z, rather than having the model determine the direction of flow for longitudinal, transverse horizontal, and transverse vertical. Both are possible options in FEHM’s tracer transport module. Therefore, the closest alignment of flow direction to this coordinate system and the direction of expected anisotropy for each material is used to define the corresponding dispersivity distribution that is drawn.

In the RRM, x most closely aligns with the flow direction (west to east), so it is assigned longitudinal dispersivity (αL). The y-direction draws from the transverse horizontal distribution (αH). As the material is highly anisotropic in z, flow is primarily lateral, so this is assigned the transverse vertical distribution (αV). The same distribution is used for the regional aquifer in the RVZM, whether in the Puye or Tschicoma formations. For unsaturated flow in the RVZM, the direction of flow is primarily vertical, so z is assigned longitudinal dispersivity (αL). Because x and y are isotropic compared with the vertical dimension, both are assigned the transverse horizontal distribution (αH).

For horizontal transport in the Puye Formation in the regional aquifer, length scale would be defined by the distance between the plume source at the regional aquifer and the point of interest for measurement, and/or target locations. This is assumed to range from 500 m to several (up to 6) km, the distance to several water-supply wells (PM-2, PM-4, PM-5). Target data locations are much closer, within a few hundred meters, so length scales overall for the saturated regional aquifer zone are allowed to range from 125 to 6000 m. For the RVZM, scale lengths are the thicknesses of the geologic units and range from 1 to 300 m depending on the unit.

Weighting

For distribution development, a weighting scheme was developed to account for the source quality and relevance of the data for the given dispersivity grouping in Table C-2.2-14. The variables in the database used to implement the weighting are value type (e.g., experimental, or value used in another model), rock type, zone type (saturated or unsaturated), and site. Other types of data (e.g., those tabulated as part of a literature review) are considered based on their similarities to these categories and are usually considered as “values used.”

Data of the type “values used” in another model are weighted lower because these are considered the lowest quality information and may be based on data from other sources already in the database. Although considerable expert judgment may have gone into their selection, it is often difficult to know how much subjectivity has been used (e.g., whether the value was selected to be “conservative” or to meet other desired requirements, and is not necessarily reflective of the conditions believed to exist at a site).

Because limited data are available for unsaturated and saturated conditions, all the data are retained within both the VZ and SZ categories for distribution development and are simply up-weighted or down-weighted according to the quality and relevance. The RRM domain is entirely saturated within the regional aquifer, so saturated zone sources are weighted more heavily than unsaturated zone sources for the regional model distribution, while the opposite is true for the RVZM distributions.

The final list of weights used for the sources is given in Table C-2.2-14, along with the length scales represented by that source. The weights were developed using subject matter expertise and professional knowledge about relevance to the site, including soil types used in a study, environmental conditions (e.g., level of saturation), type of study (e.g., laboratory, field, modeling), and reliability. A weight of 1 can be thought of as perfectly representing site conditions.

MC Simulation and Bootstrapping

An approach combining MC simulation and bootstrapping (i.e., sampling with replacement) is used to approximate the distributions of the estimated mean aqueous dispersivity as a function of scale length, using the weighting of data sources described above. Separate distributions are developed for the RRM and the RVZM through the use of different weights for the sources. The following steps are taken to develop each distribution, using the associated weights:

1. Sample a source (i.e., reference article or report) with probability proportional to the weights assigned to the sources (see Table C-2.2-14).
2. Sample a record (i.e., row from the database) from the source chosen in Step 1 and obtain a dispersivity and scale length pair according to the rules in the next step.
3. Record a scale length and dispersivity pair as follows:
    a. If the record (a row in the dataset) provides both scale length and estimated dispersivity, record the pair of values.
    b. If the selected record provides a “value used” for dispersivity, an associated scale length thought to represent the context within which the value was developed is used. This information is contained as the x-value associated with these dispersivities in Figure C-2.2-32. Record the associated scale length along with the “value used” dispersivity.

   c. If the selected record reports a distribution for dispersivity at a given scale length, then the reported scale length is used and a random draw from the associated dispersivity distribution is used to obtain a value for dispersivity. Record the reported scale length and the random dispersivity value.
   d. If the selected record provides a formula relating scale length and dispersivity with no specific recorded scale length (Neuman 1990, 090184), then draw a random scale length from a uniform distribution over the range of relevant scale lengths given in Neuman (1990, 090184). Predict the dispersivity from the selected scale length using the stated relationship. Predict the dispersivity by drawing from the predictive distribution at the value of the selected scale length. Record the random draw of scale length and the associated predicted dispersivity.

4. Repeat Steps 1–3 to create a single bootstrap sample of the same size as the available number of records by sampling with replacement from all the available records with weights for the sources as described previously.
5. Fit a regression model of dispersivity on scale length to the bootstrap sample, on the log10-log10 scale to obtain an estimated intercept and an estimated slope for the bootstrap sample.
6. Repeat Steps 1–5 2000 times to obtain 2000 pairs of bootstrap intercepts and slopes making up the bootstrap distributions of the regression coefficients describing the relationship between the scale length and mean dispersivity. The estimated means, standard errors, and estimated covariance from these distributions are used to specify the final distributions used in the models that describe the distribution of mean aqueous dispersivity for a given scale length.

The bootstrap distributions for the estimated slopes and intercepts, along with the covariance between the two, are used to obtain the distribution for the estimated mean aqueous dispersivity for a given scale length. The variance of the distribution reflects the uncertainty in estimating the mean as a function of length from available information under the weighting.

The general equations used to describe the distributions developed for the two models as a function of scale length (*L*) are:

$$\hat{\mu}(L) = \log_{10}\alpha_w \sim \mathrm{N}\left[\hat{\mu}(L), \mathrm{SE}_{\hat{\mu}}(L)\right] \qquad \textbf{Equation C-6}$$

Where

$$\hat{\mu}(L) = \widehat{\log_{10}\beta_1} + \hat{\beta}_2 \log_{10}(L) = \hat{\gamma}_1 + \hat{\gamma}_2 \log_{10}(L) \qquad \textbf{Equation C-7}$$

and

$$\mathrm{SE}_{\hat{\mu}}(L) = \mathrm{sqrt}[\mathrm{SE}(\widehat{\gamma_1})^2 + (\log_{10} L)^2\, \mathrm{SE}(\widehat{\gamma_2})^2 + 2\log_{10}(L)\, \mathrm{Cov}(\widehat{\gamma_1}, \widehat{\gamma_2})]. \qquad \textbf{Equation C-8}$$

Longitudinal Dispersivity Distributions

The bootstrap estimated regression lines for each bootstrap sample are displayed in Figure C-2.2-34. For the RRM, only data with scale lengths between 10 and 1e5 m were used to describe the distance from an RDX source to current wells or potential locations of interest to an order of magnitude approximation. For the RVZM, only data with scale lengths between 1 and 500 m were used as an order magnitude approximation of the distance from the ground surface to the top of the saturated zone. The spread of the collection of red lines associated with a particular scale length represents the spread of the distribution of longitudinal aqueous dispersivity at that scale length.

The values estimated for the distributions are given in Table C-2.2-15. Values for the RRM apply to length scales from 100 to 10,000 m. Draws from this multivariate distribution provide a representative average value of aqueous dispersivity on the log10 scale for a given scale length associated with a given geologic unit, which is then back-transformed to the original scale before use in the FEHM model.

Transverse Dispersivity Distributions

The distributions describing the relationship between transverse and longitudinal dispersivity were developed from paired data. However, the only paired data available come from Gelhar et al. (1992, 102465), for which equal weights were used for unsaturated zone (UZ) and SZ distributions; therefore, a single distribution was developed for each direction and each observation was weighted equally. The bootstrap estimated regression lines for each bootstrap sample are displayed in Figure C-2.2-35. The spread of the collection of red lines associated with a longitudinal dispersivity value represents the spread of the distribution of transverse dispersivity at that longitudinal dispersivity. The values estimated for the distributions are given in Table C-2.2-16.

Draws from these multivariate distributions provide a representative average value of transverse dispersivity in each direction on the log10 scale for a given scale length associated with a given geologic unit, which is then back transformed to the original scale before use in the FEHM model. Figure C-2.2-36 displays distributions on the original scale and log10 scale for selected scale lengths for illustration.

Ultimately, these distributions were used to develop three independent distributions for dispersivity, one for each of the three directions. Distributions were fit to plausible values for each of the three directions. These values were developed using the following process:

1. A representative scale length was drawn from a uniform distribution, with the minimum at 125 m and the maximum at 6000 m, the estimated range of length scales in the Puye Formation (Table C-2.2-14).
2. A draw from the multivariate normal distribution developed for the relationship between length scale and longitudinal dispersivity (Regional) was taken. The length scale from (1) was transformed into a longitudinal dispersivity using the draws for β_0 and β_1.
3. A draw from the multivariate normal distribution developed for the relationship between transverse horizontal and longitudinal dispersivity was taken. The longitudinal dispersivity from (2) was transformed into a transverse horizontal dispersivity using the draws for β_0 and β_1.
4. A draw from the multivariate normal distribution developed for the relationship between transverse vertical and longitudinal dispersivity was taken. The longitudinal dispersivity from (2) was transformed into a transverse vertical dispersivity using the draws for β_0 and β_1.
5. Steps 1-4 were repeated 10,000 times, and the 10,000 values for each direction were combined. A lognormal distribution was fit to each set of values.

The final distributions developed are shown in Figure C-2.2-37 and displayed in Table C-2.2-17.

C-2.2.3.2 Hydraulic Window Parameters

The RRM domain begins at the top of the regional aquifer, where it is assumed that RDX has traveled through the VZ (including the perched zones) to the regional water table. These pathways are referred to as “hydraulic windows” or “drip points.” Their footprint on the regional aquifer is referred to as the “source” of RDX at the water table. This is distinct from the source of RDX at the land surface. The hydraulic windows in the RRM are characterized as ellipses parameterized by a multivariate normal distribution.

Several parameters relating to size, shape, location, RDX concentration, and recharge rate define the source ellipses. Below, each of these characteristics and its distribution development are described in detail.

C-2.2.3.2.1 Source Location

Multiple lines of evidence are used to develop probability distributions characterizing the location of the source center at the water table. Geostatistical analyses are carried out to combine lines of evidence into a probabilistic representation of the location.

The lines of evidence pointing to the location of the primary source are the concentrations at well screens in the regional aquifer, conceptual model information, and conceptual knowledge regarding location of a possible upgradient source. The lines of evidence pointing to the location of the secondary sources are 800-foot buffer boxes around the low and medium surface sources, and results from the P&D tool.

The outline of the centroid of RDX mass at the regional aquifer, defined by concentrations in the regional aquifer, is the strongest line of evidence for source location. It is the kidney bean shape with the leading edge at R-18, labeled “C” in Figure C-2.2-38. The CSM information is perhaps the most difficult to capture quantitatively. Geological surfaces and physical structures (faults) likely play a role in transport. Currently, a bounding box is developed to quantitatively describe the limits of source location and is labeled “CSM” in Figure C-2.2-38. The northern boundary of the box is based on an estimation of the possible northern boundary of the source, and it is identified by the northing of well R-18. The southern boundary is based on the nondetect RDX concentrations at the R-25 screen in the regional aquifer. Given that the local gradient is southwest–northeast (as opposed to the regional west–east gradient), a more focused polygon representing a possible upgradient location for the source is developed by Neptune and Company (Neptune) expert opinion, and is labeled “UpGrad” in Figure C-2.2-38.

For the secondary source, polygons representing 800-ft buffers around each low and medium concentration surface source location identified in LANL (2012, 213573) are used to quantitatively capture uncertainty in the location of surface sources shown in Figure C-2.2-39. These are labeled “SS_Low” and “SS_Med” in Figure C-2.2-40. The choice of 800 ft as a buffer size was based on likely migration distances during infiltration to the water table. The P&D tool also directly provides quantitative information regarding the possible source centers. To incorporate this information into distribution development for source location, a convex hull was drawn around the source centers generated from the P&D model. The source center is assumed to be equally likely at any location in the convex hull. The convex hulls derived from the P&D tool output for the secondary source are pictured in Figure C-2.2-40, labeled “PD2” (LANL 2018, 602963). The P&D output for the stronger source is slightly farther north and is not used in distribution development.

Several lines of evidence are omitted and are not used to inform the location of the primary source. The P&D model output for the primary source is not ultimately used to inform primary source location because site experts deemed the locations too far north to be realistic. Additionally, the 800-ft buffer boxes around the 260 Outfall and the losing reach of Cañon de Valle are classified as high concentration surface source locations, but are not used to inform the subsurface location of the primary source. This is because it is likely that the “hotdog” footprint along Cañon de Valle has moved by the time the contamination has infiltrated to the depth of the water table. Lastly, RVZM results are not used as a line of evidence to define source location. The RVZM has a limited extent that does not include the location where the highest RDX has been measured in the regional aquifer, so it is not a line of evidence that can be effectively used to constrain source location.

A regular grid is laid over the area depicted in Figure C-2.2-38 and the number of lines of evidence is recorded for each grid cell. Cells with more overlapping lines of evidence are assumed to have higher probability of being the source center. All lines of evidence are weighted equally, assuming each line of evidence is comparable in its reliability of information. A multivariate normal distribution is fit to the data, where the density is assumed to be represented by the number of overlaps at a grid cell. The method of moments is used to fit the distribution, where the weighted longitude and the weighted latitudes define the mean vector. The weights are the number of overlaps for a given grid cell. The diagonals of the covariance matrix are defined by the weighted variances of the latitudes and longitudes, and the covariance is calculated from a weighted correlation. The weights in all calculations are defined by the number of overlaps for a given grid cell. The wtd.mean() and wtd.var() functions in the Hmisc R package, as well as the corr() function in the boot R package, are used to calculate these quantities.

The density of the fitted multivariate normal distribution on the regular grid is displayed in Figure C-2.2-41, with the color gradient indicating density. The orange ellipse indicates the 68th percentile of the distribution, and the yellow ellipse indicates the 95th percentile of the distribution. Since the MADS framework (https://mads.lanl.gov/) requires hard constraints on both latitude and longitude with no correlation, a bounding box is defined based on the 95th percentile ellipse. The bounding box is slightly larger in area than the ellipse.

It is important to note that the size of the ellipses in Figure C-2.2-41 and Figure C-2.2-42 do not represent the sizes of the sources. Rather, the size of the ellipses represents uncertainty in the source center (x0, y0). It is coincidental that we are using a multivariate normal distribution to quantify uncertainty in the locations of the source centers, as well as to describe the shape of the sources. Distribution development for the radii and source eccentricity are described in section C-2.2.3.2.2.

C-2.2.3.2.2 Source Size and Shape

The distributions for source radii in the *x* and *y* directions are informed by the P&D analysis (section C-2.2.2.3), RVZM results (section C-2.2.2.2), and the region of high concentrations observed in the regional aquifer (section C-1.2.3).

Results from the P&D analysis (Figure C-2.2-43 and Figure C-2.2-44) illustrate that there is large uncertainty in the source size, depending on both source location and the time of source onset. The first P&D source ranges in size from very small to about 150 meters in r_x and about 175 meters in r_y. The second source is similar to the first in terms of r_x, but may be larger in r_y, ranging from very small to about 300 meters.

Results from the RVZM are also highly variable with time. The sources identified in the RVZM, discussed in section C-2.2.3.2.3, are typically smaller in earlier years, and grow with time (Figure C-2.2-45). The size of the secondary source in the *x*-direction (r_x) is generally smaller than the primary source initially but is larger than the primary source in the later time steps (near 2050).

Since source radius is not allowed to vary with time in the RRM, a distribution for the average radius over time in the *x* and *y* directions is developed. Similar to source location, one distribution is developed to represent size of the primary source, and a second distribution is developed to represent size of the secondary source. Results from three lines of evidence—the RVZM, the P&D analysis, and well concentrations—are combined to develop one distribution for radius in the *x* and *y* directions.

First, separate distributions are developed for the VZ and P&D tool results, and then the distributions are combined to select a final distribution. The mean of each individual distribution is set to the average radius, and the standard error is the standard deviation divided by the square root of the number of “data” points. The number of “data” points in the P&D model is the number of realizations, and the number of “data” points in the RVZM is the number of time steps.

The distributions are combined in a way so as to retain the variance among the models as a representation of model uncertainty. The mean of the combined distribution is set to the average of the means of the P&D and RVZM distributions. The standard deviation of the combined distribution is calculated by subtracting the smallest 2.5th percentile from the radius defining the kidney bean shape in the regional aquifer and dividing by 4.

The same process is followed for the secondary source, using the same concentration data but using RVZM and P&D results for the secondary source. The *x*-radius of the secondary source has a smaller mean than the primary source, but distributions are fairly comparable (Figure C-2.2-46 and Figure C-2.2-47).

Source shape is highly correlated with source size and source location. Source shape depends heavily on the physical features that are present at specific locations. Although sources are in general expected to have low eccentricity, certain physical features such as the alluvial aquifer at Cañon de Valle, fractures, faults, and perched zones may lead to more elongated shapes. These shapes are highly correlated to the locations of these physical features.

The lines of evidence informing source shape are the results of the P&D tool as well as the RVZM. Source shape somewhat varies with location in the P&D output (Figure C-2.2-43). The source shape identified by the RVZM is also highly dependent upon the fixed source locations.

Source centers (x_0, y_0) are not restricted to a discrete set of locations; rather, center is represented by a bivariate continuous probability distribution. It is thus difficult to correlate center with shape in a continuous way when combining information from lines of evidence that are variable and discrete in both location and shape. For this reason, source shape is characterized by a uniform distribution with a minimum of -0.9 and a maximum of 0.9, reflecting the knowledge that no shape (other than perfectly linear) can be excluded and the difficulties in characterizing a source shape that could apply to location in a continuous way. The selection of a uniform distribution also allows the calibration more freedom in initialization. This allows exploration of a wider domain of shapes than might be explored if a distribution with more restrictive percentiles were used to constrain the starting values allowed in the calibration.

C-2.2.3.2.3 Source Concentration

Source hydraulic windows have a concentration of RDX when the contaminant plume reaches the surface of the regional aquifer. These sources are conceptualized as having a maximum concentration at the center of the window, which decreases according to a bivariate normal distribution out to the 68th-percentile isopleth. The quantity estimated by this distribution is the peak concentration in the center of the source hydraulic window.

Transport of RDX is calculated via the advection-dispersion equation (Zyvoloski 2007, 700904). Because of its relatively low solubility, RDX is conceptualized as an aqueous-phase solute, with no variation in density based on concentration. RDX is simulated exclusively in the aqueous phase because the maximum concentration of RDX will not exceed the solubility limit. Transport is assumed to be conservative (i.e., no chemical reactions occur or RDX degradation occurs). The degradation of RDX is dependent on environmental variables. RDX has been shown to degrade at higher levels of pH and under anaerobic condition. The regional aquifer in the vicinity of the RDX plume has a neutral pH of 7.5 (Heerspink et al. 2017, 602560). Groundwater in the regional aquifer is well oxygenated (dissolved oxygen varying from 5–7 mg/L) (LANL 2018, 602963). Therefore, no RDX degradation is assumed to occur in the RRM.

There is limited raw data to inform the concentration of RDX once it reaches the regional aquifer. At the surface, it was assumed that RDX was released at its solubility limit. Transport through the large VZ is complex and will alter the concentration upon reaching the regional aquifer. Some concentration data have been collected in both the VZ and regional aquifer, providing a small amount of data with which to constrain a distribution. However, these data are sparse and spread out in both time and space, making them useful mostly by comparison to modeled estimates and for use as input to modeling tools for concentration estimates. Given the inability to gather spatially distributed data at the interface of the VZ and the regional aquifer, the main source of information to inform the distribution will be abstracted model results.

The RDX-contaminated sources are conceptualized as a primary source, which is responsible for the consistent, low-noise trend observed in R-18 and the high values at R-68 and R-69. The primary source location is described in section C-2.2.3.2.1. A secondary source is also developed, since it is unknown how many sources arrive at the regional aquifer. This source has more flexibility, both in location and size (section C-2.2.3.2.1). Both recharge and concentration have the ability in the model to range from zero to nonzero values, so the calibration can essentially remove the secondary source if this results in better matches to the data. The secondary source is also described by likely preferential recharge below Cañon de Valle, which is described in more detail in section C-2.2.2.2.5.

Distributions for RDX concentration at the primary and secondary source windows (Figure C-2.2-48) were developed using modeled concentrations from 18 different runs of the VZ model. Within each run, concentrations were extracted at the regional aquifer z-slice, assumed to be at 1920 m, at each time point from 1950 to 2072 (i.e., the time scale of the RRM). The primary source location was identified as the node with the highest concentration within year 2070. The secondary source location was identified as the node with the highest concentration within year 2070 after excluding the primary source node with a 10-node radius buffer. Because each source distribution represents an average concentration over time, primary and secondary source concentrations were averaged from the year of onset to 2070. The year of onset was defined as the time point where RDX concentrations at each source first exceeded 0.1 ppb. Because of the physical lower bound of zero for concentration, a truncated normal distribution was fit to the 19 average concentrations. Simultaneous estimation of the truncated normal parameters using maximum likelihood resulted in physically unrealistic values for the mean. Therefore, the distribution mean was instead set equal to the sample median of the average concentrations. The median was used as a robust measure of center because of the skewness present in the average concentration values (Figure C-2.2-48). Conditional on the lower truncation point of zero and mean equal to the sample median, the standard deviation was estimated using maximum likelihood.

The highest measured concentration in the VZ is around 150 ppb. While this is the highest observation, it is not likely that one of a very sparse set of spatial locations happens to coincide with maximum RDX in the VZ model. Therefore, the range of values for the primary source from 0 up to ~380 ppb at the 99th percentile, with a mean centered (93 ppb) at less than the highest VZ observation and more than the highest regional observation, is consistent with the limited observed data.

C-2.2.3.2.4 Source Recharge

The purpose of this section is to describe parameter distribution development for drip points to the regional aquifer below the RDX project area at LANL. The parameter describes water reaching the saturated zone at the surface of the water table, which is the definition of recharge (e.g., Freeze and Cherry 1979, 088742, p. 211), so the term recharge will be used in this document. Recharge may occur from other directions besides the vertical, i.e., from water that has infiltrated upstream and reaches the aquifer laterally or at an angle from the surface. This parameter is alternatively called “infiltration” in model files and reports (e.g., LANL 2018, 602963, Attachment 8). However, “infiltration” is a misnomer for this parameter. Infiltration describes the entry of water into the subsurface from the ground surface (e.g., Freeze and Cherry 1979, 088742, p. 211), and it is distinct from recharge in locations with an unsaturated zone overlying the saturated zone such as occurs in the RDX project area.

Recharge velocity impacts the rate at which RDX transport occurs. Recharge water may dilute discharged RDX concentrations from the LANL TA-16 260 facility outfall, change the water table elevation (i.e., causing “mounding” with locally high saturated elevations below recharge points), and impact head values at the top boundary of the model. These processes have the potential to alter system hydraulics (e.g., increasing porewater velocities, changing direction of groundwater flow, affecting local vertical gradients).

For recharge in the RDX RRM, the spatial scale of interest encompasses all zones where hydraulic windows may occur below the RDX project area. Therefore, it includes parts of Cañon de Valle and extensive upstream surface and groundwater sources such as (1) MBR, which is diffuse subsurface recharge over the mountain block that percolates into the subsurface and flows as groundwater into the basin, and (2) MFR, which is overland flow in mountainous terrain that infiltrates at the mountain front. The terrain of interest includes mountains, mesas, and canyons, which leads to spatial variability in recharge rates. For the RRM, the recharge parameter is held constant over the time period of simulation, which is decades to hundreds of years; therefore, the value must represent an average over that time.

A distribution of recharge rates is needed because of the uncertainty in infiltration rates at the ground surface and the fact that flow through the highly heterogeneous VZ separating the ground surface from the water table is not well characterized. This zone is composed of unsaturated regions and perched saturated zones in geologic strata of variable permeability and porosity. Distribution development for recharge at the RDX site must therefore account for the high level of uncertainty in the available information and processes that affect rates of recharge to the regional groundwater aquifer. Recharge distributions, which are used as inputs for the RRM, are based on the output of forward runs of the RVZM, whose water balance is constrained by surface infiltration distributions (section C-2.2.2.2.3), calibrating to observed water levels, and flow physics.

Recharge to the regional aquifer is conceptualized as a combination of background and preferential flow paths. This conceptualization in consistent with the CSM as well as with results from the RVZM, which show regions of preferential flow (Figure C-2.2-49). Background recharge is applied throughout the area of interest using a large, circular source. While this distribution could be applied throughout the entire model, the surface infiltration distributions developed for the RVZM (section C-2.2.2.2.3), and the transport for the RVZM, are specific to the immediate area near the plume, and it was determined that background infiltration should be applied only in the area of interest.

Background Recharge Location

Background recharge is applied with a source center at (493500, 538000) near the center of the area of interest, which includes regional wells with measured RDX concentrations and regions directly downgradient of these. Since the dominant direction of flow is west to east, aligning with the x-axis, a longer x-radius is set than y-radius, though both are large enough to cover the entire area of interest. X-radius is set at 3000 m and y-radius is set at 2000 m.

Distribution development for the rate of background recharge uses RVZM results and will be discussed below in conjunction with discussion of the preferential recharge distribution.

Preferential Recharge Locations

The geology in the region suggests that certain preferential hydraulic windows of recharge may occur at the regional aquifer. In the RRM, these are conceptualized as three windows: a potential primary and secondary source of RDX and a clean region of higher recharge below Cañon de Valle, called the preferential recharge source hereafter. The three windows could be locations that consolidate small regions of fractured or highly preferential flow from the surface, parts of the unsaturated zone, or parts of the perched zone. Geochemical lines of evidence can provide constraints on the percentage of recharge from each of the three sources out of the total, so distributions for these percentages are developed as well as distributions of preferential recharge.

The primary source is likely to be relatively compact with higher concentrations, based on the clear, low-noise trend in RDX concentrations observed at R-18, coupled with high values of RDX concentrations at R-68 and R-69 and no observed RDX at R-47 above detection limits (Figure C-2.2-50; also see section C-2.3.3.3). Given the proximity of these wells to each other, and the fact that they contain the highest measured RDX, it is hypothesized that some primary source is responsible for the trends observed. Given the high concentrations arriving at the regional aquifer through a vertically extensive, 300–400 m VZ, this source is conceptualized as arriving at the regional aquifer via preferential pathways and is conceptualized as having primarily surface infiltration as the water source.

Geochemical studies analyzed water from the regional aquifer and the perched VZ to determine relative contributions from different surface sources, including alluvial, spring, and canyon sources (LANL 2018, 602963). A simple binary mixing model was employed in conjunction with chloride, a conservative tracer. End members of the mixing model used average chloride concentrations from well R-26 screen 1 to represent MBR. This location was selected because of the proximity of R-26 to the mountain front and geochemical results suggesting a lack of local recharge (i.e., no RDX concentrations and no tritium). Additional end members were: (1) average chloride concentrations of Cañon de Valle surface water, (2) alluvial groundwater, and (3) concentrations from springs. Between 86–99% of the regional aquifer water is associated with MBR, leaving between 1–14% from surface sources (LANL 2018, 602963). Additionally, an increasing Ca trend attributed to snowmelt was observed in a deep well (R-25 screen 4), which demonstrates a fast pathway from the Cañon de Valle bottom to the regional aquifer (LANL 2018, 602963). To account for uncertainty in the conceptual model, as well as the potential for a surface source to mix with perched water during migration from the surface to the regional aquifer, an additional 5% was added to the range representing alluvial water reaching the regional aquifer through a preferential pathway. Therefore, the primary source is associated with between 1–19% of the total preferential infiltration. Given that there is very little information to further characterize the likelihood of specific proportions of infiltration sources within this range, a uniform distribution is used.

Preferential Recharge Source

The preferential recharge source described in the previous section likely arrives at the regional aquifer somewhere below Cañon de Valle and the VZ perched zones. Evidence for this source includes localized mounding near R-25 (LANL 2018, 602963; N3B 2019, 700561); a deviation of the regional flow gradient from primarily west–east to southwest–northeast near the wells where RDX is observed in the regional aquifer; preferential surface infiltration in Cañon de Valle; and the large extent of perched zones below Cañon de Valle (N3B 2019, 700561).

Distributions were generated for preferential recharge based on the conceptual model and spatial locations of relevant features. Figure C-2.2-50 shows a base map reproduced from Figure 3.2-5 (N3B 2019, 700561) with the distributions for preferential, uncontaminated recharge (“preferential recharge source”) plotted over the figure. Surface features and topography are plotted, detailing the location of

Cañon de Valle relative to the wells in the regional aquifer. The approximate extent of the VZ perched zones is also plotted. These zones are recharged by MBR primarily and secondarily by MFR and preferential surface infiltration under Cañon de Valle. Without much information to constrain the location of the preferential recharge source, uniform distributions are chosen that overlap the conceptual model understanding of the system and provide enough flexibility to account for uncertainty in this CSM.

Preferential recharge source-center x-coordinates can be anywhere from R-25 to as far downgradient as R-47 x-coordinate. Source center y-coordinates are set from R-25 to as far north as CdV-9-1(i). Y-coordinates are selected to cover the higher water table elevations observed near the mounding at R-25. The extents of these distributions are shown in the rectangle constrained by the dotted red line in Figure C-2.2-50.

The size of the source is difficult to constrain. However, some general qualitative features are available. First, based on the west-east orientation of Cañon de Valle and of the water table gradients, the x-radius is likely to be significantly larger than the y-radius. Given the uncertainty in source area, a large range of potential radii are allowed (see Figure C-2.2-50). The largest x- and y-radii are plotted as a large ellipse centered at the middle of the location distribution (dotted rectangle). The smallest x- and y-radii ellipse is also shown. No correlation structure is specified between x-radius and y-radius as there is no information to constrain one. The source can vary widely in elliptical shape as a result. If the smallest x-radius is drawn simultaneously to the largest y-radius, there is potential for a longer y-axis in the ellipse. However, the number of draws from the x- and y-radius distributions where this would occur is small. No tilt or “corr” parameter is defined because there is no information to inform this. Additionally, if the shape parameter is allowed to vary, the conceptual constraint on having a smaller y-radius than x-radius across most draws no longer remains, so the shape parameter is fixed at 0 for the preferential recharge source.

The percentage of total infiltration used by the preferential recharge source is constrained using geochemical studies. As discussed above, the primary source can use between 1–19% of the total preferential infiltration. As a result, the rest of preferential infiltration must occupy between 81–99% of recharge. This percentage is conceptualized as being shared between the preferential recharge source described above as clean, and a secondary source, which is potentially mixed with contaminated perched water before reaching the regional aquifer. The existence of a contaminated secondary source is uncertain. Therefore, the proportion of total recharge allocated to the secondary source is allowed to range anywhere from 0–34%. This leaves 65–81% recharge in the preferential clean source.

Implementation of the percentages is achieved by defining uniform distributions for the primary source, Uniform (0.1,0.19), and for the preferential recharge source, Uniform (0.65,0.81). When the maximum of both distributions is drawn the secondary source is set to 0, essentially removing it as an input to the RRM. For all other draws the secondary source is calculated as the remaining percentage after the primary and preferential clean sources have been drawn.

This setup for recharge allows for significant flexibility in the model to place sources of varying rates. It also constrains the sources using the limited available data (geochemical) and incorporates qualitative information from the CSM. The RVZM then informs the possible amount of recharge, making these values dependent on the physics in the system to move water from the surface, MFR, and MBR to the regional aquifer in the area of interest.

Rate of Recharge—Preferential and Background

Distributions for background and preferential recharge rates (Figure C-2.2-51) were developed using estimated steady-state flux (mm/yr) (converted from $m^3/yr*m^2$) from 19 different runs of the RVZM. Within each run, fluxes were extracted at the regional aquifer z-slice, the highest saturated elevation of which was assumed to be at 1920 m amsl. Because of the structure and domain of the RVZM, nonlinear edge effects arise that are not representative of the fluxes entering the regional aquifer (Figure C-2.2-49). To lessen the impact of edge effects on recharge, a 2-node buffer was applied to the extent of the model and each node was spatially averaged using a 1-node radius (40-m) window.

Exploratory data analysis and the CSM both support the assumption that fluxes into the regional aquifer can be characterized as being either background or preferential recharge. Plots of the empirical cumulative distribution function for each of the 19 model runs indicated that the 80th percentile was a reasonable delineation between the two categories (Figure C-2.2-52). Because each distribution represents an average recharge flux over time, average values were computed for both background and preferential fluxes. Although there can be an upward flux of water from the regional aquifer into the VZ because of capillary pressure in dry areas, this was assumed to be minimal and average flux was truncated at 0 and fit with a truncated normal distribution using maximum likelihood.

C-2.2.3.2.5 Source Timing

Source timing describes the time at which RDX first reaches the surface of the regional aquifer. Three different sources of information were considered to develop a distribution of year of onset for RDX arrival at the regional aquifer: (1) historical data (section C-2.2.2.1), (2) P&D screening tool (section C-2.2.2.3), (3) FEHM VZ modeling results (section C-2.2.2.2). Because of the lack of available historical data, the P&D tool results are combined with the RVZM results and are used to develop the distribution. The distribution is then validated against the available historical data.

P&D Tool

The P&D tool is a screening tool that uses analytical solutions to link together an arbitrary number of UZs with an arbitrary number of SZs to estimate flow through a complex VZ with perched zone elements. VZ elements are conceptualized as slow vertical flow (pipes) using 1-D advection and dispersion, while SZ elements are conceptualized as more rapid flow (disks) using either two-dimensional or 3-D fully saturated advection and dispersion (section C-2.2.2.3). A full description and set of equations for the P&D tool has been documented by prior work (LANL 2018, 602963, Attachment 8, Section 2.1) and is summarized in section C-2.2.2.3.

Measured concentrations at R-18 and R-68 were used to constrain P&D tool results, which was run for both single and double source cases. It should be noted that groundwater flow velocity is a highly uncertain, but highly sensitive, input to the P&D tool. In the analyses presented here, both high and low groundwater velocities were tested to represent a wider range of possible arrival times. More detail about the P&D analysis can be found in the RDX compendium (LANL 2018, 602963).

Results from the P&D tool are shown in Figure C-2.2-53 and Figure C-2.2-54. Figure C-2.2-53 is based on a single source of RDX released at the surface, and the time of onset represents the time at which that source arrives at the regional aquifer. The P&D tool was also run with two different surface sources, with each resulting in an independent time of onset (Figure C-2.2-54). Unlike the RRM, there is no “primary” source in the sense that each of the two surface sources in the P&D tool results contributes equally to contamination at the site.

The results of the single source P&D tool (Figure C-2.2-53) suggest that the time of onset is skewed left, and is never greater than 1990. This iteration of the P&D tool was calibrated using historical data from R-18 and one data point from R-68. The results of the double source P&D tool (Figure C-2.2-54) show higher density in the center that divides the plot into four quadrants. Both S1 and S2 can have times of onset as early as 1960 and as late as 2010; however, the lack of points in the upper right indicates that it is only possible for one of two sources to have a time of onset as late as 2010 data if the other source has a time of onset before 1990.

The RVZM is also used to produce representative values for time of onset at the regional aquifer. Unlike the P&D tool, the RVZM results constrain the path of contamination from the surface through 3-D physics and intensive calibration efforts (section C-2.2.2.2). Time of onset was derived for both sources using modeled concentrations from 18 different calibration fits of the RVZM. Concentrations were extracted from each model fit at the regional aquifer z-slice for each time point from 1950 to 2072. The primary source location was identified as the node with the highest concentration within year 2072. The secondary source location was identified as the node with the highest concentration in year 2072 after excluding the primary source node with a 10-node radius buffer. The year of onset was defined as the time point when RDX concentrations at each respective source first exceeded the assumed detection limit of 0.1 ppb. The time of onset results from the RVZM are given in Figure C-2.2-55. The “Source 1” results are used to inform the primary source distribution, and the “Source 2” results are used to inform the secondary source distribution.

In the RRM, one source is treated as the “primary” source which contributes to the majority of RDX contamination, while the other source contributes to less contamination (sections C-2.2.3.2.3, C-2.2.3.2.4). Therefore, the structure of the RRM is more closely approximated by the double source P&D tool in the sense that there are multiple sources of RDX included in the simulation, and each source gets a unique draw from the distribution for time of onset for each simulation.

While the full range of values (1960–2010) may be reasonable to apply to the secondary source of RDX, the same cannot be said for the primary source. The single source P&D tool shows a narrower range (1964–1989), indicating the majority of contamination likely arrived at the regional aquifer at that time, making it most appropriate to describe the primary source distribution. Therefore, two distributions are developed: one for the primary source using the single source results, and one for the secondary source using the double source results. For each simulation in the RRM, a single draw will be taken from the distribution of time of onset for the primary source, and a separate independent draw will be taken from the distribution of time of onset for the secondary source.

The distribution does not represent a spatial average because different draws are taken for each source. The underlying distribution for time of onset will be used in the model, rather than developing the distribution for the average.

Primary Source

The single-source P&D results are shown in Figure C-2.2-56 alongside the RVZM results for the primary source. Various distributions were fit to the data using the fitdistr function in the fitdistrplus package in R. Weights were developed such that each model could be weighted equally in distribution development. Because there were many more results available from the P&D tool (28 times as many), each result from the RVZM was given a weight of 28, while each result from the P&D tool was given a weight of 1. Weibull, gamma, normal, and lognormal distributions were tested and evaluated alongside the data by visual examination. The lognormal distribution was chosen as the most appropriate fit to the data from both lines of evidence (Figure C-2.2-56).

Secondary Source

The distribution for the secondary source was developed using the double-source P&D results and the RVZM results from the second source. Because the underlying distribution, rather than the distribution of the mean, is of interest, the times of onset for both sources were pooled to develop the distribution. The

P&D results are shown in Figure C-2.2-57 alongside the RVZM results. As in the development of the primary source, many distributions were tested using the fitdistr package, and weights were developed such that each line of evidence could be weighted equally in distribution development. Because there were many more results available from the P&D tool (56 times as many), each result from the RVZM was given a weight of 56 while each result from the P&D tool was given a weight of 1. As with the primary source, a lognormal distribution was chosen as the most appropriate fit to the data (Figure C-2.2-57).

Historical data indicate that RDX from either the primary or secondary source reached the regional aquifer at least by the year 2000 (LANL 2009, 106939). The probability of both independent draws from these distributions being after the year 2000 is less than 0.001; therefore, it was determined that the distributions are reasonable considering the historical data.

C-2.2.3.3 Other Parameters

C-2.2.3.3.1 Western and Eastern Model Boundary Condition—Constant Head

Boundary conditions for the RRM (section C-2.1.3) include the head condition prescribed at the western and eastern edges of the model. The dominant direction of flow regionally is from west to east (mountain block to Rio Grande) so these boundary conditions are used to define the regional flow gradient. It is not known whether this gradient is due west to east, so the values set along the western and eastern boundaries are allowed to vary linearly as described below.

Water level and hydraulic head coincide at the water table of an unconfined aquifer, where no additional gauge pressure is present (other than the weight of the atmosphere, which is assumed to be 0.1 MPa). Shallow depths of the regional aquifer (where most wells are located) are generally characterized as unconfined, and therefore water level and hydraulic head are considered equal at most locations. “Water level” is used to refer to the location of the water table (interface between saturated and unsaturated conditions), whether in terms of depth below ground surface or relative to a geologic boundary, or in terms of height amsl (i.e., relative to a fixed datum). “Hydraulic head,” or “head,” is used to refer to the sum of elevation (z) above a datum (e.g., in this case amsl—above mean sea level) and pressure head, $p/\rho g$, where p is referred to as “gauge” pressure (Franke et al. 1987, 700886):

$$h = z + p/\rho g. \qquad \textbf{Equation C-9}$$

Temporal variation in pressure head can be attributed to three main sources: (1) seasonal variation as a muted response to land surface seasonality; (2) variation in response to human pumping activities; and (3) gradual changes in pressure head over time. These temporal variations are small compared with the spatial variability over the time frame of the model (less than 100 yr) and so the flow field of the model is computed as a steady state representation of 2014 conditions (section C-2.1.3). No temporal variability is represented in the current iteration of the model; however, if water level data indicate large changes in the time frame of the modeling (< 100 yr), transient water levels could be included in a future iteration of the model. The year 2014 was selected because water level targets (section C-2.2.3.3.1) are a temporal average of February 2014 conditions.

Spatially, the east and west boundary conditions for the model are applied to every z-coordinate along a boundary edge. While there are no data points near the edges of the modeling domain, water table maps were generated in 2014 based on all available water level data, topography, and geologic expertise to estimate the water table (Figure C-2.2-58). These contours serve as the main source of information for both west and east head distributions, which are discussed independently below.

While the dominant direction of flow is from west to east, the gradient varies throughout the region. In order to capture this variability, two draws are made for west head—at the northernmost and southernmost points of the model—and similarly two draws are made for east head. The gradient between the two draws is interpolated linearly based on the y-coordinate of every node along the boundary. This method allows for a range of possible gradients that broadly move west to east. Given that the draw for head will be applied to a single point in space, the distributions developed span the range of all plausible values, including the extremes, rather than being distributions of the average.

Western Hydraulic Head

The raster data used to produce the 2014 water table maps are used as the main data source in distribution development. The distribution is developed by extracting head values from the raster data for every coordinate along the western boundary. The coordinate locations chosen were 100,000 equally spaced points in order to encompass the entire spatial domain of the boundary. The water table raster data with 10 evenly spaced points along the boundary is shown as an example in Figure C-2.2-59.

The extracted water level values at the western boundary ranged from 1864.462 to 1925.726 m (Figure C-2.2-60). Given that there is no measured data at the boundaries, and no other qualitative information to inform which parts of the distribution are most likely, a uniform distribution (minimum = 1860, maximum = 1930) is chosen to represent western hydraulic head.

Eastern Hydraulic Head

A procedure similar to that of extracting heads from the 2014 water level map for the western boundary was used to extract head values for the eastern boundary. The distribution developed for eastern head was originally intended as a distribution of the average, so the process is slightly different. Rather than extracting the head at 100,000 different equally spaced locations to represent all head values, five random locations on the eastern boundary were selected and the water level was extracted from the raster data. The average water level was then taken as a plausible value to apply over the entire eastern boundary. This process was then repeated 1000 times and a preliminary distribution was fit to the 1000 average head values. The water table raster data with five randomly selected points along the eastern boundary (yellow) is shown as an example in Figure C-2.2-61. The average water level values at the eastern boundary ranged from 1647 to 1706 m (Figure C-2.2-62).

The eastern boundary of the model, however, is much further from the RDX site than the western boundary. To the east of the RDX site, complex hydrologic and geologic conditions exist in the middle to eastern portion of model domain that result in hydraulic gradients and water table surface conditions that are very different from the RDX site. The RDX site tends to have much steeper hydraulic gradients as it approaches the mountain block. Hydrologic and geologic conditions east of the RDX site were not the focus of the model, and matching the gradient within the model area is of higher priority than accuracy at the eastern boundary, which is many miles from the plume. A lower eastern head value would force a steeper gradient that matches the RDX area gradient more closely. Therefore, a linear regression equation was used to extrapolate east heads at the model boundary to expand the eastern boundary range of values at the low end of the distribution.

Extrapolating East Head using Linear Regression

Outside of the local area of the RDX site, the aquifer system in the RRM is represented using homogeneous properties, and therefore does not capture the complex geology and hydrology across the site. Figure C-2.2-58 indicates markedly different hydraulic gradients and water table conditions in the middle and eastern portion of the RRM domain compared with the RDX site. In order to produce a representative hydraulic gradient in the RDX site, values for the eastern hydraulic head need to be able to reproduce the local hydraulic gradients in the western portion of the RRM where the RDX site is located.

Hydraulic head is estimated for the eastern boundary based on extrapolating the observed hydraulic gradient at the RDX site using hydraulic head target data. These targets are developed in section C-2.3.3.1.

Figure C-2.2-63 shows the spatial distribution of wells used for groundwater level targets in the regression analysis along with the 2014 water level contours across the RRM domain. Well targets for the RRM are shown in red, and well targets for another model being developed in the eastern portion of the domain (the Chromium regional model) are shown in green. As discussed above, the contour lines show a steeper hydraulic gradient in the RDX site compared with the Chromium site. This can also be visualized by showing the relationship between water level and well location projected along an east/west line (Figure C-2.2-64).

All wells in the RDX area with the exception of R-26 were selected to estimate the local hydraulic gradient at the RDX site. R-26 was initially used as a water level target in the RRM; however, it was ultimately excluded as it may represent semi-perched conditions. The geology complexity between R-26 and the RDX site is not captured in the model. More discussion on water level targets is available in section C-2.3.3.1.

The linear regression equation fit to the water level target data is shown in Figure C-2.2-65, and statistical summary results for the regression are shown in Table C-2.2-18. Since the eastern boundary is jagged and has multiple x-coordinates, head is estimated at three different coordinates meant to represent the southeastern and northeastern corners, as well as a point towards the middle of the eastern boundary (“east middle”). Results of the extrapolation are provided in Table C-2.2-19. The results of the regression analysis for the eastern heads were used to expand the range of values described above. The final range uses the 99th percentile from the distribution developed using the 2014 WL map (1690 m) as the upper bound, and the lower bound is set by rounding the lowest extrapolated eastern head value (1477.37 m) down to the nearest tens place (1470 m).

East and West Head Distribution Results

In the current approach, uniform distributions are used for head conditions because of the uncertainty in these parameters. The distributions used for the western and eastern hydraulic heads are included below in Table C-2.2-20.

C-2.2.3.3.2 Sorption Coefficient (K_d)

Sorption onto solid porous media is represented by solid/water partition coefficient (K_d) values. The purpose of this section is to describe parameter distribution development for the RDX K_d distributions used in the RRM and RVZM. Migration of dissolved contaminants may be impacted by sorption onto the solid phase of minerals within the geologic materials present at the site. Sorption consists of several physicochemical processes including ion exchange, adsorption, and chemisorption. Mineralogy, organic carbon content, particle size and texture, element speciation, pore water pH, redox conditions and the concentrations of other constituents in pore water contribute to variability in K_d values, as do differing assumptions underlying the calculations used in the various literature sources. Sources of temporal variability in the regional aquifer sediments are expected to be negligible over the time scale of the model.

K_d values used in the RRM and RVZM are determined using distribution development and probabilistic sampling. For each realization of the RRM, a single K_d is sampled from a distribution and is applied to all model cells in the domain, regardless of actual geologic material. Because the area of interest is primarily in the Puye Formation, the distribution is intended to be representative of RDX sorption onto Puye sediments. The spatial scale of the RRM is approximately 220 km^2 in area by 800 m thick, with temporal scale ranging from tens of years to approximately 100 yr. For each realization of the RVZM, one K_d will be sampled for volcanic materials (tuff, dacite, pumice) and one for sedimentary materials, and the single draw will be applied to all geologic units assigned to those materials. Within those categories, K_d values are assumed homogeneous in space and constant in time. The spatial scales within the RVZM are approximately 3 km between the eastern and western boundaries, 1 km from north to south, and 650 m deep, extending from the land surface to ~40 m below the water table. The temporal scale is the same as the RRM. Because it is expected that realistic variability in site K_d values will occur at spatial scales much smaller than the model domains over which they are applied, the distributions are intended to represent possible average values. There are no physical limits on possible measured K_d values, but negative K_d values will not be entered into the RVZM and RRM.

The development of a K_d distribution for RDX in volcanic and sedimentary materials follows an approach previously used for other contaminated sites (Gains-Germain et al. 2018, 700888). A literature review of RDX K_d values was conducted to identify all potentially relevant information, and was then filtered depending on the applicability, quality, and quantity of the information. RDX sorption onto various geologic materials is presented in the literature for both sites external to LANL and specifically onto LANL borehole samples (LANL 2011, 207069; Heerspink et al. 2017, 602560). Data were entered from the LANL studies only, because of priority of site-specific information.

Assumptions

Strata are lumped broadly into volcanics (V) or sedimentary materials (S). Table C-2.2-21 lists the geologic units found in the RVZM, and to which group they are applied. The Cerro Toledo Formation (Qct), although sedimentary, is grouped with the volcanics because it is composed of reworked Otowi material, pumice, and rhyolite. The RRM is given a K_d sampled from the sedimentary distribution.

The groundwater used in the site-specific RDX K_d experiments in Heerspink et al. (2017, 602560) was obtained from well CdV-16-4ip, with a screened interval in the Puye Formation in the intermediate aquifer. This water is assumed to be appropriately representative of the regional aquifer groundwater across the model domain, as the groundwater chemistry in the intermediate and regional aquifers are “very similar” with slight differences in major cation and anion concentrations (LANL 2018, 602963). The shallow alluvial aquifer system near the ground surface may have substantially different water chemistry and redox conditions than the intermediate and regional aquifers, in which case distributions developed for the deeper aquifers may not be applicable in the shallow alluvial aquifer.

The K_d information entered for RDX included several types of records:

- Data from batch experiments on geologic and separated mineral samples;
- Estimated values from laboratory column experiments; and
- Large-scale model-calibrated values based on observed RDX concentration data and a physics-based flow and transport model.

Batch and column experiments were assumed to be small-scale in the spatial categorization scheme in Gains-Germain et al. (2018, 700888), while the model-calibrated values are considered site-scale.

The RDX data in the database were evaluated for suitability using exploratory data analysis. The site-scale calibrated values from a prior version of the LANL RDX RVZM were excluded because of the underlying assumptions (e.g., model accuracy and calibration uniqueness) inherent in the use of that information. Across all rock types in the RVZM, these values spanned a greater range (2.30×10^{-6} to 4.41 mL/g) (LANL 2018, 602963) than the batch- and column-experimental data (0 to 0.7 mL/g) (Heerspink et al. 2017, 602560).

Heerspink et al. (2017, 602560) describe the results of experiments on core materials from the LANL site. Three samples from two boreholes were used. The boreholes are SHB3, located to the west of the main RDX area, and R25b. At SHB3, sections of core were taken from the Otowi formation and from the upper Puye Formation. The SHB3 Puye sample was intended to be representative of materials in the portion of Puye in which the upper perched zone is found (Heerspink et al. 2017, 602560). However, after additional consultation, it was determined that the SHB3 upper Puye sample was unlikely to be representative of upper Puye in the RDX plume area. At SHB3, the sample was taken from a fine-grained sandstone layer that has not been observed in boreholes in the main section of the RDX plume, where the uppermost Puye contains larger cobbles and gravels. If present, the sandstone layer would be expected to comprise only a very small percentage of the entire portion of the Puye in the model. Therefore, the SHB3 Puye data were excluded.

The SHB3 Otowi data are used to develop distributions for the volcanic materials at the site, while the R-25b Puye data are used for sedimentary materials (i.e., Puye) in the RVZM and RRM. For each of these cores, batch and column experiments are performed on the bulk material, and batch experiments are also performed on hand-picked separates. The hand-picked separates for the SHB3 Otowi core include pumice, fines (volcanic glass), and dacite lava fragments. For the R-25b Puye core, the separates are red and black dacite lava fragments. The hand-picked separates are tested for K_d separately from the bulk sediments to distinguish between the individual materials in a geologic formation with respect to K_d values. This can be used to extrapolate or infer the behavior of other materials in which some of the same minerals are found, assuming an estimation may be made of the mass or volume percentages of the separates in the bulk materials. The hand-picked separates generally have higher K_d values than the bulk materials, particularly for the fines. Using the incorrect assumptions about the impact of these separates on the bulk or upscaled K_d can significantly affect the distribution and bias K_d values too high.

For the batch experiments performed on the bulk samples, K_d values are essentially zero, with a standard deviation estimated at 0.050 mL/g (Heerspink et al. 2017, 602560). Values of calibrated parameters are given for the best calibration with the lowest value of the OF (Calibration 3) in Tables C-2.2-3 through C-2.2-7. These tables also include values of calibrated parameters of earlier calibrations reported in the RDX compendium (LANL 2018, 602963, Attachment 8, Tables 4.0-1 and 4.0-2), and an improved calibration from LANL-EES (Neptune 2018, 700878), for comparison. In general, calibrated values show similar trends to earlier calibrations. Results from calibrations indicate that many possible combinations of parameter values yield good fits to the data and, thus, more than one set of parameter values is possible. Note that Calibration 3 yields overall smaller values of sorption coefficients (Table C-2.2-6) in accord with data. Calibrations 2 and 3, which assign three dispersivities to each of the hydrostratigraphic units, also seem to yield a better fit. For the column experiments on bulk materials, estimated K_d values were slightly higher, with K_d = 0.047 mL/g for SHB3 Otowi tuff and K_d = 0.059 mL/g for R25b Puye formation.

The K_d values in Heerspink et al. (2017, 602560) are reported as mean values with error. Following correspondence with the authors, it was clarified that the number of replicates for each batch experiment was 3 and the error represents 1 standard deviation. Because of the singular source of data, and based on the manner in which the data were collected, spatial scaling was not considered to be a necessary component of the distribution development. Discussion of the creation of the distribution of the average K_d is as follows.

The observed K_d values for bulk samples are selected and are shown in Figure C-2.2-66. The dots represent the mean values as reported and the horizontal lines represent error bars surrounding the estimate extending two standard errors in both directions ($SE = \frac{SD}{\sqrt{n}}$, where $n =$ sample size and $SD =$ standard deviation) to reflect an approximate 95% confidence interval for the mean. If an estimate for spread was not reported, then no error bars are included. The two Otowi bulk tuff records are used to inform the distribution for volcanic materials and the two Puye bulk sediment records from R-25b are used to inform the distribution for sedimentary materials.

Distribution Development

A Monte Carlo simulation approach is used to generate distributions for the mean K_d value for RDX in volcanic materials and in sedimentary materials. As observed in Figure C-2.2-66, the observed K_d values were higher in the column experiments than in the batch experiments. Additionally, there is no reported uncertainty for column experiment records, unlike for batch experiments.

The distribution for volcanic materials was obtained by combining the Otowi bulk tuff estimates from both batch and column experiments. The representative mean K_d value is equal to: (w) × (column K_d value) + (1 – w) × b, where w is the weight assigned to the column value, and b is a random draw from a normal distribution with the reported mean from the batch experiment (0) and standard deviation equal to the standard error for Otowi bulk tuff. This process is repeated 10,000 times to obtain 10,000 representative, mean K_d values for volcanic materials. The weights assigned to the column K_d value were equally spaced values between 0 and 1, in order to incorporate uncertainty in the reliability of each estimate. This approach was taken to allow for the distributions to be informed by the different methods using varying degrees, allowing some of the draws to be less impacted by the point estimate of the batch experiment and others to be largely impacted by the point estimate of the batch experiment.

Variable weights are assigned to the column experiment records and batch experiments weights under the condition that the weights sum to 1. This approach was taken to allow for the distributions to be informed by the different methods using varying degrees, allowing some of the draws to be less impacted by the point estimate of the batch experiment and others to be largely impacted by the point estimate of the batch experiment. A histogram of the weighted average K_d value for volcanic materials obtained from the process is shown in Figure C-2.2-67, with the observed K_d values from the Otowi bulk tuff materials shown below the histogram. A normal distribution was fit to the histogram, where the mean of the distribution is equal to the average of the collection of weighted means. The standard deviation, in this case, is equal to the standard deviation of the weighted means.

The same process is repeated for sedimentary materials (S), but swapping details regarding Otowi bulk tuff with details regarding Puye bulk sediments. A histogram of the weighted average K_d value for sedimentary materials obtained from the bootstrapping process is shown in Figure C-2.2-68 with the observed K_d values from the Puye bulk sediments shown below the histogram. A normal distribution was then fit to the histogram to represent sedimentary K_d values.

Final distributions for K_d are shown in Table C-2.2-22. Distributions developed may result in negative draws. Negative K_d draws are not allowable in the model, and, as a result, the distributions will be bulldozed at 0 mL/g. Bulldozing, in this sense, refers to the action of taking a negative draw and assigning the draw a value of 0 mL/g. This process will create zero-inflated distributions. Table C-2.2-22 includes the parameters for the normal distributions used for both volcanic and sedimentary materials. The 1st and 99th percentiles of the distribution are given, and the probability of a draw from the distribution being less than 0 mL/g is also included in the table. Figure C-2.2-69 shows the final "bulldozed" distributions for K_d.

C-2.2.3.3.3 Effective Diffusion Coefficient (D_e)

As described in section C-2.2.2.2.3, the effective diffusion coefficient (D_e) is used for calculating the movement of solutes in water because of differences in concentration gradient in a porous medium. This section assembles background information about the effective diffusion coefficient, provides an equation for how it is calculated from other parameters, describes data compilation and calculations used to inform distribution development, and documents the approach taken to produce input distributions for contaminants in the probabilistic model. The purpose is to describe parameter distribution development for the RDX D_e distribution used in the RRM and RVZM.

For transport calculations in porous media, the free water diffusion coefficient, D_w, is scaled by a tortuosity factor and the water content to give the effective diffusion coefficient, D_e, as entered into FEHM as a constant:

$$D_e = D_w \tau_w, \qquad \textbf{Equation C-10}$$

Where D_w is the free water diffusion coefficient [m^2/s],

τ_w is the aqueous-phase tortuosity, and

θ_w is the volumetric water content [–].

Distributions are developed here for the parameter D_e, including effects of tortuosity. Transport by advection in porous media is also subject to dispersion, which is discussed in section C-2.2.3.1.4.

Information available for D_e and D_w of RDX is extremely limited. A single value is available for D_e in LANL-area materials (3.88×10^{-9} m^2/s) (LANL 2018, 602963), and two values are available for RDX D_w (2.2×10^{-10} and 7.15×10^{-10} m^2/s). Because of the limited availability of information on D_e, the two D_w values are used in conjunction with the distribution developed for porosity and an estimation of tortuosity in order to calculate a distribution for D_e using Equation C-10.

Multiple models for estimating tortuosity exist in the literature, including, for example, the Millington–Quirk model (Millington and Quirk 1961, 110521), where tortuosity in water (τ_w) is computed as

$$\tau_w = \theta_w^{7/3}/\phi^2 \qquad \textbf{Equation C-11}$$

Where ϕ is porosity of the mixture [–].

In saturated conditions, θ_w is equal to porosity in Equation C-11, and it reduces to

$$\tau_w = \phi^{1/3} \qquad \textbf{Equation C-12}$$

The porosity distribution is used for ϕ in Equation C-12. The distribution developed is then compared with the single value from the RDX compendium (LANL 2018, 602963).

A single draw from the distribution developed for D_e will be applied to the entire model spatial and temporal domain. The distribution is therefore intended to represent a distribution of the average D_e across all space and time in the model. Although D_e is correlated with porosity, not enough information is available to allow the two parameters to be correlated in the model at the time of distribution development. Independent draws are taken from each distribution and applied separately (porosity and D_e) in the model.

The distributions for D_e are used for several purposes in the RRM:

1. They will be used to inform the ranges (uniform draws) allowed in the classical calibration.
2. They will be used as priors in the Bayesian calibration.

For the RRM, the distribution for D_e is developed using a Monte Carlo simulation technique. For each of the two D_w values available, an independent random value is drawn from the distribution developed for porosity to calculate tortuosity using Equation C-12. The independent random draws for each are multiplied by the value for D_w to obtain a value for D_e. It is assumed that each D_e is equally representative of conditions at the site, so the two D_e values are then averaged to obtain a plausible average, and this process is repeated 1000 times to obtain 1000 averages. Finally, a normal distribution is fit to the 1000 averages. Because the D_w values are relatively close in magnitude, the variation in the final distribution is driven largely by uncertainty in porosity. The low sample size also contributes to the width of the final distribution. The distribution developed is shown in Figure C-2.2-70.

Although the single value for D_e from LANL (2008, 103165), (3.88×10^{-9} m^2/s), does not fall within the distribution, the resulting distribution was considered by professional judgement to be reasonable.

C-2.3 Calibration

C-2.3.1 Overview and Purpose

Classical calibration is the process of fitting a non-linear regression model to data. The RDX model is calibrated first with the LM algorithm—a numerical optimization routine that minimizes the sum of squared differences between targets. Though the LM algorithm is shown to converge on solutions faster than the gradient descent method, numerical difficulties still exist because of the high dimensionality of the RRM parameter space. This results in difficulty estimating standard errors in the regression model. Because of these difficulties, MCMC calibration methods are also employed to estimate uncertainty associated with a given solution from the classical calibration. Results from the MCMC sampler are interpreted in a Bayesian fashion and are then used in forward modeling to generate predictive distributions at locations of interest.

C-2.3.2 Levenberg-Marquardt Optimization

The LM algorithm is used extensively for solving nonlinear, least squares problems in groundwater inverse modeling. In this application, the LM algorithm is used to numerically solve the minimization problem:

$$\widehat{\boldsymbol{\beta}} = \arg\min_{\boldsymbol{\beta}}\{\| \mathbf{y} - \mathrm{f}(\boldsymbol{\beta})\|_2^2\}\,, \qquad \textbf{Equation C-12}$$

where y represents the observed data vector (i.e., targets, see section C-2.3.3), $\mathrm{f}(\boldsymbol{\beta})$ is the predicted data vector, $\mathrm{f}(\cdot)$ is the nonlinear FEHM forward modeling operator, and $\widehat{\boldsymbol{\beta}}$ is the inverted or fitted model parameter vector.

The sum of squared deviations loss function $\|\cdot\|_2^2$ is commonly referred to as the OF, and it represents the degree of misfit between the observed (targets) and predicted data (hereafter referred to as pairs). Because of differences in both the scale of the targets and the priority of individual pair fits, a weighting and normalization scheme is imposed upon the OF to mediate the contributions of each pair within the OF. First, each pair is normalized by dividing by a quantity referred to as a meaningful difference (md). This step places each pair on the same scale and facilitates meaningful comparisons of fit across groups of targets. Meaningful difference values are determined for each group (see section C-2.3.3 for target groups) through a combination of expert judgement and quantifying the variability of differences within the target groups using preliminary fits of the FEHM forward model. Second, pairs are weighted within groups (see section C-2.3.3 for group definitions) using preference weights (pw) which dictate the relative contribution of each pair within a given group. Finally, group weights (gw) are applied to each respective group. The normalization and weights therefore result in a weighted nonlinear least squares problem (i.e., $\arg\min_{\boldsymbol{\beta}}\{\| \mathbf{w}[\mathbf{y} - \mathrm{f}(\boldsymbol{\beta})]\|_2^2\}$), with weights equal to:

$$\mathrm{w}_{\mathrm{i[j]}} = \sqrt{\left(\frac{\mathrm{gw_i}}{\sum \mathrm{gw_i}}\right)\left(\frac{\mathrm{pw_{i[j]}}}{\sum \mathrm{pw_{i[j]}}}\right)\left(\frac{1}{\mathrm{md_i}}\right)}, \qquad \textbf{Equation C-13}$$

where i denotes the ith group and i[j] the jth pair within group i.

Before the LM algorithm's iterative minimization procedure, the parameter vector $\boldsymbol{\beta}$ is initialized using either manually specified values (e.g., $\widehat{\boldsymbol{\beta}}$ from a previous calibration) or random draws from the prior distributions detailed in section C-2.2.3. Sampling from the prior distributions is restricted to be within the 1st and 99th percentiles of each distribution. At each iteration step, the parameter vector $\boldsymbol{\beta}$ is adaptively updated by either a gradient descent or Gauss–Newton update. The method used at each step is determined by the damping parameter λ, where small values result in a Gauss–Newton update and large values result in a gradient descent update. The damping factor is adjusted at each iteration based upon the resulting change in the residual. Because of the computational burden associated with this highly parameterized model, an efficient parallel LM algorithm implemented in the MADS computational framework (https://mads.lanl.gov/) is used in order to avoid the sequential selection of λ at each iteration (Lin et al. 2016, 700889). Instead, many damping parameters are generated at each iteration and the algorithm proceeds in the search direction, thus yielding the smallest OF value (which are each computed in parallel). The algorithm iterates until either the specified max number of iterations or tolerance thresholds are met.

As is the case with many optimization algorithms, the solution found by the LM algorithm is only guaranteed to be a local minimum. Because of the high dimensionality of the parameter space, multiple minima exist, and the algorithm will only converge to the global minimum if the algorithm is initialized sufficiently close to it. Because of the computational cost of running a single calibration (i.e., completion time for a single LM iteration is on the order of 1–3 hours), repeated random initializations of calibrations is not an effective strategy to explore the parameter space. Instead, candidate parameter vector initializations are identified by computing the OF for many fits of the FEHM forward model (see section C-2.4.2 for additional details). The candidate parameter vector with the smallest OF value is then subsequently used to initialize the MCMC calibration (section C-2.3.4).

C-2.3.3 Target Development

The OF is composed of target variables. These targets relate model results to observed data or known model characteristics, and the OF is a measurement of difference between model results and the target values. The main form of data available for the RRM is from wells drilled at the LANL site. Water level data and chemical data with concentrations of RDX are available for hundreds of screened intervals in wells or boreholes drilled on the Pajarito Plateau. The data from these wells is made available publicly on the Intellus website (https://intellusnm.com).

Target development takes place alongside distribution development in an iterative process. The spatial and temporal scale of targets is important to represent the observed data at a scale similar to the model for a successful calibration. Currently, the RRM uses targets that can be classified into the following four groups:

1. Hydraulic head within each well screen for February 2014.
2. Hydraulic head gradients between wells of interest.
3. RDX concentration for each well screen for each observed year.
4. RDX concentration trend for each well screen.

Each of these groups of targets can be weighted differently in order to define an OF that is most appropriate for the calibration (section C-2.3.2). For example, if the calibration can match hydraulic head targets but not RDX concentration targets, weights for concentration data can be increased relative to the hydraulic head targets. These are called the “group weights.” Within each grouping, individual targets (certain wells, or certain times) can also be weighted differently. These are called the “preference weights.” The weights and the targets are also standardized, so that different units of measurement or scales of data do not have a different impact on the OF. This is called the “meaningful difference” between targets. The OF therefore is a grouped, weighted average of residuals that measure how closely the simulation matches the observed data.

Targets and weights are altered in successive calibrations based on (1) calibration results, (2) sensitivity results from mid-calibration analyses, and (3) results from individual forward runs. The goal of the OF is to guide the computation in identifying appropriate minima in parameter space that closely match data points critical to understanding the migration of the RDX plume in both space and time.

C-2.3.3.1 Average Hydraulic Head Targets

Hydraulic head targets provide a value for each well screen that represents average conditions at each well screen location during the month of February 2014. In order to achieve a representative average, hydraulic head values for each well screen are averaged by 2-hour interval. Next, the 2-hour interval values are averaged within each calendar day to obtain a daily average for each well screen. Finally, the daily averages are averaged for each well screen to obtain a monthly average. The estimated average hydraulic head values for February 2014 are then selected for each well screen and are used as the hydraulic head targets for each well.

For well screens lacking hydraulic head data during the February 2014 time period, a nearby well with a long record of water level data is selected to impute an estimated February 2014 hydraulic head. For wells that have a long record of head data, but lack data specifically during February 2014, the head data for that well is used to impute an estimated February 2014 hydraulic head.

To impute hydraulic head for wells lacking February 2014 data, the following steps are taken:

1. The average head and average date are calculated for the well lacking data during the February 2014 time period.
2. A linear regression equation is fit to the data of a nearby well with a long record of hydraulic head data.
3. The slope from the linear regression equation is applied to the average hydraulic head and date to impute a value back to February 2014.

Head data for well R-47 begins at the end of 2014 and continues to present. R-47's own hydraulic head record was used to impute an estimate for February 2014, and the results are shown in Figure C-2.3-1. Wells R-58, R-68, and R-69 (screen 1 and screen 2) used well data from neighboring wells in order to impute an estimated February 2014 hydraulic head. For R-58, head data from CdV-R-37-2 screen 2 was used (Figure C-2.3-2). For R-68, water level data from R-63 was used (Figure C-2.3-3). For R-69, water level data from R-18 was used for both screen 1 and screen 2 (Figure C-2.3-4 and Figure C-2.3-5). Table C-2.3-1 provides the wells used for hydraulic head targets, the method used to calculate the target value, and the estimated February 2014 hydraulic head.

C-2.3.3.2 Hydraulic Head Gradient Targets

In addition to water levels, the model is structured to also match the observed hydraulic gradient based on a subset of wells located in the area of interest. The hydraulic gradient is a vector quantity that consists of both the magnitude (change in head per change in distance) and direction (angle from due North, or azimuth) of groundwater movement. The subset of wells used to construct hydraulic head gradient targets includes R-25 S5, R-68, R-63, R-69 S1, R-18, and R-47 (Figure C-2.3-6). Using these six wells, four hydraulic gradients were computed, thus resulting in both four magnitude targets and four direction targets (Table C-2.3-2).

The gradient computation detailed in Heath (1983, 700907) is used to derive the hydraulic gradient target values using water level targets (section C-2.3.3.1). This method requires a set of three wells, each with known water level and geographic location (Figure C-2.3-7). A summary of the steps to compute the hydraulic gradient is as follows:

1. Rank wells based on water level: high, intermediate, low.
2. Draw a line between the high and low wells. Calculate location on this line where the water level is equal to the intermediate well's water level.
3. Draw a line (contour) from the intermediate well through the location computed in step 2.
4. Draw a line perpendicular to the contour in step 3 through the low well's location.
5. Magnitude is equal to the difference in head between the intermediate and low wells, divided by the distance between the low well and the contour. Direction is equal to the azimuth of the line from step 4.

C-2.3.3.3 RDX Concentration and Trend Targets

Concentration targets are developed using data pulled from the publicly available Intellus database (https://intellusnm.com). The data were obtained in December 2019 and include sample results through November 1st, 2019. Experts advised removal of the following records: sample purpose of TEST, EQB, PEB, FB; sample type of WIP, WS, EM, R, S, "Qbt"; sample usage code of CLN, COMP, CONST, DEV, ENVSUR, PUMT, QC, REHAB, SCR, TEST, TRACER, WST; sample matrix of SD, SO; validation qualifier of R; and location IDs with "OB" or "WST" prefixes. The initial expert-based filtering resulted in the inclusion of the following records: sample purpose of REG and FD; sample type of W, WG; sample usage code of INV and QC (for FD only); sample matrix of W; and validation qualifier not equal to R (rejected). The sample and field duplicate pairs were matched by location identification, screen top depth, and sample date. The sample and field duplicate results were averaged by analyte for each location identification, screen top depth, and sample date combination. After this initial filtering and processing, several data points were removed based on a conversation with a site expert familiar with the wells, drilling, and data. The removed points are displayed in red in Figure C-2.3-8. These data points were deemed non-representative by expert opinion, based on conceptual knowledge of well construction and site dynamics. Data points were removed for the following well screens:

1. CdV-R-15-3 S4: two J-qualified detections occurring in 9/13 and 12/13.
2. R-25 S5 and R-25 S6: data before 2007 believed to be a result of contamination during drilling.
3. R-18: the first sample, a nondetect, collected 8/25/2005.
4. R-63: the first sample collected on 1/27/11.
5. R-68: all data collected before 9/6/17.
6. R-69: all data before 2019.

Calibration targets are developed by averaging all results for a given year at each well with detectable levels of RDX. If only nondetections are observed at a given well, a calibration target of zero is used for each year having nondetect data. The wells with zero calibration targets are CdV-R-15-3 S4, CdV-R-37-2 S2, R-60, R-17 S1, R-17 S2, R-29, R-19 S3, R-19 S4, R-19 S5, R-47, R-48, and R-58. For wells with both nondetections and detections, the yearly average of the sample results defines the calibration target for that year. Results from both detected and nondetected samples are used in calculating the average. Using all the data irrelevant of detection status has been shown to provide the most accurate estimate of the mean in comparison to other methods for analyzing censored data. If no samples were collected in a given year, no calibration target is developed for that year. The wells with detected RDX and non-zero calibration targets are R-25 S5, R-25 S6, R-18, R-63, R-68, R-69 S1, and R-69 S2 (Figure C-2.3-8).

Concentration Trends

In addition to RDX concentrations, concentration trends with time are also used as targets. This is intended to allow the calibration to separately weight behavior such as rising or falling concentrations independently from the raw concentrations themselves.

Slopes are calculated from the RDX concentration targets for wells with a long enough time history to support trend analysis. The wells with concentration trend targets are listed in Table C-2.3-3. The slopes are calculated by polynomial fitting with degree of 1 (i.e., a linear fit to the time/concentration data). Preference weights for the calibration are assigned based on the years of data and relative degree of confidence in the trend (Table C-2.3-3). The group weight for concentration slopes in the LM calibration is 0.2. Figure C-2.3-9 shows the computed slopes against the target data.

C-2.3.4 Markov Chain Monte Carlo

Markov Chain Monte Carlo algorithms can be used to evaluate complex high dimensional integrals; such as joint probability distributions. This is accomplished by probabilistically generating samples from random variables in the target joint probability distribution. MCMC applied to the RRM generates samples from the marginal posterior parameter distributions based on how well parameters values allow the RRM to match data. The MCMC algorithm used here is based on the Affine-Invariant Ensemble Sampler of Goodman and Weare (2010, 700890) (emcee). The emcee algorithm uses a complementary ensemble of chains, or walkers, to explore the parameter space. Each walker receives an initial parameter set, and initial values must differ for each walker. The emcee algorithm is initialized based on the best calibrated parameter set from the LM calibration process. At each iteration, the MCMC makes a multivariate proposal for each walker, given its previous position and a scaled difference in position by parameter between the current walker and another randomly selected walker.

The proposal is then accepted or rejected in a Metropolis step. In this step, the ratio of the likelihood in the current iteration to the likelihood in the previous iteration is compared with a draw from a random uniform distribution. If the ratio meets or exceeds the random uniform draw, the proposal is accepted. This method allows the walker to move towards higher or lower likelihood, with greater probability of moving towards higher likelihood. The ensemble methods combined with an affine transformation have been shown, in simple examples with known solutions, to converge more quickly than other methods.

The result is a collection of parameter sets that provide an optimization alternative to LM optimization. Forward modeling is conducted with the collection of posterior parameter sets developed by the MCMC calibration. The frequency of each parameter set in the MCMC output is taken into account when interpreting the forward modeling results.

C-2.4 Analysis to Diagnose and Improve Model Performance

Model development is an iterative process targeted at evolving the CSM and its implementation in the RRM. This process includes both qualitative and quantitative components that span lines of evidence based on subject matter expert knowledge, monitoring data, laboratory experiments, and geophysical data. The RRM integrates these lines of evidence by providing a quantitative calibration of the conceptual model to data (Figure C-1.3-1). Calibration is a learning process that employs several qualitative and quantitative approaches. The RRM is a complex computer resource intensive model; thus, several structural and SA approaches are employed to guide the model calibration. The following sections outline these various analytical tools and analyses.

C-2.4.1 Manual Calibration

Manual calibration refers to the process of altering parameters one at a time by hand, running individual models, and looking at results individually in great detail. In essence this is a one-at-a-time SA that is critical for building a better understanding of the model’s hydrology through space and time. Additionally, it offers insight into parameter sensitivity and relationships within the RRM.

Manual calibration was carried out in a “scrum” framework used most commonly in software development teams. Scrums are defined as an agile process framework for managing complex knowledge work. They rely on cross-functional teams to deliver in short cycles which enables fast feedback, continuous improvement, rapid adaptation to change, and accelerated delivery. Instead of a traditional linear, structured approach to workflow, a scrum allows for organic exploration of a complex problem and is facilitated by collocation and coworking in one space. For the RDX project, four hydrologists and one geologist on staff held an intensive three-day meeting conducting manual calibrations and leveraging idea sharing with white board space and visualizations. One of the hydrologists who participated was not involved in the RDX work before the scrum and so was able to bring fresh perspective and ideas to the process.

The modeling team planned and monitored the progress and results of these manual-forward iterations using shared tracking documents. By testing hydrologist-supplied theories, within and outside the bounds of the team’s statistical distributions (section C-2.2), these manual calibrations proved to be an efficient method for exploring parameter space, specifically in areas where the model structure (section C-2.1) or distributions (section C-2.2) needed to be improved. A suite of specialized visualization tools was developed in order to quickly analyze and compare the results of the manual forward runs. The model was set up to output more data and these scripts pulled spatiotemporal data from every point in space and time. These outputs were then plotted with concentration, water level, and head targets at desired wells, in order to identify how responsiveness varied across different runs. Results were also visualized in ParaView, a tool for visualizing complex, 3-D data.

During the manual calibration effort, parameter values were systematically altered with the new sets and were initiated as individual forward model runs. An iterative process, this manual forward run testing was also employed throughout calibration development in order to QA certain model conditions or tests and to improve the model structure. These manual calibrations also provided a verification step, ensuring that the model was behaving in a physically realistic manner and that post processing scripts were pulling the correct data. It was key in confirming that there were no nonlinear behaviors in nonphysical regions (for example, porosity ϕ >1 or regions of shifting positive and negative water additions because of a poorly structured boundary). This process also helped establish proof of concept for the CSM and the effects of boundary conditions. These individual parameter tests aided in verifying the functionality of new iterations of the mesh, and other assumptions regarding parameters.

Parameter alterations were done manually within the MADS input file (https://mads.lanl.gov/). By changing which MADS file was being used to initialize FEHM, modelers were able to run specified and iterative tests starting from specific calibrations and seeds. By isolating the parameter variability to a single or a few field(s), specific end-state concentration and head levels could be directly targeted. Once these tests moved model results closer to observed targets, this new information was incorporated into the distribution development or calibration workflow. The process proved to be particularly useful in refining the model in areas where the heterogeneity of localized physical and hydraulic properties caused irregularities.

Through this individual inspection of the hydrologic and physical parameters within the model, project experts are able to verify that the structure and assumptions of the model adequately portray the site and address the problem.

C-2.4.2 Forward Model Suites

Suites of forward models are launched in serial in order to better understand the parameter space defined by distribution development (section C-2.2). In this context, “forward” refers to any run or set of runs where inverse history-matching methods (such as LM) are not used to determine the input parameter values. The suites described here are different from the predictive forward modeling (section C-2.5) because the parameter sets used as inputs may span large sections of parameter space, where the final predictive forward modeling uses a specific parameter set determined by the results of the LM and MCMC calibrations. Here, results from these suites are used to evaluate parameter sensitivity and behavior, and to identify good starting places for the LM algorithm, which is highly sensitive to initialization state (section C-2.3.2). Within the distribution-dictated parameter space, the suites draw initial values and then launch forward runs from a set of parameter values. Input parameter sets are sampled using different methods including Latin Hypercube Sampling (LHS) from uniform distributions, MC from prior distributions, and LHS from prior distributions.

The MC method of sampling consists of randomly drawing N samples from each input parameter distribution. Each draw is independent of the other parameter draws in the space. Given that this method samples the space randomly, it may not be the most efficient because there could be some points clustered in one part of parameter space, while another part of parameter space is less densely sampled. LHS methods attempt to address this inefficiency by dividing the distribution into N intervals of equal probability and drawing from each of them in turn. For this work we are using an LHS method described in Bates et al. (2004, 700895) and implemented in Julia (https://github.com/MrUrq/LatinHypercubeSampling.jl). One of the challenges with the LHS sampling method is that, at high N, the time for the code to sample the distributions increases. At high *N*, MC methods may approach LHS methods in terms of sampling error. However, for large real-world problems there is conflicting evidence, both that LHS is superior to MC and also that it does not improve the sampling error in a meaningful way (Keramat and Kielbasa 1997, 700908; Manteufel 2000, 700909; Aistleitner et al. 2012, 700896). For this work the sampling method was dependent on the feasibility of differing computational times between methods. For *N* = 10,000, LHS sampling was on the order of a few hours, which is fast enough to use to generate input parameter sets for forward suites. However, at *N* = 50,000, the computation exceeded three days and was not a feasible method for a potential small improvement in sampling error. In future iterations a more thorough scaling study could be conducted, the code could be made more efficient, or alternative algorithms could be tested. Based on the computational time, “small” sets (up to *N* = 10,000) forward suites used the LHS method, and “large” sets (*N* > 10,000) used an MC method.

These suites of forward model runs, generally between 1000 and 50,000 simulations, provide an extensive amount of data that can be used for multiple purposes within the modeling workflow. First, they can help determine whether the parameter space covers all potential targets in the model. If, for example, none of 10,000 runs across LHS draws from the input parameter space, conducted across uniform distributions representing the 1% through the 99% points of the distributions, or matches the data at a given target, it is likely there is a structural or conceptual error in the model that is preventing a match to data. Once this mismatch is identified, manual calibrations can be conducted to diagnose the reasons for the model’s inability to match the target data (section C-2.4.1). Identifying specific parameters and targets where the model is unable to match the targets provides a starting place in the 200-dimensional parameter space to start investigating structural patterns and behaviors in the model. Without this starting place, the manual calibration step is unlikely to be effective in finding these mismatches. Uniform LHS forward suites allow the hydrologists the opportunity to visualize results across the extent of the input parameter space, bounded by the minimum and maximum of the distributions. Once it is verified that the input space is able to reach all of the targets, a more targeted approach to forward runs—drawing from input distributions instead of from wide uniform distributions—is used.

Secondly, the best matches from each batch and selection method are analyzed and can then be used as a starting point for new LM calibrations. For this step the prior distributions are used since they are much more informative than a uniform distribution. Depending on the number of samples needed for the set of forwards, either the LHS or MC method is employed (see above). Visualization of these forward suites’ matches in relation to the target data was conducted by sorting forward runs based on their OF. Top runs are all explored and altered using Manual Calibration to see if they can be improved before initializing the computationally expensive LM calibration. This method provides effective starting points for the LM calibration, which aids in the search for a global, vs. a local, minimum in parameter space.

Thirdly, the forward run suites can be used to test various weighting schemes and model sensitivity. As described above, the runs are sorted based on their OF. By altering the weights in the script which calculates the OF for the forward runs, the runs selected as *best* change. This allows the modeler to identify which targets are most important to match and then to select weights that appropriately prioritize among the many targets. This exploration is helpful in identifying the weighting choices for each calibration target described in section C-2.3.3.

Compared with the LM calibrations and MCMC calibrations, the computational demand of the forward suites is more manageable and they cover a much larger portion of parameter space. This makes the forward suites a critical tool for diagnosing the distribution development, improving the weighting scheme that directs the LM algorithm, and identifying appropriate initialization states that provide the LM better opportunities to reach a global minimum.

C-2.4.3 Machine Learning Meta Model

Machine learning (ML) approaches applied to RRM output can be used to abstract the most important or sensitive features to a simplified machine learning meta model (MLMM). This simplification allows the uncertainties associated with the key processes of the RRM to be studied in a computationally more efficient manner. The MLMM is applied to both calibration and forward model runs, thus taking advantage of all model simulations. Several ML approaches were explored for use in RRM abstraction, ultimately resulting in the use of extreme gradient boosting (XGB) (Chen and Guestrin 2016, 700897). The XGB approach uses boosting of binary recursive partitioning algorithms, which deconstruct a response into the relative influence from a given set of explanatory variables (i.e., model input parameters). The deconstruction breaks the model into separate parts (branches of the regression tree), and each part is examined separately. This process is repeated with smaller and smaller parts, each analyzed for the relationship between the explanatory variables and the model output (i.e., the response of interest). The deconstructed parts are then collected together to provide estimates of the sensitivity of each exploratory variable for a specific response variable from the model. The XGB approach identifies the most influential explanatory variables within the context of the observed uncertainty of the model output or response. Critically, the XGB method also identifies the range over which the influence is strongest; this can be used to better understand the full effect of a sensitive explanatory variable on the output results. Variance decomposition of the XGB fit is then used to estimate sensitivity indices. Under this decomposition approach, the goal is to identify the most influential explanatory variables within a model.

An advantage of the XGB MLMM approach is that non-linear causal relationships can be mined and extracted without the constraint of distributional assumptions. A key feature of the XGB meta model is the use of parameter partial dependencies which represent the marginal contribution of a parameter to predicting the model response. These partial dependencies can be used to understand how complex non-linear relationships are manifested in the model response. The partial dependencies can be used in a value of information analysis to optimize the allocation of resources to reduce uncertainty.

Finally, since the MLMM is an abstraction of the RRM that focuses on the most important causal processes, its runtime for a single simulation for the MLMM is much faster than the runtime for the RRM. Embedding MLMM in an MCMC simulation is used to more quickly explore parameter sensitivities through the evolution of the posterior distributions. This analysis was used in a qualitative fashion to help understand model sensitivities.

C-2.4.4 Consistent Bayes

A Consistent Bayes (CB) (Butler et al. 2018, 700905) approach is used to help explore and identify parameter sets for both calibration and forward runs that match well targets for single wells (univariate distribution) as well as combinations of wells (multivariate distribution). The CB approach to solving inverse problems constructs a probability measure on the model parameters that is consistent with both the model and the observed data. Consistency is defined in terms of matching the “push-forward” probabilities from the model (i.e., Monte Carlo generated forward RRM runs) and the probability measure on the data (i.e., the probability distribution of the data). In a Bayesian fashion, the parameter prior densities are propagated through the model to generate the push-forward probability distribution. “Pull-back” probability distributions for the model parameters are then generated through rejection sampling of the push-forward probability distribution that exactly matches the observed data distribution.

The CB approach is implemented in two steps:

1. Propagate the parameter prior distributions through the RRM using Monte Carlo simulation to generate the push-forward distribution.
2. Conduct rejection sampling on the push-forward realizations with the acceptance ratio based on the ratio of the model and data densities.

Step 1 (above) can take advantage of existing calibration and forward runs for the push-forward distribution. Step 2 is then a matter of rejection sampling on the existing model runs similar to the Metropolis step in the MCMC approach described in section C-2.3.4. Similar to the LM and MCMC calibrations, the CB approach is heavily weighted towards matching the data.

The CB rejection sampling are used to explore model runs that fit monitoring data both one well at a time (univariate distribution sampling) and various combinations of wells (multivariate sampling). The CB rejection sampling also generates posterior parameter distributions that can provide a comparison with MCMC-generated posterior distributions. The approach requires specifying a distribution for the observed data. Only wells with concentrations above the detection limit were included in the CB analysis and a normal distribution assumption was made for well data densities.

C-2.4.5 ModelWatcher Visualization Suite

ModelWatcher is a tool developed to track calibration or forward modeling progress in real-time. ModelWatcher both parses model output and creates visuals of results. The primary benefit of this is that it streamlines the testing and exploration of various models (VZ, RRM, or forward suites of runs) and of various model configurations. ModelWatcher is an independent software package developed by Neptune that can be used for data management and visualization under any model framework.

For the RRM, calibration and forward model output are stored in text files. These text files are regularly copied from the HPC cluster performing the computations to a server used for model development and research. The files are parsed, and the relevant information, including estimated parameter values, predicted RDX concentrations, and water levels at observation wells and decision locations, are gathered into csv file format in preparation for analysis and visualization. The code for creating the visuals is written within an *R* notebook. The *R* notebook is rendered to html for each seed within a calibration and each forward modeling effort, and a simple webpage provides links to each individual html page. The dashboard provides a straightforward presentation of results that is critical to the model development and calibration process as well as the analysis and interpretation of forward modeling results.

C-2.5 Predictive Forward Modeling

To make final predictions of RDX concentrations in space and time in the RRM, a probabilistic suite of forward models is launched from the posterior parameter distributions developed in the MCMC calibration. While the prior parameter distributions, discussed extensively in section C-2.2, represent the compilation of the prior knowledge for those values for a given parameter based on all existing lines of evidence, the posteriors represent the parameter values weighted towards matching the target data. Samples from the marginal posterior parameter distributions produced during the MCMC calibration are used to launch predictive (i.e., model end time is in the future) model runs. The end time for the model was set at 2070 for these results. If review warrants a longer analysis, this can be re-run in the future.

These forward runs can then be analyzed at critical times and places where decision makers need predictions of plume migration and concentration. At a given time and place of interest, the forward runs are combined into a probability distribution which identifies a predicted scenario of plume migration that characterizes the uncertainty associated with that prediction, providing much more useful context for decision makers.

Sensitivity analysis is helpful for evaluating various aspects of this decision context. As discussed in section C-2.4.3, MLMM SA of the final forward runs generates partial dependencies for each parameter. These partial dependencies indicate where within its posterior distribution the parameter has the most influence on the model response. Thus, these partial dependencies can be used in a value of information (VOI) analysis to guide decisions on reducing uncertainty in the modeling as well as monitoring. The VOI essentially assigns a “cost” to reducing each parameter’s uncertainty across the distributional range of the parameter. This gives the value of collecting more information on a parameter in terms of reducing the predictive distribution uncertainty and, in turn, the decision uncertainty. A VOI analysis was not conducted as part of this study but could help guide, or optimize, future modeling and monitoring studies if the need to reduce decision uncertainty is an outcome of the risk assessment.

C-2.5.1 Decision Context

The purpose of the modeling is to predict RDX transport in space and time, especially as it relates to the potential for contamination to reach community supply wells. Five locations were added to the full time series output, in addition to existing monitoring well locations, to consider as potential locations where concentration information could be used to inform decision making. The main three are the nearest water supply wells, which are 4.7–6.3 km downgradient from R-69, where the highest concentration of RDX has been measured in the regional aquifer. These wells are PM-5, 4.7 km from R-69; PM-4, 5.8 km from R-69; and PM-2, 6.3 km from R-69.

Additionally, output is produced at two locations which, along with existing wells, form an arc between the observed RDX in the regional aquifer and the water-supply wells (Figure C-2.4-1). These locations could serve as an early warning of RDX transport. For the purposes of this report they are named “D-A,” for decision location A, and “D-C,” for decision location C. An existing well, “CdV-R-15-3,” is also used as a decision location. Figure C-2.4-1 shows the wells used in calibration, along with the decision locations selected for modeled output. Although the RRM is well below the land surface, two surface features—the 260 Outfall and Cañon de Valle—are plotted for spatial reference. In this figure dotted lines are used to connect regions where monitoring could occur in the future to track plume movement and compare with modeled results.

For the purposes of this report and the risk assessment, RDX concentration results at these six locations will be presented (PM-2, PM-4, PM-5, D-A, D-C, and CdV-R-15-3). Input decks for all runs, as well as a significant amount of output, are retained for future work. Any run presented in this report can be rerun with additional or alternative output specified to understand transport in space and time should the need or interest arise in the future for other locations within the RRM.

C-3.0 RESULTS

C-3.1 LM Calibration Results

The LM calibration is measured by the minimum of the OF (section C-2.3.2). This minimum OF is in turn a metric of how well the simulation matches the target datasets given the weighting scheme (section C-2.3.3). Many different starting points are selected based on the best forward runs available, including some manually calibrated starting locations. The LM calibration gradually improves the matches to data through iterations of runs. Below are results from the best LM calibration, which in turn becomes the initialization state for the MCMC calibration.

Matching concentrations of RDX in the regional aquifer is the main priority for the simulation. Figure C-3.1-1 shows the results of the LM calibration plotted against the raw and target data. Raw data are plotted in black, and target data points (derived from raw data in section C-2.3.3.3) are plotted as green triangles. The OF compares simulated results only to target data (not to raw data), so the best results are ones in which the simulation matches the green data points as well as possible.

The highest measured concentrations at R-68 and R-69 screen 2 have excellent matches to data. While the exact points are not matched in R-68, the trend observed across these three years is likely noise and not signal. The simulation finds a solution between all three target data points. Likewise, the simulation at R-69 screen 1 finds a very close match to the target, which is well within the noise observed in the raw data. A notable result is that R-69 has very different observed values in screen 1 (13.4 ppb) and screen 2 (19.2 ppb) in 2019, and the simulation is able to match both screens. This result suggests that a vertical concentration gradient has been established in R-69 and that the simulation is doing well matching data vertically as well as laterally.

R-18 has the most pronounced trend, increasing with little noise from the first data point (2006) up to the most recent (2019). Again, the simulation matches the data here nearly perfectly, hitting the values at the beginning, middle, and end of a non-linear trend. Another important well, R-47, has only nondetections in the data, but the nondetections go as high as 0.3 ppb. This well is important because, despite being close to wells with high levels of RDX, and also directly east of these wells, no RDX has been detected to the present day. Therefore, R-47 provides a constraint on the eastern edge of the plume and adds evidence of a northeast gradient local to the plume. The simulation results range from just over 0.02–0.03 ppb, which matches the target data of 0 because these values are well below the RDX detection limits.

R-63 and R-25 have lower concentrations than the wells described previously; however, they are still important to match. The simulation is able to match the data at R-63 as well as at R-25. Both screen 5 and screen 6 in R-25 have close matches, which, like R-69, have different RDX concentrations with depth. Results at R-25 are marginally less accurate than results at other wells; however, the RDX measured at R-25 is very low compared with any other well (<1 ppb), and the data are also noisy.

Water levels in the LM calibration also match exceptionally well in the area local to the plume, with residuals no more than -3 m to 1 m in all wells as far east as CdV-R-15-3. East of CdV-R-15-3 results are less accurate, with residuals as high as 10 m and as low as -11 m. The model is designed to capture heterogeneity local to the plume, and the ability to represent this complexity is reduced when moving further from the plume to the east where data are more sparse. This is also by design, as incorporating heterogeneity everywhere throughout such a large model would quickly become an intractable computational problem; each additional pilot point adds three dimensions of hydraulic conductivity (Kx, Ky, and Kz) to the already 200-dimensional parameter space. The pilot point density is shown in Figure C-2.2-26, demonstrating that the density drops off east of CdV-R-15-3, ending in a homogenous K field east of R-60, R-17, and R-19. Additionally, the model does not represent potential preferential pathways of water to the regional aquifer outside the region near the plume. These pathways likely add complexity to the water tables observed in the real system, but there is little to no data to inform complexity this far east of the RDX plume. Figure C-3.1-2 shows the LM results compared with hydraulic head targets, and Figure C-3.1-3 presents this same data spatially.

In addition to the water levels, the hydraulic gradient local to the plume is also an important target. Gradient targets are especially critical because the dominant direction of flow in the model is west to east; however, local to the plume the gradient is southwest to northeast, so an accurate representation of plume transport is dependent on representing this gradient. Figure C-3.1-4 shows the hydraulic gradient targets (as orange arrows), and shows the water level results from the LM calibration as contours. The simulation gradients are plotted as black arrows and are difficult to see below the target arrows because the results are nearly perfect in both magnitude and direction.

Another important metric that can be used to understand and analyze the LM results is the source locations in the context of the CSM. Figure C-3.1-5 shows the final locations of the primary (s1), secondary (s2), and preferential recharge source (s3) for the LM calibration.

The locations of the sources are consistent with the CSM. The preferential recharge source is located just south of the east-west axis of Cañon de Valle, well within the conceptualization of the source described in section C-2.2.3.2.4. The primary source is long and narrow, with a mostly west to east axis, which could be the result of spill-off from the perched zone in the RVZM, though it is slightly south of the current conceptualization of the perched zone. The secondary source falls in the middle of the preferential recharge source.

Inventory results are just above the upper end described in the Deep Groundwater Investigation Report, which estimates between 35 and 415 kg of RDX in 2017 (N3B 2019, 700878). These results have an inventory of 417 kg for the primary source and 12 kg for the secondary source in 2020, for a total predicted inventory of 429 kg in the simulation. Inventory estimates for the entire hydrologic system at TA-16 range from 1533 kg to 3608 kg. If the sources estimated by the LM calibration were to continue at the same rate linearly, that would mean that the total RDX in the system would all have moved to the regional aquifer sometime between 2070 and 2150.

Overall the matches to data from the LM calibration are excellent. Concentrations, water levels, and hydraulic gradients near the plume match the data nearly perfectly. The hydraulic window locations are very consistent with the CSM. Further east of the plume, water level matches are less accurate, but are still within 11 m of the data, despite being in a region with very few degrees of freedom in the model. These results are the lowest OF achieved across many calibrations and are used to initialize the MCMC calibration.

C-3.2 MCMC Calibration Results

The Affine Invariant MCMC ensemble sampler described in section C-2.3.4 is initialized using the LM calibration result. Because of computational requirements, the MCMC is run with 120 walkers and 50 iterations each rather than rather than the recommended 2 times the number of parameters Iterations and walkers for the MCMC are described in section C-2.3.4. Forward modeling is then conducted with the resulting set of accepted parameter sets (section C-2.5).

One of the 120 walkers is initialized at the LM calibration result, and the remaining walkers are initialized by a draw from a generalized beta distribution, with a mean equal to the LM calibration result and a standard deviation of 0.0001. In each step of the algorithm, an affine transformation is applied with an “a” tuning, and the walker movement takes place in the transformed space. The “a” parameter provides control over the region of the multi-dimensional parameter space that is explored and thus allows tuning of the walker proposal acceptance rate; “a” = 2 is used following Foreman-Mackey et al. (2013, 700906). The proposed set of parameter values for an individual walker depends both on the previous parameter set for that walker, and on the position of the other walkers in the ensemble.

The movement of each walker, with each iteration, is displayed in Figure C-3.2-1. Walker 7 is highlighted by a red line as an example of walker movement through space, and accepted iterations for this walker are indicated by a yellow circle. The algorithm had an acceptance rate of 16.3%, indicating that the walker moved to the proposed set in 16.3% of all iterations. If the proposed parameter set was rejected, the walker stayed in place, resulting in the horizontal lines in Figure C-3.2-1. Higher posterior density is indicated by parameter sets where the walker remains stuck for multiple iterations. Though the algorithm does allow a walker to move from higher to lower likelihood, it is much more likely to move towards higher likelihood (or lower log likelihood). This method leads to posterior distributions with higher density in regions that tend to increase the likelihood function. The method also gives more weight to parameter sets that are most consistent with observed data. It does not, however, exclude the possibility of parameter sets that could, but are less likely to, have produced the observed RDX concentrations. In general, because of the high dimension of the parameter space and the initialization of the parameters with the generalized beta distribution, the MCMC algorithm is highly sensitive to the parameter set where it is initialized. The LM calibration is used to find a suitable parameter set that is consistent with conceptual site knowledge and minimizes the OF, and the MCMC algorithm then explores the local space to estimate parameter uncertainty.

Marginal posterior distributions for all parameters are displayed in Figure C-3.2-2, though hydraulic conductivity (***K***) distributions are plotted separately (Figure C-3.2-3) because of how many different targets these represent across all anchor and pilot points described in section C-2.2.3.1.1. Marginal posterior distributions are relatively narrow, reflecting the approach of local exploration around the LM calibrated parameter set. Much of the predictive uncertainty results from the complexity of the parameter space and the myriad possibilities of parameter combinations.

The MCMC results are processed to develop a unique “chain” of parameter sets for predictive modeling. After duplicates were removed from the 6000 parameter sets, 1018 unique sets remained. Predictive forward runs are launched from each unique set, and final results are weighted by the frequency of occurrence of the parameter set from which they were derived.

C-3.3 Predictive Forward Results

The chain produced from the MCMC calibration resulted in parameter sets for 1018 model runs that capture a spread of uncertainty around the LM calibration results (section C-3.2). These runs were set up to run into the future out to the year 2070. Full probabilistic time series were produced at all wells used for calibration, as well as at the decision locations described in section C-2.5.1. Spatial output at every node was produced for two years—2020 (present day conditions), and 2070 (end of simulation conditions)—in order to plot the extent of the plume in three dimensions.

Comparison of probabilistic time series results to targets are shown in Figure C-3.3-1. In these plots, all simulated values below 0.1 ppb (lower than the detection limits of RDX in the system) are plotted as 0. These plots show good matches to target data (green triangles), with the highest density of predictive forwards falling over the target data. Uncertainty is quantified as the maximum absolute difference between the target and simulated data. This uncertainty for each well is shown in Table C-2.3-4.

Results at R-68 suggest that the peak concentration has already arrived, and that concentrations are not likely to increase (beyond the presented uncertainty) in the future. Uncertainty around estimates at R-68 gets as high as 20.6 ppb (Table C-2.3-4). Simulations that matched the upper data point well did not match the lower two well, and vise-versa. It is possible that for this reason the MCMC accepted parameter combinations for both matches (high and low) but not for the intermediate values. No obvious bi-modal relationships were observed in the posterior parameter distributions that might otherwise explain this behavior.

Results at R-69 similarly match the data well, with the bulk of the predictive forwards falling directly over the target data. The vertical concentration gradient observed in R-69, with higher concentrations at depth, is well represented in the predictive forwards. Screen 1 shows a narrower range of uncertainty, up to 14.6 ppb, and screen 2 shows 17.6 ppb. Simulations suggest that concentrations are likely to continue increasing at R-69 screen 2, but only for a few years. At R-69 screen 1 they are less likely to increase in coming years but there is still the possibility that they will increase.

At R-18, the simulation matches the trend very well and predicts concentrations to continue increasing at that location for up to 20 yr. Concentrations are expected to reach maxima at similar values to observed data in R-68 and R-69 screen 2 over the next 20 yr.

Results at R-63 and R-25 match the data, though no trends are represented in the simulations. The data at these locations are noisy, and RDX concentrations are low. Simulations do not suggest future measured values to be observed above 2.5 ppb at R-63, 1 ppb at R-25 screen 5, and 2.5 ppb at R-25 screen 6.

All wells with targets of 0 ppb are matched by the simulated data (within the 0.1 ppb threshold described above). A few simulations at R-47 go as high as 0.15 ppb; however, the bulk of the simulations are below the 0.1 ppb threshold.

Three specific predictive forward runs were identified from the set of 1018 as representing the 5%, median, and 95% cases. They were selected as a function of the area occupied out to a 9.66 threshold (i.e., the runs where the 9.66 ppb isopleth expands furthest vs. expands least). In order to determine the area, the convex hull around marginalized values in the z-direction was estimated for every forward run and plotted as a distribution of total area. The 5%, median, and 95% runs were identified from this set and their RDX concentrations plotted as a function of their x, y coordinates. Maximum values of RDX for every z-coordinate at each x, y pair is plotted in Figure C-3.3-2. The thickness of the plume in m is plotted to the right of the plume heat map.

The differences in heat maps were minor between the 5%, median, and 95% runs, so only the median case is plotted. The extents of the 9.66 ppb (red lines) and 1 ppb (black lines) isopleths are shown for the 5% (dashed line), median (solid line), and 95% (dotted line) cases. Note that the selected 5%, median, and 95% runs are different at the 9.66 ppb isopleth than at the 1 ppb isopleth.

The small differences in area between the 5% and 95% runs (Figure C-3.3-3) suggests that plume expansion at the edges is slow, despite high concentrations at the hydraulic window. By 2070 the plume has only expanded between 783–804 m from the 2020 plume extent. No portion of the plume, even at 0.1 ppb, reaches the decision locations. This includes potential locations located approximately one-third of the total distance between the plume and the PM- wells (D-A, D-C, CdV-R-15-3) by 2070. This can also be seen in time series of all runs plotted at these decision locations (Figure C-3.3-4).

C-4.0 CONCLUSIONS

The RRM presented here is a robust approach to simulating a contaminant plume in a geologically complex region. Through a detailed process involving the incorporation of many lines of evidence in order to inform prior parameter distributions, probabilistic simulations, LM calibration, and MCMC calibration, a set of parameter distributions that matches the target data is identified and uncertainty is characterized.

Posterior parameter distributions are then used to produce a suite of predictive forward runs that estimate plume expansion over the next 50 yr.

The model is constructed with a variable mesh and boundary conditions to model transport in the area local to the plume (section C-2.1). Input parameters go through a detailed distribution development process that involves analyzing all lines of evidence—including data, literature, other models, and the CSM—to determine a distribution of possible values for each of the 196 input parameters to the RRM (section C-2.2). A classical calibration is conducted to identify the best match of simulated data to observed data, which includes RDX concentrations, hydraulic heads, concentration trends, and hydraulic gradients at the site. The deterministic results of the classical calibration are used to initialize an MCMC calibration that explores the parameter space more widely to characterize uncertainty at the site via development of posterior distributions (section C-2.3). Throughout the modeling steps described above, an extensive suite of analytical tools, both structural and statistical, are leveraged to improve, guide, and update the RRM (section C-2.4). Ultimately, calibration results are used to launch a set of predictive forwards out to the year 2070 (section C-2.5).

Results from the LM and MCMC calibrations demonstrate exceptional matches to target data for concentrations, hydraulic gradients, and hydraulic heads, providing confidence in the modeling (section C-3.0). Predictive forward results suggest that the plume does not expand quickly over the next 50 yr, with no simulations showing the plume reaching any of the specified decision locations (Figure C-3.3-4). These locations include water-supply wells (PM-2, PM-4, PM-5), as well as a set of potential monitoring locations between the plume and the water-supply wells (D-A, D-C, and CdV-R-15-3) (Figure C-2.4-1).

C-5.0 REFERENCES

The following reference list includes documents cited in this appendix. Parenthetical information following each reference provides the author(s), publication date, and ERID, ESHID, or EMID. This information is also included in text citations. ERIDs were assigned by the Laboratory's Associate Directorate for Environmental Management (IDs through 599999); ESHIDs were assigned by the Laboratory's Associate Directorate for Environment, Safety, and Health (IDs 600000 through 699999); and EMIDs are assigned by N3B (IDs 700000 and above). IDs are used to locate documents in N3B's Records Management System and in the Master Reference Set. The NMED Hazardous Waste Bureau and N3B maintain copies of the Master Reference Set. The set ensures that NMED has the references to review documents. The set is updated when new references are cited in documents.

Abbaspour, K.C., M.T. van Genuchten, R. Schulin, and E. Schläppi, August 1, 1997. "A Sequential Uncertainty Domain Inverse Procedure for Estimating Subsurface Flow and Transport Parameters," *Water Resources Research,* Vol. 33, No. 8, pp. 1879-1892. (Abbaspour et al. 1997, 700898)

Aistleitner, C., M. Hofer, and R. Tichy, 2012. "A Central Limit Theorem for Latin Hypercube Sampling with Dependence and Application to Exotic Basket Option Pricing," *International Journal of Theoretical and Applied Finance,* Vol. 15, No. 7. (Aistleitner et al. 2012, 700896)

Bates, S.J., J. Sienz, and V.V. Toropov, April 19–22, 2004. "Formulation of the Optimal Latin Hypercube Design of Experiments Using a Permutation Genetic Algorithm," 45th AIAA/ASME/ASCE/AHS/ASC Structures, Structural Dynamics and Materials Conference, April 19–22, 2004, Palm Springs, California. (Bates et al. 2004, 700895)

Birdsell, K.H., K.M. Bower, A.V. Wolfsberg, W.E. Soll, T.A. Cherry, and T.W. Orr, July 1999. “Simulations of Groundwater Flow and Radionuclide Transport in the Vadose and Saturated Zones Beneath Area G, Los Alamos National Laboratory,” Los Alamos National Laboratory report LA-13299-MS, Los Alamos, New Mexico. (Birdsell et al. 1999, 069792)

Birdsell, K.H., B.D. Newman, D.E. Broxton, and B.A. Robinson, 2005. “Conceptual Models of Vadose Zone Flow and Transport beneath the Pajarito Plateau, Los Alamos, New Mexico,” *Vadose Zone Journal,* Vol. 4, pp. 620–636. (Birdsell et al. 2005, 092048)

Black, P., K. Catlett, D. Anderson, P. Duffy, T. Stockton, and S. Van Sickle, March 3–7, 2019. “Scaling Input Distributions for Probabilistic Models-19472,” Waste Management 2019 Conference, March 3–7, 2019, Phoenix, Arizona. (Black et al. 2019, 700892)

Bromly, M., C. Hinz, and L.A.G. Aylmore, February 2007. “Relation of Dispersivity to Properties of Homogeneous Saturated Repacked Soil Columns,” *European Journal of Soil Science,* Vol. 58, No. 1, pp. 293-301. (Bromly et al. 2007, 700902)

Broxton, D., R. Warren, P. Longmire, R. Gilkeson, S. Johnson, D. Rogers, W. Stone, B. Newman, M. Everett, D. Vaniman, S. McLin, J. Skalski, and D. Larssen, March 2002. “Characterization Well R-25 Completion Report,” Los Alamos National Laboratory report LA-13909-MS, Los Alamos, New Mexico. (Broxton et al. 2002, 072640)

Butler, T., J. Jakeman, and T. Wildey, April 2018. “Combining Push-forward Measures and Bayes' Rule to Construct Consistent Solutions to Stochastic Inverse Problems,” *SIAM Journal on Scientific Computing,* Vol. 40, No. 2, pp. A984-A1011. (Butler et al. 2018, 700905)

Chen, T., and C. Guestrin, August 13-17, 2016. “XGBoost: A Scalable Tree Boosting System,” KDD '16: Proceedings of the 22nd ACM SIGKDD International Conference on Knowledge Discovery and Data Mining, August 13-17, 2016, San Francisco, California. (Chen and Guestrin 2016, 700897)

Cressie, N., 1993. *Statistics for Spatial Data*, John Wiley and Sons Inc., New York, New York. (Cressie 1993, 700911)

DOE (U.S. Department of Energy), January 2010. “Final Environmental Impact Statement for Decommissioning and/or Long-Term Stewardship at the West Valley Demonstration Project and Western New York Nuclear Service Center,” Volume 2 (Appendices A through R), DOE/EIS-0226, West Valley, New York. (DOE 2010, 700880)

Doherty, J., March-April 2003. “Ground Water Model Calibration Using Pilot Points and Regularization,” *Ground Water,* Vol. 41, No. 2, pp. 170-177. (Doherty 2003, 700894)

Fetter, C.W., *Applied Hydrogeology*, Third ed., Prentice Hall, Upper Saddle River, New Jersey. (Fetter 1994, 070942)

Fetter, C.W., 2008. *Contaminant Hydrogeology*, Second Edition, Waveland Press Inc., Long Grove, Illinois. (Fetter 2008, 700912)

Foreman-Mackey, D., D.W. Hogg, D. Lang, and J. Goodman, March 2013. “emcee: The MCMC Hammer,” *Publications of the Astonomical Society of the Pacific,* Vol. 125, No. 925, pp. 306-312. (Foreman-Mackey et al. 2013, 700906)

Franke, O.L., T.E. Reilly, and D. Bennett, 1987. “Chapter B5, Definition of Boundary and Initial Conditions in the Analysis of Saturated Ground-Water Flow Systems—An Introduction,” in *Techniques of Water-Resources Investigations of the United States Geological Survey*, United States Geological Survey, United States Government Printing Office, Washington, D.C. (Franke et al. 1987, 700886)

Freeze, R.A., and J.A. Cherry, January 1979. *Groundwater*, Prentice-Hall, Inc., Englewood Cliffs, New Jersey. (Freeze and Cherry 1979, 088742)

French, S., R. Shuman, G.L. Cole, K.J. Crowell, M.S. Day, C.W. Gable, M.O. Gard, J.J. Whicker, D.G. Levitt, B.D. Newman, B.A. Robinson, E.P. Springer, and P.H. Stauffer, October 2008. “Performance Assessment and Composite Analysis for Los Alamos National Laboratory Material Disposal, Area G, Revision 4,” Los Alamos National Laboratory document LA-UR-08-06764, Los Alamos, New Mexico. (French et al. 2008, 106890)

Fujinawa, K., 2010. “Anthroscape of the Mediterranean Coastal Area in the Context of Hydrogeology: Projected Impacts of Climate Change,” in *Sustainable Land Management*, S. Kapur, H. Eswaran, and W. Blum (Eds.), Springer, Berlin, Heidelberg. (Fujinawa 2010, 700903)

Gable, C.W., H.E. Trease, and T.A. Cherry, June 1996. “Geological Applications of Automatic Grid Generation Tools for Finite Elements Applied to Porous Flow Modeling,” in *Numerical Grid Generation in Computational Fluid Dynamics and Related Fields*, B.K. Soni, J.F. Thompson, H. Hausser, and P.R. Eiseman (Eds.), Mississippi State University Press, Jackson, Mississippi. (Gable et al. 1996, 700887)

Gains-Germain, L., A. Jordan, M. Higgs, P. Meeks, P. Black, and T. Stockton, March 18–22, 2018. “Explicitly Accounting for Multiple Spatial Scales in Data Informing Kd Distribution Development – 18414,” Waste Management 2018 Conference, March 18–22, 2018, Phoenix, Arizona. (Gains-Germain et al. 2018, 700888)

Gard, M.O., and B.D. Newman, November 2005. “The High Explosives Source Term at TA-16,” Los Alamos National Laboratory document LA-UR-05-9433, Los Alamos, New Mexico. (Gard and Newman 2005, 093651)

Gardner, J.N., A. Lavine, G. WoldeGabriel, D. Krier, J., D.T. Vaniman, F.A. Caporuscio, C.J. Lewis, M.R. Reneau, E.C. Kluk, and M.J. Snow, March 1999. “Structural Geology of the Northwestern Portion of Los Alamos National Laboratory, Rio Grande Rift, New Mexico: Implications for Seismic Surface Rupture Potential from TA-3 to TA-55,” Los Alamos National Laboratory report LA-13589-MS, Los Alamos, New Mexico. (Gardner et al. 1999, 063492)

Gelhar, L.W., C. Welty, and K.R. Rehfeldt, July 1992. “A Critical Review of Data on Field-Scale Dispersion in Aquifers,” *Water Resources Research,* Vol. 28, No. 7, pp. 1955–1974. (Gelhar et al. 1992, 102465)

Goodman, J., and J. Weare, 2010. “Ensemble Samplers with Affine Invariance,” *Communications in Applied Mathematics and Computational Science,* Vol. 5, No. 1, pp. 65-80. (Goodman and Weare 2010, 700890)

Heath, R.C., 1983. “Basic Ground-Water Hydrology,” prepared in cooperation with the North Carolina Department of Natural Resources and Community Development, U.S. Geological Survey Water-Supply Paper 2220, Reston, Virginia. (Heath 1983, 700907)

Heerspink, B.P., S. Pandey, H. Boukhalfa, D.S. Ware, O. Marina, G. Perkins, V.V. Vesselinov, and G. WoldeGabriel, May 2, 2017. “Fate and Transport of Hexahydro-1,3,5-trinitro-1,3,5-triazine (RDX) and Its Degradation Products in Sedimentary and Volcanic Rocks, Los Alamos, New Mexico,” *Chemosphere,* Vol. 182, pp. 276-283. (Heerspink et al. 2017, 602560)

Ho, C.K., R.G. Baca, S.H. Conrad, G.A. Smith, L.-J. Shyr, and T.A. Wheeler, January 1999. “Stochastic Parameter Development for PORFLOW Simulations of the Hanford AX Tank Farm,” Sandia National Laboratories Report No. SAND98-2880, Albuquerque, New Mexico. (Ho et al. 1999, 700883)

Jordan, A., S. Fitchett, K. Catlett, D. Levitt, G. Occhiogrosso, J. Tauxe, P. Meeks, M. Higgs, and P. Black, March 5–9, 2017. “Realistic Geochemical Paramater Uncertainty for Performance Assessment Modeling – 17066,” Waste Management 2017 Conference, March 5–9, 2017, Phoenix, Arizona. (Jordan et al. 2017, 700881)

Keramat, M., and R. Kielbasa, 1997. “Latin Hypercube Sampling Monte Carlo Estimation of Average Quality Index for Integrated Circuits,” *Analog Integrated Circuits and Signal Processing,* Vol. 14, pp. 131-142. (Keramat and Kielbasa 1997, 700908)

Kleinfelder, January 25, 2005. “Final Well R-26 Completion Report, Revision No. 1,” report prepared for Los Alamos National Laboratory, Project No. 37151, Albuquerque, New Mexico. (Kleinfelder 2005, 087846)

Kwicklis, E., M. Witkowski, K. Birdsell, B. Newman, and D. Walther, August 2005. “Development of an Infiltration Map for the Los Alamos Area, New Mexico,” *Vadose Zone Journal,* Vol. 4, pp. 672–693. (Kwicklis et al. 2005, 090069)

LANL (Los Alamos National Laboratory), September 1998. “Work Plan for Pajarito Canyon,” Los Alamos National Laboratory document LA-UR-98-2550, Los Alamos, New Mexico. (LANL 1998, 059577)

LANL (Los Alamos National Laboratory), September 2003. “Phase III RFI Report for Solid Waste Management Unit 16-021(c)-99,” Los Alamos National Laboratory document LA-UR-03-5248, Los Alamos, New Mexico. (LANL 2003, 077965)

LANL (Los Alamos National Laboratory), June 2008. “Supplemental Investigation Work Plan for Intermediate and Regional Groundwater at Consolidated Unit 16-021(c)-99,” Los Alamos National Laboratory document LA-UR-08-3991, Los Alamos, New Mexico. (LANL 2008, 103165)

LANL (Los Alamos National Laboratory), August 2009. “Pajarito Canyon Investigation Report, Revision 1,” Los Alamos National Laboratory document LA-UR-09-4670, Los Alamos, New Mexico. (LANL 2009, 106939)

LANL (Los Alamos National Laboratory), June 2011. “Hydrologic Testing Report for Consolidated Unit 16-021(c)-99,” Los Alamos National Laboratory document LA-UR-11-3072, Los Alamos, New Mexico. (LANL 2011, 203711)

LANL (Los Alamos National Laboratory), September 2011. “Corrective Measures Evaluation Report for Material Disposal Area G, Solid Waste Management Unit 54-013(b)-99, at Technical Area 54, Revision 3,” Los Alamos National Laboratory document LA-UR-11-4910, Los Alamos, New Mexico. (LANL 2011, 206324)

LANL (Los Alamos National Laboratory), September 2011. “Investigation Report for Water Canyon/ Cañon de Valle,” Los Alamos National Laboratory document LA-UR-11-5478, Los Alamos, New Mexico. (LANL 2011, 207069)

LANL (Los Alamos National Laboratory), March 2012. “Technical Area 16 Well Network Evaluation and Recommendations,” Los Alamos National Laboratory document LA-UR-12-1082, Los Alamos, New Mexico. (LANL 2012, 213573)

LANL (Los Alamos National Laboratory), July 27, 2017. “Completion Report for Regional Aquifer Well R-68,” Los Alamos National Laboratory document LA-UR-17-26063, Los Alamos, New Mexico. (LANL 2017, 602539)

LANL (Los Alamos National Laboratory), March 2018. “Compendium of Technical Reports Conducted Under the Work Plan for Chromium Plume Center Characterization,” Los Alamos National Laboratory document LA-UR-18-21450, Los Alamos, New Mexico. (LANL 2018, 602964)

LANL (Los Alamos National Laboratory), March 2018. “Compendium of Technical Reports Related to the Deep Groundwater Investigation for the RDX Project at Los Alamos National Laboratory,” Los Alamos National Laboratory document LA-UR-18-21326, Los Alamos, New Mexico. (LANL 2018, 602963)

Levitt, D.G., September 2011. “Modeling the Movement of Transient Moisture through Disposal Units at Los Alamos National Laboratory Technical Area 54, Area G,” Los Alamos National Laboratory document LA-UR-11-05424, Los Alamos, New Mexico. (Levitt 2011, 700879)

Lewis, C.L., J.N. Gardner, E.S. Schultz-Fellenz, A. Lavine, and S.L. Reneau, June 2009. “Fault Interaction and Along-Strike Variation in Throw in the Pajarito Fault System, Rio Grande Rift, New Mexico,” *Geosphere,* Vol. 5, No. 3, pp. 252–269. (Lewis et al. 2009, 111708)

Lin, Y., D. O'Malley, and V.V. Vesselinov, September 15, 2016. “A Computationally Efficient Parallel Levenberg-Marquardt Algorithm for Highly Parameterized Inverse Model Analyses,” *Water Resources Research,* Vol. 52, pp. 6948-6977. (Lin et al. 2016, 700889)

Manteufel, R.D., April 3-6, 2000. “Evaluating the Convergence of Latin Hypercube Sampling,” 41st Structures, Structural Dynamics, and Materials Conference and Exhibit, April 3-6, 2000, Atlanta, Georgia. (Manteufel 2000, 700909)

McGehee, E.D., S. McCarthy, K. Towery, J. Ronquillo, K.L.M. Garcia, and J. Isaacson, March 28, 2003. “Sentinels of the Atomic Dawn: A Multiple-Property Evaluation of the Remaining Manhattan Project Properties at Los Alamos (1942-1946),” Historic Building Survey Report No. 215, Los Alamos National Laboratory document LA-UR-03-0726, Los Alamos, New Mexico. (McGehee et al. 2003, 700541)

McLin, S., July 2005. “Analyses of the PM-2 Aquifer Test Using Multiple Observation Wells,” Los Alamos National Laboratory report LA-14225-MS, Los Alamos, New Mexico. (McLin 2005, 090073)

Meyer, B.R., C.A.R. Bain, A.S.M. De Jesus, and D. Stephenson, 1981. “Radiotracer Evaluation of Groundwater Dispersion in a Multi-Layered Aquifer,” *Journal of Hydrology,* Vol. 50, pp. 259-271. (Meyer et al. 1981, 700901)

Millington, R.J., and J.P. Quirk, 1961. “Permeability of Porous Solids,” *Transactions of the Faraday Society,* Vol. 57, pp. 1200–1207. (Millington and Quirk 1961, 110521)

N3B (Newport News Nuclear BWXT-Los Alamos, LLC), August 2019. “Investigation Report for Royal Demolition Explosive in Deep Groundwater,” Newport News Nuclear BWXT-Los Alamos, LLC, document EM2019-0235, Los Alamos, New Mexico. (N3B 2019, 700561)

Neptune (Neptune and Company, Inc.), September 30, 2018. “File Transfer Report for Chromium and RDX Project Hydrologic Modeling,” Neptune and Company, Inc., report no. NAC-0124_R0, Los Alamos, New Mexico. (Neptune 2018, 700878)

Neuman, S.P., August 1990. “Universal Scaling of Hydraulic Conductivities and Dispersivities in Geologic Media,” *Water Resources Research,* Vol. 26, No. 8, pp. 1749-1758. (Neuman 1990, 090184)

NRC (U.S. Nuclear Regulatory Commission), April 1987. “Modeling Study of Solute Transport in the Unsaturated Zone,” Workshop Proceedings, NUREG/CR-4615, LA-10730-MS, Washington, D.C. (NRC 1987, 700882)

O'Malley, D., and V.V. Vesselinov, March 7, 2014. “Analytical Solutions for Anomalous Dispersion Transport,” *Advances in Water Resources,* Vol. 68, pp. 13–23. (O'Malley and Vesselinov 2014, 700891)

Reimus, P.W., M.J. Haga, A.I. Adams, T.J. Callahan, H.J. Turin, and D.A. Counce, April–May 2003. “Testing and Parameterizing a Conceptual Solute Transport Model in Saturated Fractured Tuff Using Sorbing and Nonsorbing Tracers in Cross-Hole Tracer Tests,” *Journal of Contaminant Hydrology,* Vol. 62–63, pp. 613–636. (Reimus et al. 2003, 210315)

Reneau, S.L., E.V. McDonald, J.N. Gardner, T.R. Kolbe, J.S. Carney, P.M. Watt, and P.A. Longmire, 1996. “Erosion and Deposition on the Pajarito Plateau, New Mexico, and Implications for Geomorphic Responses to Late Quaternary Climatic Changes,” New Mexico Geological Society Guidebook: 47th Field Conference, Jemez Mountains Region, New Mexico, pp. 391-398. (Reneau et al. 1996, 055539)

Robinson, B.A., S.G. McLin, and H.S. Viswanathan, 2005. “Hydrologic Behavior of Unsaturated, Fractured Tuff: Interpretation and Modeling of a Wellbore Injection Test,” *Vadose Zone Journal,* Vol. 4, pp. 694–707. (Robinson et al. 2005, 092040)

Schulze-Makuch, D., D.A. Carlson, D.S. Cherkauer, and P. Malik, November--December 1999. “Scale Dependency of Hydraulic Conductivity in Heterogeneous Media,” *Ground Water,* Vol. 37, No. 6, pp. 904-919. (Schulze-Makuch et al. 1999, 700893)

Schwartz, F.W., and H. Zhang, 2002. *Fundamentals of Ground Water*, John Wiley and Sons Inc., New York, New York. (Schwartz and Zhang 2002, 700913)

Springer, E.P., 2005. “Statistical Exploration of Matrix Hydrologic Properties for the Bandelier Tuff, Los Alamos, New Mexico,” *Vadose Zone Journal,* Vol. 4, pp. 505–521. (Springer 2005, 098534)

Stephens, D.B., 1995. *Vadose Zone Hydrology*, CRC Press Inc., Boca Raton, Florida. (Stephens 1995, 700914)

Umari, A., M.F. Fahy, J.D. Earle, and P. Tucci, 2008. “Analysis of Conservative Tracer Tests in the Bullfrog, Tram, and Prow Pass Tuffs, 1996 to 1998, Yucca Mountain, Nye County, Nevada,” report prepared for the U.S. Department of the Interior and the U.S. Geological Survey in cooperation with the U.S. Department of Energy, Scientific Investigations Report 2007-5280, Weston, Virginia. (Umari et al. 2008, 700899)

Waldrop, W.R., L.W. Gelhar, A. Mantogiou, C. Welty, and K.R. Rehfeldt, August 1985. “A Review of Field-Scale Physical Solute Transport Processes In Saturated and Unsaturated Porous Media,” report prepared by Tennessee Valley Authority and Massachusetts Institute of Technology for the Electric Power Research Institute, final report EA-4190, Palo Alto, California. (Waldrop et al. 1985, 700900)

Zyvoloski, G., May 18, 2007. “FEHM: A Control Volume Finite Element Code for Simulating Subsurface Multi-Phase Multi-Fluid Heat and Mass Transfer,” Los Alamos National Laboratory document LA-UR-07-3359, Los Alamos, New Mexico. (Zyvoloski 2007, 700904)

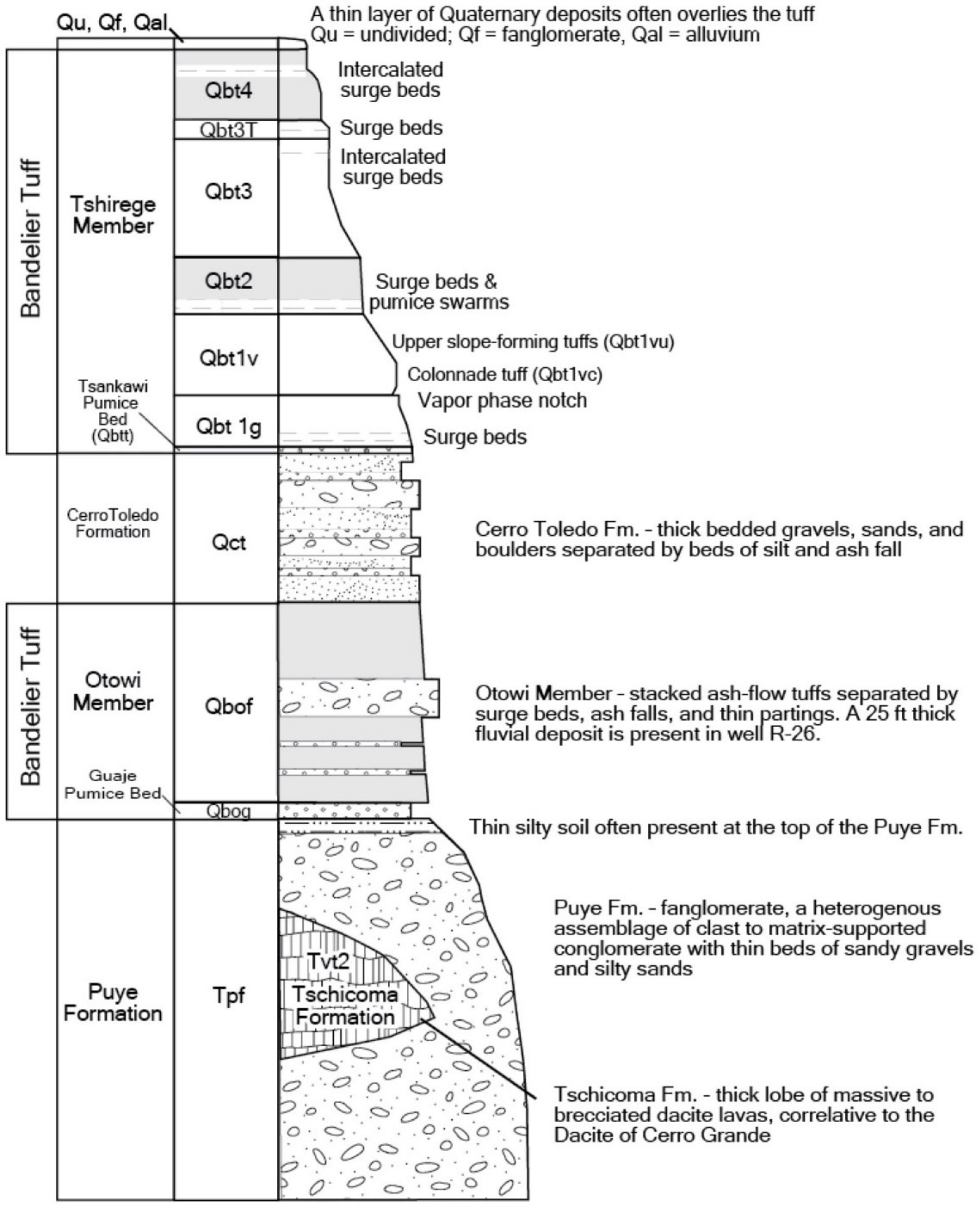

Figure C-1.2-1 Stratigraphy of the geologic units at TA-16

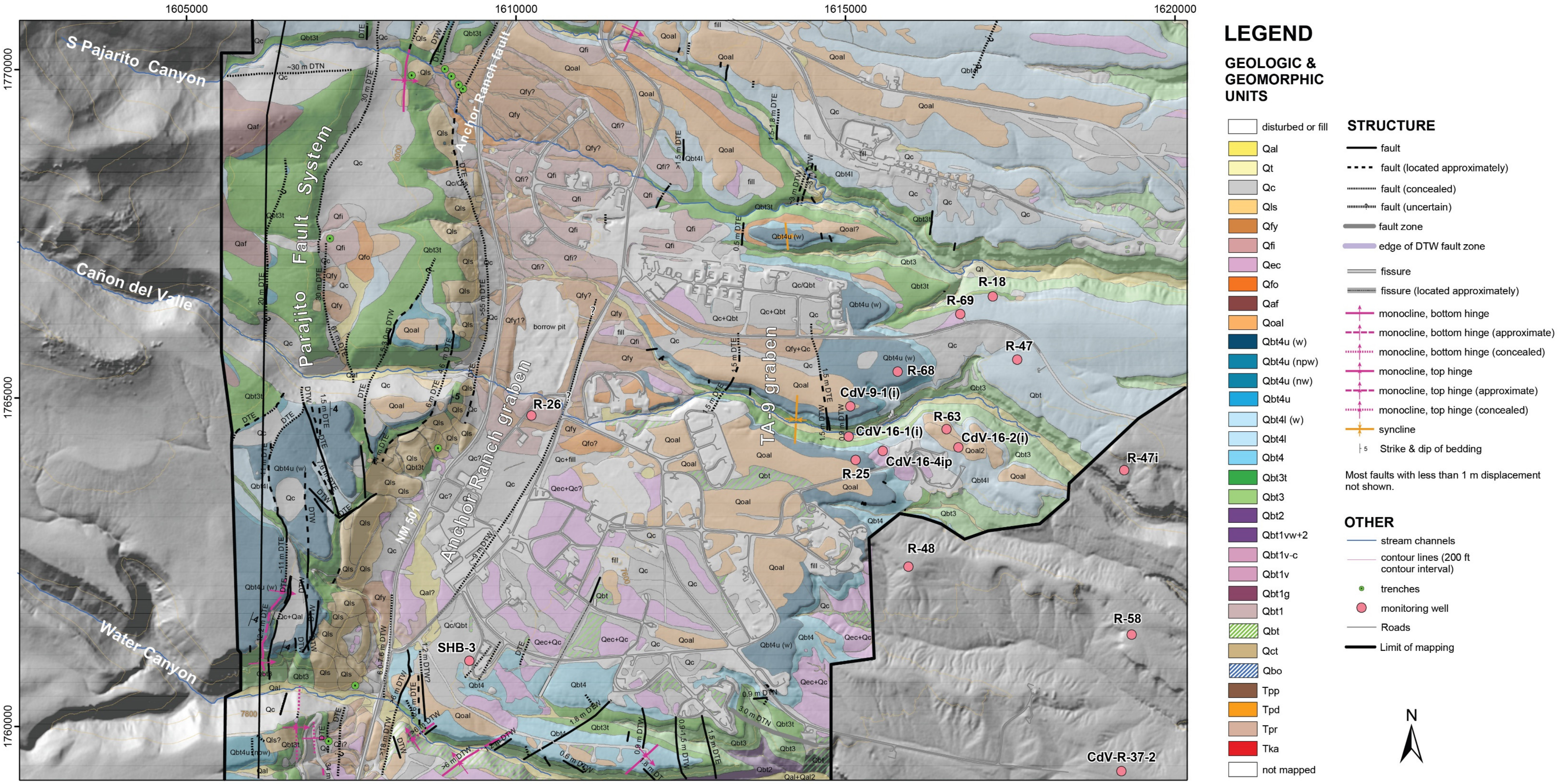

Modified from Lewis et al. 2009, 111708

Figure C-1.2-2 Surface geology and Pajarito Fault System in the vicinity of the RDX site

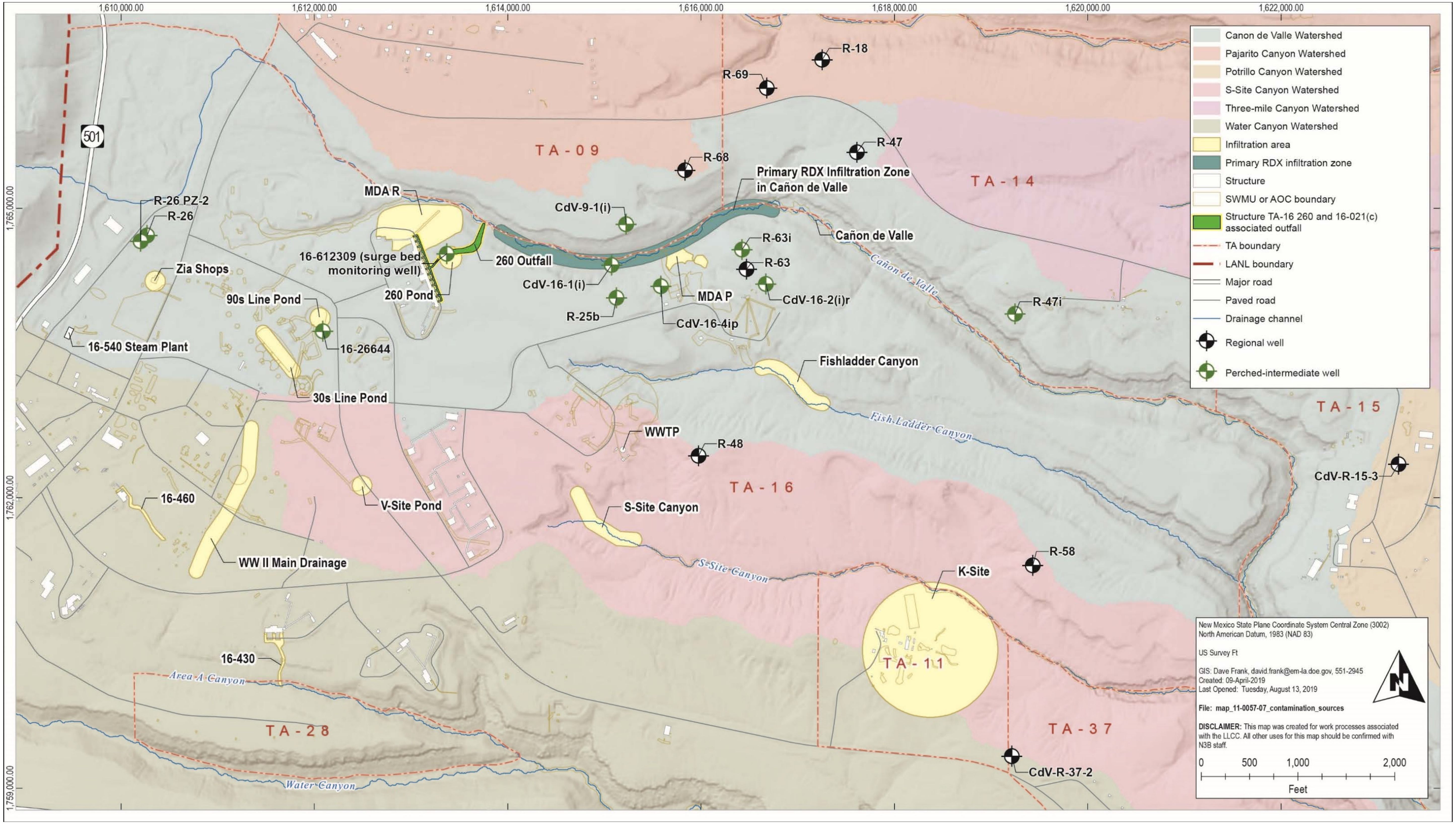

Note: RDX contaminated discharges from the 260 Outfall, combined with surface water of Cañon de Valle, were thought to infiltrate somewhere within the indicated zone.

Figure C-1.2-3 A potential area of higher infiltration of surface water is shown downcanyon of the 260 Outfall, within the area of the TA-09 graben

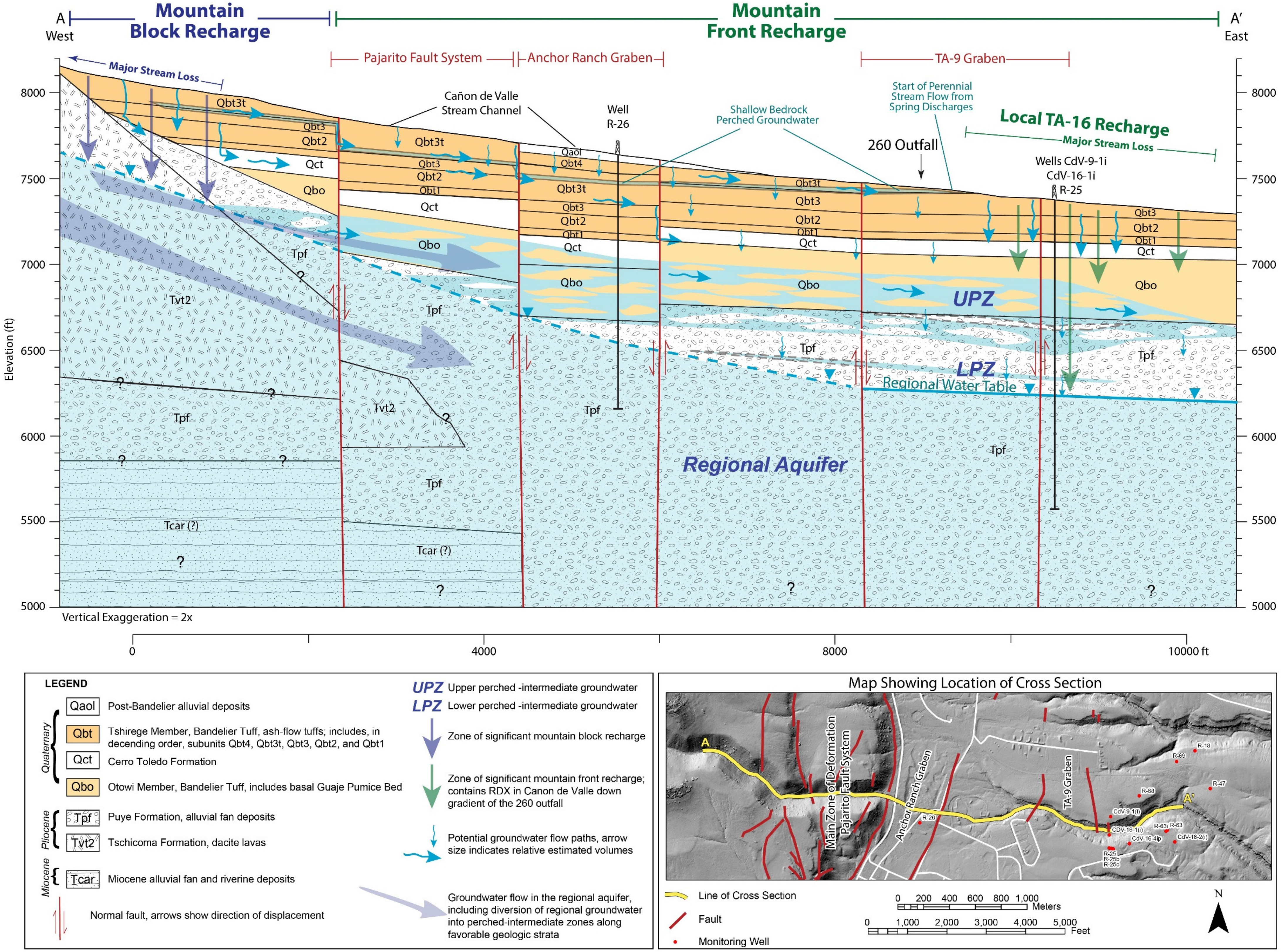

Notes: Mountain-block and mountain-front recharge are shown, along with arrows depicting dominant direction of groundwater flow. Arrows indicate a large source of recharge to the perched zones occurs from mountain-block and mountain-front recharge.

Figure C-1.2-4 Conceptual east-to-west cross-section showing the UPZ, LPZ, and regional aquifer

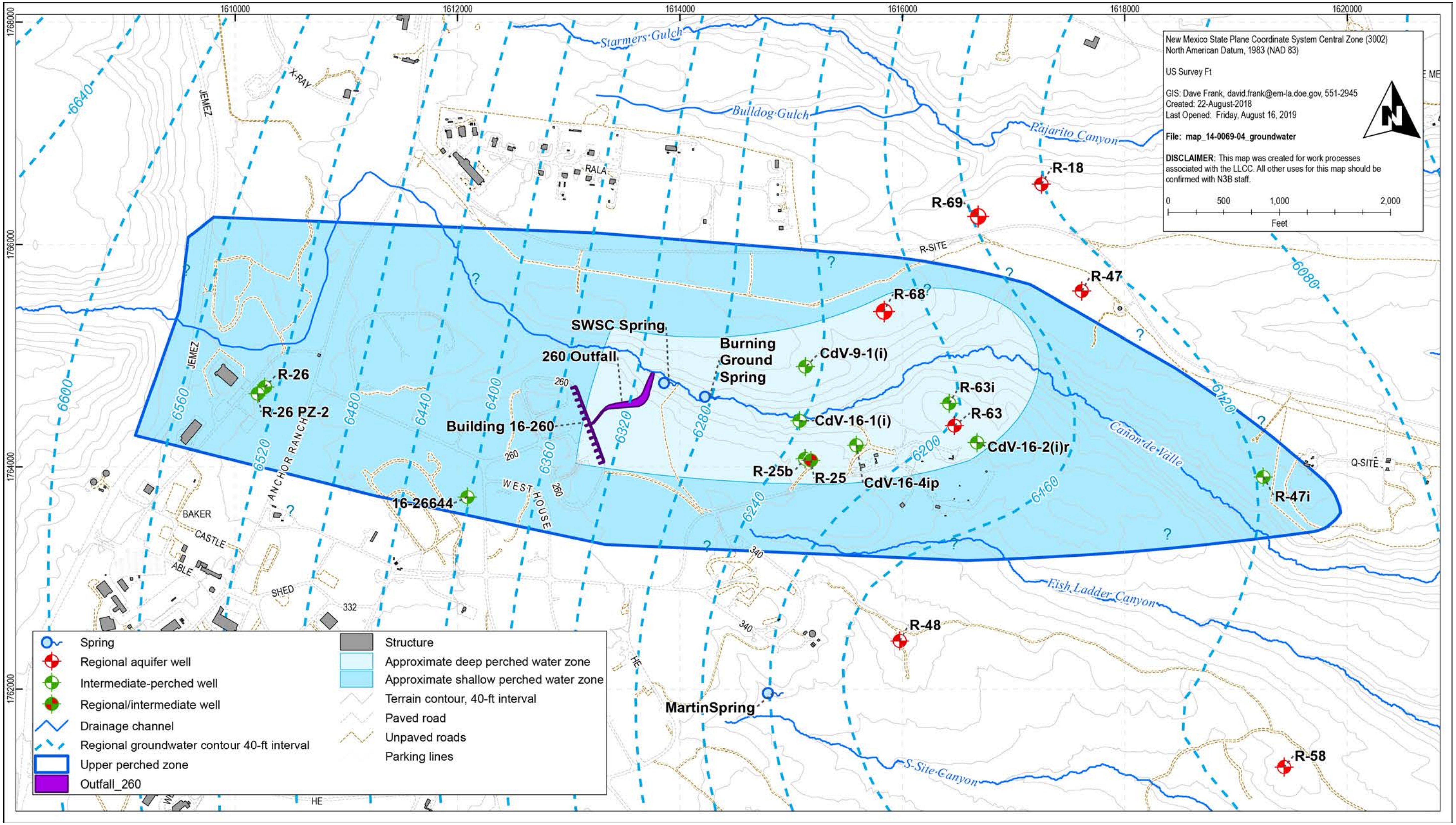

Figure C-1.2-5 Upper and lower extents of perched-intermediate aquifers with regional groundwater contours

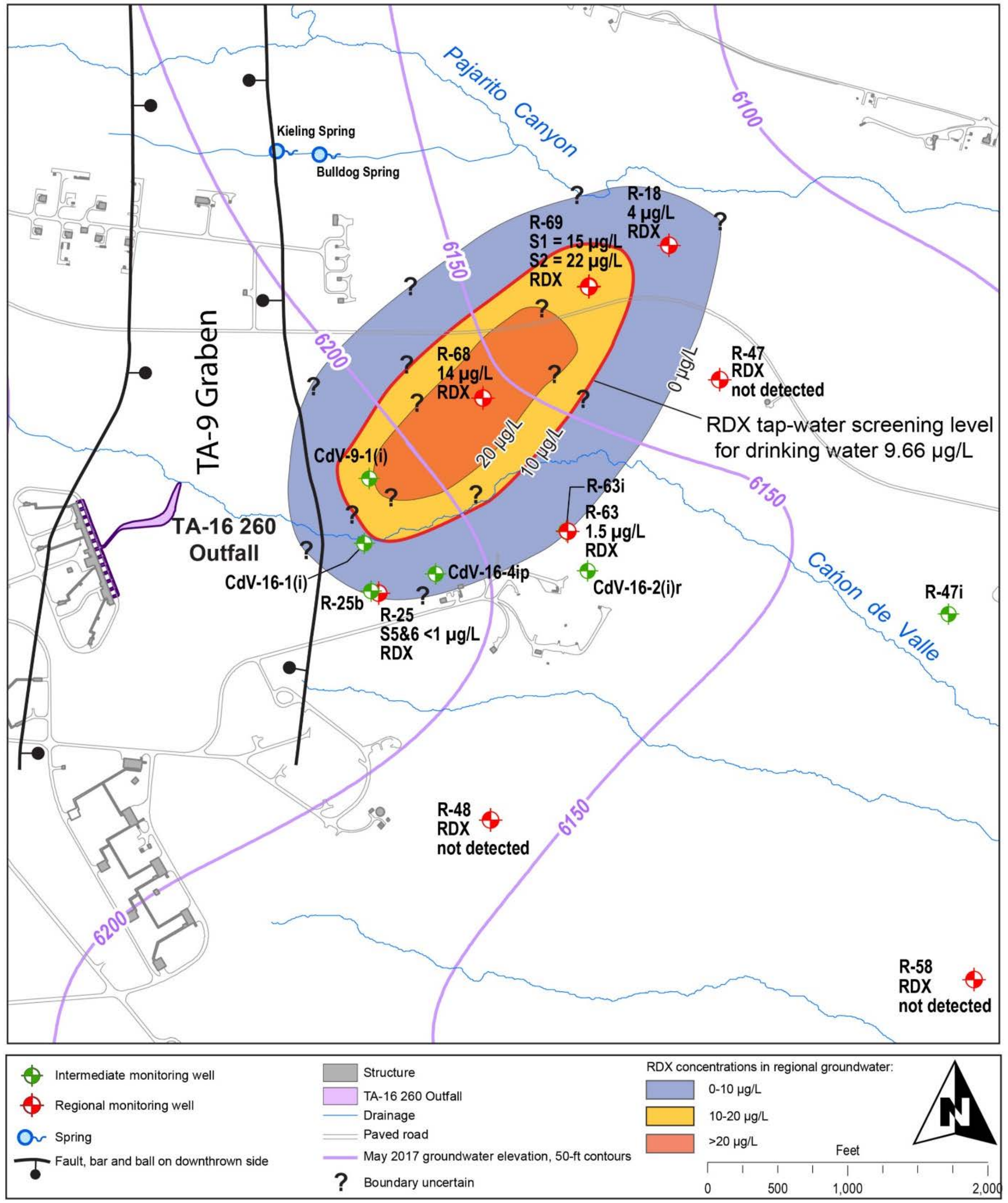

Figure C-1.2-6 Map view of RDX concentrations in the regional aquifer

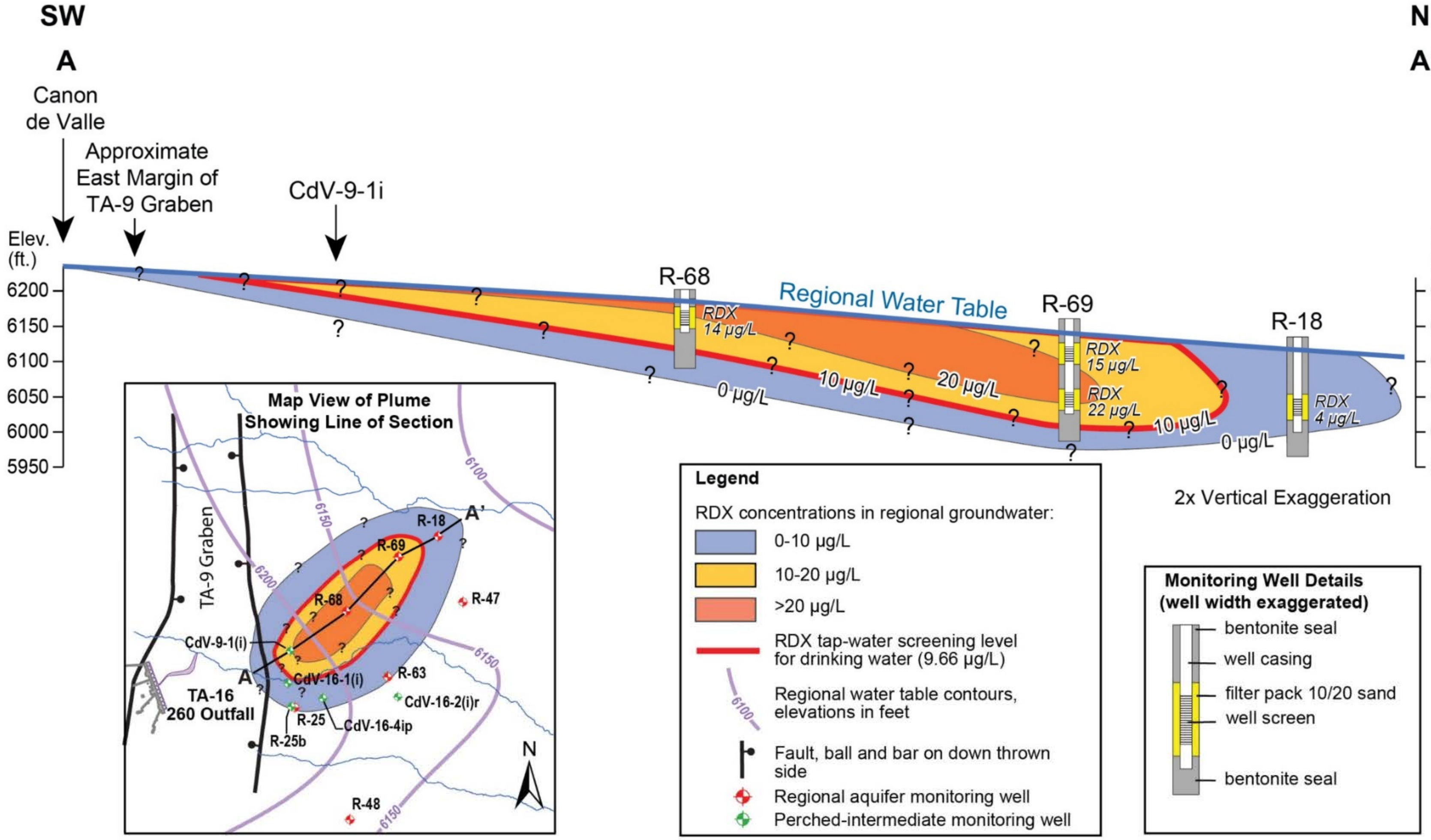

Figure C-1.2-7 Southwest to northeast cross-section of RDX concentrations in the regional aquifer

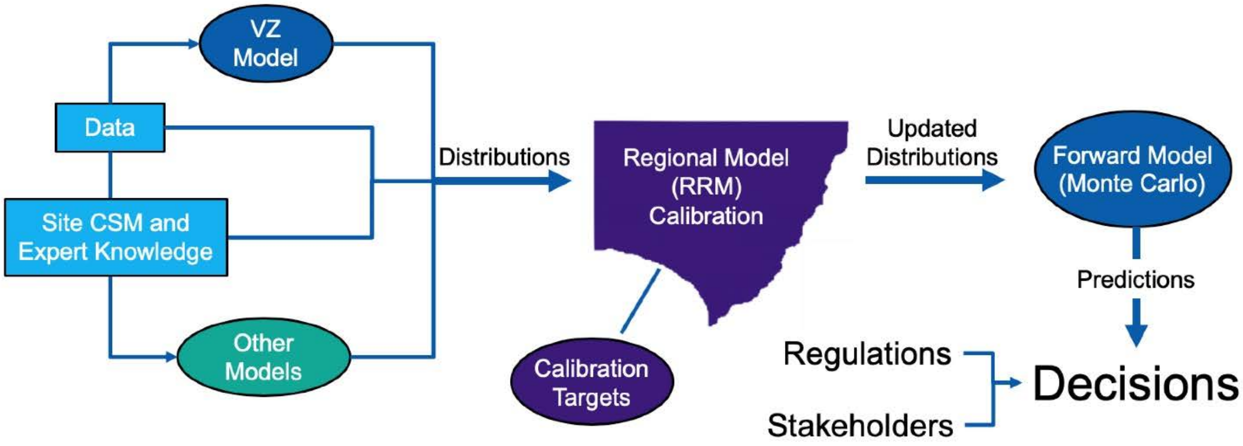

Figure C-1.3-1 Hierarchical modeling framework

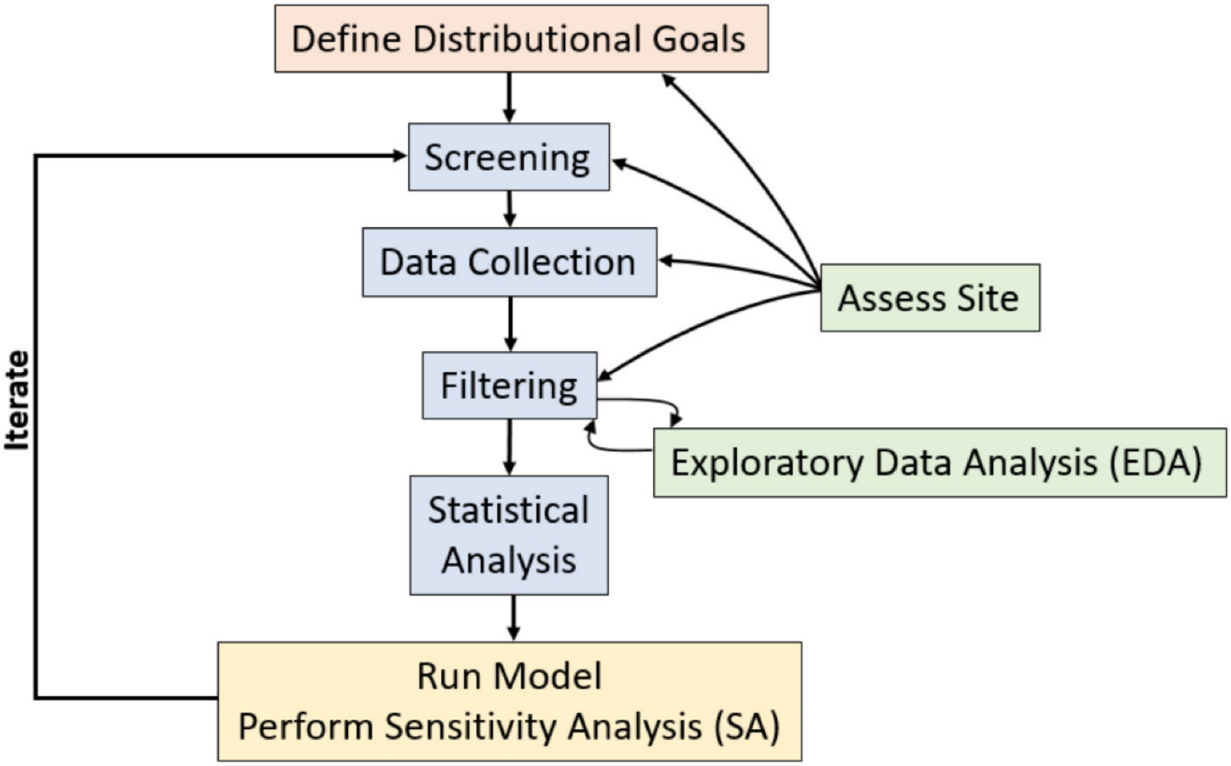

Figure C-1.3-2 Distribution development workflow

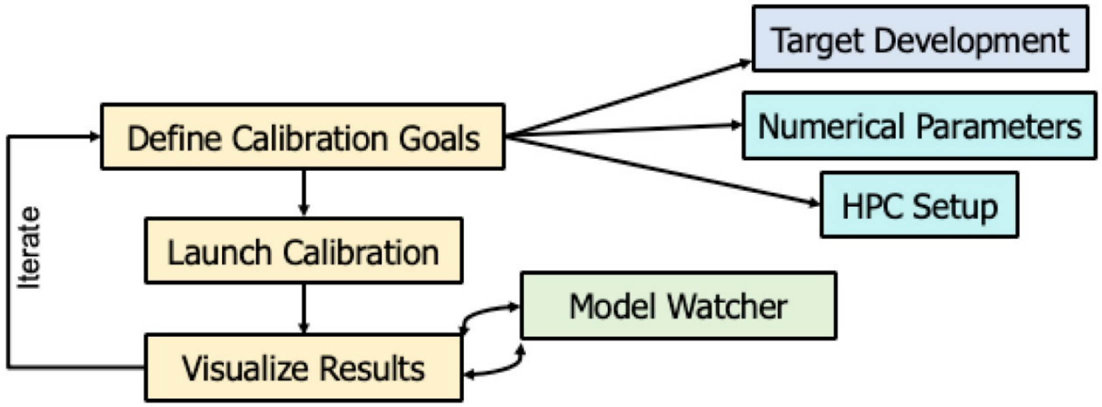

Figure C-1.3-3 **Individual calibration workflow**

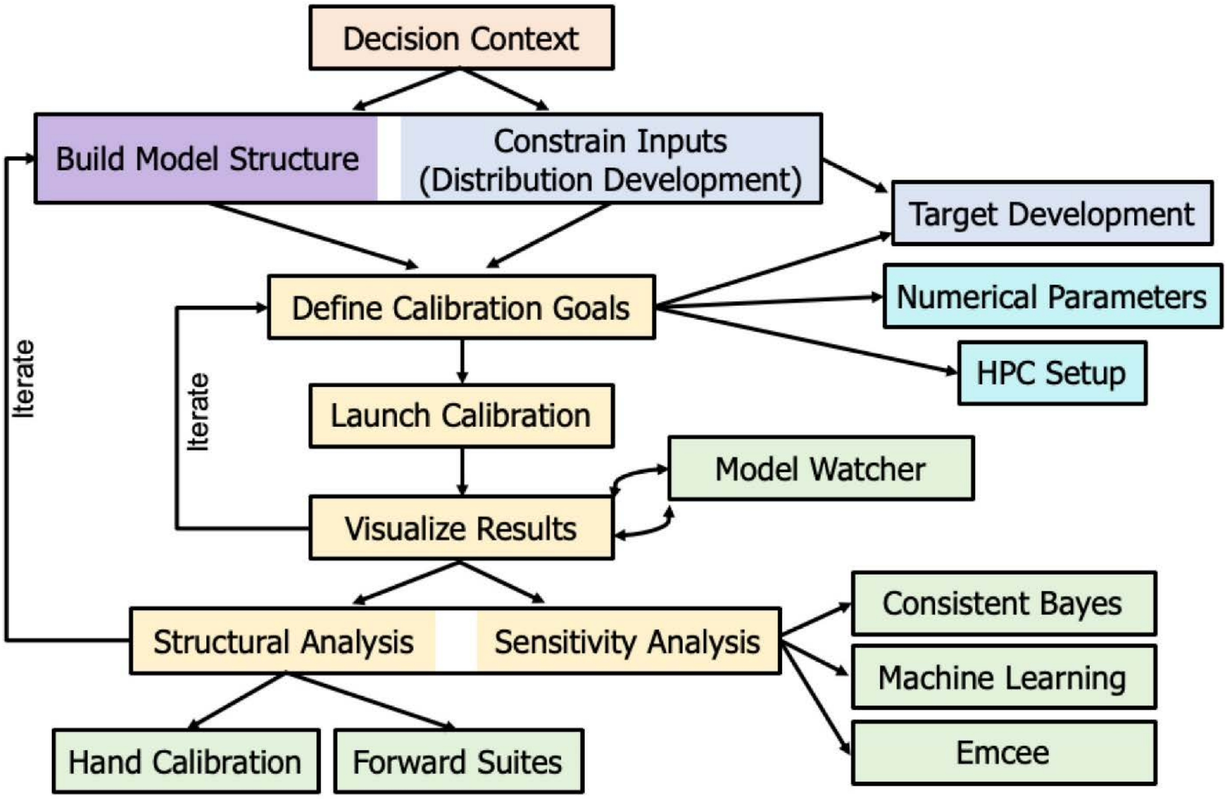

Figure C-1.3-4 **Full calibration workflow iterating back to model structure and distribution development to best understand the site**

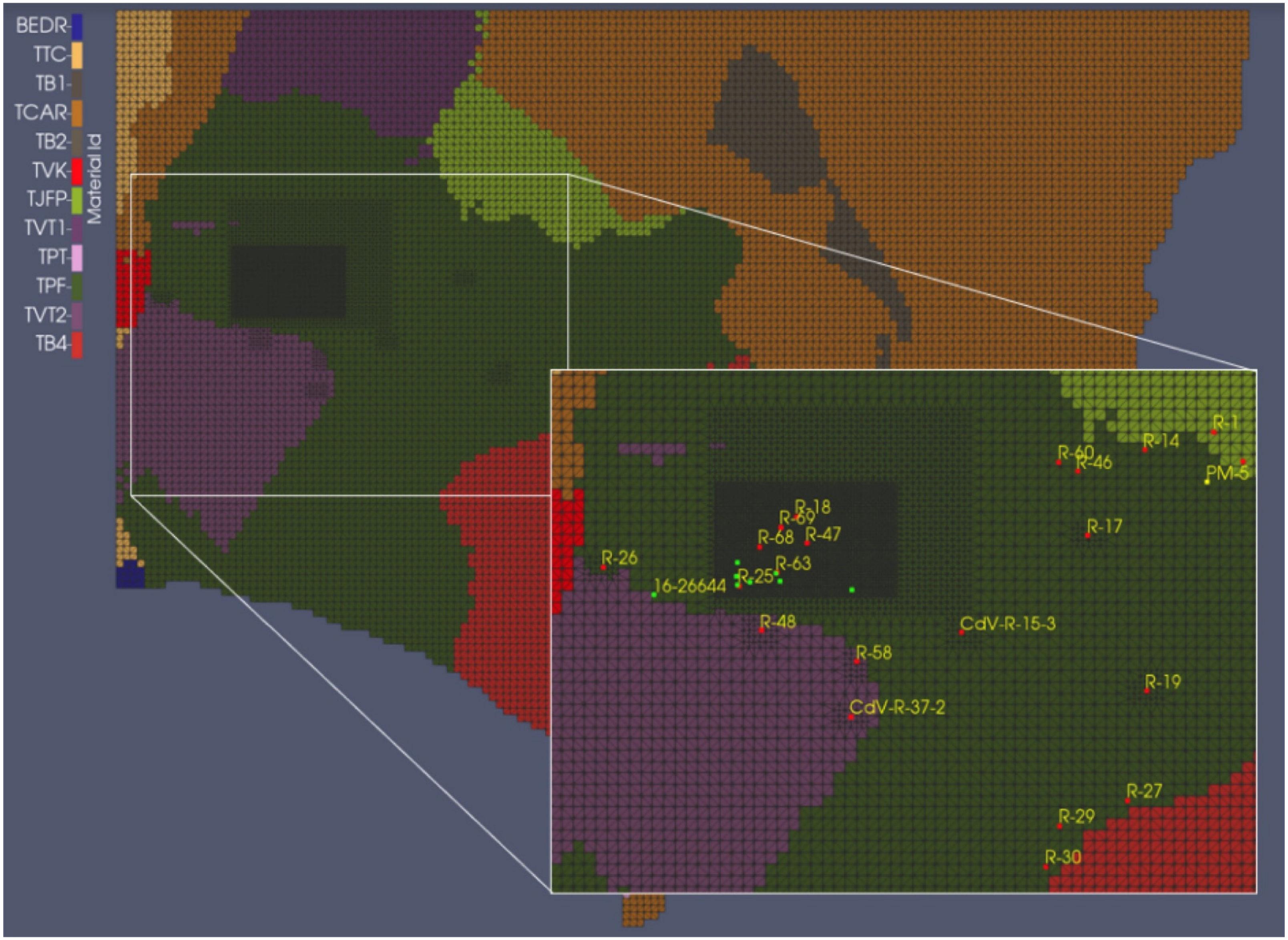

Note: Inset shows refined region with most well locations marked [well labels removed for clarity: CdV-16-4ip, CdV-9-1(i), R-47i, R-25b, CdV-16-1(i), R-63(i), and CdV-16-2(i)r].

Figure C-2.1-1 RRM discretization and geologic properties

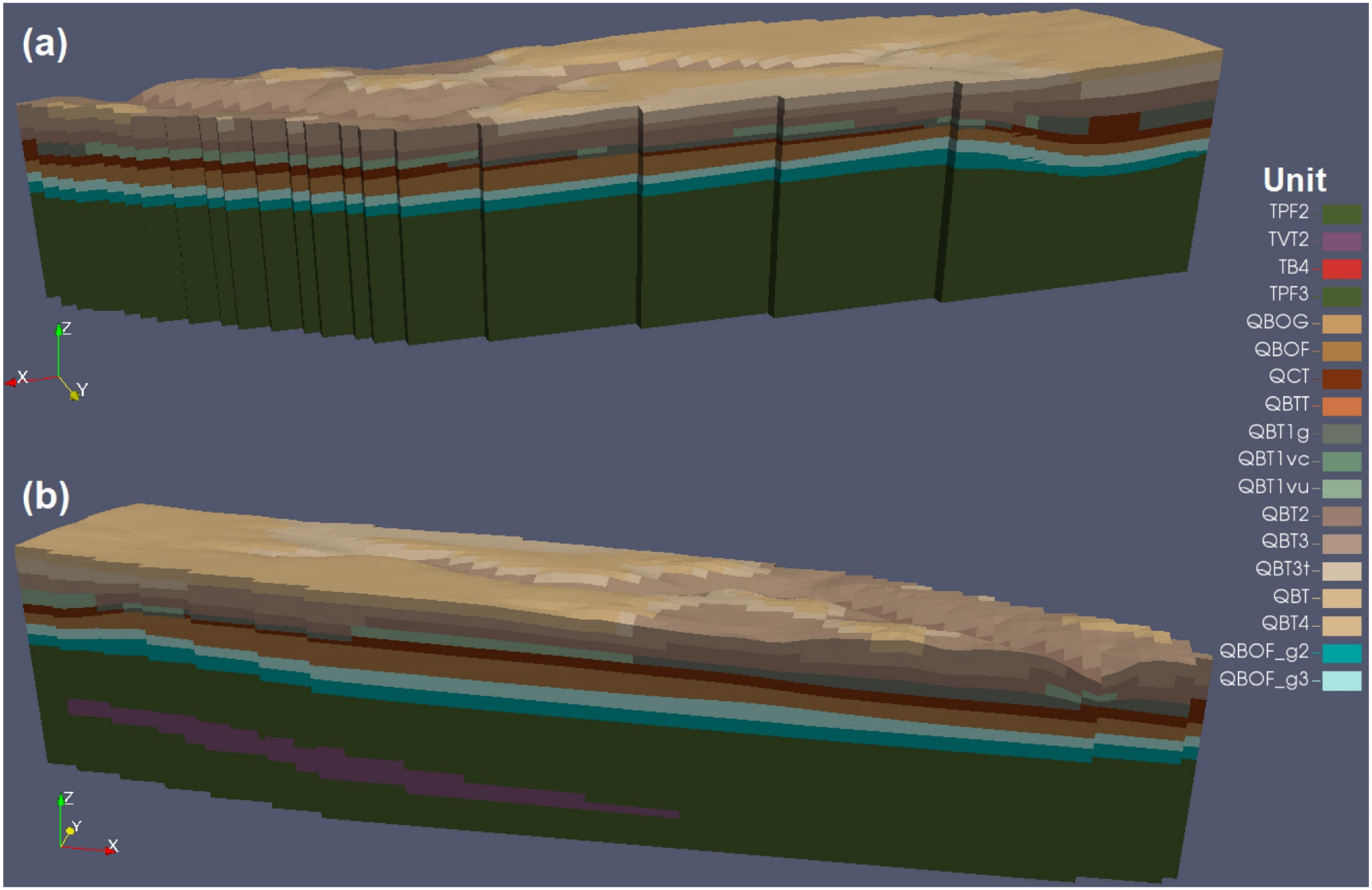

Figure C-2.2-1 RDX VZ/SZ (saturated zone) domain and geology, facing (a) the model's northern boundary and (b) the southern boundary

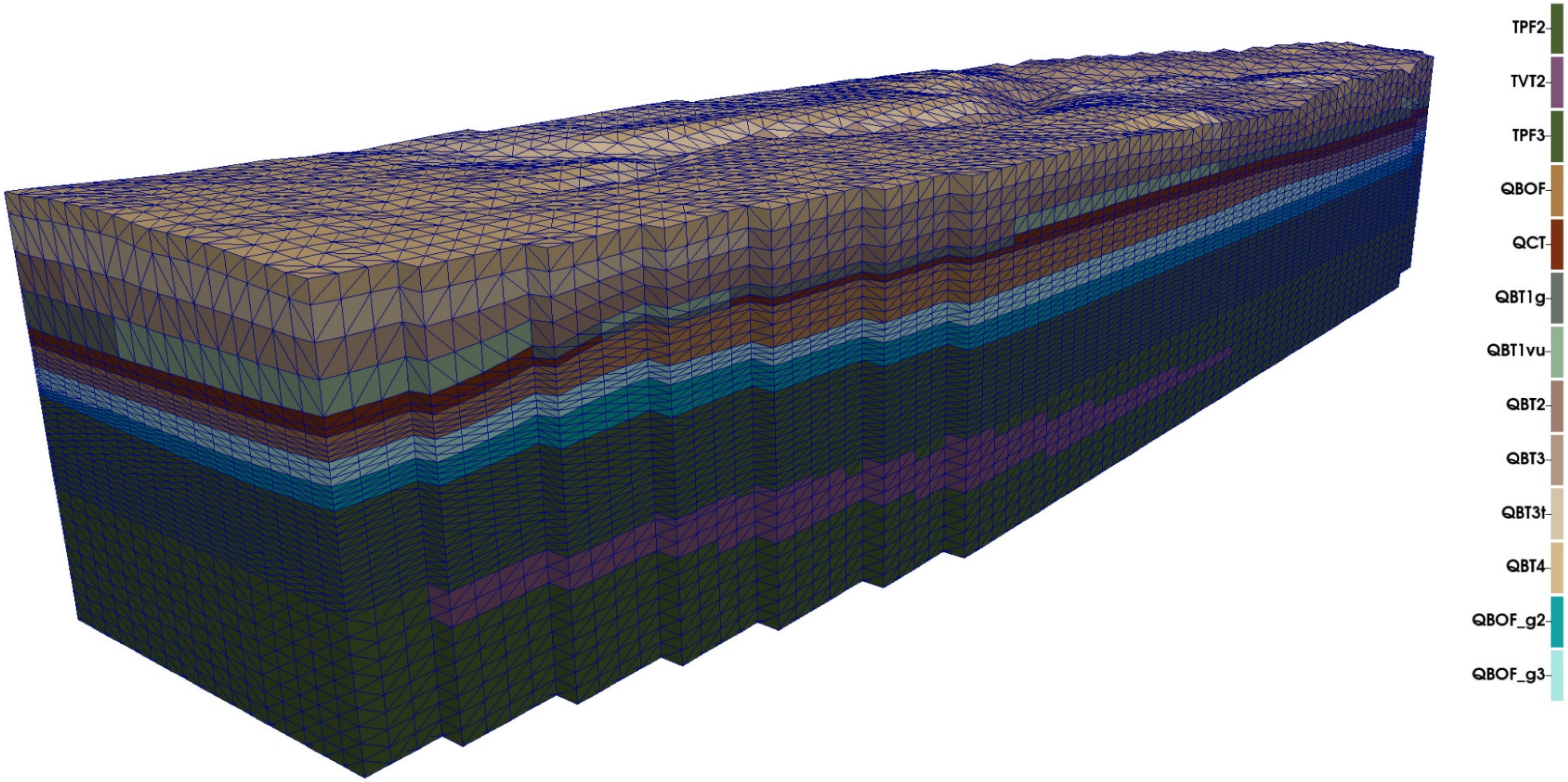

Figure C-2.2-2 RVZM mesh generated by LaGriT and plotted over the geologic framework model

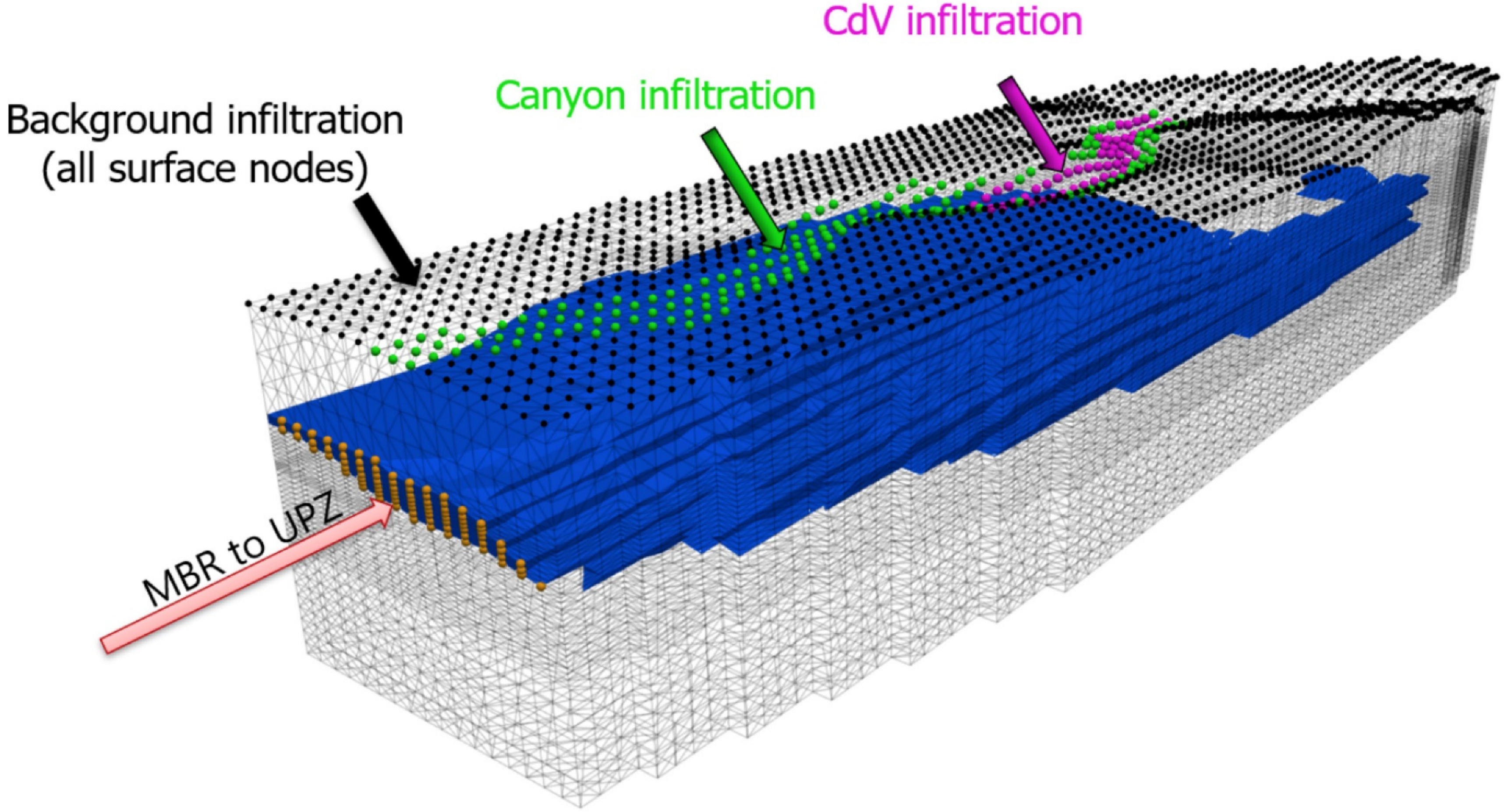

Note: MBR is mountain-block recharge; UPZ is upper perched zone, which is a saturated zone.

Figure C-2.2-3 **Variable locations of infiltration in the VZ model of the RDX site**

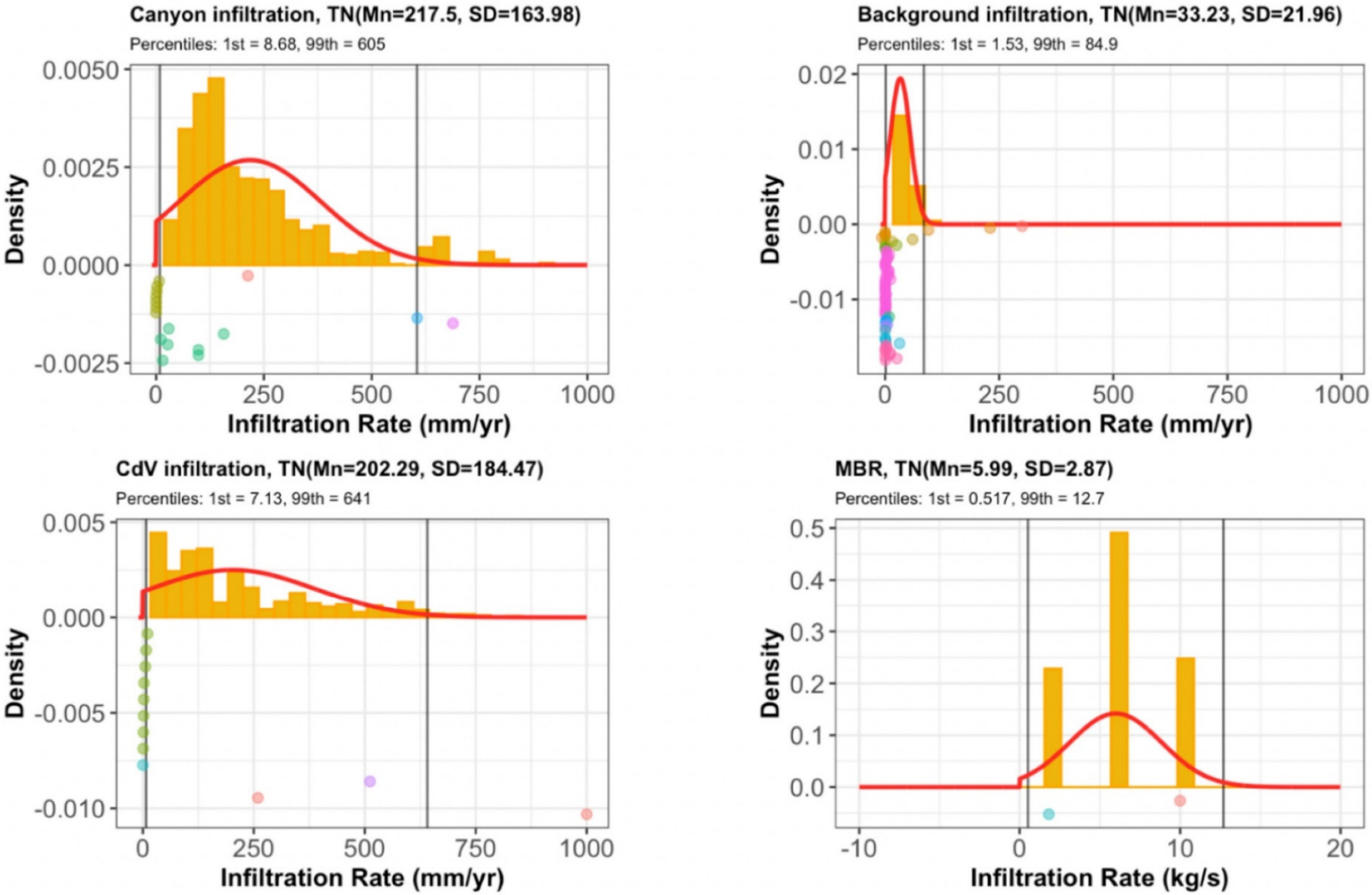

Notes: The distributions for canyon, background, and Cañon de Valle are in units of mm/yr, and the distribution for MBR is in kg/s. Data are shown below the distributions and are colored by reference source..

Figure C-2.2-4 **Probability distributions (shown as red lines) for background, canyon, Cañon de Valle, and mountain block recharge infiltration rate for use in the RVZM.**

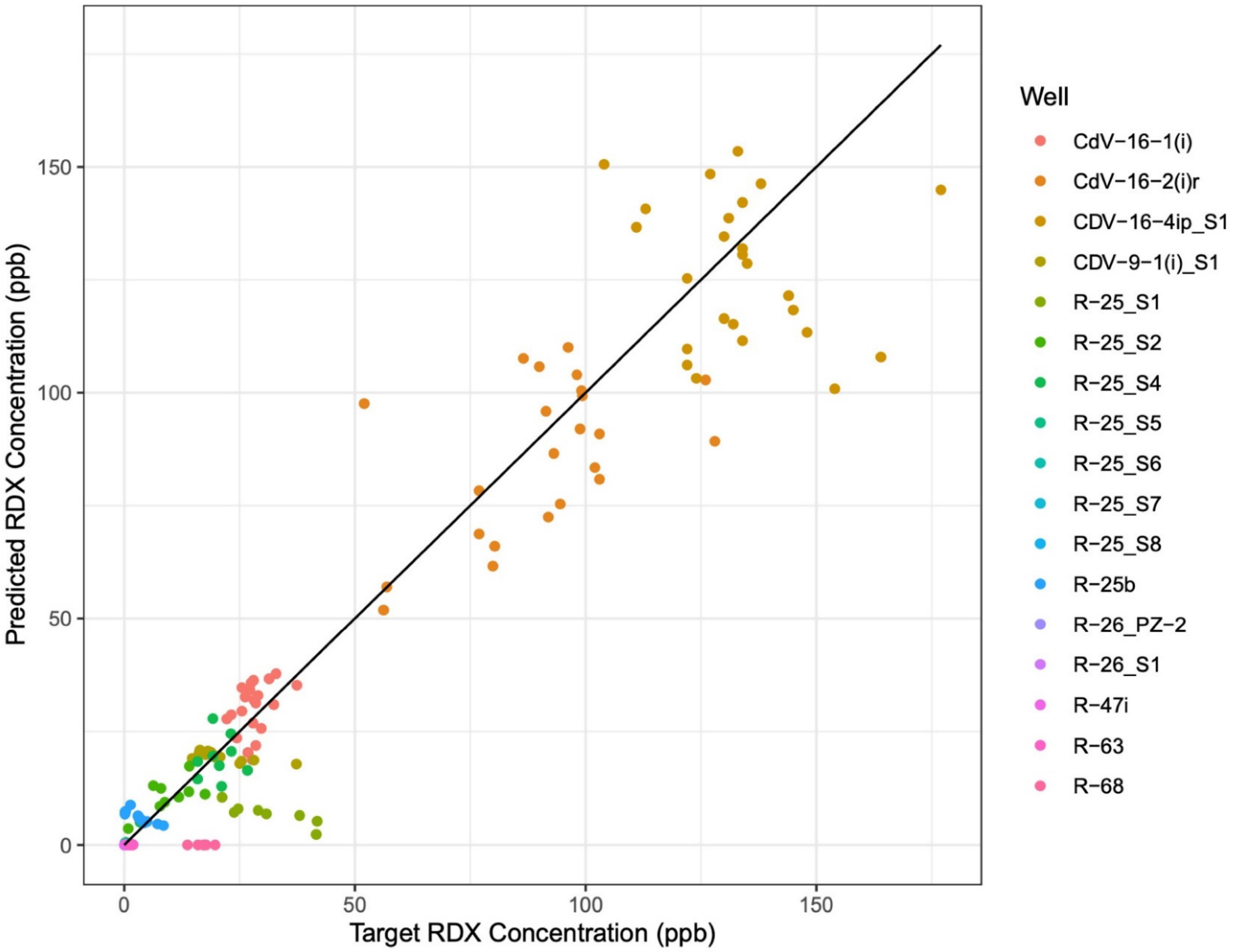

Figure C-2.2-5 Scatter-plot of targets and simulated values of RDX concentration for all wells used in Calibration 3

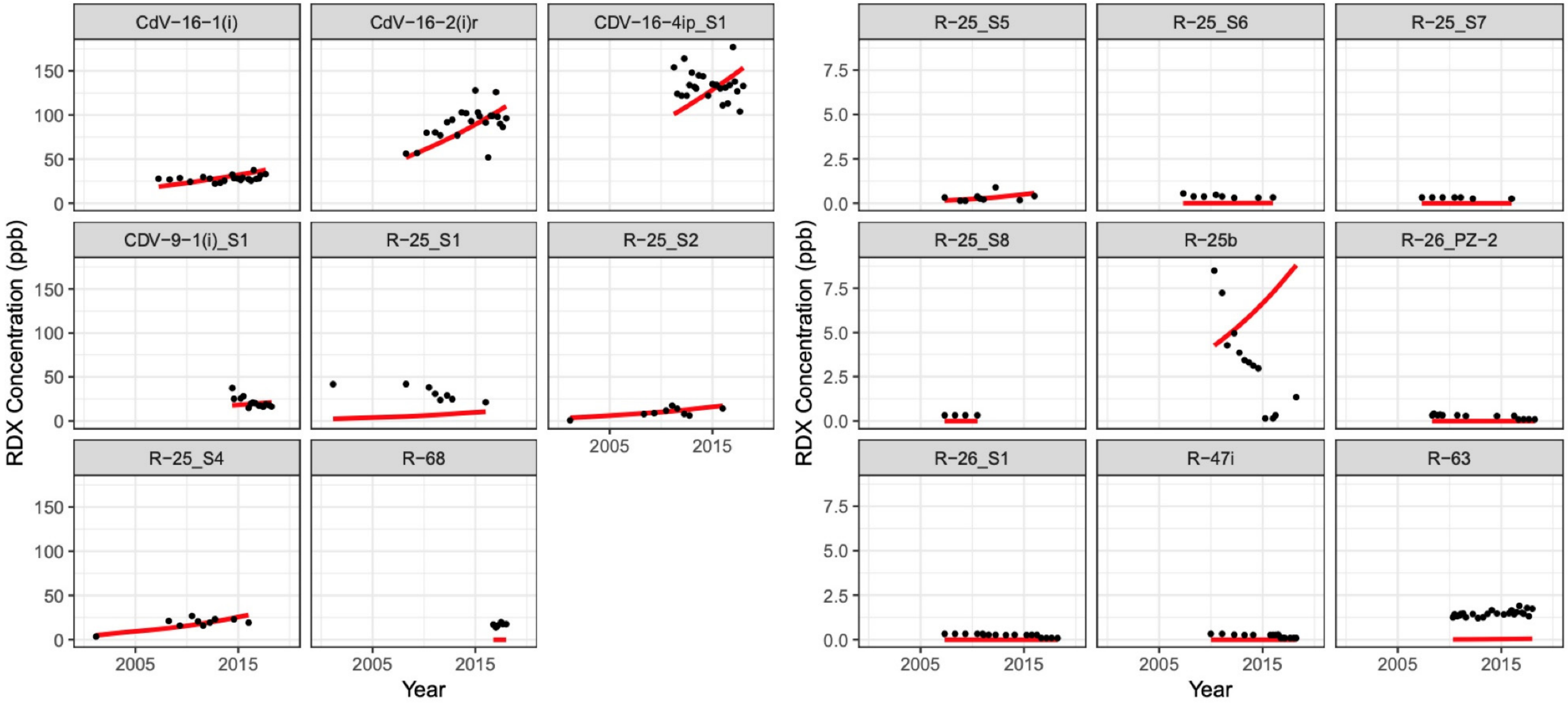

Figure C-2.2-6 Trend plots of targets and simulated values of RDX concentrations for all wells for Calibration 3

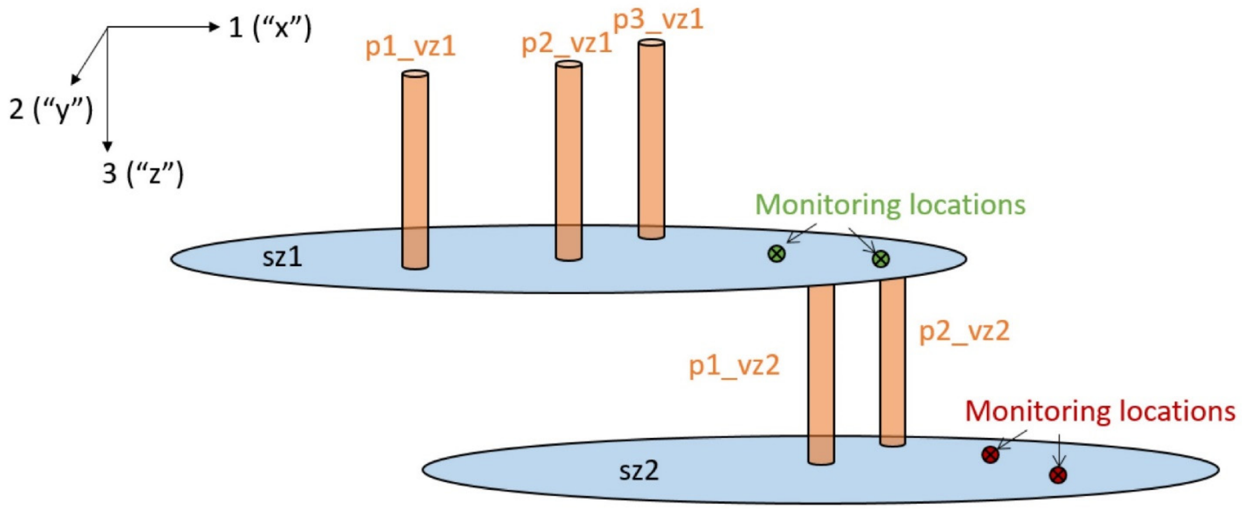

Figure C-2.2-7 The P&D screening tool allows for fast inverse analysis based on monitoring well data, based on flexible geometries of vadose zone “drip points” and perched saturated zones

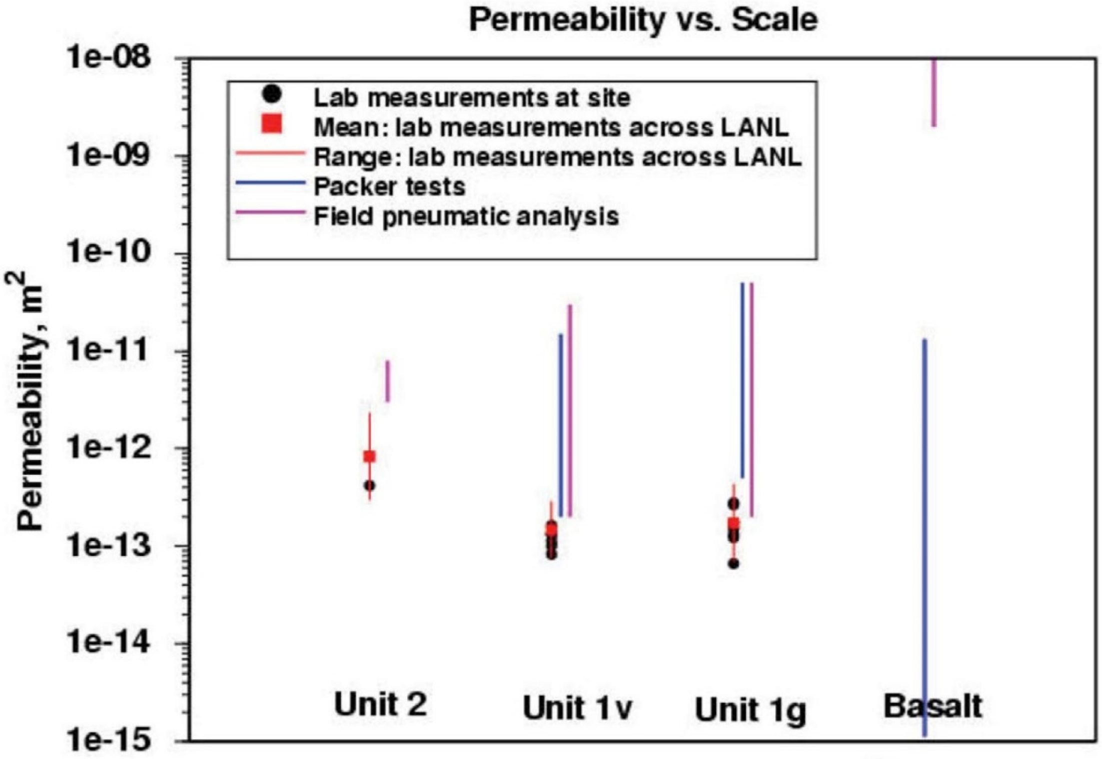

Note: Laboratory scale basalt permeability estimated to be on the order of 1e-18m^2.

Figure C-2.2-8 Permeability as a function of measurement scale for Bandelier Tuff (units Qbt 1g, Qbt 1v, and Qbt 2) and basalts

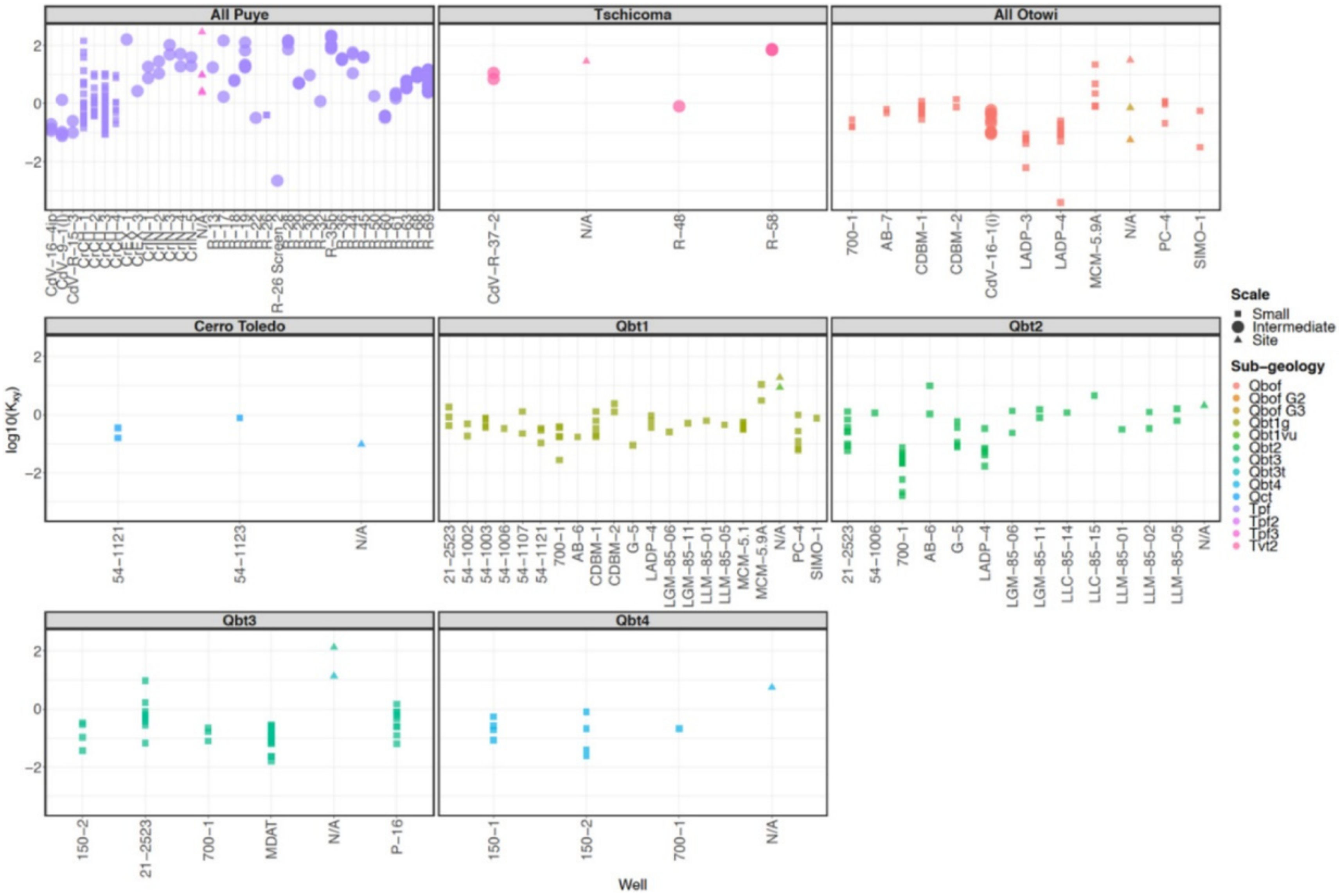

Notes: The wells are separated based on geology grouping, while colors are used to represent the specific geologic unit designation given in the original reference. The size of points represents the spatial scale of a record to draw greater attention to the points considered to provide more meaningful information.

Figure C-2.2-9 K_{xy} **(ft/day), log10 transformed, observed at each well**

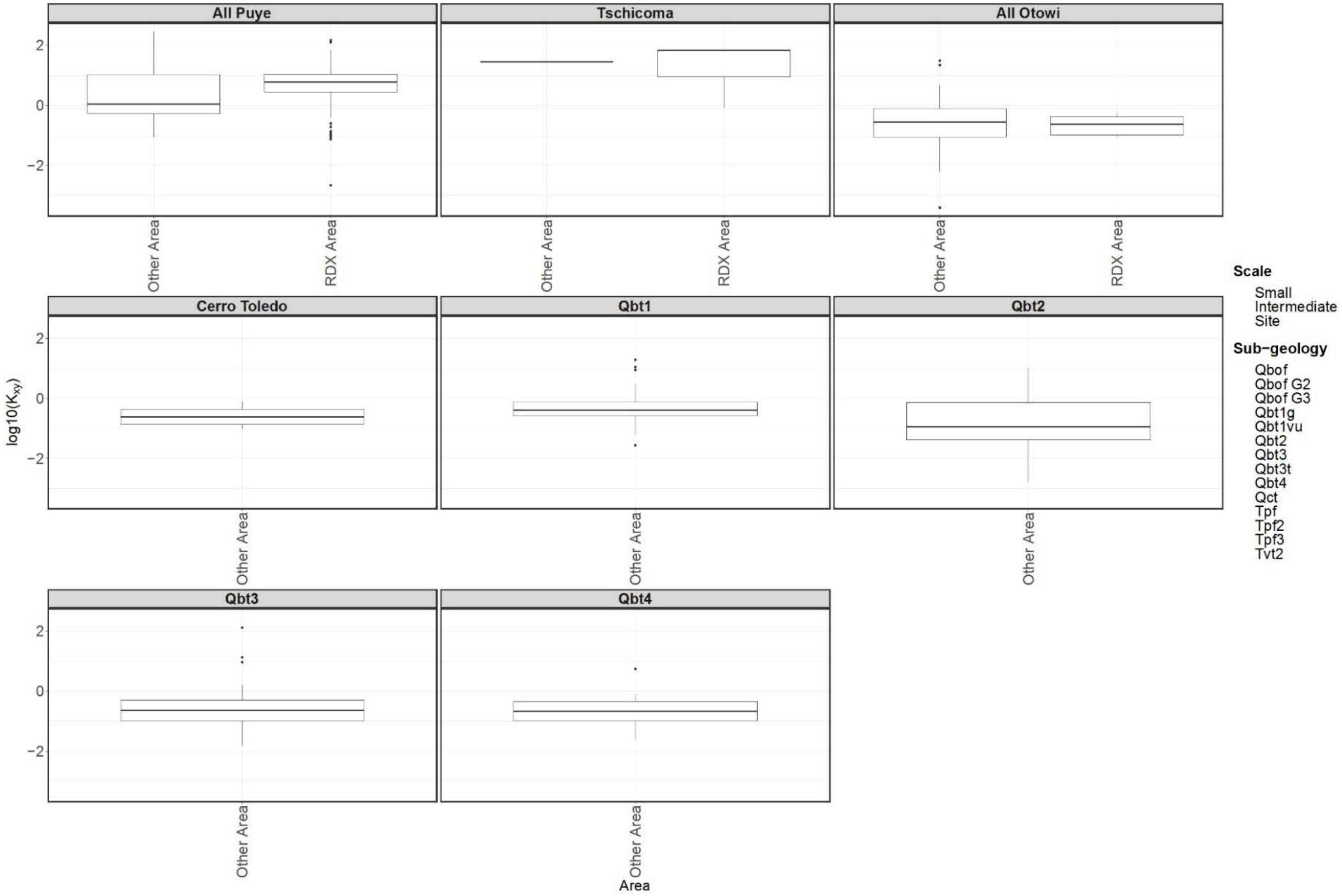

Notes: Points were provided a horizontal jitter (shift) to separate overlapping values. Boxplots are included to help compare quantiles across areas.

Figure C-2.2-10 K_{xy} data (ft/day), log10 transformed, displayed by area, geology, and scale, with separate plots for each geology group

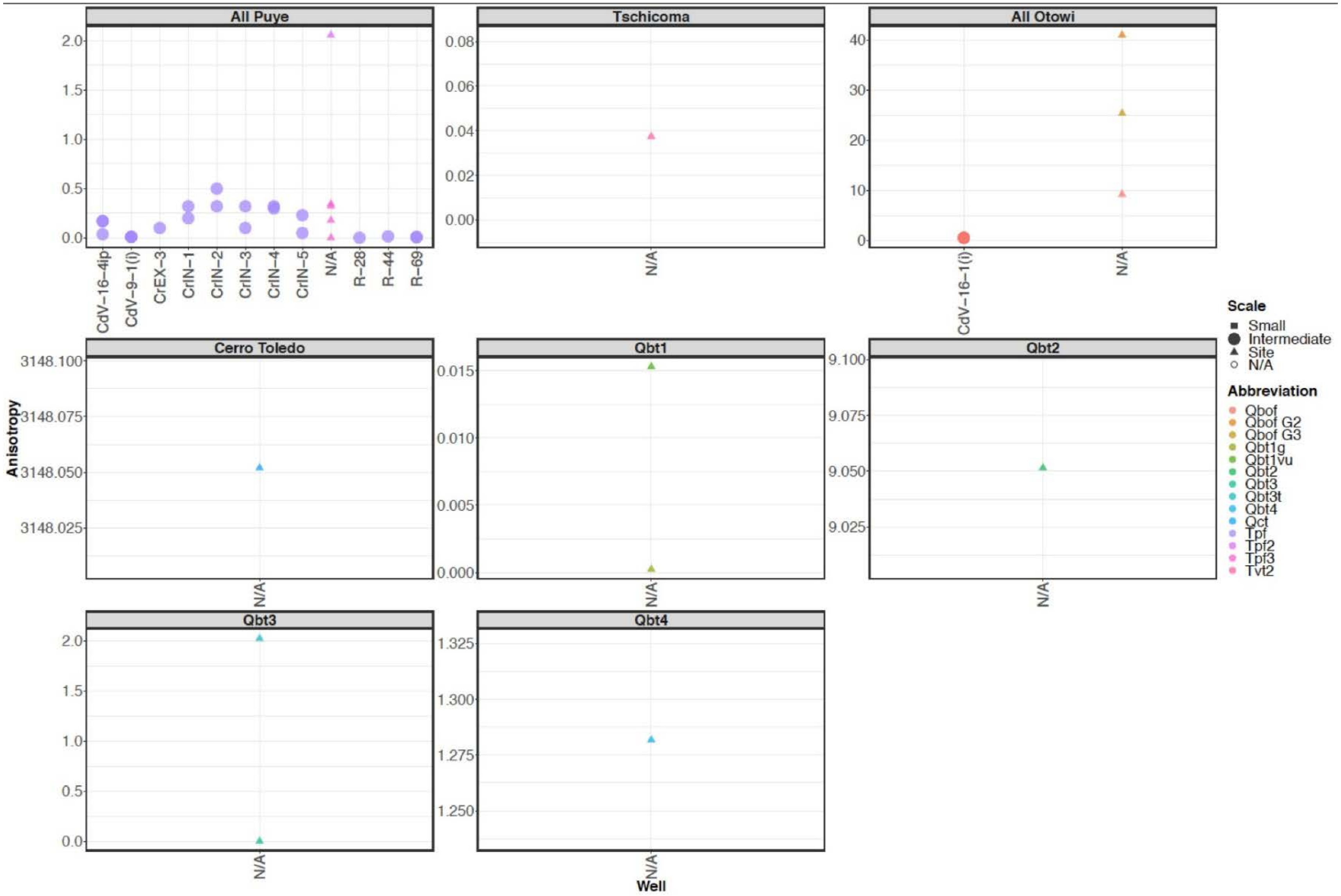

Notes: Data that are not associated with a specific well are labeled as N/A. The data are separated based on the geology group to which they belong, while colors are used to represent the specific geologic unit designation given in the original reference.

Figure C-2.2-11 Anisotropies (K_z/K_{xy}) by well

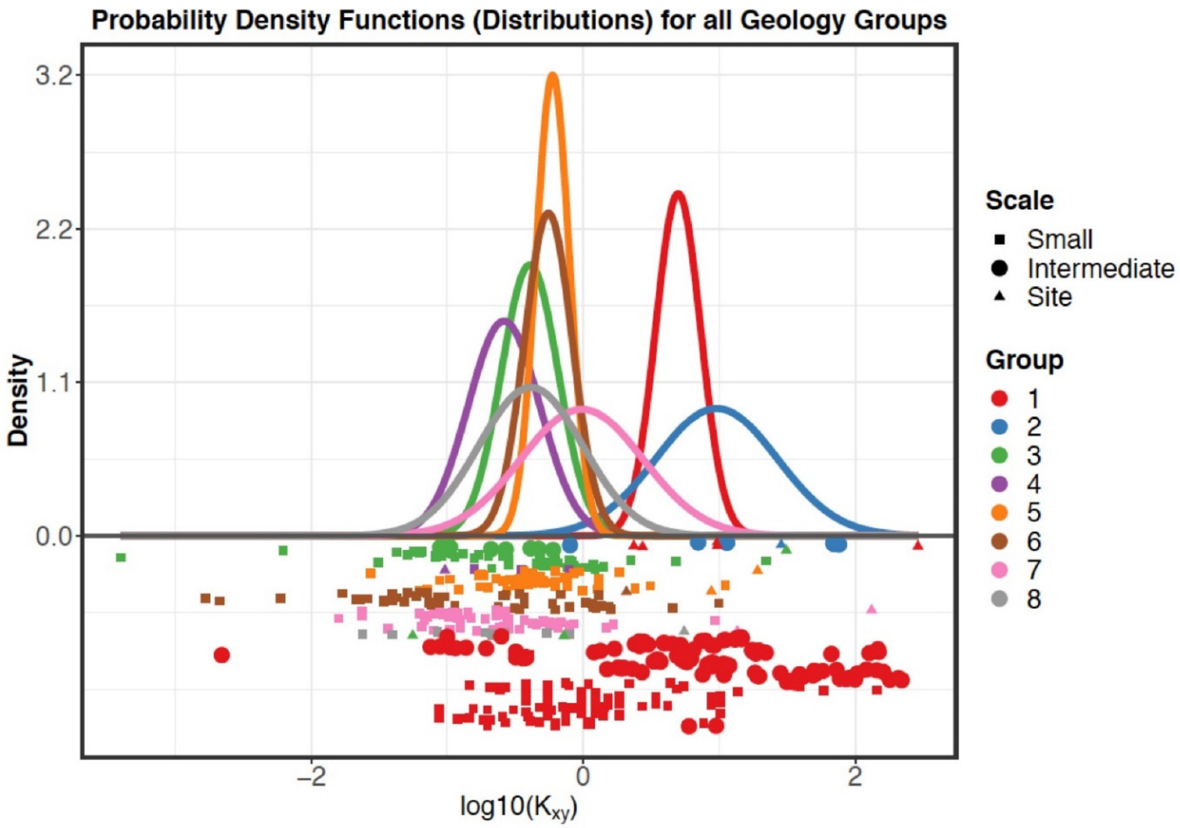

Note: Observed data are plotted alongside the distributions colored by the group they represent.

Figure C-2.2-12 Hydraulic conductivity (K_{xy}, in log10 ft/day) distributions for each geology group

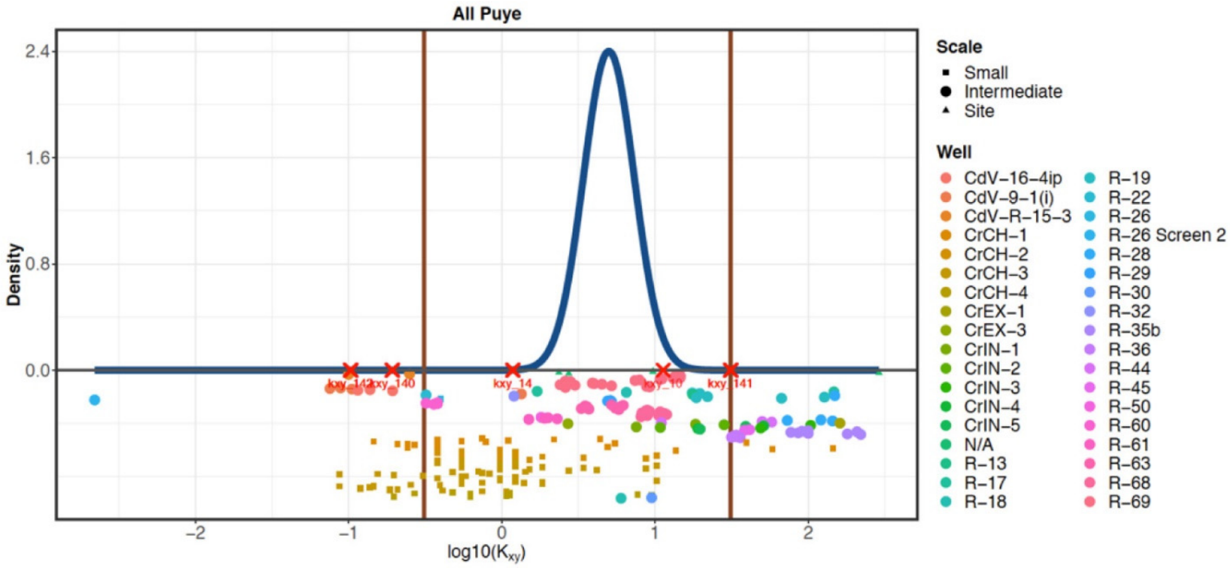

Notes: Observed data are plotted alongside the distributions colored by the well from which they were sampled. The vertical brown lines on the plots show the prior constraints used in calibration (LANL 2018b), and the red Xs are the results of that calibration for specific geologic units in the RVZM.

Figure C-2.2-13 Hydraulic conductivity (K_{xy}, in log10 ft/day) distributions for Group 1 (blue)

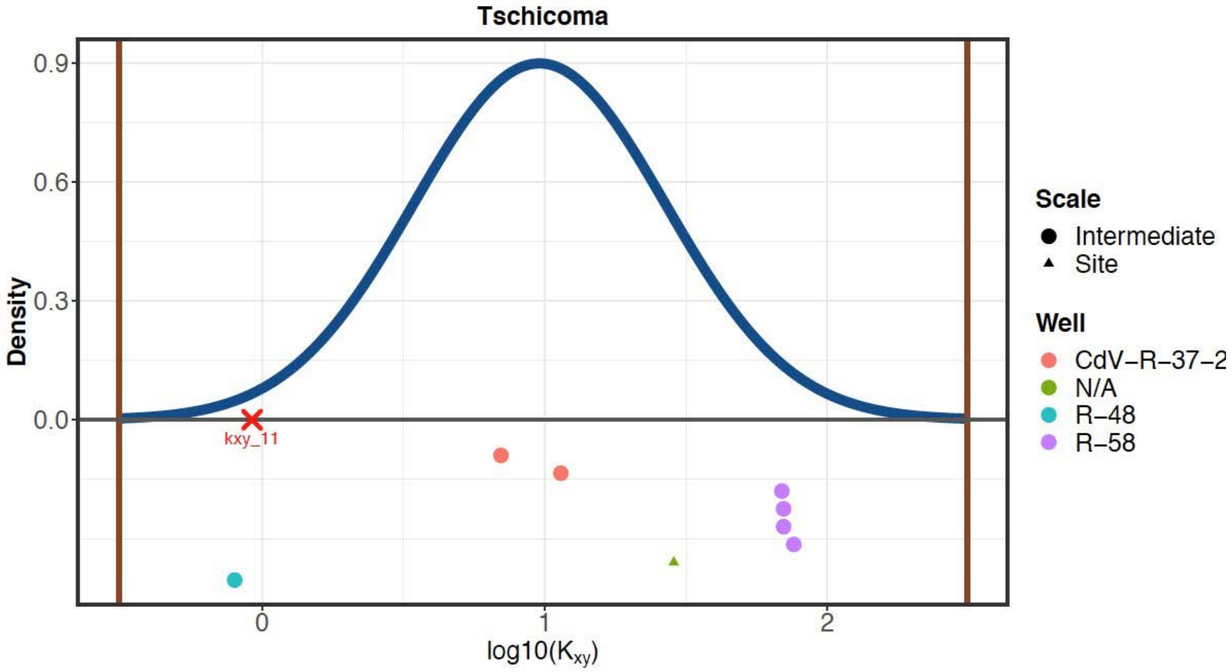

Notes: Observed data are plotted alongside the distributions colored by the well from which they were sampled. The vertical brown lines on the plots show the prior constraints used in calibration (LANL 2018b), and the red Xs are the results of that calibration for specific geologic units in the RVZM.

Figure C-2.2-14 Hydraulic conductivity (K_{xy}, in log10 ft/day) distributions for Group 2 (blue)

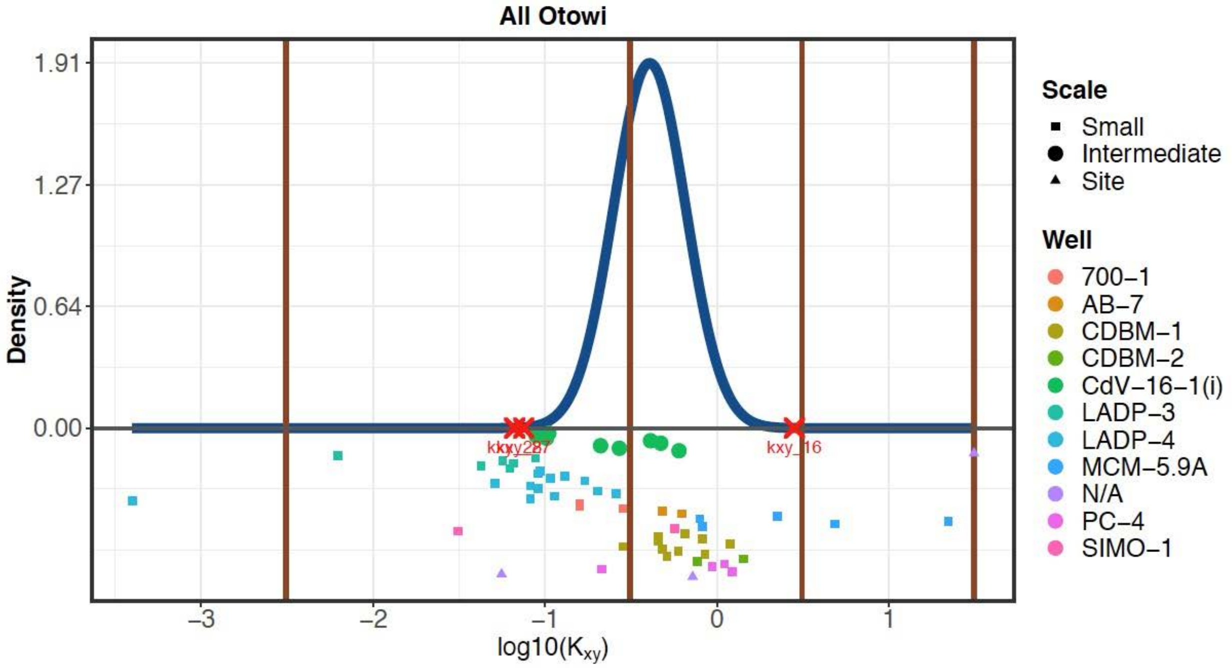

Notes: Observed data are plotted alongside the distributions colored by the well from which they were sampled. The vertical brown lines on the plots show the prior constraints used in calibration (LANL 2018b), and the red Xs are the results of that calibration for specific geologic units in the RVZM.

Figure C-2.2-15 Hydraulic conductivity (K_{xy}, in log10 ft/day) distributions for Group 3 (blue)

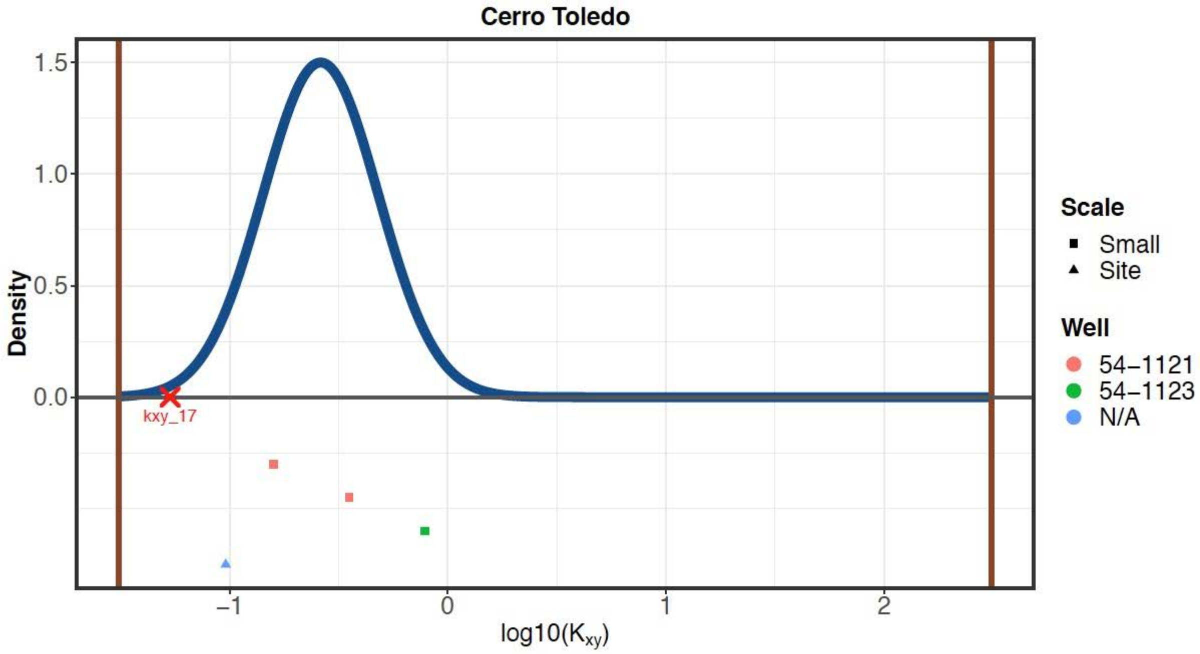

Notes: Observed data are plotted alongside the distributions colored by the well from which they were sampled. The vertical brown lines on the plots show the prior constraints used in calibration (LANL 2018b), and the red Xs are the results of that calibration for specific geologic units in the RVZM.

Figure C-2.2-16 Hydraulic conductivity (K_{xy}, in log10 ft/day) distributions for Group 4 (blue)

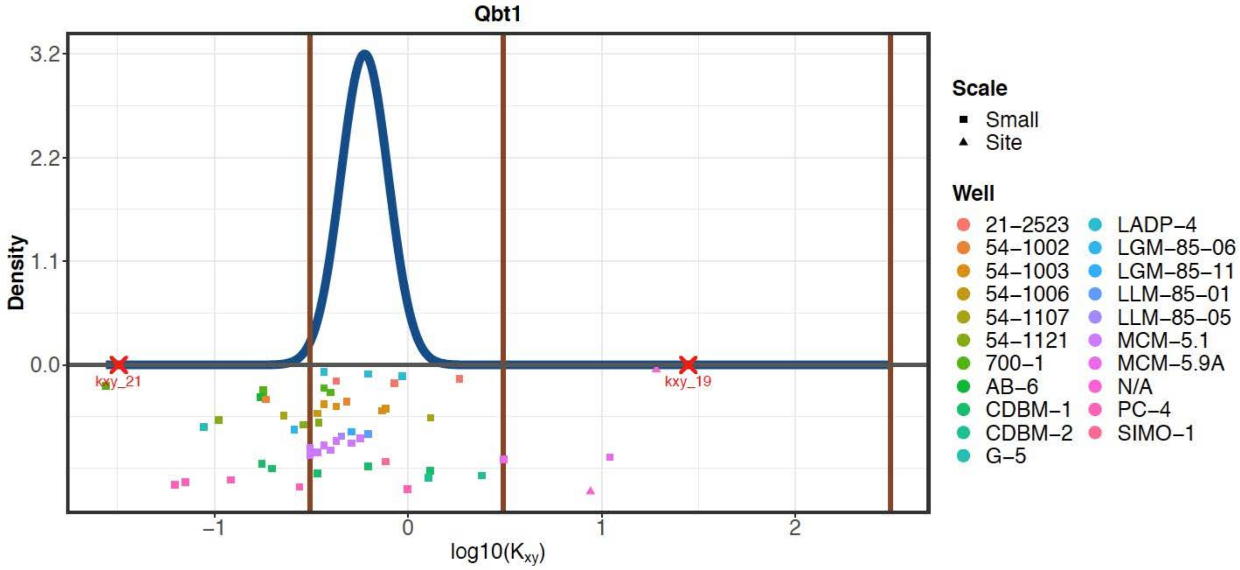

Notes: Observed data are plotted alongside the distributions colored by the well from which they were sampled. The vertical brown lines on the plots show the prior constraints used in calibration (LANL 2018b), and the red Xs are the results of that calibration for specific geologic units in the RVZM.

Figure C-2.2-17 Hydraulic conductivity (K_{xy}, in log10 ft/day) distributions for Group 5 (blue)

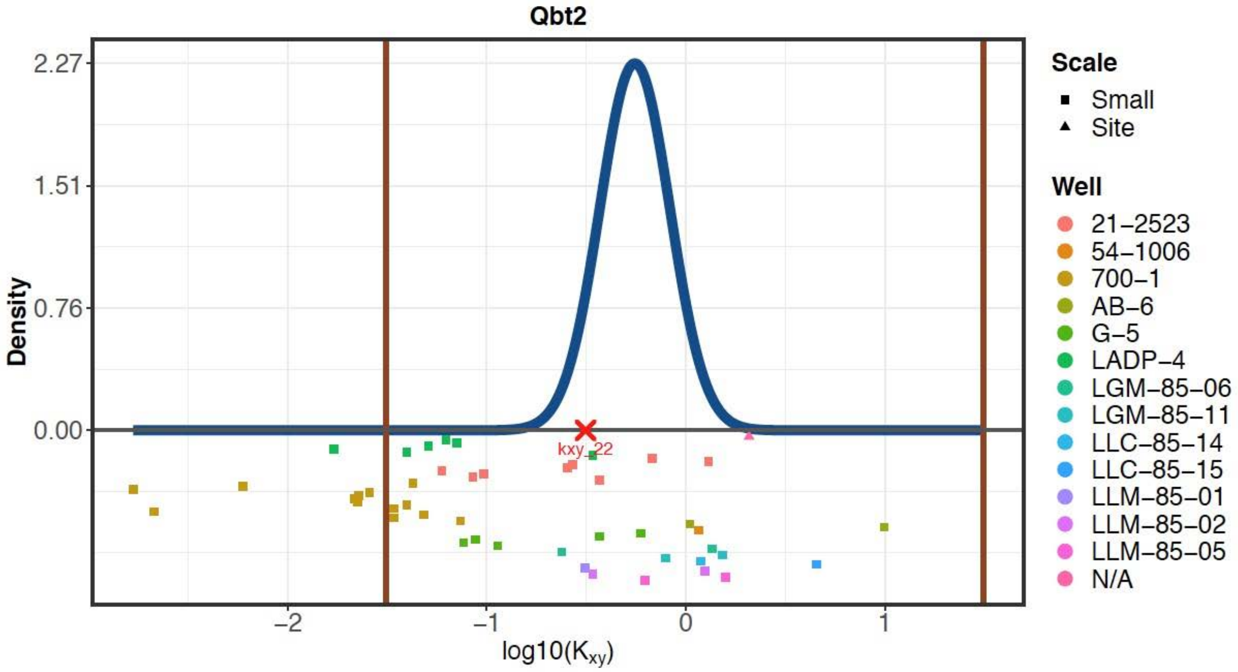

Notes: Observed data are plotted alongside the distributions colored by the well from which they were sampled. The vertical brown lines on the plots show the prior constraints used in calibration (LANL 2018b), and the red Xs are the results of that calibration for specific geologic units in the RVZM.

Figure C-2.2-18 Hydraulic conductivity (*K_{xy}*, in log10 ft/day) distributions for Group 6 (blue)

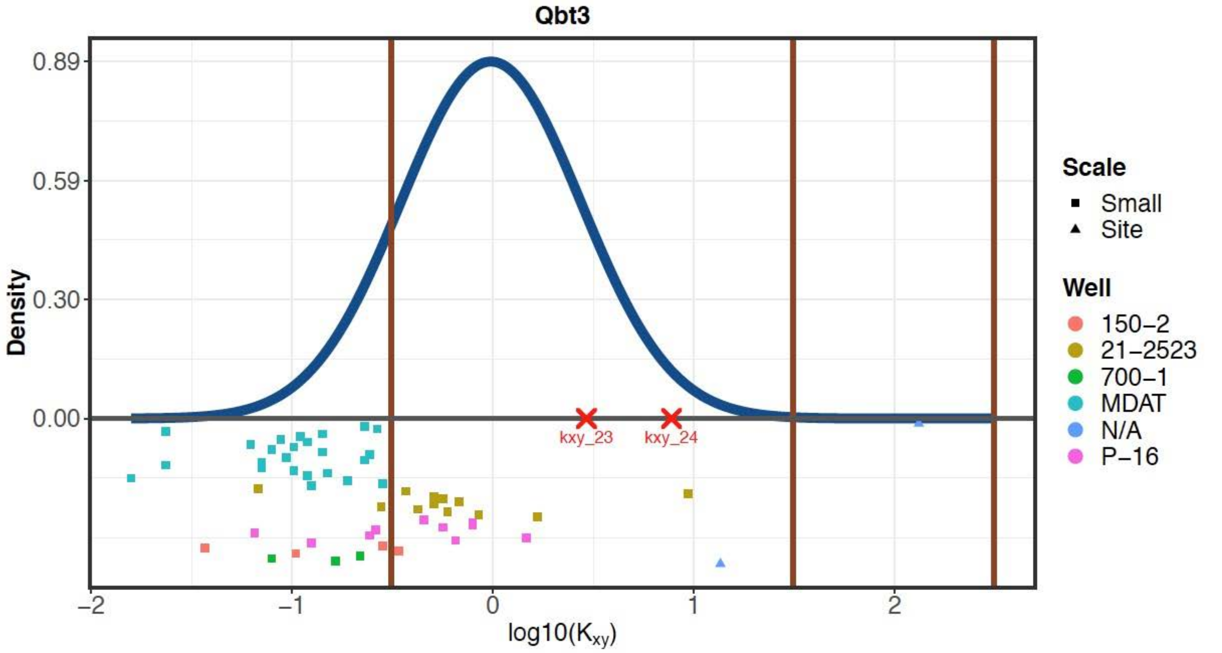

Notes: Observed data are plotted alongside the distributions colored by the well from which they were sampled. The vertical brown lines on the plots show the prior constraints used in calibration (LANL 2018b), and the red Xs are the results of that calibration for specific geologic units in the RVZM.

Figure C-2.2-19 Hydraulic conductivity (*K_{xy}*, in log10 ft/day) distributions for Group 7 (blue)

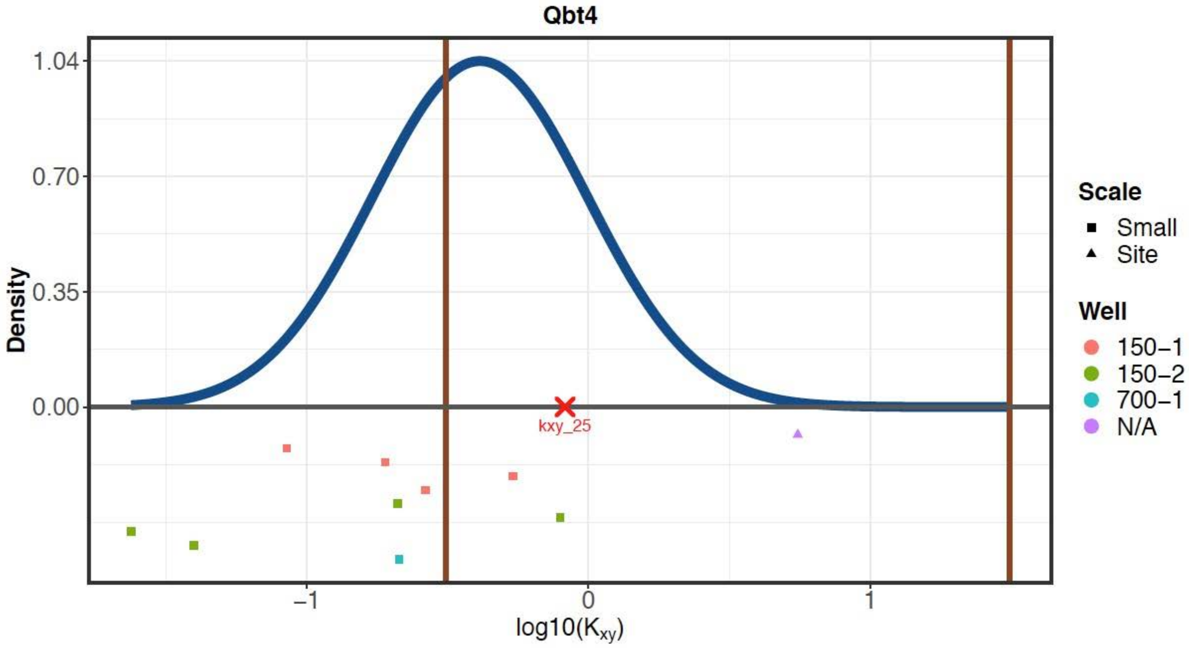

Notes: Observed data are plotted alongside the distributions colored by the well from which they were sampled. The vertical brown lines on the plots show the prior constraints used in calibration (LANL 2018b), and the red Xs are the results of that calibration for specific geologic units in the RVZM.

Figure C-2.2-20 Hydraulic conductivity (K_{xy}, in log10 ft/day) distributions for Group 8 (blue)

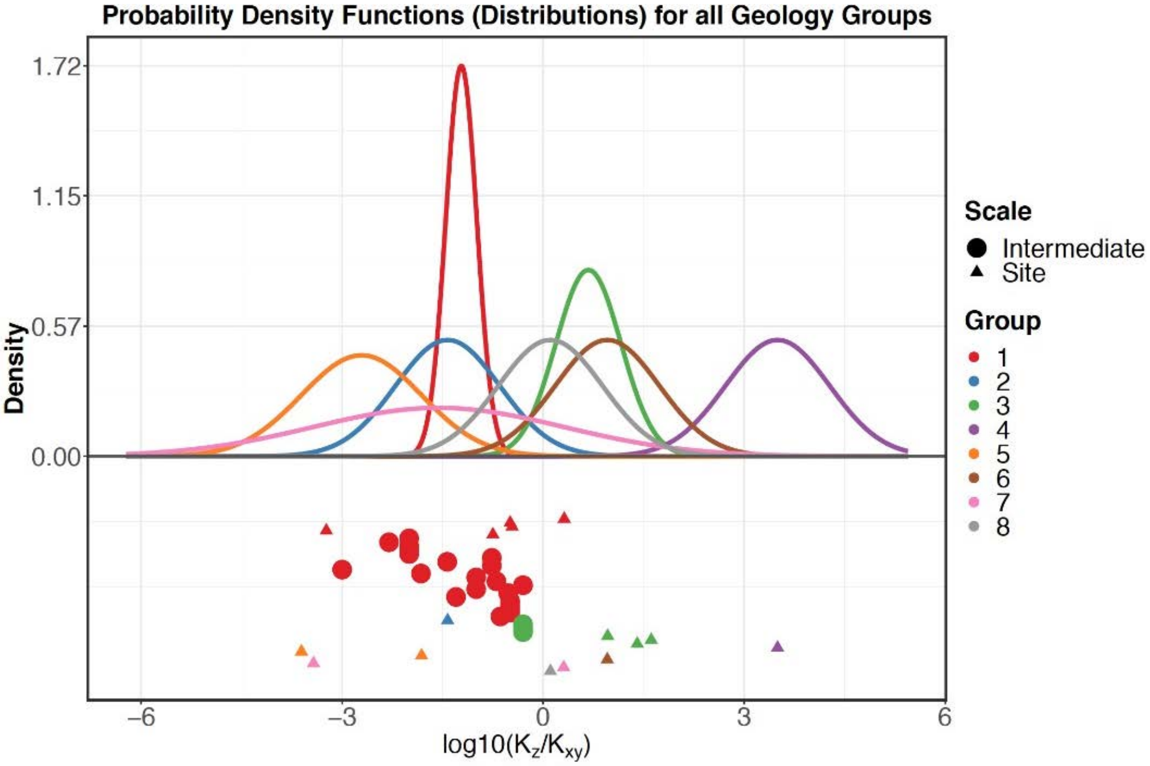

Note: Observed data are plotted alongside the distributions colored by the well from which they were sampled.

Figure C-2.2-21 Anisotropy (K_z/K_{xy}, in log10 ft/day) distributions for each geology group

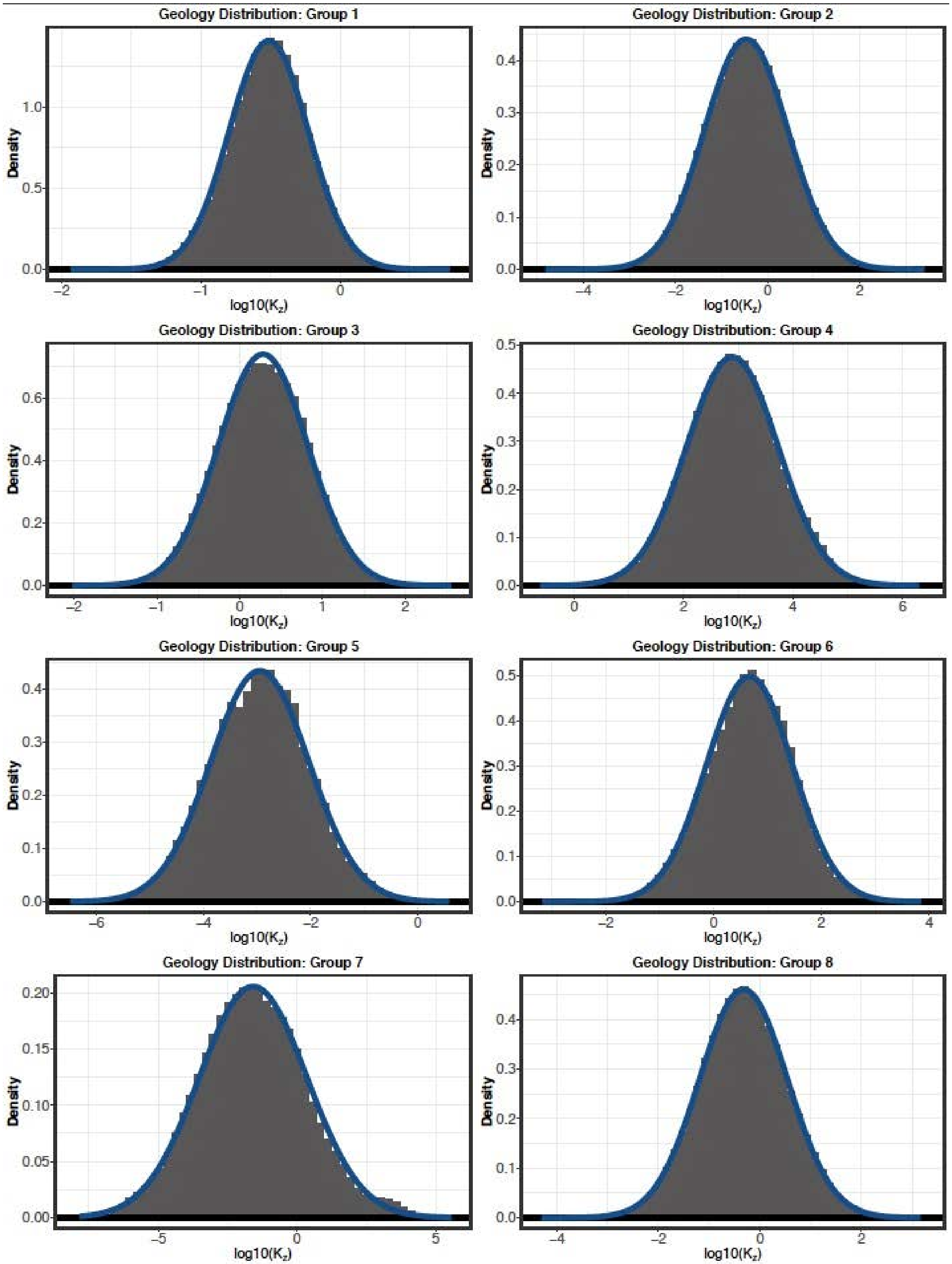

Note: Histograms of draws obtained from simulations are shown in gray.

Figure C-2.2-22 K_z (in log10 ft/day) distributions for each geology group (blue)

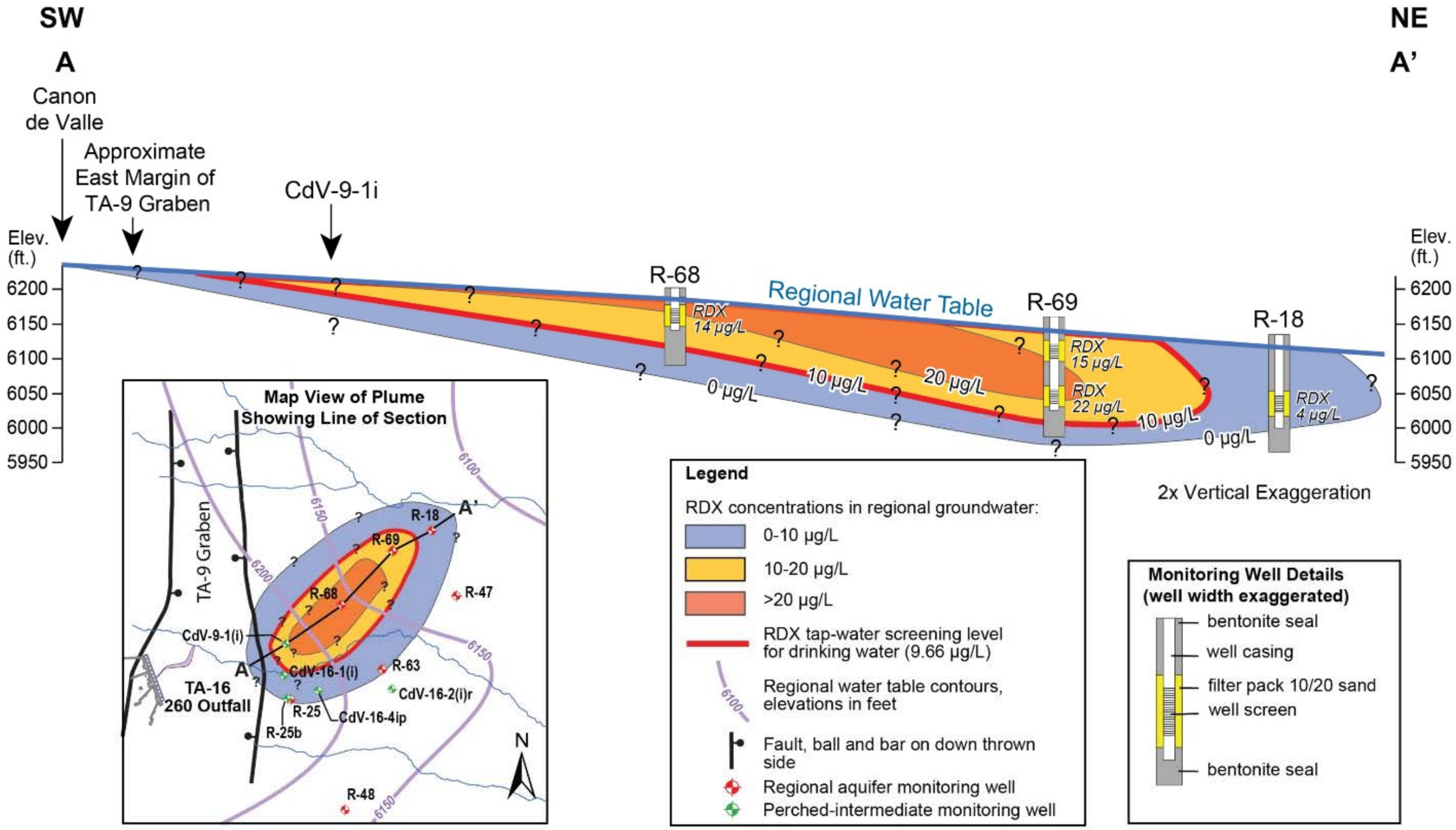

Figure C-2.2-23 Southwest to northeast cross-section of RDX contamination in the regional aquifer at TA-16

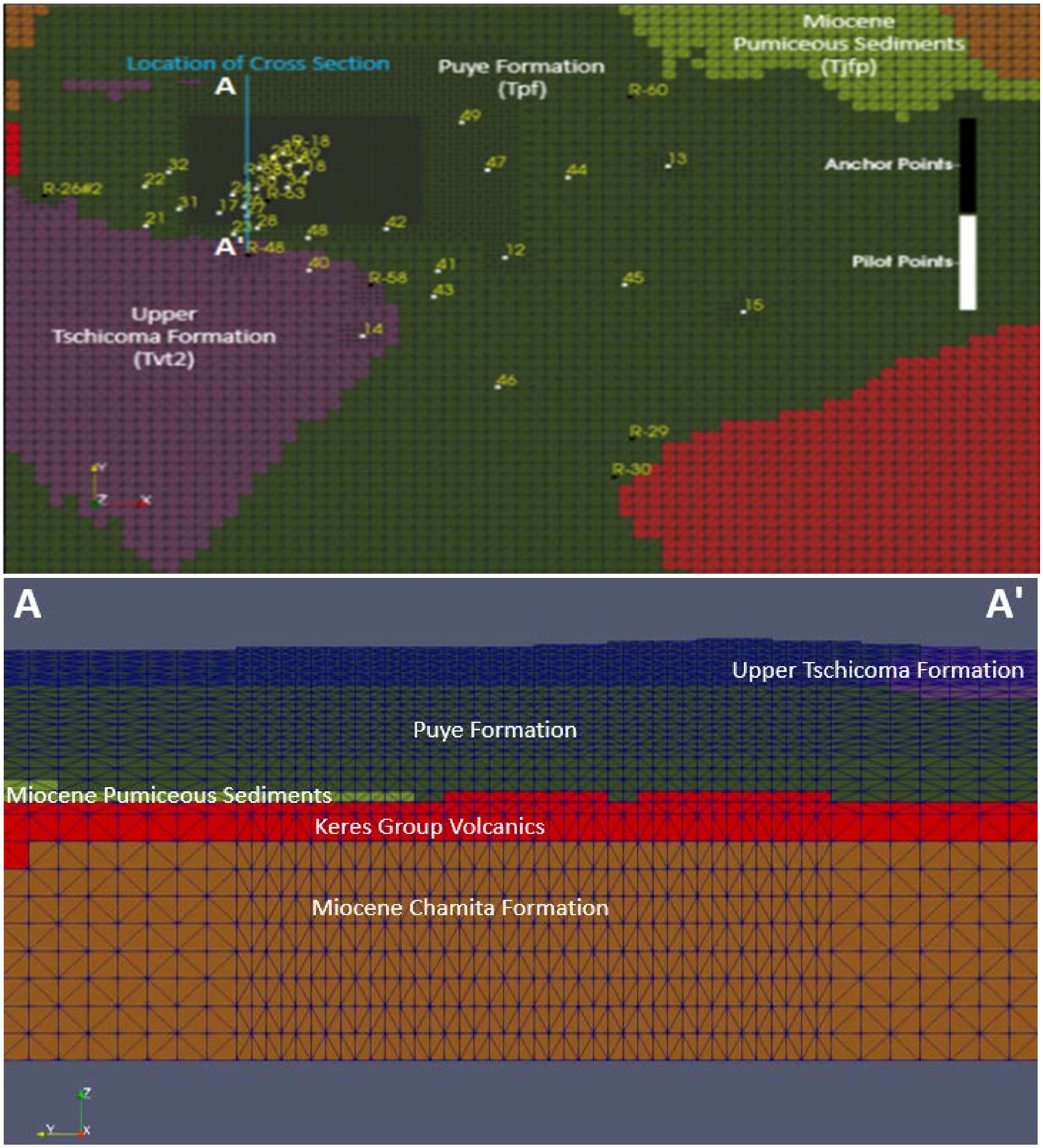

Notes: Blue line in top panel indicates location of cross-section A-A'. Bottom panel shows vertical cross section A-A'. Anchor points are shown with black squares, and pilot points are shown with white squares.

Figure C-2.2-24 Geologic units in the area of the RDX site, in plan view (top) and cross-section (bottom)

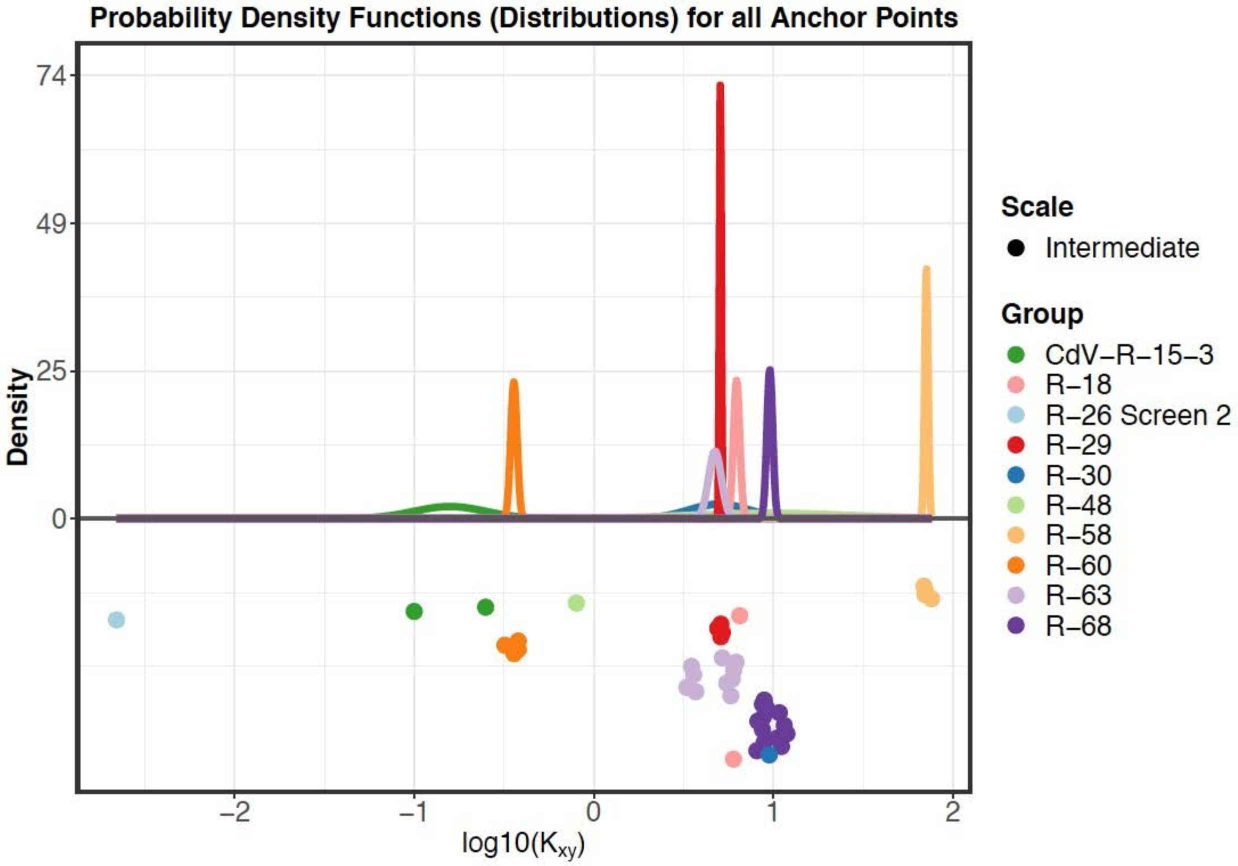

Note: Observed data are plotted alongside the distribution colored by the well from which they were sampled.

Figure C-2.2-25 Hydraulic conductivity (K_{xy}, in log10 ft/day) distributions for all anchor points

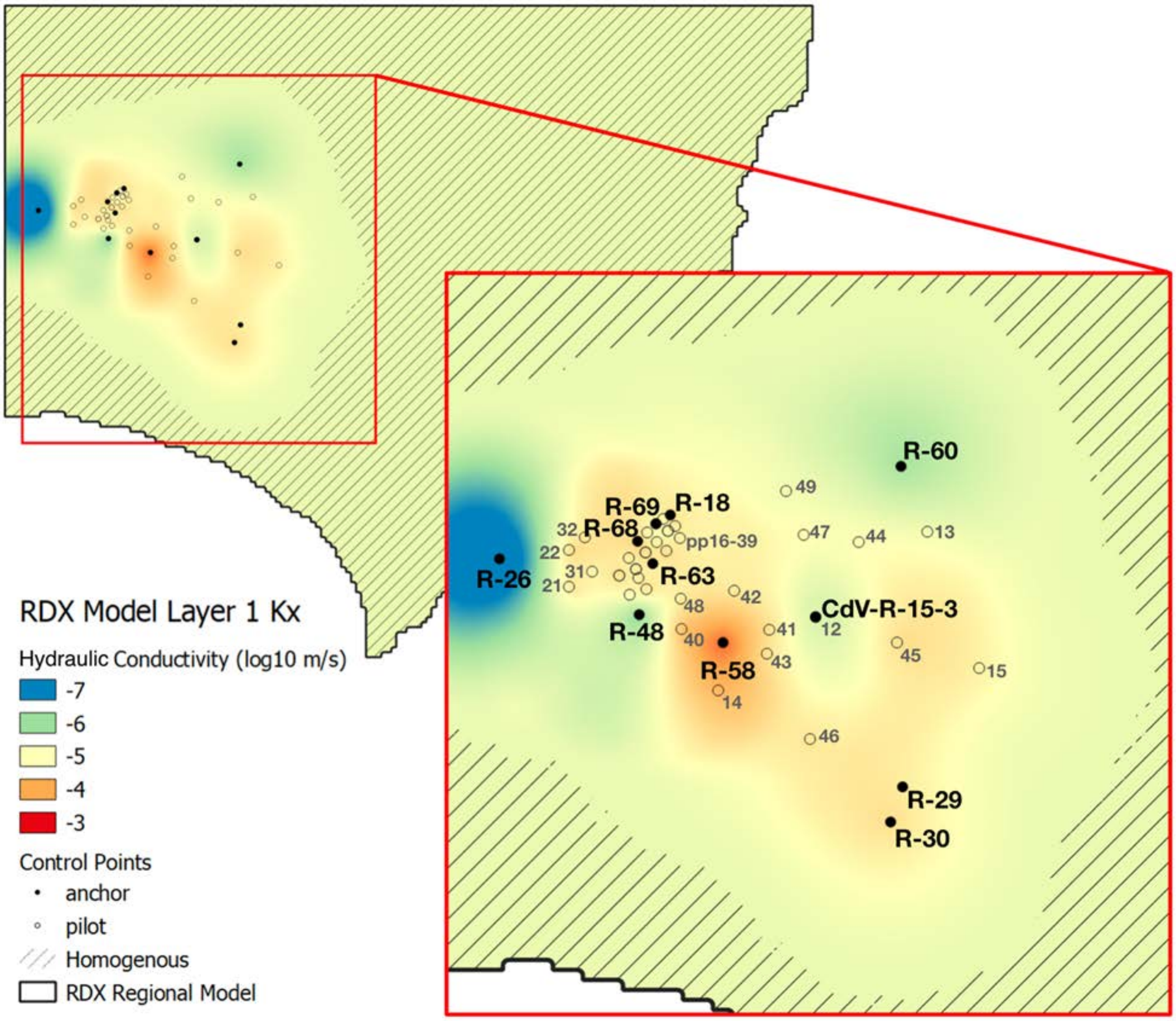

Notes: R-69 is plotted as a black dot, but it is a pilot (not an anchor) point. CdV-R-15-3 has two anchor points, one at screen 5 and one at screen 6. Pilot point 12 shares the same x,y coordinate as CdV-R-15-3 but is deeper than screen 6.

Figure C-2.2-26 Pilot and anchor point distributions as well as an example of kriged K values using the maximum krige scale and sigma from the uniform distribution

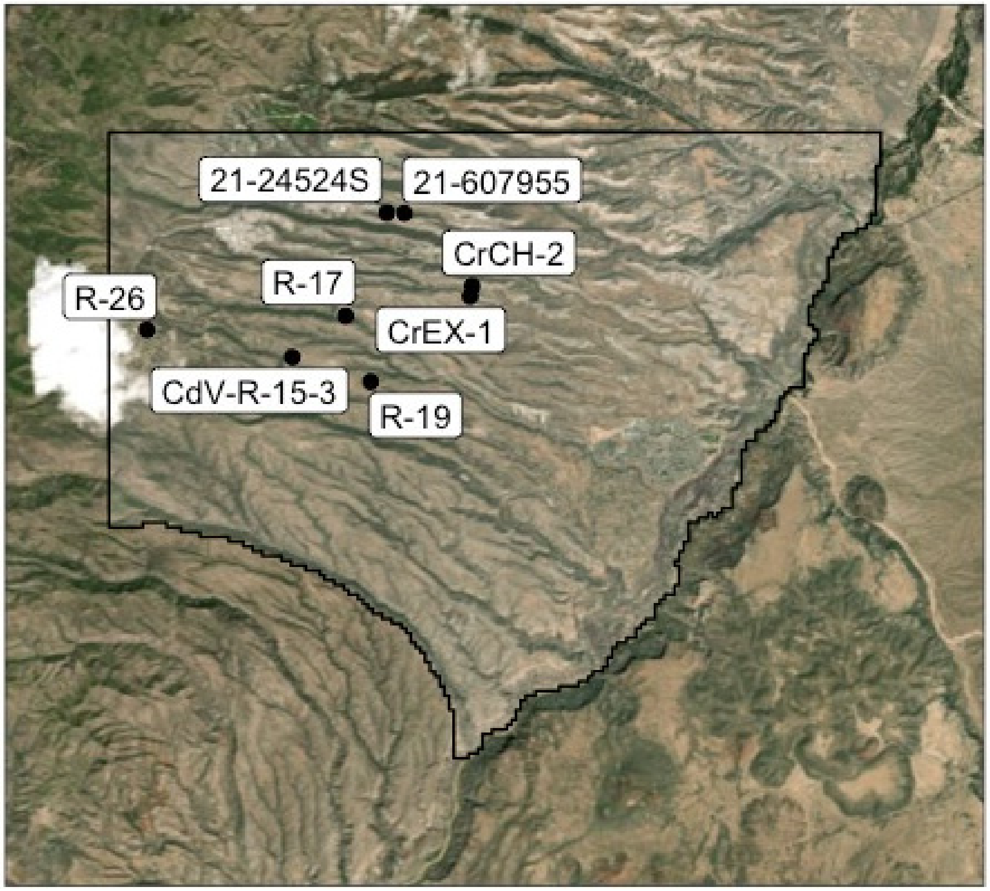

Figure C-2.2-27 Well data for porosity in the Puye Formation

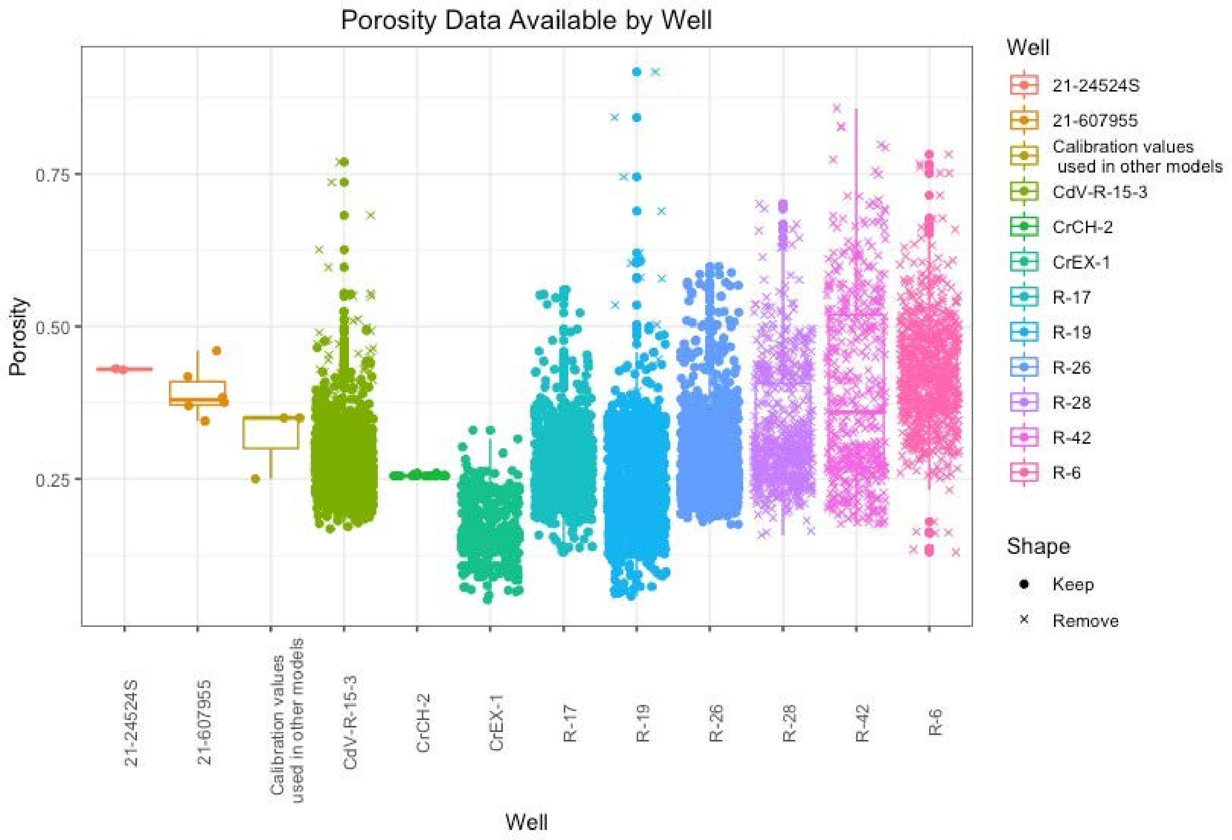

Note: X-shaped points indicate data that have been filtered out.

Figure C-2.2-28 Porosity data by well for the Puye Formation

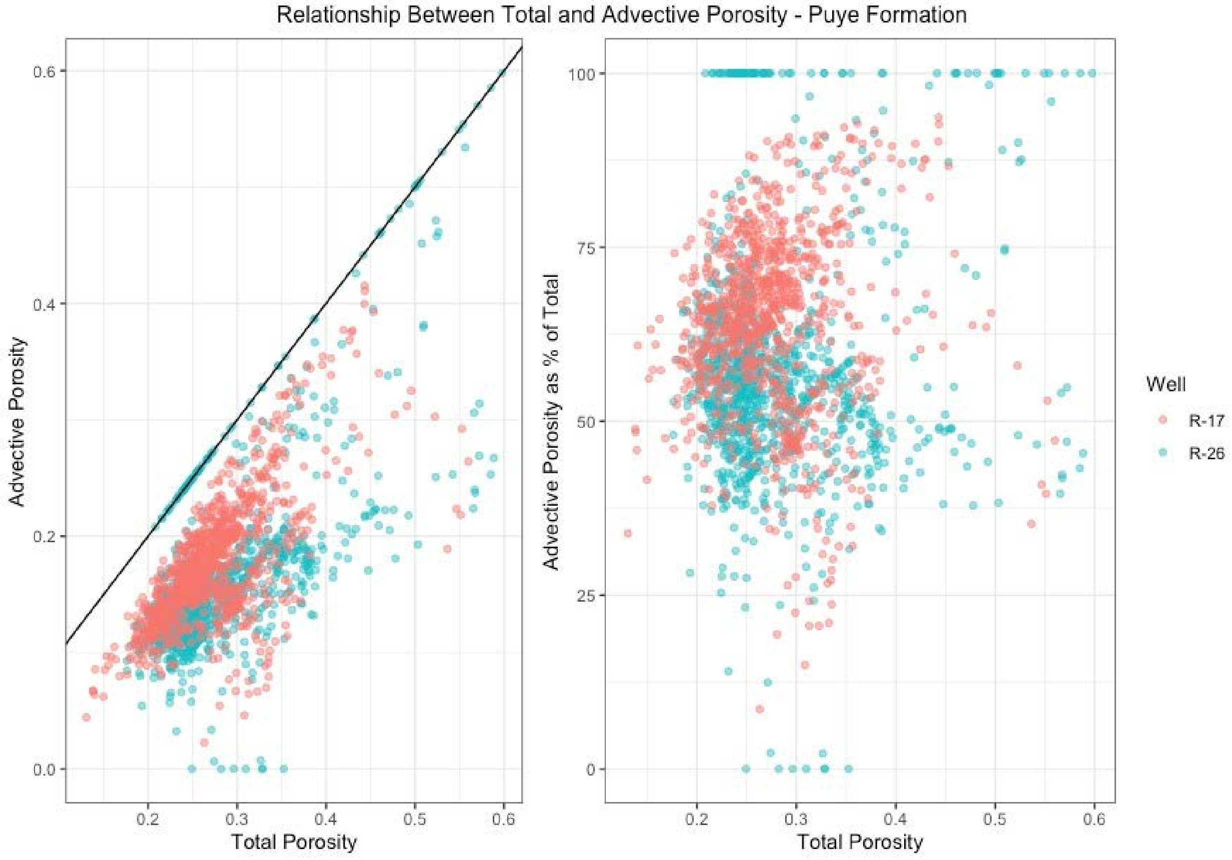

Figure C-2.2-29 Relationship between total porosity and advective porosity in the Puye formation

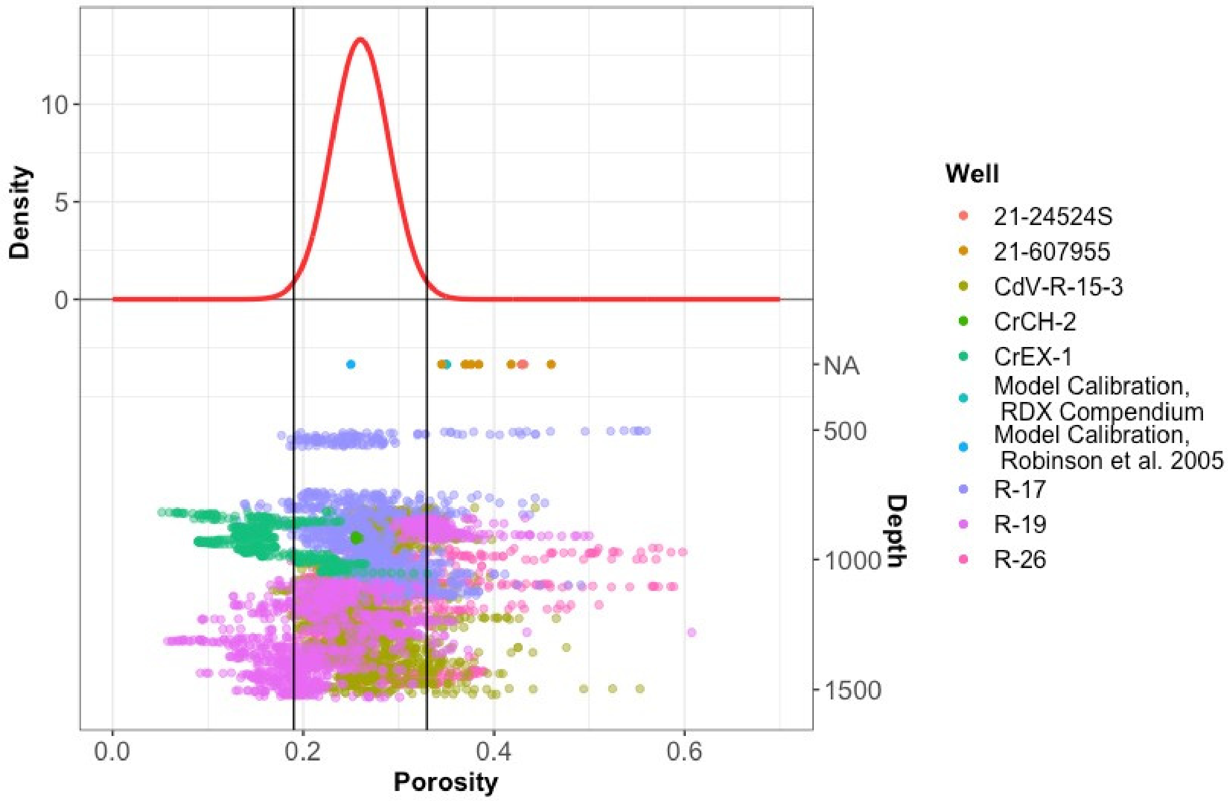

Figure C-2.2-30 Distribution developed for total porosity

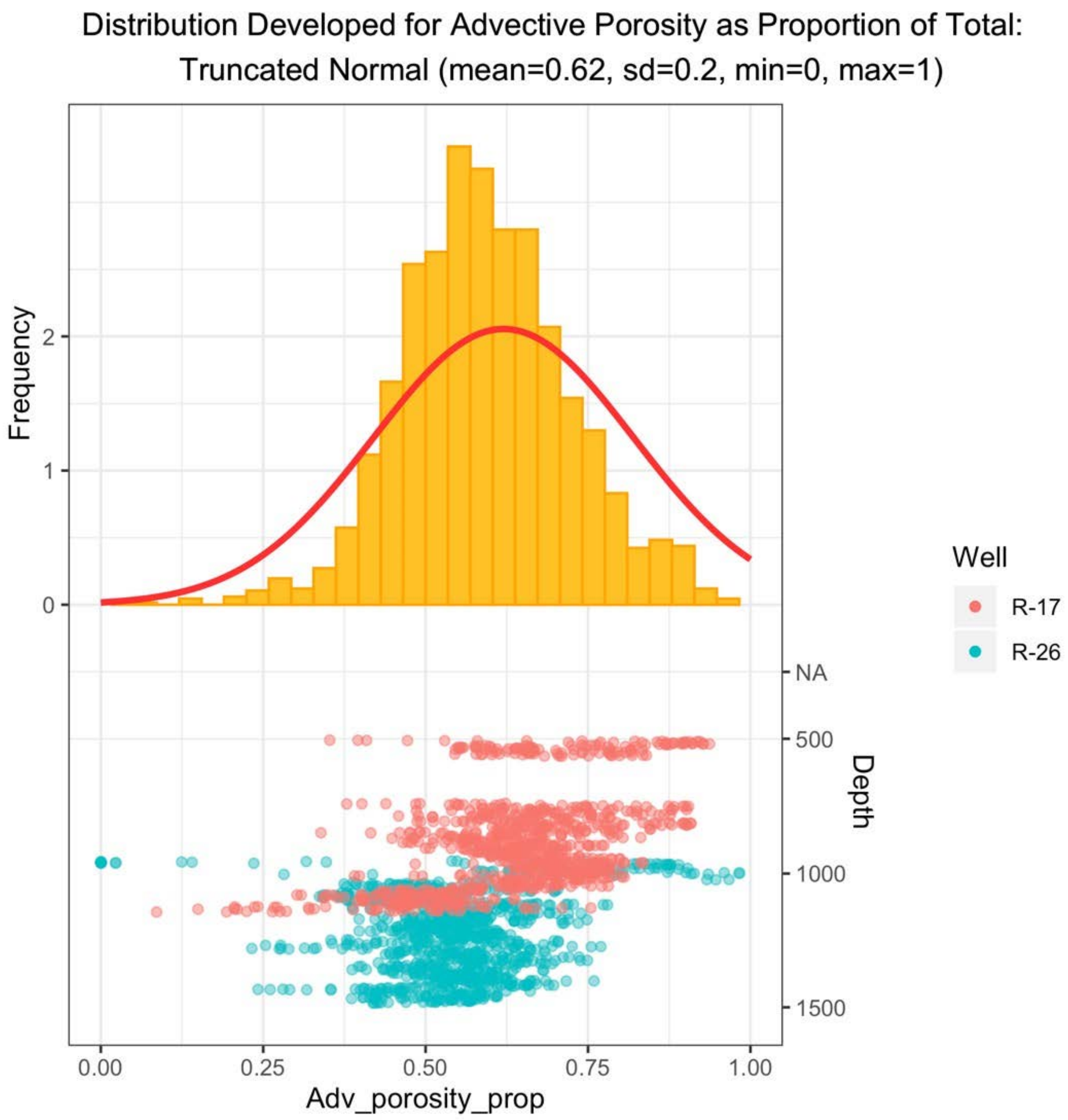

Figure C-2.2-31 Distribution developed and histogram for advective porosity as a fraction of total porosity

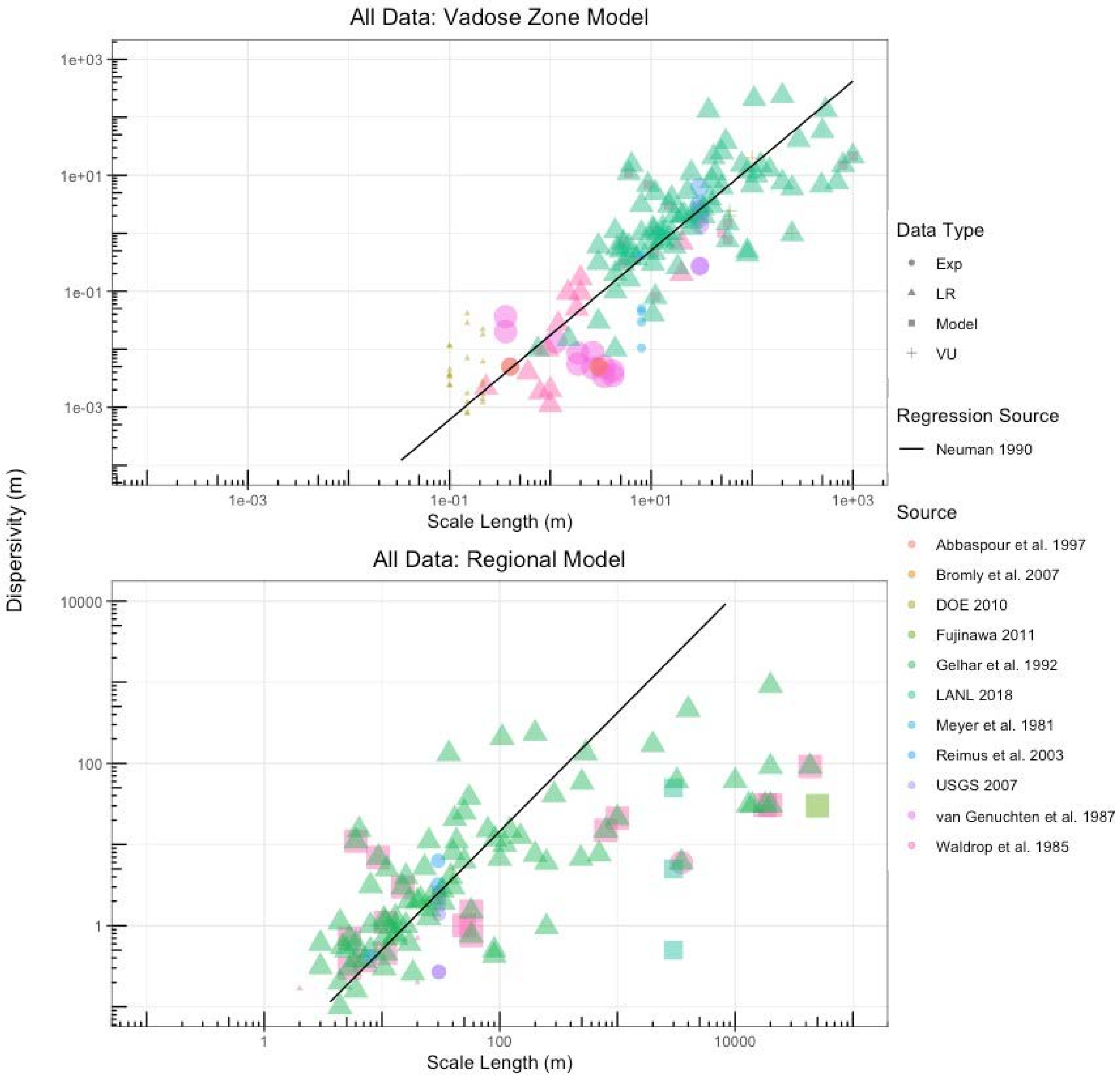

Figure C-2.2-32 Data available to inform the relationship of longitudinal dispersivity and length scale

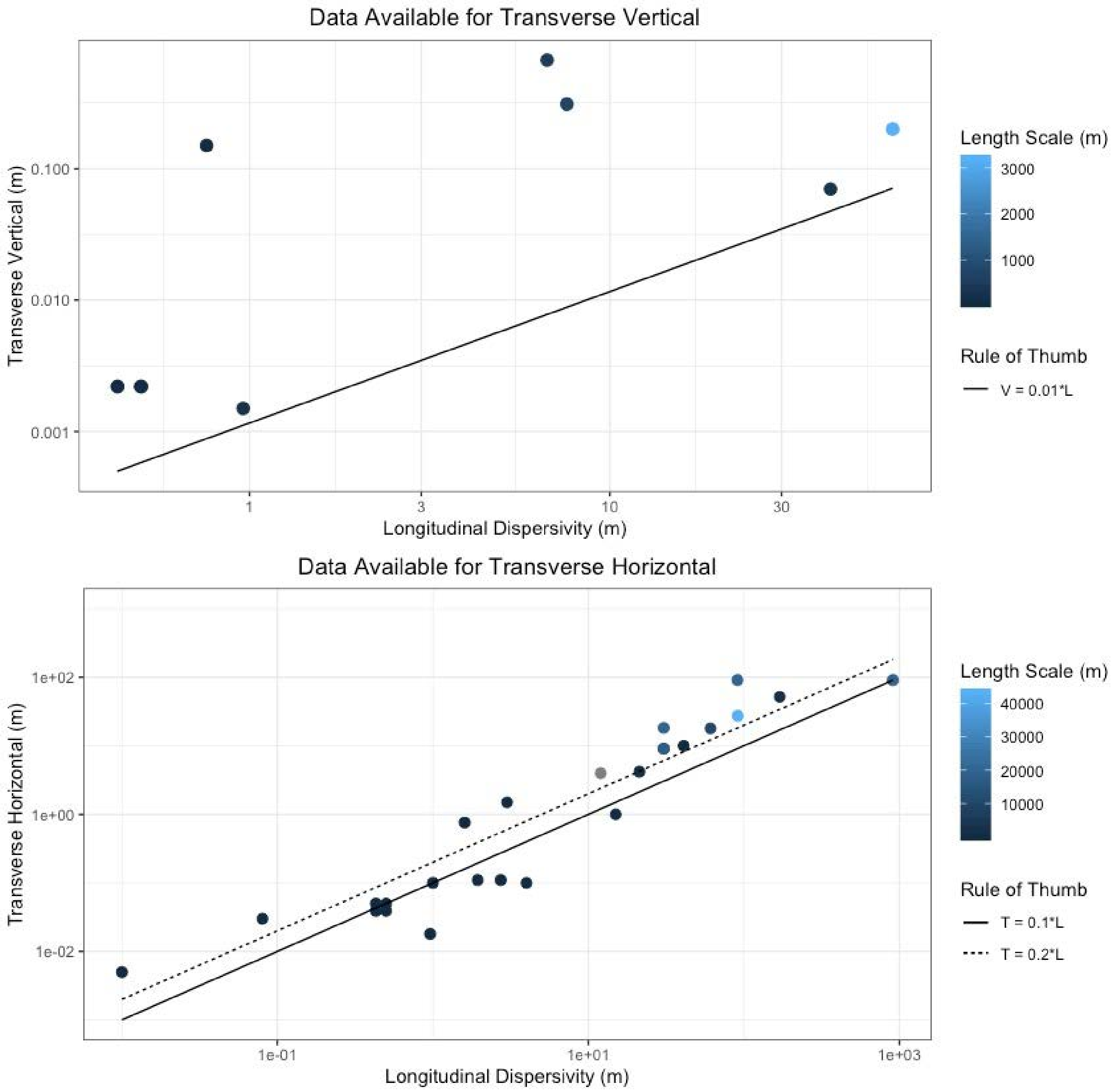

Figure C-2.2-33 Data available to inform the relationships of longitudinal dispersivity and transverse dispersivity in horizontal and vertical directions

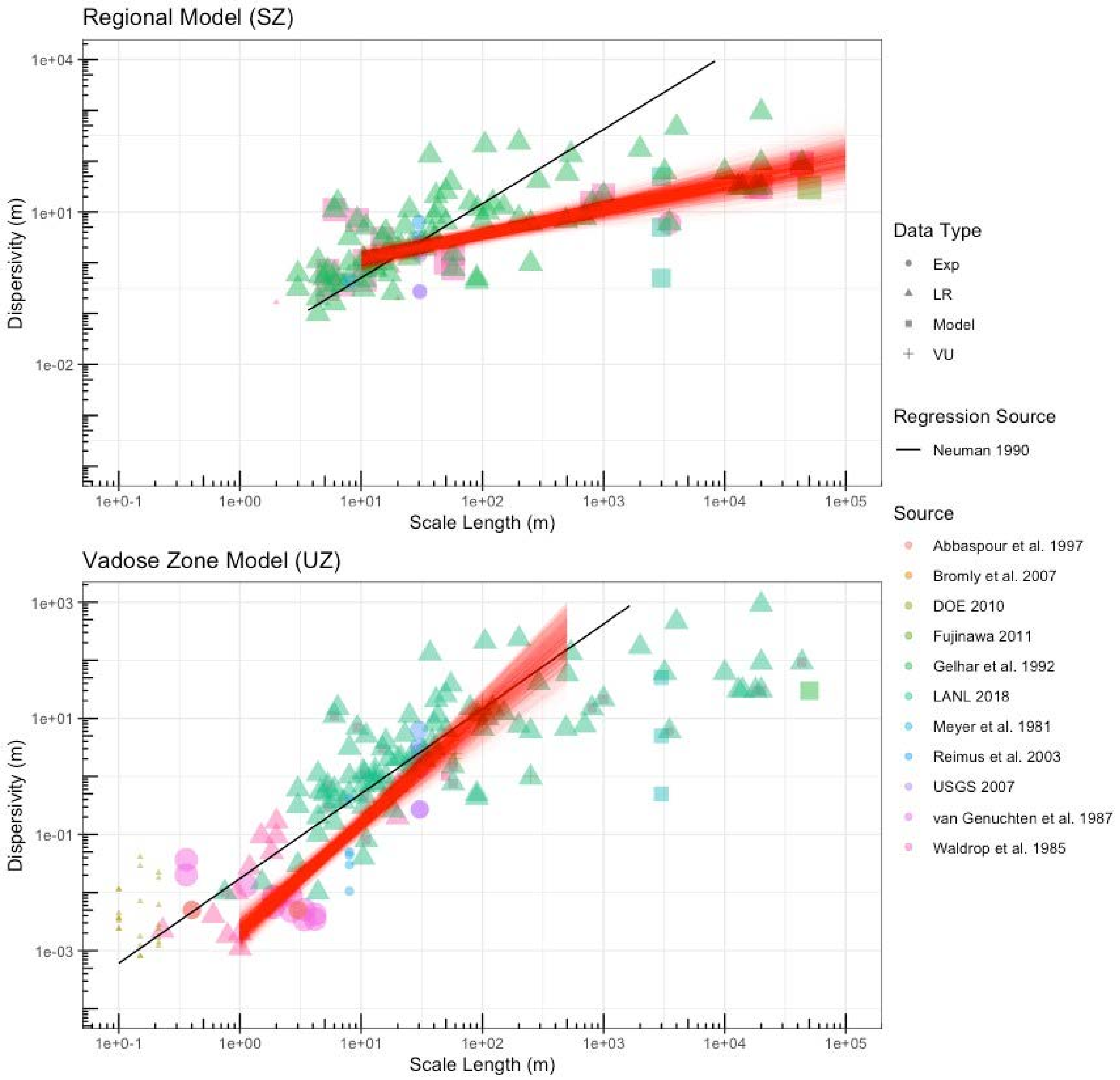

Figure C-2.2-34 Bootstrap estimated regression lines in red for the RRM

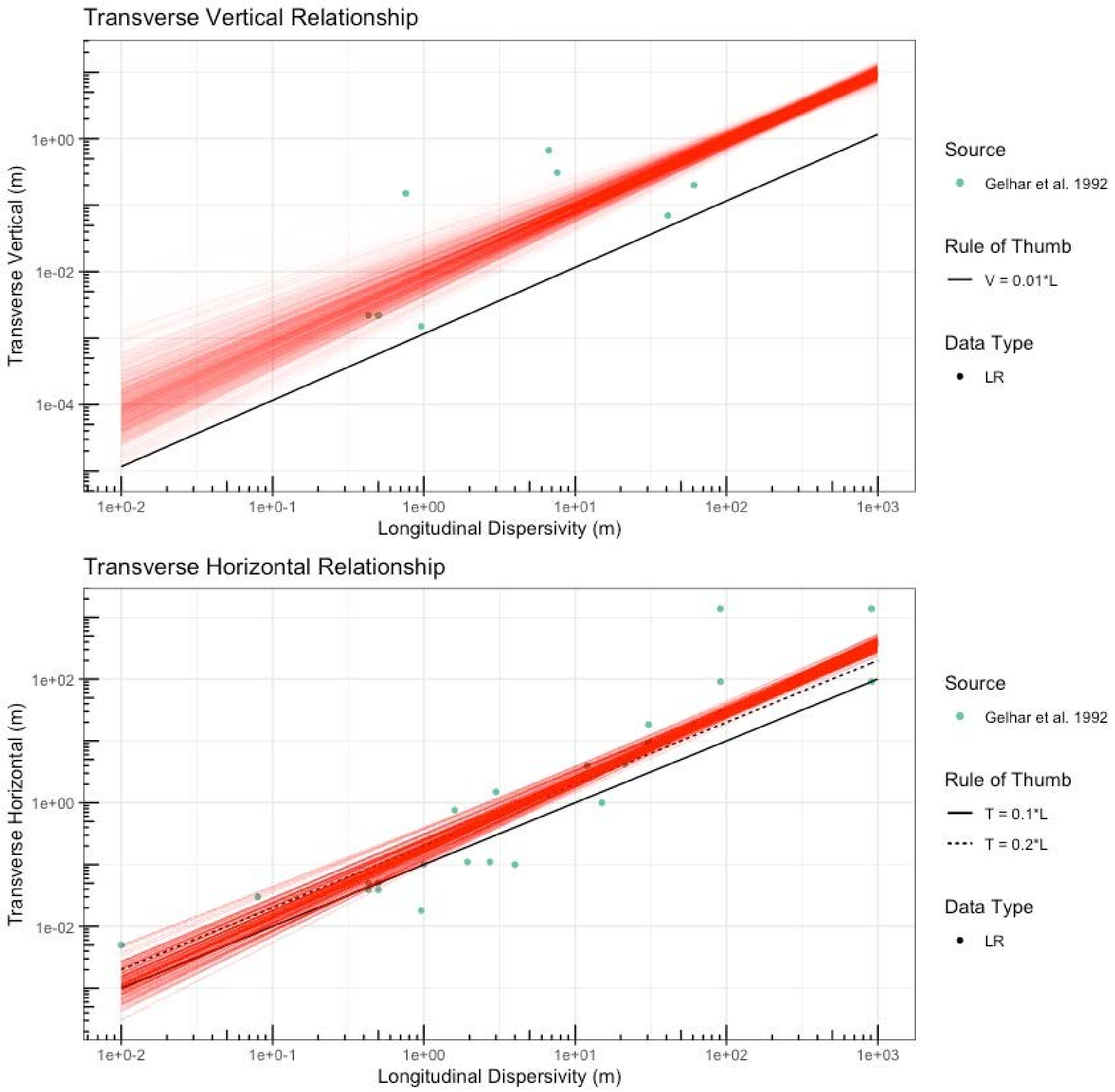

Figure C-2.2-35 Bootstrap estimated regression lines in red for transverse vertical (top) and transverse horizontal (bottom) dispersivities versus longitudinal dispersivity

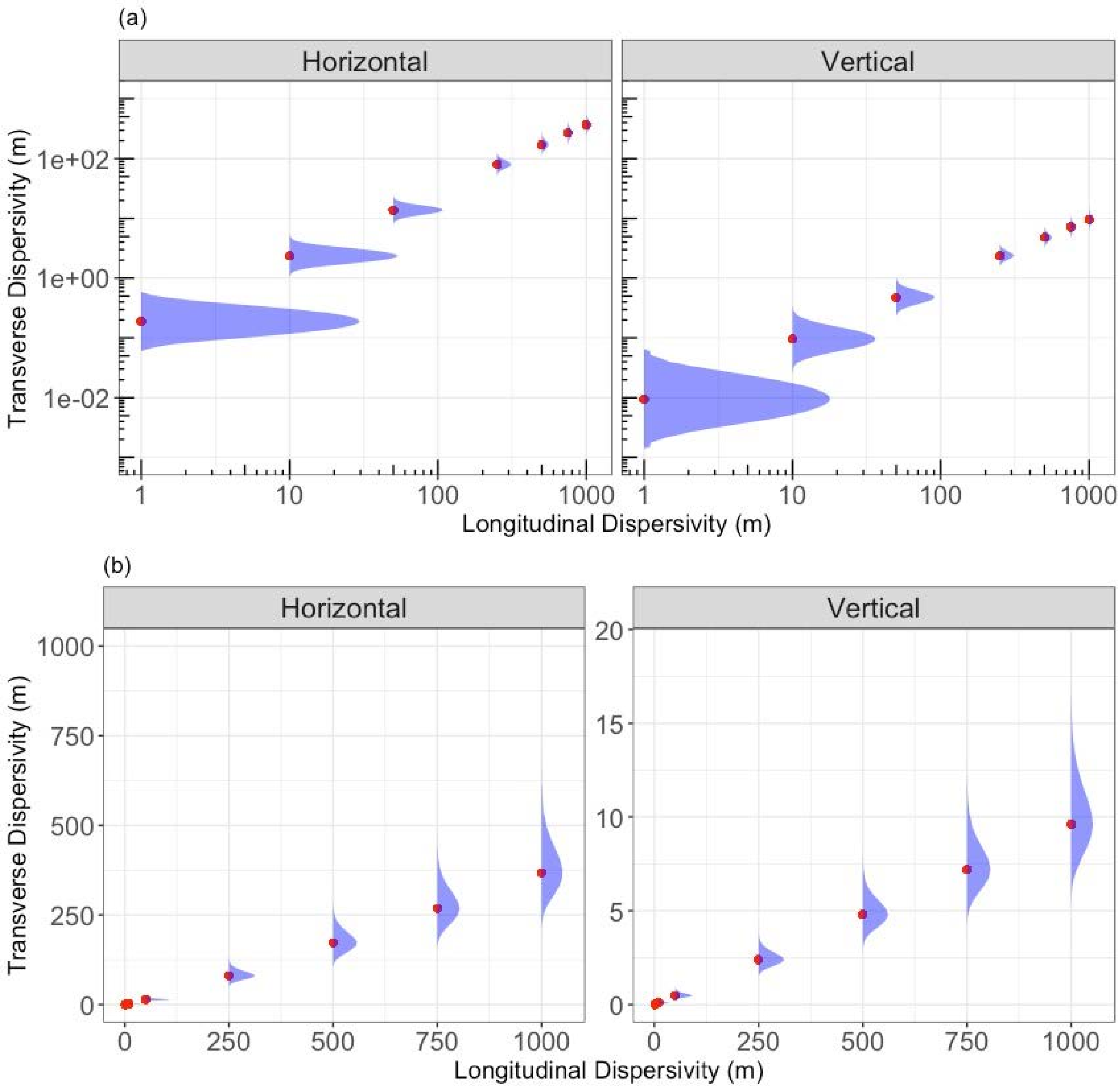

Figure C-2.2-36 **Plots of the distributions for transverse dispersivities on the (a) log10 scale and the (b) original scale for selected longitudinal dispersivities (1,10,50,250,500,750,1000 m)**

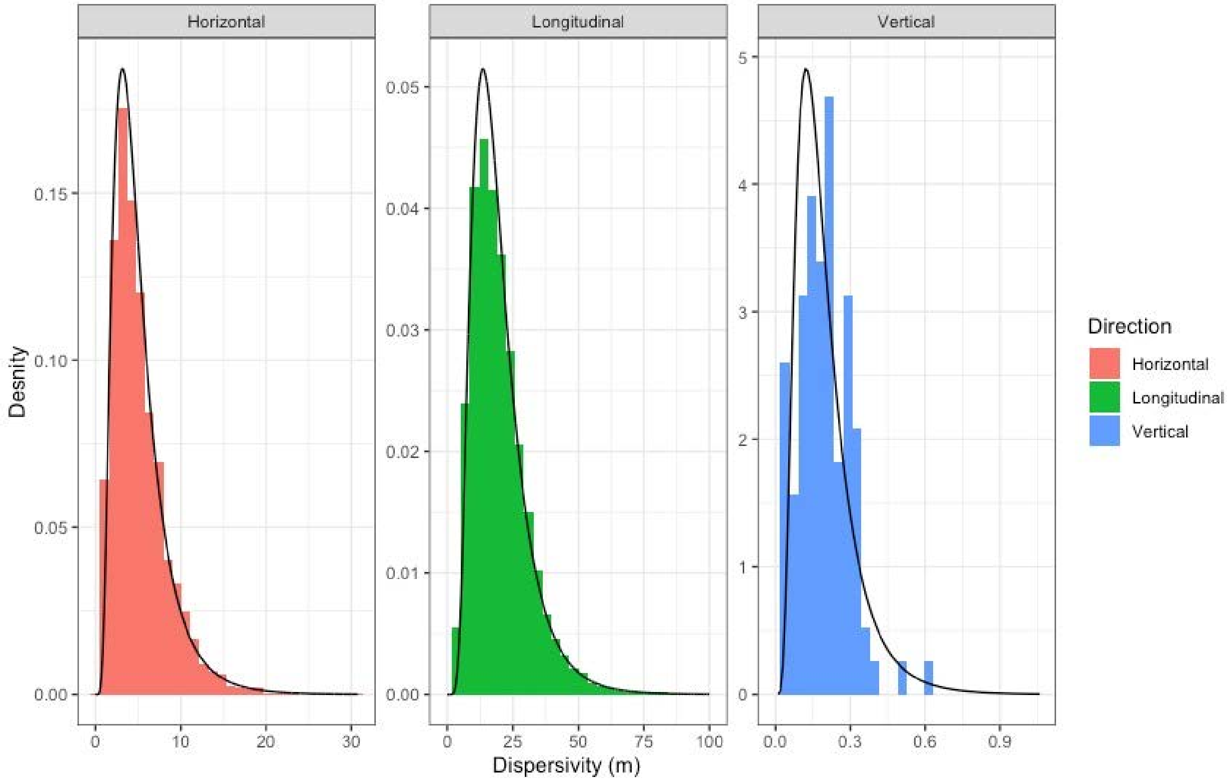

Figure C-2.2-37 Distributions developed for dispersivity in the RRM

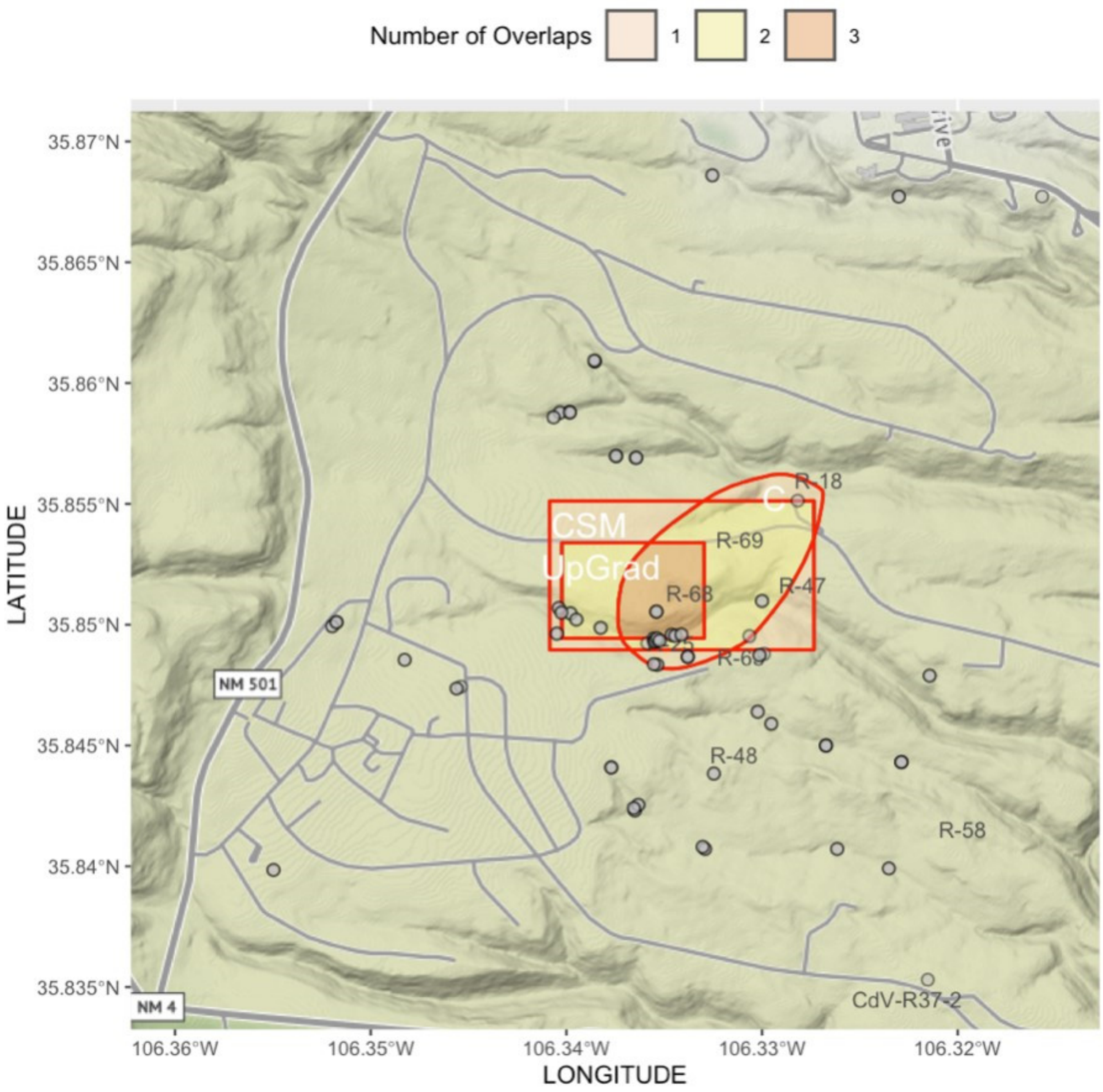

Figure C-2.2-38 Lines of evidence used to inform the primary source location

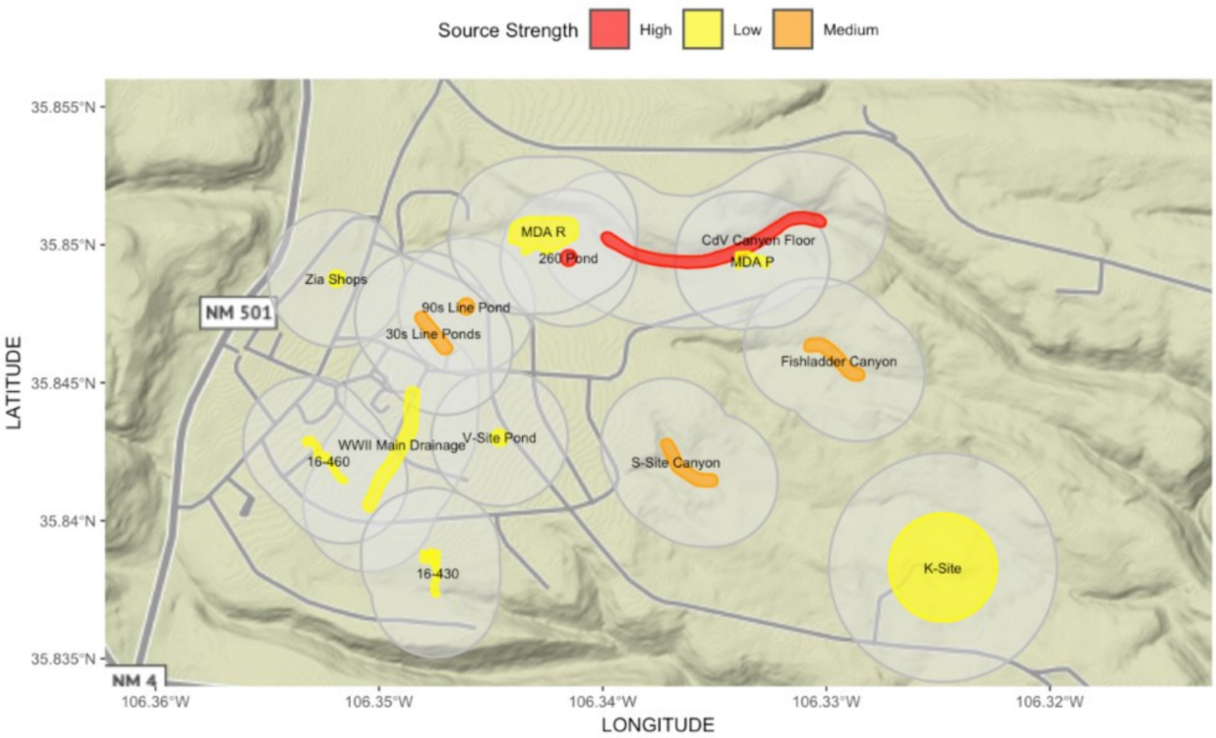

Figure C-2.2-39 **Potential sources of surface contamination ranked by their likelihood to contaminate the regional aquifer**

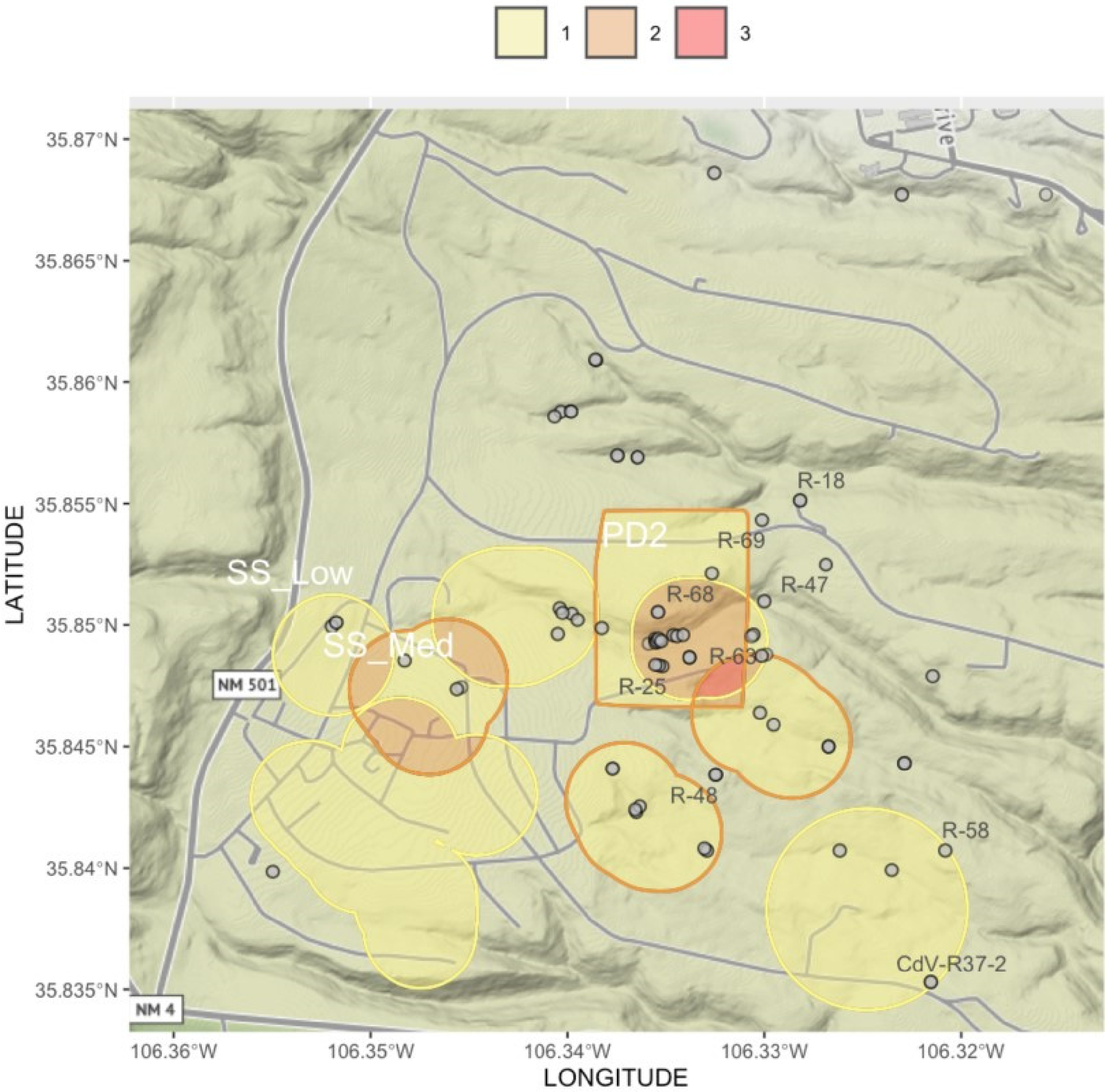

Figure C-2.2-40 Lines of evidence used to inform the secondary source location

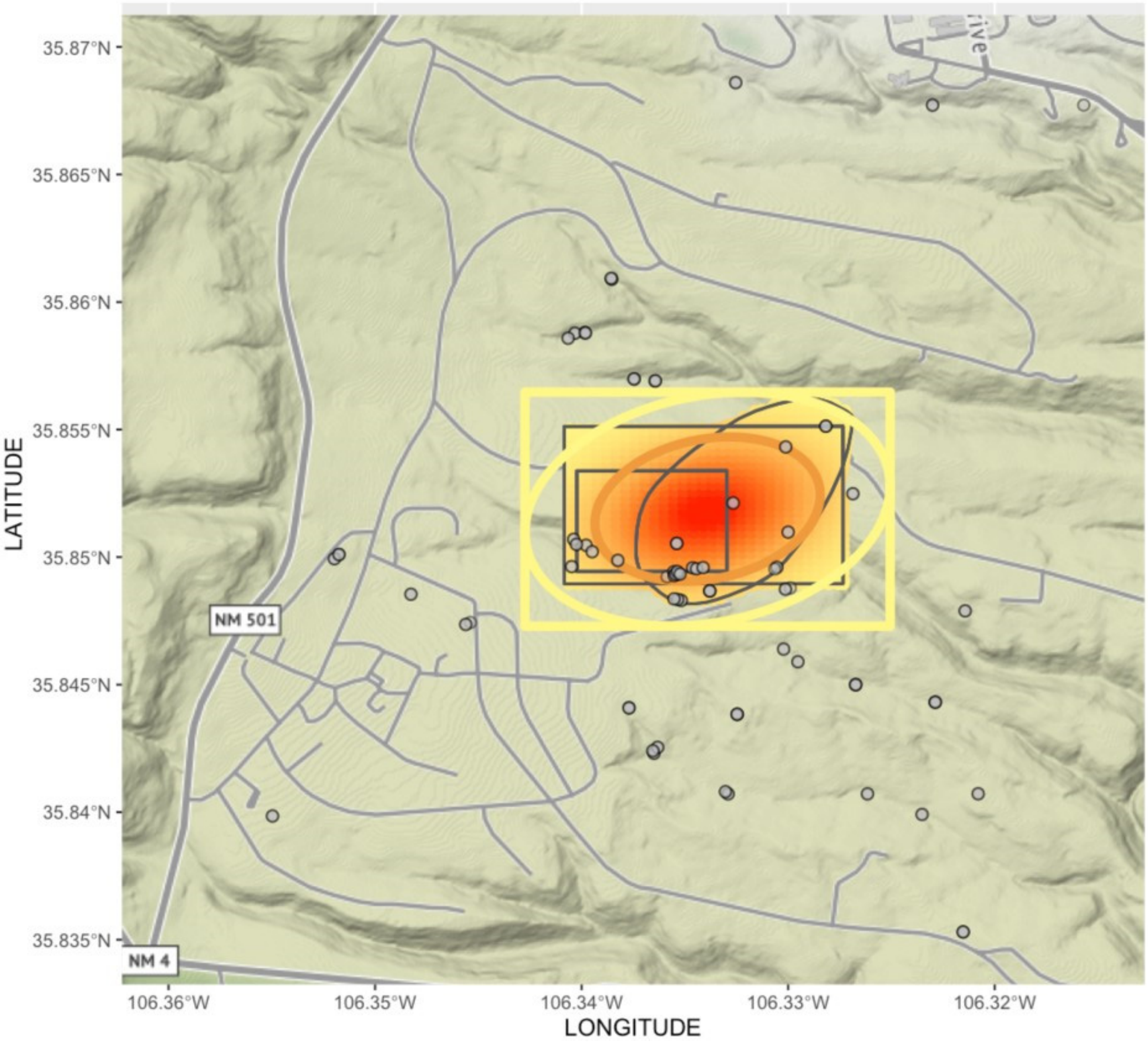

Figure C-2.2-41 Primary source distribution for source center location

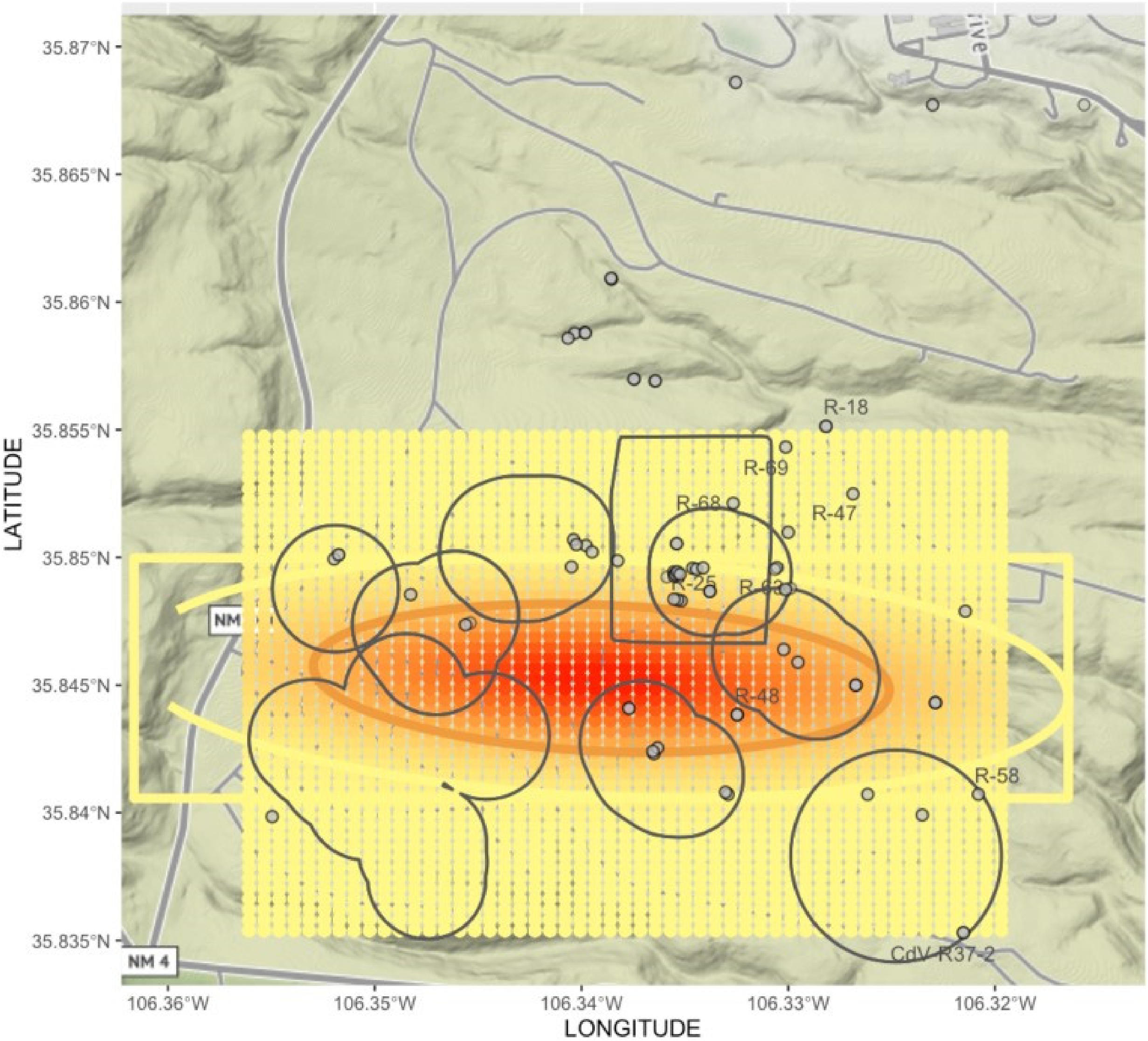

Figure C-2.2-42 **Secondary source distribution for source center location**

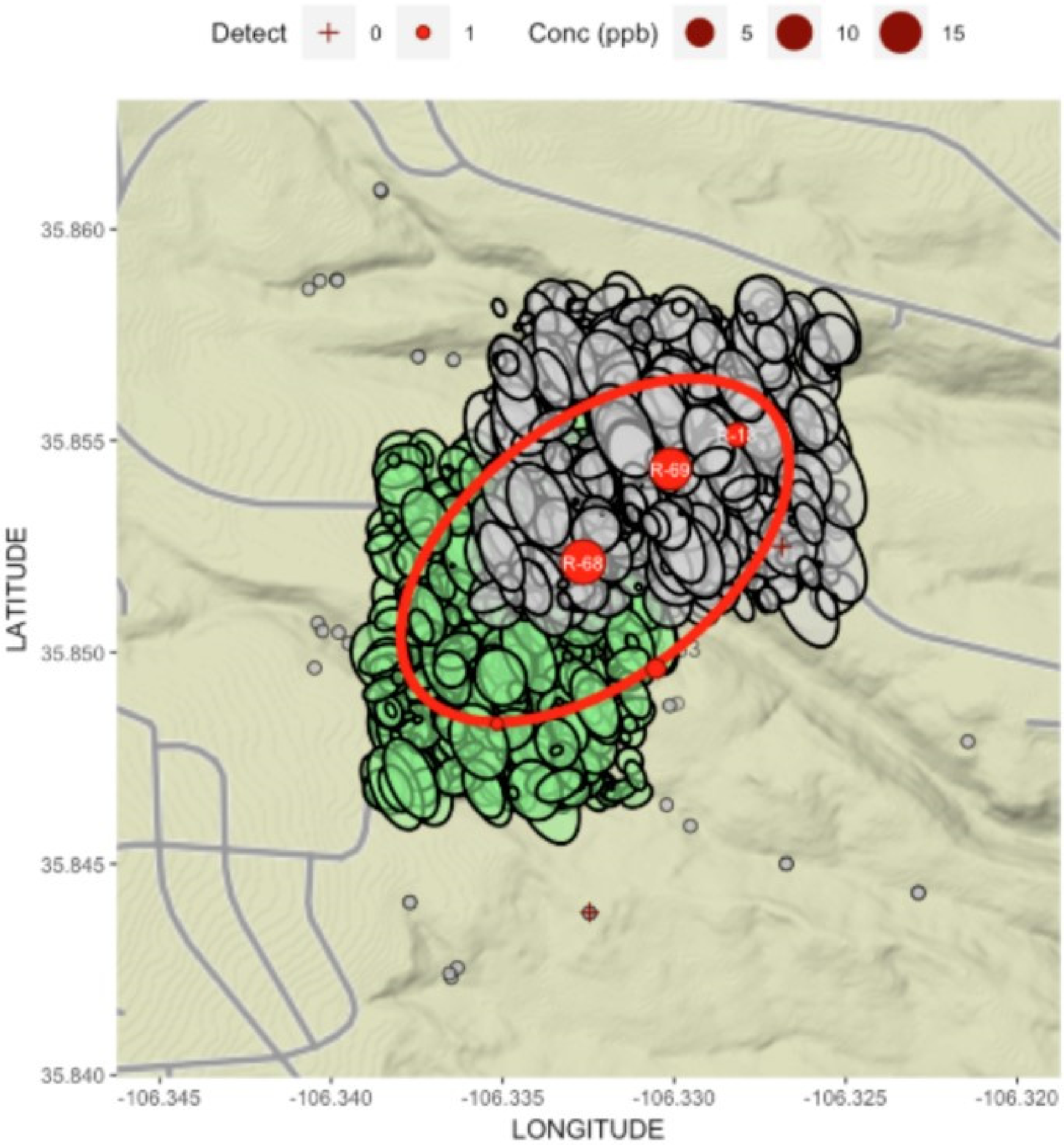

Figure C-2.2-43 **Results from the P&D analysis (section C-2.2.2.3)**

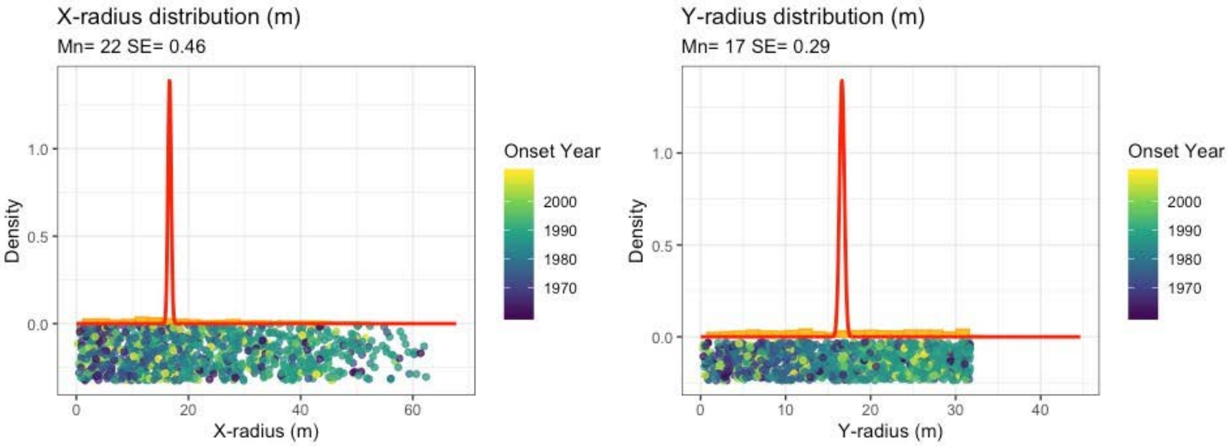

Figure C-2.2-44 Distributions developed for only the P&D analysis

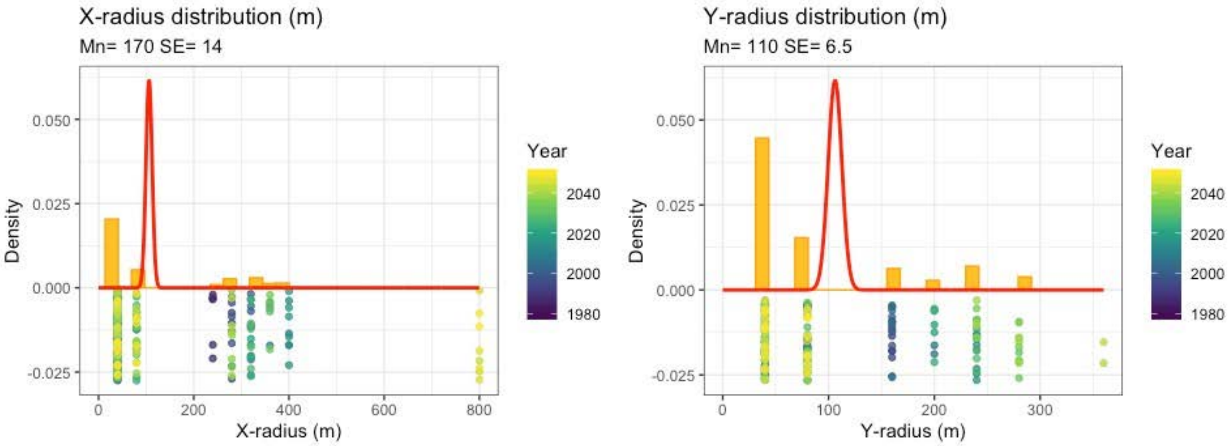

Figure C-2.2-45 Histogram of source radii from RVZM output and distribution based on only RVZM results

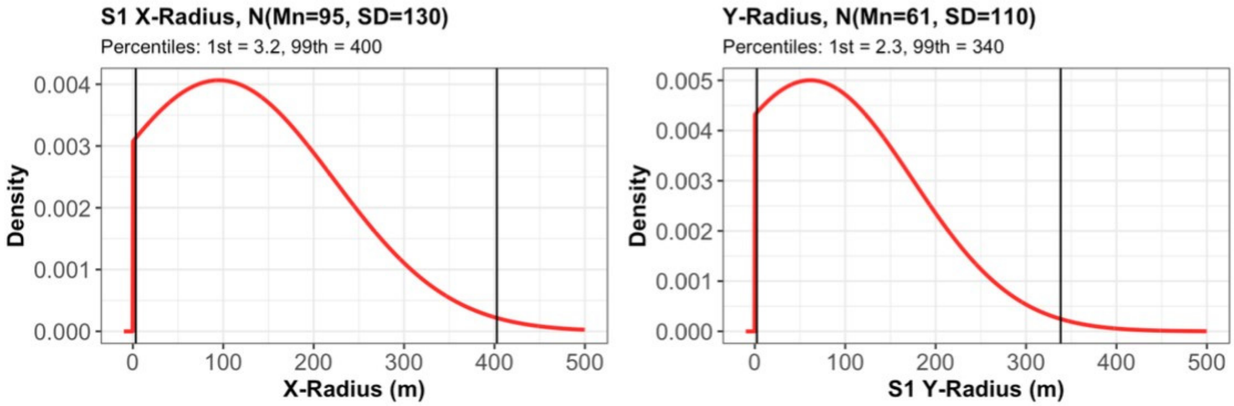

Figure C-2.2-46 Radii distributions for the primary source

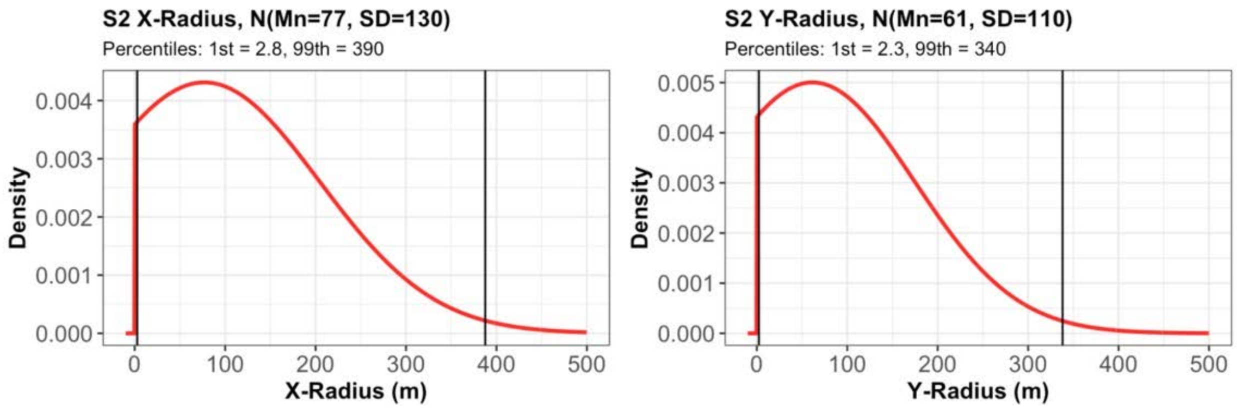

Figure C-2.2-47 **Radii distributions for the secondary source**

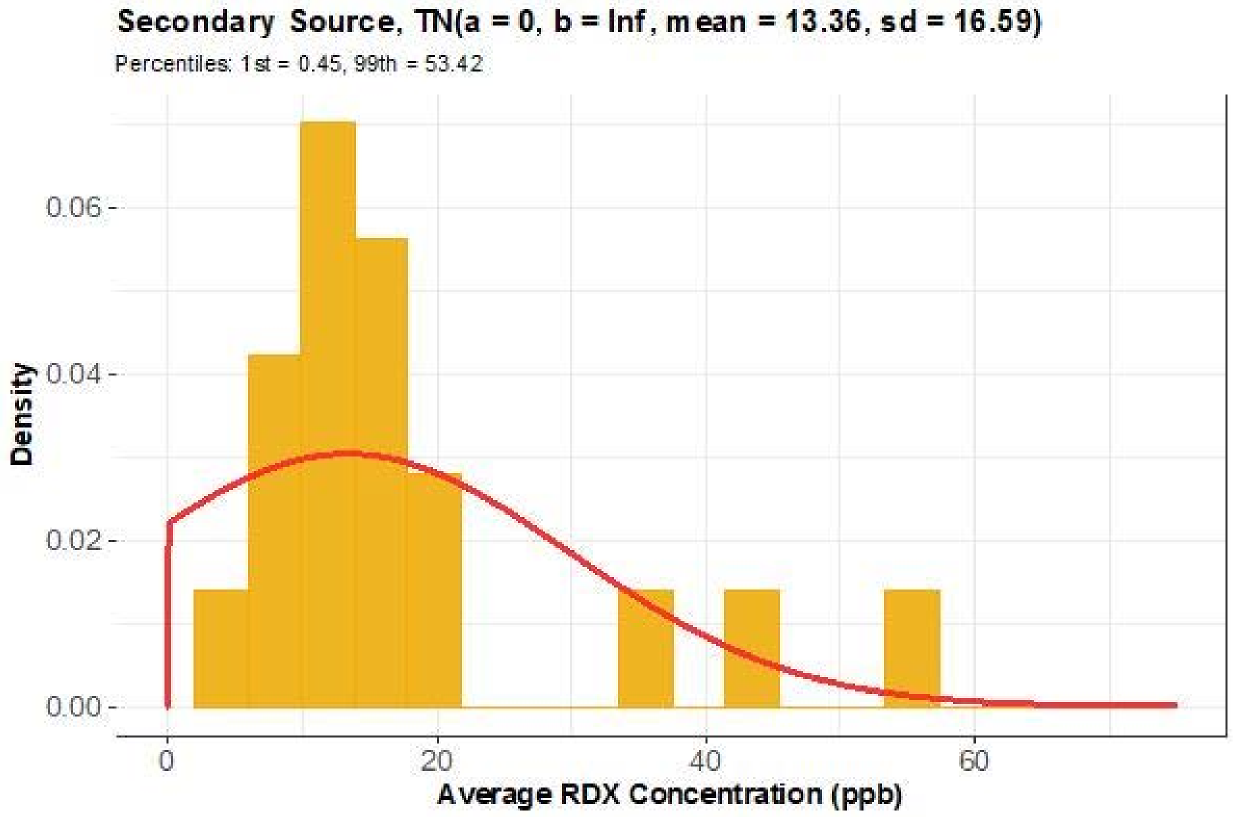

Figure C-2.2-48 **Distribution for primary and secondary source concentration at the center of the hydraulic window plotted over histograms of RVZM output used to inform distribution**

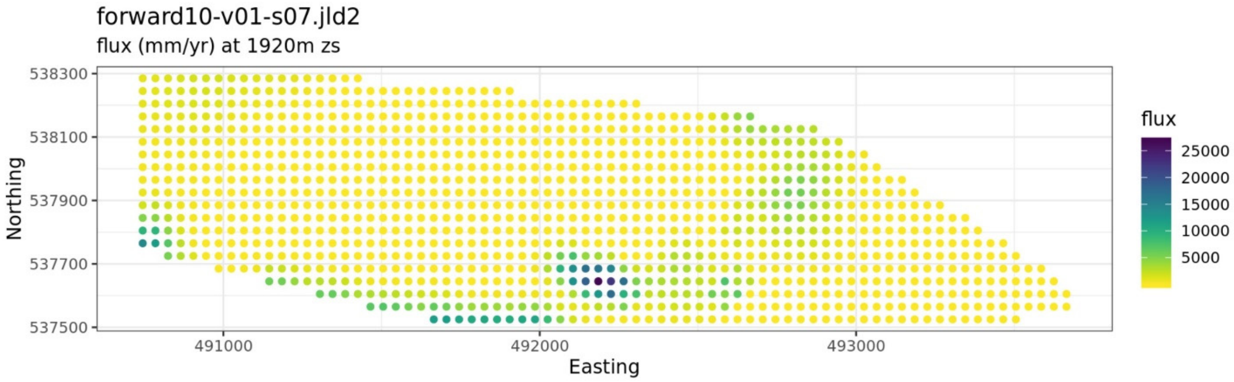

Figure C-2.2-49 **One of 19 VZ model results for recharge rate at the regional aquifer plotted in space (with boundary nodes removed) demonstrates the predictions of preferential vs. background recharge occurring at the regional aquifer**

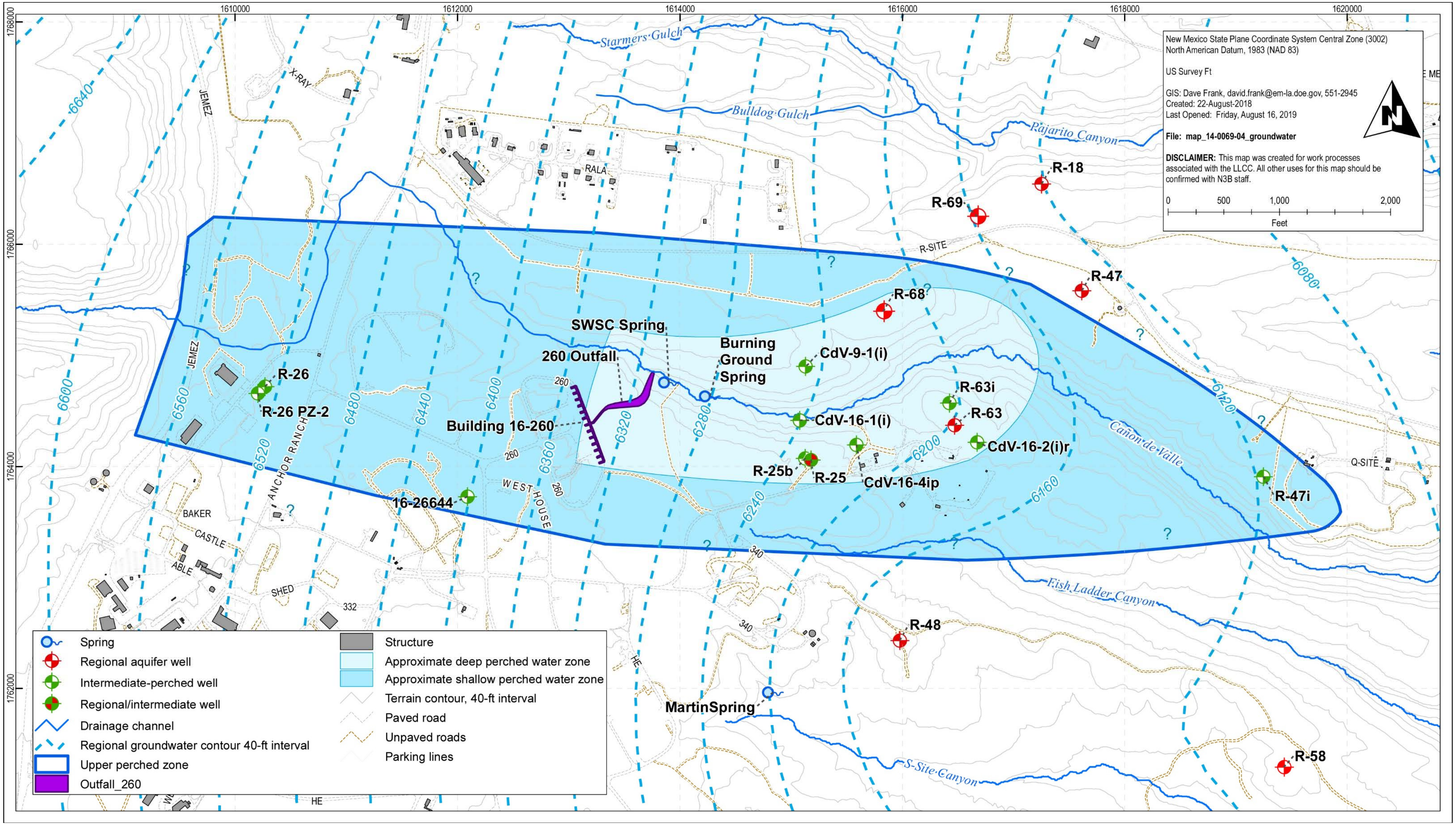

Note: The distribution for source 3 center is shown in the dotted lines, and the distribution for the size is between the maximum and minimum x and y radii plotted with the solid lines.

Figure C-2.2-50 **Regional water table contours, approximate extents of perched zones in the VZ, Cañon de Valle location, and wells in the vicinity of the regional aquifer RDX plume**

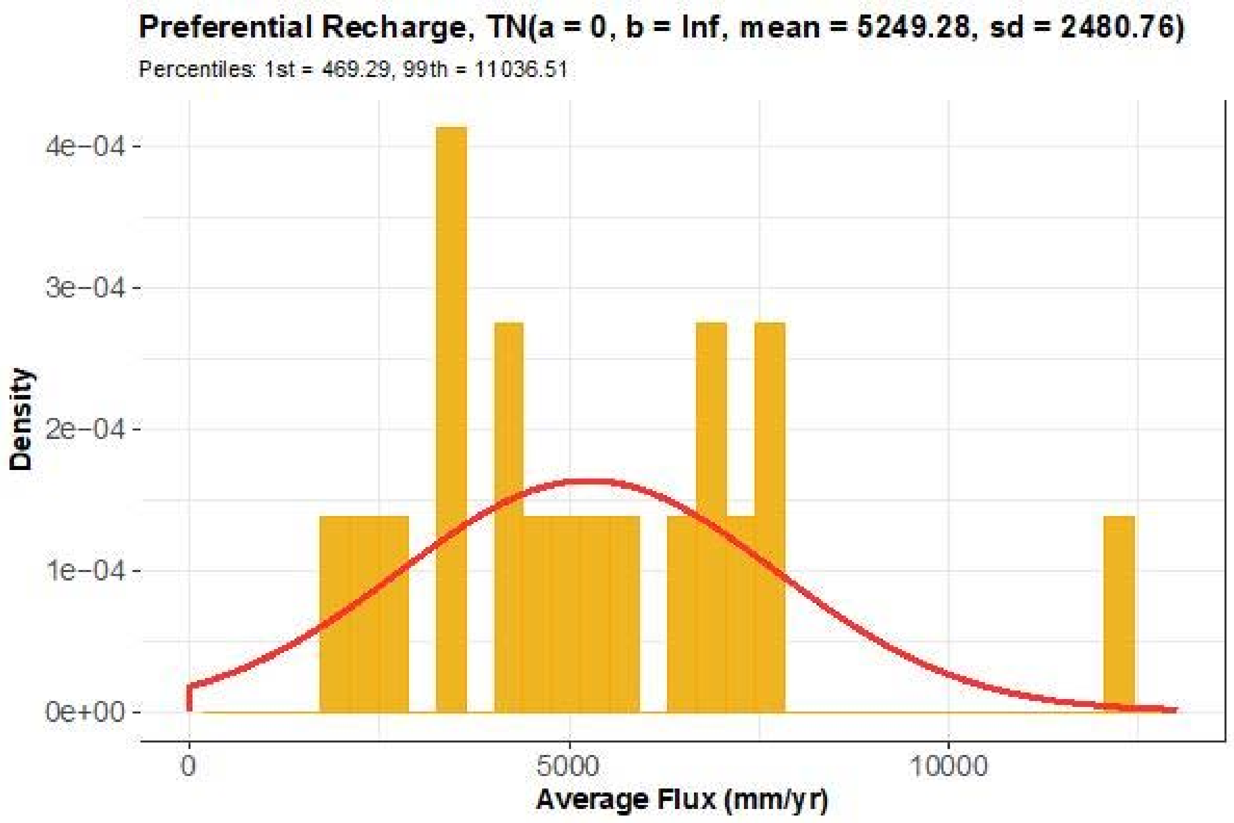

Figure C-2.2-51 Distribution for background and preferential recharge from VZ to regional aquifer (mm/year)

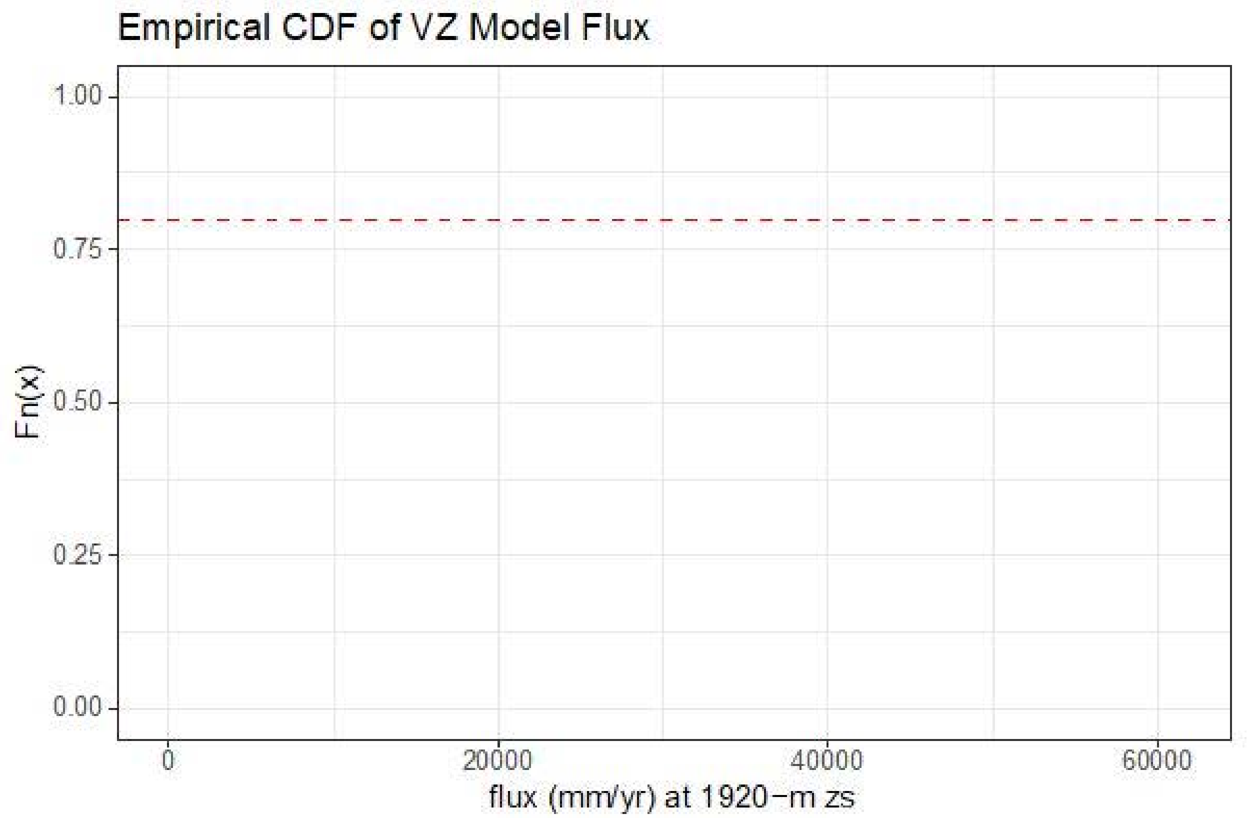

Note: Red dashed line depicts the 80th percentile.

Figure C-2.2-52 **Empirical cumulative distribution function of flux (mm/year) at the 1920-m z-slice from 19 runs of the RVZM**

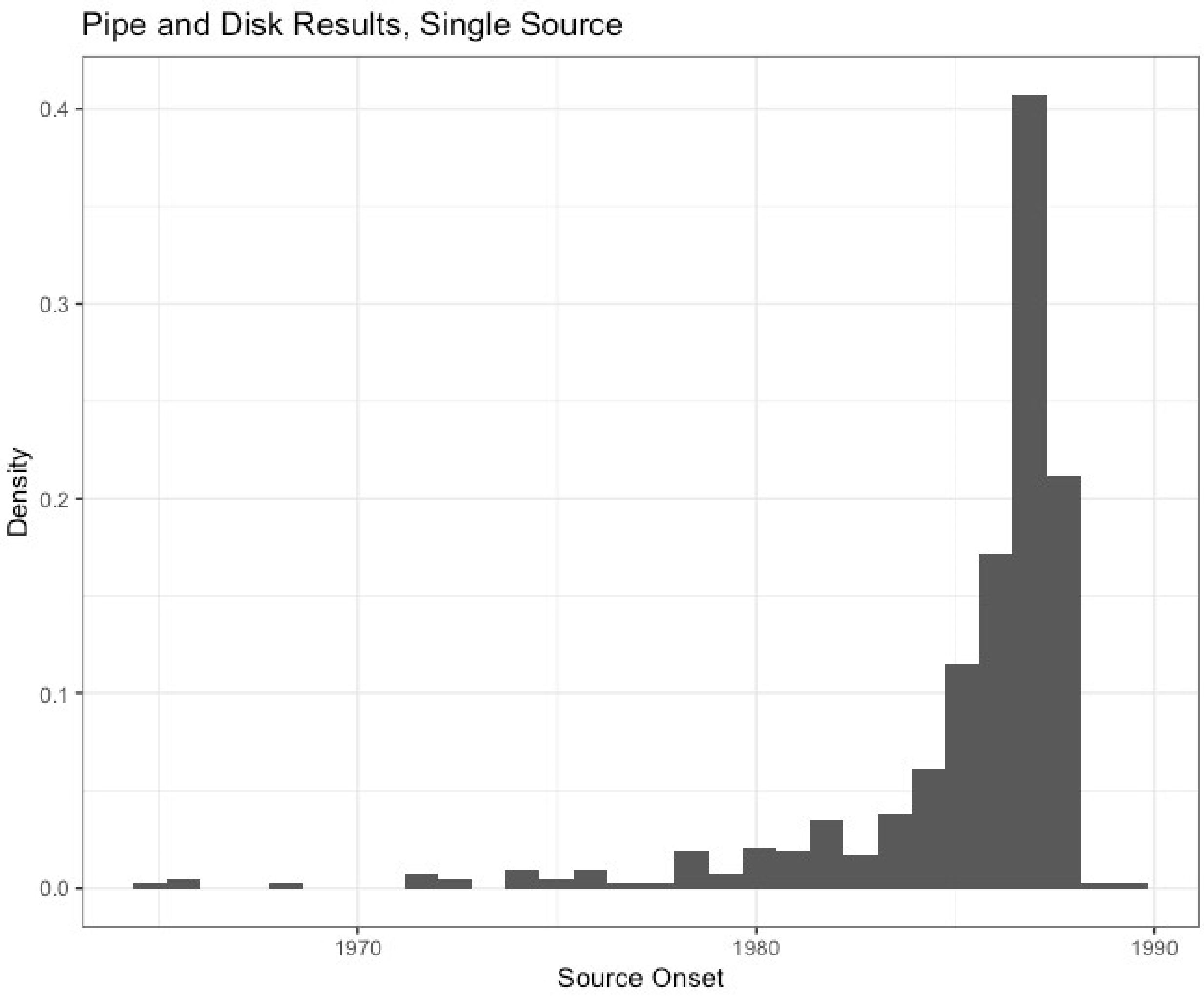

Figure C-2.2-53 Time of onset for single source P&D tool

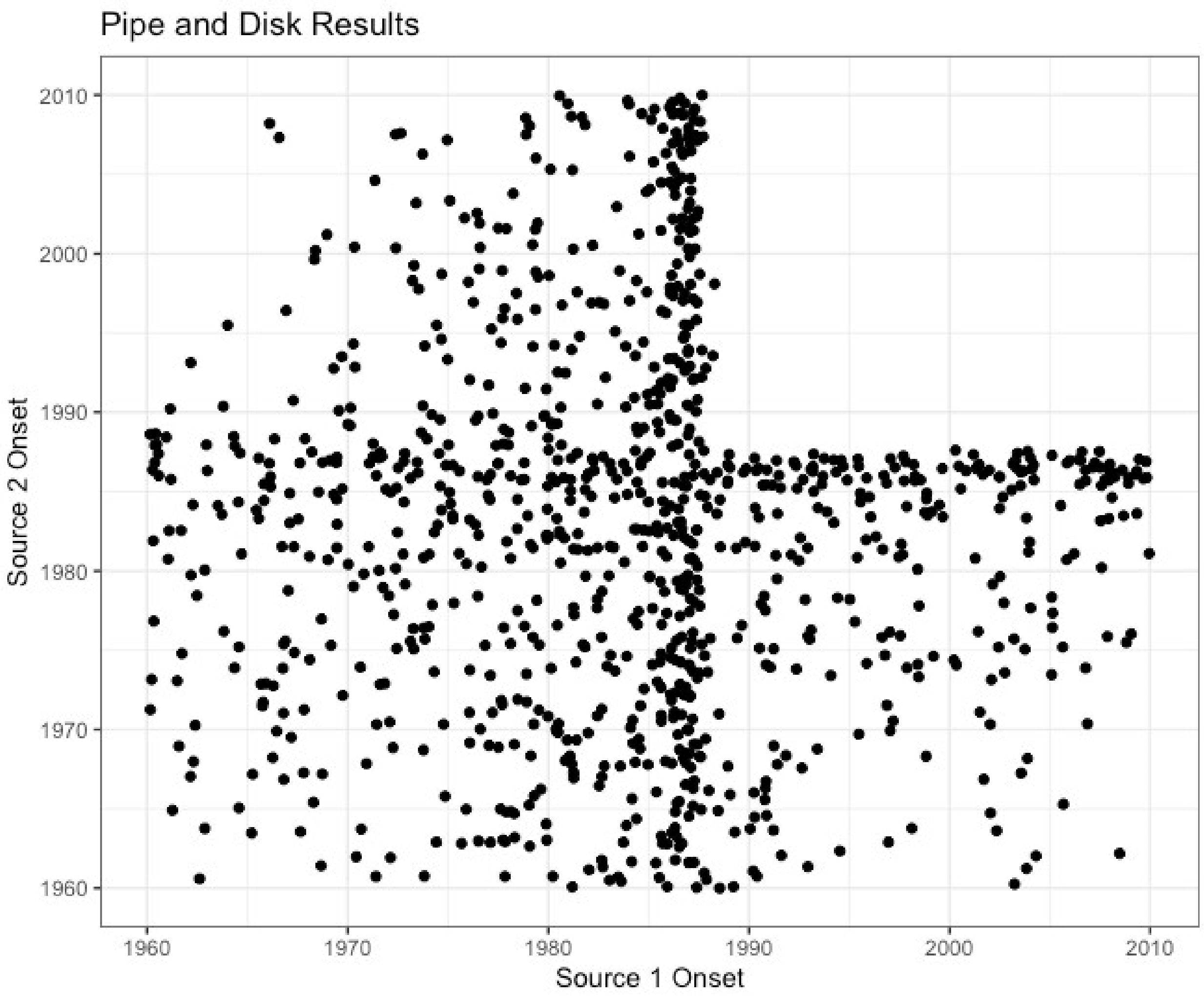

Figure C-2.2-54 Time of onset results for the double source P&D tool

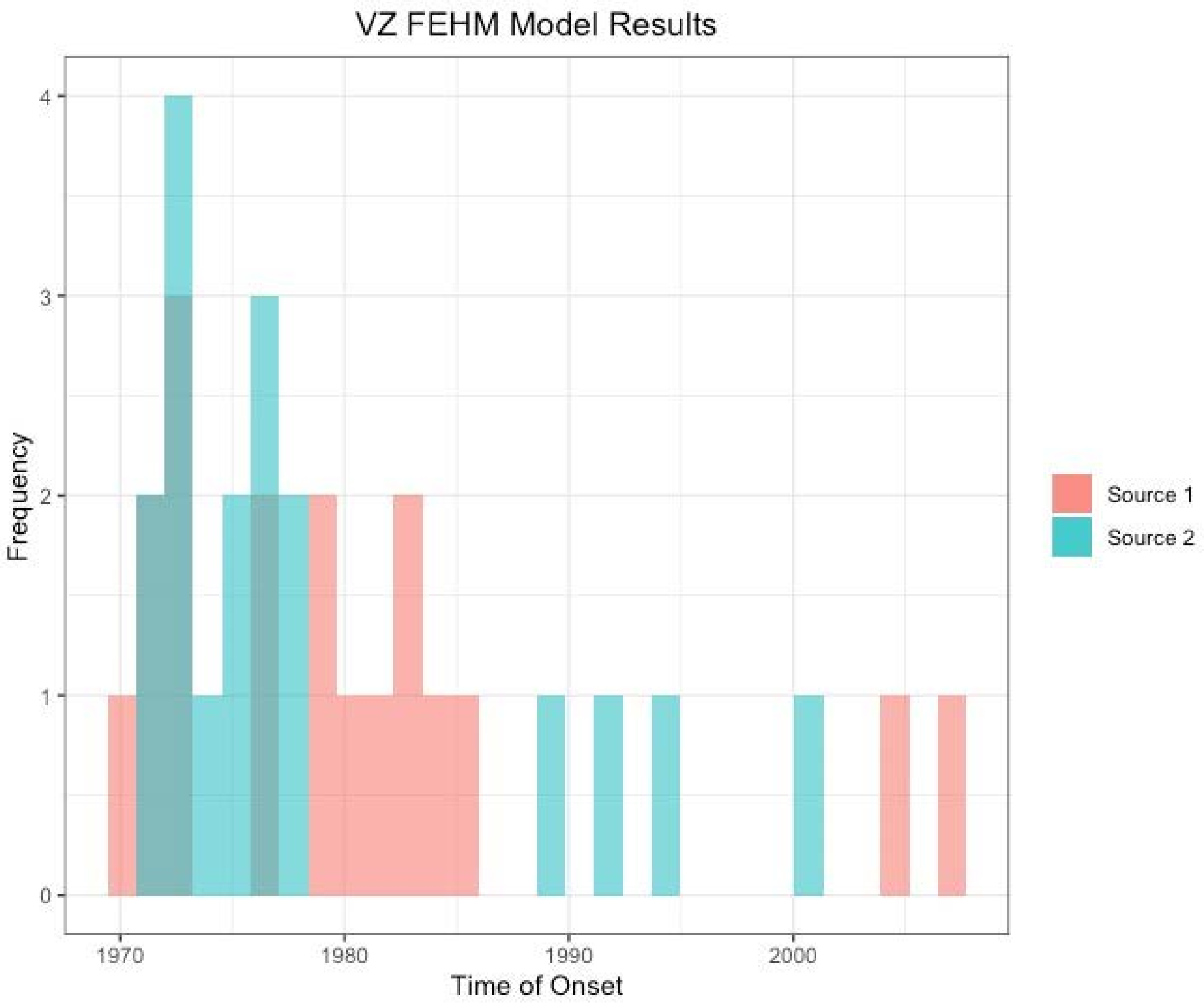

Figure C-2.2-55 Results for time of onset at the regional aquifer from the RVZM

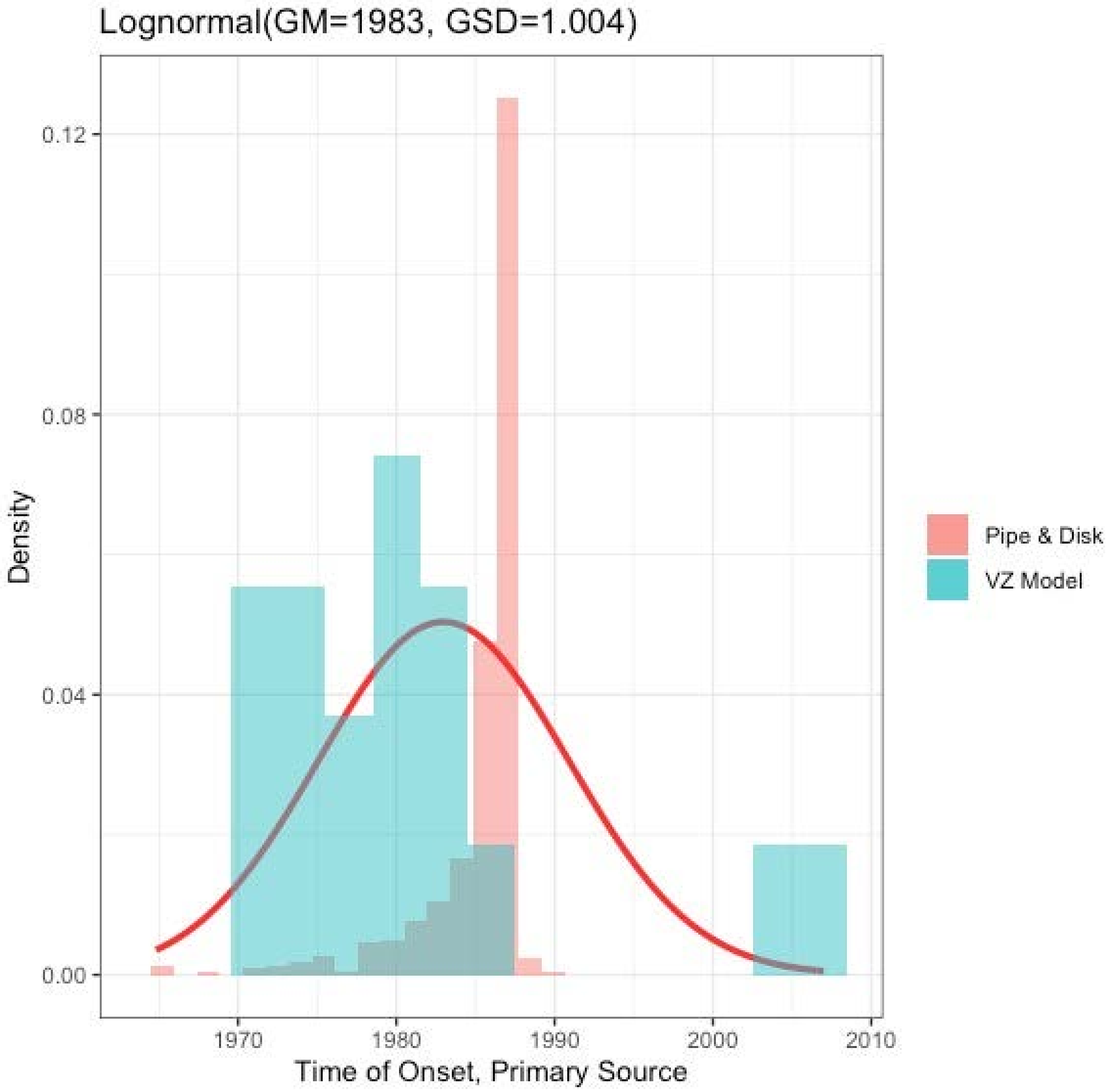

Figure C-2.2-56 **Distribution developed for time of onset for the primary source**

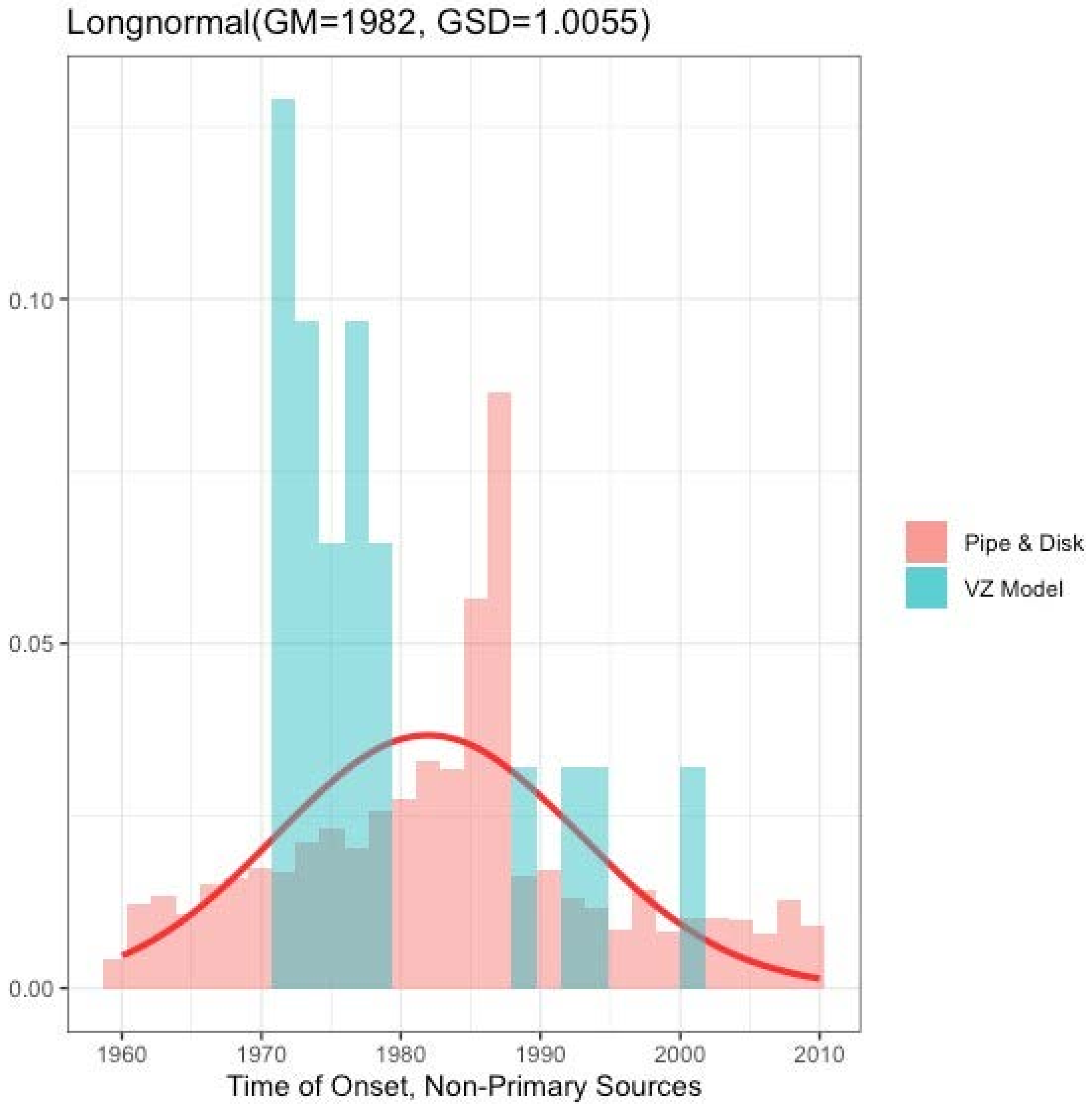

Figure C-2.2-57 **Distribution developed for time of onset for the secondary source**

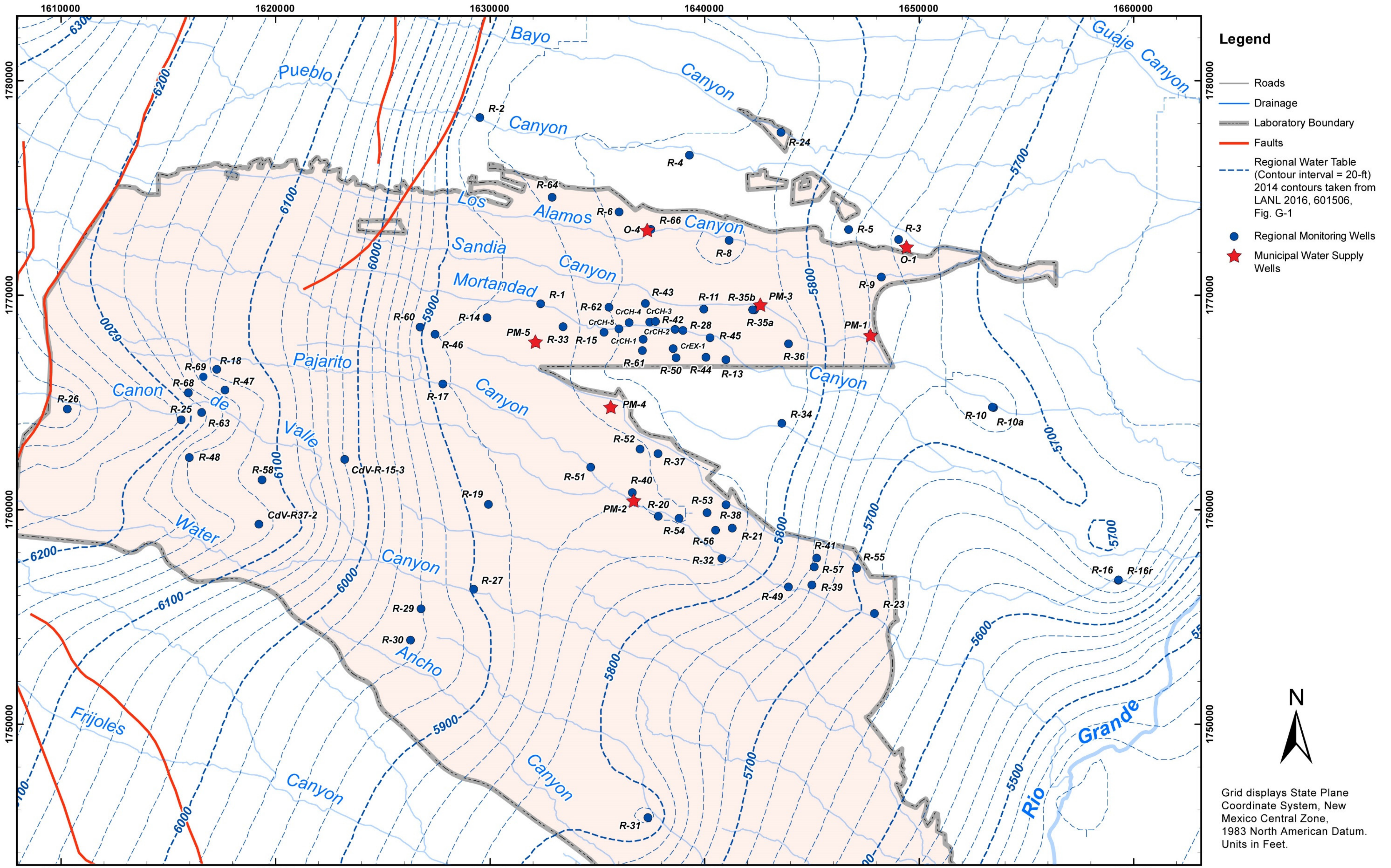

Grid displays State Plane Coordinate System, New Mexico Central Zone, 1983 North American Datum. Units in Feet.

Figure C-2.2-58 Regional water table at LANL

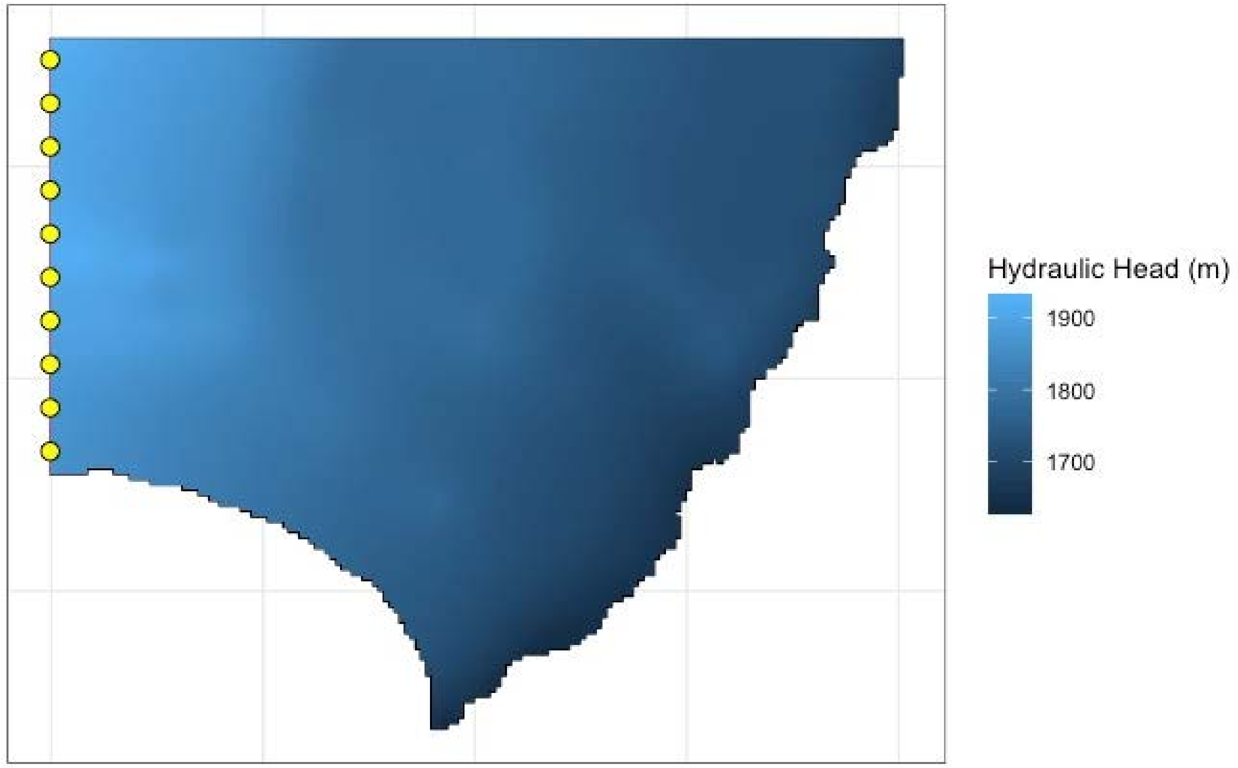

Note: Yellow dots are an example set of 10 points (actual distribution development was based on 100,000 points) selected along the western boundary.

Figure C-2.2-59 Raster data from the 2014 water table map used for distribution development for hydraulic head at the western boundary

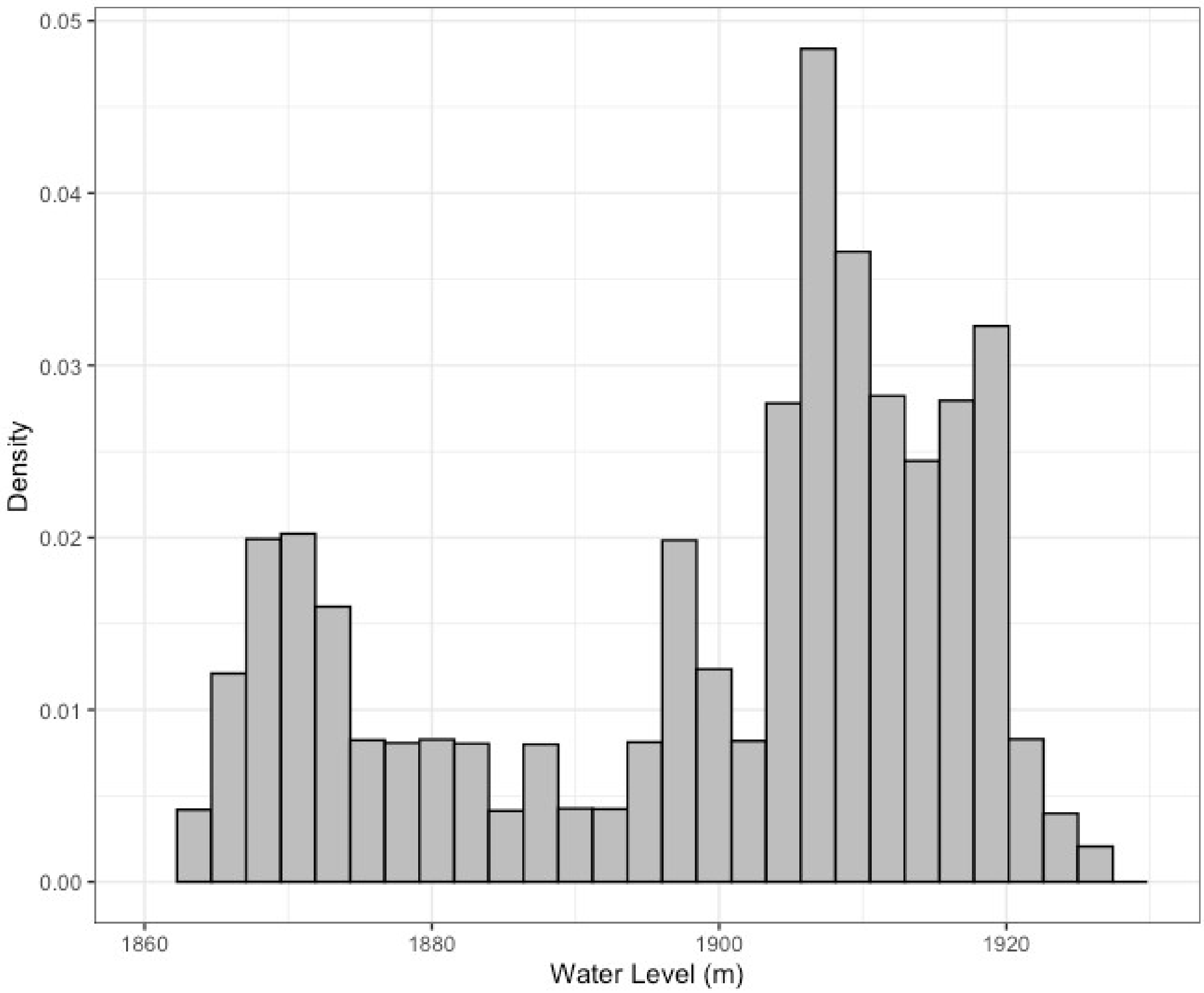

Figure C-2.2-60 Hydraulic head values at the western boundary

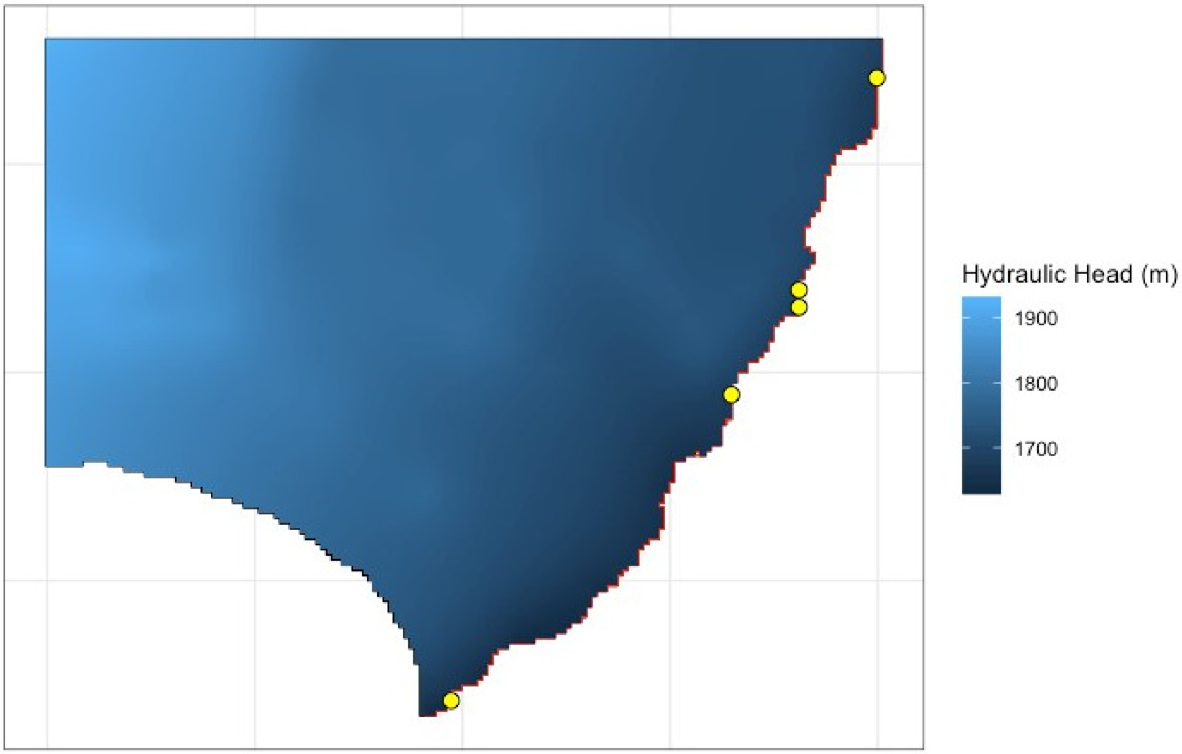

Figure C-2.2-61 **Raster data from the 2014 water table map used for distribution development for hydraulic head at the eastern boundary**

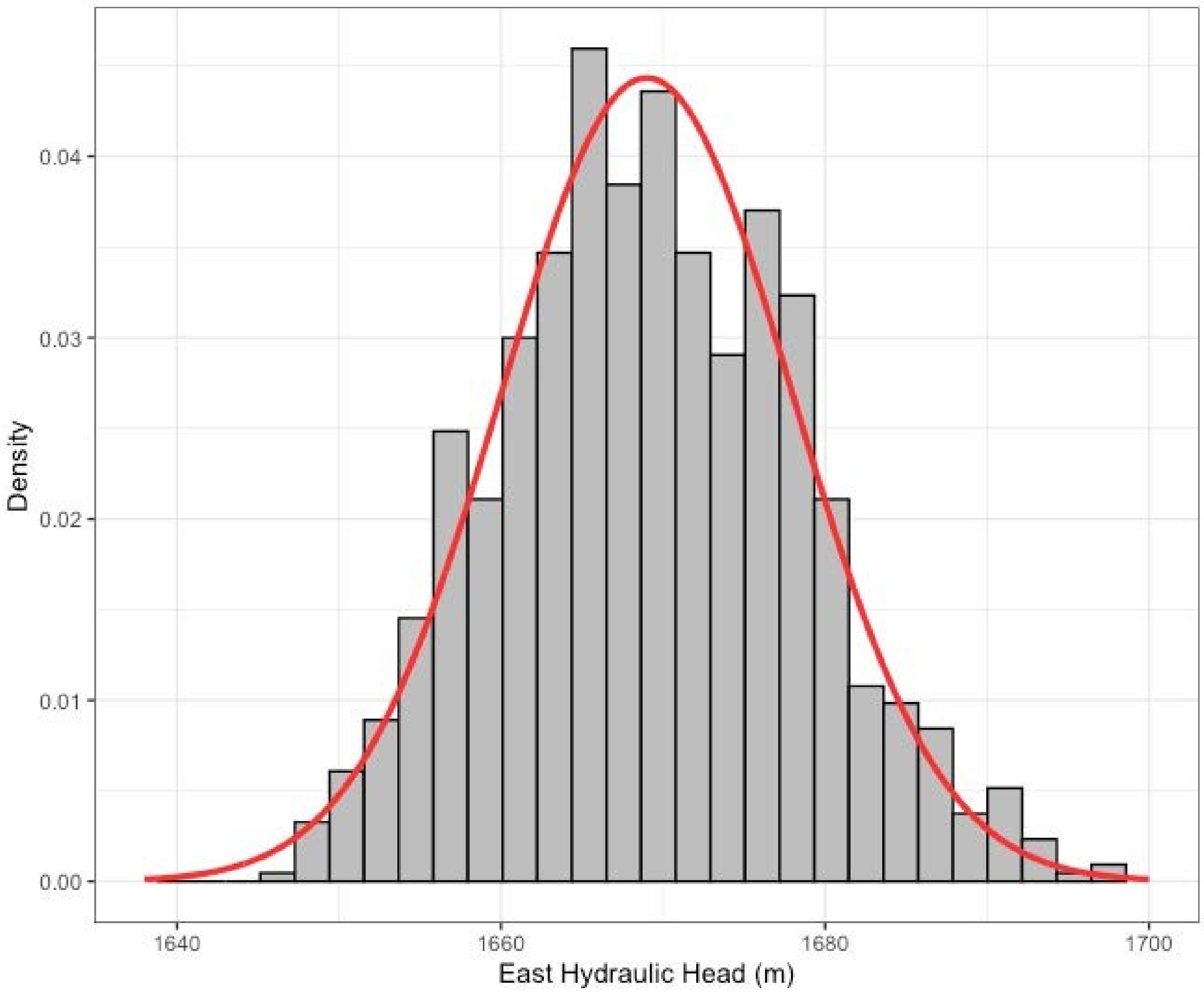

Figure C-2.2-62 **Preliminary distribution of values for hydraulic head at the eastern boundary based on the 2014 water level map**

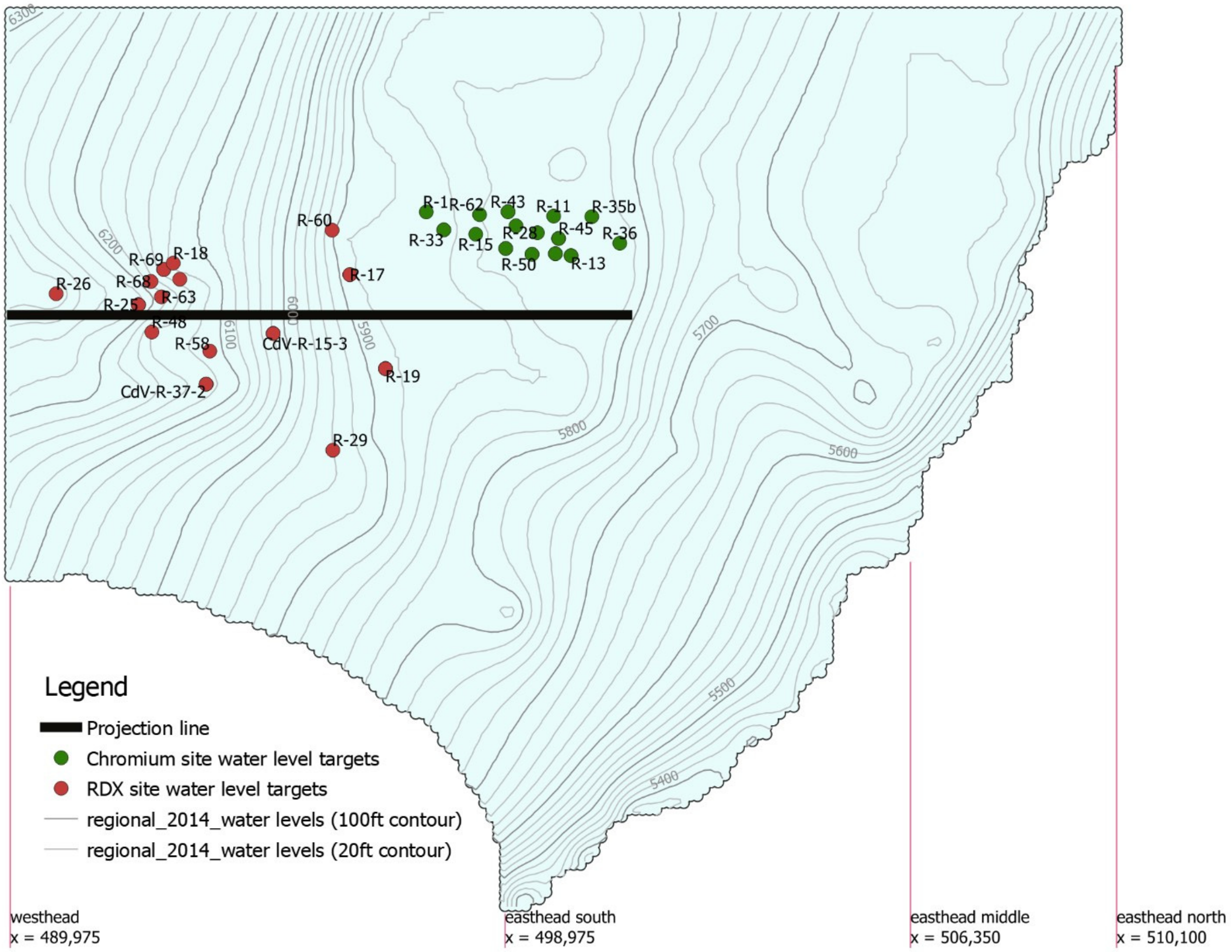

Figure C-2.2-63 Spatial distribution of wells with groundwater level targets at the RDX and chromium sites

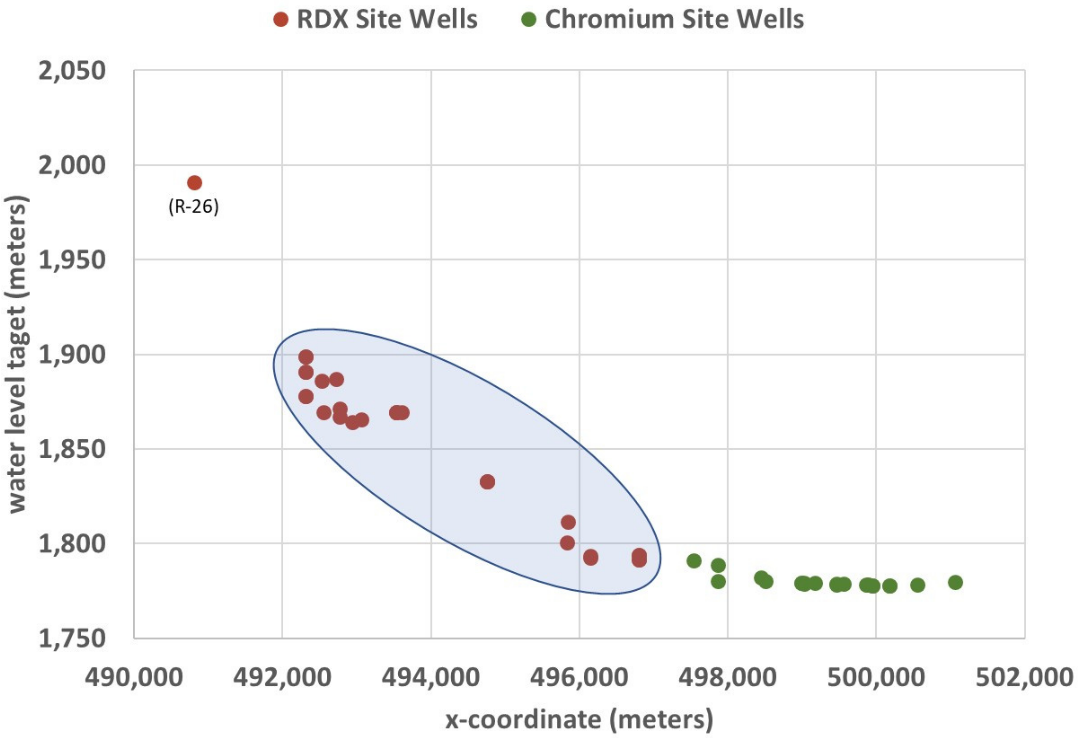

Figure C-2.2-64 Gradient in RDX versus chromium areas

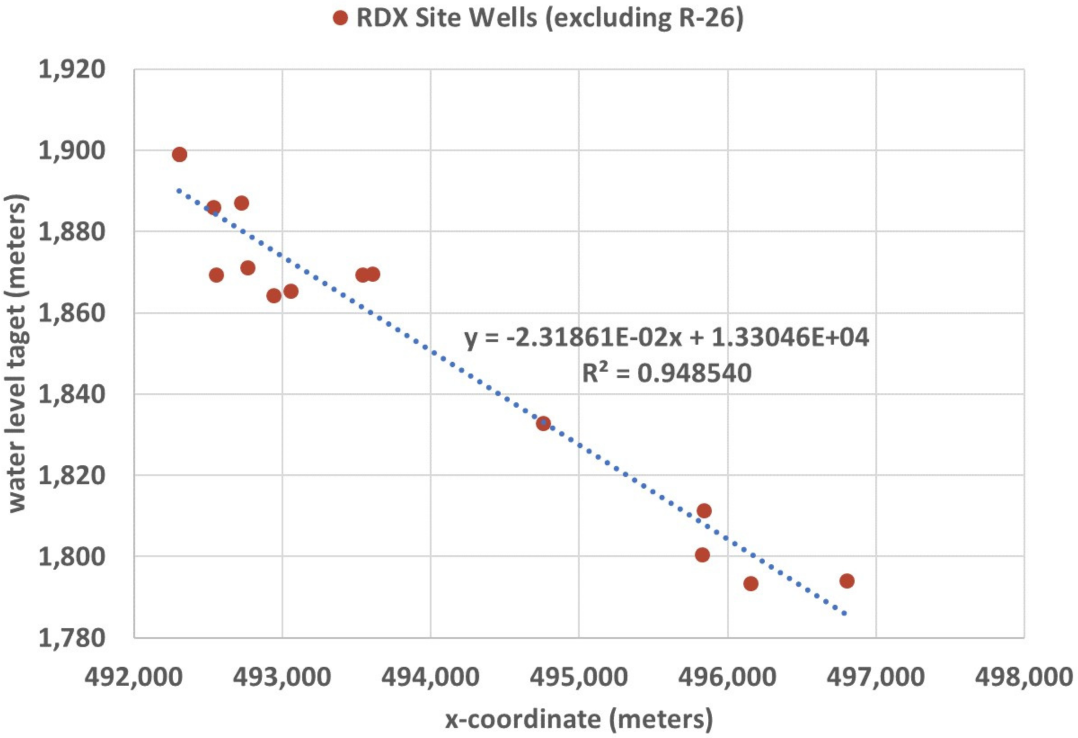

Figure C-2.2-65 Regression of RDX area wells

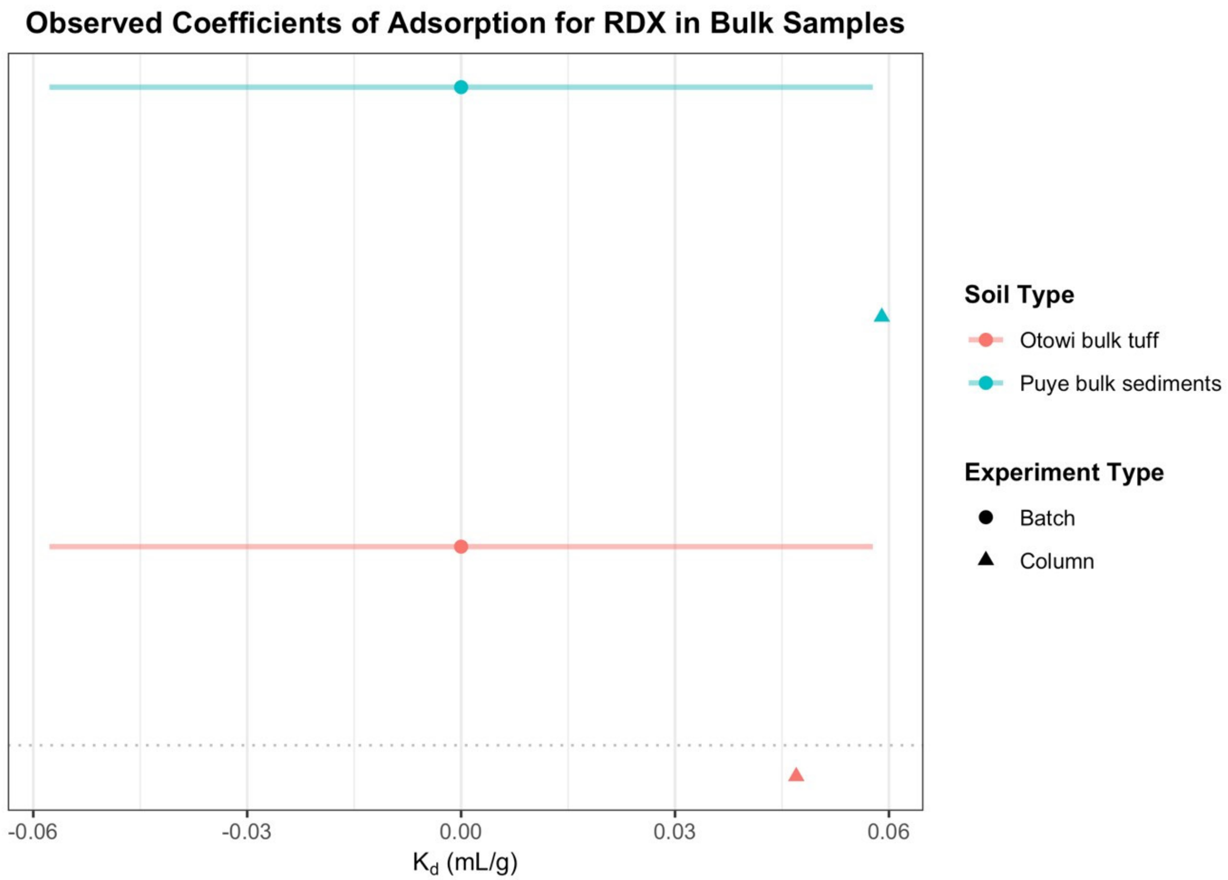

Note: The solid (colored) horizontal lines represent an approximate 95% confidence interval for the mean K_d. Some records did not have spread information, and no bars are provided for those records. Horizontal dashed lines are included to help separate the different soil types.

Figure C-2.2-66 Dot and whisker plots of the observed RDX K_d values for bulk samples

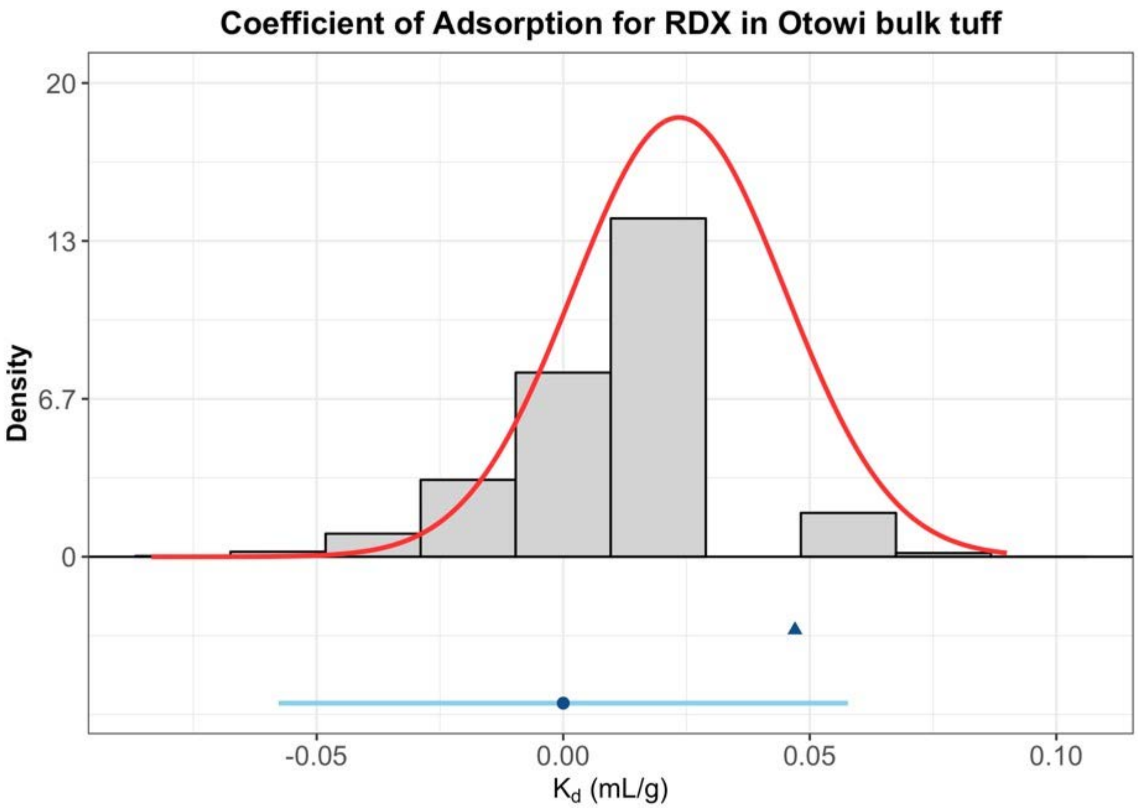

Notes: The observed mean RDX K_d values for Otowi bulk tuff are included below the plot with horizontal lines showing two standard errors in the mean for the batch experiment records. The experiment type of the record is represented on the plot by triangles (column experiment) and circles (batch experiment).

Figure C-2.2-67 Histogram of mean RDX K_d values obtained from the distribution development procedure for volcanic materials with the corresponding fitted normal distribution (red curve)

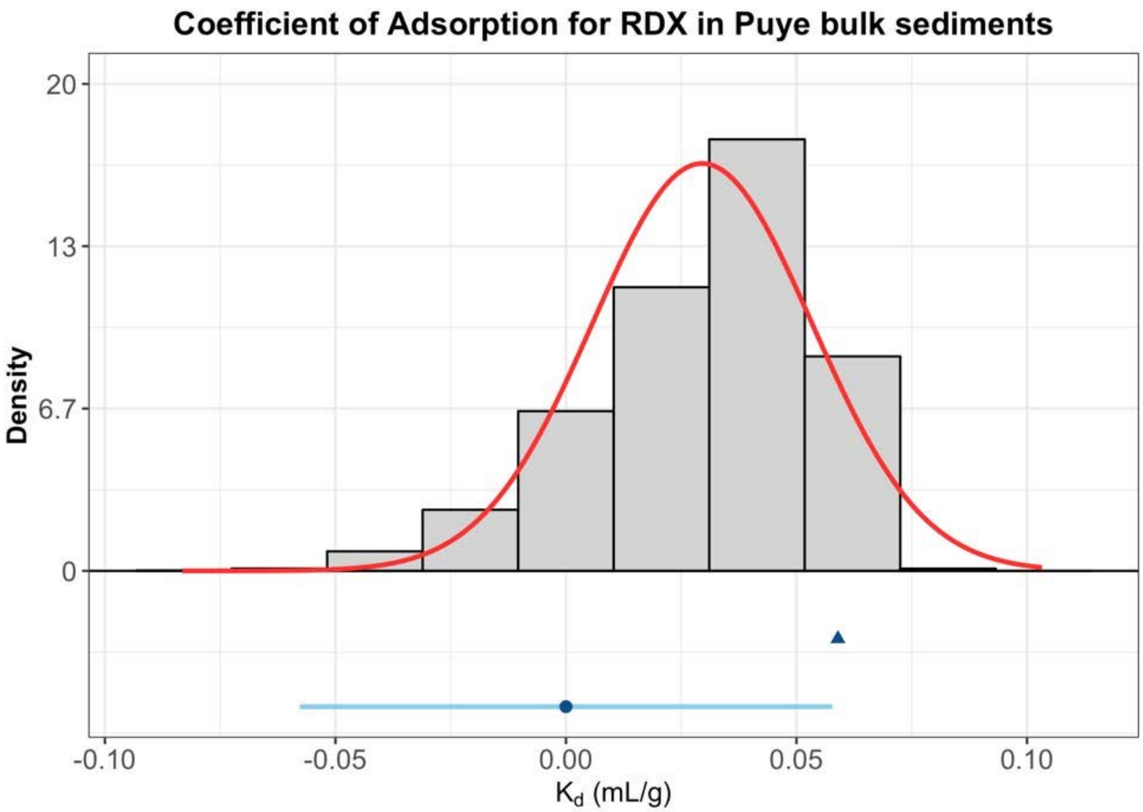

Notes: The observed mean RDX K_d values for Puye bulk sediments are included below the plot with horizontal lines showing two standard errors in the mean for the batch experiment records. The experiment type of the record is represented on the plot by triangles (column experiment) and circles (batch experiment).

Figure C-2.2-68 Histogram of mean RDX K_d values obtained from the distribution development procedure for sedimentary materials with the corresponding fitted normal distribution (red curve)

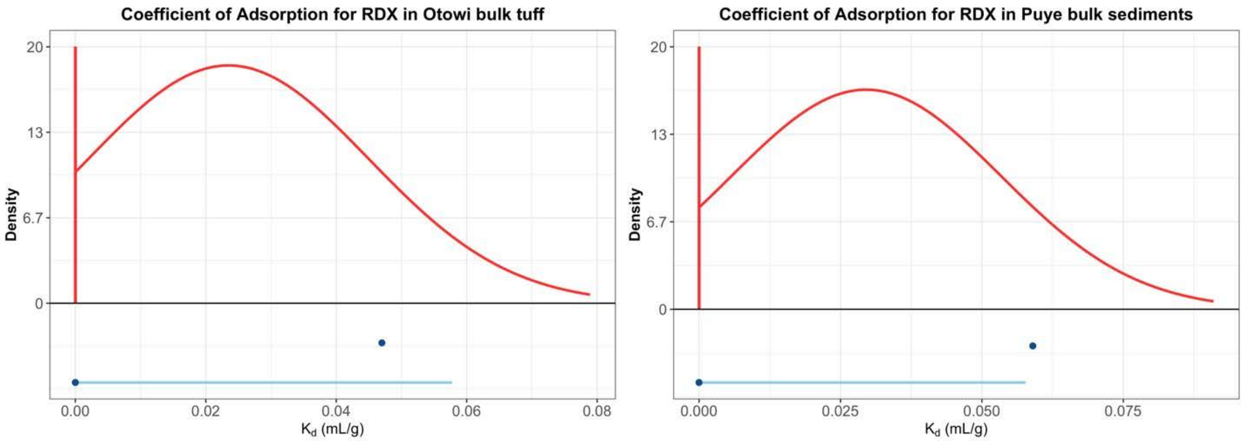

Notes: Information regarding the distributions is found in Table C-2.2-22. The vertical red lines on the left side of each plot illustrate that the distributions are bulldozed at 0 mL/g as opposed to truncated. Observed K_d coefficients are plotted below each distribution as blue points. The horizontal light-blue line extends two standard errors in the positive direction; as the distribution is bulldozed at 0 mL/g, the error bars are not displayed two standard errors in the negative direction.

Figure C-2.2-69 Final “bulldozed” distributions for average K_d coefficients of volcanic materials (left) and sedimentary materials (right)

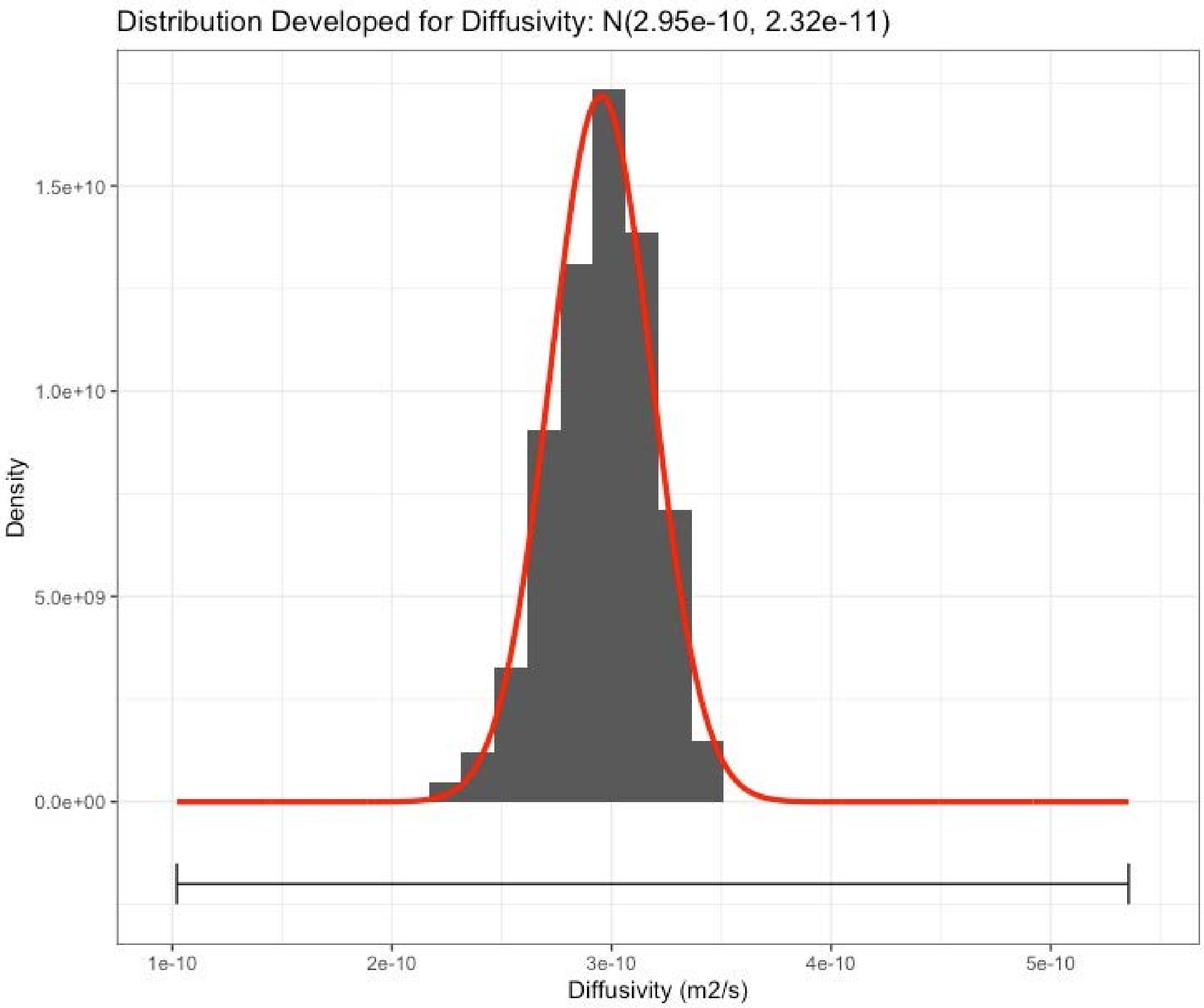

Note: The black line shows the range of possible values from which the distribution was built, using the 1st and 99th percentiles of the distribution for total porosity.

Figure C-2.2-70 Distribution developed for D_e

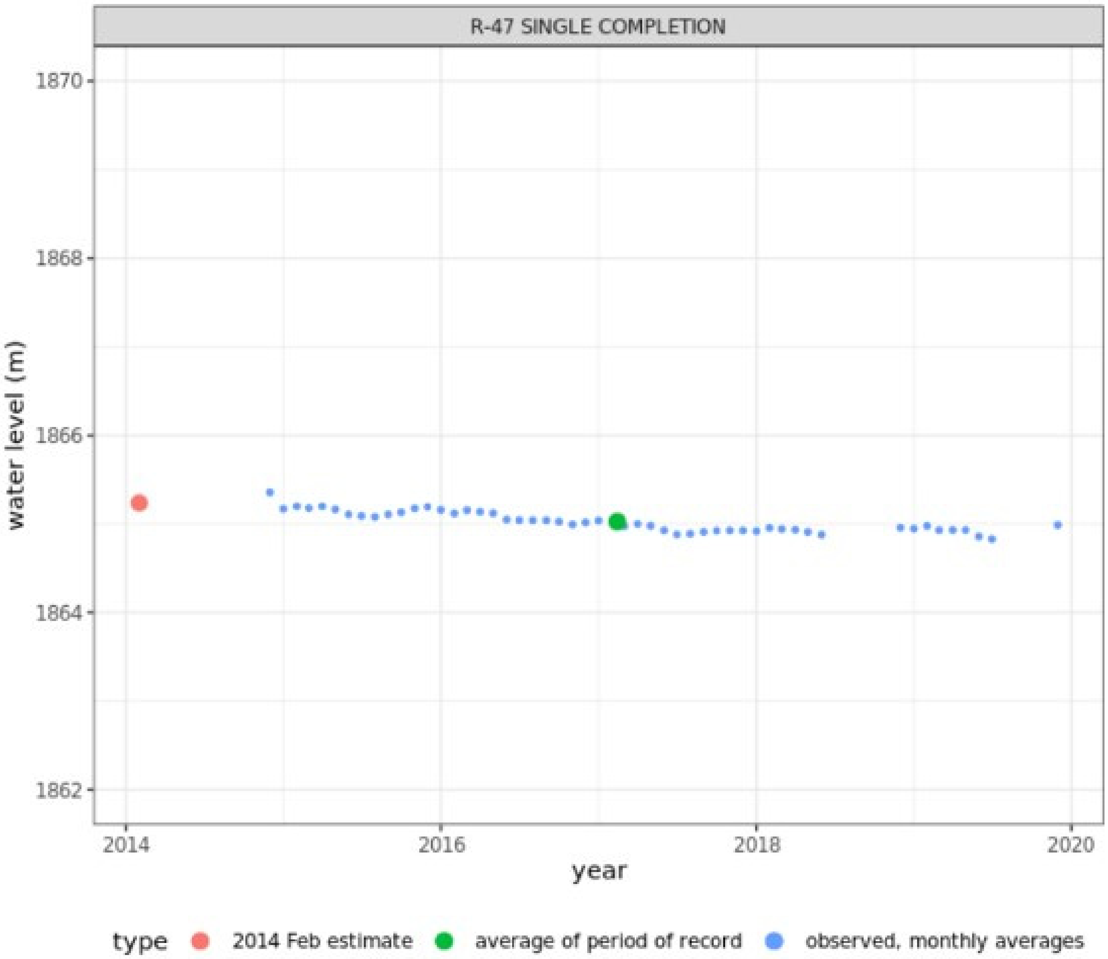

Figure C-2.3-1 R-47 imputed hydraulic head in February 2014

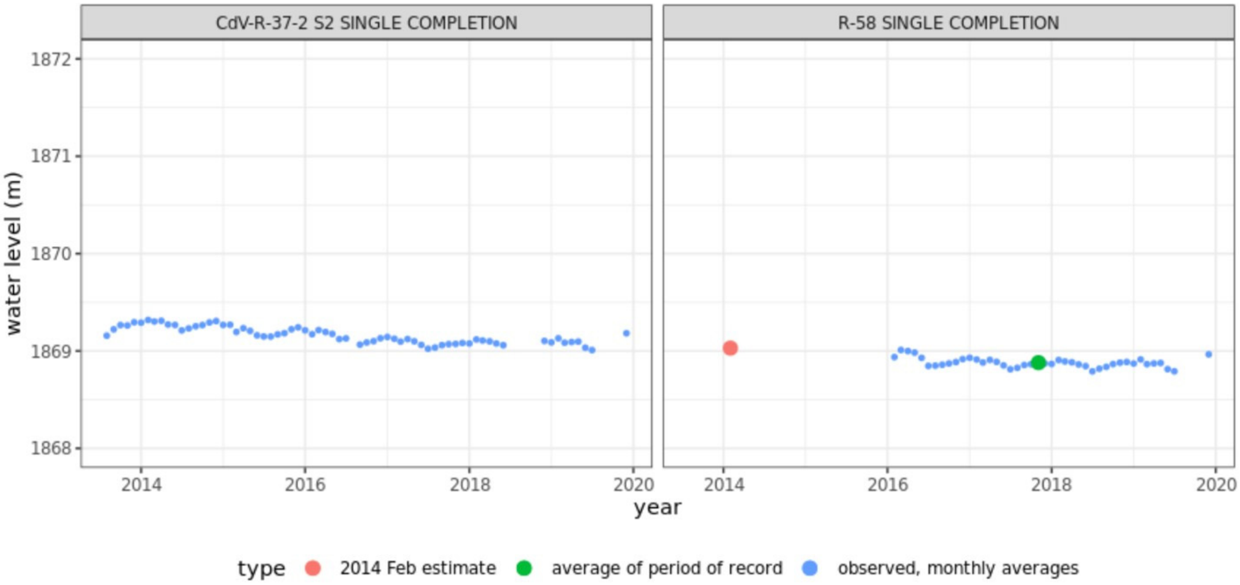

Figure C-2.3-2 CdV-R-37 screen 2 and R-58 imputed hydraulic head in February 2014

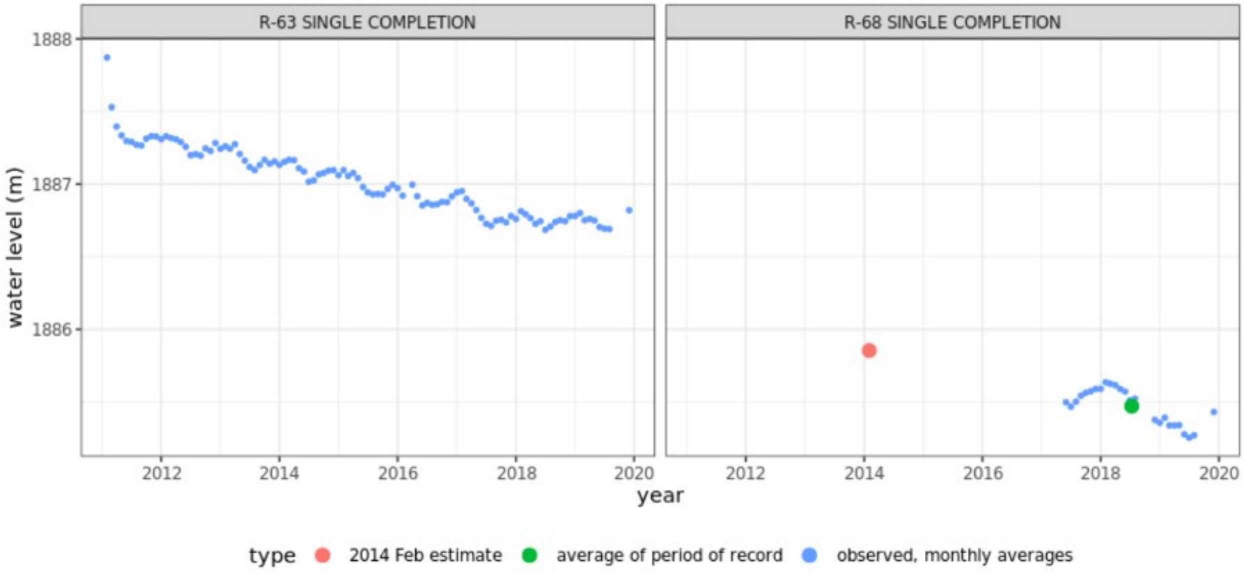

Figure C-2.3-3 R-63 and R-68 imputed hydraulic head in February 2014

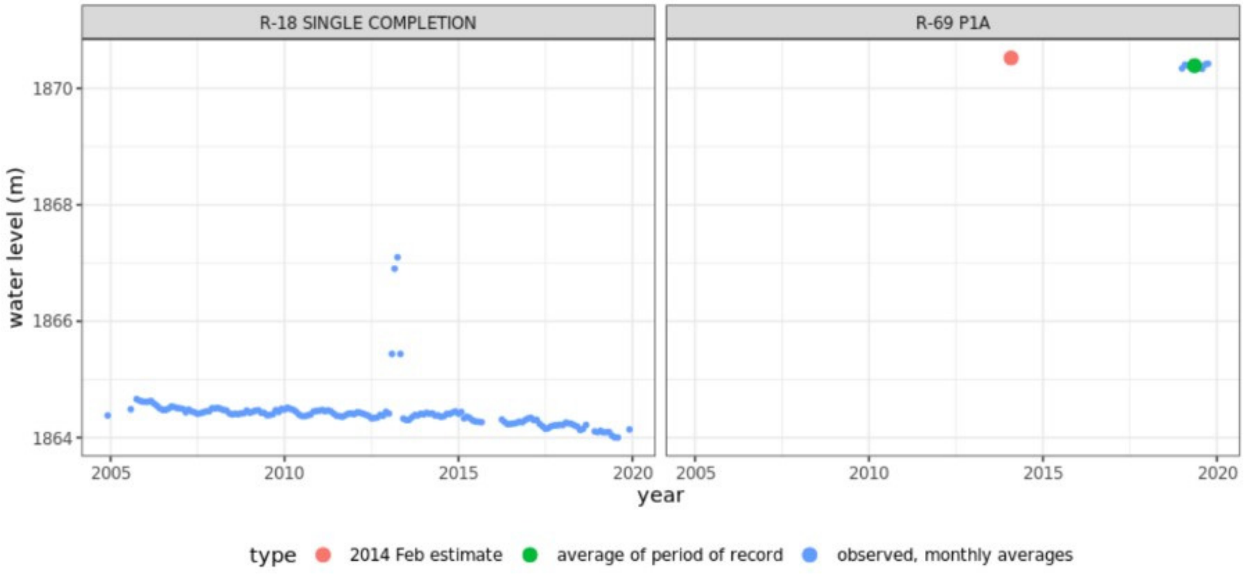

Figure C-2.3-4 R-18 and R-69 screen 1 imputed hydraulic head in February 2014

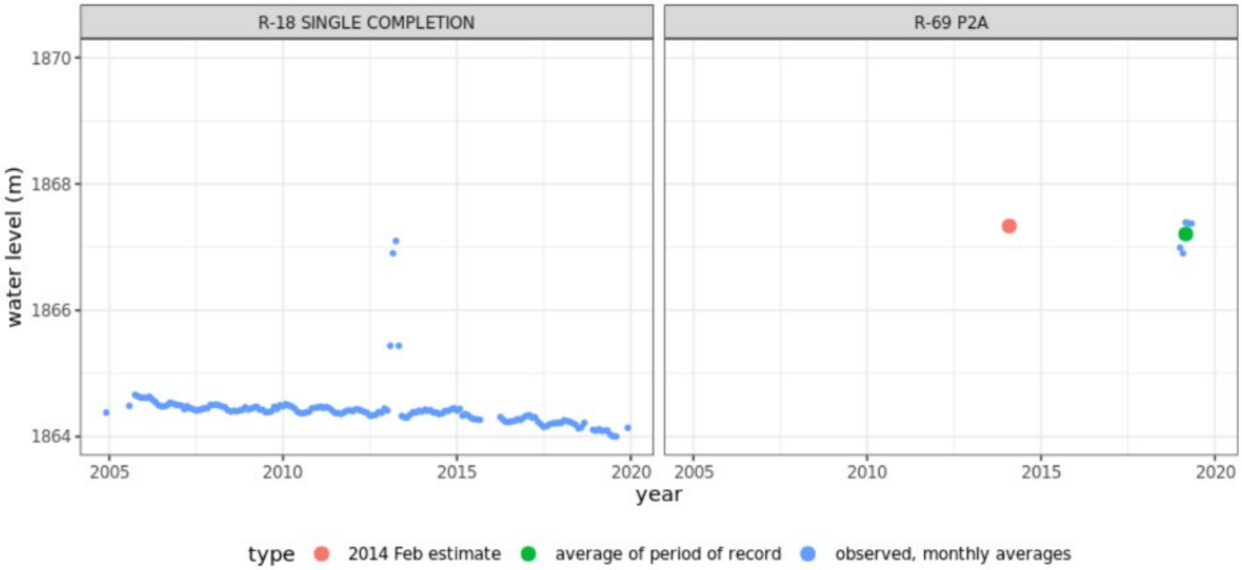

Figure C-2.3-5 **R-18 and R-69 screen 2 imputed hydraulic head in February 2014**

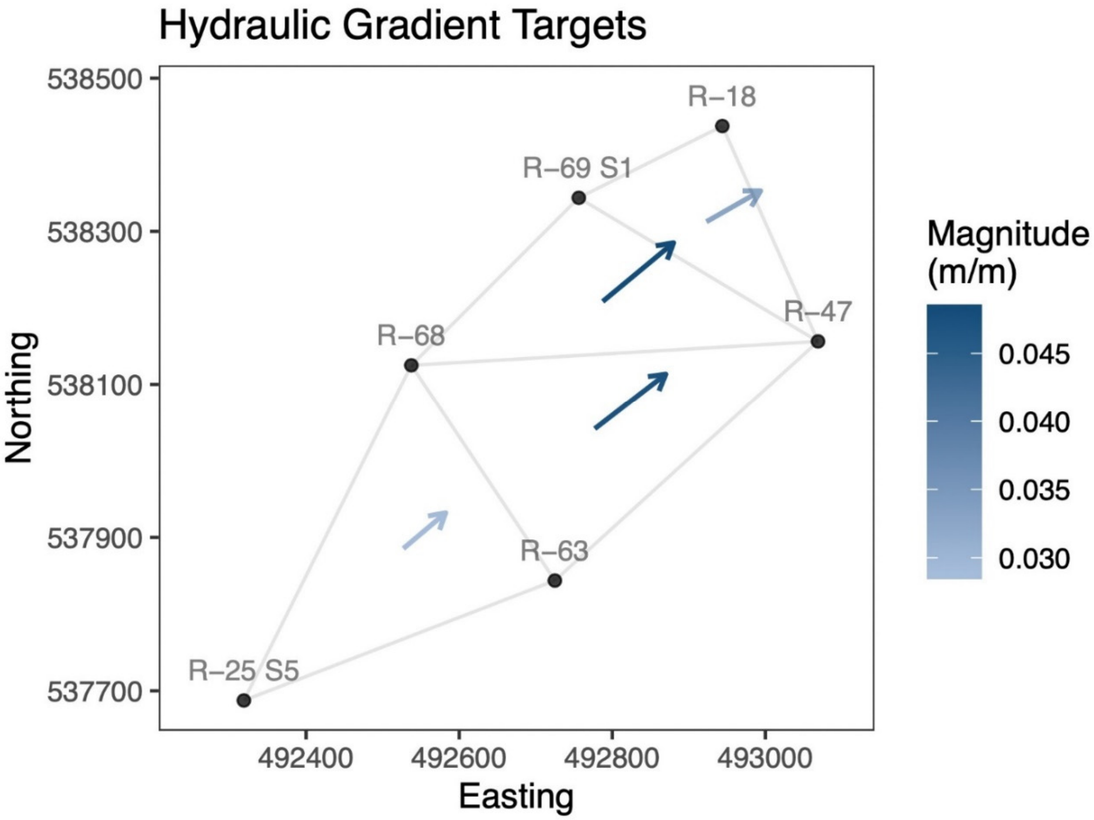

Note: Gradient vectors are anchored to the well triple centroids and relative magnitudes are indicated by a vector's length.

Figure C-2.3-6 **Graphical depiction of the hydraulic gradient vectors and subset of wells used to derive them**

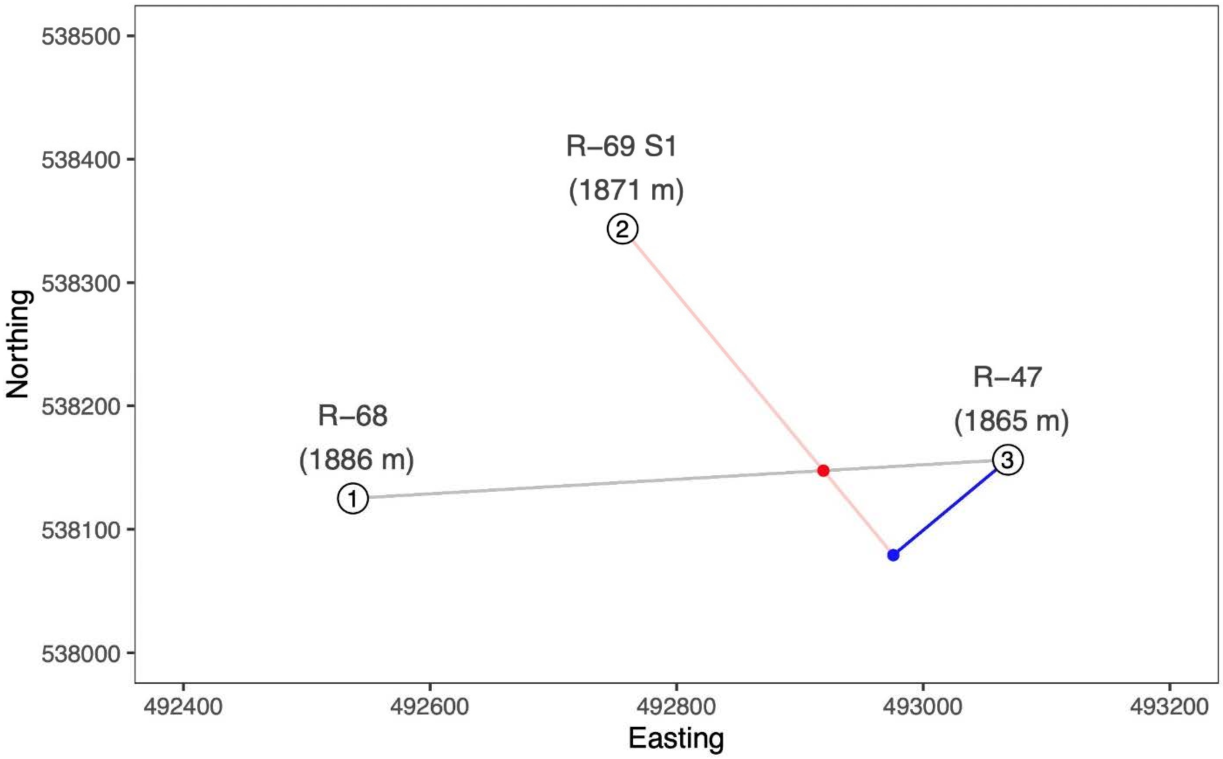

Note: Lines referenced in steps 3 and 4 are plotted in red and blue, respectively.

Figure C-2.3-7 Diagram of gradient computation for wells R-68, R-69 S1, and R-47

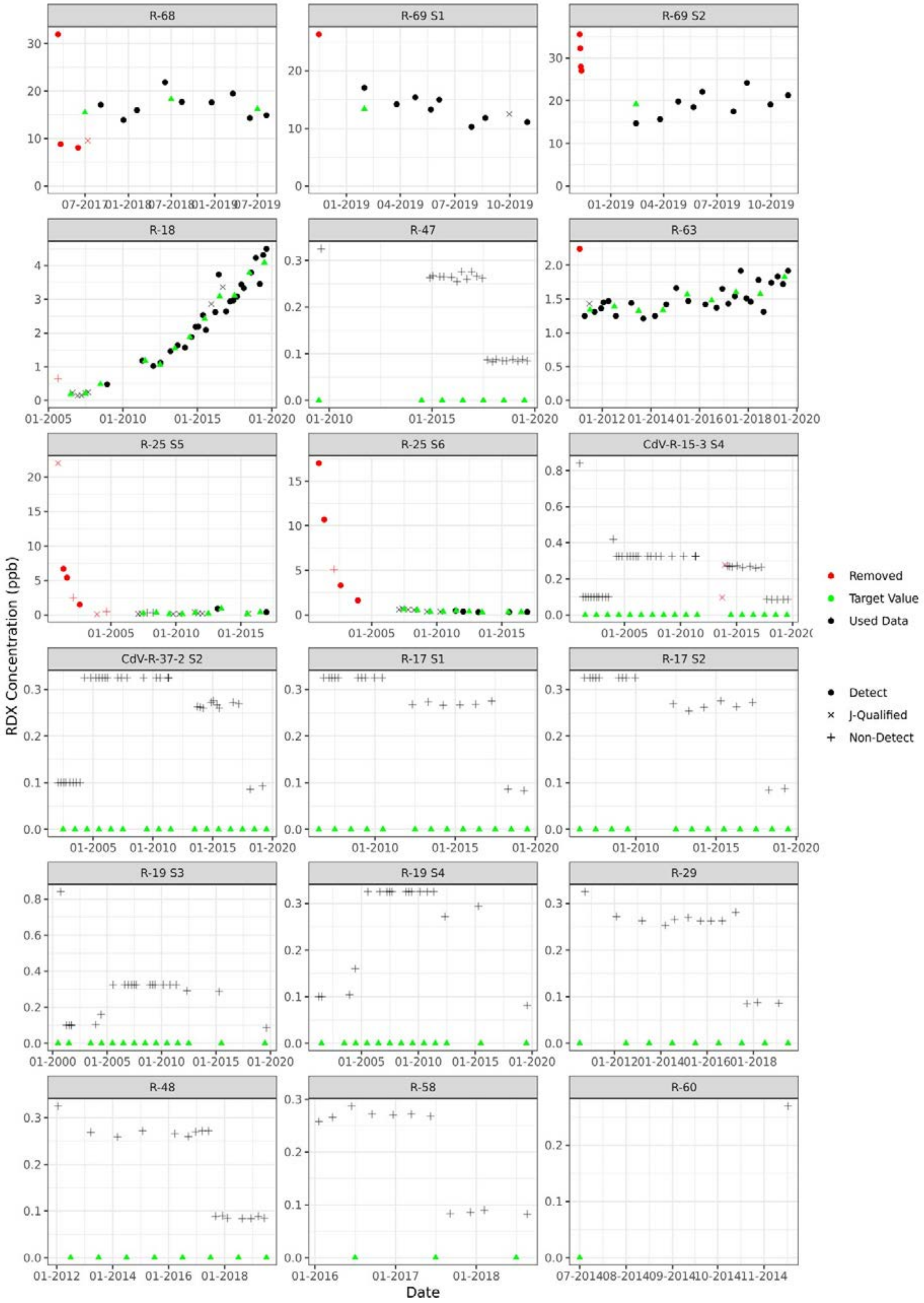

Note: Values shown in red were not included in target development on the basis of expert judgement

Figure C-2.3-8 Data used to inform yearly target values for RDX concentration in the RRM

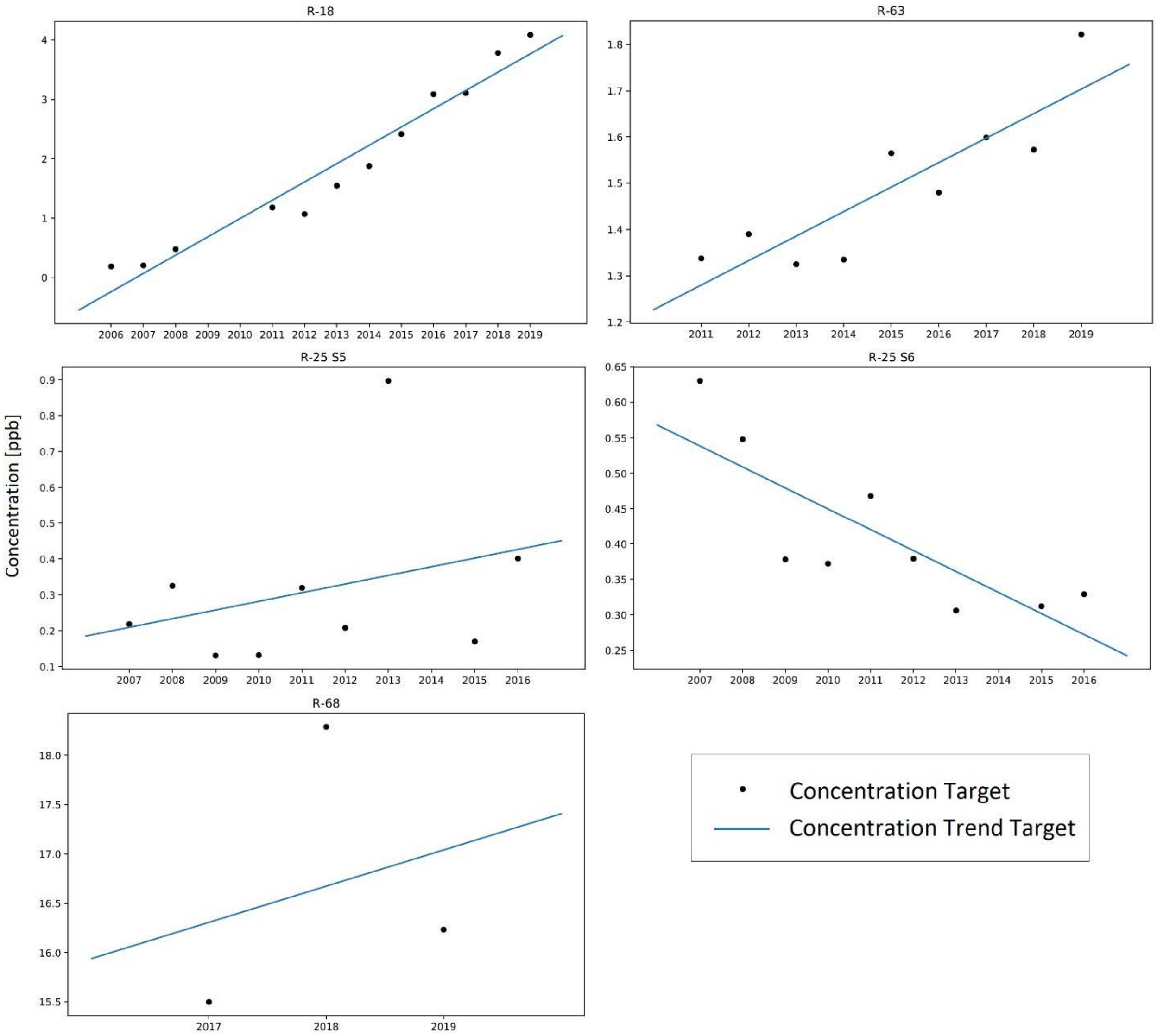

Figure C-2.3-9 **Concentration trend targets derived from the slopes of the concentration targets**

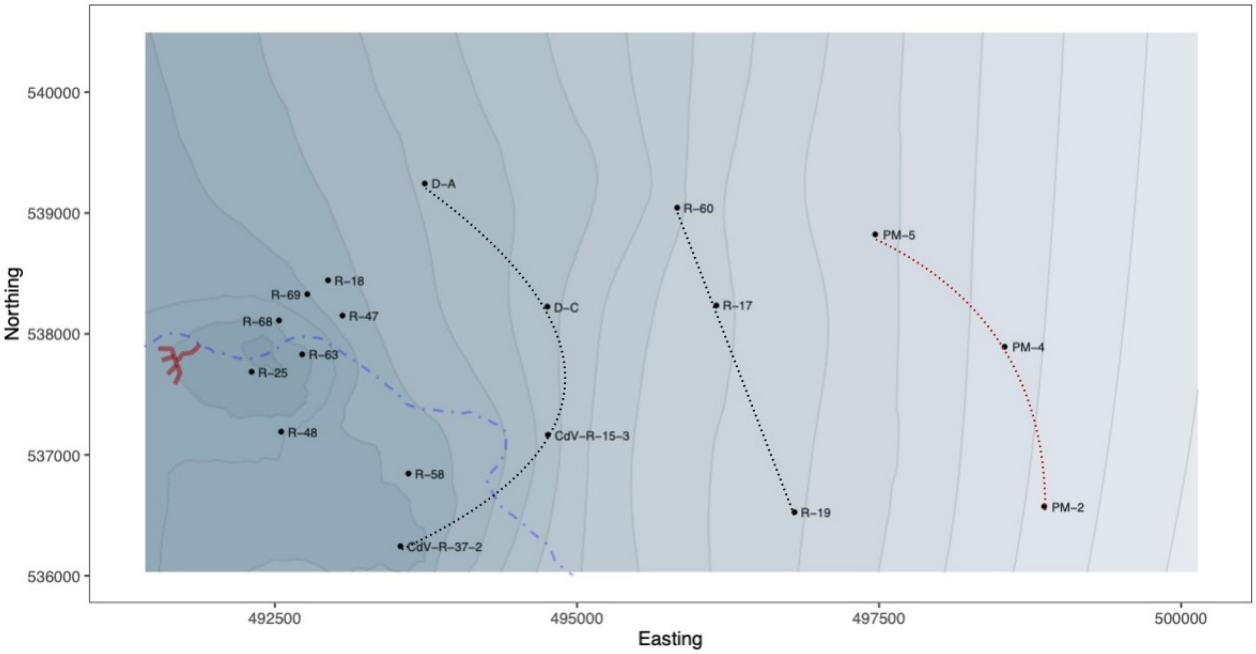

Notes: Decision locations where output is produced (PM wells, CdV-R-15-3, D-A, and D-C) are shown. The 260 Outfall and Cañon de Valle are also plotted for reference. Dotted lines represent potential regions where future monitoring could occur.

Figure C-2.4-1 Spatial location of wells used in the RDX calibration plotted over a base map of LM-calibration water table results

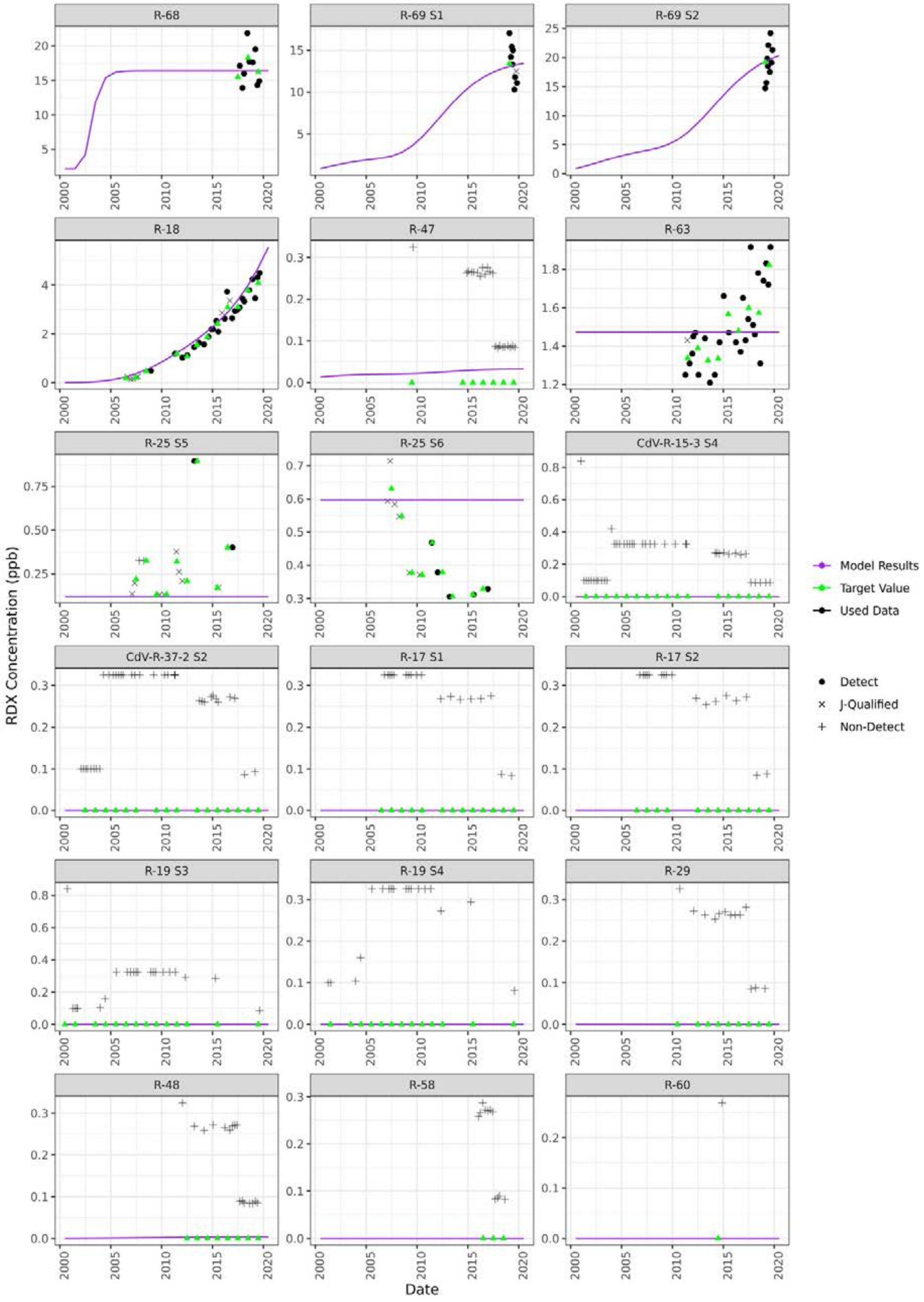

Figure C-3.1-1 **Concentration matches to data are excellent, especially at wells with higher measured RDX**

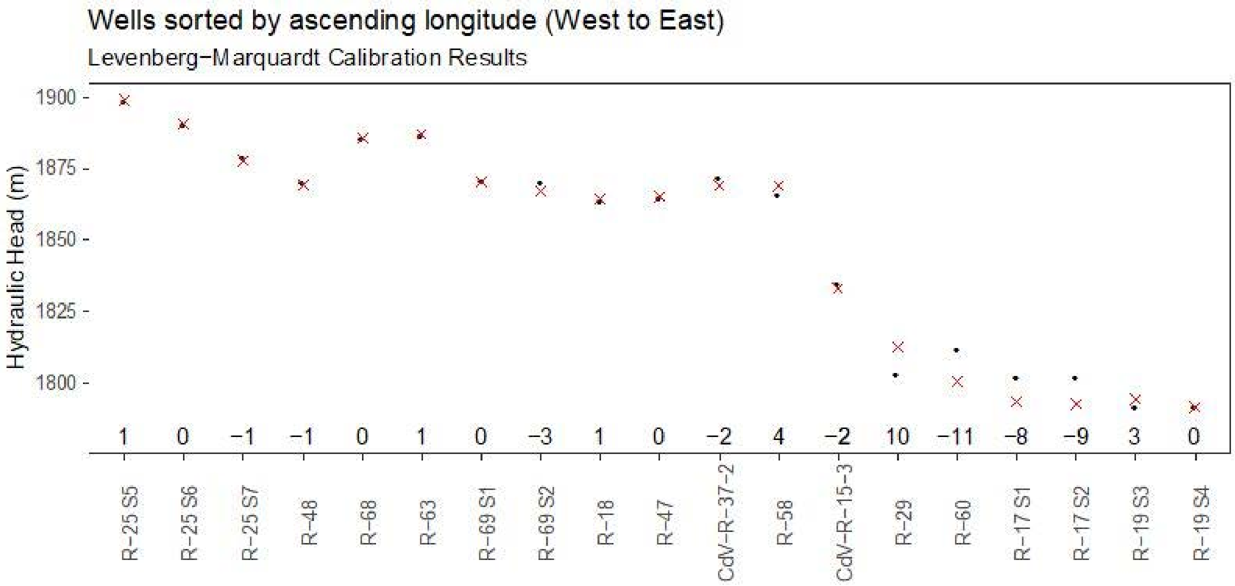

Note: Target data are shown with red Xs, and LM results are shown as black dots. Residuals (in m) are labeled above the well name along the x-axis. For a spatial representation see Figure C-3.1-3.

Figure C-3.1-2 **Hydraulic head matches to data are within 3 m local to the plume, and within 11 m downgradient of the plume**

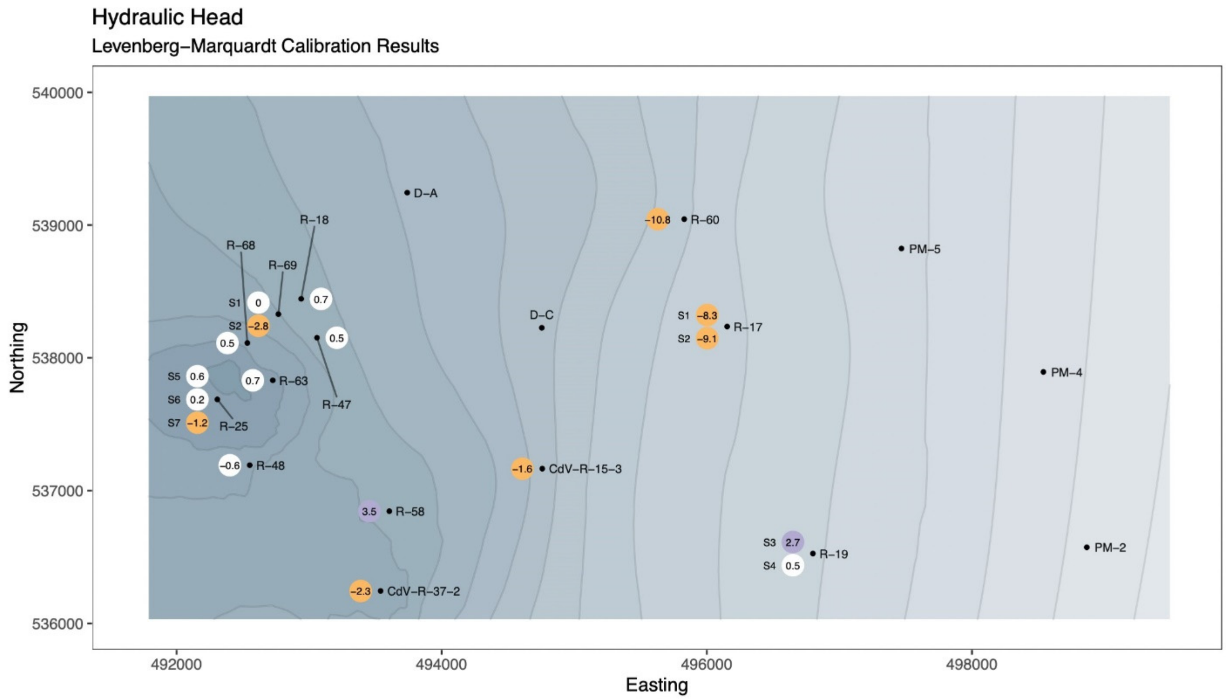

Note: Residuals (simulation–target) are shown in white if they are within 1 m, in blue if the simulation estimate is lower than the data, and in orange if the simulation is higher than the data. Residual values are plotted in the circles. The contours show the water level in the LM calibration results.

Figure C-3.1-3 Hydraulic head matches to data are within 3 m local to the plume, and within 11 m downgradient of the plume

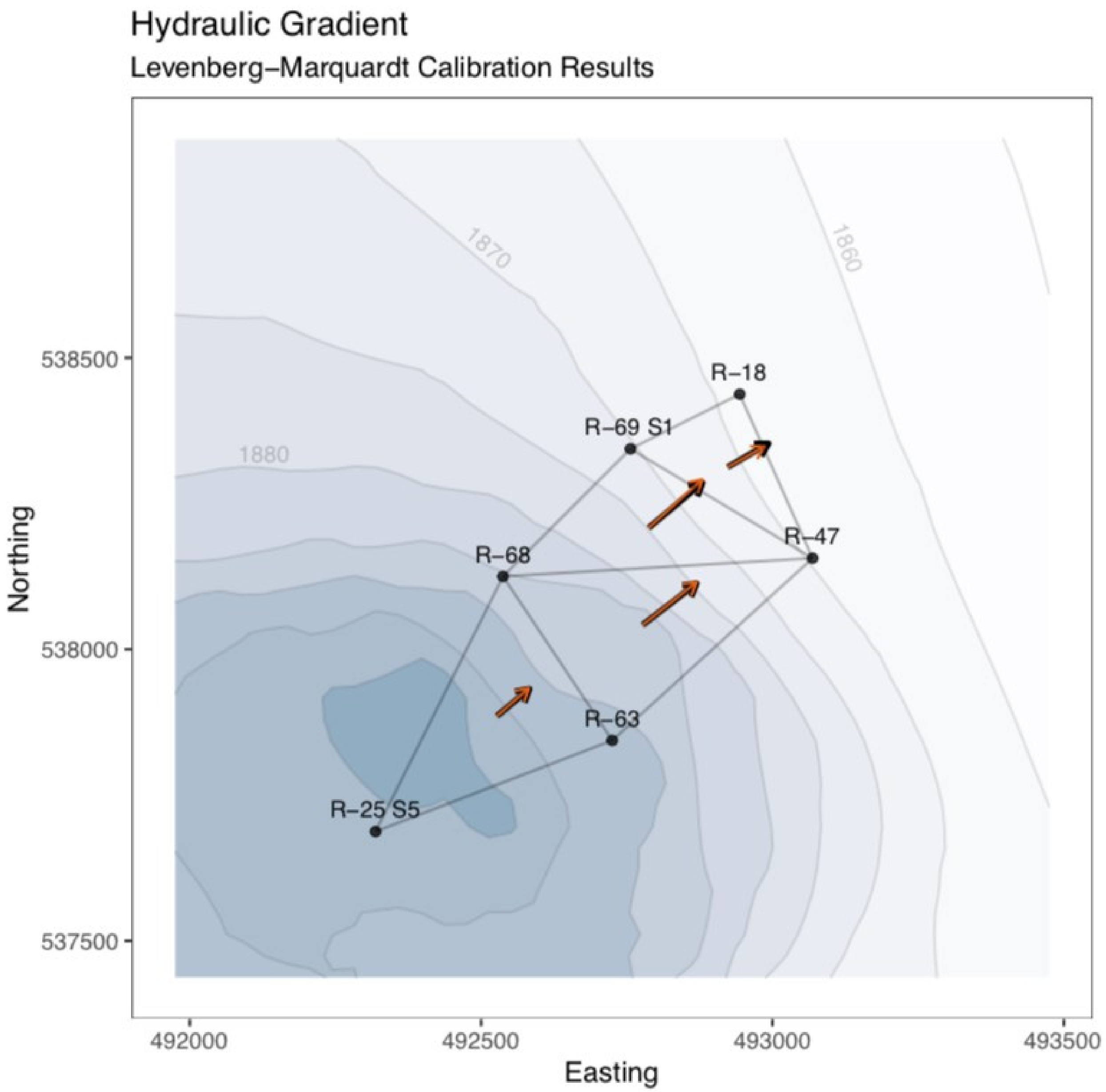

Notes: Derivation of gradient targets is described in section C-2.3.3.2. Contours of water level results from the simulation are also plotted below the gradient map.

Figure C-3.1-4 **LM calibration results (black arrows) match hydraulic gradient targets (orange arrows) nearly perfectly in both magnitude and direction**

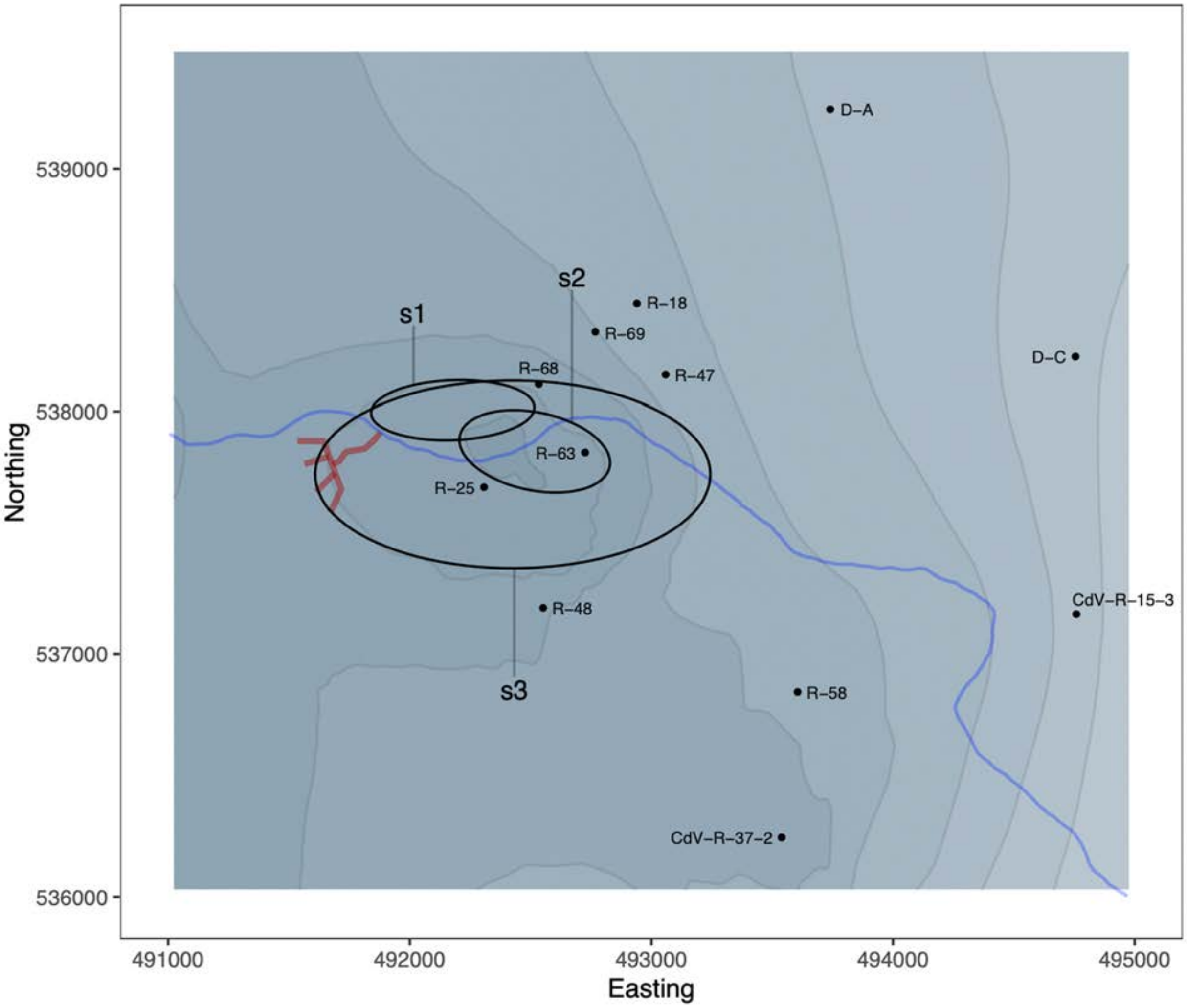

Figure C-3.1-5 **Final primary (s1), secondary (s2), and preferential recharge (s3) hydraulic window locations**

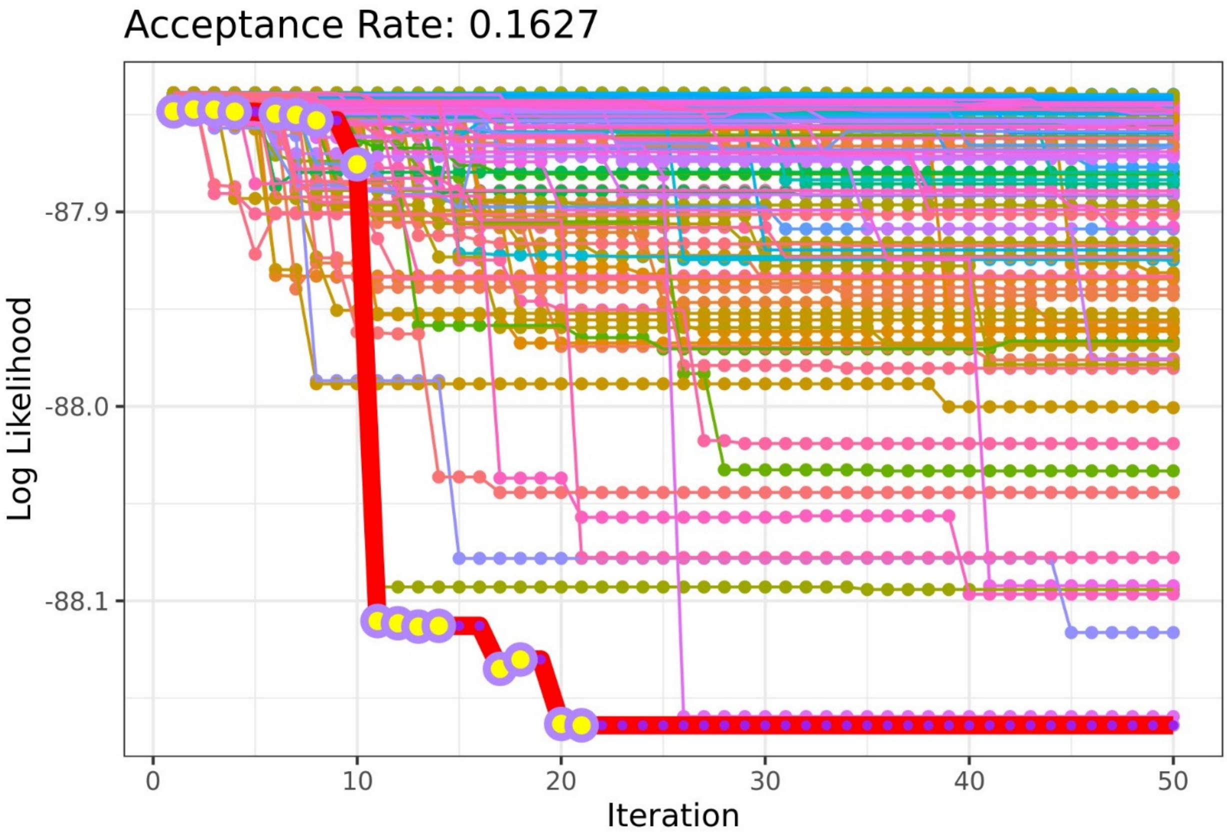

Notes: One hundred and twenty walkers were run with 50 iterations each. Walker 7 is highlighted by a red line as an example of walker movement. The yellow circles along the red line indicate iterations in which the proposed parameter set was accepted. The acceptance rate over all walkers is 16.3%.

Figure C-3.2-1 The log likelihood for each walker and each iteration in the MCMC algorithm

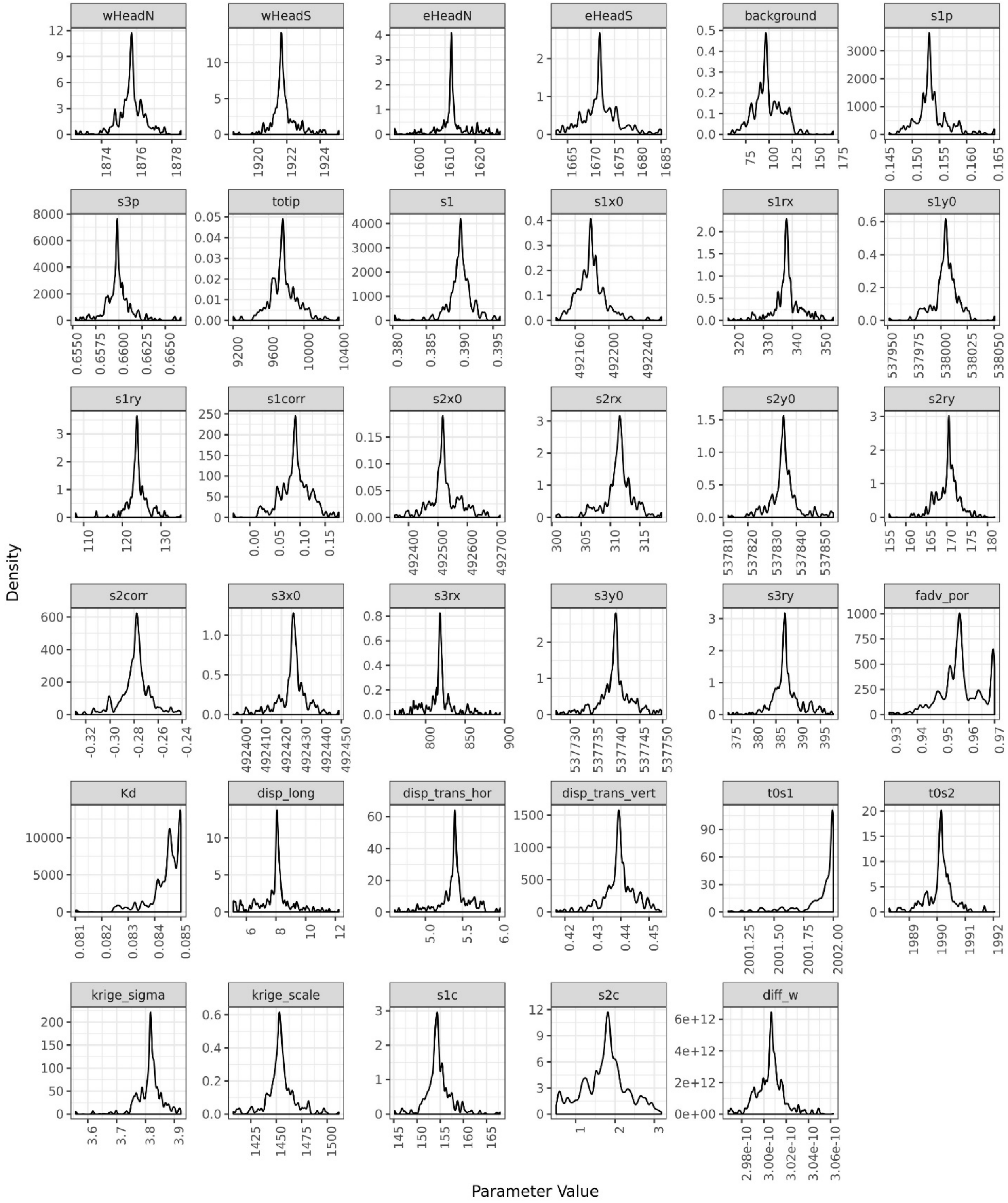

Figure C-3.2-2 Marginal posterior parameter distributions produced by the MCMC

Figure C-3.2-3 **Distributions for all posterior distributions of hydraulic conductivity (Kx, Ky, and Kz) at every anchor (1–11) and pilot (12–49) point**

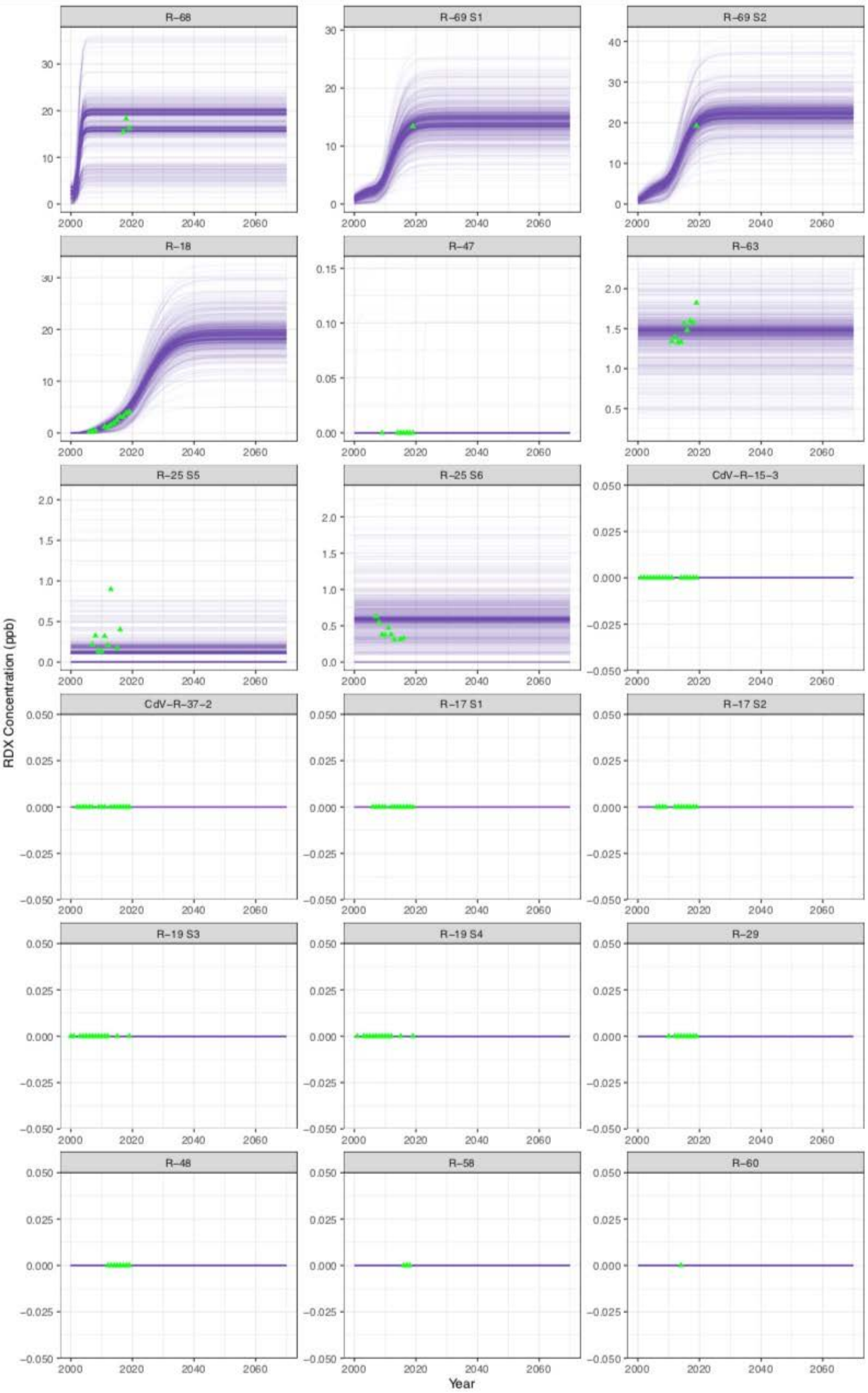

Figure C-3.3-1 **Predictive forward simulation results at every well location used for model calibration compared with target data**

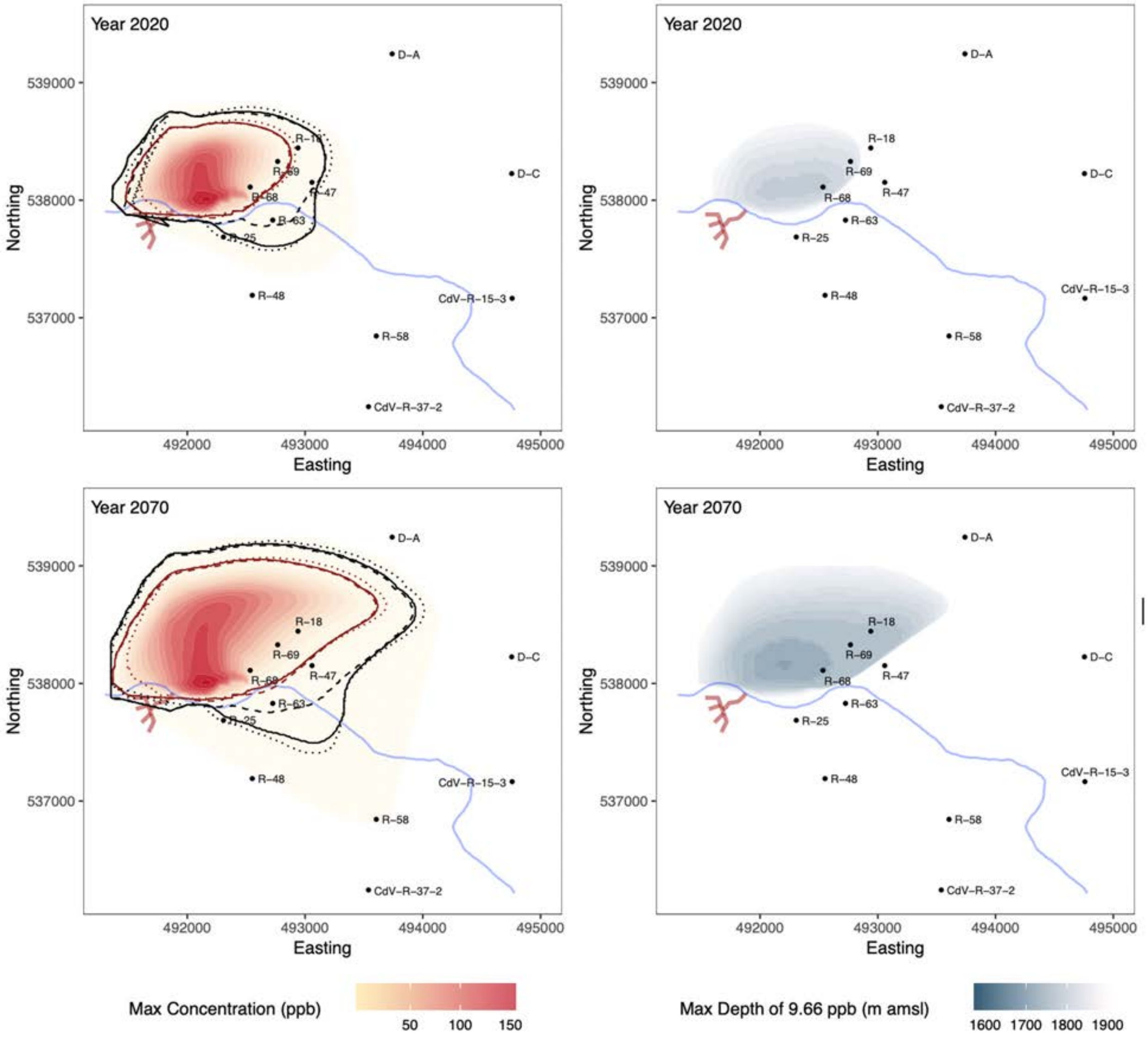

Notes: Max concentration (in any z-column) is plotted as a heat map for the median run based on the 9.66 ppb isopleth. Lines showing the uncertainty of the plume extent between simulations are added. Concentrations out to 0.1 ppb are plotted in the heat map.

Figure C-3.3-2 RDX concentrations and plume thickness plotted in years 2020 and 2070

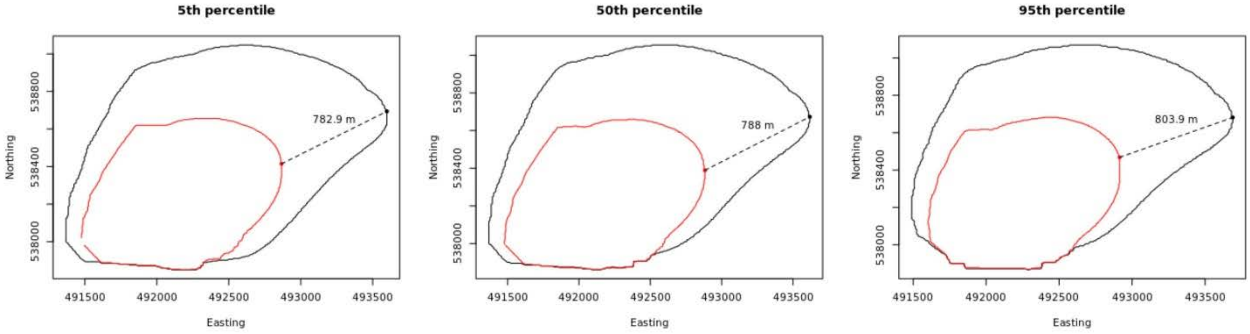

Figure C-3.3-3 **Expansion of plume from 2020 to 2070 in 5th percentile, median, and 95th percentile cases**

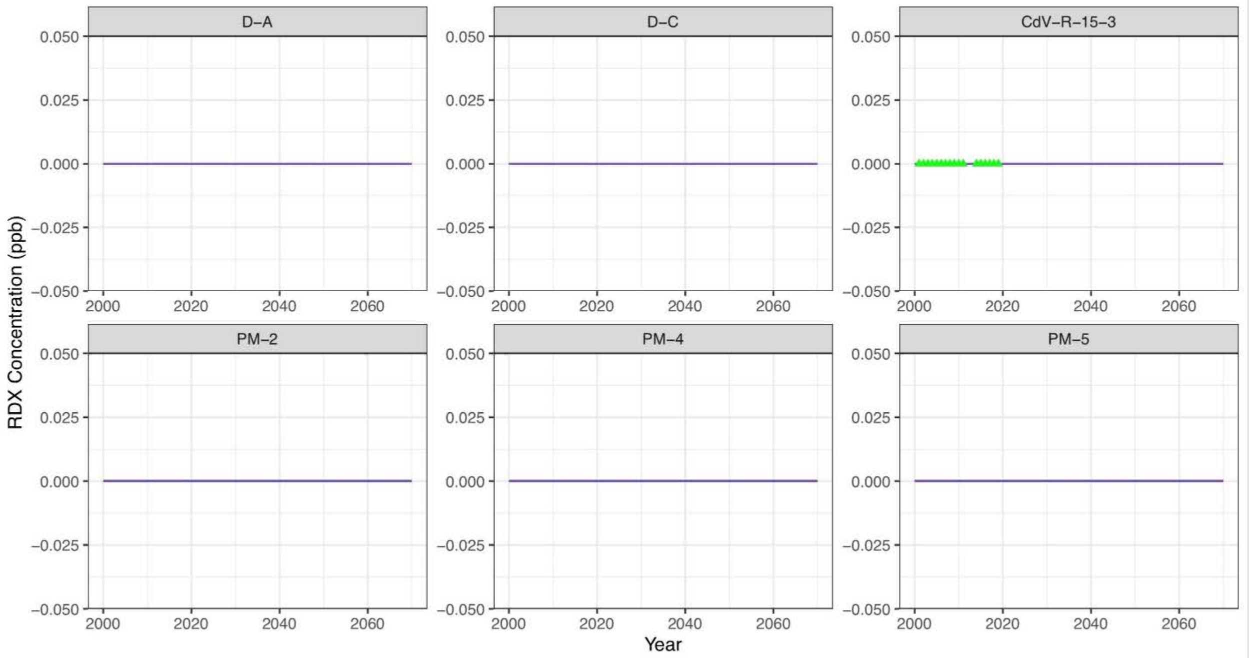

Notes: Results are plotted in the center of the frames for clarity; however, no negative concentrations were modeled. Locations of these wells are shown in Figure C-2.4-1.

Figure C-3.3-4 **No decision location selected for time series simulation output registers any RDX above a 0.1 ppb threshold by 2070**

Table C-2.2-1
Distributions for Geologic Groups

Parameter	Geology Group	Distribution	Mean	Standard Deviation	1st (%)	99th (%)
K_{xy} [log10 m/s]	1	Normal	-4.75	0.17	-5.14	-4.37
	2	Normal	-4.47	0.44	-5.51	-3.44
	3	Normal	-5.85	0.21	-6.33	-5.36
	4	Normal	-6.03	0.26	-6.65	-5.42
	5	Normal	-5.68	0.12	-5.96	-5.39
	6	Normal	-5.71	0.18	-6.12	-5.30
	7	Normal	-5.46	0.45	-6.50	-4.42
	8	Normal	-5.84	0.38	-6.73	-4.95
K_z [log10 m/s]	1	Normal	-5.97	0.28	-6.63	-5.31
	2	Normal	-5.92	0.91	-8.03	-3.81
	3	Normal	-5.17	0.54	-6.43	-3.92
	4	Normal	-2.56	0.84	-4.52	-0.61
	5	Normal	-8.40	0.92	-10.54	-6.27
	6	Normal	-4.79	0.80	-6.65	-2.92
	7	Normal	-7.04	1.94	-11.55	-2.53
	8	Normal	-5.78	0.87	-7.79	-3.76

Table C-2.2-2
Fixed Hydraulic Properties for RVZM

Formation	Density (kg/m^3)	Porosity	Residual Saturation	van Genuchten alpha (1/m)	van Genuchten n
Tpf 2	1200	0.35	0.01	5	2.68
Tvt 2	2000	0.05	0.066	0.1	2
Tpf 3	1200	0.35	0.01	5	2.68
Qbof	1200	0.44	0.043	0.59	1.76
Qct	1200	0.45	0.007	1.3	1.5
Qbt 1g	1150	0.46	0.022	0.5	1.75
Qbt 1v-u	1170	0.49	0.006	0.36	1.74
Qbt 2	1400	0.41	0.024	0.47	2.06
Qbt 3	1470	0.469	0.045	0.29	1.884
Qbt 3t	1470	0.466	0	2.57	1.332
Qbt 4	1350	0.478	0.000377	0.667	1.685
Qbof	1200	0.44	0	0.081	4.03
Qbof	1200	0.44	0	0.081	4.03

Table C-2.2-3
Calibrated Dispersivity

Unit ID	Formation	Calibration 3			Attachment 8[a]			LANL-EES[b]		
		αx	αy	αz	αx	αy	αz	αx	αy	αz
10	Tpf 2	1.602	4.958	21.531	0.102	0.288	15.000	1.200E-01	0.328	14.644
11	Tvt 2	1.679	2.214	2.539						
14	Tpf 3	1.984	2.202	12.723						
16	Qbof	3.517	1.386	22.053						
17	Qct	1.884	2.141	3.844						
19	Qbt 1g	1.403	1.237	18.218						
21	Qbt1 v-u	4.979	3.589	2.498						
22	Qbt 2	1.363	1.272	23.058						
23	Qbt 3	2.846	2.888	9.021						
24	Qbt 3t	2.695	4.000	7.188						
25	Qbt 4	0.328	2.431	1.456						
27	Qbof	1.438	3.313	2.139						
28	Qbof	2.819	2.655	8.974						
Regional Aquifer	Tpf	177.450	58.920	4.741	—[c]	—	—	—	—	—

Note: Units are meters.

[a] From “Compendium of Technical Reports Related to the Deep Groundwater Investigation for the RDX Project at Los Alamos National Laboratory,” Attachment 8 (LANL 2018, 602963).

[b] From “File Transfer Report for Chromium and RDX Project Hydrologic Modeling” (Neptune 2018, 700878).

[c] No data available.

Table C-2.2-4
Calibrated Water Fluxes and Permeability Reduction Coefficients at the Bottom of Perched Zones

Parameter	Calibration 3	Attachment 8[a]	LANL-EES[b]
Background infiltration	0.0207	0.0332	0.0772
Flux into Cañon de Valle	0.9889	1.75E-05	6.4898
Flux into other canyons	2.9824	5.71001	1.8166
MBR	4.6007	9.99312	1.2062
Permeability reduction coefficient UPZ	4.16E-04	1.13E-05	4.06E-05
Permeability reduction coefficient LPZ	2.32E-04	4.83E-04	9.58E-05
Permeability reduction coefficient UPZ window	5.95E-04	4.49E-05	1.41E-05

Note: Calibrated water fluxes are in kilograms per second.

[a] From “Compendium of Technical Reports Related to the Deep Groundwater Investigation for the RDX Project at Los Alamos National Laboratory,” Attachment 8 (LANL 2018, 602963).

[b] From “File Transfer Report for Chromium and RDX Project Hydrologic Modeling” (Neptune 2018, 700878).

Table C-2.2-5
Calibrated Permeability

Unit ID	Formation	Calibration 3		Attachment 8[a]		LANL-EES[b]	
		Kxy	**Kz**	**Kxy**	**Kz**	**Kxy**	**Kz**
10	Tpf 2	3.414E-12	1.468E-13	3.105E-12	6.394E-12	3.631E-12	3.631E-12
11	Tvt 2	1.041E-12	1.371E-11	9.164E-12	3.433E-13	2.960E-13	2.943E-13
14	Tpf 3	2.543E-12	1.026E-13	3.107E-12	9.995E-13	3.787E-13	1.055E-13
16	Qbof	1.123E-13	1.262E-12	9.999E-12	9.158E-11	9.030E-13	2.675E-12
17	Qct	3.428E-13	9.254E-09	3.080E-14	9.696E-11	1.716E-14	9.913E-12
19	Qbt 1g	3.458E-13	1.501E-15	6.139E-12	1.515E-15	8.999E-12	1.333E-14
21	Qbt 1v-u	2.272E-13	2.557E-14	2.807E-12	4.295E-14	1.029E-14	4.202E-12
22	Qbt 2	7.951E-14	2.512E-14	6.663E-13	6.031E-12	1.008E-13	1.195E-12
23	Qbt 3	3.970E-12	8.198E-13	4.229E-11	1.582E-14	9.389E-13	1.284E-13
24	Qbt 3t	2.004E-13	1.693E-12	4.350E-12	8.804E-12	2.488E-12	7.688E-12
25	Qbt 4	7.674E-14	2.169E-15	1.771E-12	2.270E-12	2.650E-13	1.415E-14
27	Qbof	5.180E-14	4.103E-12	1.786E-14	7.321E-13	2.409E-14	2.012E-14
28	Qbof	9.858E-14	7.998E-12	2.310E-13	5.860E-12	2.134E-14	2.193E-13
140	Tpf 3	3.905E-12	1.544E-13	7.553E-13	2.595E-13	6.193E-14	4.130E-14
141	Tpf 3	3.826E-12	5.218E-14	9.283E-11	5.386E-14	1.000E-11	3.778E-12
142	Tpf 3	1.254E-12	2.864E-13	8.758E-13	1.556E-13	3.314E-14	3.499E-14

Note: Units are in square meters.

[a] From “Compendium of Technical Reports Related to the Deep Groundwater Investigation for the RDX Project at Los Alamos National Laboratory,” Attachment 8 (LANL 2018, 602963).

[b] From “File Transfer Report for Chromium and RDX Project Hydrologic Modeling” (Neptune 2018, 700878).

Table C-2.2-6
Calibrated Sorption Coefficient

Unit ID	Formation	Calibration 3	Attachment 8[a]	LANL-EES[b]
10	Tpf 2	0.0997	0.0004	0.00002
11	Tvt 2	0.0276	0.5000	0.5
14	Tpf 3	0.0964	3.9900	0.27993
16	Qbof	0.0791	0.000002	0.00959
17	Qct	0.0416	0.4070	1.99835
19	Qbt 1g	0.0912	1.6360	1.76414
21	Qbt 1v-u	0.0706	0.00001	0.20414
22	Qbt 2	0.052	0.00009	0.00067
23	Qbt 3	0.0505	4.4050	1.97998
24	Qbt 3t	0.0505	4.4050	1.97998
25	Qbt 4	0.0688	0.5670	0.49990
27	Qbof	0.0791	0.000002	0.00959
28	Qbof	0.0791	0.000002	0.00959
Regional Aquifer	—[c]	0.0079	—	—

Note: Units are in milliliters per gram.

[a] From “Compendium of Technical Reports Related to the Deep Groundwater Investigation for the RDX Project at Los Alamos National Laboratory,” Attachment 8 (LANL 2018, 602963).

[b] From “File Transfer Report for Chromium and RDX Project Hydrologic Modeling” (Neptune 2018, 700878).

[c] — = Not applicable.

Table C-2.2-7
Calibrated Matrix Diffusion Coefficient

Calibration 3	Attachment 8[a]	LANL-EES[b]
1.2627E-11	3.88E-10	4.0274E-10

Note: Units are in square meters per second.

[a] From “Compendium of Technical Reports Related to the Deep Groundwater Investigation for the RDX Project at Los Alamos National Laboratory,” Attachment 8 (LANL 2018, 602963).

[b] From “File Transfer Report for Chromium and RDX Project Hydrologic Modeling” (Neptune 2018, 700878).

Table C-2.2-8
Unique Distributions for All Input Parameters to the RRM

Long Name	Parameter Name	Central Value	Unit	Sources of Information
Material Properties Parameters				
Hydraulic Conductivity(1)				
Puye Formation	(Kx, Ky)_Tpf	1.67E-05	m/s	Well data, literature
Tschicoma Formation	(Kx, Ky)_Tvt	5.63E-05	m/s	Well data, literature
Anchor points 1–11	(Kx, Ky)_(1-11)	2.51E-04 - 7.76E-09	m/s	Well data, literature
Krige Scale(2)	krige_scale	50-2000	m	Literature
Krige Sigma(2)	krige_sigma	0.1-4.0	m/s	Literature
Porosity(3)	s1	0.26	—*	Well data, literature
Advective porosity(3)	fadv_por	0.62	—	Well data, literature
Dispersivity(1)				
Longitudinal	disp_long	17.5	m	Literature
Transverse Horizontal	disp_trans_hor	4.4	m	Literature
Transverse Vertical	disp_trans_vert	0.2	m	Literature
Hydraulic Window Parameters				
Primary source centroid coordinates	s1(x,y)0	(492421.48, 538082.69)	m, State Plane NAD83	Well data, CSM, hydraulic gradient, P&D
Secondary source centroid coordinates	s2(x,y)0	(491956.15, 537350.48)	m, State Plane NAD83	CSM, surface locations, P&D
Primary source ellipse radii	s1r(x,y)	94.98, 61.37	m	RVZM, P&D, CSM
Secondary source ellipse radii	s2r(x,y)	77.04, 61.49	m	RVZM, P&D, CSM
Source shape (eccentricity)(2)	s(1-2)corr	0	—	RVZM, P&D
Primary source RDX concentration(3)	s1c	93.39	ppb	RVZM
Secondary source RDX concentration(3)	s2c	13.36	ppb	RVZM
Preferential recharge(3)	totip	-5249.28	mm/yr	RVZM
Background recharge(3)	background	-222.17	mm/yr	RVZM
Preferential recharge source centroid coordinates(2)	s3(x,y)0	(492489.16, 538296.55)	m, State Plane NAD83	CSM
Preferential recharge source radii(2)	s3r(x,y)	94.98, 61.37	m	CSM

Table C-2.2-8 (continued)

Long Name	Parameter Name	Central Value	Unit	Sources of Information
Primary percentage recharge	s1p	17.5	—	Literature, CSM
Secondary percentage recharge	s2p	17.5	—	Literature, CSM
Preferential percentage recharge	s3p	4.4	—	Literature, CSM
Primary source arrival time$^{(1)}$	t0s1	1983	year	RVZM, P&D
Secondary source arrival time$^{(1)}$	t0s2	1982	year	RVZM, P&D
Other Parameters				
Eastern constant head$^{(2)}$	easthead	1669	m	Data, literature, modeling
Western constant head$^{(2)}$	westhead	2094	m	Well data, literature
Sorption Coefficient	Kd	0.0296	mL/g	Literature
Effective Diffusion Coefficient	diff_w	2.96E-10	m^2/s	Literature

Note: Parameter distributions are normal unless marked with superscripts: (1) lognormal, (2) uniform, (3) truncnormal.

* — = Not applicable.

Table C-2.2-9
Geologic Groups for the RDX Site

Group	Name	Sub-geologies Included
1	All Puye	Tf, Tpf, Tpf 2, Tpf 3
2	Tschicoma	Tvt 1, Tvt 2, Tt, Tt 2
3	All Otowi	Qbof, Qbof G2, Qbof G3, Qbo, Qbog
4	Cerro Toledo	Qct
5	Tshirege Unit 1	Qbt 1g, Qbt 1v, Qbt1 v-u
6	Tshirege Unit 2	Qbt 2
7	Tshirege Unit 3	Qbt 3, Qbt 3t
8	Tshirege Unit 4	Qbt 4

Table C-2.2-10
Summary Statistics of K_{xy} for Each Group Calculated on the $\log_{10}$ Scale

Group	# Obs.	# Sm.	# Int.	# Site	# Unk.	# Geo.	# Wells	Min	Max	Med	Mean	SD*
1	236	112	119	5	0	3	36	0.002	290.0	2.500	17.200	40.200
2	8	0	7	1	0	1	4	0.800	76.0	48.80	41.600	32.700
3	58	47	8	3	0	3	11	0.000	31.2	0.277	1.400	4.940
4	4	3	0	1	0	1	3	0.096	0.785	0.257	0.349	0.311
5	54	52	0	2	0	2	21	0.028	19.20	0.397	1.260	3.110
6	47	46	0	1	0	1	14	0.002	9.920	0.113	0.708	1.590
7	55	53	0	2	0	2	6	0.016	132.0	0.230	3.110	17.800
8	10	9	0	1	0	1	4	0.024	5.530	0.211	0.788	1.680

Note: Units are feet per day.

* SD = Standard deviation.

Table C-2.2-11
Summary Statistics of Anisotropies for Each Group

Group	# Obs.	# Geo Types	# Wells	Min	Max	Med	Mean	SD[a]
1	26	3	12	0.001	2.060	0.171	0.235	0.399
2	1	1	1	0.038	0.038	0.038	0.038	n/a[b]
3	6	3	2	0.499	41.000	4.830	12.800	16.900
4	1	1	1	3148.052	3148.052	3148.052	3148.052	n/a
5	2	2	1	0.000247	0.015	0.008	0.008	0.011
6	1	1	1	9.050	9.050	9.050	9.050	NA
7	2	2	1	0.000374	2.020	1.010	1.010	1.430
8	1	1	1	1.280	1.280	1.280	1.280	n/a

[a] SD = Standard deviation.

[b] n/a = Not applicable.

Table C-2.2-12
Distributions for Anchor Points

Parameter	Geology	Well	Dist.	Mean	Standard Deviation	1st [%]	99th [%]
K_{xy} [log10 m/s]	Puye	R-26 screen 2	Uniform	-8.11	1.85	-12.42	-3.80
	Puye	R-30	Normal	-4.75	0.17	-5.14	-4.37
	Tschicoma	R-48	Normal	-4.47	0.44	-5.51	-3.44
	Puye	CdV-R-15-3 screen 5	Normal	-6.25	0.20	-6.72	-5.79
	Puye	CdV-R-15-3 screen 6	Normal	-6.25	0.20	-6.72	-5.79
	Puye	R-18	Normal	-4.66	0.02	-4.70	-4.62
	Puye	R-29	Normal	-4.75	0.01	-4.76	-4.73
	Tschicoma	R-58	Normal	-3.60	0.01	-3.62	-3.58
	Puye	R-60	Normal	-5.90	0.02	-5.94	-5.86
	Puye	R-63	Normal	-4.78	0.04	-4.86	-4.69
	Puye	R-68	Normal	-4.47	0.02	-4.51	-4.43
K_z [log10 m/s]	Puye	R-26 screen 2	Uniform	-9.16	1.94	-13.69	-4.64
	Puye	R-30	Normal	-5.96	0.28	-6.62	-5.31
	Tschicoma	R-48	Normal	-5.83	0.90	-7.92	-3.75
	Puye	CdV-R-15-3 screen 5	Normal	-7.48	0.30	-8.19	-6.78
	Puye	CdV-R-15-3 screen 6	Normal	-7.48	0.30	-8.19	-6.78
	Puye	R-18	Normal	-5.89	0.23	-6.43	-5.34
	Puye	R-29	Normal	-5.97	0.23	-6.52	-5.43
	Tschicoma	R-58	Normal	-5.05	0.80	-6.90	-3.19
	Puye	R-60	Normal	-7.11	0.23	-7.65	-6.57
	Puye	R-63	Normal	-6.01	0.24	-6.56	-5.45
	Puye	R-68	Normal	-5.70	0.22	-6.22	-5.18

Table C-2.2-13
Pilot Point and the Geology Group Assignments Based on Nearest Anchor Points

Type of Pilot Point	Name	Group
PP Well	pp12CdV-R-15-3	Puye
PP Well	pp13R-17	Puye
PP Well	pp14CdV-R-37-2	Tschicoma
PP Well	pp15R-19	Puye
PP Well	pp16R-25	Puye
PP Well	pp17R-25 deep	Puye
PP Well	pp18R-47	Puye
PP Well	pp19R-69	Puye
PP Well	pp20R-69 deep	Puye
Pilot Point	pp21	Tschicoma
Pilot Point	pp22	Puye
Pilot Point	pp23	Tschicoma
Pilot Point	pp24	Puye
Pilot Point	pp25	Puye
Pilot Point	pp26	Puye
Pilot Point	pp27	Puye
Pilot Point	pp28	Puye
Pilot Point	pp29	Puye
Pilot Point	pp30	Puye
Pilot Point	pp31	Puye
Pilot Point	pp32	Puye
Pilot Point	pp33	Puye
Pilot Point	pp34	Puye
Pilot Point	pp35	Puye
Pilot Point	pp36	Puye
Pilot Point	pp37	Puye
Pilot Point	pp38	Puye
Pilot Point	pp39	Puye
Pilot Point	pp40	Tschicoma
Pilot Point	pp41	Puye
Pilot Point	pp42	Tschicoma
Pilot Point	pp43	Tschicoma
Pilot Point	pp44	Puye
Pilot Point	pp45	Puye
Pilot Point	pp46	Puye
Pilot Point	pp47	Puye
Pilot Point	pp48	Puye
Pilot Point	pp49	Puye

Table C-2.2-14
Distribution Development Weighting and Length Scales Used in References

Reference	VZ Weight	SZ Weight	Length Scale (m)
Neuman 1990, 090184	0.5	0.5	0.1–100,000
Abbaspour et al. 1997, 700896	0.5	0.1	0.4–3
van Genuchten et al. 1987 ("Analysis and Prediction of Water and Solute Transport in a Large Lysimeter" from NRC 1987, 700882)	0.9	0.1	0.36–4.15
Umari et al. 2008, 700899	0.5	0.3	30.4
Waldrop et al. 1985, 700900	0.1	0.8	3500–3500
Reimus et al. 2003, 210315	0.5	0.3	30
Meyer et al. 1981, 700901	0.1	0.3	8
Bromly et al. 2007, 700902	0.05	0.7	0.051–0.3
Bromly et al. 2007, 700902	0.05	0.2	0.1–0.213
Gelhar et al. 1992, 102465	0.5	0.5	<= 115–91
Waldrop et al. 1985, 700900	0.5	0.1	0.23–20
Waldrop et al. 1985, 700900	0.1	0.3	<115–28
Waldrop et al. 1985, 700900	0.1	0.8	0.75–9.3
LANL 2018, 602963	0.3	0.5	3000
Fujinawa 2010, 100903	0.5	0.8	50000
French et al. 2008, 106890	0.1	0	60
Birdsell et al. 1999, 069792	0.1	0	100–250
DOE 2010, 700880	0	0.1	40

Table C-2.2-15
Distribution Values for Longitudinal Dispersivity

Value	RVZM (VZ)	RRM (SZ)
Length scale of application (*L*)	1–500 m	100–10,000 m
$\log_{10}\widehat{\beta_1} = \hat{\gamma}_1$, Equation C-7	-2.68	-0.43
$\widehat{\beta_2} = \hat{\gamma}_2$, Equation C-7	1.88	0.49
$\mathrm{SE}(\widehat{\gamma_1})$, Equation C-9	0.18	0.17
$\mathrm{SE}(\widehat{\gamma_2})$, Equation C-9	0.20	0.08
$\mathrm{Cov}(\widehat{\gamma_1}, \widehat{\gamma_2})$, Equation C-9	-0.03	-0.01

Table C-2.2-16
Distribution Values for the Transverse Dispersivity Directions

Value	Transverse Horizontal	Transverse Vertical
$\log_{10}\widehat{\beta_1} = \hat{\gamma}_1$, Equation C-7	-0.72	-2.02
$\widehat{\beta_2} = \hat{\gamma}_2$, Equation C-7	1.10	1.00
$\mathrm{SE}(\widehat{\gamma_1})$, Equation C-9	0.14	0.24
$\mathrm{SE}(\widehat{\gamma_2})$, Equation C-9	0.06	0.09
$\mathrm{Cov}(\widehat{\gamma_1}, \widehat{\gamma_2})$, Equation C-9	-0.007	-0.02

Table C-2.2-17
Distributions for Aqueous Dispersivity Needed for the RDX Area on the log10 Scale

Model, Direction	Distribution	Mean [–]*	Standard Deviation [–]
Regional, Longitudinal	N	$\boldsymbol{x}\begin{bmatrix}-0.43\\0.49\end{bmatrix}$	$\sqrt{\left(\boldsymbol{x}\begin{bmatrix}2.9E\text{-}2 & \text{-}1.3E\text{-}2\\ \text{-}1.3E\text{-}2 & 6.8E\text{-}3\end{bmatrix}\boldsymbol{x}^{\boldsymbol{T}}\right)}$
Both, Transverse Horizontal	N	$\boldsymbol{x}\begin{bmatrix}\text{-}072\\1.10\end{bmatrix}$	$\sqrt{\left(\boldsymbol{x}\begin{bmatrix}1.9E\text{-}2 & -7.1E\text{-}3\\ \text{-}7.1E\text{-}3 & 3.3E\text{-}3\end{bmatrix}\boldsymbol{x}^{\boldsymbol{T}}\right)}$
Both, Transverse Vertical	N	$\boldsymbol{x}\begin{bmatrix}\text{-}2.02\\1.00\end{bmatrix}$	$\sqrt{\left(\boldsymbol{x}\begin{bmatrix}5.6E\text{-}2 & \text{-}2.0E\text{-}2\\ \text{-}2.0E\text{-}2 & 8.1E\text{-}3\end{bmatrix}\boldsymbol{x}^{\boldsymbol{T}}\right)}$

* The vector ***x*** is a row vector of the form $\boldsymbol{x} = [1 \quad \log_{10} L]$.

Table C-2.2-18
Linear Regression Statistics

Estimate	Coefficient	SE	Confidence Interval	t Statistic	p-value
Intercept	13304.63	739.70	(11706.59, 14902.66)	17.99	<0.001
Slope	-0.023	0.001	(-0.026, -0.020)	-15.48	<0.001

Table C-2.2-19
Extrapolation of Water Levels

Location	x-coordinate	Water Level (m)
Southeast	498975	1735.32
East middle	506350	1564.32
Northeast	510100	1477.37

Table C-2.2-20
Distribution Developed for Hydraulic Head Boundary Conditions

Parameter	Distribution	Minimum	Maximum
Hydraulic head at western boundary	Uniform	1860	1930
Hydraulic head at eastern boundary	Uniform	1470	1690

Table C-2.2-21
RVZM Geologic Unit Groupings

Name	Abbreviation	Unit ID	Kd Group
Puye Formation, Lower	Tpf 2	10	S
Tschicoma Formation, Upper	Tvt 2	11	V
Puye Formation, Upper	Tpf 3	14	S
Otowi Member of the Bandelier Tuff	Qbof	16	V
Cerro Toledo Formation	Qct	17	V
Tshirege Member of the Bandelier Tuff, subunit 1g	Qbt 1g	19	V
Tshirege Member of the Bandelier Tuff, subunit 1vu	Qbt 1v-u	21	V
Tshirege Member of the Bandelier Tuff, subunit 2	Qbt 2	22	V
Tshirege Member of the Bandelier Tuff, subunit 3	Qbt 3	23	V
Tshirege Member of the Bandelier Tuff, subunit 3t (transition zone)	Qbt 3t	24	V
Tshirege Member of the Bandelier Tuff, subunit 4	Qbt 4	25	V
Otowi Member, Ash Flow	Qbof G2	27	V
Otowi Member, Ash Flow	Qbof G3	28	V
Puye Formation, Upper	Tpf 3	140	S
Puye Formation, Upper	Tpf 3	141	S
Puye Formation, Upper	Tpf 3	142	S

Table C-2.2-22
Final K_d Distributions

Material	Dist.	Mean K_d Value (mL/g)	Standard Deviation (mL/g)	1st (mL/g)	99th (mL/g)	Note	Pr(X<0) (%)
(V) Volcanic Materials	Normal	0.0235	0.0215	-0.0266	0.0735	Bulldoze at 0 mL/g	13.7
(S) Sedimentary Materials	Normal	0.0296	0.0238	-0.0259	0.0850	Bulldoze at 0 mL/g	10.8

Table C-2.3-1
Hydraulic Head Target Data

Well	Method	February 2014 Water Level
CDV-R-15-3 S5	February 2014 monthly mean	1833.12
CDV-R-37-2 S2	February 2014 monthly mean	1869.32
R-13	February 2014 monthly mean	1777.85
R-17 S1	February 2014 monthly mean	1793.51
R-17 S2	February 2014 monthly mean	1792.62
R-18	February 2014 monthly mean	1864.43
R-19 S3	February 2014 monthly mean	1794.06
R-19 S4	February 2014 monthly mean	1791.67
R-25 S5	February 2014 monthly mean	1899.05
R-25 S6	February 2014 monthly mean	1890.69
R-25 S7	February 2014 monthly mean	1877.80
R-48	February 2014 monthly mean	1869.41
R-60	February 2014 monthly mean	1800.55
R-63	February 2014 monthly mean	1887.15
R-29	February 2014 monthly mean	1812.76
R-47	imputed using R-47	1865.24
R-58	imputed using CdV-R-37-2 S2	1869.03
R-68	imputed using R-63	1885.85
R-69 S1	imputed using R-18	1870.52
R-69 S2	imputed using R-18	1867.33

Table C-2.3-2
Summary of the Hydraulic Gradient Magnitude and Direction Target Values

Well Triple	Magnitude (m/m)	Direction (deg.)
R-25 S5, R-68, R-63	0.0289	49.9
R-68, R-63, R-47	0.0469	52.3
R-68, R-69 S1, R-47	0.0481	50.3
R-69 S1, R-18, R-47	0.0326	60.3

Table C-2.3-3
Summary of the Concentration Trend Target Values

Well	Slope (ppb/yr)	Preference Weight
R-18	0.31	5
R-25 S5	0.024	0.5
R-25 S6	-0.030	0.5
R-63	0.053	3
R-68	0.37	1

Table C-2.3-4
Uncertainty Quantified by Maximum Absolute Difference between Simulations and Targets at Each Well with Targets above the Detection Limit of 0.1 ppb

Well	Max delta abs(simulation—target) (ppb)
R-68	20.6
R-69 screen 2	17.6
R-69 screen 1	14.6
R-18	5.6
R-25 screen 6	2.0
R-25 screen 5	2.0
R-63	1.6

Appendix D

Perched-Intermediate Groundwater Database Query
(on CD included with this document)